3-29-2019

Synthesis And Metalation Of Internally Alkylated Porphyrinoids

Alissa Nicole Latham
Illinois State University, alissa.latham1@gmail.com

SYNTHESIS AND METALATION OF INTERNALLY ALKYLATED PORPHYRINOIDS

ALISSA NICOLE LATHAM

310 pages

The mechanism for alkyl group migration in palladium(II) benzocarbaporphyrins was investigated by synthesizing a 23-methylcarbaporphyrin and reacting it with palladium(II) acetate. It was found that palladium insertion led to methyl group migration to C21 and it is proposed that this occurs through an oxidative addition onto the palladium metal center, followed by a reductive elimination to transfer the methyl to the internal carbon. A similar rearrangement was observed when 23-methylcarbaporphyrin was reacted with $[Rh(CO)_2Cl]_2$ and this resulted in the formation of a rhodium(III) complex containing a three-membered rhodacycle. The syntheses of rhodium(I) and rhodium(III) derivatives of other carbaporphyrins, including 21- and 22-methylbenzo-carbaporphyrins, were probed and four of these metalated complexes were characterized by X-ray crystallography. To further investigate the effect of internal substituents on porphyrinoid systems, a series of *N*-methylated porphyrinoids were synthesized using the versatile '3+1' variant of the MacDonald condensation. The spectroscopic data for the internally methylated derivatives were compared to their *N*-unsubstituted counterparts. It was found that internal alkylation greatly affects the chromophore of these systems, as is evident by bathochromic shifts and peak broadening in the UV-Vis spectra. However, the aromatic character of these systems is fully retained after the introduction of an internal substituent, and proton NMR spectroscopy shows the presence of large macrocyclic ring currents.

KEYWORDS: carbaporphyrin, rhodium, aromaticity, metalation, alkylation, rearrangement, crystallography

SYNTHESIS AND METALATION OF INTERNALLY ALKYLATED PORPHYRINOIDS

ALISSA NICOLE LATHAM

A Thesis Submitted in Partial
Fulfilment of the Requirements for
the Degree of

MASTER OF SCIENCE

Department of Chemistry

ILLINOIS STATE UNIVERSITY

2019

SYNTHESIS AND METALATION OF INTERNALLY ALKYLATED PORPHYRINOIDS

ALISSA NICOLE LATHAM

COMMITTEE MEMBERS:

Timothy D. Lash, Chair

Gregory M. Ferrence

Shawn R. Hitchcock

ACKNOWLEDGMENTS

The author would like to acknowledge the members of her research group and thank them for their support throughout the duration of her time at Illinois State University. The author would also like to thank Dr. Timothy D. Lash for his endless patience, guidance and encouragement throughout the time she spent working with him. The writer acknowledges financial support from the National Science Foundation under grants no. CHE-1212691 and CHE-1465049 and the Petroleum Research Fund. The author also thanks NSF grant no. CHE-1039689 for funding the X-ray diffractometer.

The writer would also like to thank the members of her committee. Dr. Gregory M. Ferrence for his assistance in obtaining all the X-ray crystal structures and his guidance, and Dr. Shawn R. Hitchcock for his encouragement and support. Finally, the author thanks her parents for their unending love and encouragement and her dog Nala for always lifting her spirits.

A. N. L

CONTENTS

		Page
ACKNOWLEDGMENTS		i
CHARTS		iv
FIGURES		v
SCHEMES		x
CHAPTERS		
I.	INTRODUCTION	1
II.	ALKYL GROUP MIGRATION IN INTERNALLY METHYLATED PALLADIUM(II) BENZOCARBAPORPHYRINS	32
	Introduction	32
	Results and Discussion	36
	Conclusion	51
	Experimental	52
III.	RHODIUM COMPLEXES OF CARBAPORPHYRINOID SYSTEMS	59
	Introduction	59
	Results and Discussion	61
	Conclusion	94
	Experimental	95
IV.	SYNTHESIS AND CHARACTERIZATION OF *N*-METHYLATED PORPHYRINOIDS	102
	Introduction	102
	Results and Discussion	102

Conclusion 133

Experimental 134

V. CONCLUSIONS 144

REFERENCES 147

APPENDIX A: SPECTROSCOPIC DATA FOR PYRROLIC INTERMEDIATES 163

APPENDIX B: SPECTROSCOPIC DATA FOR
23-METHYLBENZOCARBAPORPHYRIN AND PALLADIUM(II) COMPLEXES 178

APPENDIX C: SPECTROSCOPIC DATA FOR RHODIUM COMPLEXES 203

APPENDIX D: SPECTROSCOPIC DATA FOR *N*-METHYLATED PORPHYRINOIDS 249

CHARTS

Chart	Page
1. Examples of porphyrin and porphyrin analogues	3
2. Organometallic benzocarbaporphyrins	4
3. Organometallic complexes of benziporphyrin and azuliporphyrin	4
4. Rhodium(III) and iridium(III) azuliporphyrins	5
5. Porphyrin analogues and their metal complexes	6
6. Hetero- and diheteroporphyrinoids	9
7. Common π-electron delocalization pathways observed in porphyrinoids	12
8. Examples of methylated N-confused porphyrins	26
9. Examples of metalated azuliporphyrins	61

FIGURES

Figure Page

1. Shielding and deshielding regions due to porphyrin ring current 13
2. Dipolar resonance structure for azuliporphyrins 17
3. 500 MHz ^{1}H NMR spectrum of pyrrole ester **78** in $CDCl_3$. The multiplet at 5.23 ppm corresponds to a small amount of the related isopropyl ester pyrrole (ca. 3%) that results from the transesterification with the solvent 2-propanol 38
4. 500 MHz ^{1}H NMR spectrum of 23-methylbenzocarbaporphyrin **76** in $CDCl_3$ 42
5. UV-vis spectra of 23-methylcarbaporphyrin **76** in 1% triethylamine-dichloromethane (free base, red line) and 1% TFA-dichloromethane (monocation **76**H^+, purple line) 43
6. Color POV-Ray rendered ORTEP III drawing (50% probability level, hydrogen atoms rendered arbitrarily small for clarity) of 23-methylcarbaporphyrin **76** 43
7. UV-vis spectra of palladium(II) carbaporphyrin complexes **84** (23-methyl, red line) and **72** (21-methyl, blue line) 46
8. Downfield region for the ^{1}H NMR spectra of 23-methyl palladium complex **84** (top spectrum) and 21-methyl palladium complex **72** (bottom spectrum) 47
9. Color POV-Ray rendered ORTEP III drawing (50% probability level, hydrogen atoms rendered arbitrarily for clarity) of 21-methyl palladium(II) complex **72** 48
10. Time course experiments on the rate of alkyl group migration, showing the conversion of **84** (black line) into **72** (red line) **a)** Timed reflux reactions **b)** Reaction of **84** in d_3-acetonitrile at 70 °C in an NMR tube within a 500 MHz NMR instrument 50
11. 500 MHz ^{1}H NMR spectrum of rhodium(I) carbaporphyrin diester **89** in $CDCl_3$ 64
12. 125 MHz ^{13}C NMR spectrum of rhodium(I) carbaporphyrin diester **89** in $CDCl_3$ 64

13. IR spectrum of rhodium(I) carbaporphyrin diester **89** 65

14. UV-Vis spectrum of rhodium(I) carbaporphyrin diester **89** 65

15. Color POV-Ray rendered ORTEP III drawing (50% probability level, hydrogen atoms rendered arbitrarily small for clarity) of rhodium(I) carbaporphyrin **89** 67

16. 500 MHz ^{1}H NMR spectrum of rhodium(III) carbaporphyrin diester **90** in d_6-benzene 68

17. UV-Vis spectrum of rhodium(III) carbaporphyrin diester **90** 69

18. Color POV-Ray rendered ORTEP III drawing (50% probability level, hydrogen atoms rendered arbitrarily small or omitted for clarity) of rhodium(III) complex **90** 71

19. 500 MHz ^{1}H NMR spectrum of rhodium(I) naphthocarbaporphyrin **91** in $CDCl_3$ 74

20. 125 MHz ^{13}C NMR spectrum of rhodium(I) naphthocarbaporphyrin **91** in $CDCl_3$ 74

21. IR spectrum of rhodium(I) naphthocarbaporphyrin **91** 75

22. UV-Vis spectrum of rhodium(I) naphthocarbaporphyrin **91** 75

23. Color POV-Ray rendered ORTEP III drawing (50% probability level, hydrogen atoms rendered arbitrarily small for clarity) of rhodium(I) naphthocarbaporphyrin **91** 77

24. 500 MHz ^{1}H NMR spectrum of rhodium(III) naphthocarbaporphyrin **92** in d_6-benzene 79

25. 125 MHz ^{13}C NMR spectrum of rhodium(III) naphthocarbaporphyrin **92** in d_6-benzene 79

26. UV-Vis spectrum of rhodium(III) naphthocarbaporphyrin **92** 80

27. 500 MHz ^{1}H NMR spectrum of rhodium(I) 22-methylbenzocarbaporphyrin **93** in $CDCl_3$ 83

28. 125 MHz ^{13}C NMR spectrum of rhodium(I) 22-methylbenzocarbaporphyrin **93** in $CDCl_3$ 84

29. IR spectrum of rhodium(I) 22-methylbenzocarbaporphyrin **93** 84

30. UV-Vis spectrum of rhodium(I) 22-methylbenzocarbaporphyrin **93** 85

31. 500 MHz ^{1}H NMR spectrum of rhodium(I) 21-methylbenzocarbaporphyrin **94** in $CDCl_3$ 86

32. 125 MHz ^{13}C NMR spectrum of rhodium(I) 21-methylbenzocarbaporphyrin **94** in $CDCl_3$ 87

33. IR spectrum of rhodium(I) 21-methylbenzocarbaporphyrin **94** 87

34. UV-Vis spectrum of rhodium(I) 21-methylbenzocarbaporphyrin **94** 88

35. 400 MHz ^{1}H NMR spectrum of bridged rhodium(III) complex **95** in $CDCl_3$ 90

36. 100 MHz ^{13}C NMR spectrum of bridged rhodium(III) complex **95** in $CDCl_3$ 90

37. UV-Vis spectrum of bridged rhodium(III) complex **95** 91

38. Color POV-Ray rendered ORTEP III drawing (50% probability level, hydrogen atoms rendered arbitrarily small for clarity) of methylene-bridged rhodium(III) carbaporphyrin **95** 93

39. 500 MHz ^{1}H NMR spectrum of 23-methyl-21-oxaporphyrin **96b** in $CDCl_3$ 105

40. 125 MHz ^{13}C NMR spectrum of 23-methyl-21-oxaporphyrin **96b** in $CDCl_3$ 106

41. UV-Vis spectra of **96b** in 1% triethylamine-dichloromethane (free base, pink line) and **96a** in 1% triethylamine-dichloromethane (free base, black line) 106

42. UV-Vis spectra of **96a** in 1% triethylamine-dichloromethane (free base, dark blue line) or 1% TFA-dichloromethane (dication, light blue line), and **96b** in 1% triethylamine-dichloromethane (free base, red line) or 1% TFA-dichloromethane (dication, pink line) 107

43. 500 MHz ^{1}H NMR spectrum of *N*-methyl thiaporphyrin **97b** in $CDCl_3$ 110

44. 125 MHz ^{13}C NMR spectrum of *N*-methyl thiaporphyrin **97b** in $CDCl_3$ 111

45. UV-Vis spectra of **97b** in 1% triethylamine-dichloromethane (free base, purple line) and **97a** in 1% triethylamine-dichloromethane (free base, black line) 111

46. UV-Vis spectra of **97b** in 1% triethylamine-dichloromethane (free base, blue line) and 1% TFA-dichloromethane (dication, green line), and **97a** in 1% triethylamine-dichloromethane (free base, purple line) and 1% TFA-dichloromethane (dication, red line) 112
47. 500 MHz ^{1}H NMR spectrum of *N*-methyl porphyrin **99b** in $CDCl_3$ 115
48. 125 MHz ^{13}C NMR spectrum of *N*-methyl porphyrin **99b** in $CDCl_3$ 115
49. UV-Vis spectra of *N*-methyl porphyrin **99b** (red line) and *N*-unsubstituted porphyrin **99a** (black line) 116
50. UV-Vis spectra of **99b** in 1% triethylamine-dichloromethane (free base, black line) and 1% TFA-dichloromethane (dication, purple line) 116
51. 500 MHz ^{1}H NMR spectrum of *N*-methyloxybenziporphyrin **100a** in $CDCl_3$ 119
52. 125 MHz ^{13}C NMR spectrum of *N*-methyloxybenziporphyrin **100a** in $CDCl_3$ 120
53. UV-Vis spectra of *N*-methyloxybenziporphyrin **100a** (blue line) and *N*-unsubstituted oxybenziporphyrin **7a** (black line) 120
54. UV-Vis spectra of **100a** in 1% triethylamine-dichloromethane (free base, black line) and 1% TFA-dichloromethane (dication, blue line) 121
55. IR spectrum of *N*-methyloxybenziporphyrin **100a** 121
56. 500 MHz ^{1}H NMR spectrum of palladium(II) oxybenziporphyrin complex **102** in $CDCl_3$ 123
57. 125 MHz ^{13}C NMR spectrum of palladium(II) oxybenziporphyrin complex **102** in $CDCl_3$ 123
58. IR spectrum of palladium(II) oxybenziporphyrin complex **102** 124
59. 500 MHz ^{1}H NMR spectrum of *N*-methyloxypyriporphyrin **100b** in $CDCl_3$ 126

60. 125 MHz ^{13}C NMR spectrum of *N*-methyloxypyriporphyrin **100b** in $CDCl_3$ 126

61. IR spectrum of *N*-methyloxypyriporphyrin **100b** 127

62. UV-Vis spectra of *N*-methyloxypyriporphyrin **100b** (green line) and the *N*-unsubstituted oxypyriporphyrin **7b** (black line) 127

63. UV-Vis spectra of **100b** in 1% triethylamine-dichloromethane (free base, black line) and 1% TFA-dichloromethane (monocation, green line) 128

64. 500 MHz ^{1}H NMR spectrum of *tert*-butyl azuliporphyrin **103**H_2^{2+} in TFA-d_6-DMSO 131

65. 125 MHz ^{13}C NMR spectrum of *tert*-butyl azuliporphyrin **103**H_2^{2+} in TFA-d_6-DMSO 131

66. UV-Vis spectra of **103a** in 1% triethylamine-dichloromethane (free base, black line) and **103b** in 1% triethylamine-dichloromethane (free base, purple line) 132

67. UV-Vis spectra of **103b** in 1% triethylamine-dichloromethane (free base, black line) and in 1% TFA-dichloromethane (dication, red line) 132

SCHEMES

Scheme Page

1. Formation of palladium(II) complexes of 23-oxa-, 23-thia- and 23-selena-21-benzocarbaporphyrins 8
2. Formation of nickel(II) complexes **24a,b** and oxyheterocarbaporphyrin 8
3. C-H activation of aryl units by Rh(III) porphyrins 10
4. Ring contraction of Rh(III) benziporphyrins into Rh(III) carbaporphyrins containing a three-membered rhodacycle 11
5. Mono- and diprotonation of benzocarbaporphyrin **3** 15
6. Protonation of tropiporphyrin **9** 16
7. Protonation of benziporphyrin **5** 18
8. Protonation of dimethoxybenziporphyrin **8** 18
9. Tetramerization of monopyrroles to produce porphyrins 21
10. Etioporphyrin type-isomers from the acid-catalyzed tetramerization of a pyrrole 21
11. '2+2' MacDonald condensation reaction 22
12. '3+1'variant of the MacDonald Condensation 23
13. Synthesis of a tripyrrane 24
14. Synthesis of heteroporphyrins through the '3+1' variant of the MacDonald reaction 25
15. Methylation of NCP to give a *N*,*N*-dimethyl NCP 26
16. Alkylation of an oxidized benziporphyrin derivative 27
17. Alkylation of palladium(II) oxybenziporphyrin 28
18. Base-promoted rearrangement of palladium(II) *p*-benziporphyrin to palladium(II) carbaporphyrin 29

19. Alkyl group migration in a palladium(II) benzocarbaporphyrin complex 30

20. Preparation of benzocarbaporphyrin via the '3+1' MacDonald condensation 33

21. Methylation of benzocarbaporphyrin **73** 33

22. Proposed [1,5] sigmatropic rearrangement for alkyl group migration 35

23. Synthesis and protonation of 23-methylbenzocarbaporphyrin **76** 36

24. Barton-Zard synthesis and methylation of a pyrrole precursor 37

25. Synthesis of acetoxymethylpyrrole **80** 39

26. Synthesis of *N*-methyl tripyrrane **54d** 40

27. Metalation of 23-methylbenzocarbaporphyrin to give 23- and 21-methyl palladium(II) complexes 45

28. Proposed mechanism for migration of an alkyl group from the 23- to 21-position of benzocarbaporphyrins 50

29. Metalation of benzocarbaporphyrin **3** to give rhodium(I) and rhodium(III) derivatives 60

30. Rhodium(I) and rhodium(III) complexes of carbaporphyrin diester **88** 62

31. Rhodium(I) and rhodium(III) complexes of naphthocarbaporphyrin **87** 72

32. Formation of 21- and 22-methyl rhodium(I) derivatives **94** and **93** 81

33. Formation of rhodium derivative **95** of 23-methylcarbaporphyrin **76** 89

34. '3+1' Synthesis of 23-methyl-21-oxaporphyrin **96** 103

35. '3+1' Synthesis of 23-methyl-21-thiaporphyrin **97** 108

36. '3+1' Synthesis of 23-methylporphyrin **99** 113

37. '3+1' Synthesis of *N*-methylated and *N*-unsubstituted oxybenzi- and oxypyriporphyrins 117

38. Metalation of *N*-methyloxybenziporphyrin **100a** with palladium(II) acetate 122

39. Synthesis of *N*-methylazuliporphyrin **103b**H_2^{2+} 129

CHAPTER I: INTRODUCTION

Porphyrins **1** (Chart 1) and metalloporphyrins have been widely investigated, due not only to their biological importance, but also to their numerous applications. Metalloporphyrins provide important functions in nature, including oxygen transportation by hemoglobin and photosynthesis with chlorophyll, oxidation reactions with the cytochromes, and many redox functions as well.[1,2-5] Porphyrins and closely related phthalocyanines are two classes of conjugated systems that are used in areas such as dyes and inks, as well as in the development of optical materials with potential use in optical recording technology.[1,6] Metalloporphyrins, incorporating numerous different metals, have been investigated in the development of artificial molecular recognition receptors, enzyme mimics, DNA cleaving agents, chiral catalysts for asymmetric synthesis, materials, and in the discovery of new reactions.[2,5, 7-11] Certain porphyrins are also known for their applications as photosensitizers within the medical field, because of their high affinity for tumor cells and ability to produce singlet oxygen in Photodynamic Therapy (PDT).[12]

To act as a photosensitizer, the compound needs to absorb energy from light, which it then uses to produce the singlet oxygen. Unfortunately, light is strongly absorbed by bodily tissue over much of the visible region, which places limitations on clinical applications.[6] Light has the greatest penetration at higher wavelengths, specifically between 650-800 nm, which is the reason there has been extensive research directed towards developing photosensitizers that absorb in this range of wavelengths. Therefore, modifying porphyrin and porphyrin analogue structures has been explored in an attempt to produce molecules that absorb within the needed wavelength range. Investigations into modifying the porphyrin chromophore also gives insights into the coordination

chemistry of porphyrin-like systems, as well as the nature of conjugation and aromaticity seen in these macrocyclic molecules.[6]

Porphyrin is one of nature's most versatile ligands, forming coordination complexes with virtually every known metal.[13] The majority of elements in the periodic table can form complexes with porphyrins, and many of them can also take on additional axial ligands.[14] These macrocyclic compounds possess an internal cavity that contains four nitrogen atoms and this allows for the flexibility in coordination. However, the internal atoms of this cavity can be altered, which gives rise to a number of different porphyrin derivatives. Carbaporphyrins[15-18] are porphyrin analogues in which one or more of the internal nitrogen atoms are replaced with a carbon atom, and include true carbaporphyrins such as **2** and **3**,[16,18] azuliporphyrins **4**,[19] benziporphyrins **5**,[20] N-confused porphyrins **6**,[21] oxybenziporphyrins **7a**,[22,23] dimethoxybenziporphyrins **8**[24] and tropiporphyrins **9**[25] (Chart 1).

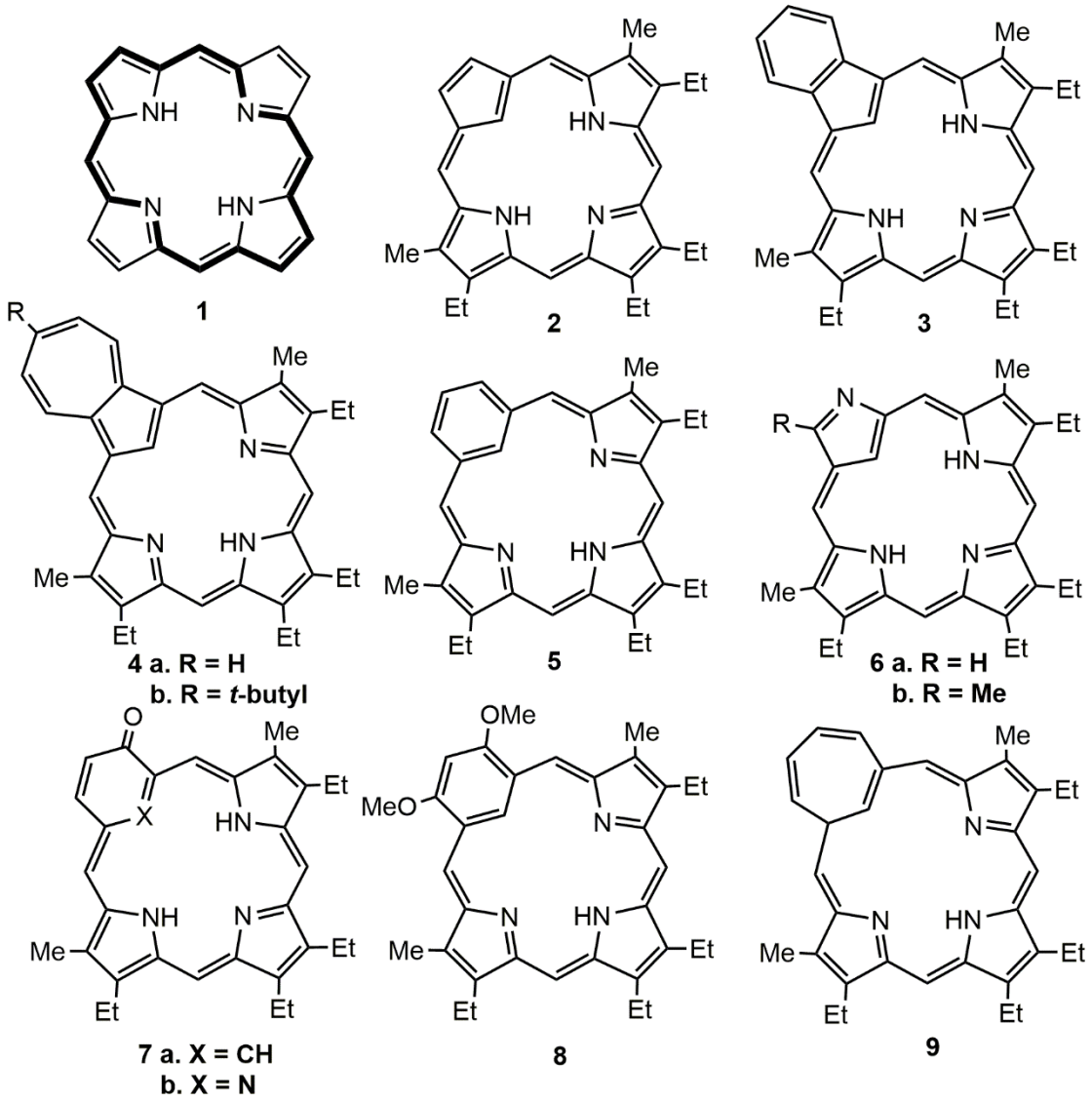

Chart 1. Examples of porphyrin and porphyrin analogues

Even with the modified core, these carbaporphyrinoids still undergo metal coordination, albeit with a smaller number of mainly late transition metals.[26] True carbaporphyrins, such as **2** and **3**, normally act as trianionic ligands. Benzocarbaporphyrin **3** has been shown to form complexes with metals such as Ag(III),[27-29] Au(III),[28] Rh(III)[30] and Ir(III)[30] to give organometallic derivatives such as **10a,b** and **11a,b** (Chart 2). On the other hand, benziporphyrins[31] act as dianionic ligands affording metal complexes such as **12a-c**, and azuliporphyrins similarly react to

afford Ni(II),[32] Pd(II)[32] and Pt(II)[32] complexes **13a-c**, as well as Ru(II) derivative **14**[33] (Chart 3). Azuliporphyrins can also form Rh(III) complexes **15a-c** and **16**, and Ir(III) derivatives **17a-d** (Chart 4), but these metal centers have an additional axial ligand.[34,35]

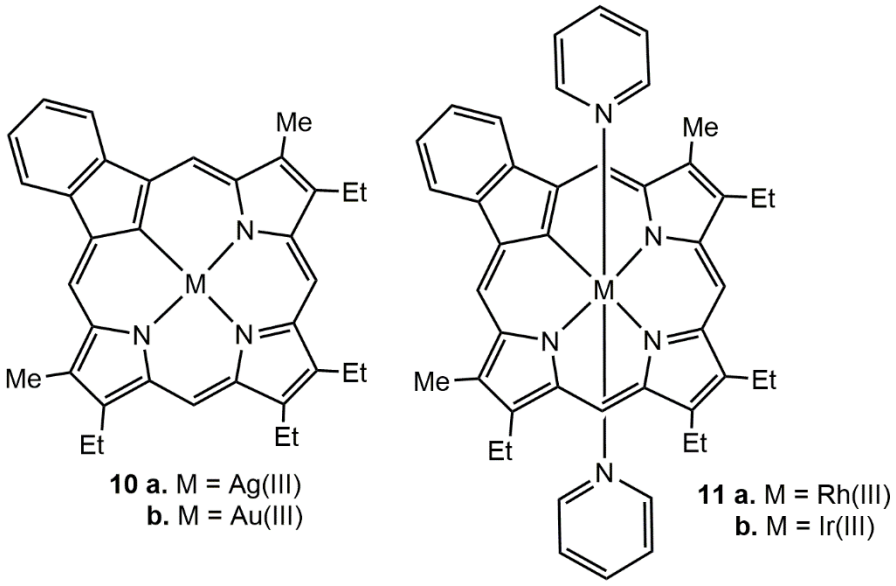

Chart 2. Organometallic benzocarbaporphyrins

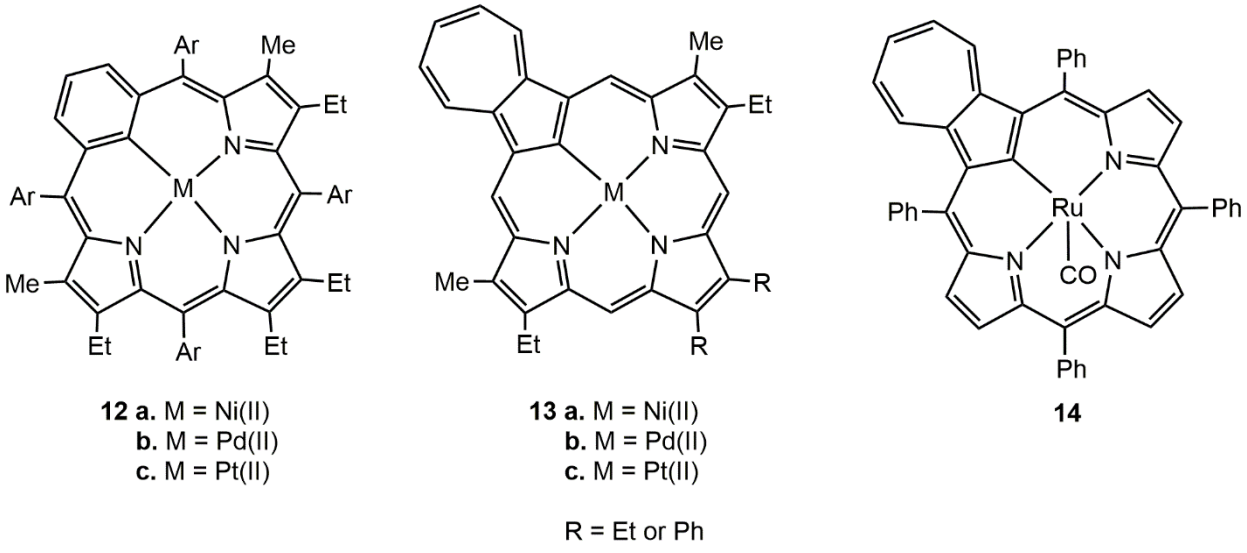

Chart 3. Organometallic complexes of benziporphyrin and azuliporphyrin

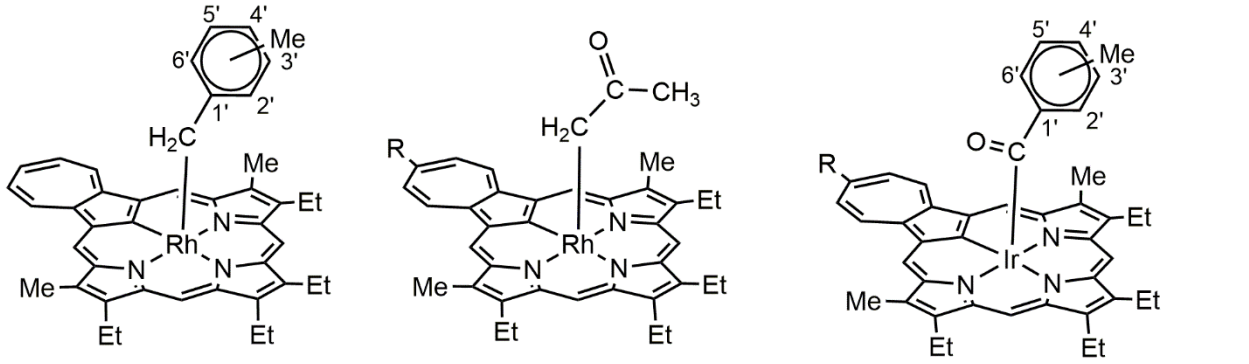

Chart 4. Rhodium(III) and iridium(III) azuliporphyrins

N-confused porphyrins (NCPs)[36] typically act as both dianionic and trianionic ligands. Reaction of *N*-confused porphyrin with nickel(II) chloride in refluxing chloroform/methanol gave a nickel(II) complex where one of the NH protons had moved to the external nitrogen.[37] An example of *N*-confused porphyrin acting as a trianionic ligand can be seen in the reaction of NCP with silver(I) trifluoracetate, which affords the Ag(III) complex.[38] Oxybenziporphyrin also gave Ag(III) complex **18a** (Chart 5) when treated with silver(I) acetate,[39] but also reacted with palladium(II) chloride to form an anionic Pd(II) complex **19a**.[40] Oxybenziporphyrin also formed a related anionic platinum(II) complex **19b** when reacted with platinum(II) chloride.[41] Tetraaryloxybenziporphyrins not only formed Ag(III) derivatives **18b**, but also gave Au(III) complexes **18c** [42] (Chart 5). Dimethoxy benziporphyrins **20a,b** and **21a,b** formed nickel(II) complexes **22a-d** when reacted with nickel(II) acetate.[43,44] They also reacted with palladium(II) acetate to afford the related palladium(II) complexes **23a-d**[44] (Chart 5). Similarly, dimethoxybenziporphyrins with two *meso*-substituents were prepared and reacted with palladium(II) acetate to give the corresponding palladium(II) complexes.[45] When tropiporphyrins

9 were reacted with silver(I) acetate at room temperature, only trace amounts of the corresponding silver complexes were formed. However, when they were refluxed with silver(I) acetate and DBU in pyridine, the corresponding silver(III) complexes were obtained in good yields.[46]

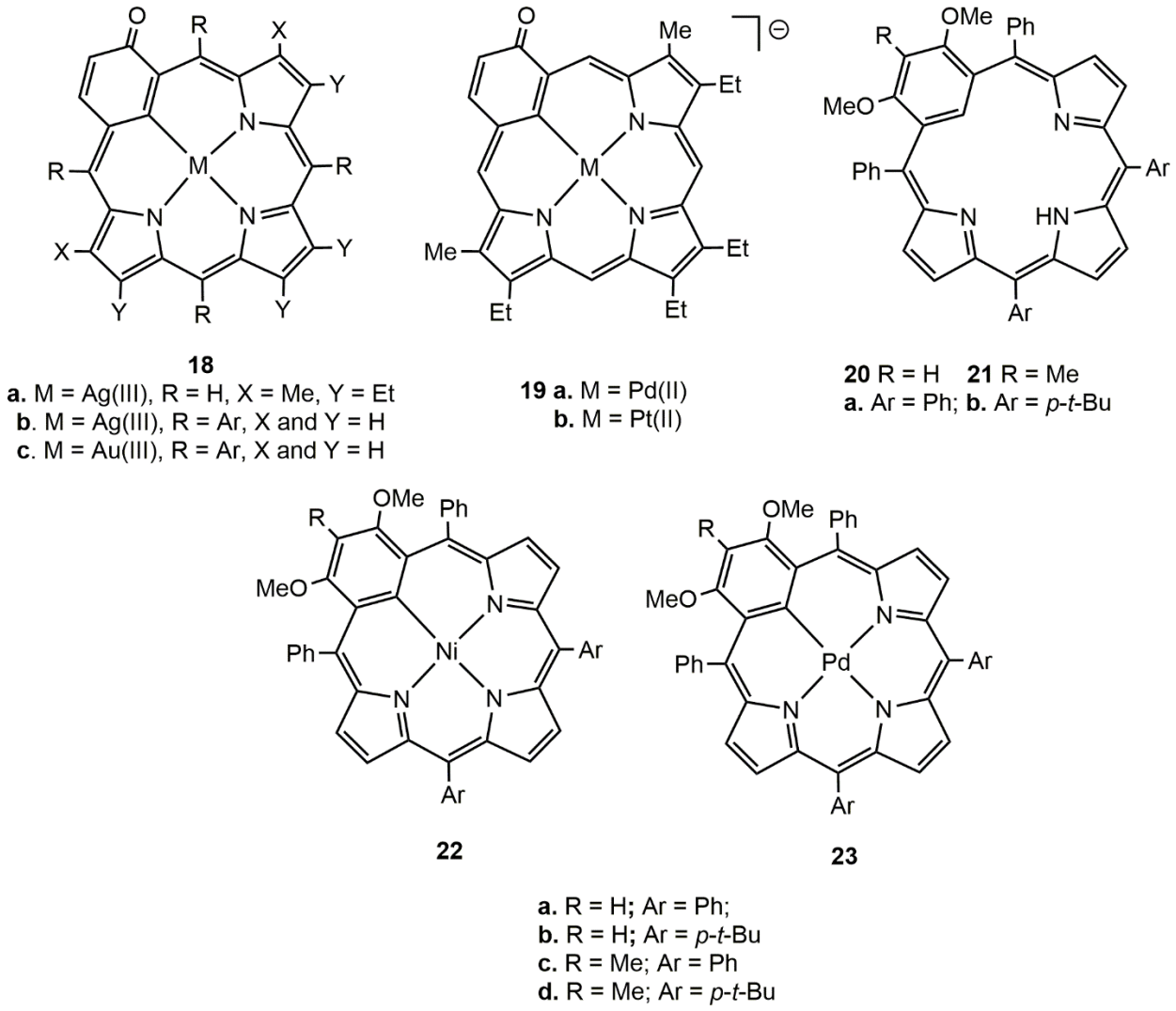

Chart 5. Porphyrin analogues and their metal complexes

Further modifications to the reactivity of carbaporphyrins have been observed in heterocarbaporphyrins, where the internal cavity of 21-benzocarbaporphyrins **3** not only contains nitrogen and carbon atoms, but also oxygen, sulfur or selenium atoms **24a-c**[46] at the 23-position

(Scheme 1). Normally, benzocarbaporphyrins are trianionic, possessing three internal hydrogens that can be given up in favor of coordinating with metal centers. 23-Oxa-, 23-thia- and 23-selena-21-benzocarbaporphyrins **24a-c** were reacted with palladium(II) acetate to afford the corresponding palladium(II) complexes **25a-c** (Scheme 1), where the porphyrin was shown to act as a dianionic ligand instead.[46] This is due to there being one fewer internal hydrogens when one of the remaining nitrogen atoms is replaced by the oxygen, sulfur or selenium. The same dianionic character was seen when the same benzocarbaporphyrins were reacted with nickel(II) acetate in DMF, affording the corresponding nickel(II) complexes **26a,b**. However, in the presence of air oxidation to oxyheterocarbaporphyrins **27** was observed (Scheme 2).[46] Heteroporphyrins with an internal core of XNNN **28a-d** (Chart 6), in general, have much lower reactivity towards metalation, which is due in part to the reduced planarity of the macrocycle.[47] Furthermore, incorporation of larger heteroatoms (S, Se and Te) result in a change in the cavity size, which plays a role in reducing metal-binding in heteroporphyrins.[48] However, despite this weaker metal-binding behavior, examples of metalated heteroporphyrins do exist. For example, Latos-Grazynski and co-workers reported the first synthesis of Cu(II), Fe(II) and Ni(II) complexes **29a-c** of tetraphenyl-21-thiaporphyrin **30** by treating the free-base with copper, iron and nickel chloride salts under reflux conditions (Chart 6).[49]

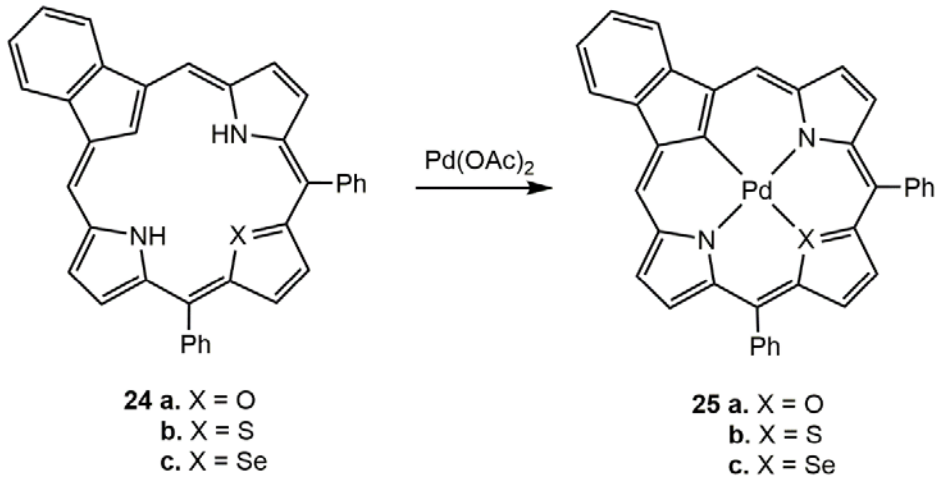

24 a. X = O
b. X = S
c. X = Se

25 a. X = O
b. X = S
c. X = Se

Scheme 1. Formation of palladium(II) complexes of 23-oxa-, 23-thia- and 23-selena-21-benzocarbaporphyrins

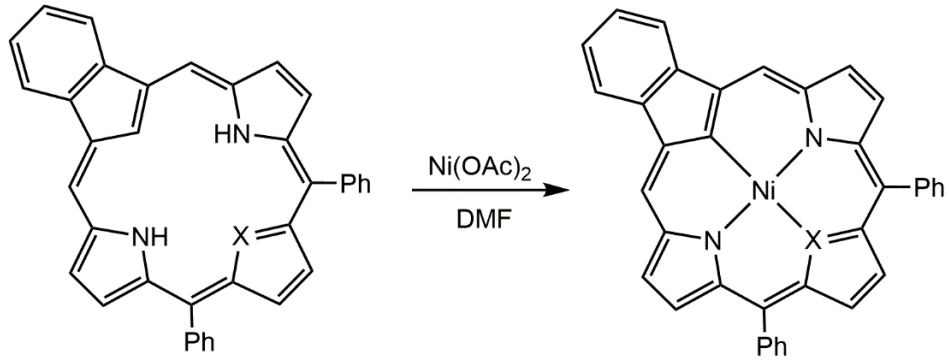

24 a. X = O
b. X = S

26 a. X = O
b. X = S

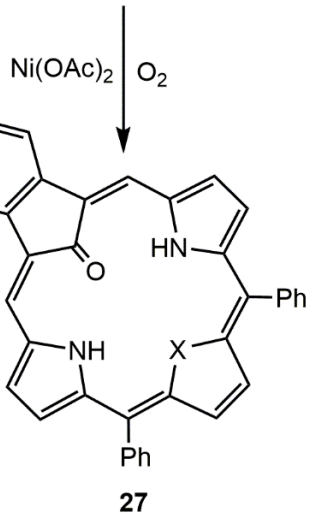

27

Scheme 2. Formation of nickel(II) complexes **24a,b** and oxyheterocarbaporphyrin

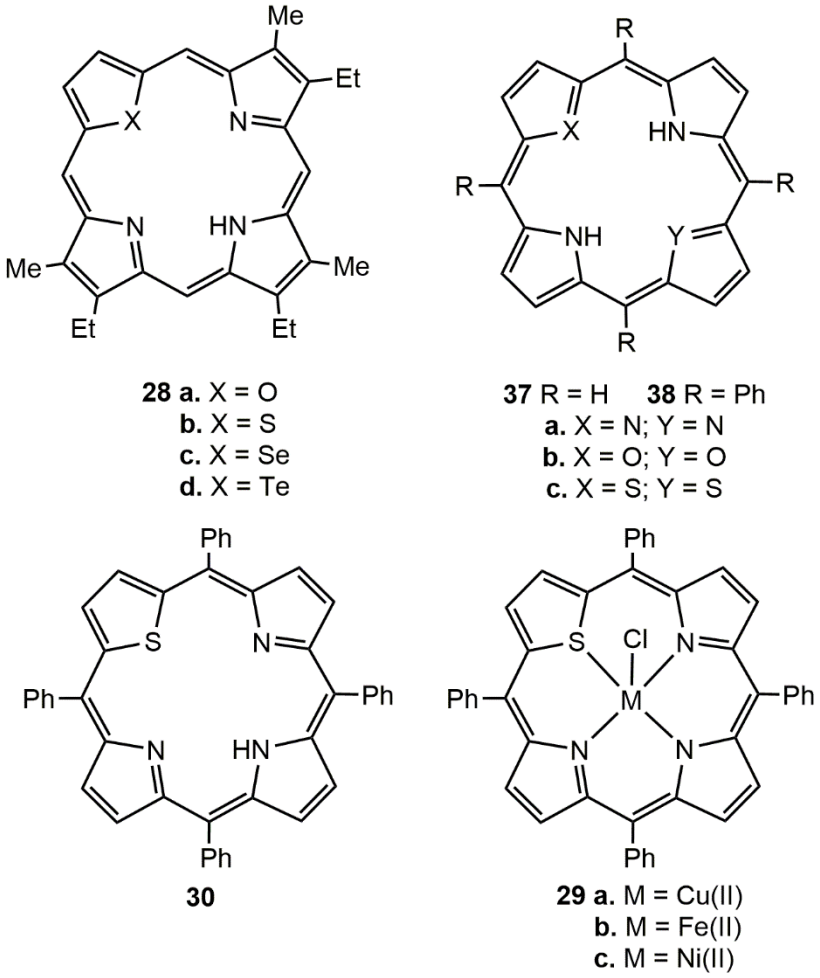

Chart 6. Hetero- and diheteroporphyrinoids

All three of these metal complexes incorporated chloride as an axial ligand and were stable in the solid state. However, the Fe(II) complex demetalated in solution upon standing.[47] Similarly, the palladium(II) complex was obtained by refluxing 21-thiaporphyrin with palladium(II) chloride. Rh(III)[50] and Ru(III)[51] complexes were also reported for the same heteroporphyrin, along with many other metals.[52-54] Likewise, 21-oxaporphyrin has been shown to form Ni(II),[55] Fe(III),[56] Zn(II),[58], Re(I)[54] Mn(II),[59] Co(II)[59] and Cu(II)[59] complexes.

Rhodium complexes of porphyrins have attracted much interest and have been studied for the past 50 years, leading to important discoveries such as catalytic enantioselective

cyclopropanations, as well as more recently, selective C-H and C-C activation transformations.[1] Due to its small size in all of its oxidation states, rhodium can fit neatly into the nearly planar porphyrin ligand to form rhodium(I), rhodium(II) and rhodium(III) complexes with varying geometries. The rhodium(I) complexes possess square planar geometries, while rhodium(II) porphyrins exhibit square planar monomeric and square pyramidal dimeric geometries, and rhodium(III) porphyrins are commonly associated with square pyramidal or octahedral geometries.[1] The square planar and square pyramidal geometries of some of these rhodium complexes allow axial ligands to easily coordinate to the metal center. Rhodium coordination has been investigated thoroughly and examples of five- and six-coordinate complexes have been seen with nitrogen, sulfur, phosphorus, oxygen and carbon-based ligands.[1,60-62] The vast number of rhodium complexes is due to their high association constants, ranging from 10^5 for nitrogen-based ligands and 10^8 for phosphorus-based ligands.[1] Rhodium(III) porphyrins have been shown to facilitate carbon-hydrogen bond activation,[63-65] specifically, Rh(OEP)Cl complexes **31** (OEP = 2,3,7,8,12,13,17,18-octaethylporphyrin) were found to be prone to electrophilic cleavage of aryl C-H bonds to form aryl rhodium(III) porphyrins **32**.[66,67] This occurred through **31** being activated by either $AgClO_4$ or $AgBF_4$ to generate the electrophilic metalloporphyrin (Scheme 3).

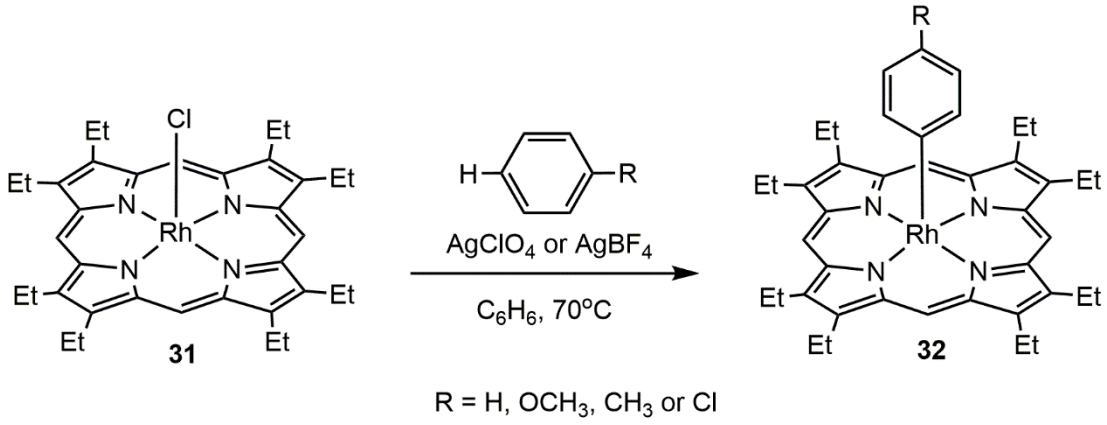

Scheme 3. C-H activation of aryl units by Rh(III) porphyrins

The resulting cationic species can then activate the C-H bonds in benzene, anisole, toluene and chlorobenzene to form the corresponding aryl species with selective metalation at the para positions.[66,67] Rhodium(III) porphyrinoid complexes have also been shown to undergo ring contractions. Specifically, *p*- and *m*- benziporphyrins ring contracted into true carbaporphyrins while also generating a three-membered ring rhodacycle **33** (Scheme 4).[68]

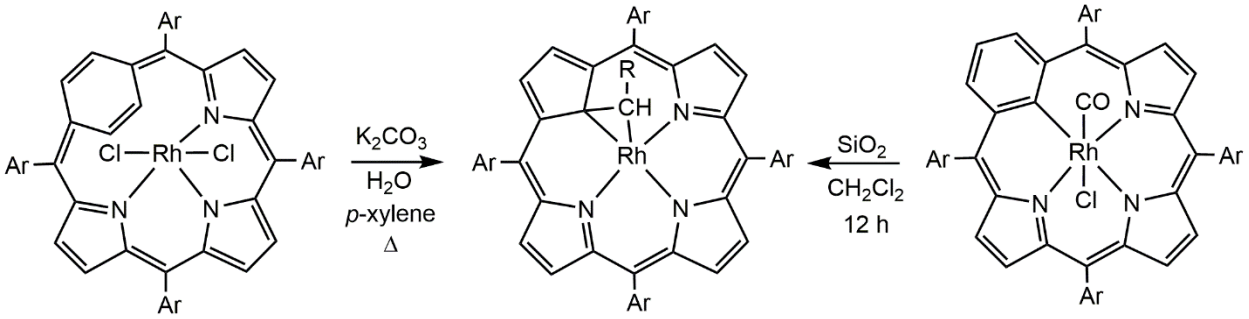

33 a. R = H
b. R = CHO

Scheme 4. Ring contraction of Rh(III) benziporphyrins into Rh(III) carbaporphyrins containing a three-membered rhodacycle

Alongside the interest that arises from studying these stable organometallic complexes, porphyrin derivatives are widely investigated for their aromatic properties. This aromatic character is evident through X-ray crystallography, where the absence of bond length alternation implies the presence of a conjugated pathway around the macrocycle, as well as from characteristic chemical shifts in proton NMR spectroscopy, and the ability of the porphyrin nucleus to maintain its integrity when analyzed by electron impact mass spectrometry.[3] However, there has been much dispute over the factors that are responsible for porphyrinoid aromaticity. The porphyrin system contains 26π electrons, which includes two "lone pairs" found on the internal nitrogens. However, it was proposed by Sondheimer,[69] and later Emmanuel Vogel[70,71] during a study on bridged annulenes, that an 18π-electron pathway (shown in bold for structure **1**, Chart 1) found within the

system resembles [18]annulene **34** (Chart 7) and is a major contributor to the aromaticity observed in porphyrinoids.

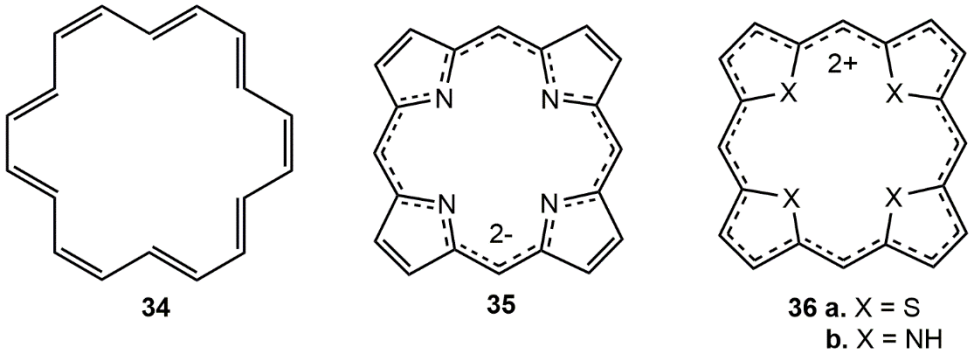

34 **35** **36 a.** X = S **b.** X = NH

Chart 7. Common π-electron delocalization pathways observed in porphyrinoids

Schleyer[72] suggested that these macrocycles are better considered to be 22π-electron systems, due to the "lone pair" electrons located on two of the pyrrole nitrogens. These lone pair electrons may give rise to multiple different π-electron pathways that could contribute to the overall aromaticity of a porphyrin. Other models have been proposed for porphyrin aromaticity, although these speculations tend to be a better fit for metalloporphyrins than free-base porphyrins.[73] A 16π electron-pathway **35** (Chart 7) related to the dianion of [16]annulene has been proposed for the porphyrin ligands,[74] and a 20-atom delocalized pathway around the outside of the system which resembles a dication of [20]annulene may play a role in dirprotonated porphyrins and related heteroporphyrins. The latter pathway was initially proposed for the tetrathiaporphyrin dication **36a**,[75] which resembles porphyrin dications **36b** (Chart 7). The delocalized pathways in **35** and **36** both consist of 18π-electrons and therefore follow Huckel's Rule, which states that a molecule possessing [4n +2] π-electrons, as well as uninterrupted conjugation and planarity, is aromatic.

Numerous examples of porphyrin analogues have been reported, each of which exhibit different degrees of aromaticity. These properties are most easily probed by proton NMR spectroscopy. Through this characterization method, the resonances corresponding to the internal and external protons of these porphyrins can help to determine the level of aromaticity that they may possess, if they possess any at all.

The π-electron pathway in porphyrins produces a diamagnetic ring current which, when in the presence of an induced magnetic field, will deshield the external protons of the macrocycle and shield the internal protons (Figure 1). This causes the external protons to shift downfield in a ^{1}H NMR spectrum, and the internal protons to shift upfield. The extent to which these peaks are shifted in their respective directions gives insights into the level of aromaticity seen in these compounds. The degree of aromatic character that these macrocycles possess can fluctuate when changes to the structure are made. These changes in aromaticity can show how alterations including the *meso*- and pyrrole unit substituents, additional rings, and changes to the internal atoms can affect the flow of electrons around the porphyrin nucleus and, in turn, its stability.

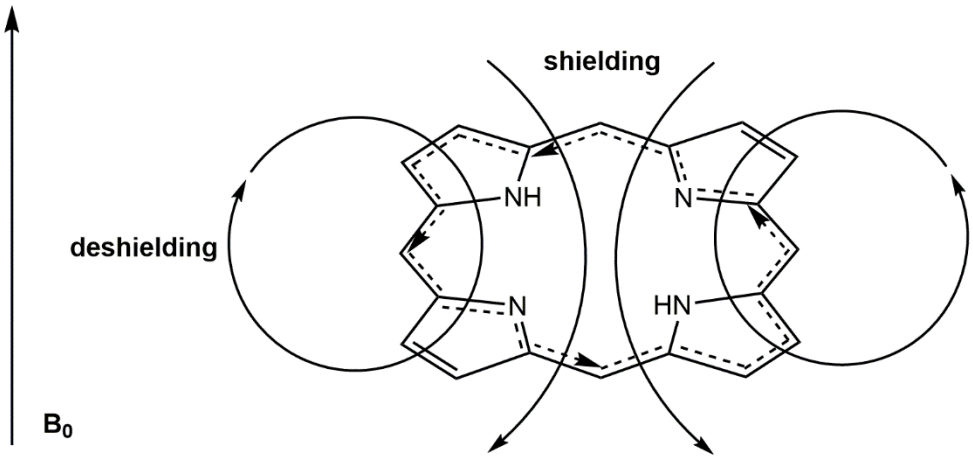

Figure 1. Shielding and deshielding regions due to porphyrin ring current

Porphyrin **1** (Chart 1), without any structural modifications, can be used as a reference point for the comparison of core-modified and substituted porphyrins. Firstly, the two major tautomers for porphyrins have been found to rapidly interconvert, resulting in the pyrrole units all being equivalent on the NMR timescale at room temperature.[76] In regards to the peaks seen in a proton NMR spectra for porphyrins, the external *meso*-protons have been found to resonate downfield near 10 ppm, while the internal NH protons give rise to a broad peak near -4 ppm.[76] These two extremely different values help to show the effect of the diatropic ring current on these macrocycles. The substituents on the pyrrole rings are also affected by the ring current. The methyl units directly attached to the porphyrin pyrroles give singlets at relatively downfield values near 3.6 ppm.[76] Upon modifying the core of the porphyrin to introduce an internal carbon, the degree of aromaticity may change, but other factors also play a role. Carbaporphyrinoids such as benzocarbaporphyrins **3**, azuliporphyrins **4**, tropiporphyrins **9**, benziporphyrins **5** dimethoxybenziporphyrins **8** and oxybenziporphyrins **7a** (Chart 1), show a wide range of aromatic properties and while **3** and **7a** are strongly aromatic, **5** is essentially non-aromatic.

Benzocarbaporphyrins **3** possess global aromatic character due to the presence of an 18π-electron pathway within the structure.[73] In the proton NMR spectrum of this carbaporphyrin, the internal CH gives a peak at -6.74 ppm and the internal NH protons show a broad resonance near -4.0 ppm, while the external *meso*-protons are observed downfield as two 2H singlets at 9.82 and 10.10 ppm[16,18] and the methyl groups resonate at 3.68 ppm as a 6H singlet.[73] The addition of trace amounts of TFA gave a monocationic species that retained comparable aromatic properties, showing the internal CH at -6.75 ppm, the NHs as broad peaks at -4.61 ppm (1H) and -3.22 ppm (2H), and the *meso*-protons at 10.06 and 10.33 ppm (two 2H singlets). In 50% TFA-$CDCl_3$, a dicationic structure $\mathbf{3H_2}^{2+}$ (Scheme 5) was observed that also retained macrocyclic aromatic

character, with the internal methylene and three NH protons resonating at -5.15 and -1.5 ppm, respectively, and the external *meso*-protons giving peaks at 10.45 and 11.10 ppm, and the methyl protons showing up at 3.60 ppm.[77,78]

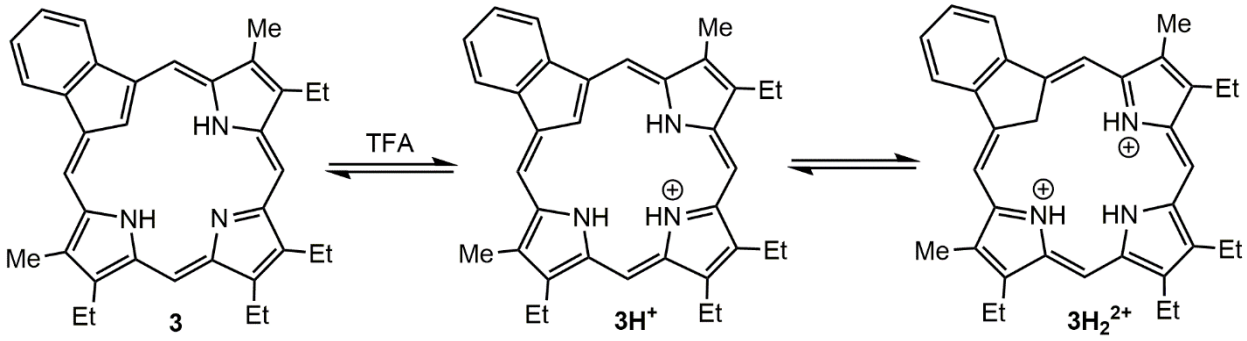

Scheme 5. Mono- and diprotonation of benzocarbaporphyrin **3**

Tropiporphyrins **9** are carbaporphyrins containing a cycloheptatriene ring.[25] These compounds exhibit slightly reduced aromaticity due to the presence of a strained seven-membered ring within the porphyrin structure. This reduced aromatic character results in upfield shifts to the proton resonances of the external *meso*-protons and methyl substituents, which give peaks at 8.0, 9.2 and 3.2 ppm, respectively. However, the internal CH is still strongly shielded and appears at -7 ppm.[25] The results indicate that the diatropic ring current in tropiporphyrins is reduced compared to regular porphyrins or benzocarbaporphyrin. Tropiporphyrins are protonated with trace TFA to give monocationic species $\mathbf{9H^+}$ that exhibit slightly enhanced diatropic character. However, further protonation by the addition of more TFA leads to a non-aromatic dicationic species $\mathbf{9H_2^{2+}}$ (Scheme 6).[25]

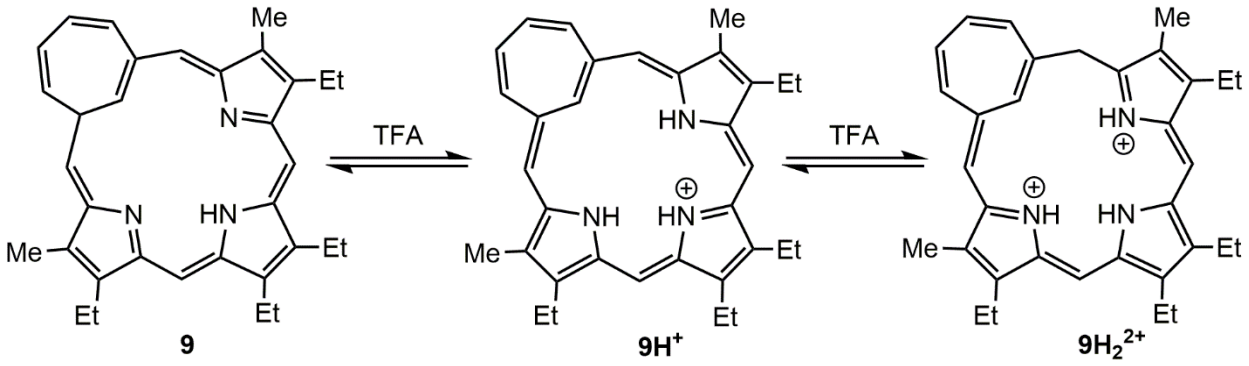

Scheme 6. Protonation of tropiporphyrin **9**

Azuliporphyrins **4** also show reduced aromatic character due to the cross conjugated azulene unit that is present.[73] Azuliporphyrin **4a** is not very soluble in organic solvents, and the internal CH resonance could not be located in the proton NMR spectrum. However, *tert*-butyl subsitituted azuliporphyrins **4b** were more soluble, and their proton NMR spectra showed the internal CH and NH peaks between 2.8 and 2.9 ppm, while the *meso*-protons were observed at 8.15 and 9.05 ppm.[79] Despite being cross conjugated, these carbaporphyrins still exhibit significant diatropic character. This observation was attributed to dipolar resonance contributors such as **4'** (Figure 2), which give the system its porphyrin-like delocalization pathway, as well as tropylium character.[79-81] The significance of this dipolar resonance contributor is also supported by the polar nature of azuliporphyrins compared to benzocarbaporphyrins and benziporphyrins.[73]

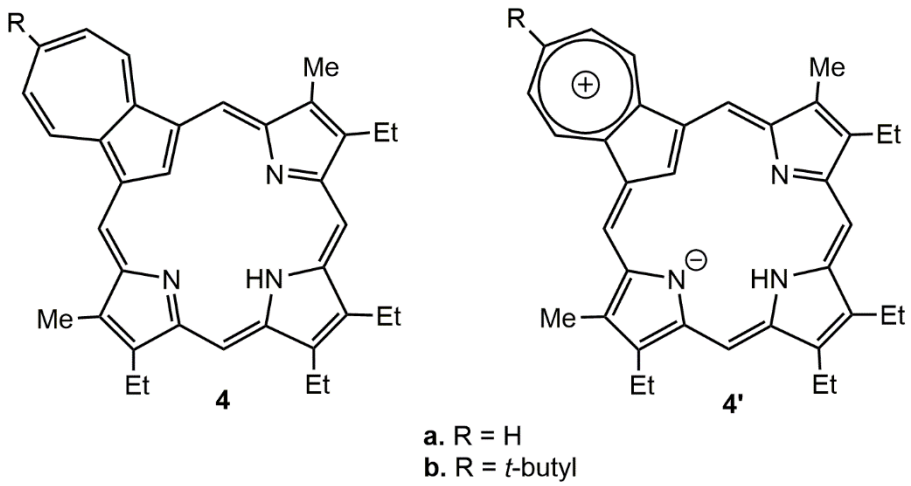

Figure 2. Dipolar resonance structure in azuliporphyrins

In contrast to azuliporphyrins, the cross conjugation resulting from the presence of a benzene ring in benziporphyrins **5** produces a non-aromatic system. The internal CH shows up as a poorly resolved triplet at 7.90 ppm, while the external benzene protons are observed as a triplet and doublet of doublets at 7.75 and 7.98 ppm, respectively, demonstrating the absence of a global aromatic ring current.[23] In addition, the *meso*-protons gave two 2H singlets at 6.57 and 7.27 ppm, respectively, and the external methyls were observed as a 6H singlet at 2.43 ppm, values that are far upfield from those observed for a porphyrin.[22] Benziporphyrins are non-aromatic because they would have to forfeit the aromaticity of the benzene ring in order for the entire system to be aromatic, and this is unlikely to be favorable.[73] However, addition of TFA afforded a diprotonated dication $\mathbf{5H_2}^{2+}$, that displayed weakly diatropic character, shifting the *meso*-protons downfield to 7 and 8 ppm, while the internal CH was shifted upfield to near 5 ppm.[23] The observed diatropic character was proposed to arise from resonance contributors such as $\mathbf{5'H_2}^{2+}$ that enable delocalization of charge as well as the formation of the 18π-electron delocalization pathway (Scheme 7).[73]

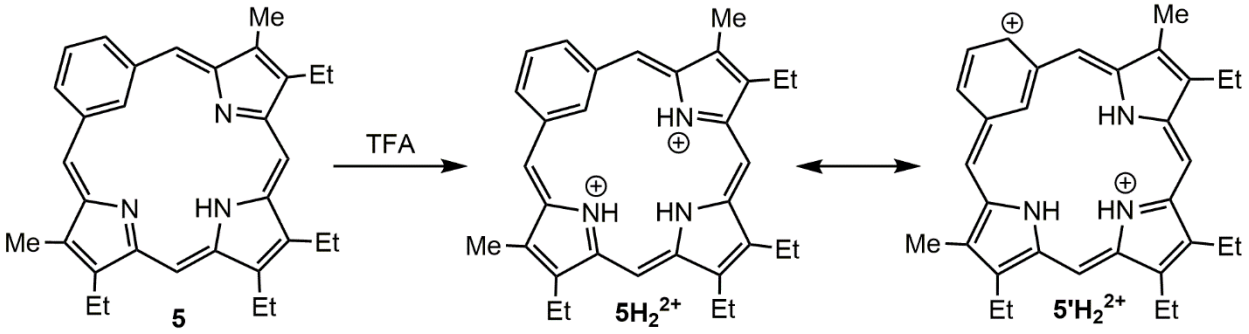

Scheme 7. Protonation of benziporphyrin **5**

Closely related benziporphyrin-like structures have also been investigated, including dimethoxybenziporphyrin **8**. Unlike **5**, **8** was found to possess a weak diatropic ring current as a free base, but when the compound was diprotonated with TFA much larger shifts were seen in the proton NMR spectra. The interior CH for **8** was observed upfield at -0.68 ppm, while the *meso*-protons were shifted downfield to give two 2H singlets at 8.44 and 9.60 ppm.[82] This increase in diatropic character can be explained by the presence of the electron-donating methoxy groups, which provide favorable resonance contributors such as **8'H$_2^{2+}$** that possess 18π-electron delocalization pathways (Scheme 8).[73]

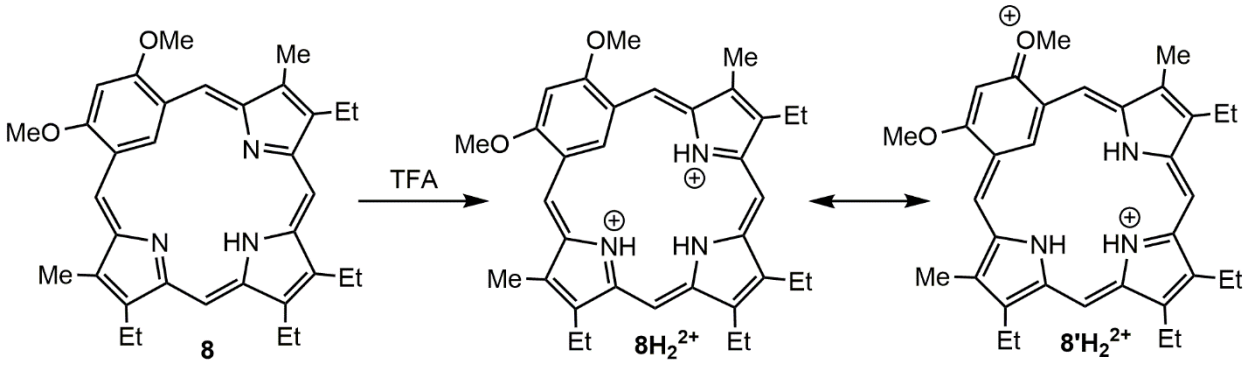

Scheme 8. Protonation of dimethoxybenziporphyrin **8**

Another variation on the benziporphyrin structure is oxybenziporphyrin **7a**, which is highly diatropic because the six-membered ring favors a tautomer with a conjugated carbonyl group, allowing an aromatic delocalization pathway to be present in the system.[22,23,73] Furthermore, related oxypyriporphyrins **7b** are also well known and exhibit the necessary 18π-electron delocalization pathway to possess porphyrinoid aromaticity.[23,77,78]

Heteroporphyrins **28** (Chart 6) are porphyrin analogues in which one or more of the internal nitrogen atoms are replaced by a different atom. 21-Thia **28b** and 21-oxaporphyrins **28a** are examples of heteroporphyrins, and were first synthesized in 1971, along with related diheteroporphyrins **37** and **38** (Chart 6).[57] It was found that 21-thiaporphyrin **25b** showed the *meso*-proton resonances between 9.98-10.06 ppm, while the internal NH proton resonated at -4.98 ppm.[57] The 21-oxaporphyrin **25a** contained *meso*-protons that were observed between 9.69 and 10.12 ppm, but the internal NH proton could not be detected.[57] Little data for *meso*-unsubstituted monoheteroporphyrins has been reported, although *meso*-substituted heteroporphyrins and diheteroporphyrins have been far better studied. When the proton NMR spectrum of porphyrin **37a** was compared to that of the related 21,23-dioxa- **37b** and 21,23-dithiaporphyrins **37c** (Chart 6, page 99), it was found that the *meso*-proton peaks were shifted downfield from 9.55 ppm to 10.98 and 10.71 ppm, respectively.[83] Tetraphenylporphyrin **38a** (TPP) was also compared to its 21,23-diheteroatom derivatives, containing both oxygen **38b** (2OTPP) and sulfur **35c** (2STPP) atoms (Chart 6). The *β*-protons for TPP were observed at 8.72 ppm, while those for 2OTPP and 2STPP were seen at 9.37 and 9.63, respectively, showing similar downfield shifts.[84] These results indicate that the diheteratom derivatives were more aromatic than the original porphyrins.

Porphyrins and porphyrin analogues possess varying diatropic characteristics that can easily be identified, in part, through proton NMR spectroscopy. Changes made to the porphyrin

macrocycle can result in changes in the properties of these structures and are therefore important to investigate. Carbaporphyrins, in particular, are of interest because their structures can easily be varied using specific synthetic methods, and all of them include modified internal core atoms. Additional changes to these porphyrin analogues can provide important insights into how much change a porphyrin can undergo while maintaining its characteristic chemical properties.

Porphyrins have been synthesized in many ways over the years, and the route chosen for synthesis depends on the type of porphyrinoid being targeted and whether or not the macrocycle is symmetrical. The most common method of synthesizing simple symmetrical porphyrins is through the tetramerization of a monopyrrole. This route was first reported by Rothemund, and this methodology allowed tetraphenyl porphyrin (TPP) to be prepared by reacting pyrrole **39** with benzaldehyde[84,85] (Scheme 9). Another example of this type of synthesis involves the reaction of 3,4-diethylpyrrole with formaldehyde to produce octaethylporphyrin **40** (OEP)[86] (Scheme 9). Monopyrrole tetramerization works best with pyrroles that possess identical 3- and 4-substituents, otherwise mixtures will arise to due acid-catalyzed scrambling reactions.[87,88] An example of this production of mixtures can be seen through the acid-catalyzed tetramerization of pyrrole **41**, which gives four etioporphyrin type-isomers **42-45** (Scheme 10).[89]

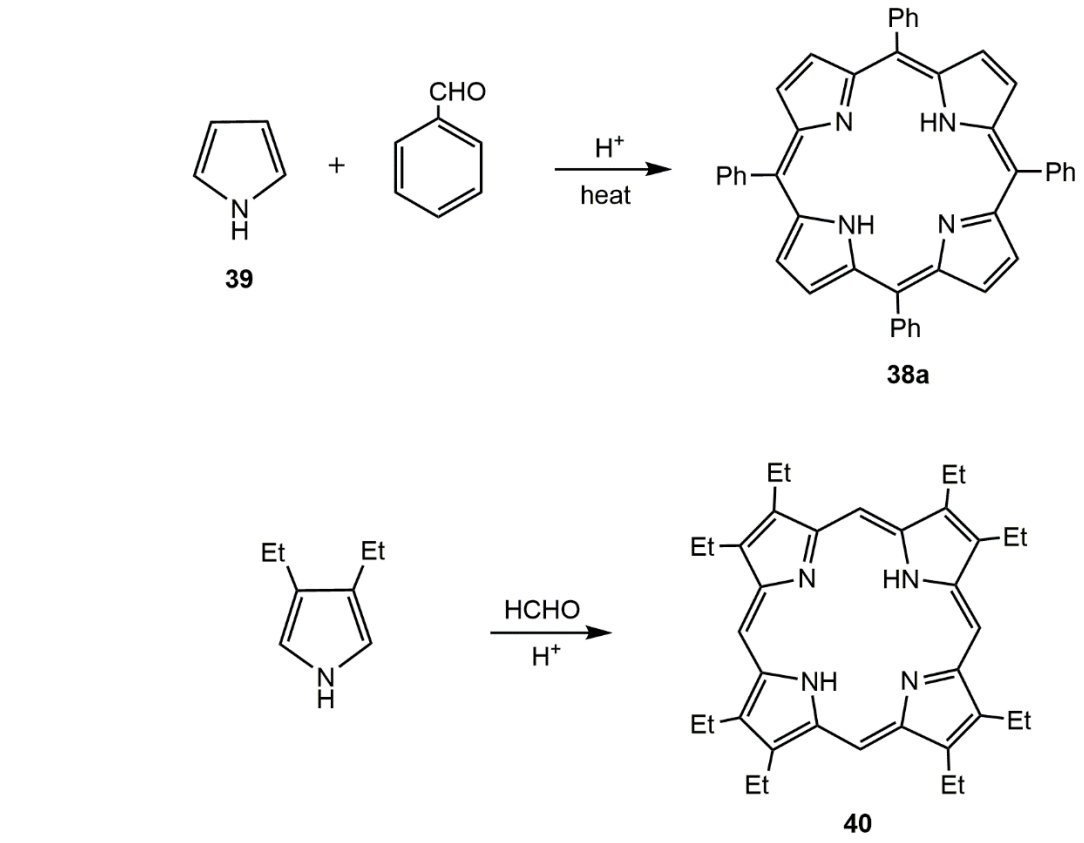

Scheme 9. Tetramerization of monopyrroles to produce porphyrins

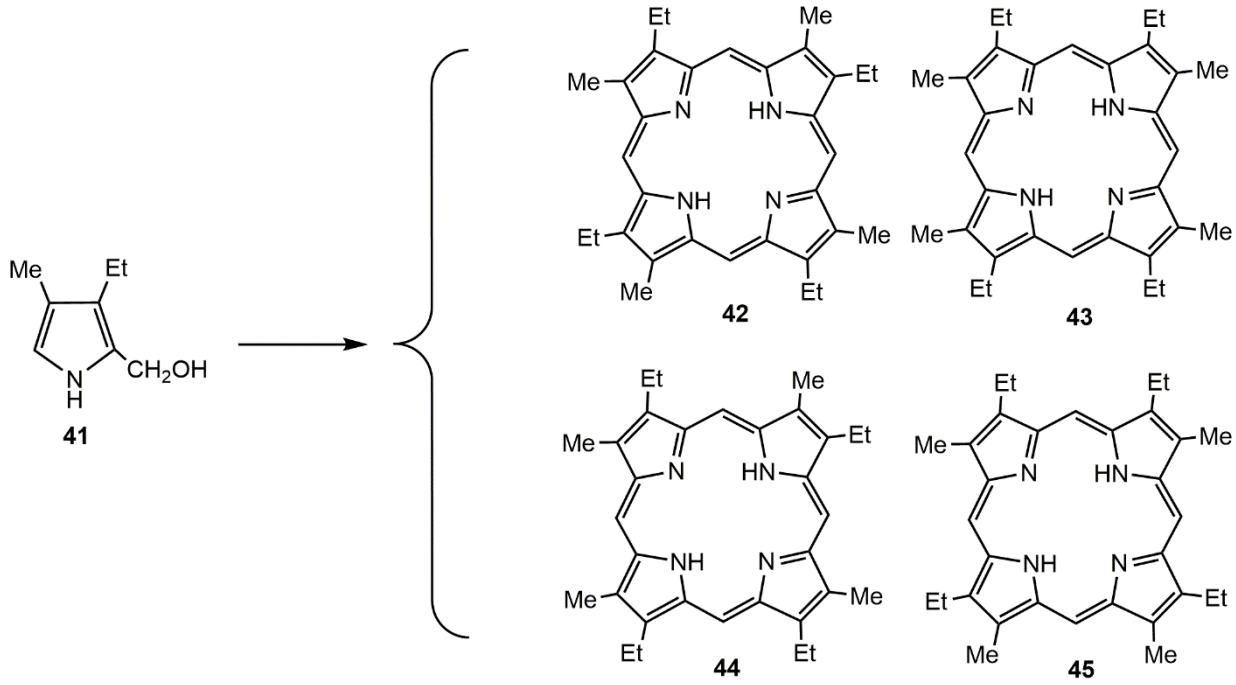

Scheme 10. Etioporphyrin type-isomers from the acid-catalyzed tetramerization of a pyrrole

Another common method used for porphyrin synthesis is the MacDonald '2+2' condensation. For this approach, two dipyrrolic components, commonly dipyrromethanes, are key intermediates. The use of two unsymmetrical dipyrromethanes would result in two different porphyrins, due to the possibility of one of the dipyrrolic units reacting in either of two orientations, related by a 180° flip.[89] However, it was found that this can be avoided by ensuring one of the dipyrromethane units is symmetrical. MacDonald and coworkers demonstrated this by reacting a symmetrical 1,9-diformyldipyrromethane **46** with a 1,9-di-unsubstituted dipyrromethane **47a**, or its corresponding dicarboxylic acid **47b**, in the presence of an acid catalyst to give pure porphyrin **48** in very high yields (Scheme 11).[90]

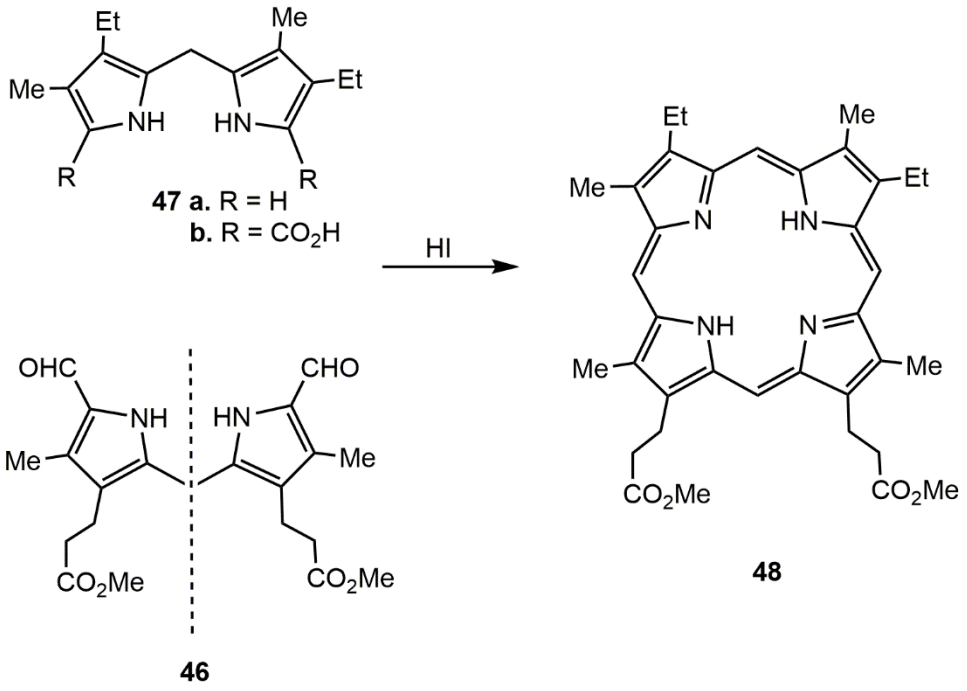

Scheme 11. '2+2' MacDonald condensation reaction

A variant of the '2+2' condensation, developed by Johnson and coworkers,[57] and known as the '3+1' route, involves the reaction of a tripyrrolic unit, such as tripyrrane **49**, with a monopyrrole bearing two aldehyde groups (e.g. **50**) in the presences of an acid catalyst to give

porphyrin **51**[89] (Scheme 12). In most cases, the '3+1' chemistry is carried out by reacting a tripyrrane unit with a monopyrrole in the form of a dialdehyde. However, there are examples where this is reversed, and a tripyrrane dialdehyde is condensed with a simple monopyrrole.[91]

The popularity of this method is, in part, due to the simplicity in constructing the aforementioned tripyrrane unit. Sessler and coworkers developed a convenient synthesis of tripyrranes, that afforded symmetrically substituted structures such as **49**[92] (Scheme 12). Even though this approach is limited by the symmetry of the intermediates, the ease and success of the reactions, as well as the abundance of porphyrinoids it can produce, makes up for this deficiency.

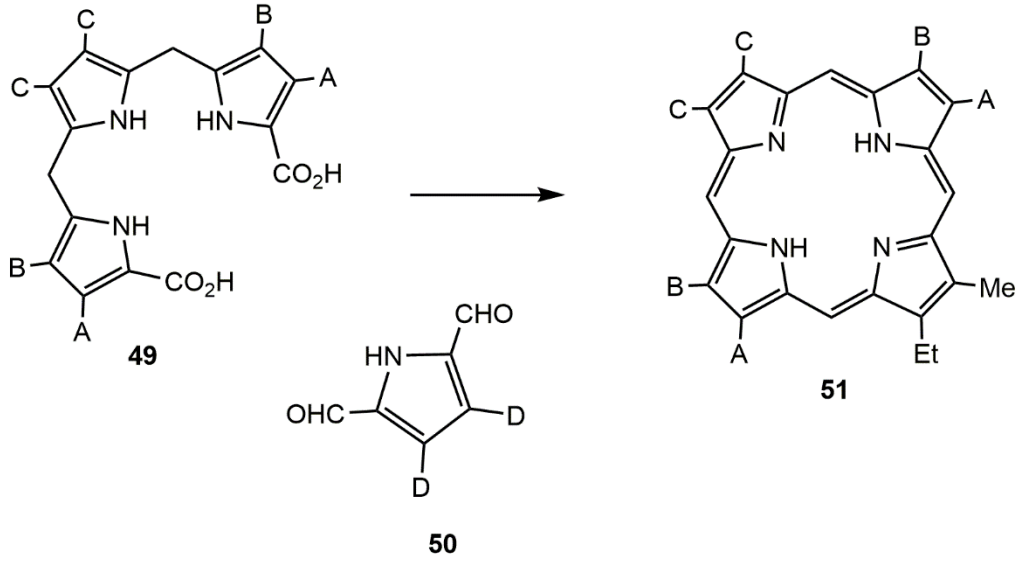

Scheme 12. '3+1'variant of the MacDonald Condensation

By reacting two equivalents of acetoxymethyl pyrrole **52** with one equivalent of diethylpyrrole **53a** under acidic conditions, tripyrrane **54a** can be isolated in >70% yield (Scheme 13). Subsequent cleavage of the protective benzyl ester groups with Pd/C under an atmosphere of hydrogen gives the corresponding tripyrrane dicarboxylic acid **54b** (Scheme 13), which can be

used in the ‘3+1’ syntheses. It has also been found that the identity of the substituents on the tripyrrane can greatly influence the efficiency of these cyclization reactions.[91,93,94]

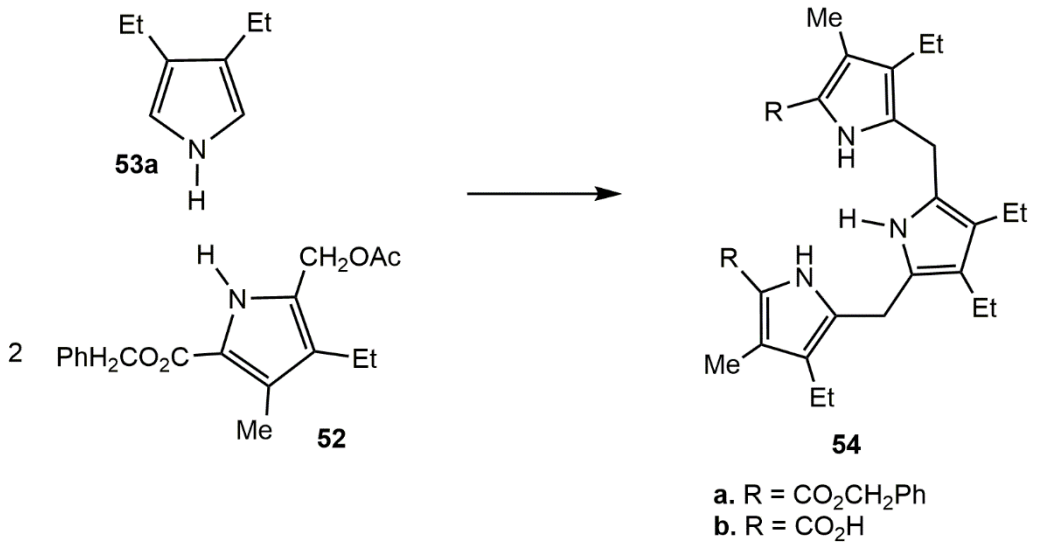

Scheme 13. Synthesis of a tripyrrane

The ease in varying the dialdehyde unit is another factor that contributes to the popularity of the ‘3+1’ method. This paved the way for the synthesis of numerous porphyrinoids that possess unique functionality based on the identity of the inserted dialdehyde unit. Furthermore, the central pyrrole unit of the tripyrrane can be changed so that alternative heterocyclic or carbocyclic rings can be introduced. For example, in the study that first introduced the ‘3+1’ methodology, Johnson condensed tripyrrane **55a** or heterotripyrrane **55b,c** with furan dialdehyde **56a** or thiophene dialdehyde **56b** in the presence of HBr to give a series of heteroporphyrins **57a-d** (Scheme 14).[57] This method has also been very successful in the synthesis of carbaporphyrinoid systems,[22] either by using carbocyclic dialdehydes or tripyrrance analogues that incorporate carbocyclic rings. This approach allows the synthesis of porphyrinoids that would not be accessible from the ‘2+2’ MacDonald reaction, therefore reinforcing the importance of this method for the development of novel porphyrin analogues.

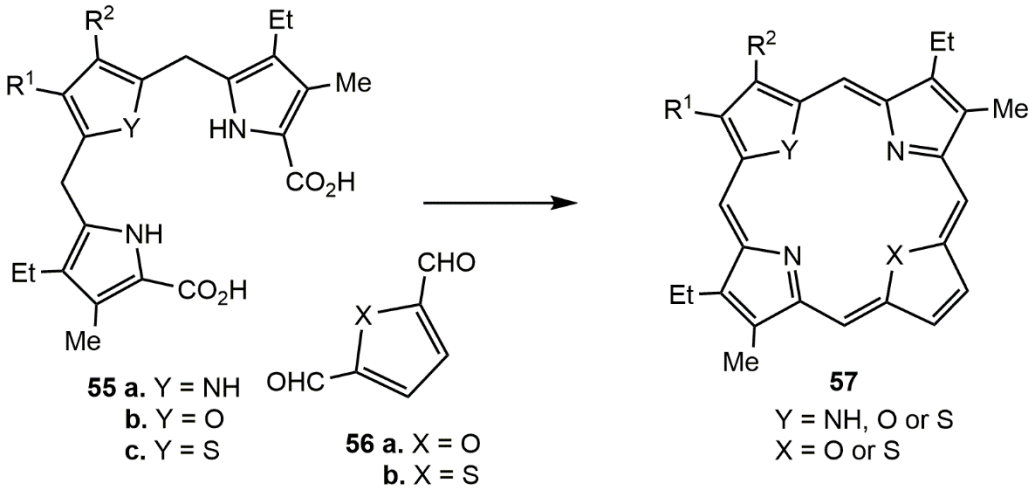

Scheme 14. Synthesis of heteroporphyrins through the '3+1' variant of the MacDonald reaction

The internal cavity of porphyrinoids determines the abilities of these ligands to coordinate to metal centers. Often times, if the atoms and available bonding locations are altered within these macrocycles, their coordinating nature will be changed as well. Alkylation of carbaporphyrins has been well documented[95-97,98] and this can greatly alter the coordination properties of these ligands. When N-confused porphyrin (NCP) **58** was reacted with methyl iodide in the presence of Na_2CO_3, the major product was *N*,*N*'-dimethyl NCP **59** (Scheme 15) with methyl groups on the external nitrogen as well as the internal nitrogen at the 24-position.[96] This alkylation reaction was interesting, as it introduced methyl groups on two nitrogen positions rather than just one, and demonstrated that not only are internally alkylated NCPs stable but also that the external nitrogen can easily be alkylated as well. This porphyrinoid was found to generate singlet oxygen after being irradiated at long wavelengths in the visible region, thereby showing that this compound has potential as a photosensitizer for photodynamic therapy (PDT).[96]

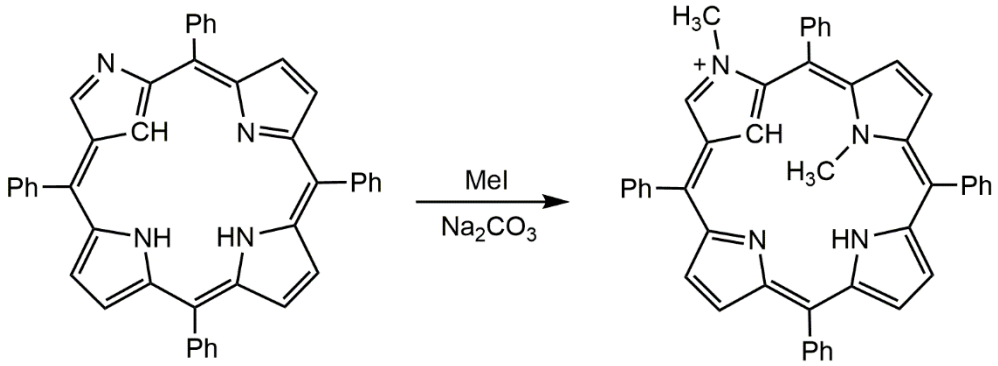

58 **59**

Scheme 15. Methylation of NCP to give a *N*,*N*-dimethyl NCP

Other work on NCPs by Latos-Grazynski and co-workers resulted in the preparation of outer *N*-methylated NCP **60**, *C*-methylated NCP **61**, *C*,*N*-dimethylated NCP **62** and their nickel(II) derivatives[95,98] (Chart 8).

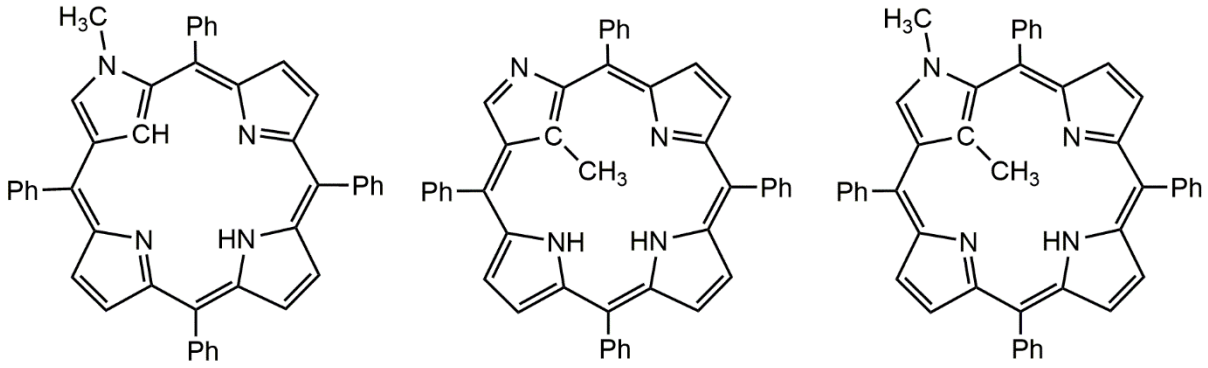

60 **61** **62**

Chart 8. Examples of methylated N-confused porphyrins

An oxidized benziporphyrin derivative **63** was alkylated with methyl and ethyl iodide to give the corresponding *N*-methyl or *N*-ethyl products **64**, with selective alkylation on the 23-position[97] (Scheme 16). Alkylation of the anionic palladium(II) complex of oxybenziporphyrin **65**

could take place on the oxygen as well as the internal carbon.[99] When reacted with *n*-butyl iodide, a mixture of *O*-butyl **66** and *C*-butyl **67a** products was obtained, but when reacted with methyl iodide only the internal carbon atom alkylated to give **67b**[99] (Scheme 17). *N*-alkylporphyrins in general are of interest due to their role in a significant pathway for physiological porphyrin destruction.[100] The *N*-alkylation of benzocarbaporphyrins resulted in *N*- and *C*-alkylated products, and also allowed these systems to act as a dianionic ligands instead of exhibiting their usual trianionic character.[101]

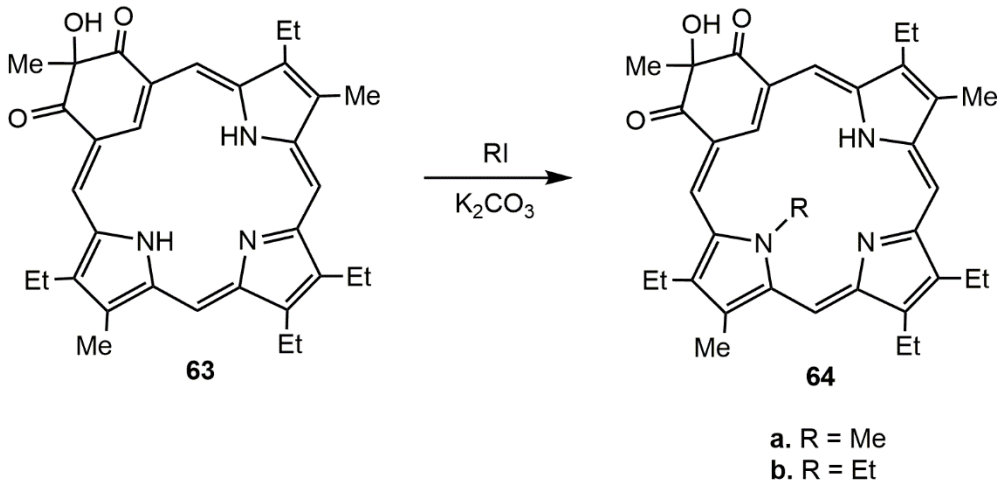

Scheme 16. Alkylation of an oxidized benziporphyrin derivative

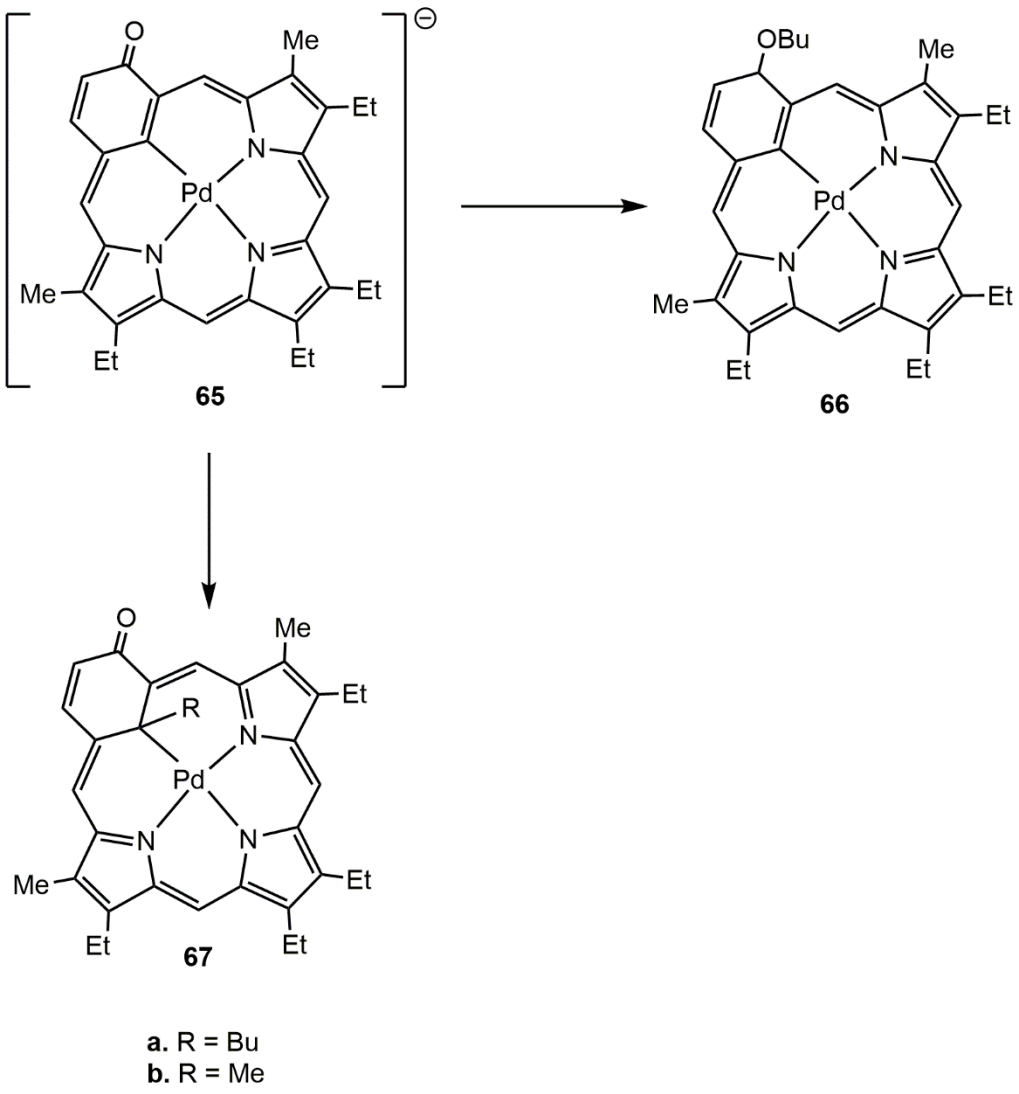

Scheme 17. Alkylation of palladium(II) oxybenziporphyrin

The coordination chemistry of alkylated porphyrins and related macrocyclic systems involves a number of interesting reactions. For instance, metalated *N*-methylporphyrins have been observed to undergo demethylation of the pyrrolic nitrogen, and transfer of the methyl cation to another nitrogen base present in solution.[102-105] Another case involved palladium(II) *p*-benziporphyrin complexes **68** undergoing a base promoted rearrangement to give the corresponding palladium(II) carbaporphyrins **69a,b** (Scheme 18).[106] Furthermore, the metalation

of methylbenzocarbaporphyrin **70** with palladium(II) acetate resulted in an unexpected alkyl group migration, where the internal methyl was seen to move from the 22-position in **71** to the 21-position in **72**[101] (Scheme 19). The mechanism behind this migration is unknown, but was proposed to involve a [1,5]sigmatropic rearrangement which could, in part, be due to the proximity of the alkyl group on the 22-nitrogen to the internal 21-carbon atom. Similar rearrangements were also observed for carbaporphyrins without fused benzo-units[107] and with naphthocarba[2,3-*b*]porphyrins.[108] Palladium-mediated rearrangements of vactaporphyrin[109] and some expanded porphyrins have also been noted.[110] Alongside palladium metal, rhodium(III) metal cations present within the cavity of benziporphyrins have been seen to promote the ring contraction of the benzene ring to a cyclopentadiene with the additional formation of a three-membered rhodacycle bridging the metal center and the internal carbon atom.[68]

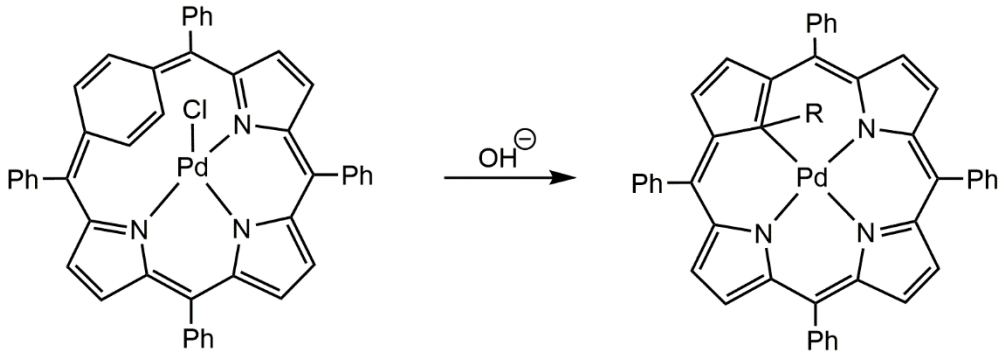

68 **69**

a. R = CHO
b. R = H

Scheme 18. Base-promoted rearrangement of palladium(II) *p*-benziporphyrin to palladium(II) carbaporphyrin

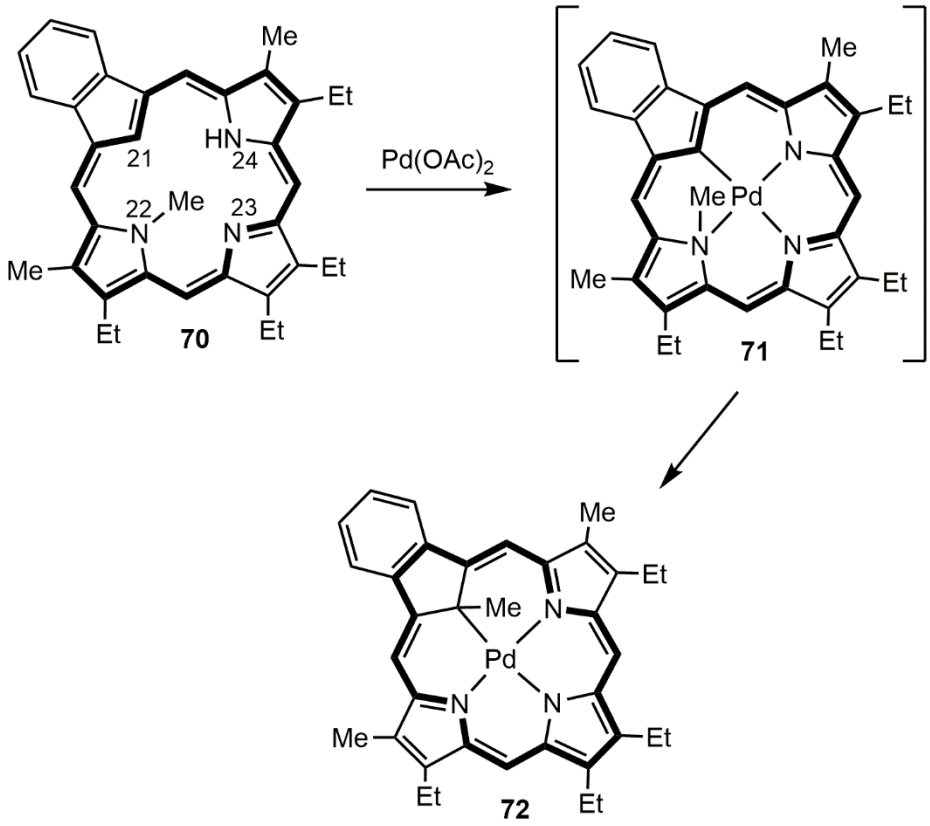

Scheme 19. Alkyl group migration in a palladium(II) benzocarbaporphyrin complex

Therefore, reactions of this type appear to have considerable significance and show that there is still much to investigate in regards to the coordination chemistry and reactivity of organometallic porphyrinoids. To further probe this chemistry, a 23-methylbenzocarbaporphyrin **73** was synthesized and its reactivity with palladium(II) acetate was compared to that of the 22-methylbenzocarbaporphyrin **71**. Metalation of the 23-methyl derivative provides insights into the significance of the alkyl group position within the porphyrinoid cavity, as well as the overall mechanism that is occurring. Furthermore, considering the C-H activation properties of rhodium(III) porphyrins, and the known formation of rhodacycle moieties within rhodium(III) carbaporphyrins, metalation of the 23-methylbenzocarbaporphyrin with rhodium complexes is also of interest. The introduction of internal alkyl groups may lead to deformation of porphyrinoid

macrocycles and the influences of these structural changes on the spectroscopic properties of these systems is worthy of study. The convenience of the '3+1' method allows for the construction of a series of *N*-methyl porphyrinoids. This not only allows investigations into the coordination chemistry of a multitude of internally methylated porphyrin analogues, but also enables variations in the electronic properties of these macrocycles to be assessed.

CHAPTER II: ALKYL GROUP MIGRATION IN INTERNALLY METHYLATED PALLADIUM(II) BENZOCARBAPORPHYRINS

Introduction

Carbaporphyrinoid systems form stable organometallic complexes with late transition metal cations.[26] True carbaporphyrins such as **73** are trianionic ligands and have been shown to form stable Ag(III) and Au(III) derivatives.[27-29] In order to modify the reactivity of this system, internal alkyl substituents have been introduced that could potentially enable this macrocyclic platform to act as a dianionic ligand. Benzocarbaporphyrin **73** was previously prepared by condensing a tripyrrane dicarboxylic acid **54b** with indene dialdehyde **74** in the presence of TFA[101] (Scheme 20). After purification by column chromatography and recrystallization, benzocarbaporphyrin **73** was reacted with methyl iodide in a suspension of potassium carbonate and refluxing acetone to give two alkylation products. The minor product **75** had the methyl group on the 21-position, while the major product **70** had the methyl located on the 22-position[101] (Scheme 21). These two products were isolated in 10% and 62% yields, respectively, but no trace of the hypothetical 23-alkyl product was observed.[101]

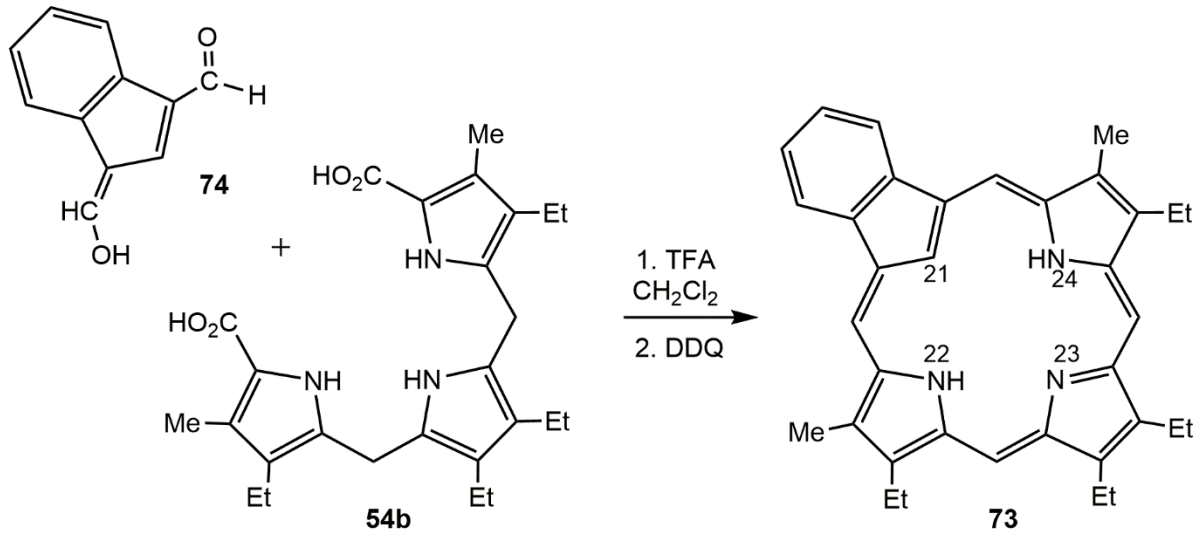

Scheme 20. Preparation of benzocarbaporphyrin via the '3+1' MacDonald condensation

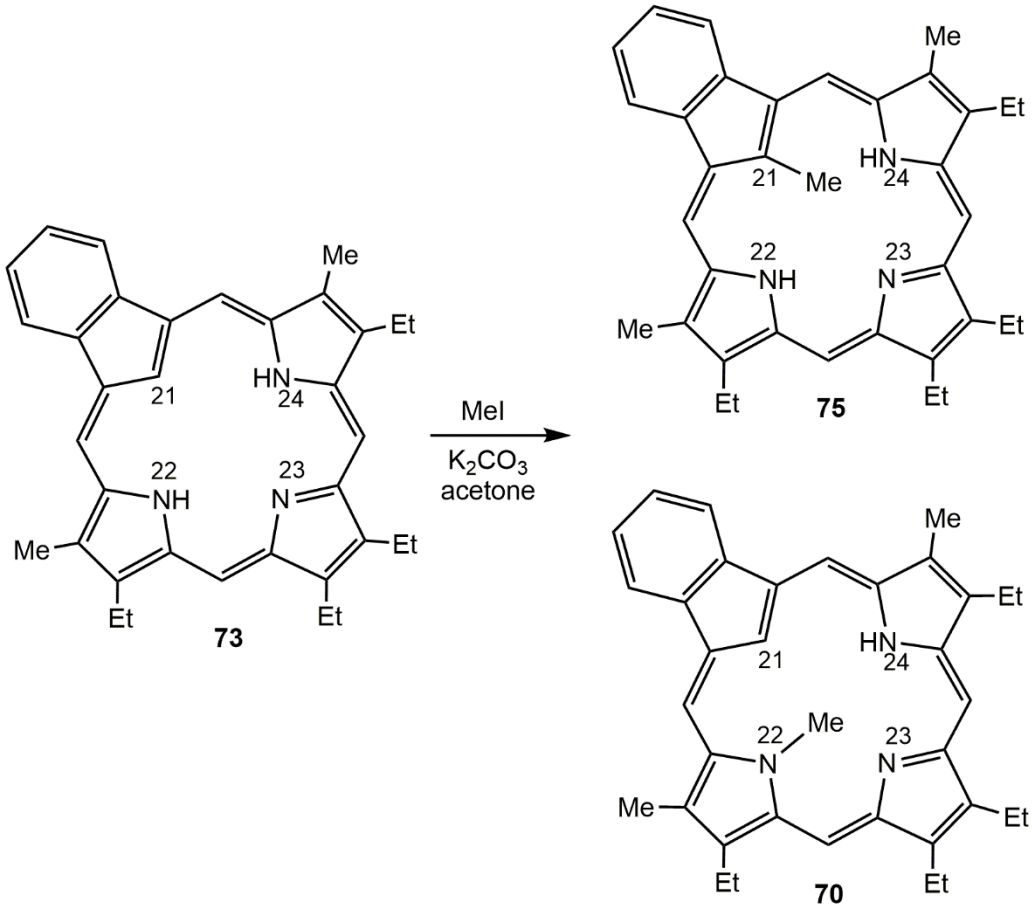

Scheme 21. Methylation of benzocarbaporphyrin **73**

Having replaced one of the inner hydrogens with a methyl group in **70** and **75**, it was thought that the porphyrin analogues would now act as dianionic ligands. Reaction of **70** with palladium(II) acetate in refluxing acetonitrile initially gave *N*-methyl palladium(II) complex **71**, but unexpectedly this rapidly rearranged to give the C-methyl palladium(II) complex **72** (Scheme 19). When the reaction time was reduced to 5 minutes the major product was *N*-methyl palladium(II) complex **71**, but after 30 minutes virtually all of the material had converted into **72**. Attempts to purify the *N*-methyl palladium(II) complex **71** by column chromatography were unsuccessful as this led to almost complete conversion to the C-methyl derivative **72**. Therefore, this compound could not be isolated in pure form due to the persistence of alkyl group migration at room temperature. However, owing to the difference in symmetry between the two structures, it could be determined by proton NMR spectroscopy that C-methyl palladium complex **72** was being formed. The *N*-methyl palladium complex is asymmetrical, while the C-methyl palladium complex has a plane of symmetry, therefore the latter produces a smaller number of peaks in the NMR spectrum.

It was proposed that the alkyl group migration could have occurred through a Pd-alkyl intermediate, where the methyl group moves from one position to the other by hopping onto the metal center. This migration could have also occurred via a concerted [1,5]sigmatropic rearrangement due to the close proximity of the methyl group to the 21-position[101] (Scheme 22). No intermediates were discovered to support either mechanism of migration, so it is unclear which of these was actually occurring.

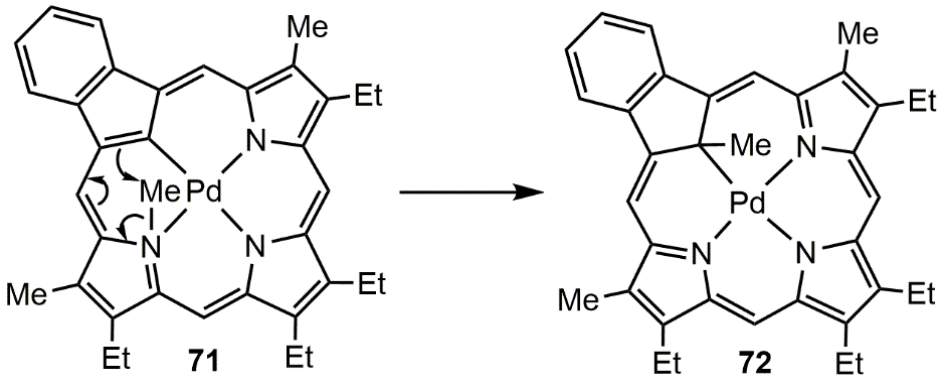

Scheme 22. Proposed [1,5] sigmatropic rearrangement for alkyl group migration

Rearrangements of this type could potentially be further investigated through the metalation of 23-methylbenzocarbaporphyrin **76**[111] (Scheme 23). Ensuring the methyl is at a position further away from the 21-position would force the alkyl group to traverse the entire porphyrinoid cavity in order to migrate in a similar fashion. If the migration still occurs upon the insertion of a palladium(II) center into the carbaporphyrin cavity, it may be easier to determine which mechanism is taking place. Since a 23-alkyl product was not observed upon methylation of benzocarbaporphyrin **73**, the desired carbaporphyrin **76** had to be constructed via the '3+1' MacDonald-type condensation of a *N*-methylated tripyrrane **54d** with indene dialdehyde **74** (Scheme 23).

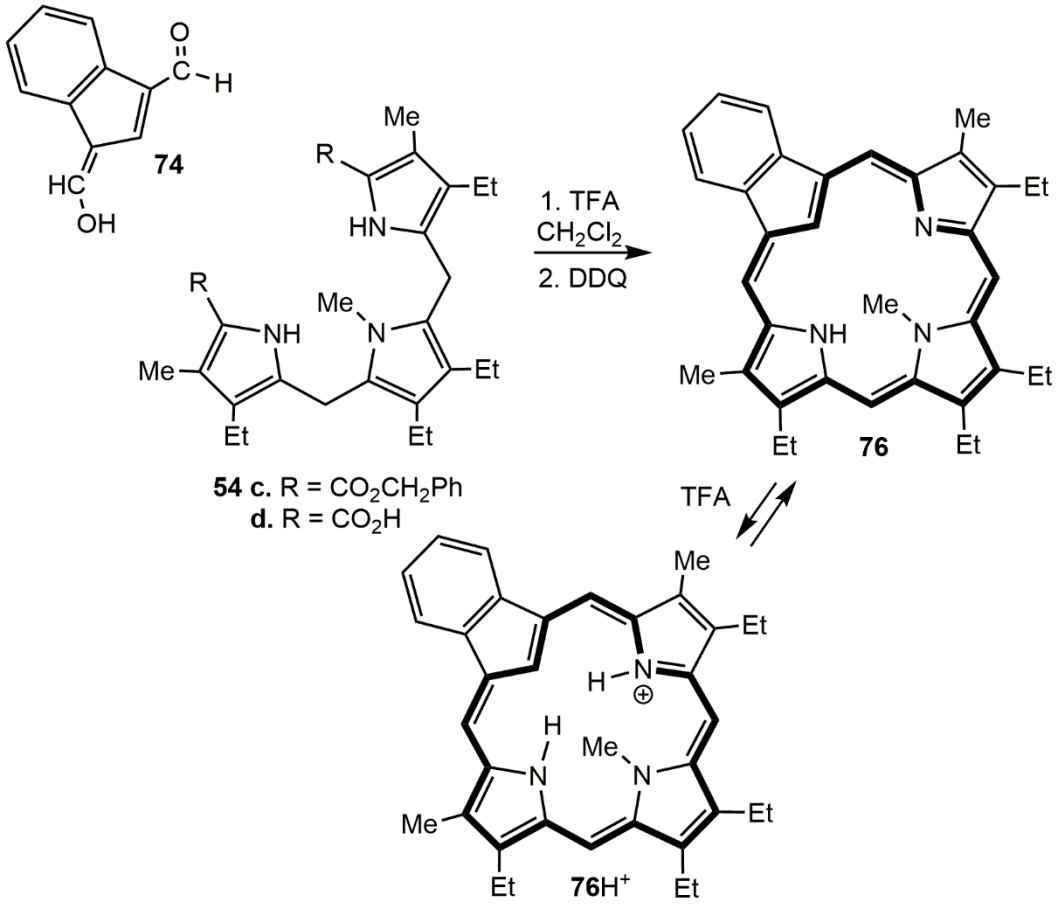

Scheme 23. Synthesis and protonation of 23-methylbenzocarbaporphyrin **76**

Results and Discussion

The synthesis of tripyrrane **54d** required the availability of two different pyrrolic precursors. The central pyrrole unit of **54d** bears an *N*-methyl substituent, but initially it was necessary to prepare an *N*-unsubstituted pyrrole ethyl ester **78**. Synthesis of this pyrrole ester began by reaction of ethyl isocyanoacetate with 3-acetoxy-4-nitrohexane and two equivalents of 1,8-diazabicyclo[5.4.0]undec-7-ene (DBU) in THF-isopropyl alcohol (Barton-Zard condensation, Scheme 24). The product **78** was isolated in 70% yield but the proton NMR spectrum (Figure 3) showed that it was contaminated with approximately 3% of the corresponding isopropyl ester due to transesterification with the 2-propanol. However, as the ester is saponified at a later stage,

pyrrole ethyl ester **78** was used in this form. Methylation of **78** was achieved by the dropwise addition of methyl iodide to a solution of the pyrrole ethyl ester and potassium hydroxide in dimethylsulfoxide (DMSO). The required *N*-methyl derivative **79** was obtained in 79% yield, but again the product was contaminated with a small amount of the related isopropyl ester. Subsequent saponification and decarboxylation of the pyrrole ester with sodium hydroxide in refluxing ethylene glycol at a temperature of 200°C for 2.5 hours produced 3,4-diethyl-1-methylpyrrole **53b** in 84% yield (Scheme 24). Pyrrole **53b** had previously been prepared from 1,2-dimethylhydrazine using a variation on the Fischer indole synthesis.[112] Initially, purification was carried out by vacuum distillation. However, it was later found that this was unnecessary, and pure **53b** could be obtained in higher yields by simply extracting the product into hexanes.

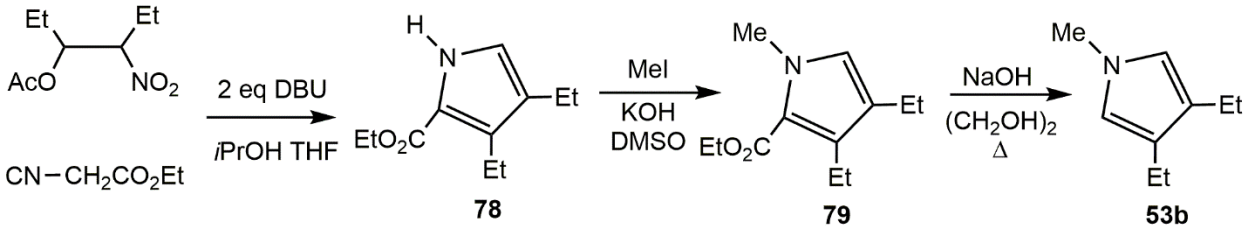

Scheme 24. Barton-Zard synthesis and methylation of a pyrrole precursor

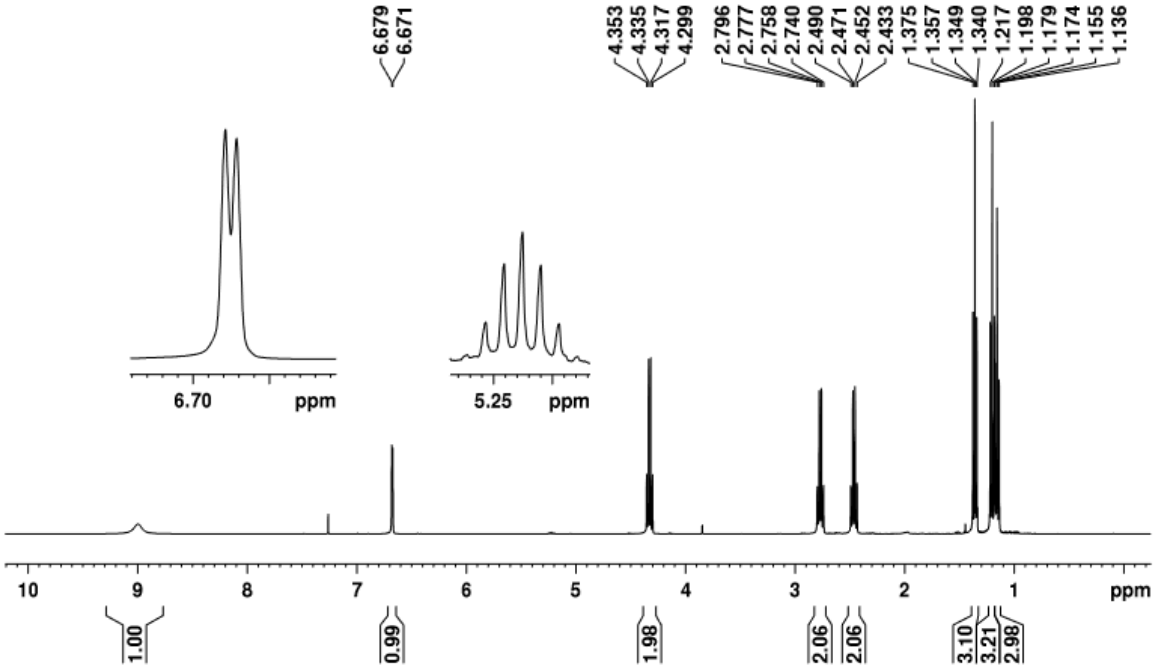

Figure 3. 500 MHz ^{1}H NMR spectrum of pyrrole ester **78** in $CDCl_3$. The multiplet at 5.23 ppm corresponds to a small amount of the related isopropyl ester pyrrole (ca. 3%) that results from the transesterification with the solvent 2-propanol

A second pyrrole unit **80** was required to synthesized the desired tripyrrane. Diethyl aminomalonate **81** was reacted with 3-ethyl-2,4-pentanedione in gently boiling acetic acid for 2 hours to give the ethyl ester pyrrole **82**. Subsequent transesterification with sodium benzyloxide in benzyl alcohol afforded the benzyl ester derivative **83**, which was then reacted overnight with lead tetraacetate in acetic acid and acetic anhydride to give acetoxymethylpyrrole **80** (Scheme 25).

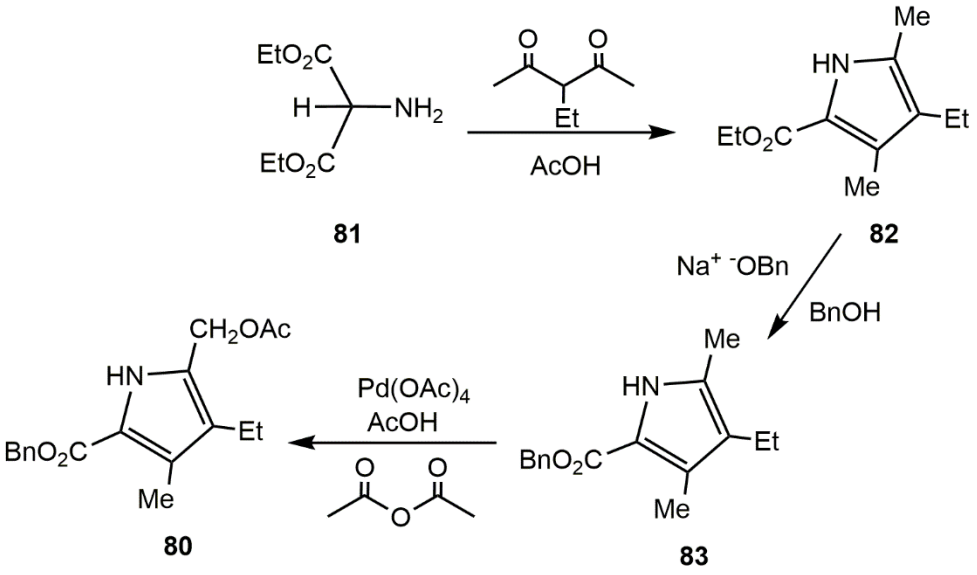

Scheme 25. Synthesis of acetoxymethylpyrrole **80**

Tripyrranes can be prepared by condensing α,α'-diunsubstituted pyrroles with two equivalents of an acetoxymethylpyrrole such as **80** in the presence of an acid catalyst.[92] However, attempts to react **53b** with **80** in the presences of Montmorillonite clay[113] gave poor results, and reactions with acetic acid in ethanol or other alcohol solvents[114] also gave low yields of the desire tripyrrolic product **54c** (Scheme 26). It was speculated that ethanol might be replacing the acetoxy groups present on **80** to give ethyl ether by-products, which in turn lowered the yield of the desire product by consuming one of the intermediates. Superior results were obtained by reacting **53b** and **80** in a 1:2 ratio with acetic acid in refluxing acetonitrile under nitrogen. *N*-Unsubstituted tripyrranes commonly precipitate from solution, but this was not observed with *N*-methyl tripyrrane **54c** and therefore the crude product had to be purified by column chromatography. Some tripyrranes have been known to decompose during chromatography, but in the case of **54c** it could be isolated as an oil that solidified in the freezer (Scheme 26). However, the purification of this tripyrrane by column chromatography proved difficult. Pure samples were hard to acquire, even

after several runs through silica columns eluting with 80% dichloromethane-hexanes. It was found that triethylamine aided in stabilizing the tripyrrane during column chromatography. When the reaction product was columned on silica gel and eluted with 80:20:1 dichloromethane/hexanes/triethylamine, pure samples of the tripyrrane were obtained after two chromatographic purifications. The benzyl ester protective groups of **54c** were then cleaved by hydrogenolysis over Pd/C, to give the *N*-methyltripyrrane dicarboxylic acid **54d** (Scheme 26).

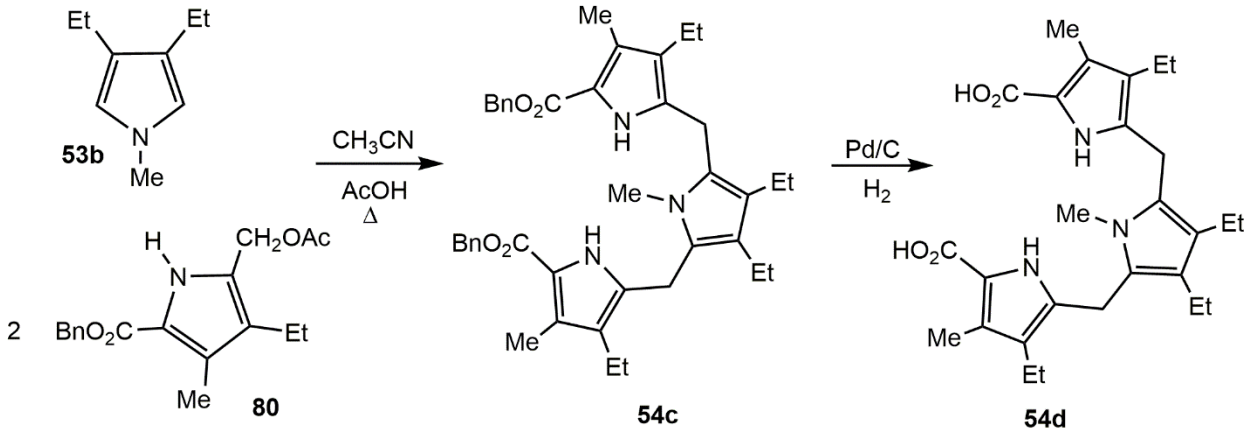

Scheme 26. Synthesis of *N*-methyl tripyrrane **54d**

N-Alkyl tripyrranes had not previously been applied to the preparation of porphyrinoid products. However, '2+2' MacDonald condensation of a *N*-methyldipyrrylmethane with a dipyrrylmethane dialdehyde had been used to synthesize a *N*-methylporphyrin,[115] and related porphyrins were prepared from *a,c*-biladiene intermediates.[116] The steric bulk associated with presence of an internal substituent might inhibit the cyclization reaction, and given the instability of tripyrranes under the acidic conditions used to carry out these reactions, there was a possibility that decomposition would ensue. Fortunately, acid catalyzed condensation of **54d** with indene dialdehyde **74**, followed by oxidation with 2,3-dichloro-5,6-dicyano-1,4-benzoquinone (DDQ)

gave the desired 23-methylcarbaporphyrin **76** in 32% yield (Scheme 23). Fairly concentrated conditions were used (less than 20 mL of dichloromethane for every 100 mg of tripyrrane), but it was found that dilution did not afford any higher yields. The carbaporphyrin was chromatographed twice on grade 3 neutral alumina, eluting with dichloromethane and then chloroform, and a dark band was collected each time. The product was recrystallized from chloroform-methanol to yield purple-blue crystals. The *N*-substituted carbaporphyrin retains fully aromatic characteristics, and the proton NMR spectrum (Figure 4) showed that the macrocycle is symmetrical with relatively downfield *meso*-protons resonating as two 2H singlets at 9.67 and 10.03 ppm, while the benzo-protons were observed as multiplets at 7.67-7.71 and 8.79-8.83 ppm. The internal methyl group and CH were strongly shifted upfield to give a 3H singlet and 1H singlet at -4.25 ppm and -4.95 ppm, respectively, and the internal NH appeared as a broad peak between 0 and -1 ppm. Also of note, the CH_2 protons of the ethyl substituents appeared as multiplets due to complex coupling that stems from the diastereotopic nature of these protons. Apart from the coupling effects, these results are very similar to those obtained for *N*-unsubstituted benzocarbaporphyrin. The UV-Vis of carbaporphyrin **76** (Figure 5) was typical of an aromatic porphyrinoid, showing a strong Soret absorption at 439 nm and Q bands at 538, 567, 624 and 683 nm. Addition of trifluoroacetic acid (TFA) afforded a monoprotonated species **76**H^+ that showed a diminished Soret band at 444 nm (Figure 5). Crystals of **76** that were suitable for X-ray crystallographic analysis were obtained and the results showed that the pyrrole ring bearing the internal methyl group was titled by 24.34(3)° from the macrocyclic plane, defined by atoms C1, C2, C3, C4, C5, C6, C7, C8, C9, C10, C11, C14, C15, C16, C17, C18, C19, C20 and C21 (Figure 6). The remainder of the macrocyclic framework is rather flat with the two remaining pyrrole rings and the indene subunit only tilted 0.46(3)°, 3.04(3)° and 2.96(2)°, respectively, from the macrocyclic plane. In addition, the *N*-

methyl bond is significantly bent relative to the pyrrole ring plane as evidenced by the 139.2(1)° C12-C11-N23-C25 and 137.8(1)° C13-14-N23-C25 torsion angles. These results differ from the structure obtained for a benzocarbaporphyrin without the *N*-alkyl substituent as this showed that the indene moiety was tilted by 15.5° relative to the mean macrocyclic plane, whereas the pyrrole to mean macrocyclic plane tilts were 2.5°, 4.4°, and 4.9°.[18] With the exception of the C1-C2 bond length, a Mogul geometry check validated all bond distances, angles and torsions to be within typical ranges.[117] The long 1.4822(19) Å C1-C2 and 1.4753(19) Å C3-C4 bond lengths are consistent with more single bond like character, which suggests the benzo π-system of the indene subunit is isolated from the main macrocyclic π-system.

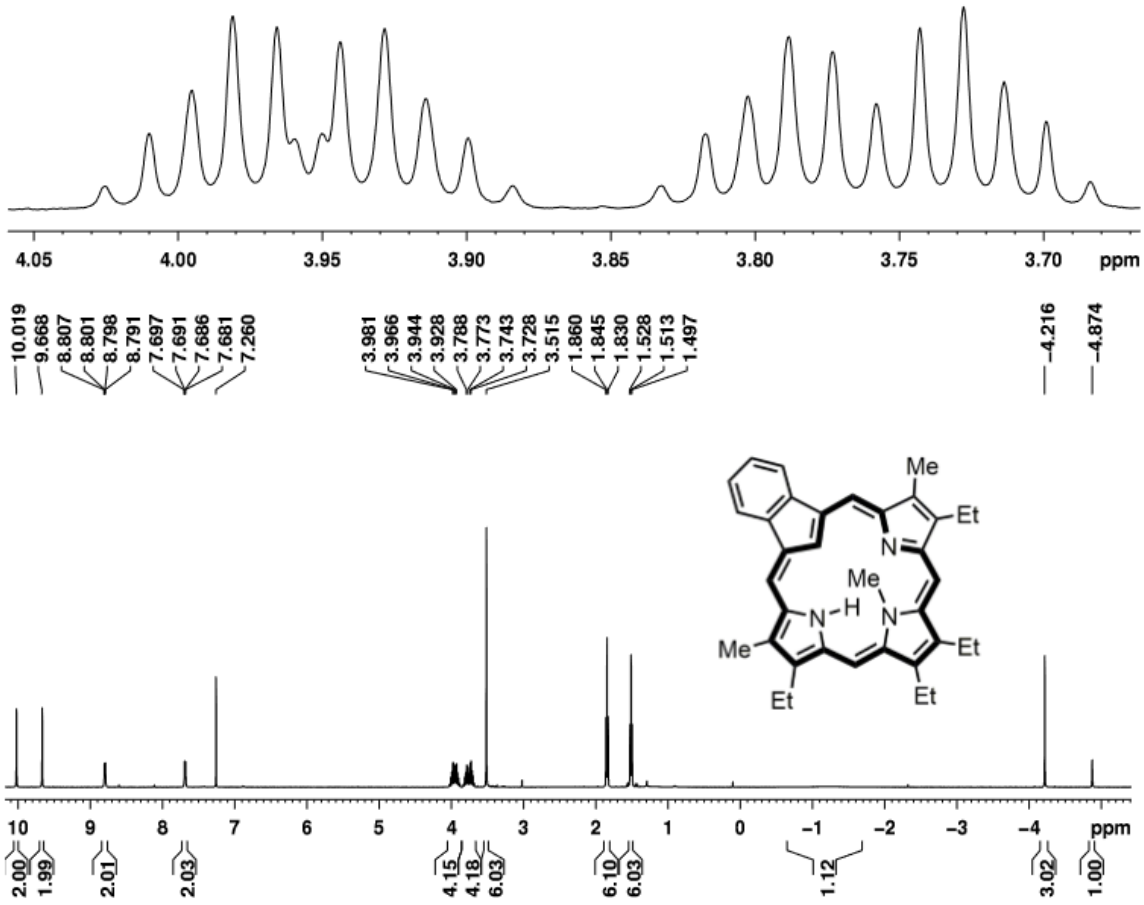

Figure 4. 500 MHz ^{1}H NMR spectrum of 23-methylbenzocarbaporphyrin **76** in $CDCl_3$

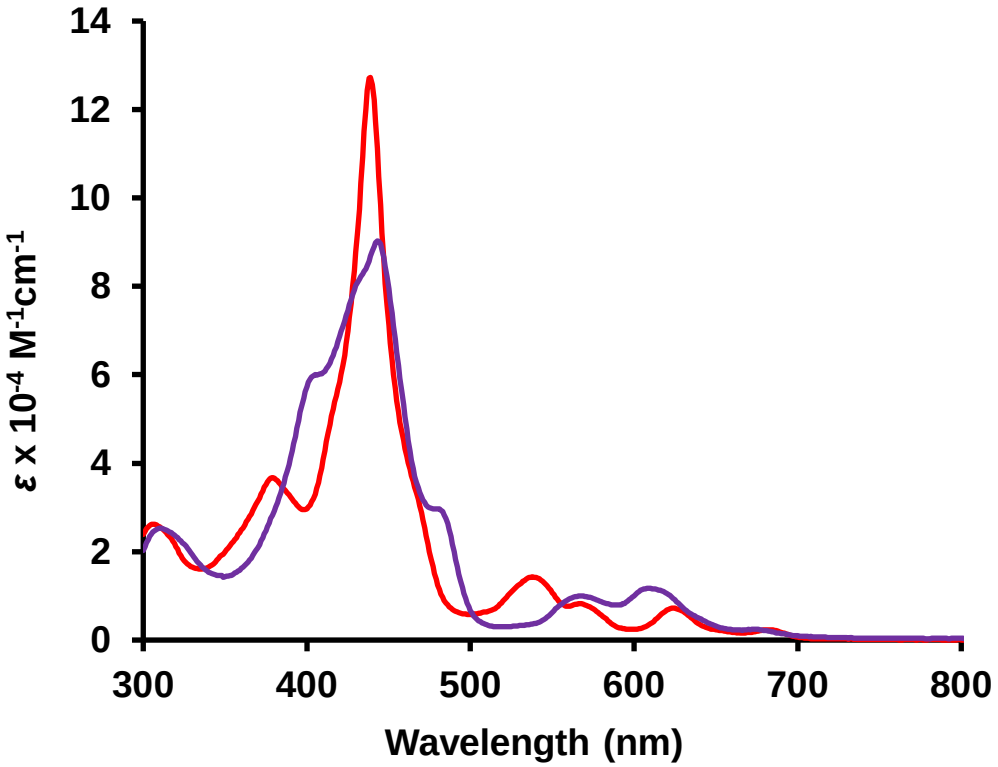

Figure 5. UV-vis spectra of 23-methylcarbaporphyrin **76** in 1% triethylamine-dichloromethane (free base, red line) and 1% TFA-dichloromethane (monocation **76**H^+, purple line)

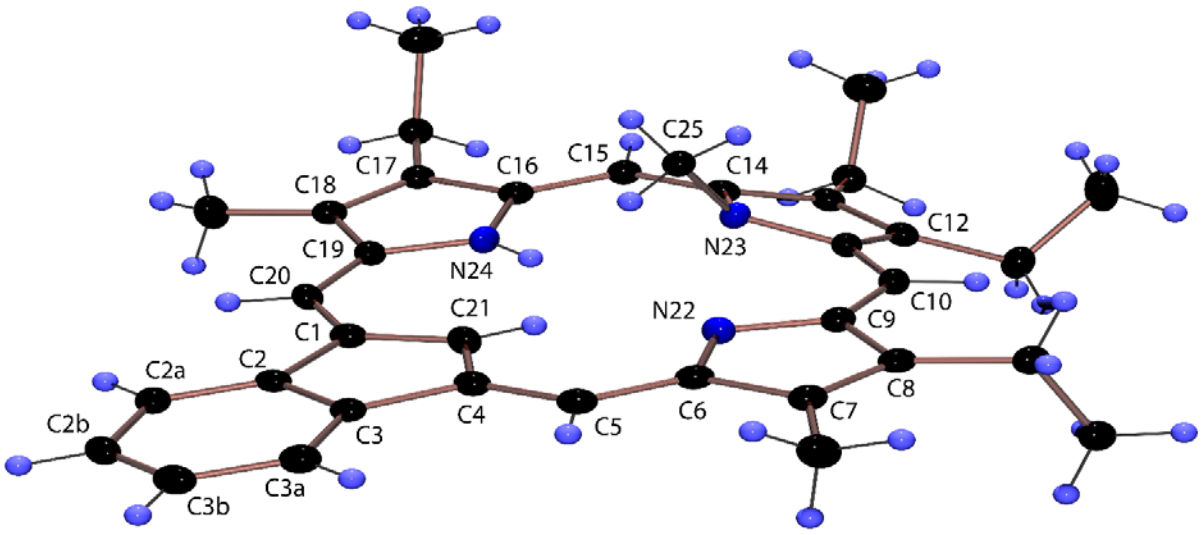

Figure 6. Color POV-Ray rendered ORTEP III drawing (50% probability level, hydrogen atoms rendered arbitrarily small for clarity) of 23-methylcarbaporphyrin **76**.

Reaction of **76** with palladium(II) acetate in refluxing acetonitrile for 30 minutes gave a mixture of metalated products. When the reaction time was reduced to 5 minutes and the crude product purified by column chromatography and recrystallized from chloroform-methanol, a *N*-methyl palladium complex **84** was isolated in 67% yield (Scheme 27). This compound retained strong aromatic character and the symmetry observed for the complex is evident in the NMR spectra. The *meso*-protons appeared downfield at 9.85 and 10.00 ppm and the internal methyl gave a 3H singlet at -2.86 ppm. The benzo-protons were observed as two 2H multiplets at 7.47 and 8.50 ppm, which demonstrates that this complex has a delocalized π-electron pathway similar to that of **76**. The UV-Vis spectrum of **84** gave several strong absorptions between 300 and 520 nm, followed by weaker, broad absorption peaks between 600 and 700 nm (Figure 7). When the reaction of **76** with palladium(II) acetate was carried out overnight, the initially formed *N*-methyl palladium complex **84** was completely converted to the C-methyl palladium(II) complex **72** (Scheme 27). Therefore, the alkyl group migration still occurs for 23-methylbenzocarbaporphyrin **76**, but at a much slower rate. The C-methyl product **72** was identical to the previously isolated product from the reaction of 22-methylbenzocarbaporphyrin with palladium(II) acetate.[102] The UV-Vis spectrum of **72** is very different from the UV-Vis spectrum of **84**, displaying a Soret band at 421 nm as well as a fairly strong absorption at 697 nm (Figure 7). The difference in UV-Vis spectra is due to the presence of a redirected π-electron pathway in **72**, where the conjugation passes through the middle of the indene unit. This relocated conjugation pathway also allows for the two palladium complexes to be easily distinguished from one another by proton NMR spectroscopy (Figure 8).

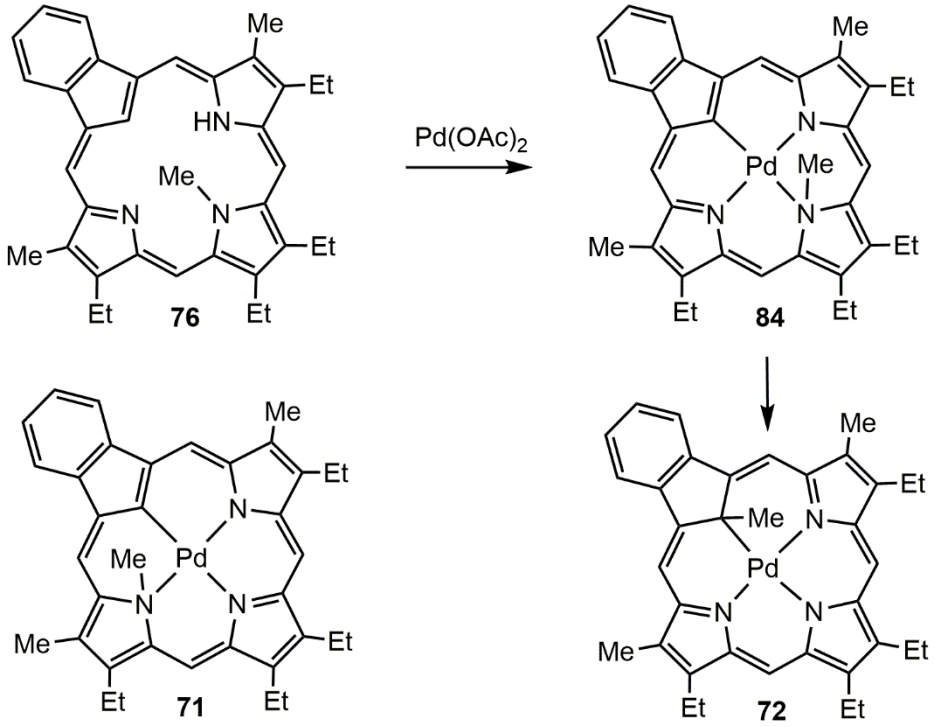

Scheme 27. Metalation of 23-methylbenzocarbaporphyrin to give 23- and 21-methyl palladium(II) complexes

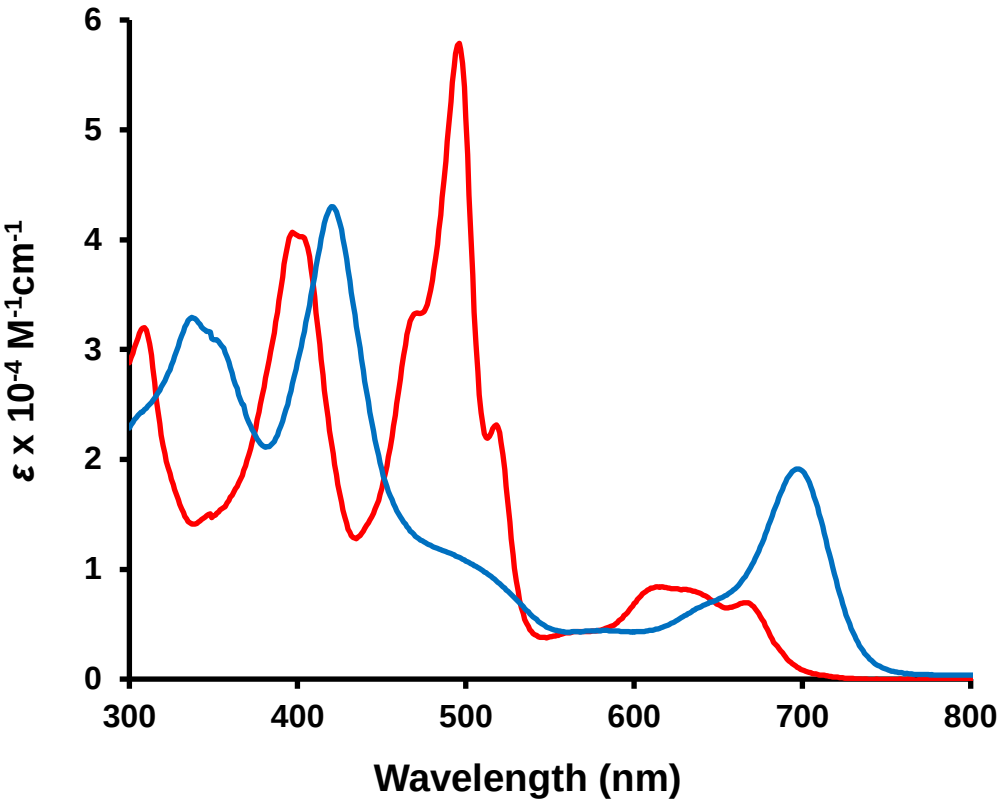

Figure 7. UV-vis spectra of palladium(II) carbaporphyrin complexes **84** (23-methyl, red line) and **72** (21-methyl, blue line)

Palladium complexes **72** and **84** both possess a plane of symmetry, but the downfield regions of their proton NMR spectra were quite different. For **84**, the benzo-protons were observed at 7.45-7.49 ppm and 8.48-8.52 ppm, but in 21-methyl palladium complex **72** the protons resonate at 8.22-8.25 ppm and 9.39-9.43 ppm. These differences can be ascribed to the differing π-electron pathways (shown in bold, Figure 8) for these metalated carbaporphyrins. The downfield shifts for **72** are due to the 18π-electron pathway passing through the benzene unit, causing the benzo-protons to experience more of the deshielding effect due to the macrocyclic ring current. The *meso*-protons of **72** were also identified as two 2H singlets resonating at 9.56 and 10.27 ppm. The internal

methyl group was seen upfield at -3.27 ppm, compared to -2.86 ppm in **84**, but this is due to the methyl group being connected to a carbon atom rather than a nitrogen.

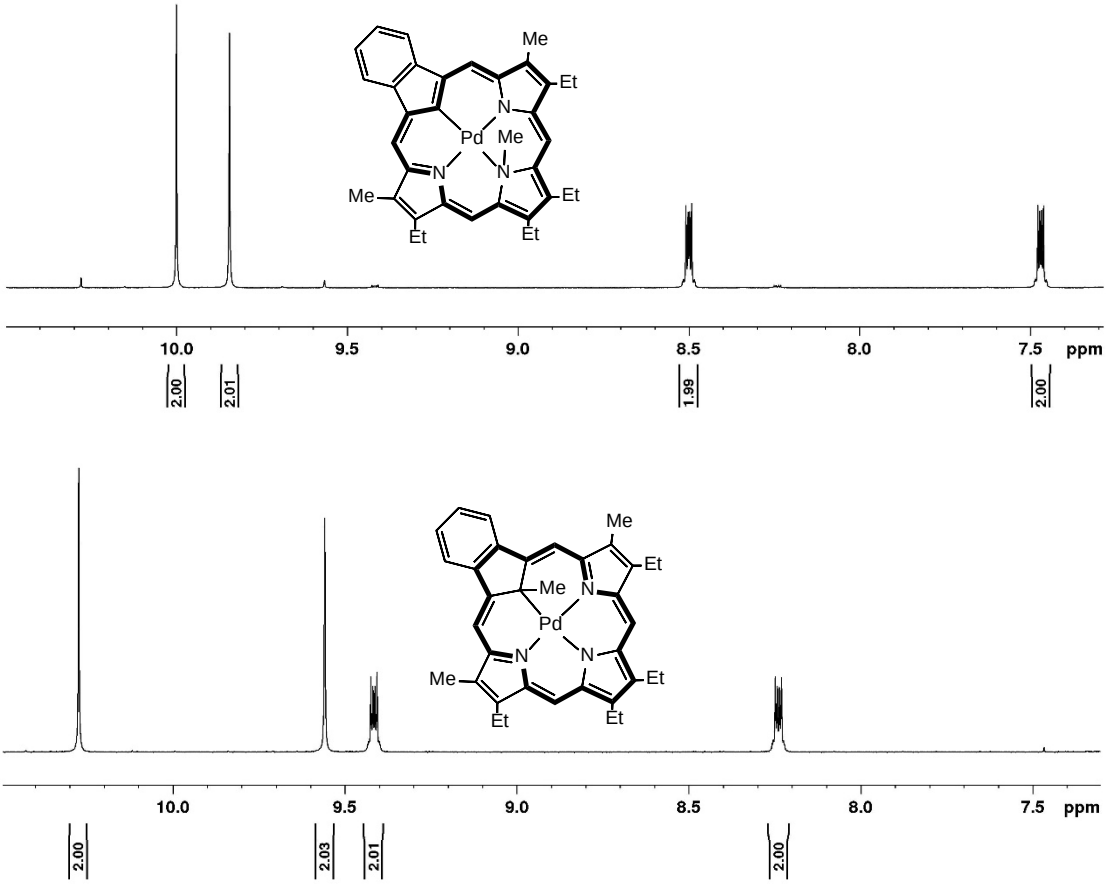

Figure 8. Downfield region for the ^{1}H NMR spectra of 23-methyl palladium complex **84** (top spectrum) and 21-methyl palladium complex **72** (bottom spectrum)

The structure of **72** was confirmed by X-ray crystallography (Figure 9). The framework of bond distances are consistent with an overall aromatic carbaporphyrin containing an sp^3 hybridized C21. The palladium(II) metal center resides in an approximately square planar coordination environment with 2.058(2) Å Pd-C21, 2.037(2) Å Pd-N22, 2.066(2) Å Pd-N23, and 2.028(1) Å Pd-N24 bond lengths. Coordination of the palladium ion and the internal alkyl to C21 results in lengthened 1.491(2) Å and 1.498(2) Å $sp^3 \rightarrow sp^2$ C21-C1 and C21-C4 bond distances. This leads

to C21 lying separate from the macrocycle's π-system. This is further supported by C21 being located 0.360(2) Å out of the PdN_3 plane, and 0.196(2) Å out of the plane defined by the other indene unit atoms. The indene unit itself is tilted 14.82(4)° from the PdN_3 plane. The carbon of the methyl group, C25, lies 1.935(2) Å out of the PdN_3 plane and 1.707(2) Å out of the plane defined by the indene unit atoms. Furthermore, the C1-C2 and C3-C4 bond lengths are ca. 0.03 Å shorter than those found in carbaporphyrin **76**, which is consistent with the π-electron pathway being relocated through the indene unit in palladium complex **72**.

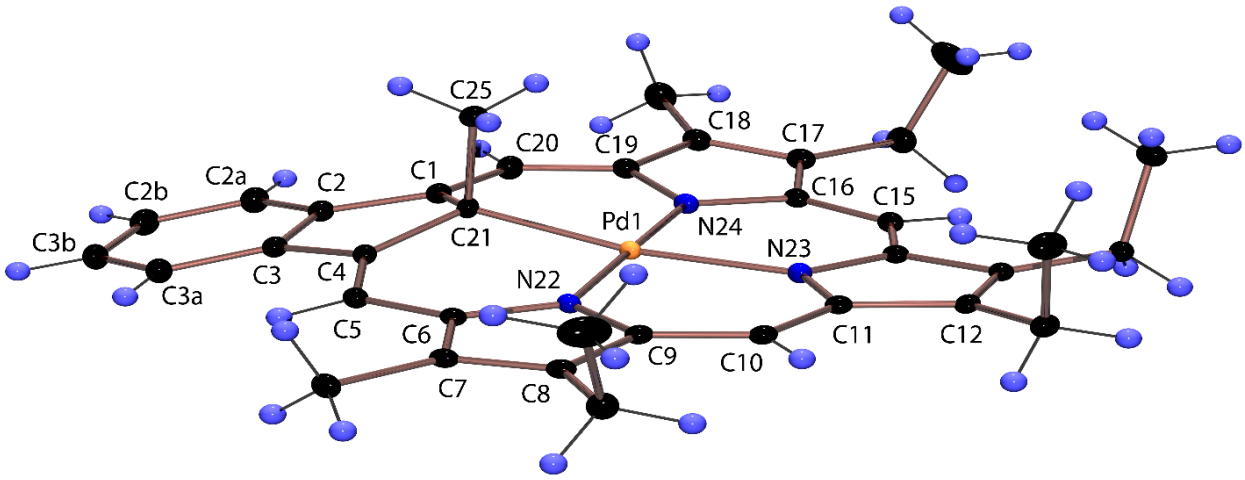

Figure 9. Color POV-Ray rendered ORTEP III drawing (50% probability level, hydrogen atoms rendered arbitrarily for clarity) of 21-methyl palladium(II) complex **72**

Two time course experiments were conducted to investigate the rate of methyl group migration. The first experiment consisted of timed reactions where **76** was refluxed with palladium(II) acetate in acetonitrile for time periods ranging from 5 minutes to overnight (ca. 16 hours). The relative proportions of the two palladium complexes were determined by comparing the integrations observed for the *meso*-, benzo-, and internal methyl protons of each compound. The percent compositions of each metal complex were graphed as a function of time (Figure 10a).

Although the formation of **84** was very rapid, it was observed that the methyl group migration was only 50% complete after refluxing for 2.5 hours in acetonitrile. This is much slower compared to the almost full conversion to **72** seen after only 30 minutes for the 22-methyl derivative **71**. It is possible that **71** could be an intermediate in the formation of **72** from **84** (Scheme 27). However, this species was not detected in any of the proton NMR spectra. As a slight excess of palladium(II) acetate is used in these reactions, there was also a possibility that this promoted the rearrangement. It was found that neither the absence or presence of palladium(II) acetate had a measurable effect on the rate of migration. This was determined by a second time course experiment where the 23-methyl palladium(II) complex **84** was dissolved in d_3-acetonitrile in a NMR tube at 70 °C and spectra were collected using a 500 MHz NMR spectrometer over a period of ca. 8 hours. The percent composition of each product was determined in the same fashion as the first experiment, and the values were plotted against increasing time. The results showed 50% conversion of **84** to **72** after 380 minutes (Figure 10b). This depicts a slower conversion due to the lower temperature but shows that the migration can occur without the presence of palladium(II) acetate. Methyl group migration without the presence of a palladium metal center was also tested by refluxing **76** in acetonitrile with no palladium(II) acetate added, and it was found that no migration occurred. Furthermore, it was found that this migration occurs even in the solid state. A crystalline sample of **84** that had been stored for approximately 1 year was found to have completely converted to the 21-methyl derivative **72**. No intermediates could be seen in any of the NMR spectra obtained during the time course experiments, and therefore the mechanism remains ambiguous. However, these new results provide some insights into these rearrangements. It is possible that the 22-methyl palladium(II) complex is formed as an intermediate, as the conversion of **71** to **72** is fast compared

to the rearrangement of **84** to **72**. However, as the migration does not occur without the presence of a palladium metal center, the intermediacy of a palladium-methyl complex is more plausible.

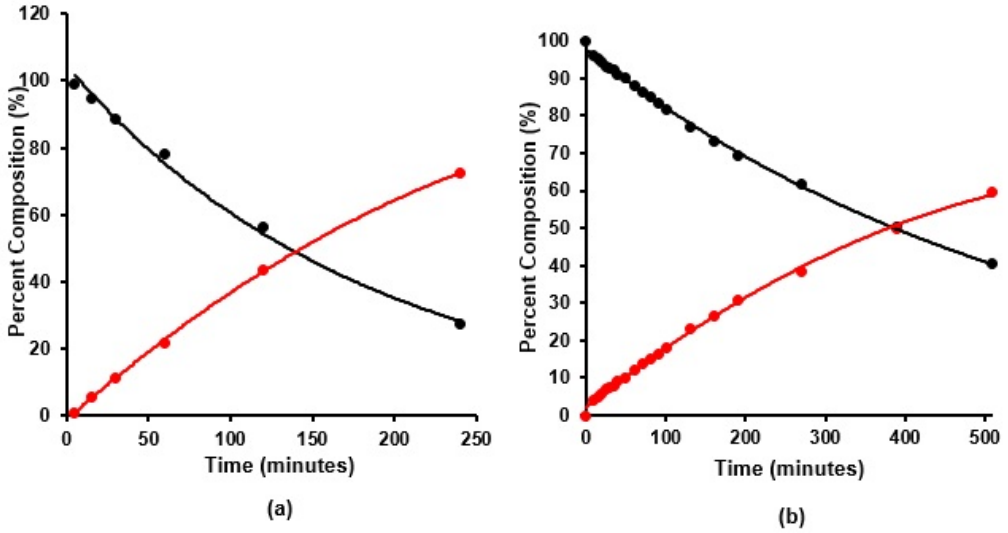

Figure 10. Timed experiments on the rate of alkyl group migration, showing the conversion of **84** (black line) into **72** (red line) **a)** Timed reflux reactions **b)** Reaction of **84** in d_3-acetonitrile at 70 °C in an NMR tube within a 500 MHz NMR instrument

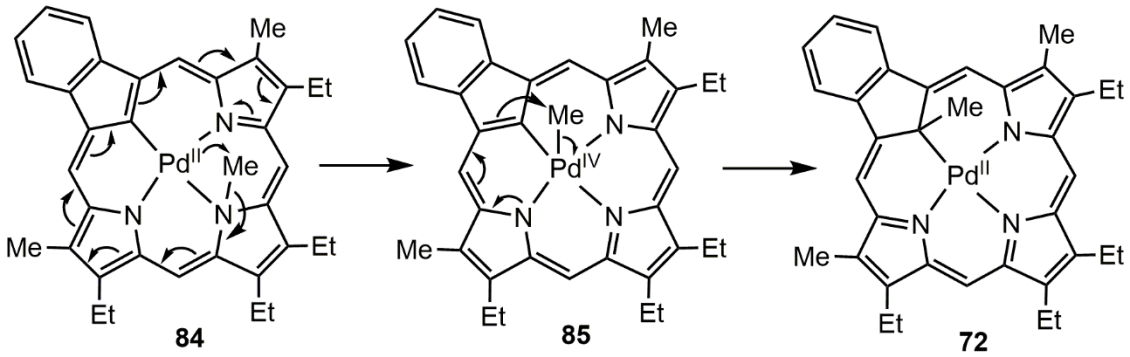

Scheme 28. Proposed mechanism for migration of an alkyl group from the 23- to 21-position of benzocarbaporphyrins

It is proposed that a palladium-methyl intermediate is formed through an oxidative addition of the alkyl group onto the metal center forming a palladium(IV) species **85**. Subsequent reductive elimination would lead to transfer of the methyl group to the 21-carbon, producing the observed product **72** and a reduction of the palladium to its original 2+ oxidation state (Scheme 28).

Conclusion

Introduction of internal methyl substituents results in benzocarbaporphyrins taking on dianonic character when reacted with metals such as palladium. Methyl group migration was also observed and investigated within these carbaporphyrinoids. It was found that methyl substituents located on two different internal nitrogens migrated to the internal carbon atom and produced the same 21-methyl palladium(II) benzocarbaporphyrin complex **72**. Due to the dramatic effects that internal alkyl moieties have on carbaporphyrin coordination with palladium cations, the next chapter focuses on the introduction of rhodium into internally methylated carbaporphyrinoid systems. Rhodium(I) and rhodium(III) complexes of benzocarbaporphyrins, a carbaporphyrin diester and a naphthocarbaporphyrin are discussed. The metalation of the 23-methylbenzocarbaporphyrin **76** with rhodium is also described, and the unexpected formation of a rhodium(III) bridged derivative is reported.

Experimental:

Melting points are uncorrected. NMR spectra were recorded using a 400 or 500 MHz NMR spectrometer and were run at 302 K unless otherwise indicated. ^{1}H NMR values are reported as chemical shifts δ, relative integral, multiplicity (s, singlet; d, doublet; t, triplet; q, quartet; m, multiplet; br, broad peak) and coupling constant (*J*). Chemical shifts are reported in parts per million (ppm) relative to $CDCl_3$ (^{1}H residual $CHCl_3$ singlet δ 7.26, ^{13}C $CDCl_3$ triplet δ 77.23) or d_6-DMSO (^{1}H residual d_5-DMSO pentet δ 2.49, ^{13}C d_6-DMSO septet δ 39.7) and coupling constants were taken directly from the spectra. NMR assignments were made with the aid of ^{1}H-^{1}H COSY, HSQC, DEPT-135 and nOe difference proton NMR spectroscopy. 2D experiments were performed using standard software. High-resolution mass spectra (HRMS) were carried out using a double focusing magnetic sector instrument. Samples of X-ray quality crystals were suspended in mineral oil at ambient temperature and a suitable crystal was selected, mounted on a MiTeGen Micromount and transferred to a Bruker AXS SMART APEXII CCD X-ray diffractometer. The X-ray diffraction data were collected at 100(2) K using Mo-Kα (λ = 0.71073 Å) radiation.

Ethyl 3,4-diethyl-1-methylpyrrole-2-carboxylate (**79**). 3-Acetoxy-4-nitrohexane (52.5 g, 0.278 mol) and ethyl isocyanoacetate (26.0 g, 0.230 mol) were mixed with THF (165 mL) and 2-propanol (67 mL) in a 3-neck round bottom flask fitted with a thermometer, addition funnel and drying tube. DBU (86.0 g, 0.565 mol) was added dropwise, maintaining the temperature between 20-30 ^{o}C with the aid of an salt-ice bath. After the addition was complete, the orange solution was stirred at room temperature overnight. The solvent was removed under reduced pressure and the residue poured into water (225 mL). Diethyl ether (225 mL) was added and the aqueous layer drawn off and extracted twice with 225 mL of diethyl ether. The combined ether layers were

washed with 10% aqueous HCl (2 x 300 mL), dried over magnesium sulfate and the solvent removed on a rotary evaporator. The residue was vacuum distilled to yield ethyl 3,4-diethylpyrrole-2-carboxylate (**17a**)[43] (31.6 g, 0.162 mol, 70%) as a pale yellow oil, bp 102-105 °C at 0.6 torr. ^{1}H NMR (400 MHz, $CDCl_3$): δ 1.16 (3H, t, $^3J_{HH}$ = 7.5 Hz), 1.20 (3H, t, $^3J_{HH}$ = 7.5 Hz) (3,4-CH_2CH_3), 1.36 (3H, t, $^3J_{HH}$ = 7.2 Hz, OCH_2CH_3), 2.46 (2H, q, $^3J_{HH}$ = 7.5 Hz, 4-CH_2CH_3), 2.77 (2H, q, $^3J_{HH}$ = 7.5 Hz, 3-CH_2CH_3), 4.33 (2H, q, $^3J_{HH}$ = 7.2 Hz, OCH_2), 6.68 (1H, d, $^3J_{HH}$ = 2.9 Hz, 5-H), 9.00 (1H, br s, NH). The proton NMR spectrum shows the presence of ca. 3% of the corresponding isopropyl ester due to transesterification with 2-propanol.

Potassium hydroxide pellets (3.84 g) were heated with dimethylsulfoxide (15 mL) until a yellow colored solution was obtained. The solution was cooled to room temperature and the foregoing pyrrole ester **17a** (3.80 g, 19.5 mmol) was added. After the mixture had been stirred for 1 h, methyl iodide (5.2 g) was added dropwise, keeping the temperature below 30 °C with the aid of a salt-ice bath. After the addition was completed, the solution was stirred for an additional 1 h, keeping the temperature below 30 °C. The solution was poured in ice/water (200 mL), and the aqueous layer was extracted with dichloromethane (2 x 200 mL). The combined dichloromethane layers were washed with water (5 x 100 mL), dried over magnesium sulfate and the solvent removed under reduced pressure. The residue was vacuum distilled to yield *N*-methylpyrrole ester **17b** (3.20 g, 15.3 mmol, 79%) as a pale yellow oil, bp 98-100°C at 1 torr. ^{1}H NMR (500 MHz, $CDCl_3$): δ 1.12 (3H, t, $^3J_{HH}$ = 7.6 Hz, 3-CH_2CH_3), 1.14 (3H, t, $^3J_{HH}$ = 7.6 Hz, 4-CH_2CH_3), 1.30 (3H, t, $^3J_{HH}$ = 7.2 Hz, OCH_2CH_3), 2.37 (2H, q, $^3J_{HH}$ = 7.6 Hz, 4-CH_2CH_3), 2.72 (2H, q, $^3J_{HH}$ = 7.6 Hz, 3-CH_2CH_3), 3.75 (3H, s, N-Me), 4.24 (2H, q, $^3J_{HH}$ = 7.2 Hz, OCH_2), 6.43 (1H, s, 5-H). ^{13}C NMR (125 MHz, $CDCl_3$): δ 13.8 (OCH_2CH_3), 14.5 (4-CH_2CH_3), 15.2 (3-CH_2CH_3), 17.4 (4-CH_2),

18.5 (3-CH_2), 36.5 (N-Me), 58.7 (OCH_2), 118.6, 123.5, 125.8 (5-CH), 133.4, 161.2 (C=O). HR-MS (EI) *m/z*: Calcd for $C_{12}H_{19}NO_2$ 209.1416; found 209.1419.

3,4-Diethyl-1-methylpyrrole (**53b**). Pyrrole ester **79** (2.82 g, 13.5 mmol) was added to sodium hydroxide (1.07 g) in ethylene glycol (11 mL), and the mixture heated for 2.5 h at 200 °C. After cooling the solution to room temperature, the mixture was partitioned between water (50 mL) and hexanes (50 mL). The aqueous layer was drawn off and further extracted with hexanes (3 x 50 mL). The combined hexanes layers were dried over magnesium sulfate and the solvent removed under reduced pressure to yield 3,4-diethyl-1-methylpyrrole (1.55 g, 11.3 mmol, 84%) as a pale yellow oil, b.p 78-80°C at 18 torr. ^{1}H NMR (500 MHz, $CDCl_3$): δ 1.46 (6H, t, $^3J_{HH}$ = 7.6 Hz, 2 x CH_2CH_3), 2.71 (4H, q, $^3J_{HH}$ = 7.6 Hz, 2 x CH_2CH_3), 3.80 (3H, s, N-Me), 6.58 (2H, s, 2,5-H). ^{13}C NMR (125 MHz, $CDCl_3$): δ 14.6 (2 x CH_2CH_3), 18.3 (2 x CH_2CH_3), 35.1 (N-Me), 118.2 (2,5-CH), 124.1 (3,4-C). HR-MS (EI) *m/z*: Calcd for $C_9H_{15}N$ 137.1204; found 137.1204.

2,5-Bis(5-benzyloxycarbonyl-3-ethyl-4-methyl-2-pyrrolylmethyl)-3,4-diethyl-1-methylpyrrole (**54c**). Benzyl 5-acetoxymethyl-4-ethyl-3-methylpyrrole-2-carboxylate (1.28 g, 4.10 mmol) and 3,4-diethyl-1-methylpyrrole (0.279 g, 2.04 mmol) were dissolved in acetonitrile (15 mL) and acetic acid (1 mL). The mixture was refluxed overnight under nitrogen. The solution was then cooled to room temperature, diluted with dichloromethane (50 mL), and then washed with water (100 mL) and aqueous 10% sodium bicarbonate solution (100 mL). The dichloromethane layer was dried over sodium sulfate and the solvent removed under reduced pressure. The residue was purified by column chromatography on silica gel, eluting with 80:20:1 dichloromethane-hexanes-triethylamine, and afforded the *N*-methyl tripyrrane (0.624 g, 0.964 mmol, 48%) as an orange oil that slowly solidified when stored in the freezer. ^{1}H NMR (500 MHz, $CDCl_3$): δ 1.05 (6H, t, $^3J_{HH}$ = 7.6 Hz, 3',3''-CH_2CH_3), 1.09 (6H, t, $^3J_{HH}$ = 7.6 Hz, 3,4-CH_2CH_3),

2.27 (6H, s, 4',4''-CH_3), 2.39-2.45 (8H, m, 4 x C*H*$_2$$CH_3$), 2.98 (3H, s, N-Me), 3.81 (4H, s, 2 x bridge-CH_2), 5.24 (4H, s, 2 x OCH_2), 7.28-7.39 (10H, m, 2 x Ph), 8.23 (2H, br s, 2 x NH). ^{13}C NMR (125 MHz, $CDCl_3$): δ 10.7 (4',4''-Me), 15.4 (3',3''-CH_2*C*H_3), 17.24 (3,4-CH_2*C*H_3), 17.28, 18.0 (4 x *C*H_2CH_3), 21.9 (2 x bridge-CH_2), 30.4 (N-Me), 65.6 (2 x OCH_2), 117.1, 122.2, 122.9, 123.4, 128.1 (Ph), 128.7 (Ph), 131.1, 136.9, 161.6 (2 x C=O). HR-MS (ESI) *m/z*: $[M + H]^+$ Calcd for $C_{41}H_{50}N_3O_4$ 648.3801; found 648.3792.

N-methyl tripyrrane dicarboxylic acid **54d**. *N*-methyl tripyrrane **54c** (0.703 g, 1.09 mmol) was placed in a hydrogenation vessel and dissolved in acetone (100 mL), methanol (34 mL) and triethylamine (14 drops). The mixture was purged with nitrogen, 10% palladium-charcoal (67 mg) was added and the solution shaken under an atmosphere of hydrogen at 40 psi at room temperature overnight. The catalyst was removed by suction filtration and the solvent removed on a rotary evaporatory while maintaining the bath temperature below 30 ^{o}C. The residue was dissolved in 5% aqueous ammonium and diluted to a final volume of 50 mL with water. The resulting solution was cooled to 0-5 ^{o}C, and then acidified by adding acetic acid dropwise while maintaining the temperature below 5 ^{o}C. The mixture was allowed to sit in a salt-ice bath for 30 min and the precipitate was then collected by suction filtration and washed multiple times with water to remove all traces of acid. The solid was dried overnight in a vacuum desiccator to yield the dicarboxylic acid (0.419 g, 0.897 mmol, 83%) as an unstable pale purple powder that was used without further purification. ^{1}H NMR (500 MHz, d_6-DMSO): δ 0.73 (6H, t, $^3J_{HH}$ = 7.5 Hz), 0.97 (6H, t, $^3J_{HH}$ = 7.5 Hz) (4 x CH_2C*H*$_3$), 2.12 (6H, s, 4',4''-CH_3), 2.11 (4H, q, $^3J_{HH}$ = 7.5 Hz), 2.35 (4H, q, $^3J_{HH}$ = 7.5 Hz) (4 x C*H*$_2$$CH_3$), 2.99 (3H, s, N-Me), 3.81 (4H, s, 2 x bridge-CH_2), 10.14 (2H, br s, 2 x NH), 11.53 (2H, v br, 2 x CO_2H). ^{13}C NMR (125 MHz, $CDCl_3$): δ 9.9 (4',4''-Me), 14.8, 16.3, 16.5, 17.2,

21.6 (2 x bridge-CH_2), 30.1 (N-Me), 116.5, 119.6, 122.6, 123.1, 125.5, 130.4, 162.1 (2 x C=O). HR-MS (ESI) *m/z*: Calcd for $C_{27}H_{37}N_3O_4$ 490.2682; found 490.2672.

8,12,13,17-Tetraethyl-7,18,23-trimethylbenzo[*b*]carbaporphyrin (**76**). *N*-methyl tripyrrane dicarboxylic acid **54d** (0.144 g, 0.308 mmol) was dissolved in TFA (1.5 mL) and stirred under nitrogen for 2 min. Dichloromethane (27 mL) was added, followed immediately by indene dialdehyde (54.0 mg, 0.314 mmol), and the solution stirred under nitrogen for 2 h. The mixture was neutralized by the dropwise addition of triethylamine, DDQ (72.0 mg, 0.317 mmol) was added, and the mixture stirred for a further 1 h. The solution was washed with water (100 mL) and then sodium bicarbonate (100 mL), and the solvent removed under reduced pressure. The residue was chromatographed twice on grade 3 neutral alumina eluting with dichloromethane and then chloroform, and a dark brown band was collected. The product was recrystallized from chloroform-methanol to yield the 23-methylbenzocarbaporphyrin (52.5 mg, 0.102 mmol, 32%) as dark purple-blue crystals, mp > 300 ^oC. UV-vis (1% Et_3N-CH_2Cl_2): λ_{max}/nm (log ε) 306 (4.42), 379 (4.56), 439 (5.10), 538 (4.15), 567 (3.91), 624 (3.86), 683 (3.36). UV-vis (1% TFA-CH_2Cl_2): λ_{max}/nm (log ε) 310 (4.42), 403 (sh, 4.77), 444 (4.97), 481 (4.47), 568 (4.01), 608 (4.08), 677 (3.26). ^{1}H NMR (500 MHz, $CDCl_3$): δ -4.95 (1H, s, 21-H), -4.25 (3H, s, N-Me), -0.63 (1H, v br, NH), 1.47 (6H, t, $^3J_{HH}$ = 7.7 Hz, 12,13-CH_2CH_3), 1.83 (6H, t, $^3J_{HH}$ = 7.7 Hz, 8,17-CH_2CH_3), 3.51 (6H, s, 7,18-Me), 3.67-3.75 (2H, m), 3.76-3.84 (2H, m) (12,13-CH_2), 3.88-4.02 (4H, m, 8,17-CH_2), 7.67-7.71 (2H, m, 2^2,3^2-H), 8.79-8.83 (2H, m, 2^1,3^1-H), 9.67 (2H, s, 10,15-H), 10.03 (2H, s, 5,20-H). ^{1}H NMR (500 MHz, TFA-$CDCl_3$): δ -6.53 (1H, br s, 21-H), -4.79 (2H, s, 2 x NH), -4.51 (3H, s, N-Me), 1.50 (6H, t, $^3J_{HH}$ = 7.7 Hz, 12,13-CH_2CH_3), 1.77 (6H, t, $^3J_{HH}$ = 7.7 Hz, 8,17-CH_2CH_3), 3.60 (6H, s, 7,18-Me), 3.69-3.80 (4H, m, 12,13-CH_2), 4.05 (4H, q, $^3J_{HH}$ = 7.7 Hz, 8,17-CH_2), 7.70-7.80 (2H, br, 2^2,3^2-H), 8.64-8.72 (2H, m, 2^1,3^1-H), 10.00 (2H, s, 10,15-H), 10.26 (2H, s, 5,20-H).

^{13}C NMR (125 MHz, $CDCl_3$): δ 11.5 (7,18-Me), 16.9 (12,13-$CH_2\mathit{C}H_3$), 17.4 (8,17-$CH_2\mathit{C}H_3$), 20.0 (8,17-CH_2), 20.1 (12,13-CH_2), 31.4 (N-Me), 96.4 (10,15-CH), 103.4 (5,20-CH), 118.8 (21-CH), 120.4 (2^1,3^1-CH), 126.5 (2^2,3^2-CH), 134.2, 135.2, 136.3, 140.7, 144.0, 147.6. ^{13}C NMR (125 MHz, TFA-$CDCl_3$): δ 11.7 (7,18-Me), 16.5 (12,13-$CH_2\mathit{C}H_3$), 16.9 (8,17-$CH_2\mathit{C}H_3$), 20.13, 20.15 (4 x $\mathit{C}H_2CH_3$), 30.7 (N-Me), 95.8 (10,15-CH), 103.6 (5,20-CH), 116.5 (21-CH), 121.9 (2^1,3^1-CH), 128.7 (2^2,3^2-CH), 136.2, 136.8, 138.8, 138.9, 140.6, 141.5, 141.7, 150.6. HR-MS (ESI) *m/z*: $[M + H]^+$ Calcd for $C_{36}H_{40}N_3$ 514.3222; found 514.3198.

[8,12,13,17-Tetraethyl-7,18,23-trimethylbenzo[*b*]carbaporphyrinato]palladium(II) (**84**). Palladium(II) acetate (10.0 mg, 0.0450 mmol) was added to a solution of 23-methylbenzocarbaporphyrin **76** (10.0 mg, 0.0195 mmol) in acetonitrile (10 mL) and heated under reflux in a pre-heated oil bath for 5 min. The solution was diluted with chloroform (30 mL) and washed with water (50 mL). The aqueous solution was back extracted with chloroform and the combined organic layers were evaporated under reduced pressure. The residue was purified by column chromatography on silica gel eluting with dichloromethane-hexanes (70:30) and a dark green band was collected. The solvent was removed on a rotary evaporator and the residue recrystallized from chloroform-methanol to give the palladium complex (8.0 mg, 0.013 mmol, 67%) as dark green crystals, mp > 300 °C. UV-vis (CH_2Cl_2): λ_{max}/nm (log ε) 309 (4.50), 397 (4.61), 404 (sh, 4.60), 470 (sh, 4.52), 496 (4.76), 518 (4.36), 561 (3.63), 613 (3.93), 635 (sh, 3.90), 667 (3.84). ^{1}H NMR (500 MHz, $CDCl_3$): δ -2.86 (3H, s, N-Me), 1.67 (6H, t, $^3J_{HH}$ = 7.7 Hz, 12,13-$CH_2C\mathit{H}_3$), 1.81 (6H, t, $^3J_{HH}$ = 7.7 Hz, 8,17-$CH_2C\mathit{H}_3$), 3.48 (6H, s, 7,18-Me), 3.84-4.00 (8H, m, 4 x $C\mathit{H}_2CH_3$), 7.45-7.49 (2H, m, 2^2,3^2-H), 8.48-8.52 (2H, m, 2^1,3^1-H), 9.85 (2H, s, 10,15-H), 10.00 (2H, s, 5,20-H). ^{13}C NMR (125 MHz, $CDCl_3$): δ 11.7 (7,18-Me), 16.5 (12,13-$CH_2\mathit{C}H_3$), 17.6 (8,17-$CH_2\mathit{C}H_3$), 20.16, 20.21 (4 x $\mathit{C}H_2CH_3$), 45.3 (N-Me), 98.9 (10,15-CH), 109.6 (5,20-CH), 118.8

(2^1,3^1-CH), 126.0 (2^2,3^2-CH), 133.8, 135.1, 136.3, 138.9, 140.7, 142.7, 145.6, 149.8. HR-MS (ESI) *m/z*: Calcd for $C_{36}H_{37}N_3Pd$ 617.2022; found 617.2044.

[8,12,13,17-Tetraethyl-7,18,21-trimethylbenzo[*b*]carbaporphyrinato]palladium(II) (**72**). Palladium(II) acetate (10 mg, 0.0450 mmol) was added to a solution of 23-methylbenzocarbaporphyrin **76** (10 mg, 0.0195 mmol) in acetonitrile (10 mL) and the mixture refluxed overnight. The solvent was removed under reduced pressure and the residue chromatographed on a silica gel column eluting with dichloromethane-hexanes (70:30). A brown band was collected and the solvent removed under reduced pressure to give **72** (10.2 mg, 0.0165 mmol, 85%) as a dark brown solid, mp >300 ^oC. ^1H NMR (500 MHz, $CDCl_3$): δ -3.21 (3H, s, 21-CH_3), 1.74 (6H, t, $^3J_{HH}$ = 7.7 Hz), 1.75 (6H, t, $^3J_{HH}$ = 7.7 Hz) (4 x CH_2CH_3), 3.33 (6H, s), 3.71-3.78 (8H, m, 4 x CH_2CH_3), 8.22-8.25 (2H, m, 2^2,3^2-H), 9.39-9.43 (2H, m, 2^1,3^1-H), 9.56 (2H, s, 10,15-H), 10.27 (2H, s, 5,20-H). The sample had identical spectroscopic properties to a previously prepared sample obtained by reacting **70** with $Pd(OAc)_2$.[101]

CHAPTER III: RHODIUM COMPLEXES OF CARBAPORPHYRINOID SYSTEMS

Introduction

Benzocarbaporphyrin **3** typically acts as a trianionic ligand, forming stable organometallic complexes **10a** and **10b** with silver(III)[27,28] and gold(III)[28], respectively (Scheme 29). However, attempts to react **3** with nickel(II), palladium(II) or platinum(II) salts were unsuccessful.[27] Azuliporphyrins, which are similar in structure, readily generated nickel(II), palladium(II) and platinum(II) complexes **13a-c**[32] and have also been seen to form stable rhodium(III) derivatives **15a-c** and **16** as well as iridium(III) complexes **17a-d** (Chart 9). Rhodium porphyrins have been widely investigated for their catalytic properties and can promote C-H and C-C bond activation,[1] and rhodium(I) and rhodium(III) benzocarbaporphyrins have recently been reported.[30] Carbaporphyrin **3** reacted with $[Rh(CO)_2Cl]_2$ in refluxing dichloromethane to afford rhodium(I) complex **86** in 90% yield (Scheme 29). The rhodium metal coordinates with the 22- and 23-nitrogen atoms of the benzocarbaporphyrin and possesses two terminal carbonyl ligands. Subsequent reaction in refluxing pyridine led to the formation of rhodium(III) complex **11a** in 50% yield. This rhodium(III) derivative incorporates two axial pyridine ligands coordinating to the metal center on opposite faces of the carbaporphyrin system. It is of interest to investigate the effect internal alkylation has on the coordination chemistry of benzocarbaporphyrins with rhodium metal. In this chapter, the syntheses and characterization of rhodium carbaporphyrin complexes are discussed. Metalation studies of 21-, 22-, and 23-methylbenzocarbaporphyrins with a rhodium(I) reagent were performed and the results were compared to those of *N*-unsubstituted

benzocarbaporphyrin **3**. Furthermore, a carbaporphyrin diester and naphthocarbaporphyrin also underwent metalation with $[Rh(CO)_2Cl]_2$ and the results of these reactions were also analyzed.

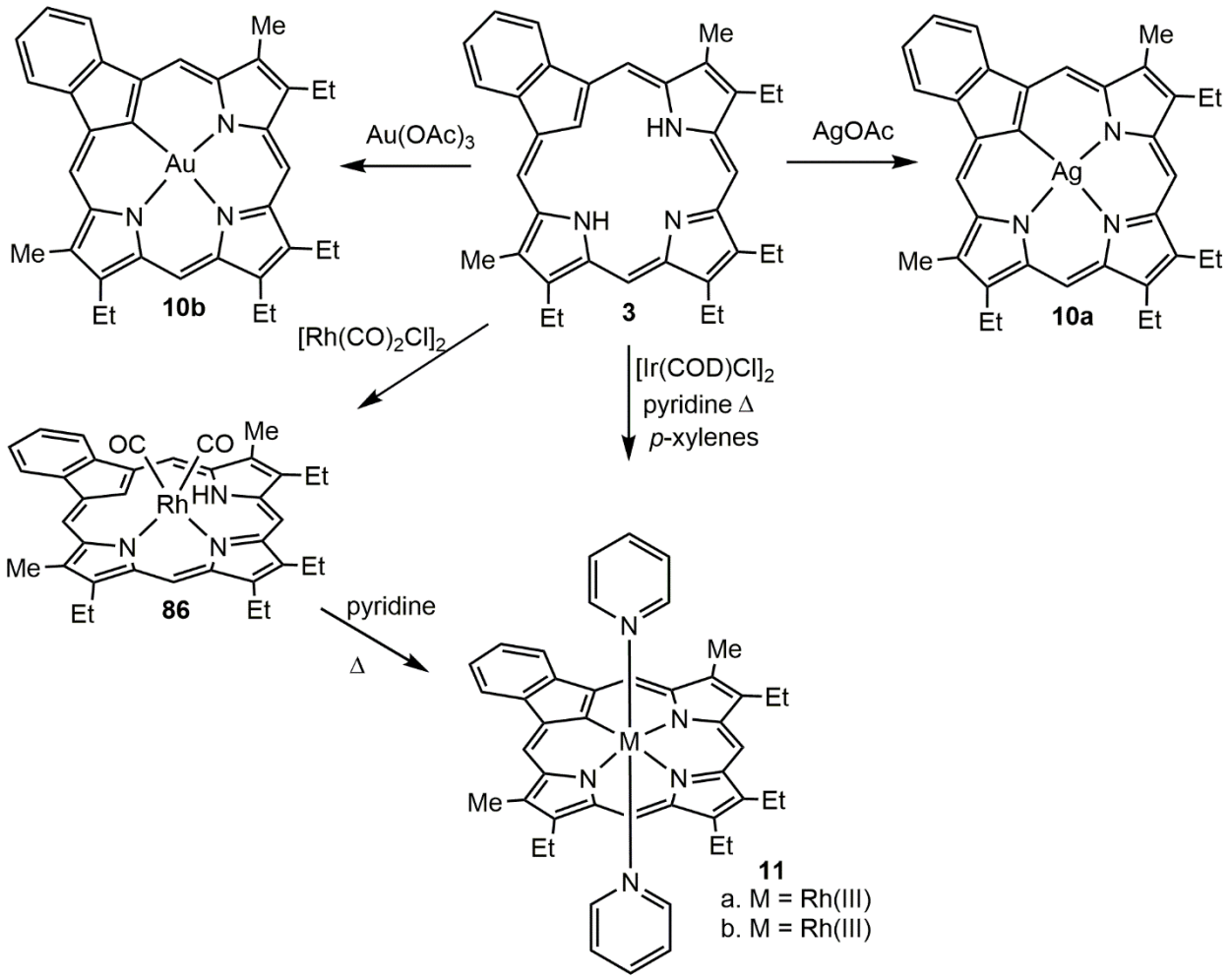

Scheme 29. Metalation of benzocarbaporphyrin **3** to give rhodium(I) and rhodium(III) derivatives

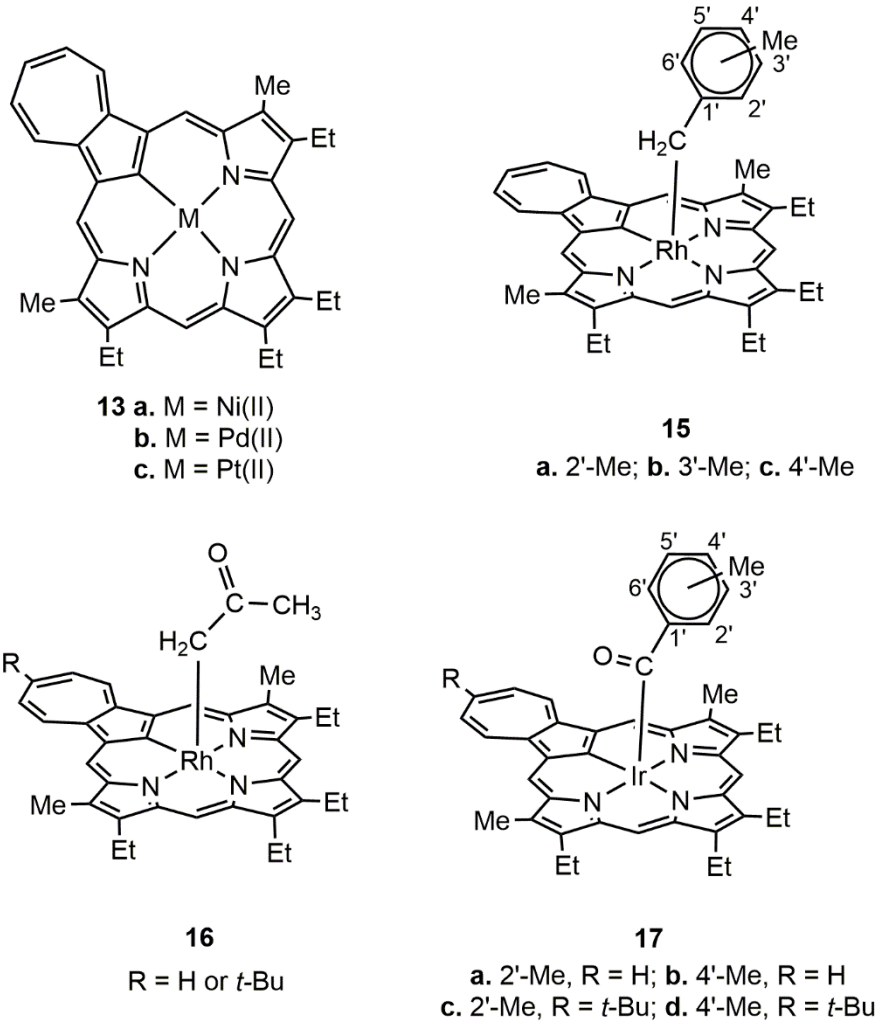

Chart 9. Examples of metalated azuliporphyrins

Results and Discussion

Recently, syntheses of naphthocarbaporphyrin **87**[108] and carbaporphyrin diester **88**[29] have been developed. Carbaporphyrin diester **88** was reacted with $[Rh(CO)_2Cl]_2$ in refluxing dichloromethane in the presence of anhydrous sodium acetate to give the corresponding rhodium(I) complex **89** (Scheme 30). The crude product was chromatographed on grade 3 neutral alumina eluting with chloroform and collected as a dark green band. The fraction was

recrystallized from chloroform-hexanes to give the pure rhodium(I) carbaporphyrin diester **89** in up to 99% yield.

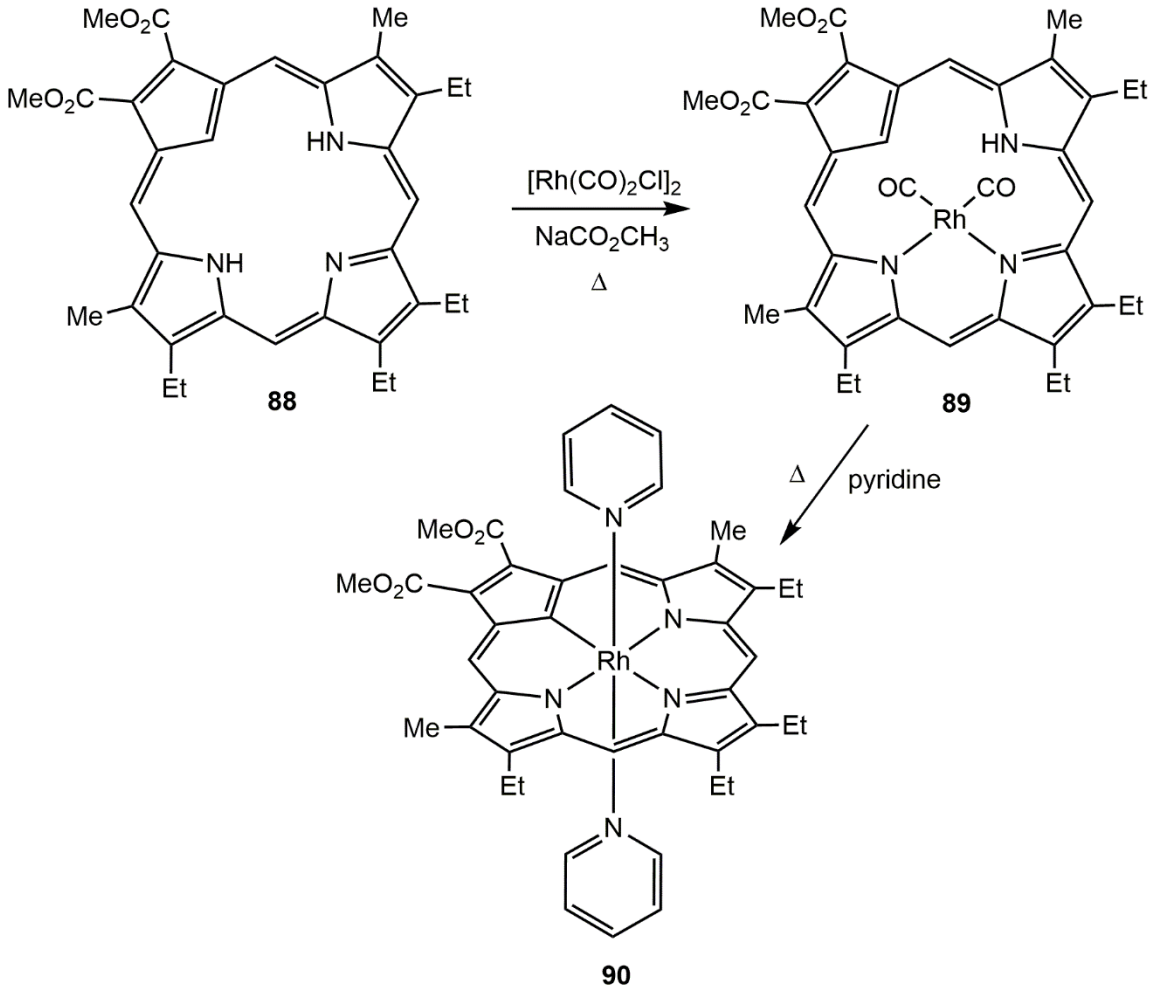

Scheme 30. Rhodium(I) and rhodium(III) complexes of carbaporphyrin diester **88**

Carbaporphyrin **88** is a symmetrical molecule, but this symmetry is lost upon introduction of the rhodium(I) metal center. This can be seen by comparison of the proton NMR spectra of the free base carbaporphyrin diester and the rhodium(I) complex. The free base (**88)** had two peaks for the *meso*-protons resonating at 9.51 and 10.24 ppm. The internal CH was observed at -6.27 ppm and the NH protons gave a broad 2H singlet at -3.12 ppm. The two external methyl groups

appeared as a 6H singlet at 3.51 ppm and the two methyl ester groups gave a 6H singlet at 4.27 ppm.[29] These results not only demonstrate that **88** possesses a plane of symmetry but also confirms the macrocyclic aromaticity for the system. When rhodium(I) is introduced into the center of the cavity, the loss of symmetry can be seen due to the duplication of many of the resonances. For instance, the *meso*-protons now produce four separate 1H singlets at 9.40, 9.44, 10.02 and 10.37 ppm. Similarly, the methyl groups afford two 3H singlets at 3.35 and 3.45 ppm, instead of the single peak observed in free base **88**. The internal CH and NH peaks for **89** were observed at -4.94 and -1.09 ppm, respectively (Figure 11). These values are shifted upfield compared to the equivalent peaks seen for free base **88**, but still indicate that **89** retains a high degree of macrocyclic aromaticity. The carbon-13 NMR spectrum for **89** further supported this lack of symmetry and gave four resonances for the *meso*-carbons at 92.4, 102.8, 107.5 and 116.7 ppm. The carbon atoms of the terminal carbonyl ligands were observed as two doublets at 177.0 and 178.7 ppm ($^{1}J_{\text{Rh-C}}$ = 69.9 and 67.7 Hz, respectively) (Figure 12). The splitting of these peaks is due to the presence of the NMR active nucleus rhodium-103 (I = ½). The IR spectrum for **89** showed two strong peaks at 2066 and 2011 cm^{-1}, which correspond to the two terminal carbonyl ligands of the rhodium(I) metal center. An additional absorption at 1698 cm^{-1} was observed due to the methyl ester carbonyl groups (Figure 13). The UV-Vis spectrum of **89** gave two relatively weak Soret-like bands at 357 and 490 nm with smaller Q bands at 569 and 611 nm (Figure 14).

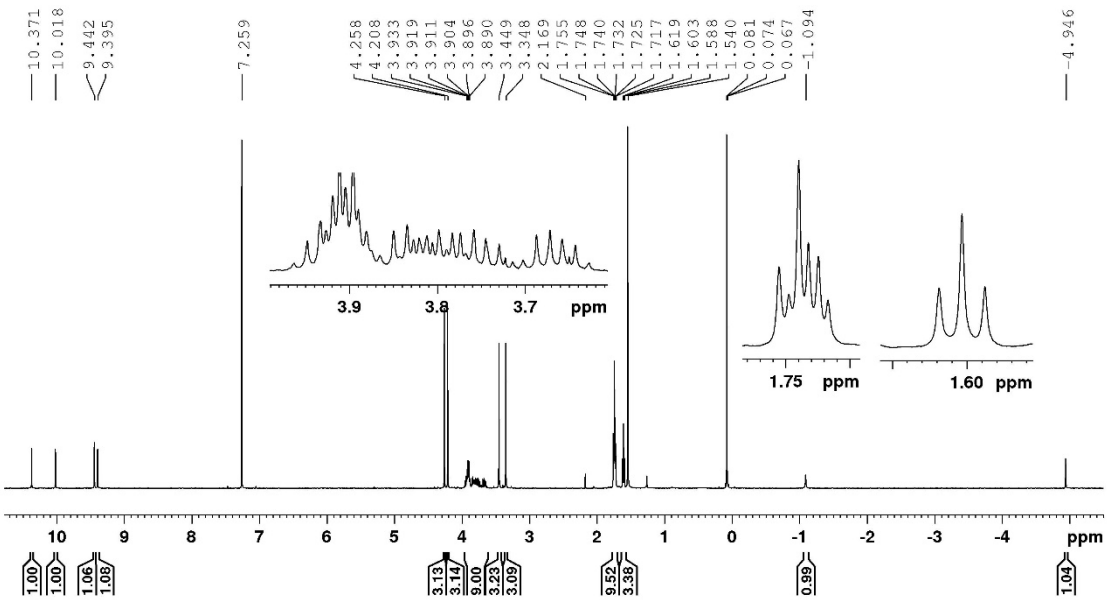

Figure 11. 500 MHz ^{1}H NMR spectrum of rhodium(I) carbaporphyrin diester **89** in $CDCl_3$

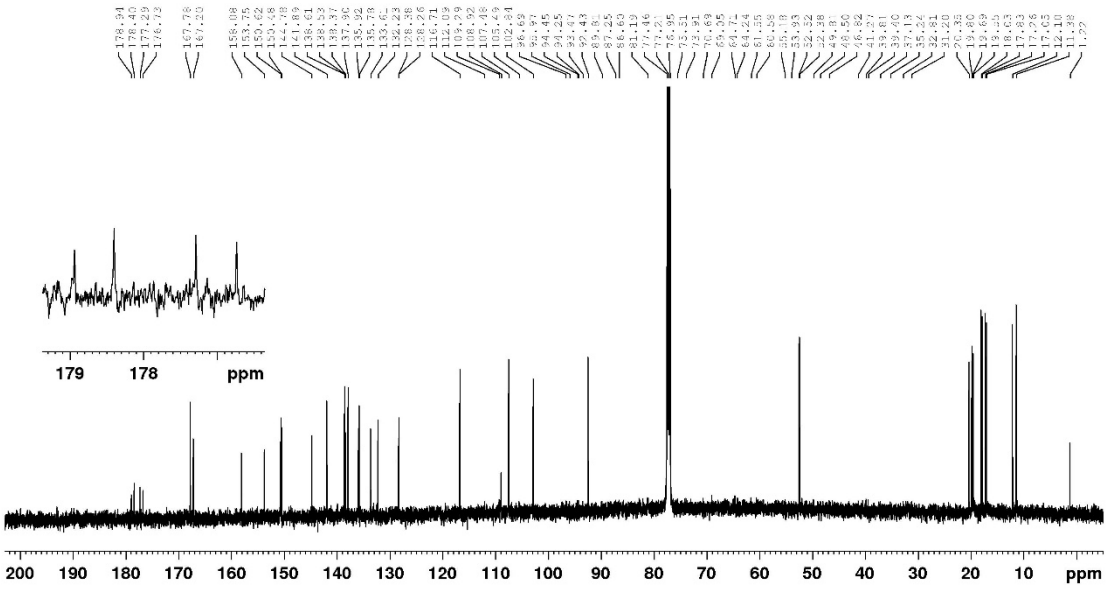

Figure 12. 125 MHz ^{13}C NMR spectrum of rhodium(I) carbaporphyrin diester **89** in $CDCl_3$

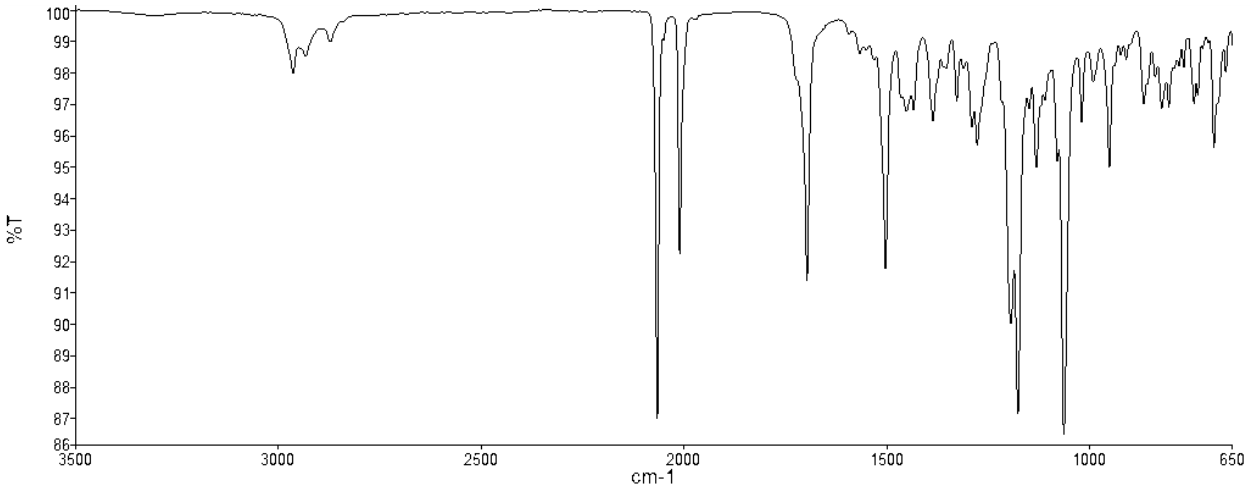

Figure 13. IR spectrum of rhodium(I) carbaporphyrin diester **89**

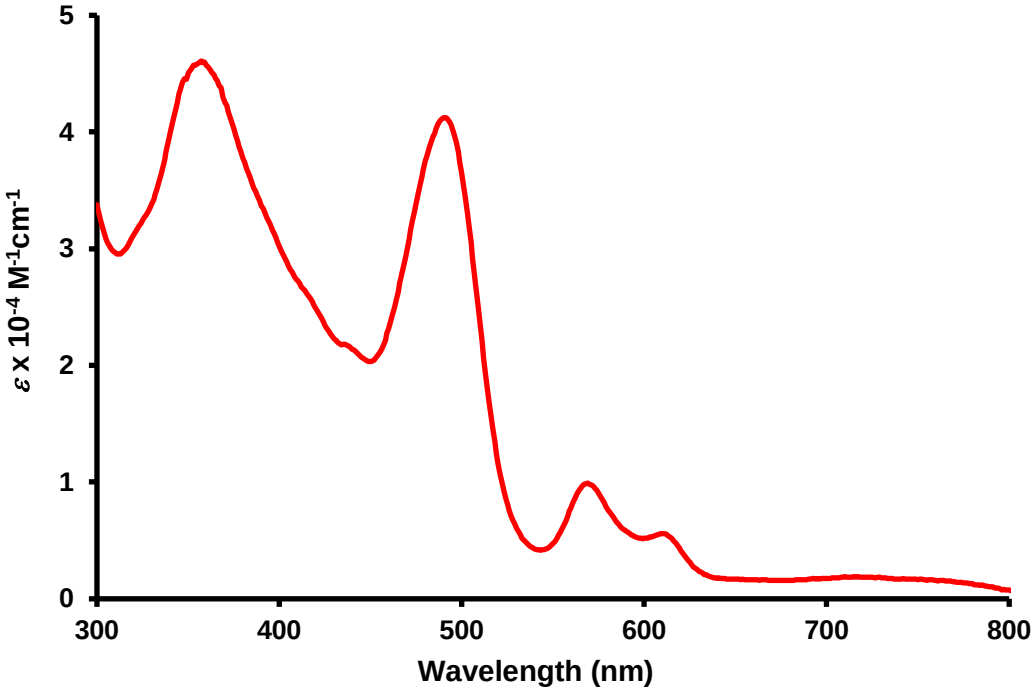

Figure 14. UV-Vis spectrum of rhodium(I) carbaporphyrin diester **89**

The structure for this complex was also confirmed by X-ray crystallography (Figure 15). The framework of bond lengths shows that this carbaporphyrin is aromatic with a delocalized π-electron pathway passing through the C21 atom. This is evidenced by the longer bond lengths of

1.462(3) Å and 1.471(3) Å for the C1-C2 and C3-C4 bonds, respectively. The bond lengths for C1-C21 and C4-C21 are found to be comparatively shorter, showing lengths of 1.407(3) Å and 1.401(3) Å, respectively, which demonstrates that the π-electron pathway is passing through these bonds. The bonds directly connected to the *meso*-carbons, C4-C5, C5-C6, C9-C10, C10-C11, C14-C15, C15-C16, C19-C20 and C20-C1, varied from 1.384-1.410 Å in reasonable agreement with expected aromatic bond lengths. The rhodium(I) metal center is coordinated to two adjacent pyrrolic nitrogen atoms in a typical square planar $L_2Rh(CO)_2$ coordination geometry, with the rhodium(I) atom displaced by 1.5623(6) Å from the 24-atom mean macrocylic plane of the porphyrinoid. Similarities in the crystal structure parameters were observed between **89** and rhodium(I) benzocarbaporphyrin **86**. The previously reported **86**[30] has its rhodium(I) metal center displaced by 1.5958(2) Å, which is only slightly larger than the displacement seen for **89**. Furthermore, the dihedral angle that the Rh1, N23, N24, C25, C26 plane makes with the mean macrocylic plane in **89** is 60.32(4)°, which is similar to the corresponding 61.78(2)° dihedral angle observed for **86**. The 0.188 Å rms distance the framework atoms lie from their mean plane indicate that **89** is relatively planar. However, the need to accommodate the two internal hydrogen atoms leads to some distortion, which is noted through the 13.8(1)°, 9.3(1)°, 13.0(1) °, and 12.0(1)° dihedral angles between the framework plane and the respective cyclopentadiene and three pyrrolic mean planes. The internal carbon and uncoordinated pyrrolic nitrogen protons were easily identifiable in the difference Fourier of the X-ray structure, allowing for a clear assignment of oxidation state to the rhodium metal center.

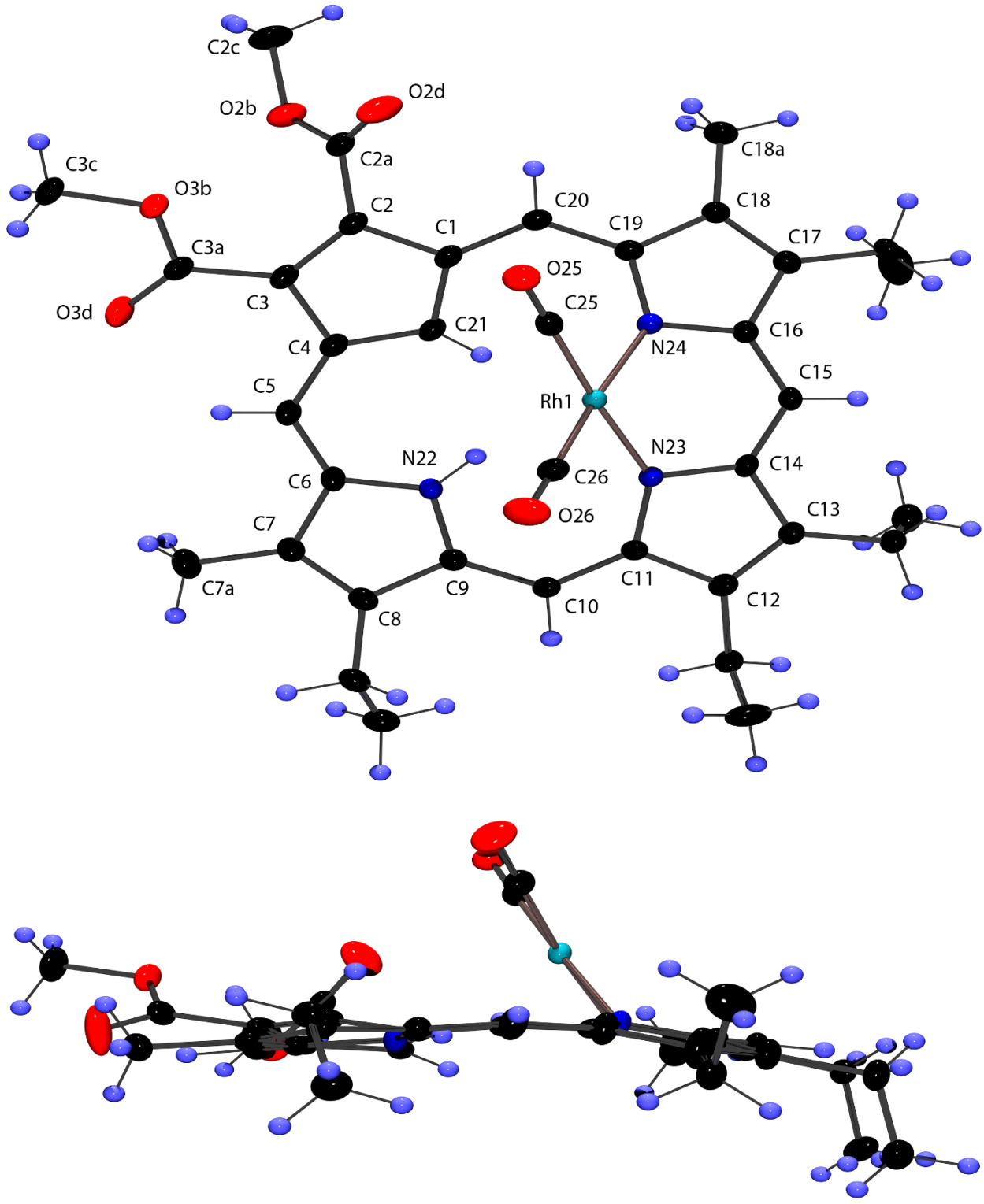

Figure 15. Color POV-Ray rendered ORTEP III drawing (50% probability level, hydrogen atoms rendered arbitrarily small for clarity) of rhodium(I) carbaporphyrin **89**

Rhodium(I) complex **89** was refluxed in pyridine for 30 minutes and gave a rhodium(III) complex **90** containing two axial pyridine ligands coordinating through the nitrogen to the metal center (Scheme 30). This compound was chromatographed on grade 3 neutral alumina eluting with toluene and a dark band was collected. Recrystallization from chloroform-hexanes gave the pure product **90** in 14% yield. The carbaporphyrin ring regains its symmetry in **90**. This rhodium(III) complex is rather insoluble in chloroform but gave reasonable NMR data in d_6-benzene, and the proton NMR spectrum confirmed the symmetry and aromatic character of the macrocycle. Two relatively downfield 2H singlets for the *meso*-protons were observed at 9.46 and 10.59 ppm. The α-protons of the two pyridine rings were shielded by the ring current of the carbaporphyrin and gave an upfield 4H multiplet at 2.33 ppm. The β- and γ-protons were less shielded by the ring current, but were still shifted upfield to 4.10 and 4.70 ppm, respectively (Figure 16). The large shielding effect the pyridine ligands are experiencing can be further appreciated through a comparison to pyridine, as this shows the α-proton resonances downfield near 9 ppm. The UV-Vis spectrum of **90** gave a strong Soret band at 481 nm and Q bands at 603 and 680 nm (Figure 17).

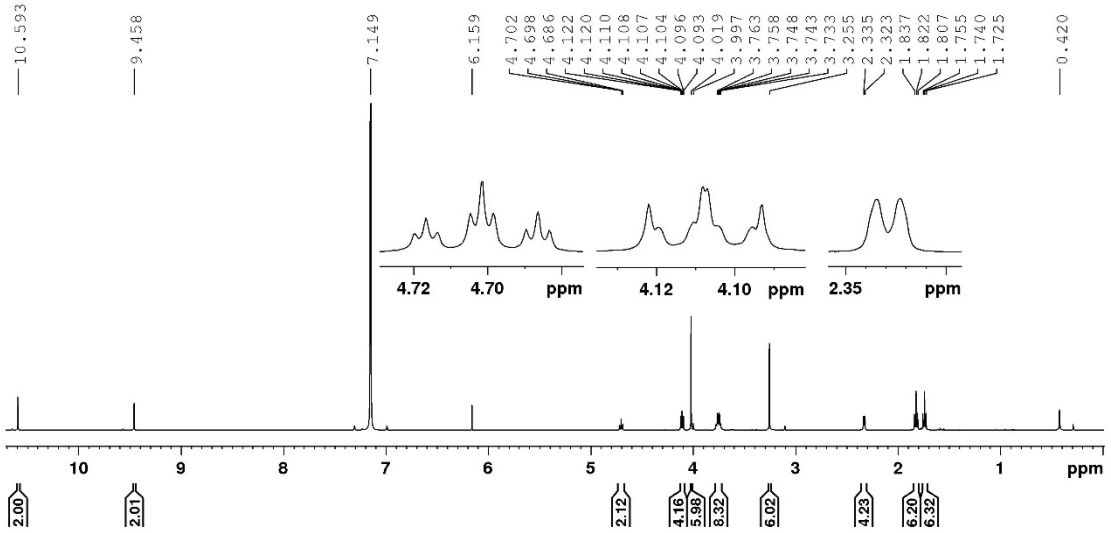

Figure 16. 500 MHz ^{1}H NMR spectrum of rhodium(III) carbaporphyrin diester **90** in d_6-benzene

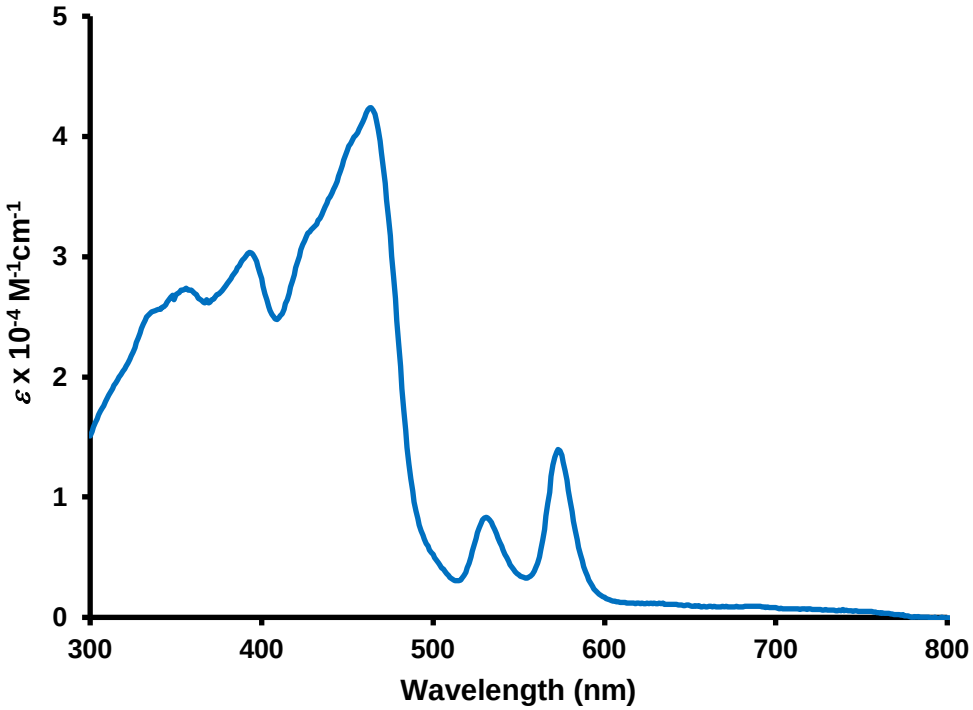

Figure 17. UV-Vis spectrum of rhodium(III) carbaporphyrin diester **90**

Crystals suitable for X-ray crystallography were obtained, and the structure of **90** was further confirmed (Figure 18). The X-ray structure demonstrated that the rhodium(III) atom is six-coordinate with the pyrrolic nitrogens and the cyclopentadienyl internal carbon atom occupying the equatorial plane, while the pyridine ligands took up each of the axial positions, resulting in a nearly idealized octahedral coordination environment. Unlike the rhodium atom seen in **89**, the rhodium(III) atom of **90** is only displaced 0.0810(5) Å from the 24-atom mean macrocyclic plane of the porphyrinoid. The 0.077 Å rms distance the framework atoms lie from their mean plane indicate the macrocycle is essentially planar, and this is further supported by the 5.0(1)°, 3.5(1)°, 5.8(1)°, and 2.7(1)° dihedral angles of the cyclopentadiene and three pyrrolic mean planes with the mean macrocyclic plane. The framework of bond lengths also show that this carbaporphyrin is aromatic with the delocalized π-electron pathway passing through the internal C21 atom. This is

supported by the longer bond lengths of 1.464(3) and 1.469(3) Å seen for the C1-C2 and C3-C4 bonds, respectively. Comparatively shorter are the more aromatic-like bond lengths of 1.416(3) and 1.413 Å that are observed for the C1-C21 and C4-C21 bonds, respectively. Furthermore, the bonds directly connected to the *meso*-carbons varied from 1.382-1.404 Å, which is expected for the bonding seen within an aromatic systems.

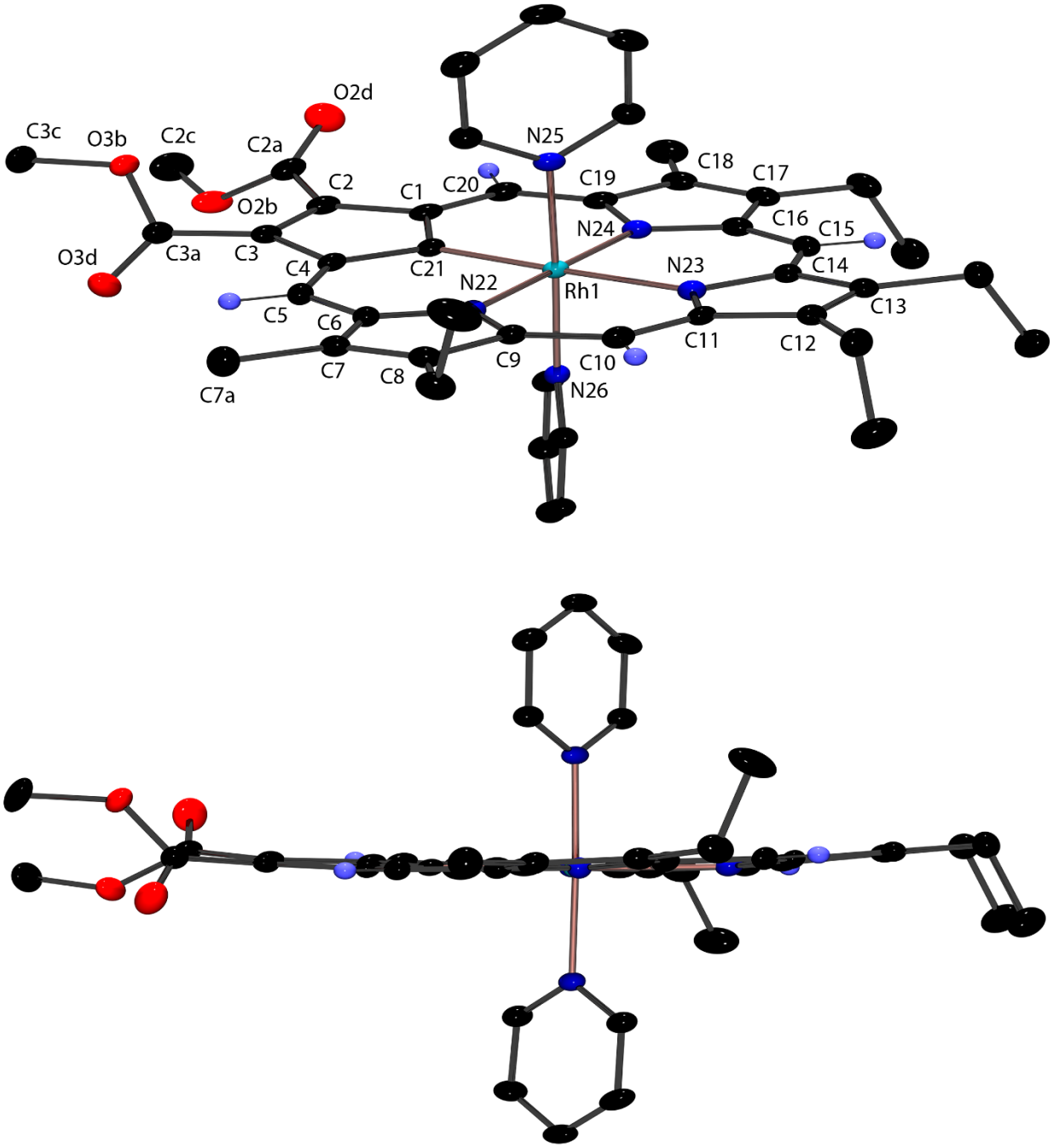

Figure 18. Color POV-Ray rendered ORTEP III drawing (50% probability level, hydrogen atoms rendered arbitrarily small or omitted for clarity) of rhodium(III) complex **90**

Naphtho[2.3-*b*]carbaporphyrin **87** was also reacted with $[Rh(CO)_2Cl]_2$ in refluxing dichloromethane to give the rhodium(I) complex **91** (Scheme 31). The crude material was purified using a silica gel column, eluting with 20:80 dichloromethane-hexanes, and a green band was collected. Subsequent recrystallization from chloroform-hexanes gave pure **91** in 72% yield.

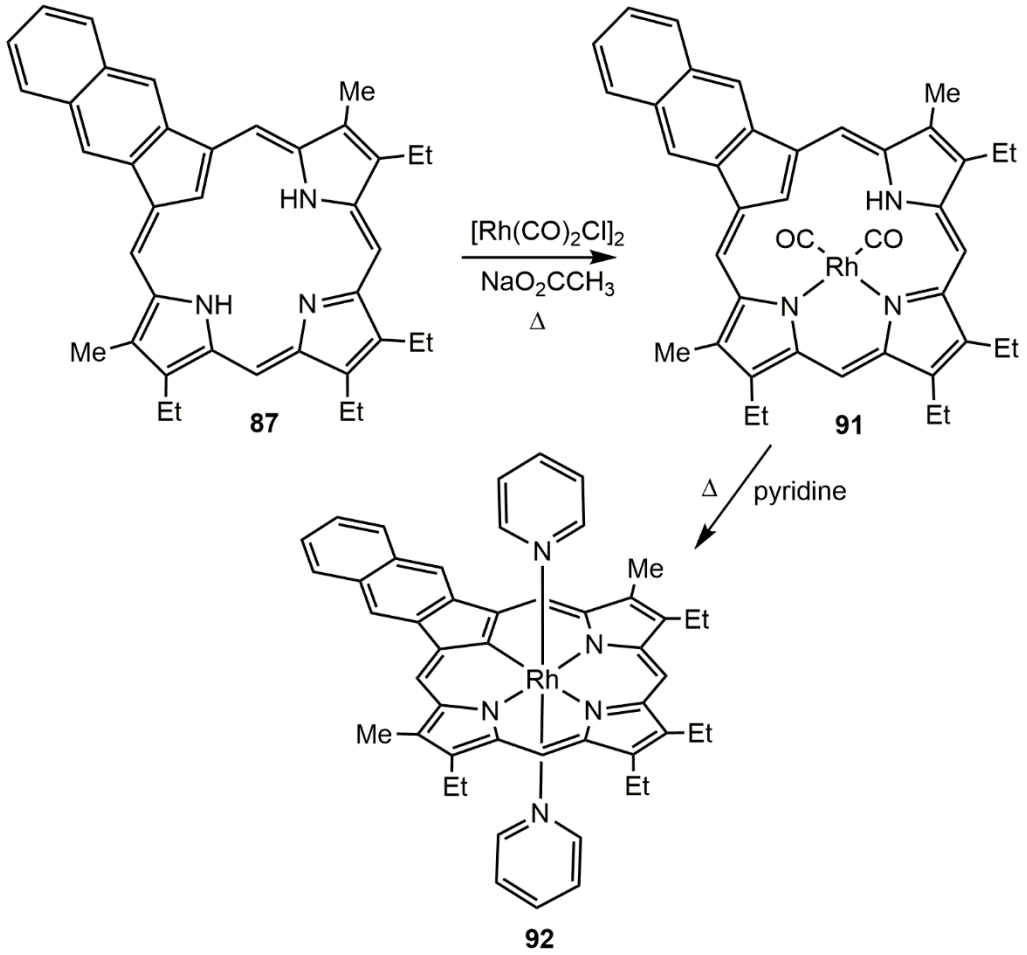

Scheme 31. Rhodium(I) and rhodium(III) complexes of naphthocarbaporphyrin **87**

Free base naphthocarbaporphyrin **87** is symmetrical and the proton NMR spectrum shows the *meso*-protons as two 2H singlets at 9.76 and 10.00 ppm, and the methyl substituents as a 6H singlet at 3.61 ppm. In addition, the internal CH for **87** gives a singlet at -6.55 ppm and the two NH protons afford a broad 2H singlet at -3.87 ppm.[108] Rhodium(I) complex **91**, in contrast, showed

four 1H singlets for the *meso*-protons between 9.78 and 10.34 ppm, demonstrating the loss of symmetry in this metalated derivative. The inner NH and CH resonances appeared at -2.48 and -5.19 ppm, respectively (Figure 19). When comparing the upfield and downfield shifts seen for free base **87** and rhodium(I) derivative **91**, it is evident that they exhibit comparable diamagnetic ring currents. The carbon-13 NMR spectrum further demonstrates the loss of symmetry seen in **95** (Figure 20). The four *meso*-protons were identified at 93.8, 97.5, 103.1 and 105.0 ppm, while the internal CH gave a peak at 123.0 ppm. The carbonyl resonances appear as two doublets at 177.6 and 178.4 ppm ($^{1}J_{\text{Rh-C}}$ = 69.0 and 67.1 Hz, respectively). Interestingly, the IR spectrum for **91** gave three peaks near 2000 cm^{-1} for carbonyl ligand stretching, rather than the two that might have been expected (Figure 21). The lower frequency bands appear to be a Fermi doublet that results from the carbonyl peak interacting with an aromatic overtone. The UV-vis spectrum for **91** was porphyrin-like and displayed a strong Soret band at 481 nm and several Q bands between 566 and 680 nm (Figure 22).

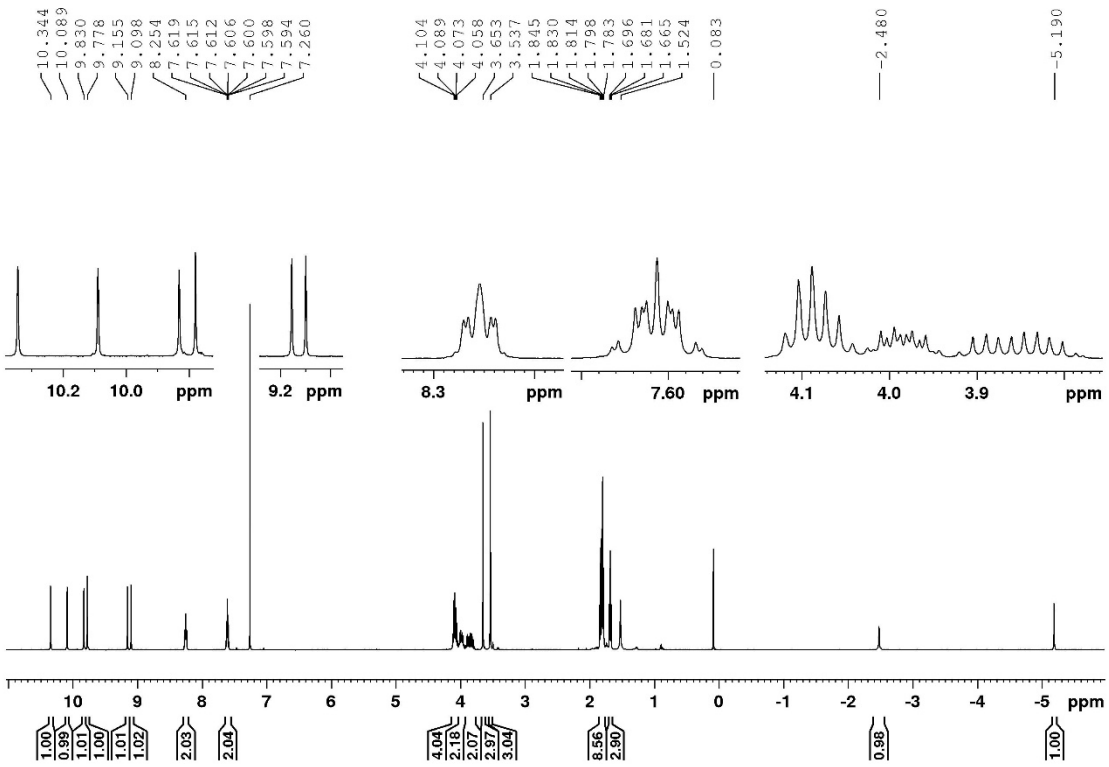

Figure 19. 500 MHz ^{1}H NMR spectrum of rhodium(I) naphthocarbaporphrin **91** in $CDCl_3$

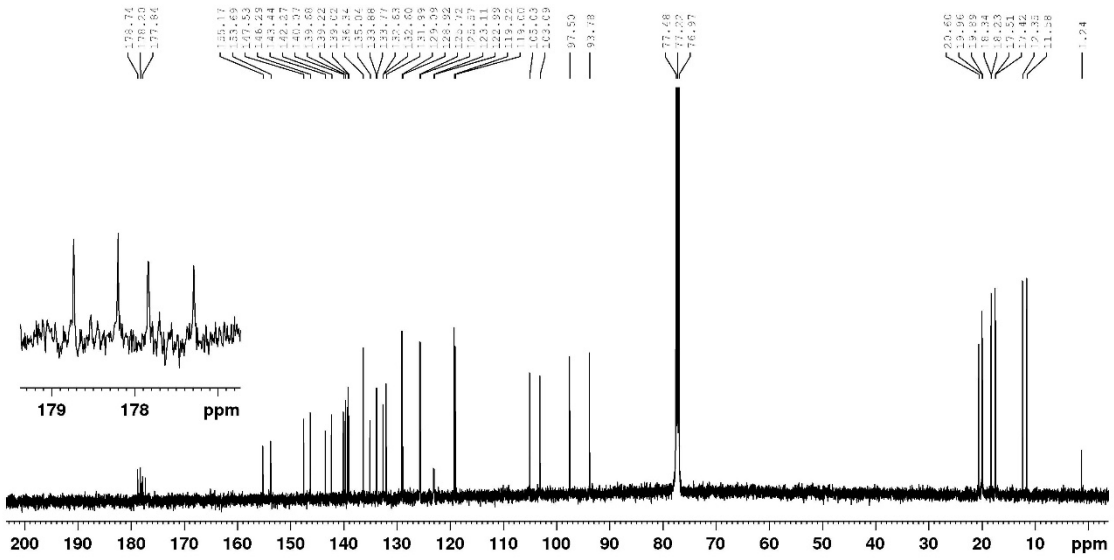

Figure 20. 125 MHz ^{13}C NMR spectrum of rhodium(I) naphthocarbaporphyrin **91** in $CDCl_3$

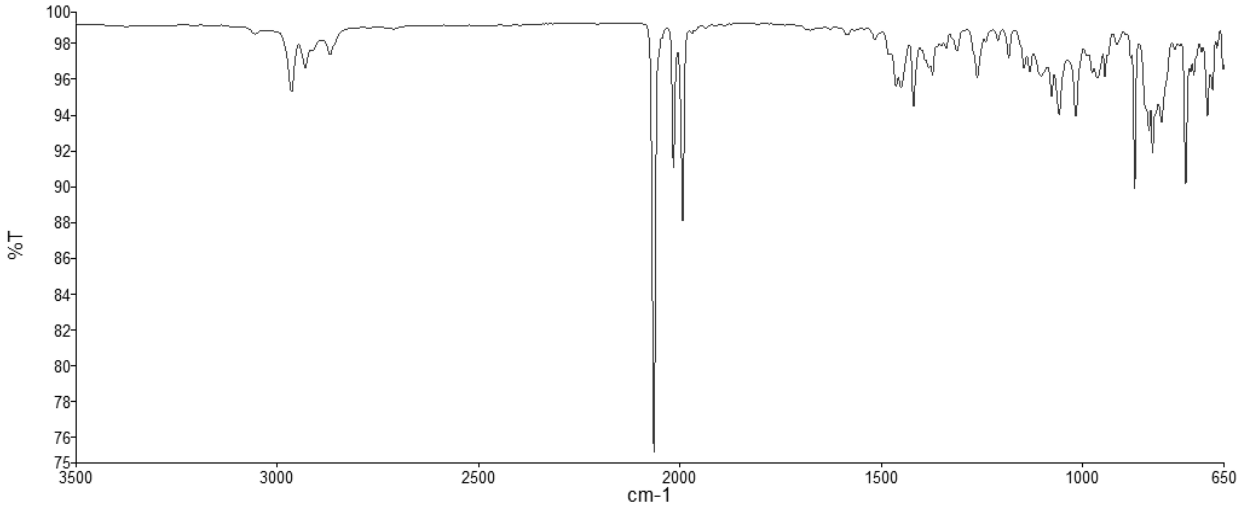

Figure 21. IR spectrum of rhodium(I) naphthocarbaporphyrin **91**

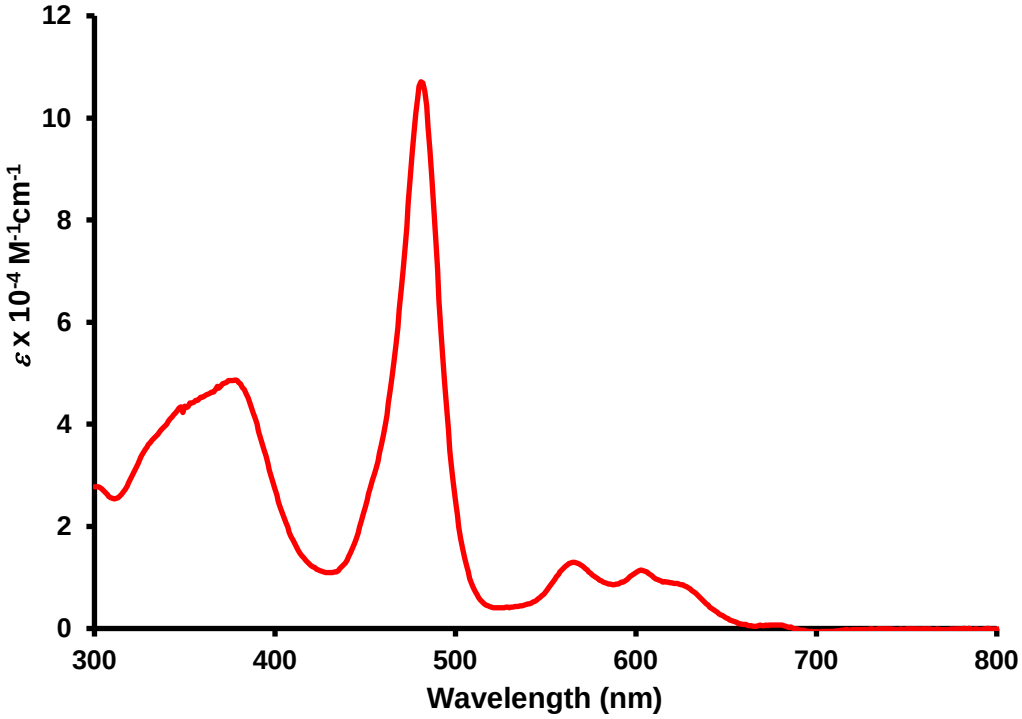

Figure 22. UV-Vis spectrum of rhodium(I) naphthocarbaporphyrin **91**

The structure of **91** was also confirmed by X-ray crystallography (Figure 23), which verified the presence of a dicarbonyl-rhodium(I) moiety coordinating to two adjacent nitrogens.

This coordination is analogous to the coordination seen in rhodium(I) benzocarbaporphyrin **86** and rhodium(I) carbaporphyrin diester **89**. Square planar $L_2Rh(CO)_2$ geometry is observed, with the rhodium(I) atom displaced by 1.5544(4) Å from the 24-atom mean macrocyclic plane. The dihedral angle the Rh, N23, N24, C25, C26 plane makes with the mean macrocyclic plane is 59.70(5)° and similar to the values seen in related rhodium(I) carbaporphyrin systems, as are the Rh-N and Rh-$C_{(CO)}$ distances. The 0.210 Å rms distance the framework atoms lie from their mean plane indicate reasonable planarity. However, there is some distortion observed through the 14.03(3)°, 12.85(7)°, 12.34(7)°, and 13.45(7)° dihedral angles of the benz[*f*]indene and three pyrrolic mean planes, respectively. This is likely due to accomodation of the two internal hydrogen atoms. Overall, the framework bond distances are consistent with an aromatic system containing a delocalized π-bonding model where the bonds directly connected to the *meso*-carbons fall within a typical aromatic bond length range of 1.389-1.409 Å. The bond lengths for C1-C2 and C3-C4 are relatively long, 1.476 and 1.479 Å, respectively, indicating that the delocalized π-system runs through the internal C21.

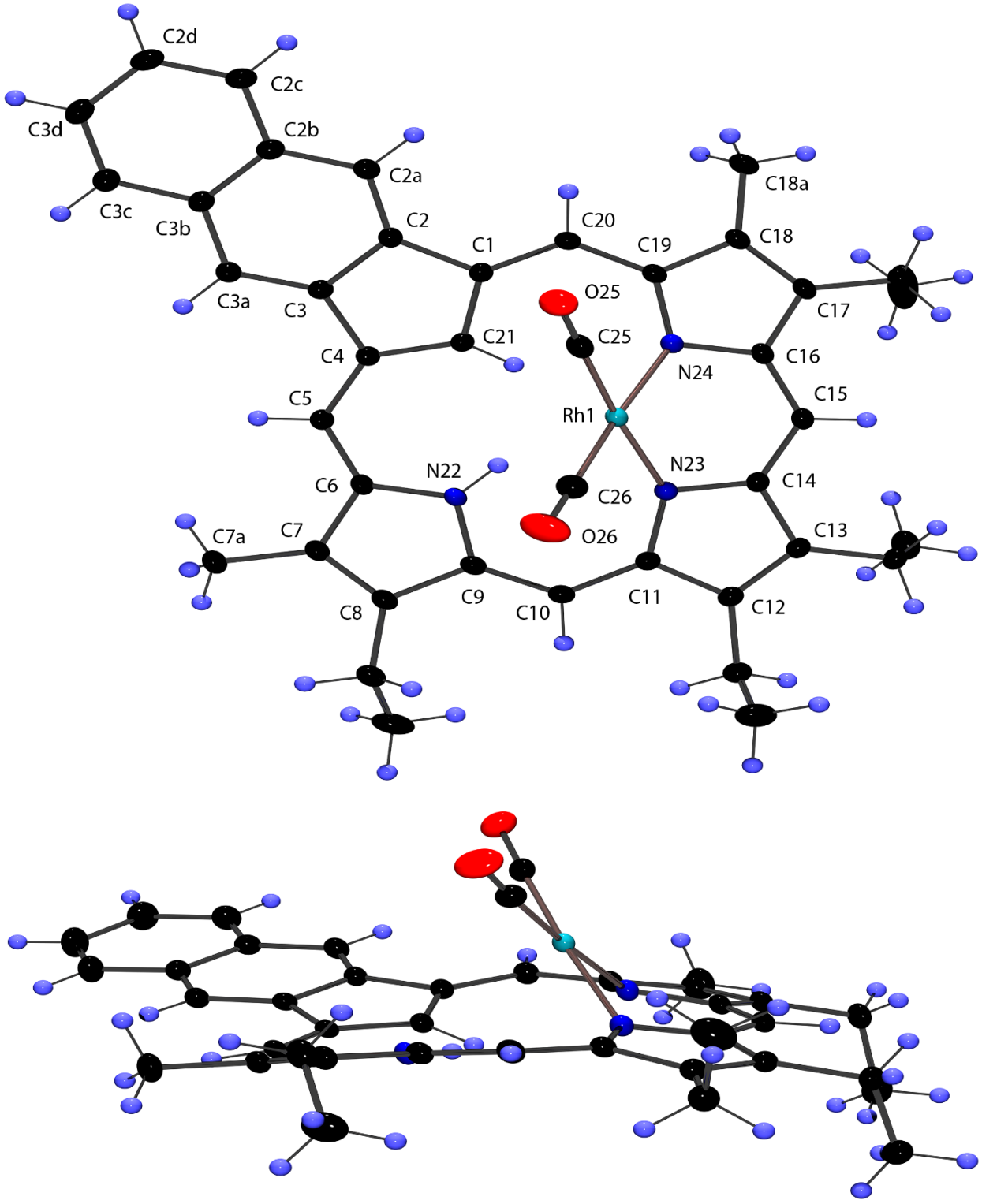

Figure 23. Color POV-Ray rendered ORTEP III drawing (50% probability level, hydrogen atoms rendered arbitrarily small for clarity) of rhodium(I) naphthocarbaporphyrin **91**

When a solution of **91** in pyridine was refluxed for one hour, rhodium(III) complex **92** was formed (Scheme 31). This compound also incorporated two axial pyridine ligands coordinating to the rhodium metal center. Purification through chromatography on alumina with 50:50 toluene-hexanes gave a light brown band that was collected and then further purified through recrystallization from chloroform-hexanes to give pure **92** in 21% yield. Like the rhodium(III) complex **90**, this compound was also insoluble in chloroform and was therefore dissolved in d_6-benzene to collect NMR spectra (Figure 24). The symmetry that was lost in the rhodium(I) complex is regained in the rhodium(III) complex, showing similarity to the free base naphthocarbaporphyrin **87**. This symmetry is supported by the presence of two 2H singlets for the *meso*-protons resonating at 10.07 and 10.56 ppm, and the external methyl groups giving a 6H singlet at 3.59 ppm. The α-, β- and γ-protons of the axial pyridine ligands are observed as a 4H doublet at 1.44 ppm, a 4H triplet at 3.92 ppm and a 2H triplet at 4.58 ppm, respectively. The large upfield shifts that these pyridine resonances demonstrate the high degree of aromatic character present in **92**. Further evidence for the aromaticity and symmetry of this compound is evident in the carbon-13 NMR spectrum (Figure 25). The *meso*-protons were observed at 94.7 and 102.8 ppm and the α-, β- and γ- pyridine resonances at 148.1, 120.6 and 133.1 ppm, respectively. The UV-Vis spectrum of **92** showed a strong Soret band at 447 nm, followed by several Q bands between 530 and 606 nm (Figure 26). The X-ray structure for this compound was not obtained, as suitable crystals for analysis could not be produced.

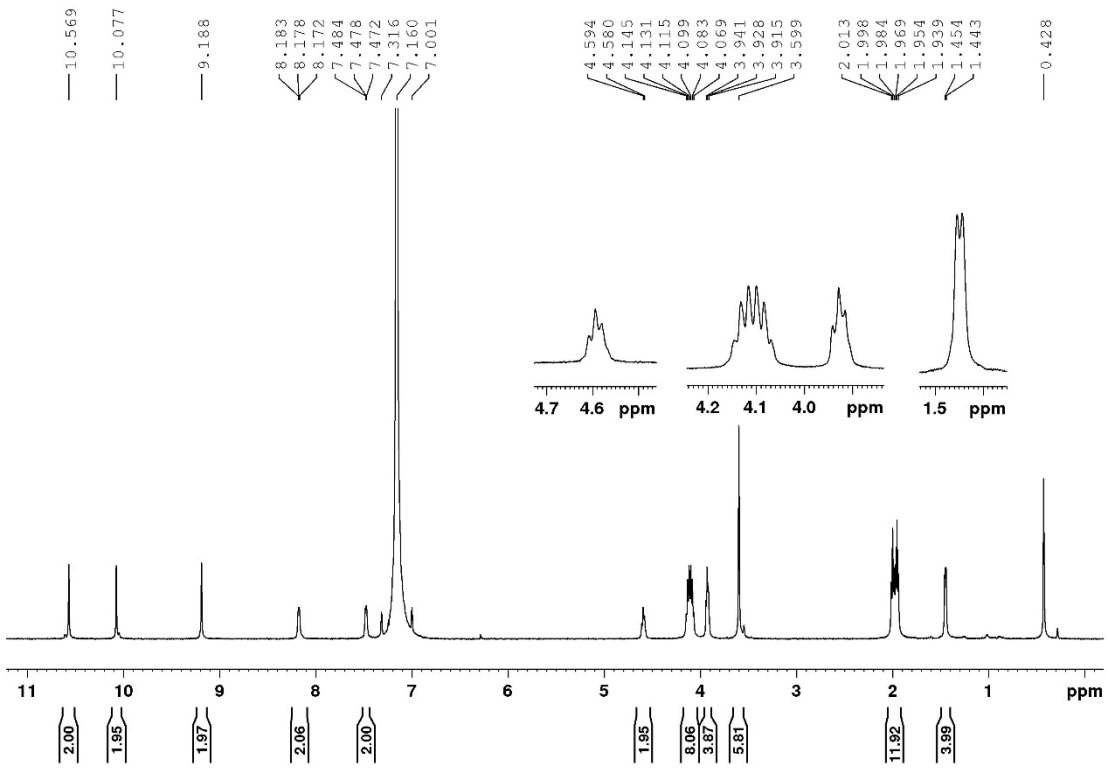

Figure 24. 500 MHz ^{1}H NMR spectrum of rhodium(III) naphthocarbaporphyrin **92** in d_6-benzene

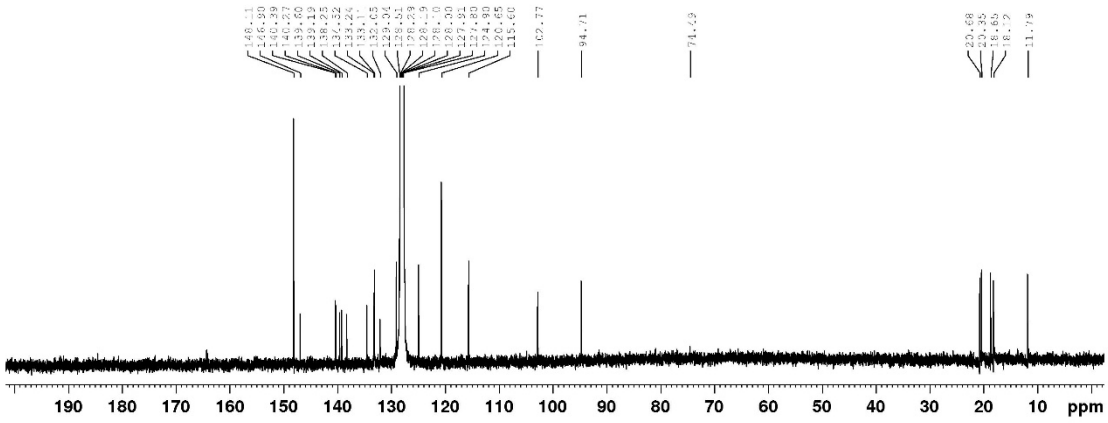

Figure 25. 125 MHz ^{13}C NMR spectrum of rhodium(III) naphthocarbaporphyrin **92** in d_6-benzene

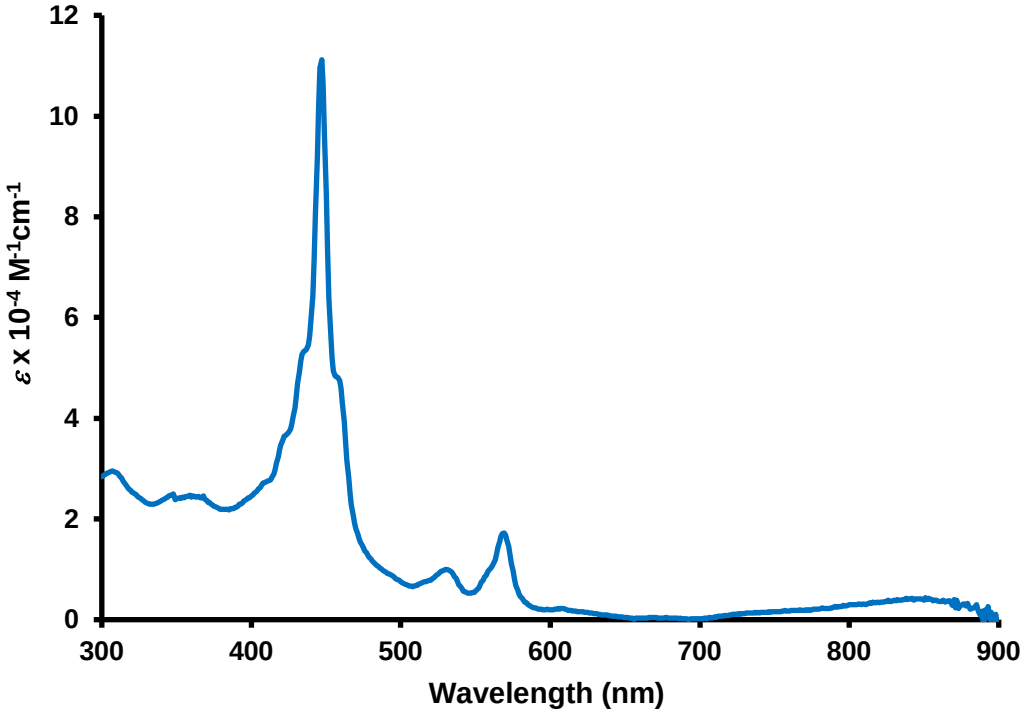

Figure 26. UV-Vis spectrum of rhodium(III) naphthocarbaporphyrin **92**

Benzocarbaporphyrin **3** was shown to form stable rhodium(I) and rhodium(III) derivatives[30], while internally methylated benzocarbaporphyrins **70** and **76** gave rise to unexpected alkyl group migrations when metalated with palladium(II) acetate.[111,101] The ability of the internally alkylated benzocarbaporphyrins to form palladium(II) complexes, as well as the observed methyl group migrations within these complexes, make systems such as **70**, **75**, and **76** important metalation targets. Internally methylated compounds such as these have the potential to undergo C-H activation upon the introduction of a rhodium(III) metal center. However, in the 23-methylcarbaporphyrin **76** the internal alkyl residue on N23 may block coordination to a rhodium(I) metal cation and it was questionable whether the formation of a rhodium(I) derivative of **76** could be possible.

In order to investigate the effects of internal alkyl substituents, 21- and 22-methylbenzocarbaporphyrins **75** and **70**, respectively, were reacted with $[Rh(CO)_2Cl]_2$ in refluxing dichloromethane overnight.[111] 22-Methylcarbaporphyrin **70** reacted under these conditions to give the corresponding rhodium(I) complex **93** (Scheme 32). The rhodium complex was purified through an alumina column, eluting with 50% dichloromethane-hexanes, and collected as a brown band. The fractions were recrystallized from chloroform-hexanes to give the pure rhodium(I) 22-methylbenzocarbaporphyrin complex **93** in 50% yield.

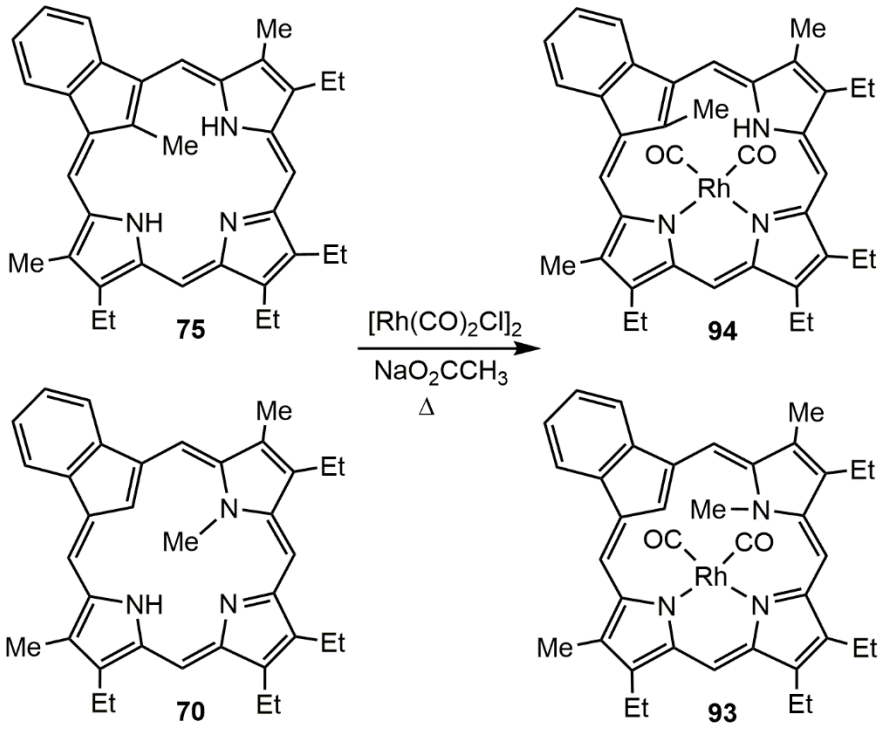

Scheme 32. Formation of 21- and 22-methyl rhodium(I) derivatives **94** and **93**

The rhodium(I) complex retains the strong aromatic character seen in **70** and the proton NMR spectrum shows the *meso*-protons downfield as four 1H singlets between 9.64 and 10.16 ppm. Furthermore, the external methyl substituents were significantly deshielded and were observed as two 3H singlets at 3.36 and 3.69 ppm, while the internal methyl group was strongly

shielded and identified as a 3H singlet at an upfield value of -4.50 ppm. The internal C-H was also relatively upfield at -4.68 ppm, resonating as a 1H singlet (Figure 27). The carbon-13 NMR spectrum showed the carbonyl resonances as doublets at 178.8 and 179.4 ppm ($^1J_{Rh-C}$ = ca. 69 Hz) due to coupling with rhodium-103 (I = ½). The *meso*-carbons gave rise to four peaks at 97.1, 102.5, 104.6 and 106.6 ppm, while the internal indene carbon appeared at 121.2 ppm (Figure 28). The presence of the terminal CO ligands is also evident from the IR spectrum, which showed two strong peaks at 1985 and 2057 cm^{-1} (Figure 29). The UV-vis spectrum for **93** displayed a Soret-like band at 481 nm and smaller absorptions at 561 and 637 nm (Figure 30).

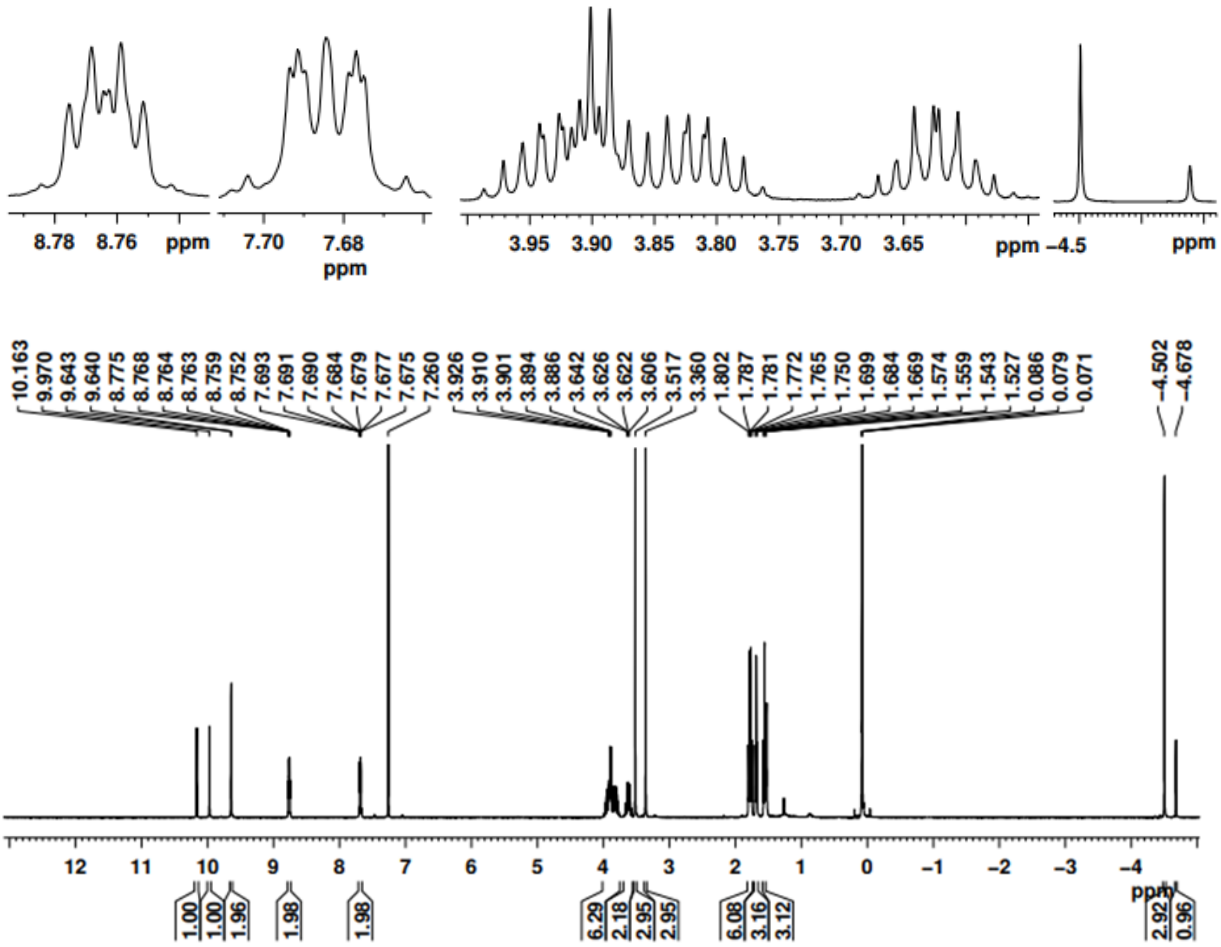

Figure 27. 500 MHz ^{1}H NMR spectrum of rhodium(I) 22-methylbenzocarbaporphyrin **93** in $CDCl_3$

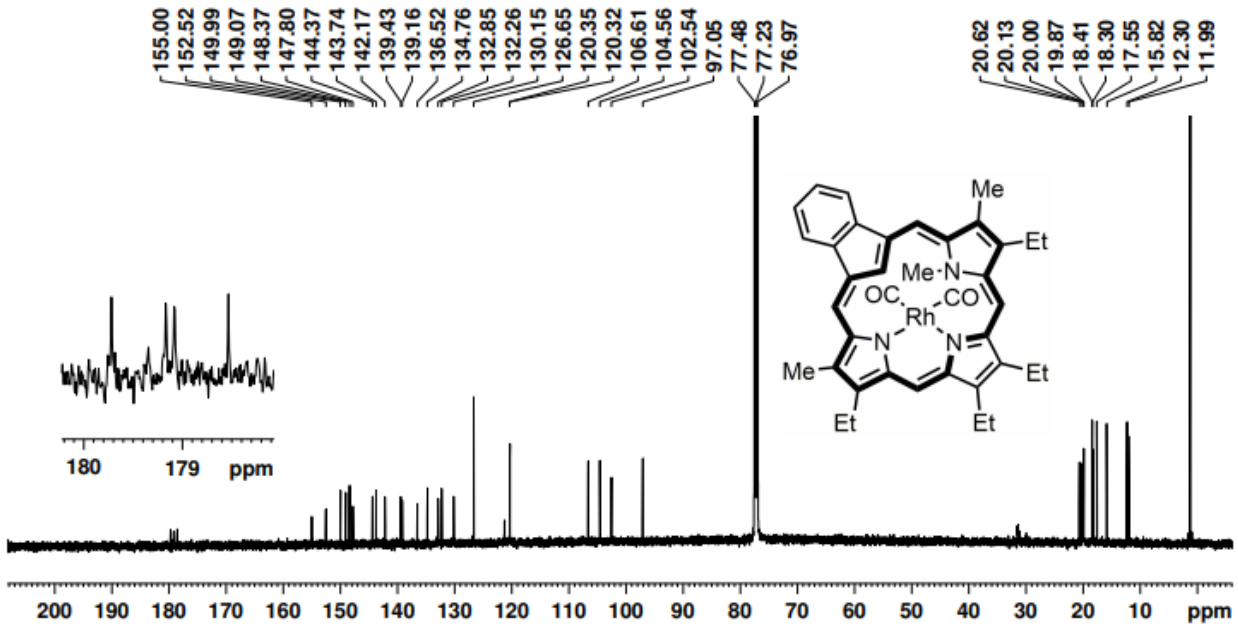

Figure 28. 125 MHz ^{13}C NMR spectrum of rhodium(I) 22-methylbenzocarbaporphyrin **93** in $CDCl_3$

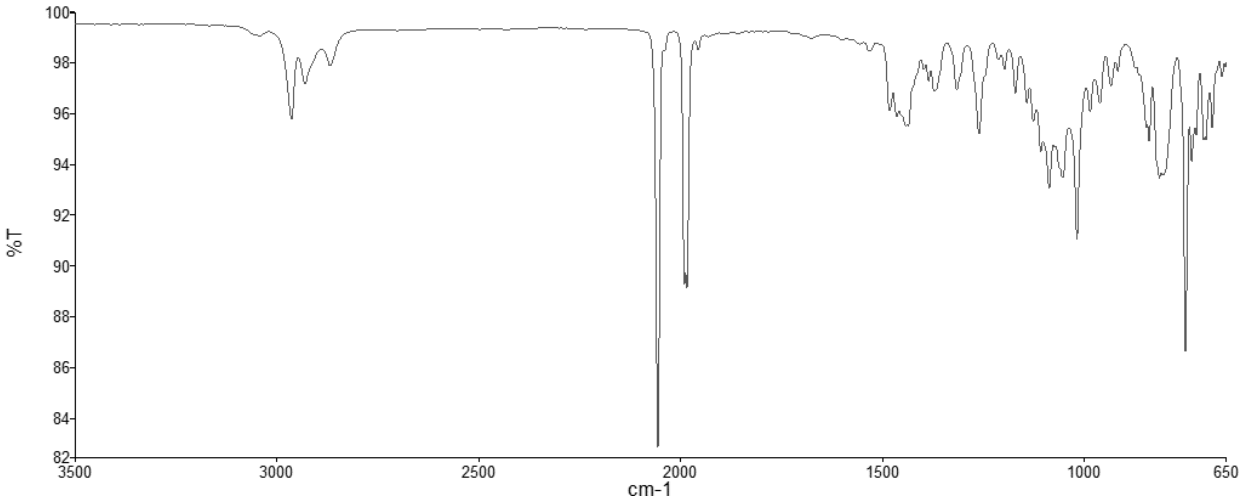

Figure 29. IR spectrum of rhodium(I) 22-methylbenzocarbaporphyrin **93**

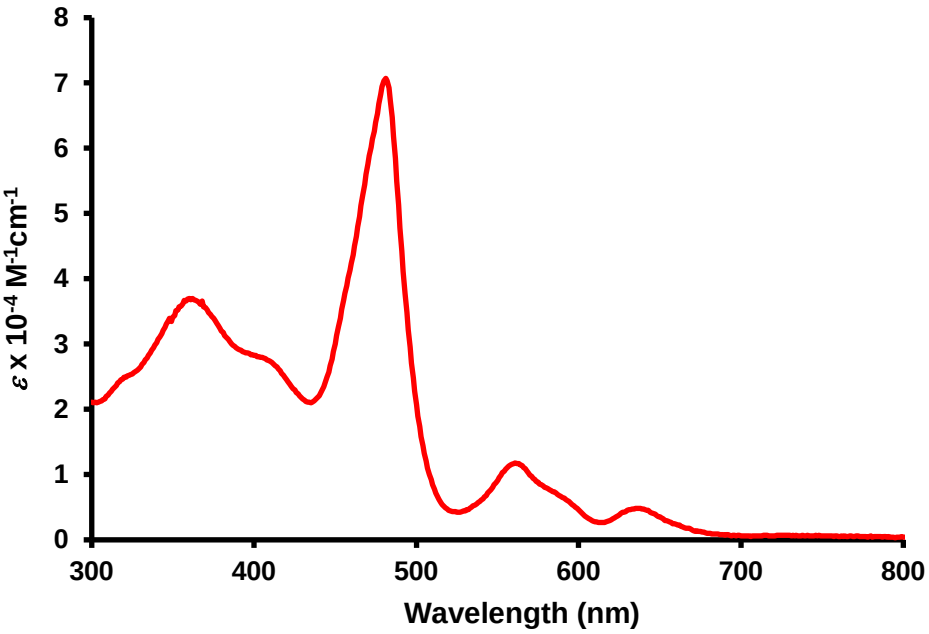

Figure 30. UV-Vis spectrum of rhodium(I) 22-methylbenzocarbaporphyrin **93**

21-Methylcarbaporphyrin **75** reacted similarly to give rhodium(I) complex **94** (Scheme 32). The crude product was purified by column chromatography on neutral alumina eluting with 50% dichloromethane-hexanes, and a green band was collected. Recrystallization from chloroform-hexanes gave the pure product **94** in 67% yield. The loss of symmetry when **75** was converted to the rhodium(I) derivative is evident in the proton NMR spectrum of **94**, where the *meso*-protons give rise to four 1H singlets at 9.52, 9.56, 9.69 and 9.82 ppm, and the internal methyl and NH protons appear upfield at -5.66 and -2.83 ppm, respectively (Figure 31). Alongside the display of asymmetry, the large downfield and upfield shifts in the spectrum provide evidence that the strong aromatic character of the macrocycle is retained. The carbon-13 NMR spectrum shows two doublets for the terminal CO ligands between 177 and 179 ppm, while the *meso*-carbons appear at 93.0, 99.9, 103.5 and 108.6 ppm (Figure 32). The IR spectrum of **94** also gave two strong peaks for the carbonyl ligands at 1996 and 2063 cm^{-1} (Figure 33). The UV-Vis spectrum for **94**

showed similarities to the spectrum of **93**, with a Soret-like band at 476 nm and weaker absorptions at 562, 604 and 627 nm (Figure 34). Attempts to form rhodium(III) derivatives from **94** and **93** in refluxing pyridine were unsuccessful.

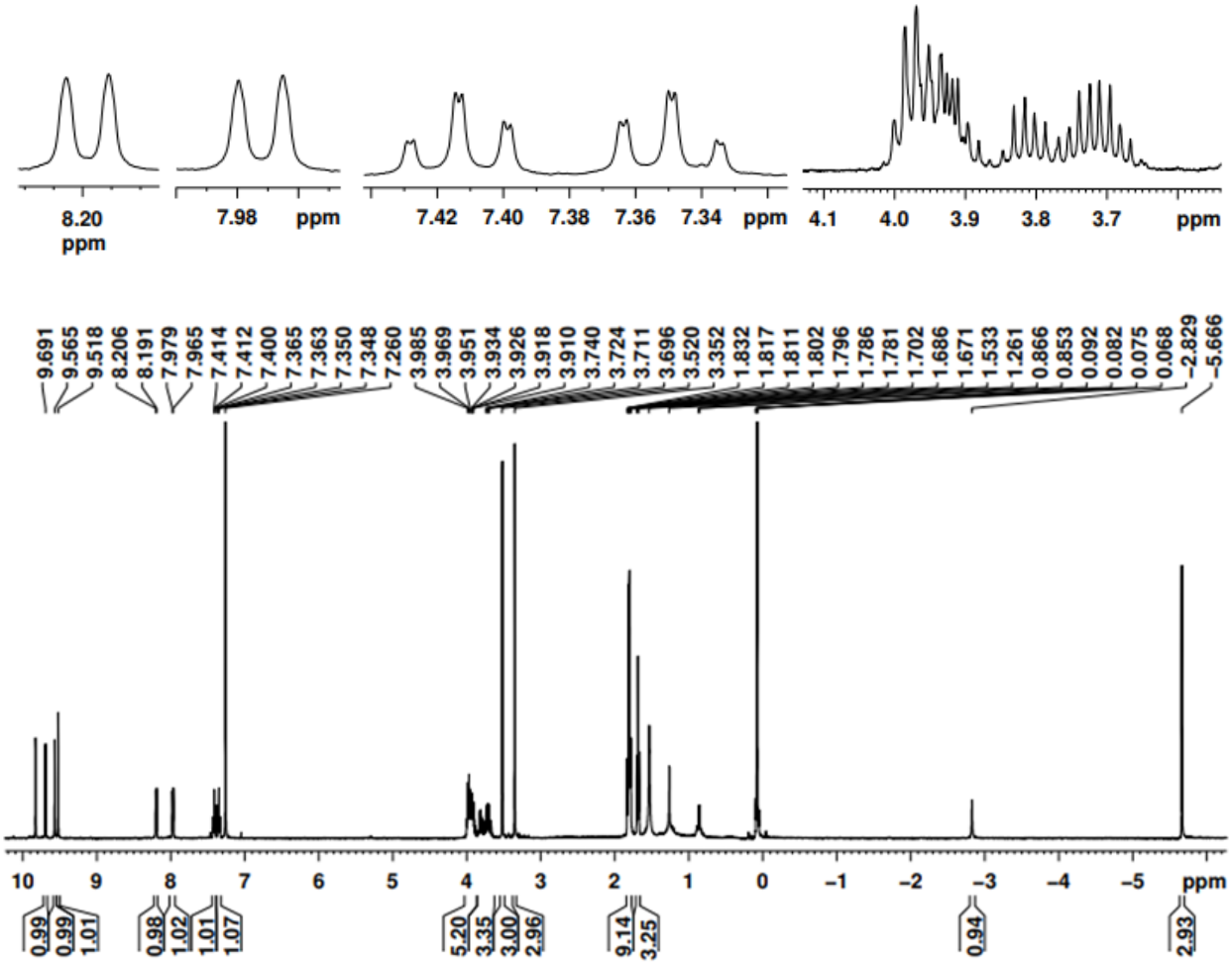

Figure 31. 500 MHz ^{1}H NMR spectrum of rhodium(I) 21-methylbenzocarbaporphyrin **94** in $CDCl_3$

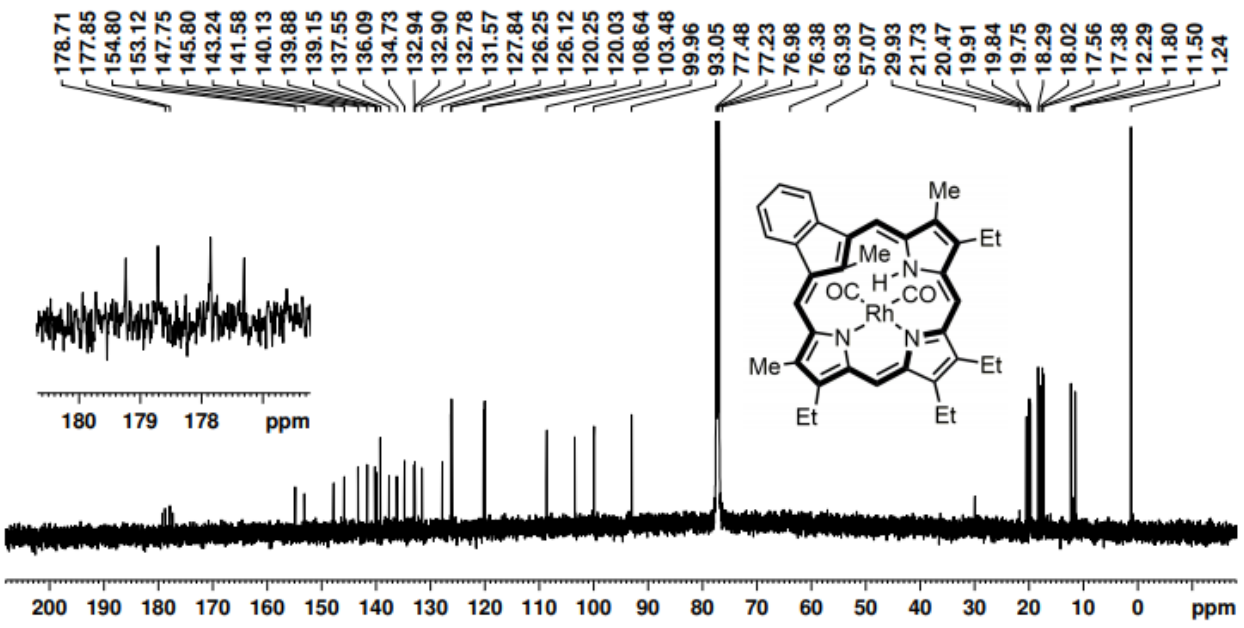

Figure 32. 125 MHz ^{13}C NMR spectrum of rhodium(I) 21-methylbenzocarbaporphyrin **94** in $CDCl_3$

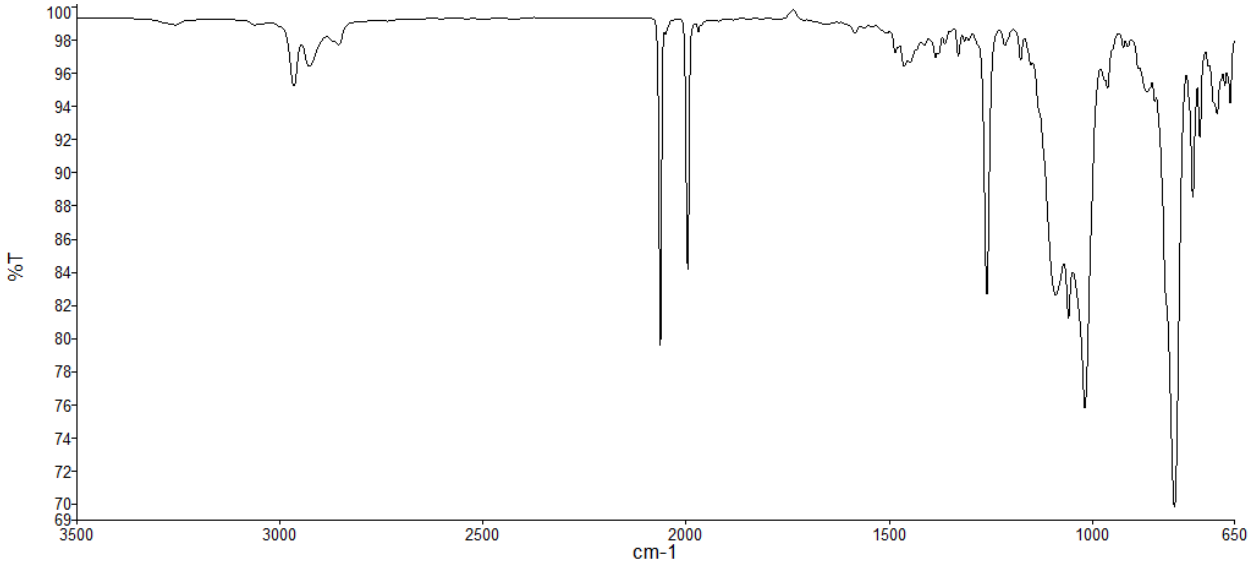

Figure 33. IR spectrum of rhodium(I) 21-methylbenzocarbaporphyrin **94**

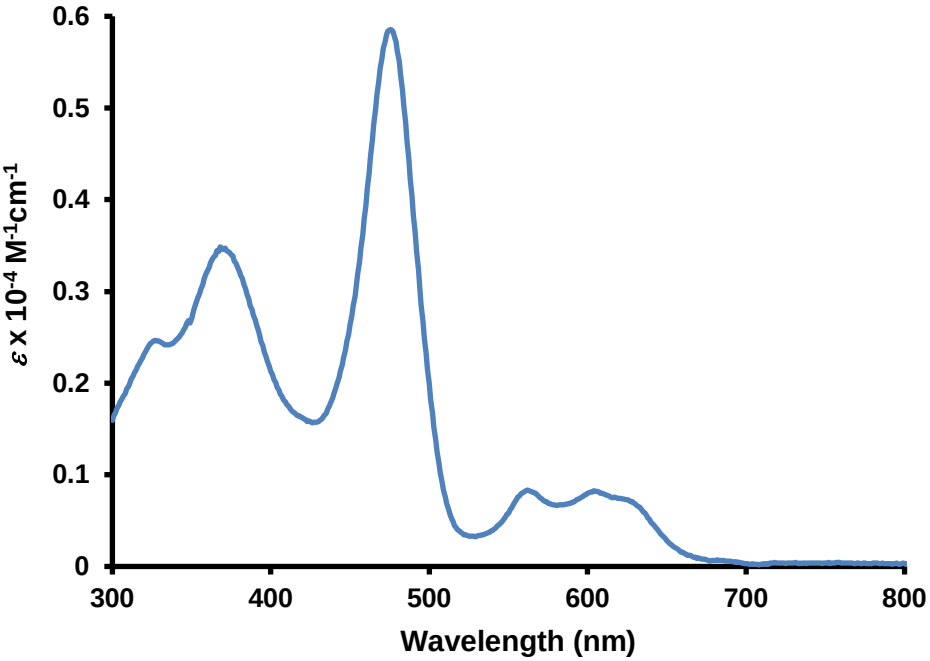

Figure 34. UV-Vis spectrum of rhodium(I) 21-methylbenzocarbaporphyrin **94**

When 23-methylbenzocarbaporphyrin **76** was reacted under the same conditions with $[Rh(CO)_2Cl]_2$, a rhodium(I) complex of the type described above was not formed.[111] This was due to the placement of the internal methyl substituent in a site that prevented coordination to two adjacent nitrogens. Nevertheless, when **76** was reacted with $[Rh(CO)_2Cl]_2$ in refluxing toluene, a bridged rhodium(III) complex **95** was generated in 31% yield (Scheme 33). The crude compound was chromatographed twice on silica gel, eluting with dichloromethane, followed by recrystallization from chloroform-hexanes to give the pure product. The formation of **95** from **76** was unexpected but may involve a similar rearrangement to the one observed for palladium(II) complex **84**, where the methyl group seemingly somersaults over the rhodium center. Related bridged rhodium(III) complexes were previously obtained by the ring contraction of benziporphyrin complexes.[68]

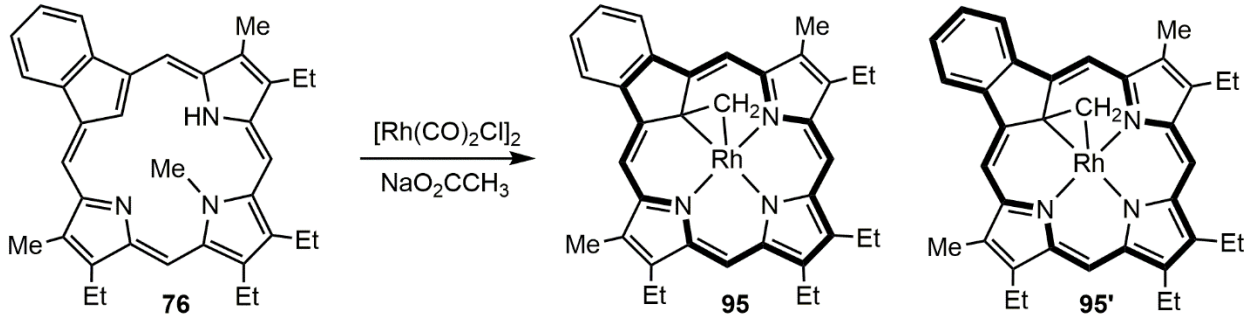

Scheme 33. Formation of rhodium derivative **95** of 23-methylcarbaporphyrin **76**

The proton NMR spectrum of **95** shows a plane of symmetry, with the *meso*-proton resonances appearing as two 2H singlets at 9.51 and 10.03 ppm (Figure 35). The benzo-protons are observed as two downfield multiplets at 8.16-8.20 and 9.37-9.41 ppm. The external methyl substituents were also shifted downfield and resonated as a 6H singlet at 3.34 ppm. The bridging CH_2 unit appears as a weakly split 2H doublet at -3.22 ppm ($^2J_{RhH}$ = 1.0 Hz) due to coupling with rhodium-103 (I = ½). The observed chemical shifts are characteristic of a strong diatropic ring current, showing that the aromaticity of the rhodium(III) bridged complex is retained. An 18π-electron pathway is emphasized in structure **95**, but a 22π-electron circuit (see **95'** in Scheme 33) may also potentially contribute to this structure. This consideration helps to explain the pronounced downfield shifts of the benzo-protons observed in the proton-NMR spectrum. The carbon-13 NMR spectrum further demonstrates the symmetry of **95**, and the *meso*-carbons gave rise to two peaks at 103.7 and 104.2 ppm (Figure 36). The internal methylene and 21-carbon peaks gave doublets at 46.3 ppm ($^1J_{RhC}$ = 21.4 Hz) and 54.5 ppm ($^1J_{RhC}$ = 14.2 Hz), respectively. The UV-Vis spectrum of **95** (Figure 37) is very different from rhodium(I) complexes **94** and **93**, showing a peak at 333 nm, followed by a series of broad absorptions ending with a moderately strong band centered on 682 nm. This spectrum was also dissimilar from the rhodium(I) and rhodium(III) derivatives of both naphthocarbaporphyrin **87** and carbaporphyrin diester **88**. This is

most likely due to the 18 or 22π-electron pathway being relocated through the periphery of the indene unit while bypassing C21.

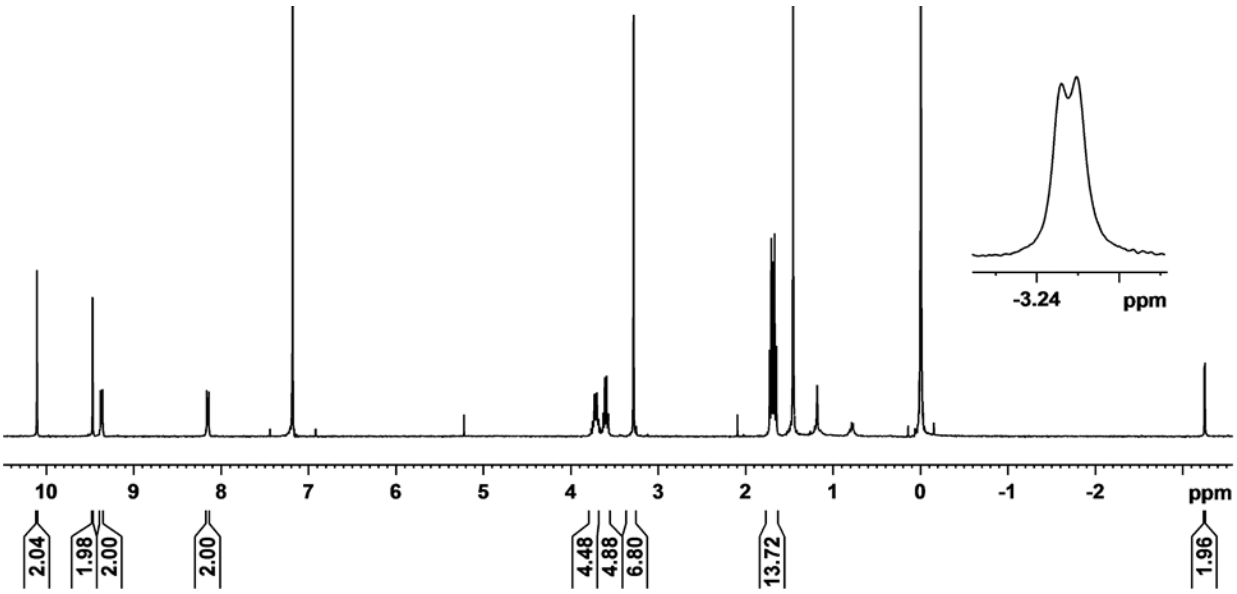

Figure 35. 400 MHz ^{1}H NMR spectrum of bridged rhodium(III) complex **95** in $CDCl_3$

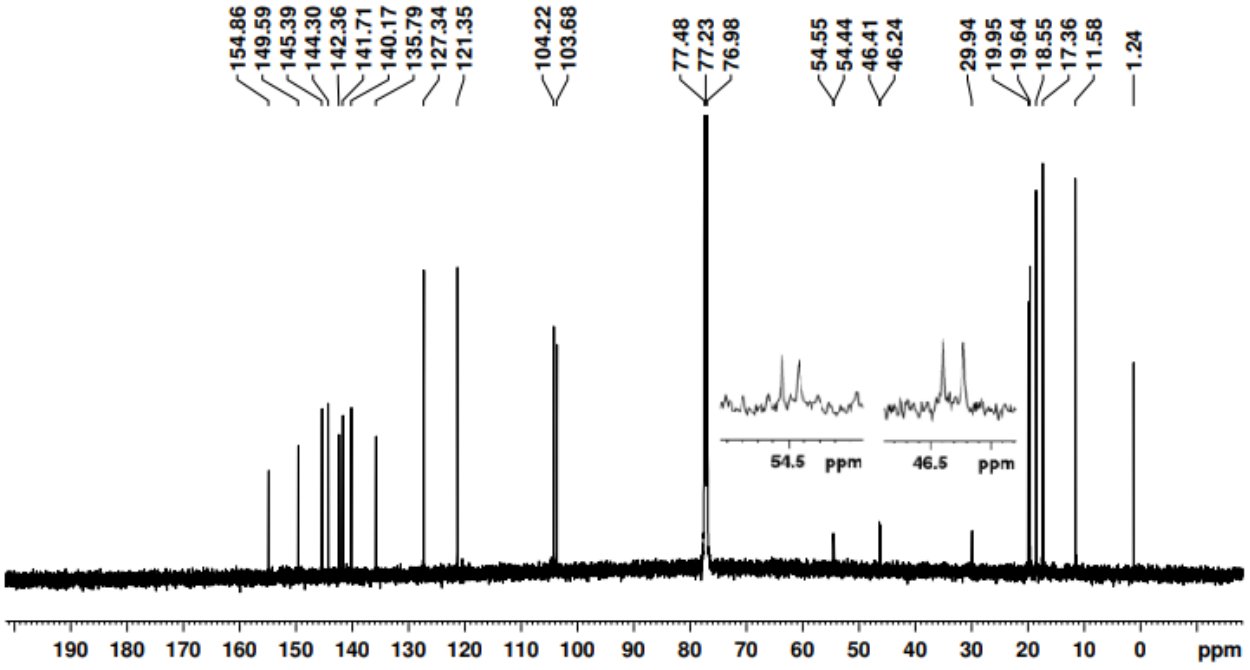

Figure 36. 100 MHz ^{13}C NMR spectrum of bridged rhodium(III) complex **95** in $CDCl_3$

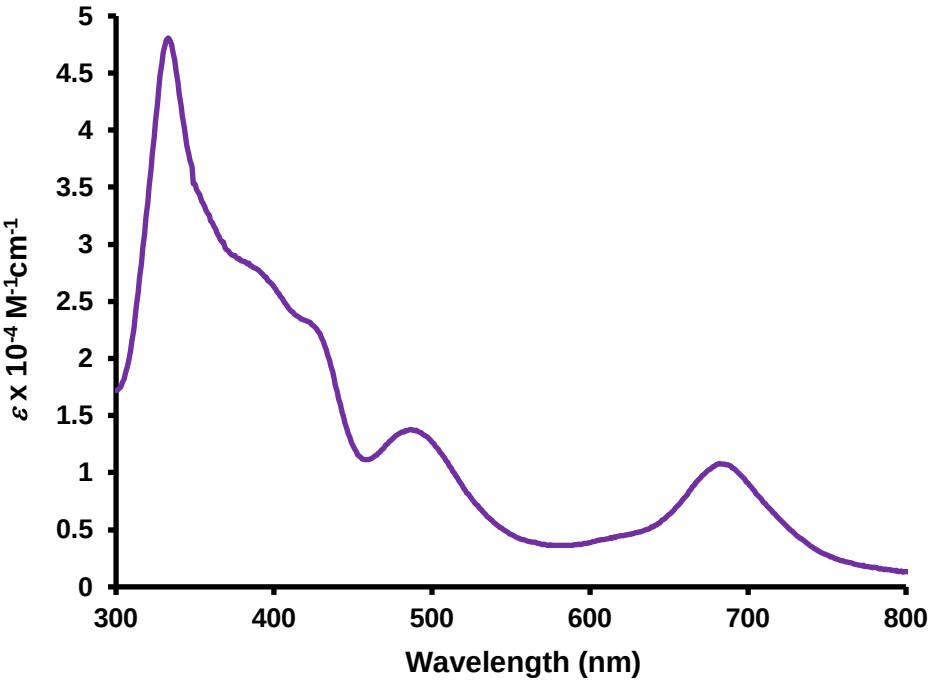

Figure 37. UV-Vis spectrum of bridged rhodium(III) complex **95**

The structure of **95** was confirmed by X-ray crystallography (Figure 38). The porphyrinoid framework is remarkably similar to that of C-methyl palladium complex **72**, with the main difference being the presence of a bridging CH_2 unit. The overall framework of bond distances is consistent with an aromatic compound possessing a π-delocalization pathway that passes through the indene unit due to the presence of the sp^3 hybridized C21 atom. The bond lengths of C1-C2 and C3-C4 are consistent with this and give smaller values of ca. 1.447 Å compared to the larger bond lengths of 1.463(2) and 1.462(2) Å that are observed for the C1-C21 and C4-C21 bonds. The rhodium(III) center resides in a distorted square pyramidal coordination environment with the equatorial plane consisting of the C21 and the three pyrrole nitrogen atoms. The bond lengths between Rh-C21, Rh-N22, Rh-N23 and Rh-N24 are 2.1329(11) Å, 2.0369(9) Å, 2.0431(9) Å and 2.0410(9) Å, respectively. Additionally, the C1-C21-C25 and C4-C21-C25 bond angles are both 120.5(1)°, while the C25-C21-Rh bond angle is 64.09(6)°, and the methylene unit C25 lies

1.585(1) Å out of the RhN_3 plane. The rhodium(III) metal center of **95** has a similar coordination environment to the one seen in the related tetraphenyl rhodium(III) carbaporphyrin complex that was formed through a ring contraction of *p*-benziporphyrins.[68] However, the methylene unit is separated from the Rh atom by 1.9932(1) Å in **95**, which is 0.04 Å shorter than was observed in the tetraphenyl rhodium(III) carbaporphyrin complex.

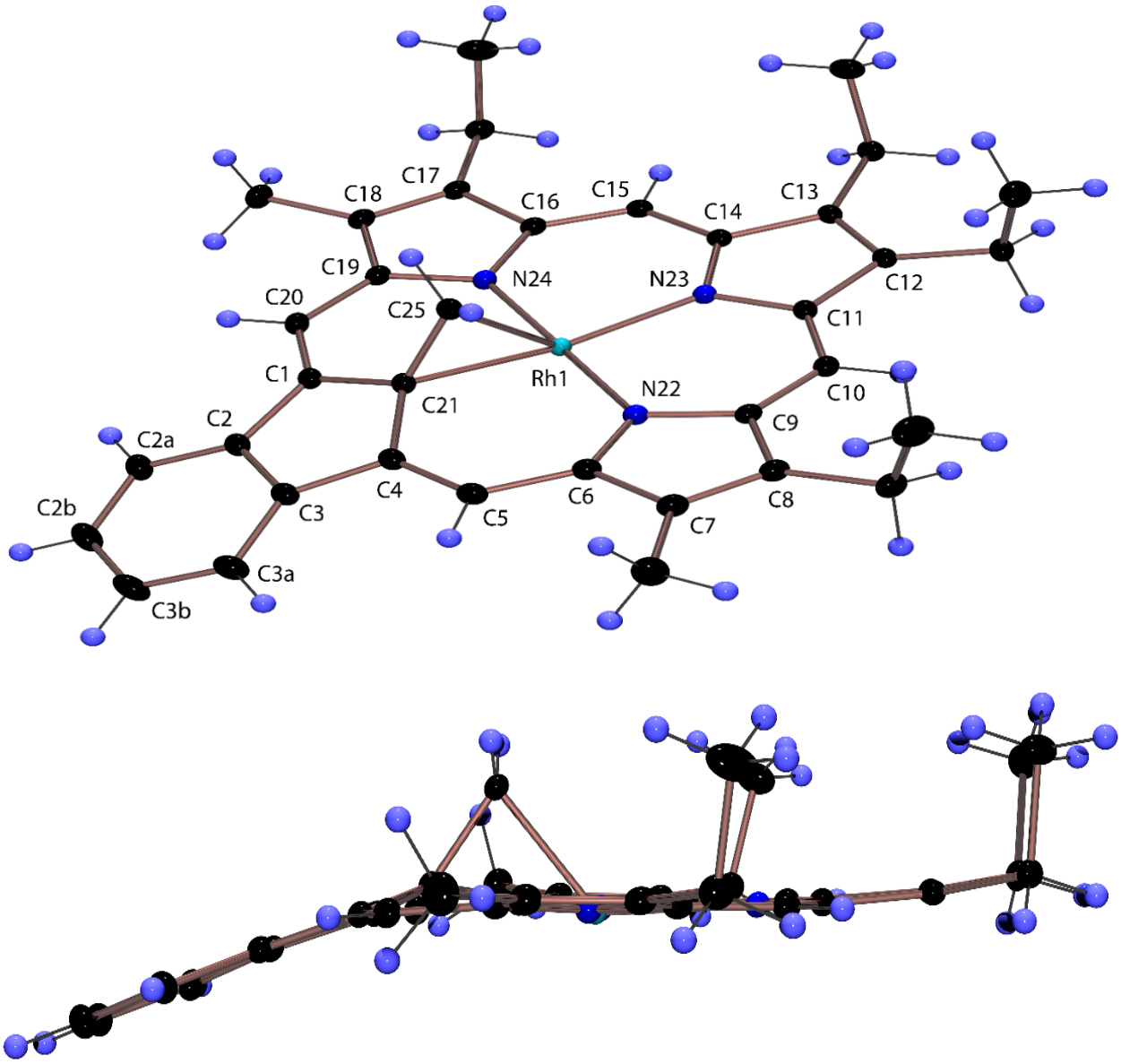

Figure 38. Color POV-Ray rendered ORTEP III drawing (50% probability level, hydrogen atoms rendered arbitrarily small for clarity) of methylene-bridged rhodium(III) carbaporphyrin **95**

Conclusion

The rhodium(I) and rhodium(III) complexes reported in this chapter greatly expand the number of carbaporphyrinoids that can form stable complexes with rhodium metal. Carbaporphyrin diester **88** and naphthocarbaporphyrin **87** formed stable rhodium(I) and rhodium(III) complexes in a similar fashion to that of benzocarbaporphyrin **3**. In contrast, it was found that internally methylated benzocarbaporphyrins reacted differently than **3** when rhodium metal was introduced into the macrocycle cavity. 21- and 22-methylbenzocarbaporphyrins **75** and **70**, respectively, formed stable rhodium(I) complexes but could not be converted into rhodium(III) derivatives. 23-Methylbenzocarbaporphyrin **76** did not even form this type of rhodium(I) complex, but instead rearranged to give a bridged rhodium(III) derivative **95**. These investigations show that the inner substituent greatly impacts the coordination chemistry of carbaporphyrin systems. In the following chapter, a series of *N*-methylated porphyrinoids are described and their properties are compared to their respective *N*-unsubstituted counterparts, in order to further demonstrate the effects internal alkylation has on a number of porphyrinoid macrocycles.

Experimental:

Melting points are uncorrected. NMR spectra were recorded using a 400 or 500 MHz NMR spectrometer and were run at 302 K unless otherwise indicated. ^{1}H NMR values are reported as chemical shifts δ, relative integral, multiplicity (s, singlet; d, doublet; t, triplet; q, quartet; m, multiplet; br, broad peak) and coupling constant (*J*). Chemical shifts are reported in parts per million (ppm) relative to $CDCl_3$ (^{1}H residual $CHCl_3$ singlet δ 7.26, ^{13}C $CDCl_3$ triplet δ 77.23) or d_6-DMSO (^{1}H residual d_5-DMSO pentet δ 2.49, ^{13}C d_6-DMSO septet δ 39.7) and coupling constants were taken directly from the spectra. NMR assignments were made with the aid of ^{1}H-^{1}H COSY, HSQC, DEPT-135 and nOe difference proton NMR spectroscopy. 2D experiments were performed using standard software. High-resolution mass spectra (HRMS) were carried out using a double focusing magnetic sector instrument. Samples of X-ray quality crystals were suspended in mineral oil at ambient temperature and a suitable crystal was selected, mounted on a MiTeGen Micromount and transferred to a Bruker AXS SMART APEXII CCD X-ray diffractometer. The X-ray diffraction data were collected at 100(2) K using Mo-Kα (λ = 0.71073 Å) radiation.

[8,12,13,17-Tetraethyl-2,3-dimethoxycarbonyl-7,18-dimethyl-21-carbaporphyrinato](dicarbonyl)rhodium(I) (**89**). Carbaporphyrin diester **88**[29] (60.2 mg, 0.106 mmol) was dissolved in dichloromethane (111 mL) under nitrogen. Anhydrous sodium acetate (84.7 mg) was then added, followed by tetracarbonyldi-μ-chlorodirhodium(I) (40.4 mg, 0.10 mmol), and the mixture refluxed overnight under nitrogen. The solvent was removed under reduce pressure and the residue was chromatographed on grade 3 alumina eluting with chloroform. A dark green band was collected, and recrystallized with chloroform-hexanes to afford the rhodium(I) carbaporphyrin (76.2 mg, 0.105 mmol, 99%) as dark crystals, mp >300 ^{o}C. IR (ZnSe): ν_{CO}/cm^{-1}

2066, 2011, 1698. UV-vis (CH_2Cl_2): λ_{max}/nm (log ε) 357 (4.66), 490 (4.61), 569 (4.00), 611 (3.74), 723 (3.27). ^{1}H NMR (500 MHz, $CDCl_3$): δ -4.94 (1H, s, 21-H), -1.09 (1H, s, NH), 1.60 (3H, t, *J* = 7.7 Hz), 1.72-1.76 (9H, m) (4 x CH_2CH_3), 3.35 (3H, s, 7-Me), 3.45 (3H, s, 18-Me), 3.63-3.71 (1H, m), 3.72-3.86 (3H, m), 3.87-3.96 (4H, m) (4 x CH_2CH_3), 4.21 (3H, s, 3-CO_2Me), 4.26 (3H, s, 2-CO_2Me), 9.40 (1H, s), 9.44 (1H, s) (10,15-H), 10.02 (1H, s, 20-H), 10.37 (1H, s, 5-H). ^{13}C NMR (125 MHz, $CDCl_3$): δ 11.4 (18-Me), 12.1 (7-Me), 17.1, 17.3, 17.8, 18.0, 19.6, 19.7, 19.8, 20.4, 52.4 (3-CO_2CH_3), 52.5 (2-CO_2CH_3), 92.4 (10- or 15-CH), 102.8 (10- or 15-CH), 107.5 (20-CH), 108.9 (21-CH), 116.7 (5-CH), 128.3, 128.4, 132.2, 133.6, 135.8, 135.9, 137.9, 138.4, 138.55, 138.63, 141.9, 144.8, 150.5, 150.6, 158.8, 158.1, 167.2 (ester C=O), 167.8 (ester C=O), 177.0 (d, $^1J_{Rh\text{-}C}$ = 69.9 Hz, CO), 178.7 (d, $^1J_{Rh\text{-}C}$ = 67.7 Hz, CO). HR-MS (ESI) *m/z*: $[M + H]^+$ calcd for $C_{37}H_{39}N_3O_6Rh$ 724.1894, found 724.1887.

[8,12,13,17-Tetraethyl-7,18-dimethyl-21-carbanaphtho[2,3-*b*]porphyrinato](dicarbonyl)rhodium(I) (**91**). Naphthocarbaporphyrin **87**[108] (20.1 mg, 0.0365 mmol) was reacted with $[Rh(CO)_2Cl]_2$ (15.2 mg, 0.039 mmol) and sodium acetate (29.8 mg) under the foregoing conditions. The product was purified on a silica gel column eluting with 20:80 dichloromethane-hexanes and a green band was collected. The solvent was evaporated and the residue recrystallized from chloroform-hexanes to yield the naphthocarbaporphyrin complex (18.5 mg, 0.0261 mmol, 72%) as dark crystals, mp >300 ºC. IR (ZnSe): ν_{CO}/cm^{-1} 2065, 2017, 1993. UV-vis (CH_2Cl_2): λ_{max}/nm (log ε) 378 (4.69), 481 (5.03), 566 (4.11), 603 (4.06), 624 (sh, 3.94), 680 (2.73). ^{1}H NMR (500 MHz, $CDCl_3$): δ -5.19 (1H, s, 21-H), -2.48 (1H, s, NH), 1.68 (3H, t, *J* = 7.7 Hz), 1.78-1.85 (9H, 3 overlapping triplets) (4 x CH_2CH_3), 3.54 (3H, s), 3.65 (3H, s) (7,18-CH_3), 3.78-3.92 (2H, m), 3.94-4.02 (2H, m), 4.04-4.12 (4H, m) (4 x CH_2CH_3), 7.58-7.63 (2H, m, 2^3,3^3-H), 8.23-8.28 (2H, m, 2^2,3^2-H), 9.10 (1H, s), 9.15 (1H, s) (2^1,3^1-H), 9.78 (1H, s), 9.83 (1H, s)

(10,15-H), 10.09 (1H, s), 10.34 (1H, s) (5,20-H). ^{13}C NMR (125 MHz, $CDCl_3$): δ 11.6, 12.3, 17.4, 17.5, 18.2, 18.3, 19.9, 19.96, 19.98, 20.6, 93.8, 97.5, 103.1, 105.0, 119.0, 119.2, 123.0 (21-CH), 125.6, 125.7, 128.9, 129.1, 132.0, 132.61, 132.63, 133.8, 133.9, 135.0. 136.3, 139.0, 139.2, 139.7, 140.1, 142.3, 143.4, 146.3, 147.5, 153.69, 153.71, 155.2, 177.6 (d, $^1J_{Rh\text{-}C}$ = 69.0 Hz, CO), 178.4 (d, $^1J_{Rh\text{-}C}$ = 67.1 Hz, CO). HR-MS (ESI) *m/z*: $[M + H]^+$ calcd for $C_{41}H_{39}N_3O_2Rh$ 708.2097, found 708.2089.

[8,12,13,17-Tetraethyl-2,3-dimethoxycarbonyl-7,18-dimethyl-21-carbaporphyrinato](dipyridine)rhodium(III) (**90**). Rhodium(I) complex **89** (10.0 mg, 0.0138 mmol) was dissolved in pyridine (10 mL) and refluxed under nitrogen in a preheated oil bath for 30 min. The solvent was removed under reduced pressure and the residue chromatographed on grade 3 alumina eluting with toluene. A dark band was collected and recrystallized with chloroform-hexanes to yield rhodium(III) carbaporphyrin **90** (3.2 mg, 0.0039 mmol, 28%) as dark crystals, mp >300 °C. UV-vis (CH_2Cl_2): λ_{max}/nm (log ε) 356 (4.44), 393 (4.43), 427 (sh, 4.50), 450 (sh, 4.59), 463 (4.63), 531 (3.92), 573 (4.14). ^{1}H NMR (500 MHz, C_6D_6): δ 1.74 (6H, t, *J* = 7.5 Hz), 1.82 (6H, t, *J* = 7.5 Hz), 2.33 (4H, d, *J* = 5.9 Hz, 4 x α-pyridine-H), 3.25 (6H, s, 17,18-Me), 3.73-3.80 (8H, m, 4 x C*H*$_2$CH$_3$), 4.02 (6H, s, 2 x OMe), 4.09-4.12 (4H, m, 4 x β-pyridine-H), 4.70 (2H, dt, J = 1.6, 7.6 Hz, 2 x γ-pyridine-H), 9.46 (2H, s, 10,15-H), 10.59 (2H, s, 5,20-H). ^{13}C NMR (125 MHz, $CDCl_3$): δ 11.3 (7,18-Me), 17.6, 18.3, 19.9, 20.2, 51.4 (2 x OMe), 94.2 (10.15-CH), 113.1 (5,20-CH), 121.2 (4 x β-pyridine-CH), 129.5, 133.6 (2 x γ-pyridine-CH), 136.2, 138.4, 139.1, 139.2, 141.8, 142.2, 142.5, 148.5 (4 x α-pyridine-CH), 167.7 (2 x C=O). HR-MS (ESI) *m/z*: calcd for $C_{45}H_{46}N_5O_4Rh$ 823.2605, found 823.2638.

[8,12,13,17-Tetraethyl-7,18-dimethyl-21-carbanaphtho[2,3-*b*]porphyrinato](dipyridine)rhodium(III) (**92**). Rhodium(I) naphthocarbaporphyrin **91** (18.5 mg, 0.0261 mmol) was dissolved in pyridine (17 mL) and refluxed under nitrogen for 1 h. The solvent was removed under reduced pressure and the residue purified on a grade 3 alumina column eluting with 50:50 toluene-hexanes. A light brown band was collected and recrystallized with chloroform-hexanes to yield the rhodium(III) complex (4.5 mg, 0.0056 mmol, 21%) as dark crystals, mp >300 ^{o}C. UV-vis (CH_2Cl_2): λ_{max}/nm (log ε) 348 (4.40), 422 (sh, 4.56), 434 (sh, 4.68), 447 (5.04), 458 (sh, 4.68), 530 (3.99), 569 (4.24), 606 (3.47), 851 (3.65). ^{1}H NMR (500 MHz, C_6D_6, 60 ^{o}C): δ 1.44 (4H, d, *J* = 6.2 Hz, 4 x α-pyridine-H), 1.94 (6H, t, *J* = 7.6 Hz), 1.99 (6H, t, *J* = 7.6 Hz) (4 x CH_2CH_3), 3.59 (6H, s, 7,18-Me), 3.92 (4H, t, *J* = 7.1 Hz, 4 x β-pyridine-H), 4.06-4.14 (8H, m, 4 x CH_2CH_3), 4.58 (2H, t, *J* = 7.1 Hz, 2 x γ-pyridine-H), 7.45-7.48 (2H, m, 2^3,3^3-H), 8.15-8.18 (2H, m, 2^2,3^2-H), 9.18 (2H, s, 2^1,3^1-H), 10.07 (2H, s, 10,15-H), 10.56 (2H, s, 5,20-H). ^{13}C NMR (125 MHz, C_6D_6, 60 ^{o}C): δ 11.8, 18.1, 18.6, 20.3, 20.7, 94.7, 102.8, 115.6, 120.6 (4 x β-pyridine-CH), 14.9, 129.0, 132.1, 133.1 (2 x γ-pyridine-CH), 133.2, 134.5, 138.2, 139.2, 139.6, 140.3, 140.4, 146.9, 148.1 (4 x α-pyridine-CH). HR-MS (ESI) *m/z*: $[M + H]^+$ calcd for $C_{49}H_{46}N_5Rh$ 807.2808, found 807.2798.

[8,12,13,17-Tetraethyl-7,18,22-trimethylbenzo[*b*]-carbaporphyrinato](dicarbonyl)rhodium(I) (**93**). 22-Methylbenzocarbaporphyrin **70** (10.4 mg, 0.0203 mmol) was dissolved in dichloromethane (22 mL) under nitrogen. Anhydrous sodium acetate (16.3 mg) was added, followed by $[Rh(CO)_2Cl]_2$ (7.8 mg, 0.0201 mmol), and the mixture was refluxed overnight under nitrogen. The solvent was removed under reduced pressure, and the residue purified by column chromatography on silica gel eluting with dichloromethane-hexanes (50:50). The rhodium complex was collected as a brown band. Recrystallization from chloroform-

hexanes afforded the **93** (6.8 mg, 0.010 mmol, 50%) as dark crystals, mp >300 °C. UV-vis (CH_2Cl_2): λ_{max}/nm (log ε) 319 (sh, 4.39), 360 (4.57), 407 (sh, 4.44), 481 (4.85), 561 (4.07), 586 (sh, 3.83), 637 (3.68). IR (ZnSe): ν_{CO} 1985, 2057 cm^{-1}. ^1H NMR (500 MHz, $CDCl_3$): δ -4.68 (1H, s, 21-H), -4.50 (3H, s, N-Me), 1.56 (3H, t, $^3J_{HH}$ = 7.7 Hz), 1.68 (3H, t, $^3J_{HH}$ = 7.7 Hz), 1.76 (3H, t, $^3J_{HH}$ = 7.7 Hz), 1.79 (3H, t, $^3J_{HH}$ = 7.7 Hz) (4 x CH_2CH_3), 3.36 (3H, s), 3.52 (3H, s) (7,18-Me), 3.56-3.69 (2H, m), 3.76-3.99 (6H, m) (4 x CH_2CH_3), 7.66-7.71 (2H, m, 2^2,3^2-H), 8.74-8.78 (2H, m, 2^1,3^1-H), 9.640 (1H, s), 9.643 (1H, s) (10,15-H), 9.97 (1H, s), 10.16 (1H, s) (5,20-H). ^{13}C NMR (125 MHz, $CDCl_3$): δ 12.0, 12.3, 15.8, 17.6, 18.3, 18.4, 19.9, 20.0, 20.1, 20.6, 97.1, 102.5, 104.6, 106.6, 120.32, 120.35, 121.2 (br), 126.6, 130.1, 132.3, 132.9, 134.8, 136.5, 139.2, 139.4, 142.2, 143.7, 144.4, 147.8, 148.4, 149.1, 150.0, 152.5, 155.0, 178.8 (d, $^1J_{RhC}$ = 68.5 Hz, CO), 179.4 (d, $^1J_{RhC}$ = 69.4 Hz, CO). HR-MS (ESI) *m/z*: $[M + H]^+$ Calcd for $C_{38}H_{39}N_3O_2Rh$ 672.2097; found 672.2104.

[8,12,13,17-Tetraethyl-7,18,21-trimethylbenzo[*b*]carbaporphyrinato](dicarbonyl)rhodium(I) (**94**). Anhydrous sodium acetate (11.4 mg) was added, followed by $[Rh(CO)_2Cl]_2$ (5.5 mg, 0.0142 mmol), to a solution of 21-methylbenzocarbaporphyrin **75** (7.0 mg, 0.0136 mmol) in dichloromethane (15 mL) under nitrogen. The resulting mixture was heated under reflux overnight. The solvent was removed under reduced pressure and the residue purified by column chromatography on silica gel eluting with dichloromethane-hexanes (50:50). The complex eluted as a green band. Recrystallization from chloroform-hexanes gave the rhodium(I) complex (6.2 mg, 0.00924 mmol, 67%) as as dark crystals, mp >300 °C. UV-vis (CH_2Cl_2): λ_{max}/nm (log ε) 327 (4.18), 368 (4.34), 476 (4.56), 562 (3.71), 604 (3.71), 627 (3.64). IR (ZnSe): ν_{CO} 1996, 2063 cm^{-1}. ^1H NMR (500 MHz, $CDCl_3$): δ -5.66 (3H, s, N-Me), -2.83 (1H, br s, NH), 1.69 (3H, t, $^3J_{HH}$ = 7.7 Hz), 1.78-1.83 (9H, 3 overlapping

triplets) (4 x CH_2CH_3), 3.35 (3H, s), 3.52 (3H, s) (7,18-Me), 3.67-3.85 (3H, m), 3.88-4.01 (5H, m) (4 x CH_2CH_3), 7.35 (1H, dt, $^4J_{HH}$ = 0.9 Hz, $^3J_{HH}$ = 7.3 Hz), 7.41 (1H, dt, $^4J_{HH}$ = 0.9 Hz, $^3J_{HH}$ = 7.4 Hz) (2^2,3^2-H), 7.97 (1H, d, $^3J_{HH}$ = 7.2 Hz), 8.20 (1H, d, $^3J_{HH}$ = 7.3 Hz) (2^1,3^1-H), 9.52 (1H, s), 9.56 (1H, s) (10,15-H), 9.69 (1H, s), 9.82 (1H, s) (5,20-H). ^{13}C NMR (125 MHz, $CDCl_3$): δ 11.5, 11.8 (21-Me), 12.3, 17.4, 17.6, 18.0, 18.3, 19.75, 19.84, 19.91, 20.5, 93.0, 99.9, 103.5, 108.6, 120.0, 120.2, 126.1, 126.2, 127.8, 131.5, 132.8, 132.89, 132.94, 134.7, 136.1, 137.5, 139.1, 139.9, 140.1, 141.6, 143.2, 145.8, 147.7, 153.1, 154.8, 177.6 (d, $^1J_{RhC}$ = 67.0 Hz, CO), 179.0 (d, $^1J_{RhC}$ = 66.2 Hz, CO). HR-MS (ESI) *m/z*: $[M + H]^+$ Calcd for $C_{38}H_{39}N_3O_2Rh$ 672.2097; found 672.2088.

[8,12,13,17-Tetraethyl-7,18-dimethyl-21-methylene-benzo[*b*]carbaporphyrinato]rhodium(III) (**95**). 23-Methylbenzocarbaporphyrin **76** (20.0 mg, 0.0390 mmol) was dissolved in toluene (40 mL) under nitrogen. Anhydrous sodium acetate (33.3 mg) was added, followed by $[Rh(CO)_2Cl]_2$ (14.3 mg, 0.0368 mmol), and the mixture refluxed overnight. The solvent was removed under reduced pressure and the residue was purified twice by column chromatography on silica gel eluting with dichloromethane. The product eluted as a dark band. Recrystallization from chloroform-methanol gave the rhodium(III) complex (7.4 mg, 0.0121 mmol, 31%) as dark crystals, mp >300 ºC. UV-vis (CH_2Cl_2): λ_{max}/nm (log ε) 333 (4.68), 386 (sh, 4.45), 424 (sh, 4.36), 486 (4.14), 682 (4.03). ^{1}H NMR (400 MHz, $CDCl_3$): δ -3.22 (2H, br d, $^2J_{RhH}$ = 1.0 Hz, Rh-CH_2), 1.74 (6H, t, $^3J_{HH}$ = 7.7 Hz, 8,17-CH_2CH_3), 1.78 (6H, t, $^3J_{HH}$ = 7.7 Hz, 12,13-CH_2CH_3), 3.34 (6H, s, 7,18-Me), 3.62-3.70 (4H, m, 8,17-CH_2), 3.72-3.83 (4H, m, 12,13-CH_2), 8.16-8.20 (2H, m, 2^2,3^2-H), 9.37-9.41 (2H, m, 2^1,3^1-H), 9.51 (2H, s, 10,15-H), 10.12 (2H, s, 5,20-H). ^{13}C NMR (100 MHz, $CDCl_3$): δ 11.6 (7,18-Me), 17.4 (8,17-CH_2CH_3), 18.5 (12,13-CH_2CH_3), 19.6 (12,13-CH_2), 19.9 (8,17-CH_2), 46.3 (d, $^1J_{RhC}$ = 21.4 Hz, Rh-CH_2), 54.5 (d, $^1J_{RhC}$ = 14.2 Hz, 21-C), 103.7 (10,15-CH), 104.2 (5,20-CH), 121.3 (2^1,3^1-CH), 127.3 (2^2,3^2-CH), 135.8, 140.2,

141.7, 142.4, 144.3, 145.4, 149.6, 154.9. HR-MS (EI) *m/z*: Calcd for $C_{36}H_{36}N_3Rh$ 613.1964; found 613.1659.

CHAPTER IV: SYNTHESIS AND CHARACTERIZATION OF *N*-METHYLATED PORPHYRINOIDS

Introduction

Upon the successful synthesis and metalation of 23-methylbenzocarbaporphyrin **76**, attempts were made to generate a series of porphyrinoids from *N*-methyl tripyrrane unit **54d**. Using the '3+1' variant of the MacDonald condensation, a number of dialdehyde units were condensed with **54d** to give porphyrinoid systems containing an internal methyl group. It is of interest to compare the spectroscopic properties of the methylated derivatives with the previously reported *N*-unsubstituted macrocycles in order to determine how the internal alkyl substituent affects these porphyrinoid systems. In this chapter, the synthesis and characterization of *N*-methylated porphyrinoids is discussed. NMR and UV-vis spectra are used to identify differences in the properties of the macrocycles due to the presence of internal alkylation.

Results and Discussion

The synthesis of oxa- or thiaporphyrins containing an internal methyl group at the 23-position will simultaneously test the effect of introducing both a heteroatom (O or S) and an *N*-alkyl substituent. 21-Oxaporphyrin **96a** and the related *N*-methylated derivative **96b** were both prepared and their properties contrasted. Reaction of tripyrrane dicarboxylic acid **54b** with furan dialdehyde **56a** under dilute conditions (99 mL of dichloromethane for 100 mg of tripyrrane) in the presence of TFA, followed by oxidation with ferric chloride, gave oxaporphyrin **96a** (Scheme 34). Tripyrrane **54d** similarly reacted with **56a** to afford the *N*-methyl analogue **96b** (Scheme 34),

although better results were obtained under fairly concentrated conditions (<20 mL dichloromethane for 100 mg of tripyrrane). Crude *N*-methyl derivative **96b** was chromatographed twice on neutral alumina eluting with chloroform, and a dark band was collected each time. The fractions were recrystallized from chloroform-hexanes to give the pure product as dark crystals in 42.3%. *N*-Unsubstituted oxaporphyrin **96a** was purified by chromatography on neutral alumina, eluting with chloroform, and a bright red/pink band was collected. The fractions were recrystallized from chloroform-hexanes to give *N*-unsubstituted oxaporphyrin **96a** in 66.2% yield. A related 21-oxaporphyrin **96c** was synthesized by Johnson et al.[57] that differed only by one of the external substituents and was isolated as a monocationic species.

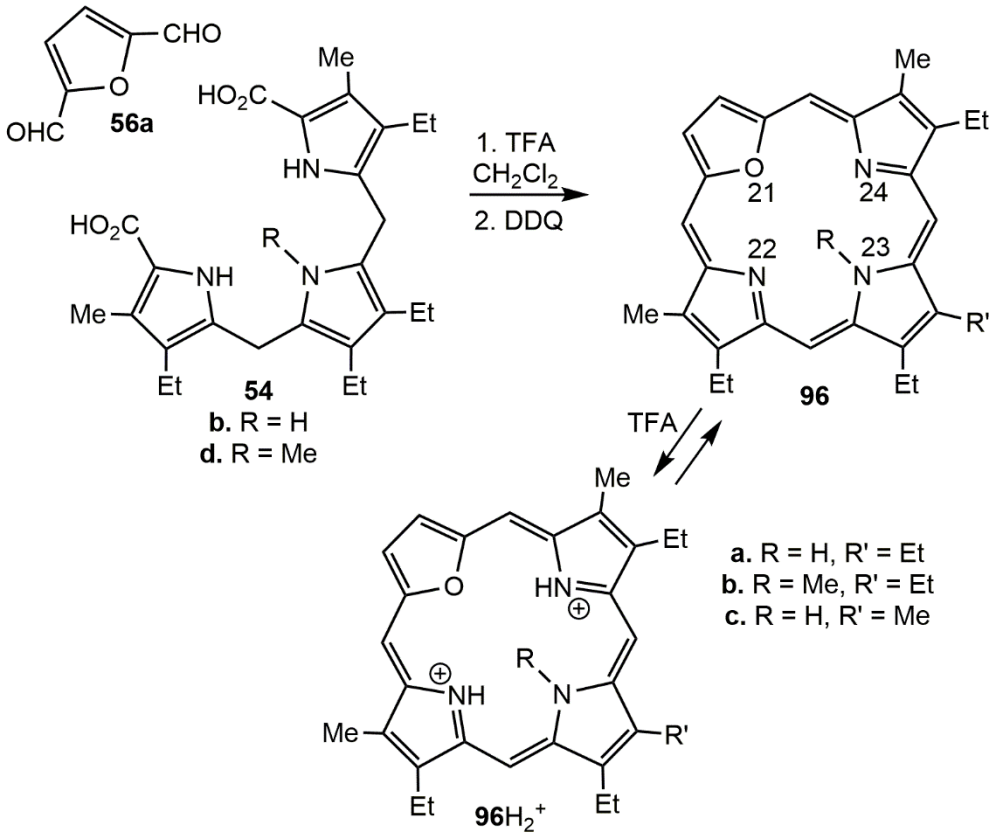

Scheme 34. '3+1' Synthesis of 23-methyl-21-oxaporphyrin **96**

The proton NMR spectrum of *N*-methyl derivative **96b** indicated that this was a symmetrical molecule showing two 2H singlets for the *meso*-protons at 10.34 and 11.10 ppm, as well as an additional 2H singlet for the two furan ring protons at 10.69 ppm. The external methyl groups were observed as a 6H singlet at 3.70 ppm, while the internal methyl group gave an upfield singlet at -5.21 ppm (Figure 39). These resonances indicate that the system possesses a strong diatropic ring current, demonstrating that the macrocycle retains strongly aromatic properties despite the introduction of an internal substituent. The carbon-13 NMR spectrum of **96b** also demonstrates the symmetry of this system, showing the *meso*-carbons at 101.46 and 102.65 ppm, while the furan CH carbons appear further downfield at 132.53 ppm (Figure 40). The internal methyl group can be seen at 32.34 ppm as a broad singlet, possibly due to incomplete decoupling of the upfield proton resonance. When **96b** was run in TFA-$CDCl_3$, a dicationic species **96b**H_2^{2+} was observed (Scheme 34). The two internal NH protons appeared as a 2H singlet at -4.28 ppm, which was not present in the free base **96b**. The internal methyl group of the dication resonated as a 3H singlet at -5.60 ppm, which was further upfield compared to the free base, while the *meso*-protons and furan protons were identified as 2H singlets downfield at 10.82, 11.10 and 10.56 ppm, respectively. *N*-Unsubstituted oxaporphyrin **96a** required the addition of TFA in $CDCl_3$ in order to obtain high quality spectra. This data showed the *meso*-protons and furan protons as two 2H singlets at 11.04, 11.18 and 10.61, respectively, while the external methyl groups resonated as a 6H singlet at 3.82 ppm. These values are shifted slightly downfield from those seen in the dication species of the *N*-methyl derivative, but overall the protonated versions of **96a** and **96b** appear to possess similar macrocyclic ring currents.

The UV-Vis spectrum of **96b** shows bathochromic shifts to longer wavelengths when compared to the *N*-unsubstituted counterpart **96a** (Figure 41). The non-methylated compound gave

two Soret bands at 371 and 392 nm, while *N*-methyl derivative **96b** afforded two Soret bands at 378 and 407 nm. The weaker Q bands of each species further demonstrates the shift to longer wavelengths. For **96a**, these absorptions are observed at 489, 520, 585 and 643 nm, whereas the bands for **96b** are broadened and centered at higher values of 501, 527, 604 and 664 nm. Addition of 5% trifluoracetic acid (TFA) to a solution of **96b** gave the related dicationic species **96b**H_2^{2+} and this produced a single, much stronger Soret band at 395 nm followed by weaker Q bands at 527, 561 and 611 nm (Figure 42). The dication for the non-methylated counterpart **96a** similarly afforded a Soret band at 394 nm, with two weaker absorptions centered at 523 and 551 nm (Figure 42). Hence, the Q bands for **96b** are bathochromically shifted, although the Soret band is only slightly modified.

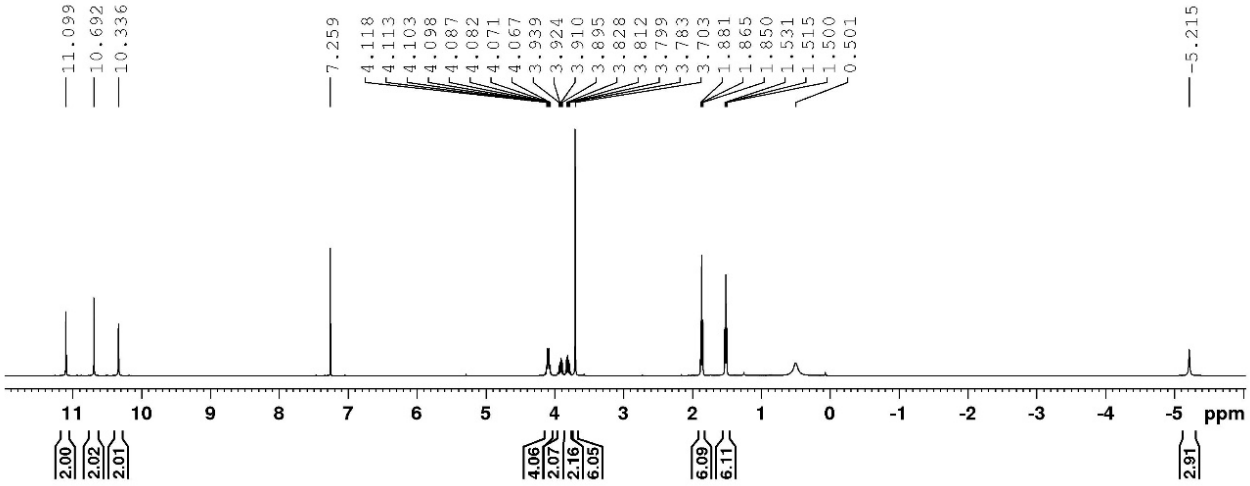

Figure 39. 500 MHz ^{1}H NMR spectrum of 23-methyl-21-oxaporphyrin **96b** in $CDCl_3$

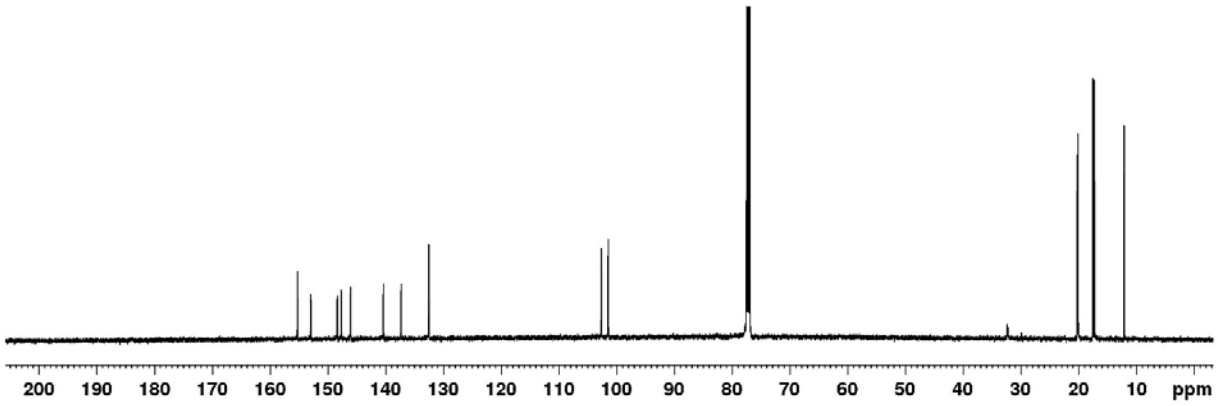

Figure 40. 125 MHz ^{13}C NMR spectrum of 23-methyl-21-oxaporphyrin **96b** in $CDCl_3$

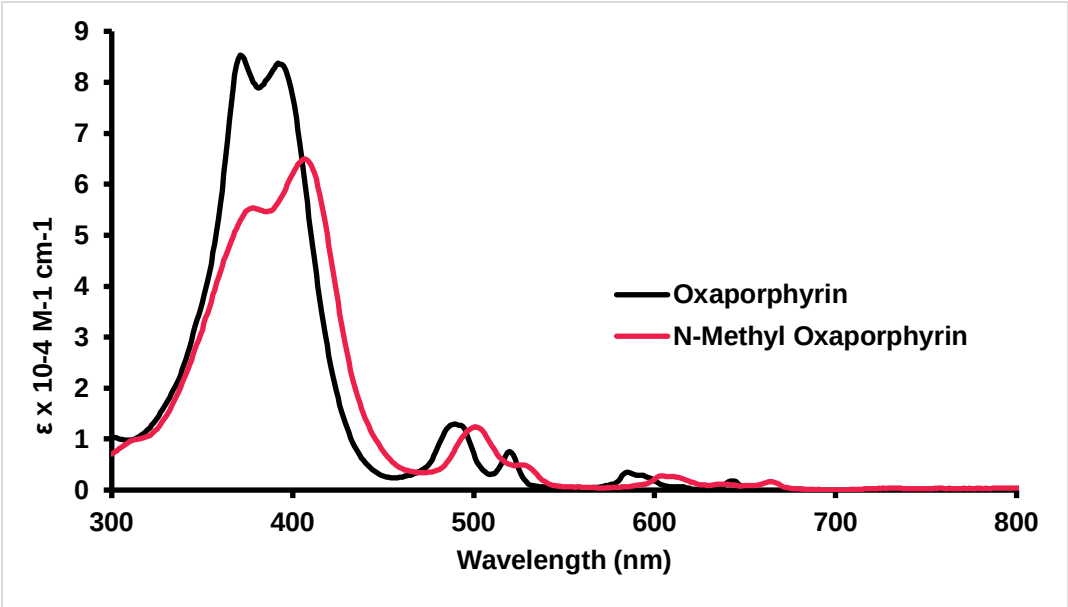

Figure 41. UV-Vis spectra of **96b** in 1% triethylamine-dichloromethane (free base, pink line) and **96a** in 1% triethylamine-dichloromethane (free base, black line)

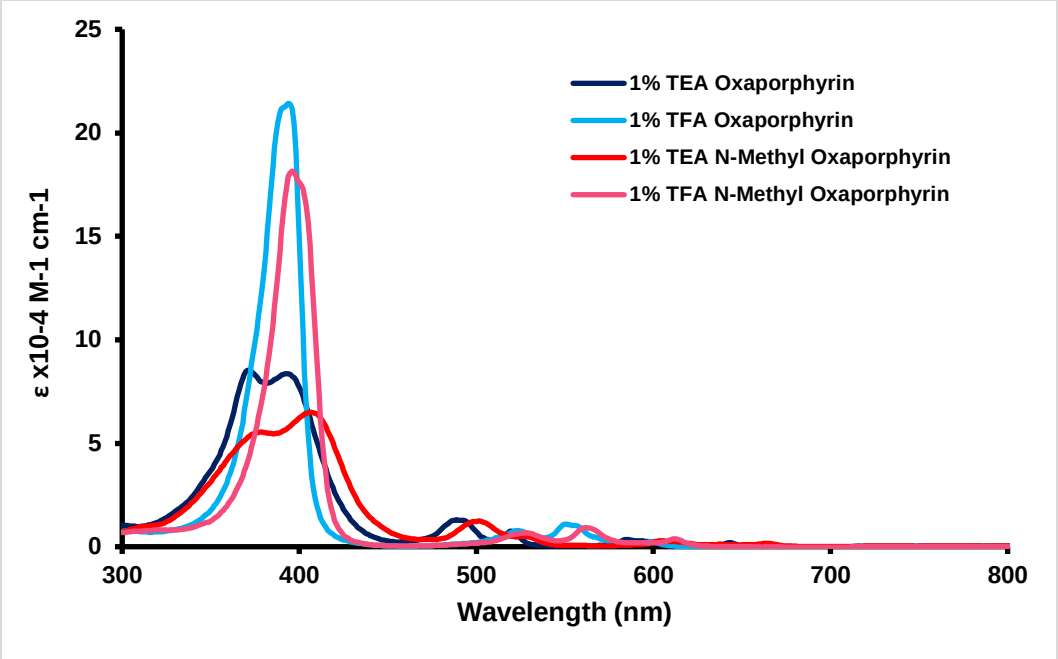

Figure 42. UV-Vis spectra of **96a** in 1% triethylamine-dichloromethane (free base, dark blue line) or 1% TFA-dichloromethane (dication, light blue line), and **96b** in 1% triethylamine-dichloromethane (free base, red line) or 1% TFA-dichloromethane (dication, pink line)

21-Thiaporphyrin **97a** and its *N*-methyl derivative **97b** were similarly synthesized and their properties contrasted. Condensation of tripyrrane **54b** with thiophene dialdehyde **56b** under dilute conditions (99 mL of dichloromethane for 100 mg of tripyrrane) in the presence of TFA, followed by oxidation with ferric chloride, gave *N*-unsubstituted thiaporphyrin **97a** in 42% yield (Scheme 35). 23-Methyl-21-thiaporphyrin **97b** was also synthesized by condensing *N*-methyl tripyrrane **54d** with thiophene dialdehyde **56b**, although concentrated conditions (<20 mL of dichloromethane for 100 mg tripyrrane) and oxidation with DDQ gave better results, and **97b** was isolated in 17% yield (Scheme 35). Both thiaporphyrin derivatives were chromatographed twice on grade 3 neutral alumina, eluting with dichloromethane. 21-Thiaporphyrin **97a** was collected as a green/yellow band while *N*-methyl thiaporphyrin **97b** was collected as a yellow/brown band.

Both compounds were highly soluble in organic solvents and were characterized without further purification. The related *N*-unsubstituted thiaporphyrin **97c**, which differs by the placement of one external substituent, was prepared in a similar fashion by Johnson and coworkers.[57] However, the authors noted that thiaporphyrin **97c** was probably obtained as a mixture of isomers, due to the presence of additional peaks in the NMR spectrum. In contrast, **97a** and **97b** were both isolated as single isomers.

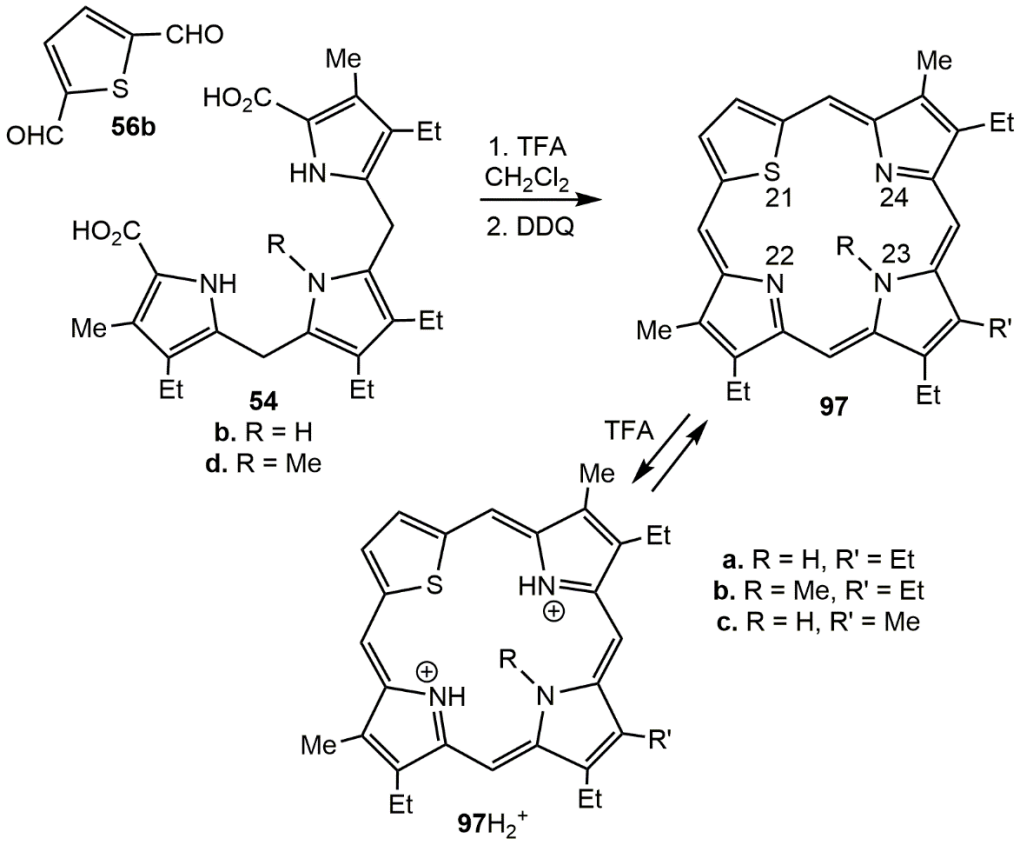

Scheme 35. '3+1' Synthesis of 23-methyl-21-thiaporphyrin **97**

The proton NMR spectrum of **97b** displayed the internal methyl as a 3H singlet at an upfield value of -4.39 ppm, while the two 2H singlets corresponding to the *meso*-protons were located downfield at 9.96 and 10.57 ppm (Figure 43). The protons on the thiophene ring also

resonated downfield as a 2H singlet at 10.00 ppm. The shifts and the number of peaks observed are consistent with a highly aromatic and symmetrical molecule. The carbon-13 NMR spectrum also supports this as the *meso*-carbons and the CH carbons of the thiophene ring resonate at 103.41, 113.15, and 133.88 ppm, respectively (Figure 44). When TFA was added to the sample, the proton NMR spectrum of dicationic species **97b**H_2^{2+} was obtained and this showed significant shifts in the proton resonances of the macrocycle. The *meso*-protons were identified as two 2H singlets at 10.72 and 11.48 ppm and the thiophene protons were observed as a 2H singlet at 10.39 ppm. The internal NH protons, which were not present in **97b**, resonated as a very broad 2H singlet centered at -4.12 ppm, while the internal methyl was identified as a 3H singlet at -4.84 ppm.

The proton NMR spectrum of non-methylated **97a** showed the *meso*-protons as two 2H singlets at 10.15 and 10.72 ppm, while the thiophene CH resonated at 10.13 ppm. The external methyl groups were identified as a 6H singlet at 3.45 ppm, and the internal NH proton was present as a broad 1H singlet at -3.87 ppm. These values suggest that **97a** possesses a slightly larger diatropic ring current than *N*-methyl derivative **97b**, although they are both strongly aromatic structures. The carbon-13 spectrum of **97a** further indicates the symmetry of the molecule, as the *meso*-carbons gave two peaks at 99.16 and 112.68 ppm. When TFA was added to **97a**, the proton-NMR spectrum of the resulting dication showed the *meso*-protons as two 2H singlets at 10.97 and 11.66 ppm, the thiophene protons as a 2H singlet at 10.60 ppm, and the external methyl groups as a 6H singlet at 3.79 ppm. Once again, the downfield shifts are slightly larger for the *N*-unsubstituted version.

The UV-Vis spectra of *N*-methyl thiaporphyrin **97b** and *N*-unsubstituted thiaporphyrin **97a** were compared (Figure 45). The non-methylated compound **97a** gave a Soret band at 398 nm, followed by several weaker Q bands from 495 nm to 649 nm. *N*-methyl derivative **97b** gave a

Soret band at 412 nm while the Q bands were identified between 505 nm and 667 nm. These values confirm that bathochromic shifts are observed for the methylated derivative, demonstrating the effect the internal alkyl group has on the chromophore. The UV-Vis spectra of the free base and dication forms of both **97a** and **97b** were also compared (Figure 46). It can be observed from these spectra that the addition of TFA affords shifts to longer wavelengths in both **97b** and **97a**, where **97b** and **97b**H_2^{2+} gave Soret bands at 412 and 423 nm, respectively, while **97a** and **97a**H_2^{2+} gave Soret bands at 398 and 418 nm, respectively.

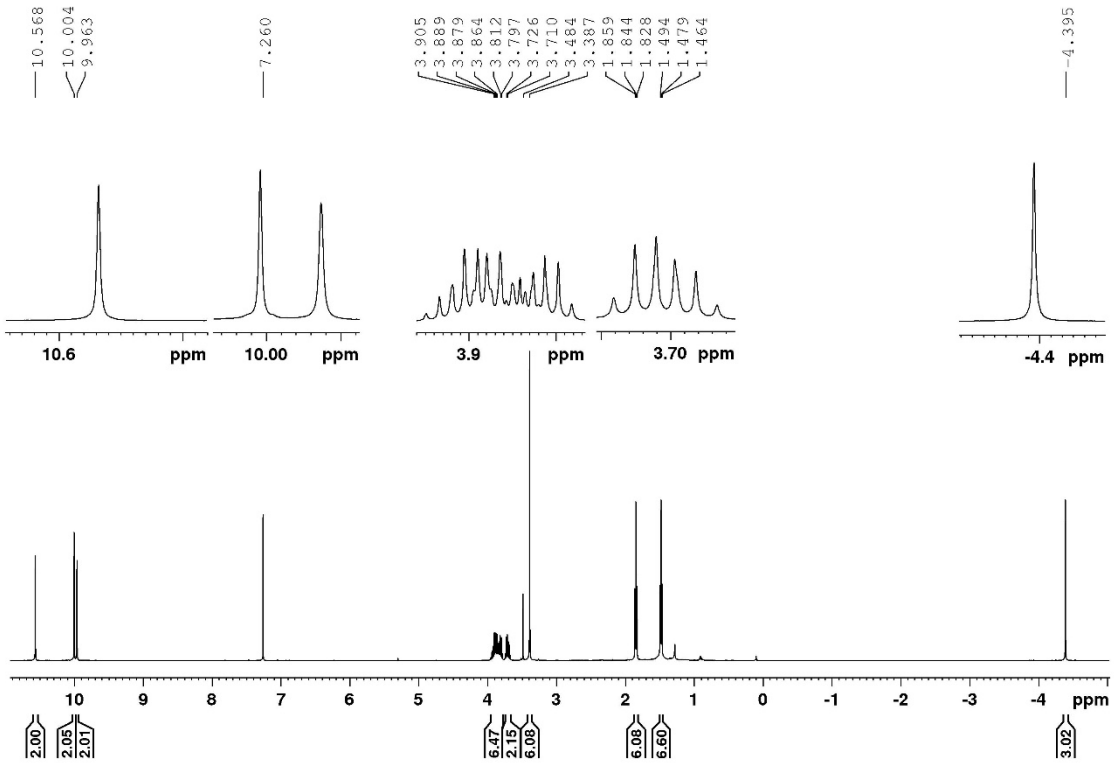

Figure 43. 500 MHz ^{1}H NMR spectrum of *N*-methyl thiaporphyrin **97b** in $CDCl_3$

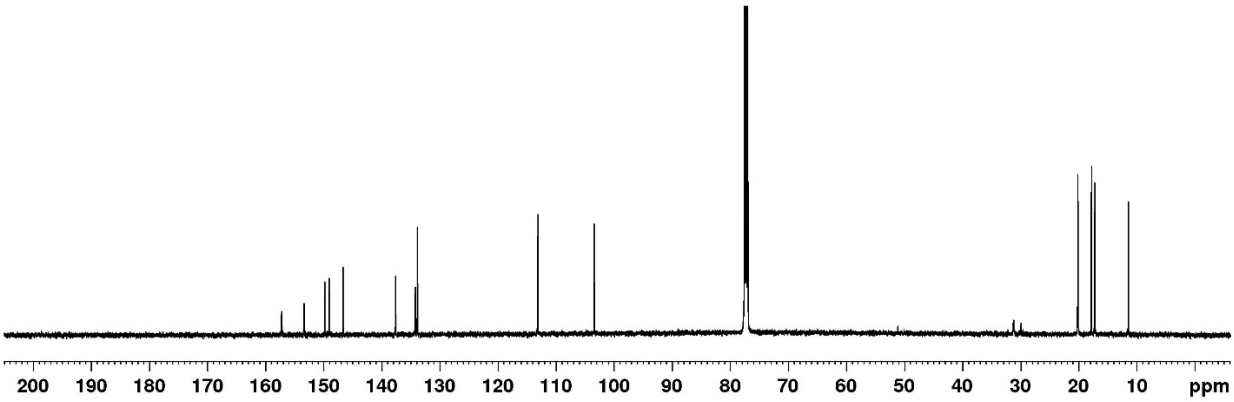

Figure 44. 125 MHz ^{13}C NMR spectrum of *N*-methyl thiaporphyrin **97b** in $CDCl_3$

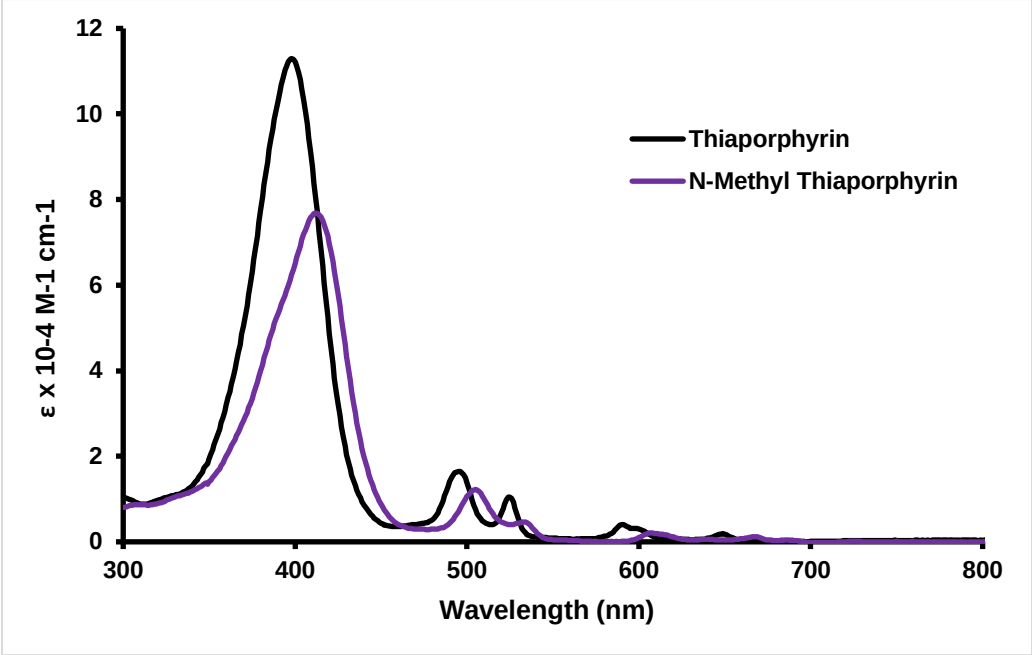

Figure 45. UV-Vis spectra of **97b** in 1% triethylamine-dichloromethane (free base, purple line) and **97a** in 1% triethylamine-dichloromethane (free base, black line)

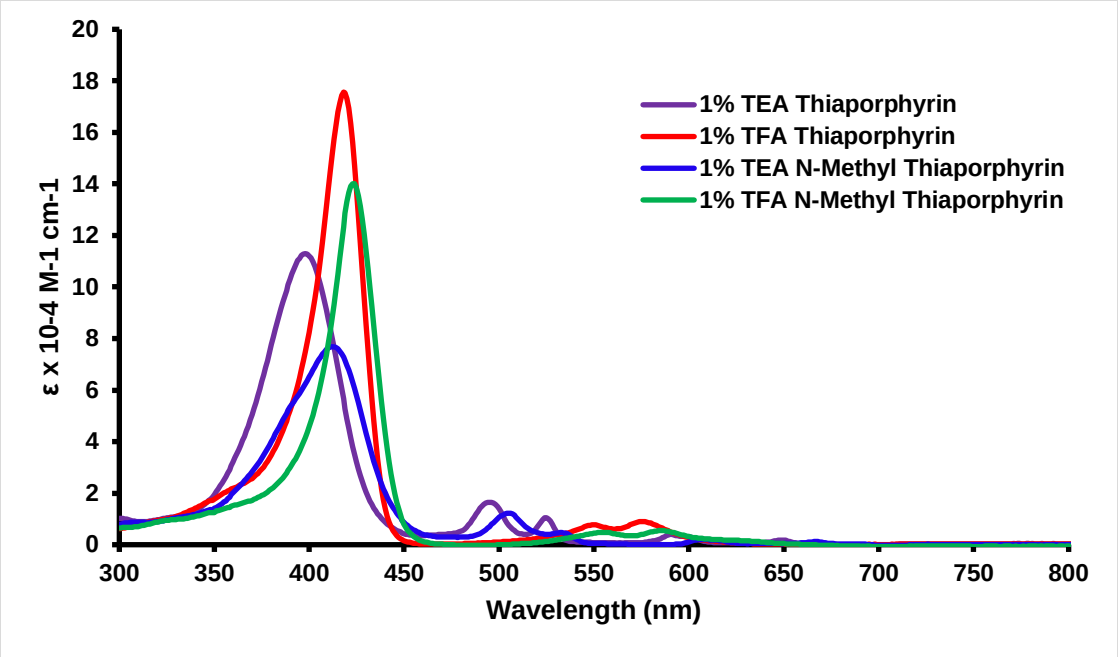

Figure 46. UV-Vis spectra of **97b** in 1% triethylamine-dichloromethane (free base, blue line) and 1% TFA-dichloromethane (dication, green line), **97a** in 1% triethylamine-dichloromethane (free base, purple line) and 1% TFA-dichloromethane (dication, red line)

In addition to heteroporphyrins, it was also of interest to investigate how internally methylated porphyrins differ from regular *N*-unsubstituted porphyrins. Condensation of *N*-methyl tripyrrane **54d** with diethyl pyrrole dialdehyde **98** gave *N*-methylporphyrin **99b** (Scheme 36). The compound was purified by column chromatography on alumina, eluting with chloroform. A dark red/pink band was collected and recrystallized from chloroform-hexanes to give the pure product as dark purple/blue crystals in 50% yield.

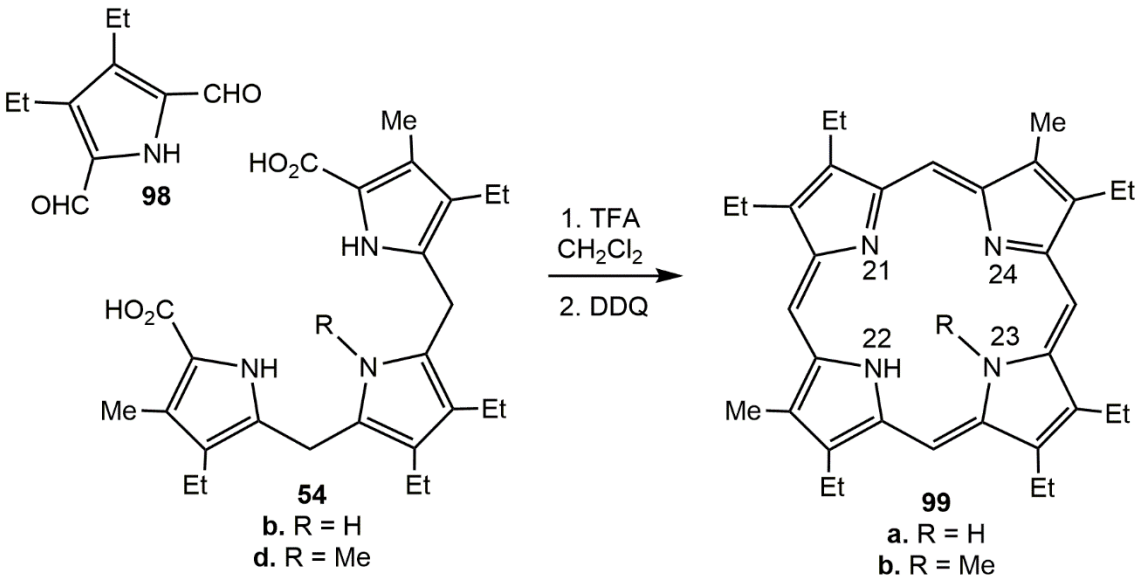

Scheme 36. '3+1' Synthesis of 23-methylporphyrin **99**

The proton NMR spectrum of **99b** demonstrated the symmetry and aromatic character of the internally methylated porphyrin (Figure 47). The *meso*-protons were identified as two 2H singlets at 9.90 and 9.94 ppm, and the external methyl groups were observed as a 6H singlet at 3.49 ppm, while the internal methyl group was seen far upfield as a 3H singlet at -4.76 ppm. These large shifts are consistent with an aromatic system and are also observed in the *N*-unsubstituted counterpart **99a**, demonstrating the preservation of aromaticity upon the insertion of an internal substituent. The *meso*-protons and the external methyl groups of **99a** were seen as a 4H singlet and a 6H singlet at 10.10 and 3.64 ppm, respectively.[118] The carbon-13 NMR spectrum of the *N*-methylated derivative (**99b**) further indicates the symmetrical nature of this compound (Figure 48). The *meso*-carbons resonate as two peaks at 96.72 and 101.59 ppm, while the internal methyl appears at 32.80 ppm. When TFA was added to the sample, a diprotonated species **99b**H_2^{2+} was formed. The proton NMR spectrum of the dication displayed the *meso*-protons as two 2H singlets at 10.61 and 10.73 ppm, while the internal methyl and NH protons appeared as a 3H singlet at -

5.59 ppm and a 2H broad singlet at -3.52 ppm, respectively. For comparison, the proton NMR spectrum of **99a** in TFA-$CDCl_3$ gave two 2H singlets at 10.69 and 10.70 ppm for the *meso*-protons, while the four internal NH protons appeared as two separate broad 2H singlets at -4.02 and -4.17 ppm. These data indicate that **99a** and **99b** have comparable diatropic properties.

The UV-Vis spectra of *N*-methyl porphyrin **99b** and *N*-unsubstituted porphyrin **99a** were also compared (Figure 49). Bathochromic shifts were observed for the methylated derivative, although overall the spectra were similar. *N*-Methyl porphyrin **99b** displayed a Soret band at 410 nm, while *N*-unsubstituted porphyrin **99a** gave a Soret band at a significantly shorter wavelength of 397 nm. Both displayed four Q bands, although the bands of **99b** are slightly broader and shifted towards the red. The UV-Vis spectra of the free base *N*-methyl porphyrin **99b** and the dication **99b**H_2^{2+} were also compared (Figure 50). Free base **99b** shows a slight shoulder at 379 nm and a strong Soret band at 410 nm, followed by a number of weaker absorptions between 505 and 641 nm. However, dication **99b**H_2^{2+} gave a much stronger Soret band at 404 nm and two Q bands at 551 and 596 nm.

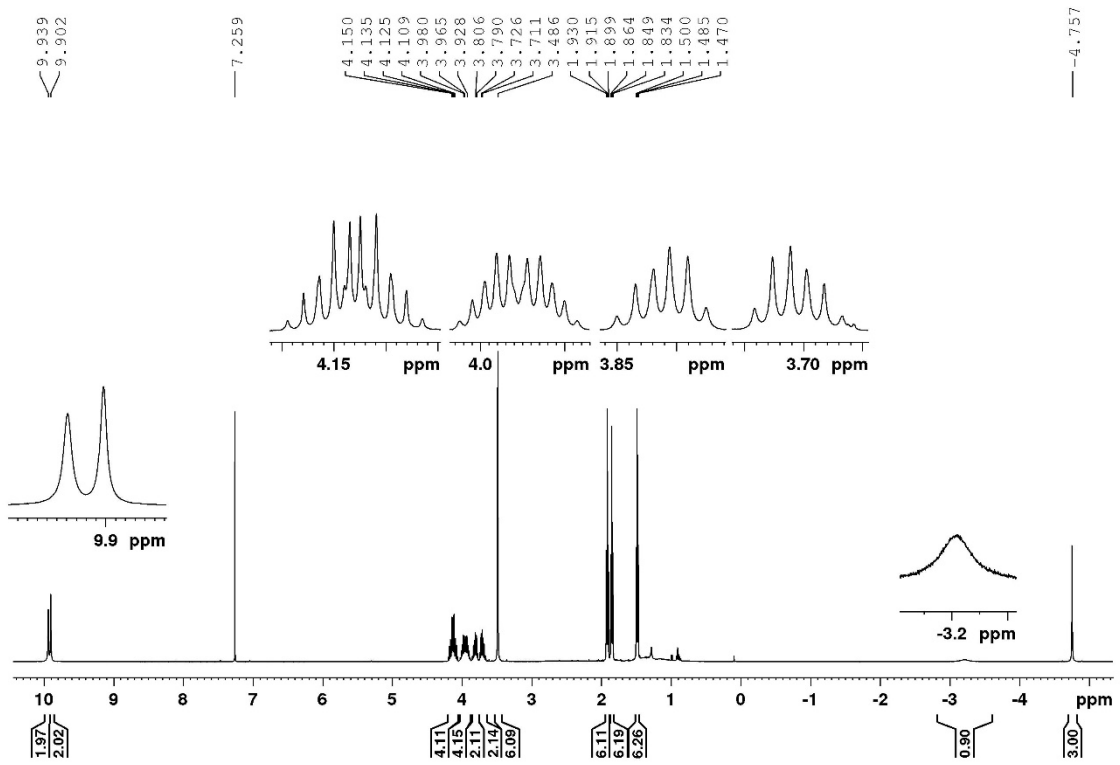

Figure 47. 500 MHz ^{1}H NMR spectrum of *N*-methyl porphyrin **99b** in $CDCl_3$

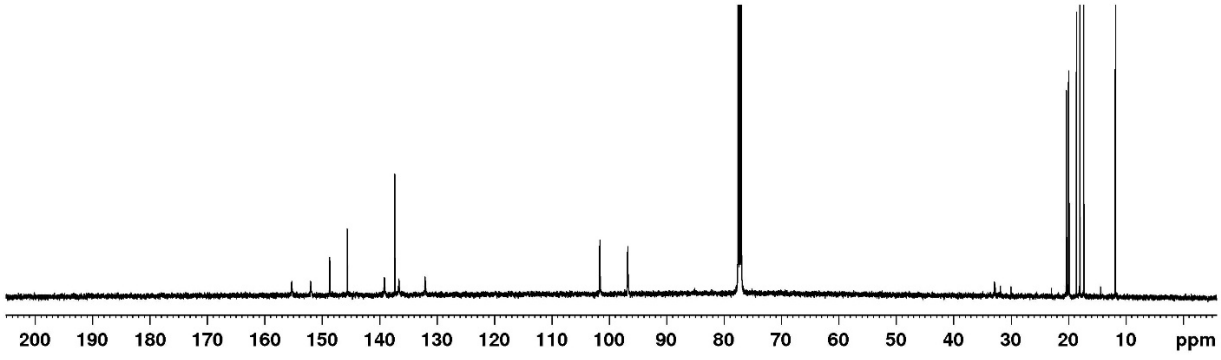

Figure 48. 125 MHz ^{13}C NMR spectrum of *N*-methyl porphyrin **99b** in $CDCl_3$

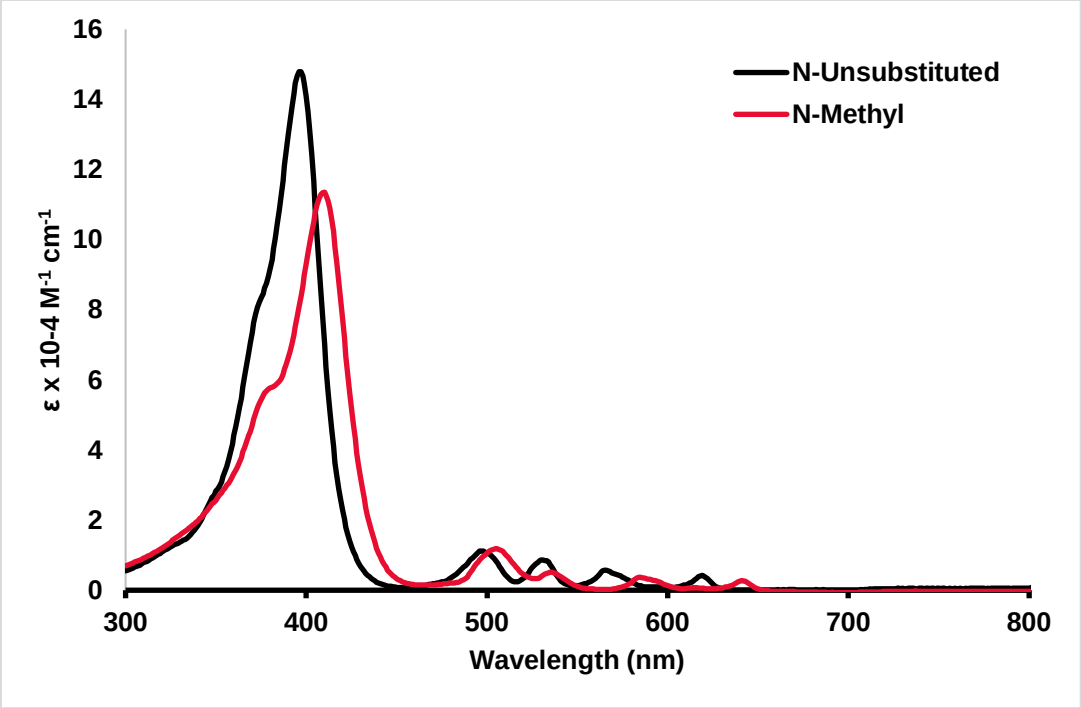

Figure 49. UV-Vis spectra of *N*-methyl porphyrin **99b** (red line) and *N*-unsubstituted porphyrin **99a** (black line)

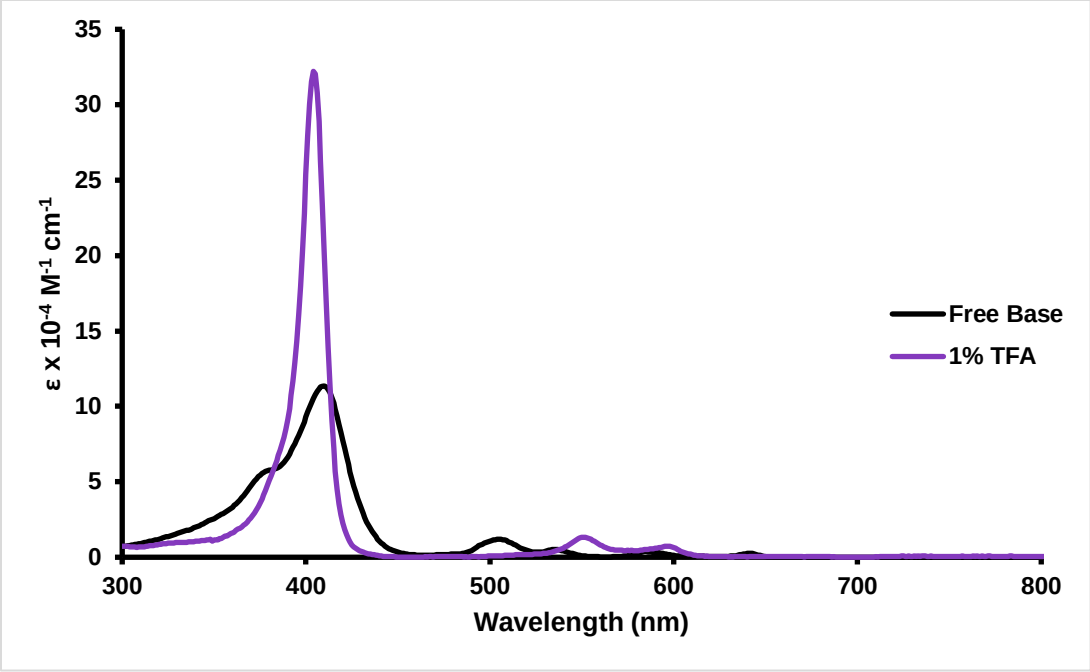

Figure 50. UV-Vis spectra of **99b** in 1% triethylamine-dichloromethane (free base, black line) and 1% TFA-dichloromethane (dication, purple line)

The *N*-methyl derivative **100a** of oxybenziporphyrin **7a** was also synthesized. This compound was formed by reaction of *N*-methyl tripyrrane **54d** in dichloromethane and TFA with dialdehyde **101a** (Scheme 37). Purification on an alumina column, eluting first with dichloromethane and then 50% chloroform-dichloromethane, followed by recrystallization from chloroform-hexanes, gave the pure product in 13% yield.

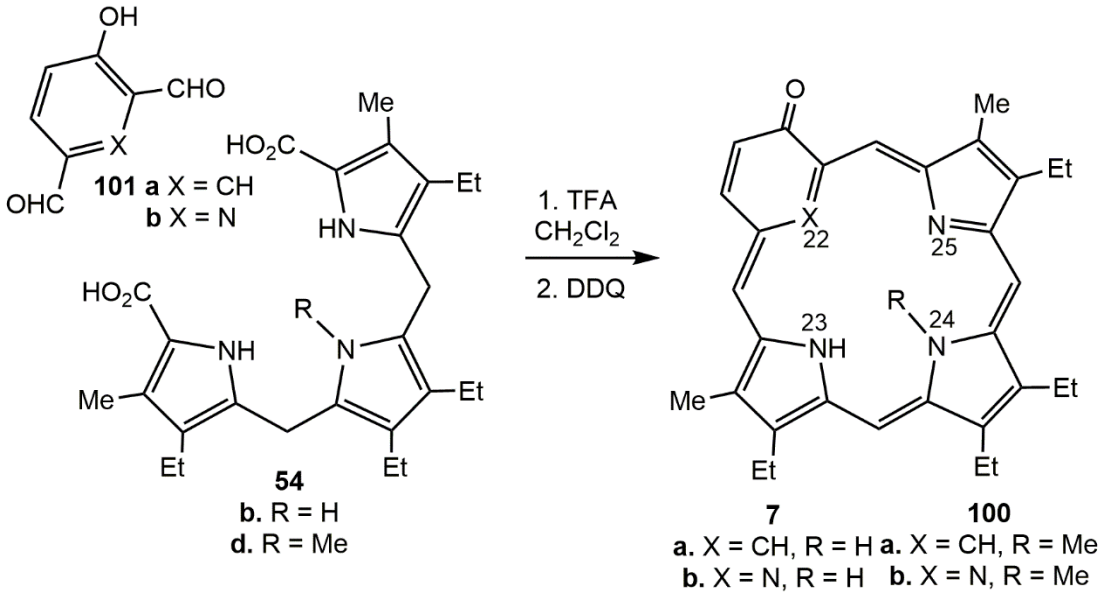

Scheme 37. '3+1' Synthesis of *N*-methylated and *N*-unsubstituted oxybenzi- and oxypyriporphyrins

The proton NMR spectrum of **100a** confirmed the asymmetry of this compound by showing an increased number of peaks for the protons on the structure (Figure 51). The four *meso*-protons present in this molecule correspond to the two 1H singlets at 10.50 and 9.20 ppm, and the 2H singlet at 9.37 ppm. Furthermore, the proton on the β-carbon relative to the carbonyl unit resonates as a doublet of doublets at 8.72 ppm, showing evidence for long-range coupling to the internal CH proton of the six membered ring. Two 3H singlets at 3.33 and 3.43 ppm correspond to the two external methyl substituents, while the internal methyl group resonated as a 3H singlet

at -3.63 ppm and the internal CH was observed at -4.14 ppm as a broad 1H singlet. In comparison, *N*-unsubstituted oxybenziporphyrin **7a** has been reported to show the *meso*-protons as four separate 1H singlets between 8.85 and 10.29 ppm, the internal CH as a weakly coupled doublet (J= 2 Hz) at -7.3 ppm, and the internal NH protons as a broad 2H peak near -4 ppm.[23] The shifts seen in the upfield region for the *N*-methyl derivative **100a** are slightly weaker than those seen in its *N*-unsubstituted counterpart **7a**, but the downfield regions for these porphyrinoids are very similar. The carbon-13 NMR spectrum of **100a** (Figure 52) shows the carbonyl carbon at 189.33 ppm, while the *meso*-carbons appear at 96.7, 99.0, 111.2 and 118.9 ppm, and the internal methyl was identified at 33.3 ppm. The carbon-13 NMR spectrum of *N*-unsubstituted oxybenziporphyrin **7a** showed the carbon of the carbonyl present on the six-membered ring at 187.94 ppm and the *meso*-carbons were located at 93.3, 94.9, 105.7 and 111.1 ppm.[23] *N*-methylated oxybenziporphyrin **100a** appears to possess a similar aromatic ring current to **7a**, and potential distortion of the macrocycle due to the presence of the *N*-methyl group does not appear to significantly affect macrocyclic diatropicity.

However, the UV-Vis spectrum of *N*-unsubstituted oxybenziporphyrin **7a** is significantly different from its *N*-methyl derivative **100a** (Figure 53). These closely related carbaporphyrinoids possess the same chromophore, but the UV-Vis spectrum for **100a** is much weaker and broader, as well as slightly shifted towards longer wavelengths, compared to its *N*-unsubstituted counterpart. A weak absorption is seen at 331 nm in **100a**, while two absorptions at 313 and 335 nm are identified for **7a**. The Soret band for **100a** is observed at 441 nm with another band shortly after at 473 nm. The same pattern is seen in **7a** but these two bands are much stronger and are observed at 426 and 452 nm. Furthermore, the four Q bands for **100a** are much broader and less distinguishable than those of **7a**. The strongest absorption within the Q bands is seen at 588 nm

for **7a** but at a much larger wavelength of 621 nm for the *N*-methyl derivative **100a**. Addition of TFA to **100a** results in the formation of a dicationic species **100a**H_2^{2+} that gives shifts in the absorption values compared to that of free base **100a** (Figure 54). The Soret band for the free base is observed at 441 nm with a second absorption close after at 473 nm, while the dication gives a single Soret band at 433 nm that is slightly weaker than that for the free base. Furthermore, the free base shows two Q bands centered at 621 and 724 nm, while the spectrum for the dication produced broader, less distinguishable Q bands between 550 and 770 nm. The IR spectrum for the *N*-methyloxybenziporphyrin **100a** gave a strong peak at 1618 cm^{-1} for the carbonyl stretching frequency (Figure 55), which is similar to the frequency of 1624 cm^{-1} that was observed for **7a**.[23]

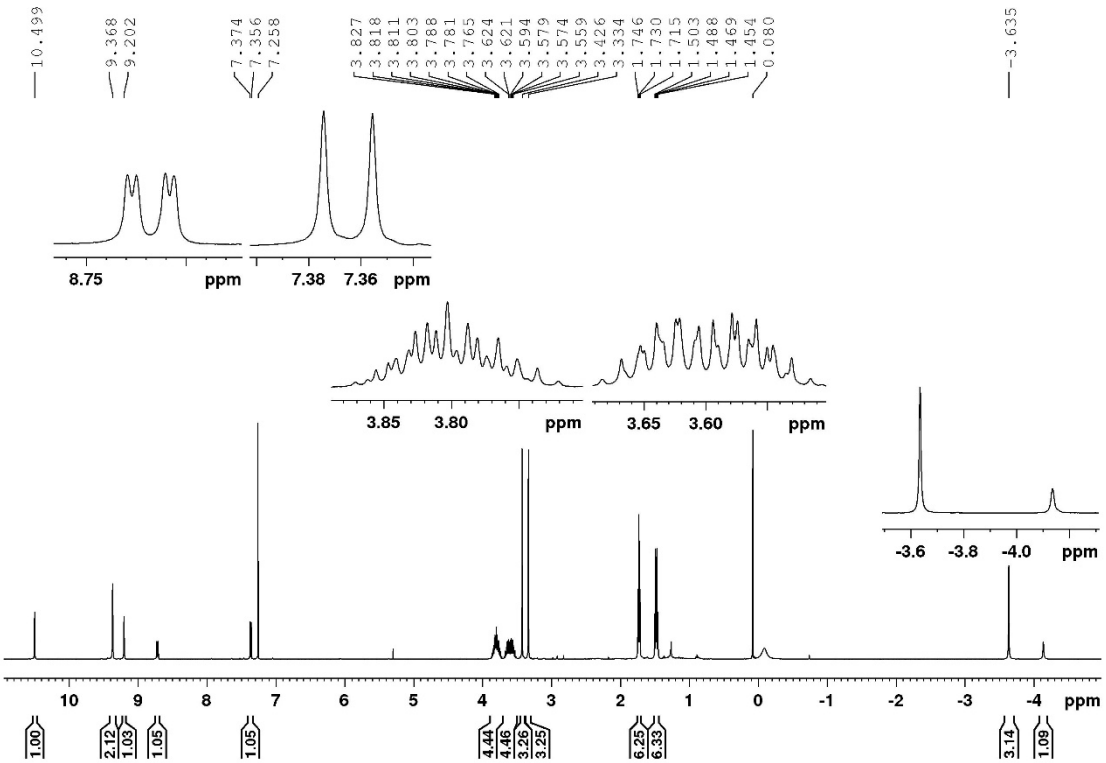

Figure 51. 500 MHz ^{1}H NMR spectrum of *N*-methyloxybenziporphyrin **100a** in $CDCl_3$

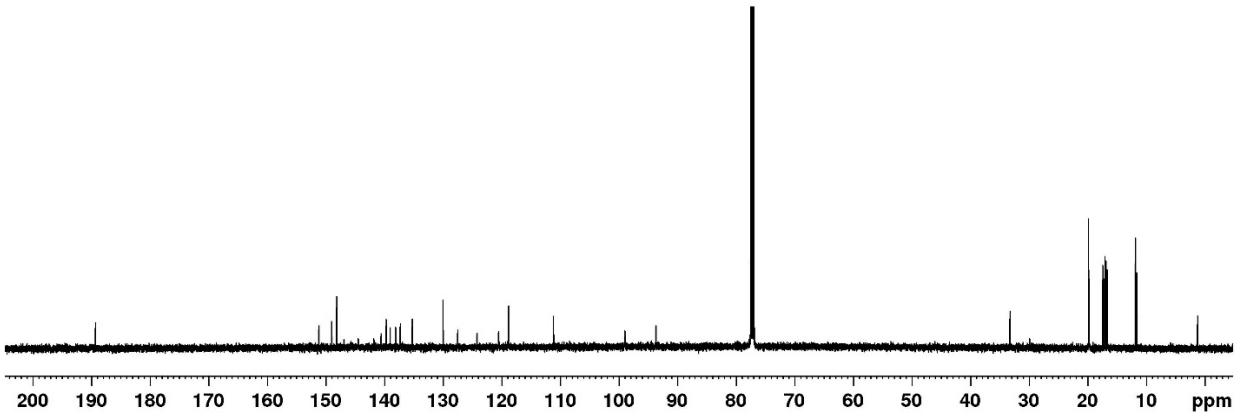

Figure 52. 125 MHz ^{13}C NMR spectrum of *N*-methyloxybenziporphyrin **100a** in $CDCl_3$

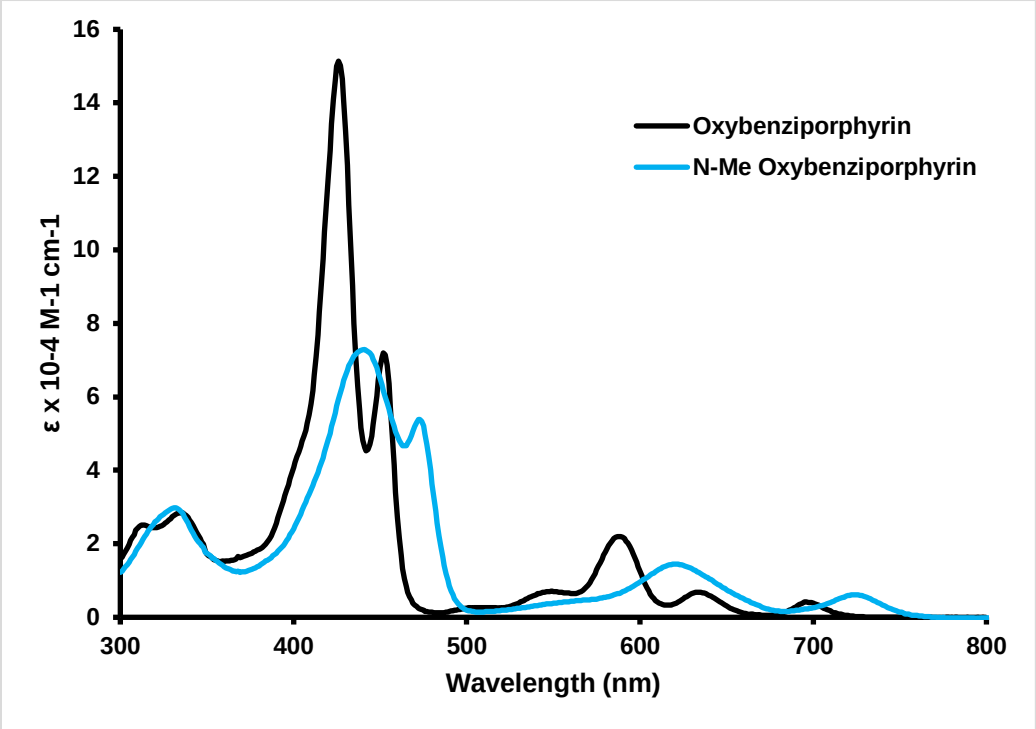

Figure 53. UV-Vis spectra of *N*-methyloxybenziporphyrin **100a** (blue line) and *N*-unsubstituted oxybenziporphyrin **7a** (black line)

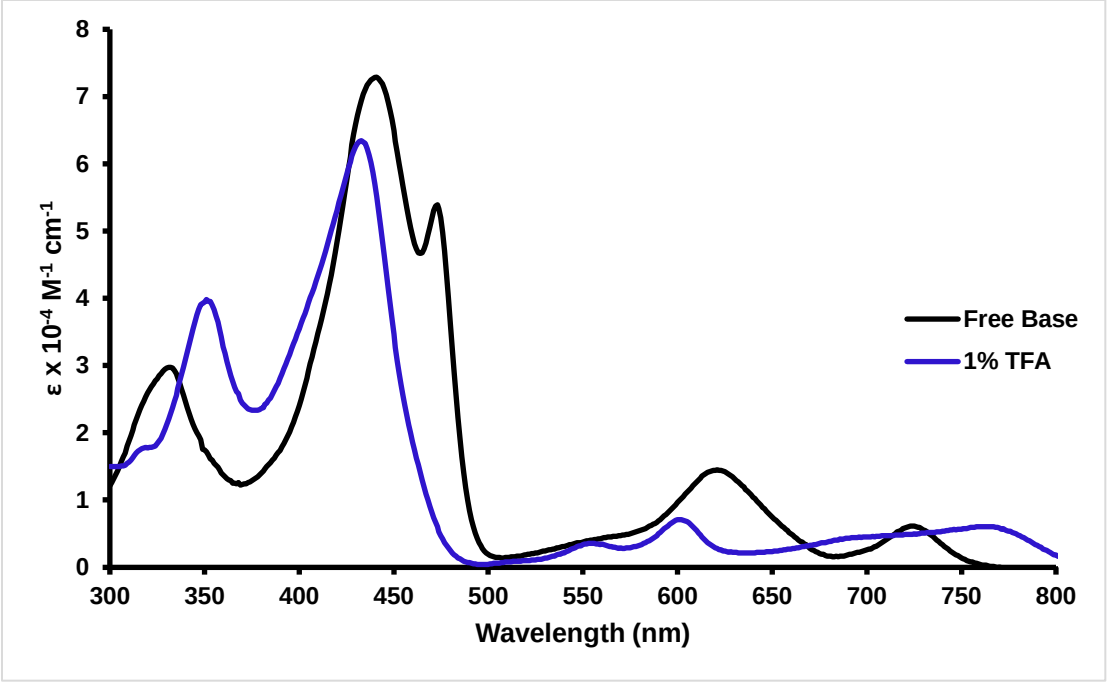

Figure 54. UV-Vis spectra of **100a** in 1% triethylamine-dichloromethane (free base, black line) and 1% TFA-dichloromethane (dication, blue line)

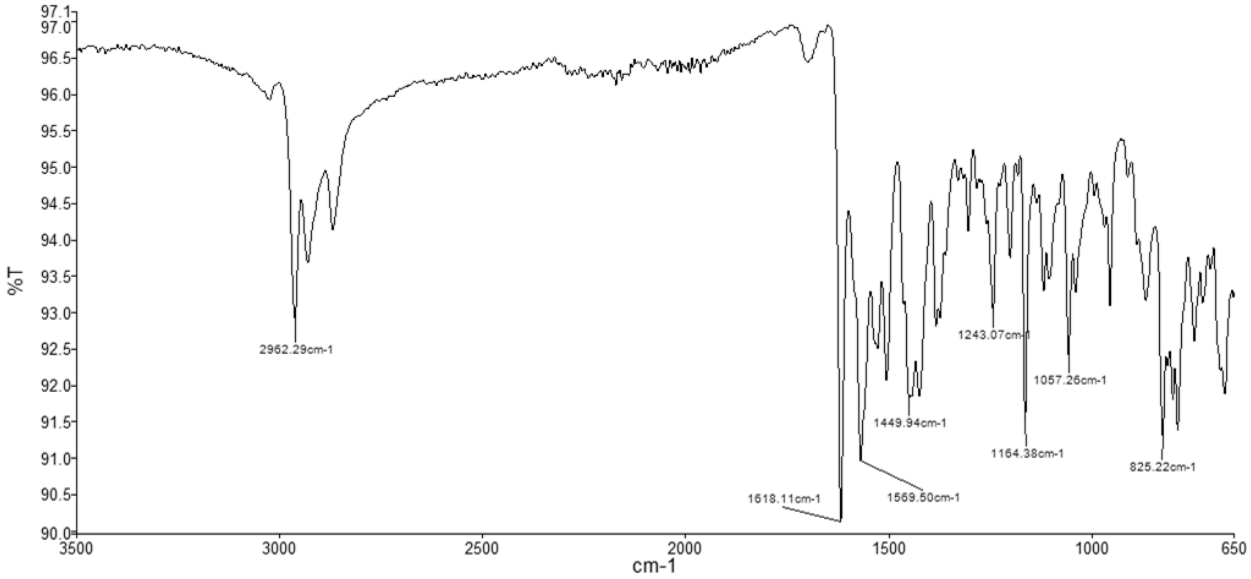

Figure 55. IR spectrum of *N*-methyloxybenziporphyrin **100a**

N-methyloxybenziporphyrin **100a** was reacted with palladium(II) acetate in refluxing acetonitrile to give the related palladium(II) complex **102** (Scheme 38), which was purified by column chromatography on grade 3 alumina eluting with chloroform. Following recrystallization from chloroform-hexanes, the pure metalated product **102** was isolated as green crystals in 36.4% yield. The proton NMR spectrum of the complex shows very similar shifts to the proton NMR spectrum of the free base compound **100a** (Figure 56). The *meso*-protons resonated as four 1H singlets at 9.22, 9.46, 9.52 and 10.58 ppm, while the external methyl substituents were observed as two 3H singlets at 3.27 and 3.32 ppm. The internal methyl was the only upfield shifted peak and was observed as a 3H singlet at -2.36 ppm. The carbon-13 NMR spectrum of **102** displayed the *meso*-carbons at 98.7, 100.2, 123.6 and 125.8 ppm, while the internal methyl and the carbonyl carbon were observed at 46.3 ppm and 190.2 ppm, respectively (Figure 57). The proton NMR resonances of **102** are shifted slightly further downfield compared to those for **100a**, indicating that a slightly stronger diatropic ring current is present within the metalated complex **102**. The IR spectrum for palladium(II) complex **102** gave a strong absorption at 1555 cm^{-1} for the carbonyl stretching frequency (Figure 58).

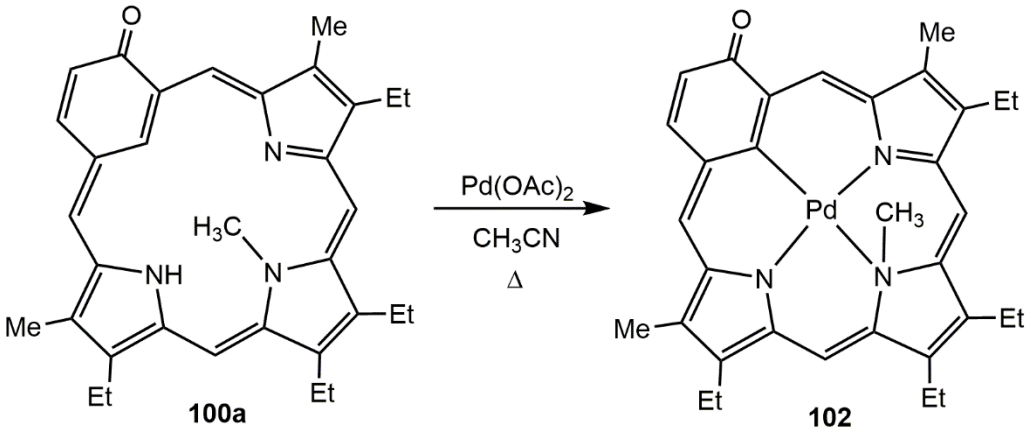

Scheme 38. Metalation of *N*-methyloxybenziporphyrin **100a** with palladium(II) acetate

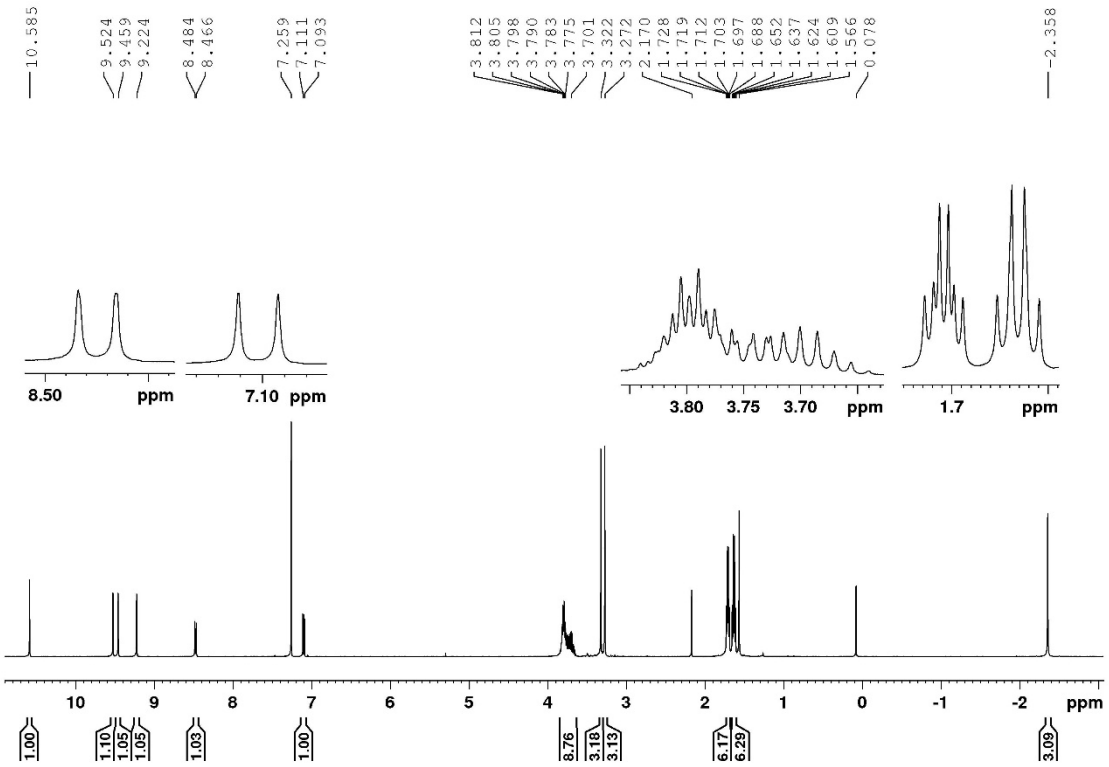

Figure 56. 500 MHz ^{1}H NMR spectrum of palladium(II) oxybenziporphyrin complex **102** in $CDCl_3$

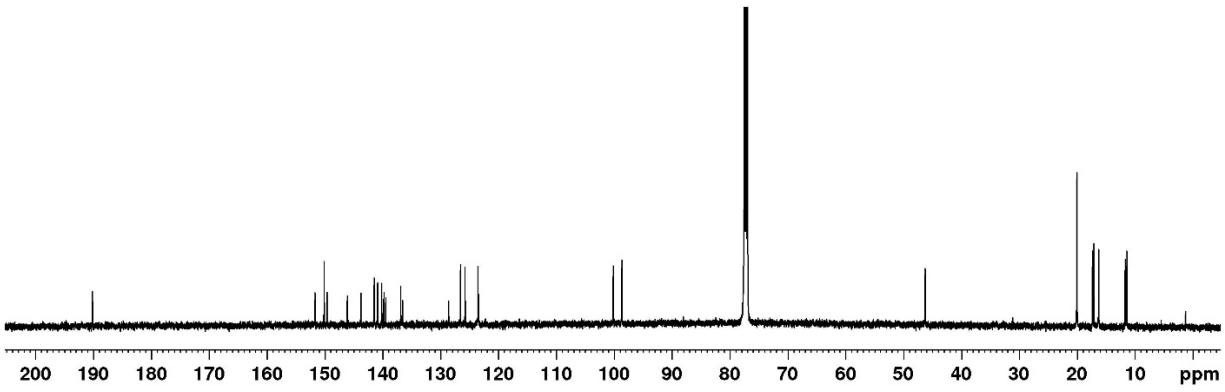

Figure 57. 125 MHz ^{13}C NMR spectrum of palladium(II) oxybenziporphyrin complex **102** in $CDCl_3$

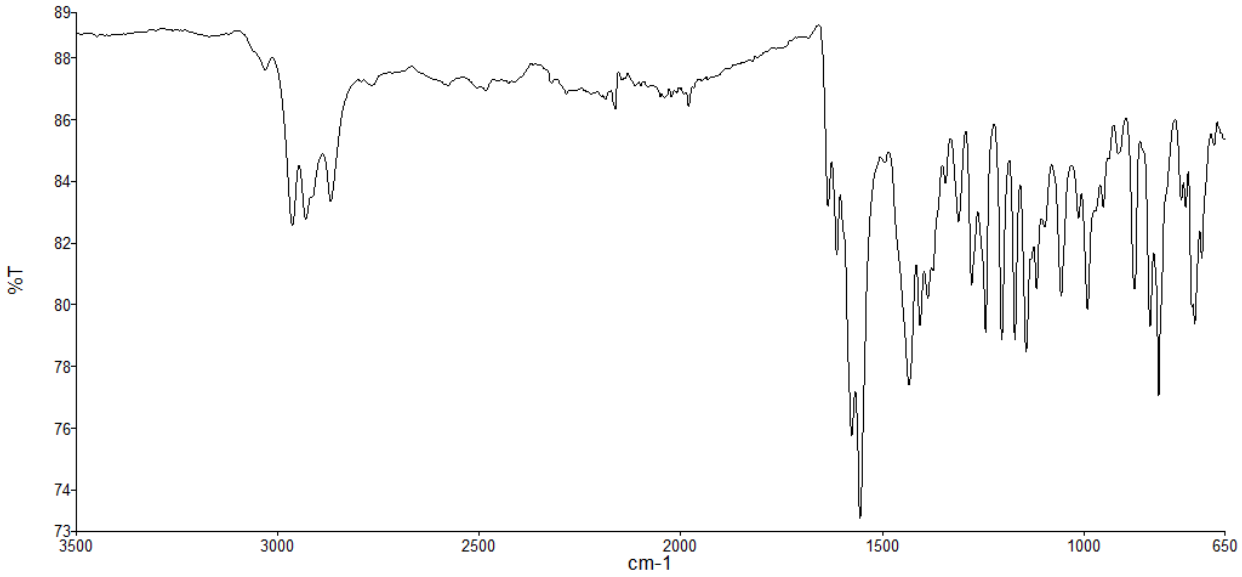

Figure 58. IR spectrum of palladium(II) oxybenziporphyrin complex **102**

N-methyloxypyriporphyrin **100b** was synthesized by reaction of *N*-methyl tripyrrane **54d** with dialdehyde **101b** in dichloromethane and TFA (Scheme 37, page 116). The crude material was chromatographed with neutral alumina, eluting with chloroform. The compound did not recrystallize well, as it was very soluble in organic solvents, and was therefore collected in 35.8% yield and characterized without further purification. The proton NMR spectrum of this compound suggests it is fairly aromatic, due to the internal *N*-methyl and NH protons appearing as a 3H singlet and 1H broad singlet at -4.20 and -1.26 ppm, respectively (Figure 59). The four *meso*-protons were observed as 1H singlets between 9.64 and 10.89 ppm and the external methyl groups were identified as two 3H singlets at downfield values of 3.44 and 3.58 ppm. For comparison, the proton NMR spectrum of *N*-unsubstituted oxypyriporphyrin[77] **7b** has previously been reported to display the *meso*-protons as four 1H singlets between 9.48 and 10.96 ppm and the external methyl groups as two 3H singlets at 4.01 and 4.04 ppm. Two broad singlets near -3.6 ppm were also observed for the NH protons, since there are two internal protons compared to the single proton

within the cavity of **100b**. The carbon-13 spectrum of **100b** (Figure 60) showed the carbonyl carbon resonating at 185.53 ppm and the *meso*-carbons at 96.8, 97.3, 113.3 and 119.8 ppm, while the carbonyl carbon of *N*-unsubstituted oxypyriporphyrin **7b** resonated at 184.9 ppm and the four *meso*-carbons were observed between 96 and 108 ppm. The IR spectrum for *N*-methyloxypyriporphyrin **100b** (Figure 61) shows a strong peak at 1626 cm^{-1}, which is similar to the peak observed at 1629 cm^{-1} for *N*-unsubstituted oxypyriporphyrin **7b**.

Although the NMR spectrum of **100b** are not significantly altered by the presence of an internal methyl group, comparison of the UV-Vis spectra of *N*-methyloxypyriporphyrin **100b** and the *N*-unsubstituted oxypyriporphyrin **7b** showed drastic differences when the internal methyl group was present (Figure 62). There are similar bathochromic shifts in the spectrum for **100b** to those seen for all of the methylated derivatives discussed above. However, much more significantly, the absorptions for **100b** were much weaker and broader than those observed for **7b**. These observations suggest that the internal methyl group induces a significant amount of distortion to the chromophore. The Soret band for the *N*-unsubstituted system was observed at 420 nm, while the Soret band for the *N*-methyl derivative was a broad band centered on 434 nm. When TFA was added to **100b** a dicationic species was formed and the peaks in the resulting UV-Vis spectrum (Figure 63) were seen to sharpen and increase in intensity, with the Soret band centered on 426 nm.

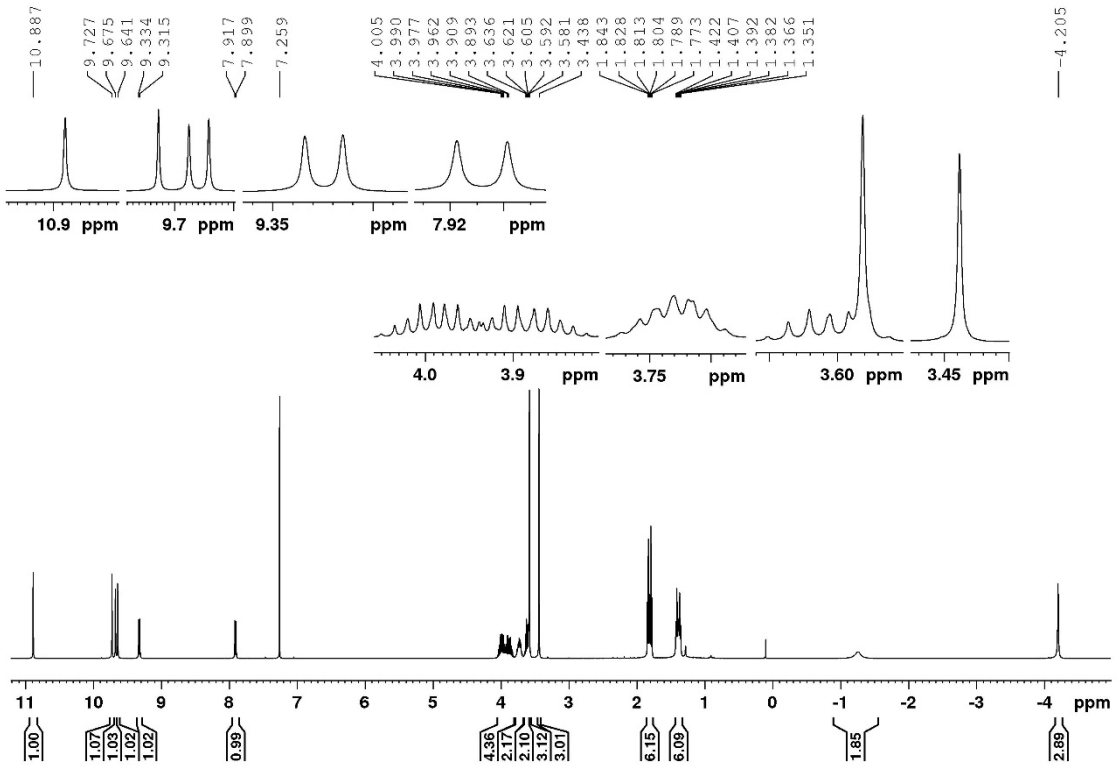

Figure 59. 500 MHz ^{1}H NMR spectrum of *N*-methyloxypyriporphyrin **100b** in $CDCl_3$

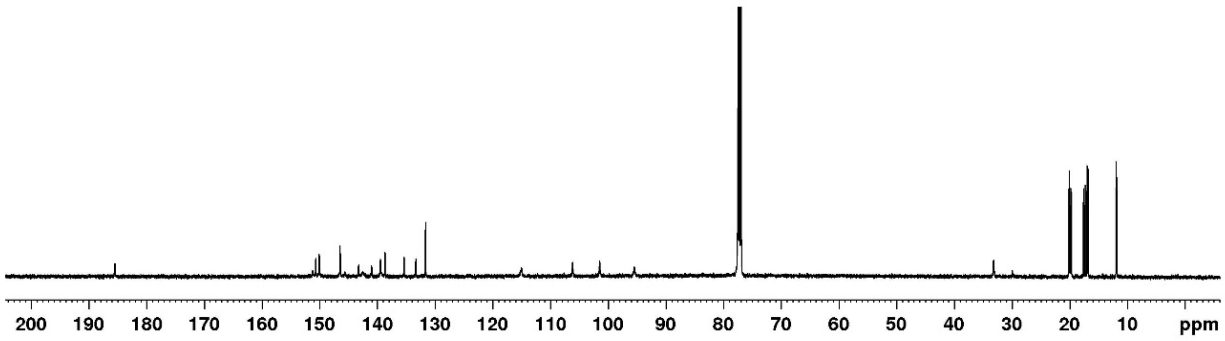

Figure 60. 125 MHz ^{13}C NMR spectrum of *N*-methyloxypyriporphyrin **100b** in $CDCl_3$

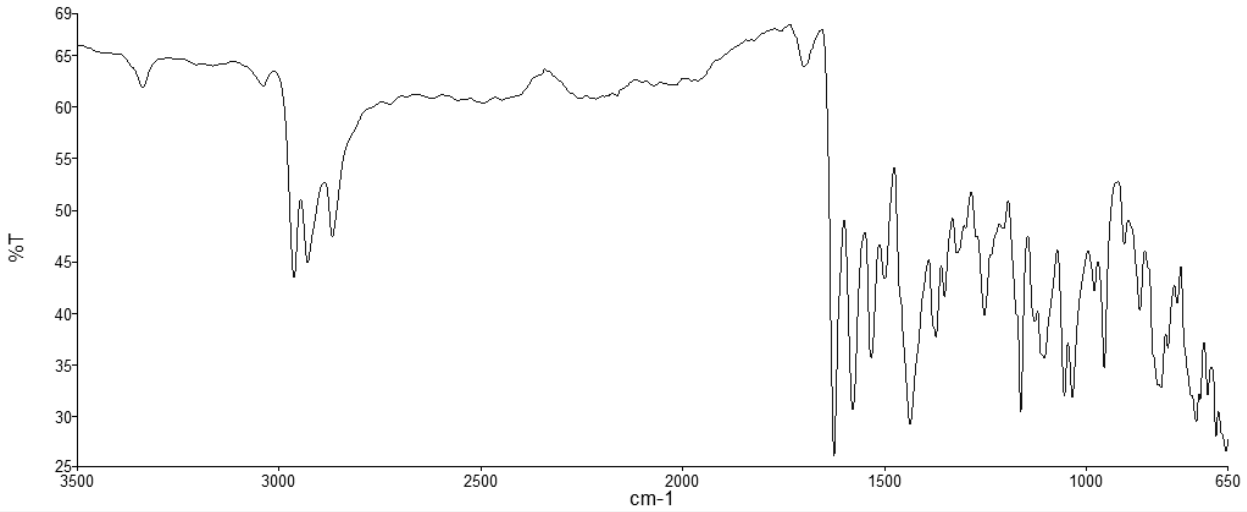

Figure 61. IR spectrum of *N*-methyloxypyriporphyrin **100b**

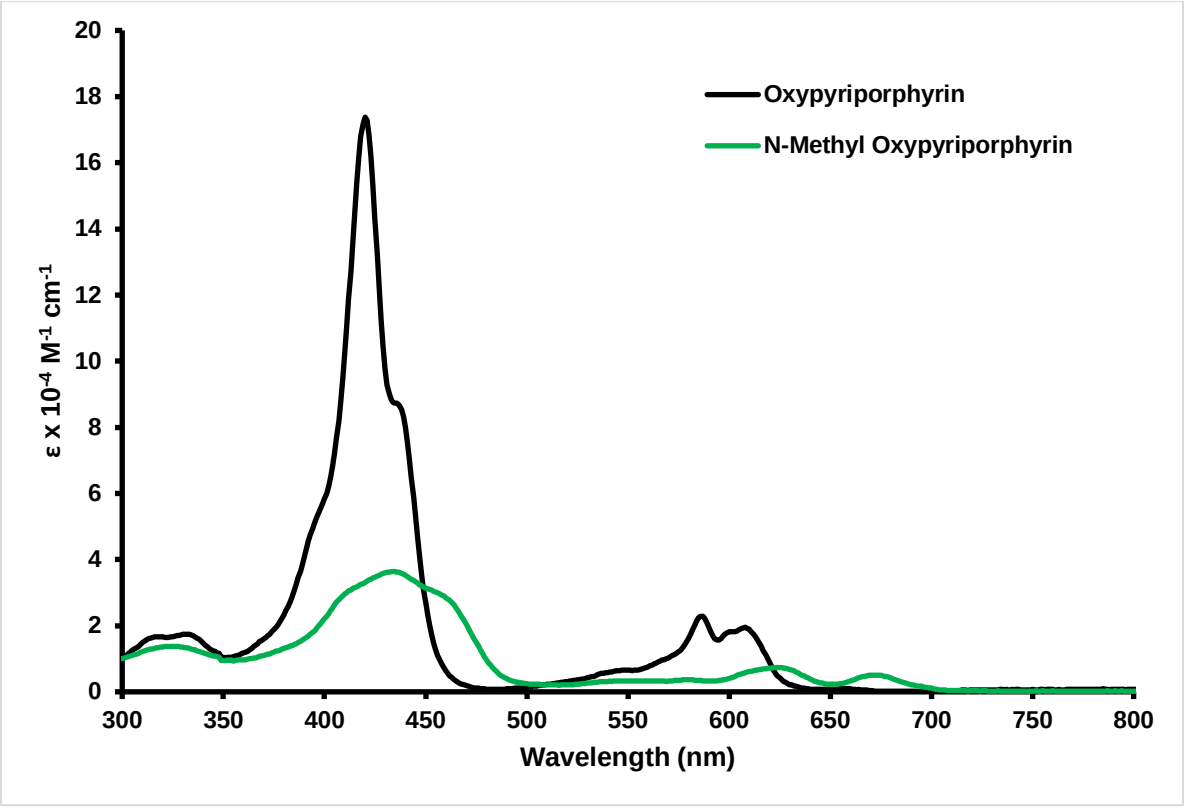

Figure 62. UV-Vis spectra of *N*-methyloxypyriporphyrin **100b** (green line) and the *N*-unsubstituted oxypyriporphyrin **7b** (black line)

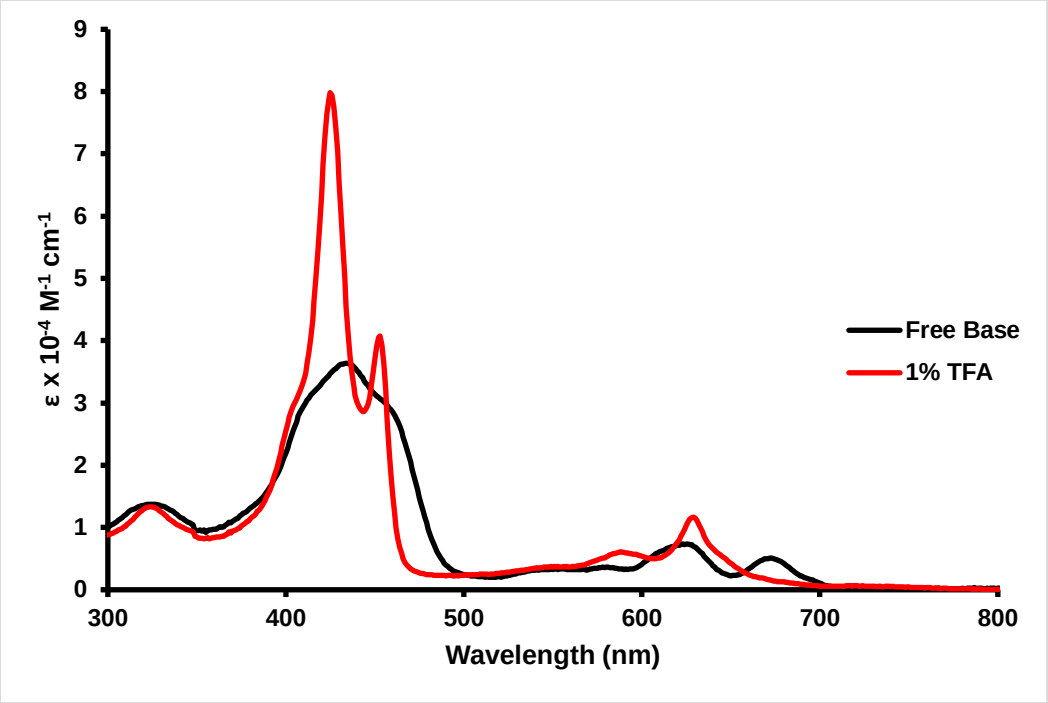

Figure 63. UV-Vis spectra of **100b** in 1% triethylamine-dichloromethane (free base, black line) and 1% TFA-dichloromethane (dication, green line)

An internally methylated azuliporphyrin **103b**H_2^{2+} was also synthesized (Scheme 39). It was found that **103b**H_2^{2+} is only stable when protonated, residing as a dicationic species. In order to optimized yields, *N*-methyl tripyrrane **54d** was condensed overnight with azulene dialdehyde **104** in dichloromethane in the presence of TFA under dilute conditions. Oxidation by ferric chloride, followed by a wash with 10% aqueous hydrochloric acid, gave the crude dihydrochloride. Recrystallization twice from chloroform-hexanes gave **103b**H_2^{2+} in 78% yield.

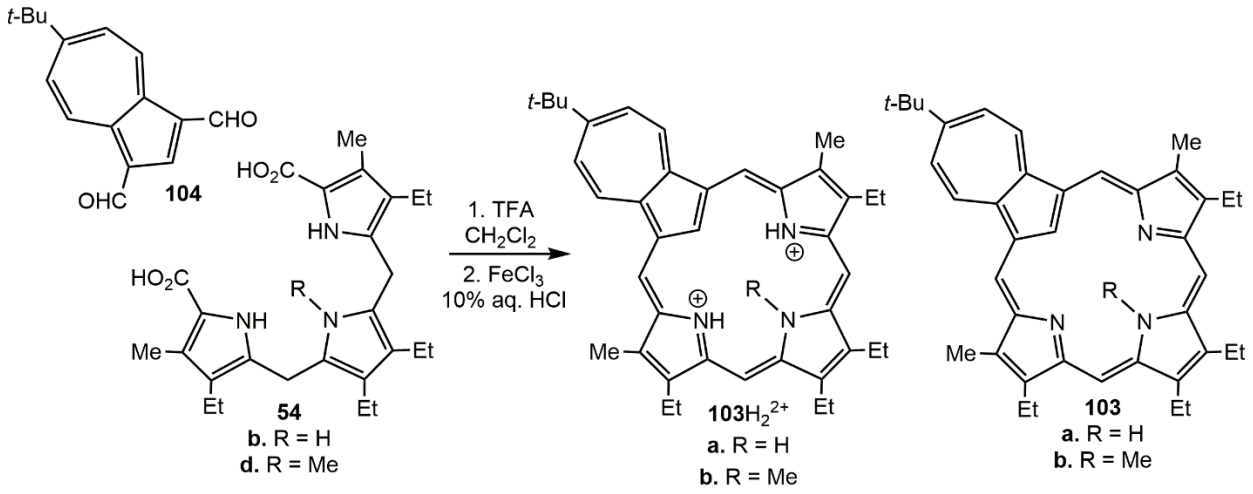

Scheme 39. Synthesis of *N*-methylazuliporphyrin **103b**H_2^{2+}

The proton NMR spectrum for **103b**H_2^{2+} demonstrated that the macrocycle posseses a plane of symmetry. This is evident in part from the two 2H singlets at 9.66 and 10.72 ppm for the *meso*-protons and the two 2H doublets at 8.89 and 10.39 ppm for the four external azulene protons (Figure 64). The external methyl groups were also observed as a 6H singlet at 3.46 ppm. These downfield shifts indicate that **103b**H_2^{2+} is a highly aromatic species. The internal methyl resonates as a 3H singlet at -3.36 ppm, while the internal CH and NH protons appear as a 1H singlet at -3.38 ppm and a 2H broad singlet at -0.36 ppm, respectively, again confirming the aromatic nature of this system. The proton NMR spectrum reported for a *N*-unsubstituted azuliporphyrin dication **103a**H_2^{2+} gave similar chemical shifts.[81] In that case, the *meso*-protons were reported as two 2H singlets at 9.93 and 10.39 ppm, while the external methyl groups were observed as a 6H singlet at 3.47 ppm. Furthermore, the internal peaks of the non-methylated counterpart were similar to those of the *N*-methyl derivative, where the internal CH is observed as a 1H singlet at -3.19 ppm, and the internal NH protons resonate as broad 1H and 2H singlets at -2.0 and -0.25 ppm, respectively. This data indicates that the methyl group does not undermine the aromaticity of the *tert*-butyl

azuliporphyrin dication. However, while azuliporphyrin **103a** lacking an internal methyl could be isolated as a free base and characterized, this was not possible for **103b**. Further evidence of the symmetry present in **103b**H_2^{2+} is provided by the carbon-13 NMR spectrum (Figure 65). The four *meso*-carbons gave two peaks at 97.2 and 111.0 ppm, while the internal methyl carbon and the quartnerary *tert*-butyl carbon resonated at 32.3 and 40.8 ppm, respectively. The three carbons of the methyl groups on the *tert*-butyl substituent appeared at 31.5 ppm.

The UV-Vis data for **103b** were obtained for the free base and the dication, and the free base spectrum in 1% triethylamine-dichloromethane was compared to the one previously reported for the *N*-unsubstituted counterpart **103a** (Figure 66). Overall, this data shows bathochromic shifts in the methylated derivative compared to its non-methylated counterpart. Each spectrum contains multiple bands, the strongest for **103b** appearing at 363 nm, while the strongest band for **103a** is observed at a slightly shorter wavelength of 358 nm. These results indicate that the presence of an internal methyl substituent does alter the *tert*-butylazuliporphyrin chromophore in a similar fashion to the other methylated porphyrinoids described above, and the effects are nowhere near as drastic as those seen for oxybenzi- and oxypyriporphyrins. The UV-Vis spectra of the *N*-methyl derivative in 1% triethylamine and 1% trifluoroacetic acid were also contrasted (Figure 67). These results show that the spectrum of the protonated species possesses stronger and sharper peaks than the spectrum of the free base, demonstrating that protonation considerably alters the azuliporphyrin chromophore. The protonated form shows a strong absorbance at 370 nm, followed by a Soret band at 468 nm. A third reasonably strong band is also seen at 647 nm. In contrast, the free base shows several mid-level absorptions between 363 and 482 nm, followed by a very broad, weaker band centered at 669 nm.

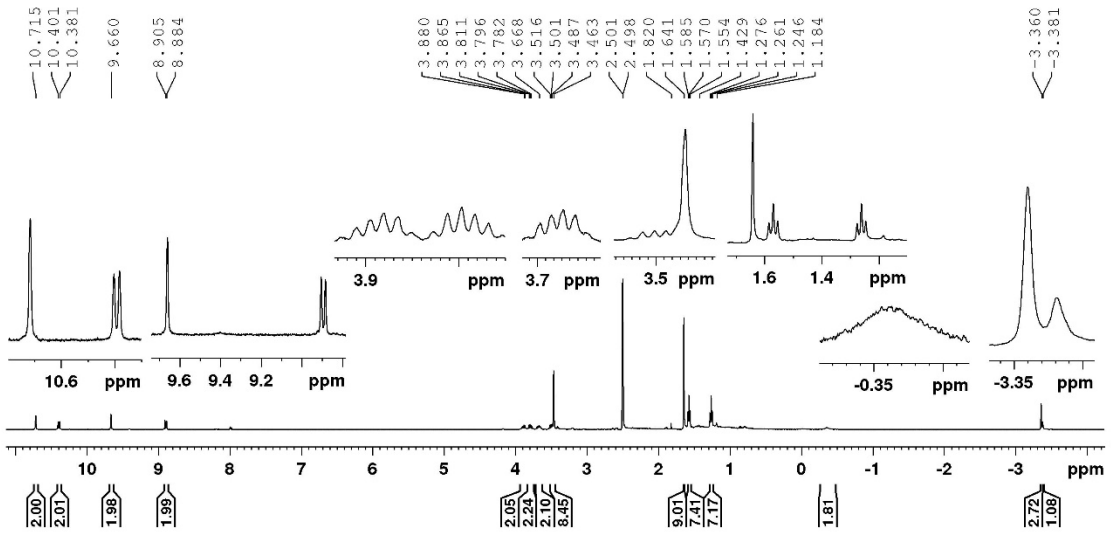

Figure 64. 500 MHz ^{1}H NMR spectrum of *tert*-butyl azuliporphyrin **103b**H_2^{2+} in TFA-d_6-DMSO

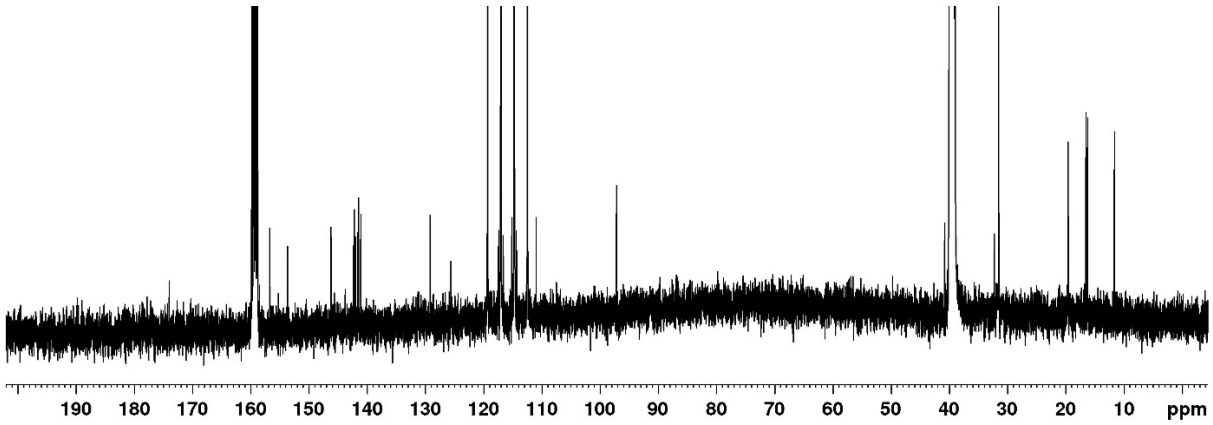

Figure 65. 125 MHz ^{13}C NMR spectrum of *tert*-butyl azuliporphyrin **103b**H_2^{2+} in TFA-d_6-DMSO

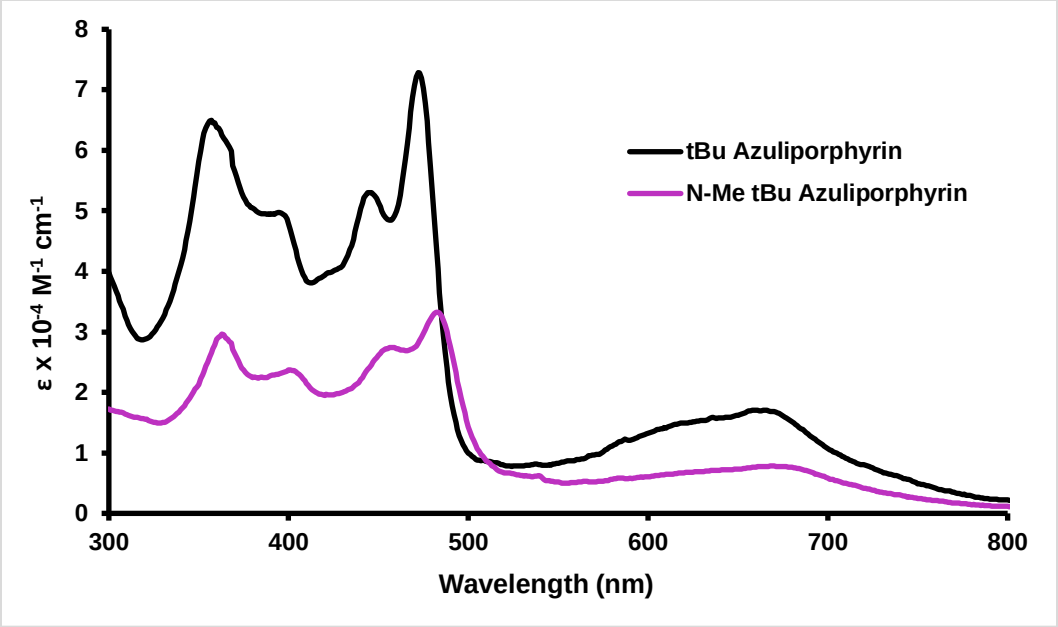

Figure 66. UV-Vis spectra of **103a** in 1% triethylamine-dichloromethane (free base, black line) and **103b** in 1% triethylamine-dichloromethane (free base, purple line).

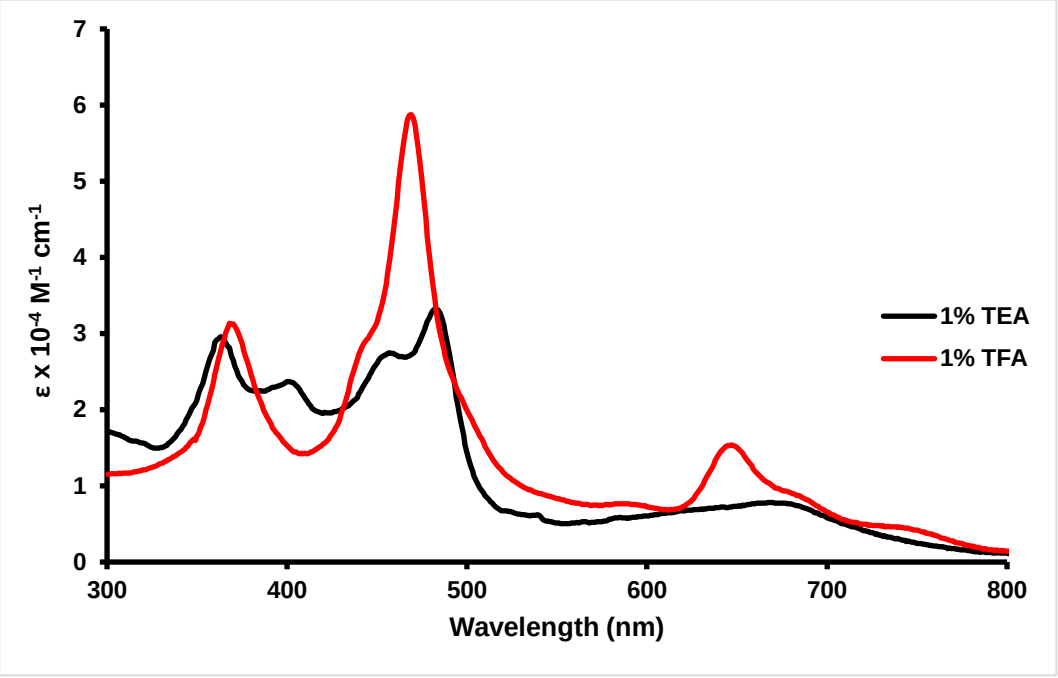

Figure 67. UV-Vis spectra of **103b** in 1% triethylamine-dichloromethane (free base, black line) and in 1% TFA-dichloromethane (dication, red line).

Conclusion

By comparing a series of porphyrin analogues with their *N*-methylated derivatives, it has been found that the introduction of an internal methyl group significantly affects the porphyrinoid chromophore, which consequently alters some of the electronic properties of these macrocycles. These effects are primarily evident in the UV-Vis spectra, where bathochromic shifts and peak broadening are observed for each of the reported *N*-methyl porphyrinoid systems. Other spectroscopic properties are not as clearly affected by the internal substituent, and only slight shifts are seen in the NMR spectra of the *N*-methylated compounds. This series of macrocycles also demonstrates that the versatile '3+1' method can successfully introduce an internal substituent into a number of different porphyrin analogues. Furthermore, the introduction of a *N*-methyl group can alter the coordination chemistry of these structures, and this was demonstrated by the formation of a palladium(II) *N*-methyloxybenziporphyrin. In this case, not only does the internal substituent not inhibit metal coordination, it also switches the carbaporphyrinoid cavity from being a trianionic ligand to a dianionic ligand.

Experimental:

Melting points are uncorrected. NMR spectra were recorded using a 400 or 500 MHz NMR spectrometer and were run at 302 K unless otherwise indicated. ^{1}H NMR values are reported as chemical shifts δ, relative integral, multiplicity (s, singlet; d, doublet; t, triplet; q, quartet; m, multiplet; br, broad peak) and coupling constant (*J*). Chemical shifts are reported in parts per million (ppm) relative to $CDCl_3$ (^{1}H residual $CHCl_3$ singlet δ 7.26, ^{13}C $CDCl_3$ triplet δ 77.23) or d_6-DMSO (^{1}H residual d_5-DMSO pentet δ 2.49, ^{13}C d_6-DMSO septet δ 39.7) and coupling constants were taken directly from the spectra. NMR assignments were made with the aid of ^{1}H-^{1}H COSY, HSQC, DEPT-135 and nOe difference proton NMR spectroscopy. 2D experiments were performed using standard software. High-resolution mass spectra (HRMS) were carried out using a double focusing magnetic sector instrument.

8,12,13,17-Tetraethyl-7,18-dimethyl-21-oxaporphyrin (**96a**). Tripyrrane dicarboxylic acid **54b** (100 mg, 0.221 mmol) was dissolved in TFA (1 mL) and stirred under nitrogen for 2 minutes. The mixture was diluted with dichloromethane (99 mL), followed by the addition of 2,5-furandicarboxaldehyde (28.2 mg, 0.227 mmol), and was left to stir overnight under nitrogen. The solution was washed with ferric chloride (0.1%, 200 mL), water and then aqueous sodium bicarbonate solution. The solvent was removed under reduced pressure and the crude material chromatographed on neutral grade 3 alumina, eluting with chloroform. A bright red/pink band was collected and recrystallized from chloroform-hexanes to give **96a** (66.0 mg, 0.133 mmol, 66%) as dark purple/blue crystals, mp > 300 °C. UV-Vis (1% Et_3N-dichloromethane): λ_{max}/nm (log ε) 371 (4.93), 392, (4.92), 489 (4.11), 520 (3.88), 585 (3.54), 643 (3.26). UV-Vis (1% TFA-dichloromethane): λ_{max}/nm (log ε) 394 (5.33), 523 (3.90), 551 (4.04), 599 (3.40). ^{1}H NMR (500 MHz, TFA-$CDCl_3$): δ -4.53 (3H, br s, 2 x NH), 1.85-1.91 (12H, m, 4 x CH_2CH_3, overlapping

triplets), 3.83 (6H, s, 7,18-Me), 4.26-4.33 (8H, m, 4 x CH_2CH$_3$), 10.61 (2H, s), 11.04 (2H, s), 11.18 (2H, s). ^{13}C NMR (125 MHz, TFA-CDCl$_3$): δ 11.89, 16.82, 17.63, 20.33, 20.50, 100.42, 101.30, 133.92, 140.92, 141.48, 142.68, 143.39, 146.30, 146.32, 147.39, 147.42, 155.31. HR-MS (ESI) m/z: [M + H]+ calcd for $C_{30}H_{34}N_3O$ 452.2702, found 452.2696.

8,12,13,17-Tetraethyl-7,18,23-trimethyl-21-oxaporphyrin (**96b**). *N*-methyl tripyrrane **54d** (200 mg, 0.428 mmol) was dissolved in TFA (2 mL) and stirred under nitrogen for 2 minutes. The solution was diluted with dichloromethane (38 mL), followed by immediate addition of 2,5-furandicarboxaldehyde (54.5 mg, 0.441 mmol), and left to stir for another 2 hours under nitrogen. The mixture was neutralized by the dropwise addition of triethylamine, DDQ (100 mg) was added, and the solution stirred for 1 hour. The mixture was washed with water and then with aqueous sodium bicarbonate solution, and the solvent removed under reduced pressure. The crude material was chromatographed twice on neutral grade 3 alumina, eluting with chloroform, and a dark purple band was collected each time. Recrystallization from chloroform-hexanes gave pure 23-methyl-21-oxaporphyrin (84.2 mg, 0.181 mmol, 42%) as dark purple/blue crystals, mp > 300 °C. UV-Vis (1% Et$_3$N-dichloromethane): λ_{max}/nm (log ε) 378 (4.74), 407 (4.81), 501 (4.09), 527 (3.69), 604 (3.45), 638 (3.08), 664 (3.23). UV-Vis (1% TFA-dichloromethane): λ_{max}/nm (log ε) 396 (5.26), 528 (3.83), 562 (3.97), 612 (3.58). UV-Vis (5% TFA-dichloromethane): λ_{max}/nm (log ε) 395 (5.27), 528 (3.86), 561 (3.99), 611 (3.64), 730 (3.29). ^{1}H NMR (500 MHz, CDCl$_3$): δ -5.21 (3H, s, N-Me), 1.52 (6H, t, $^3J_{HH}$ = 7.7 Hz, 12,13-CH$_2$CH_3), 1.87 (6H, t, $^3J_{HH}$ = 7.7 Hz, 8,17-CH$_2$CH_3), 3.70 (6H, s, 7,18-Me), 3.77-3.84 (2H, m), 3.88-3.96 (2H, m), 4.05-4.13 (4H, m) (4 x CH_2CH$_3$) 10.34 (2H, s, 10,15-H), 10.69 (2H, s, 2,3-H), 11.10 (2H, s, 5,20-H). ^{1}H NMR (500 MHz, TFA-CDCl$_3$): δ -5.60 (3H, s, N-Me), -4.28 (2H, s, 2 x NH), 1.52 (6H, t, $^3J_{HH}$ = 7.7 Hz, 12,13-CH$_2$CH_3), 1.88 (6H, t, $^3J_{HH}$ = 7.7 Hz, 8,17-CH$_2$CH_3), 3.79 (6H, s, 7,18-Me), 3.81-3.92 (4H, m, 12,13-CH$_2$),

4.23-4.28 (4H, m, 8,17-CH_2), 10.56 (2H, s, 2,3-H), 10.82 (2H, s, 10,15-H), 11.10 (2H, s, 5,20-H). ^{13}C NMR (125 MHz, $CDCl_3$): δ 12.14, 17.28, 17.55, 20.13, 20.27, 32.34 (br, N-*C*H_3), 101.46, 102.65, 132.53, 137.31, 140.38, 146.10, 147.71, 148.39, 152.96, 155.26. ^{13}C NMR (125 MHz, TFA-$CDCl_3$): δ 11.70, 16.59, 16.70, 20.27, 20.60, 30.56 (N-*C*H_3), 100.61, 102.47, 134.42, 140.45, 141.23, 141.97, 142.94, 147.40, 156.05, 156.95. HR-MS (ESI) *m/z*: $[M + H]^+$ calcd for $C_{31}H_{36}N_3O$ 466.2858, found 466.2855.

8,12,13,17-Tetraethyl-7,18-dimethyl-21-thiaporphyrin (**97a**). Tripyrrane dicarboxylic acid **54b** (100 mg, 0.221 mmol) was dissolved in TFA (1 mL) and stirred under nitrogen for 2 minutes. The mixture was diluted with dichloromethane (99 mL), followed by the addition of 2,5-thiophenedicarboxaldehyde (31.7 mg, 0.226 mmol), and left to stir overnight under nitrogen. The mixture was washed with ferric chloride (0.1%, 200 mL), water and then aqueous sodium bicarbonate solution. The solvent was removed under reduced pressure and the crude material was then chromatographed on neutral grade 3 alumina, eluting with dichloromethane. A red/pink band was collected, which was chromatographed a second time on neutral alumina, eluting with dichloromethane, and a green/brown band was collected. The solid was vacuum dried overnight to give 21-thiaporphyrin **97a** (43.0 mg, 0.0921 mmol, 42%) as a dark solid, mp > 300 °C. UV-Vis (1% Et_3N-dichloromethane): λ_{max}/nm (log ε) 398 (5.05), 495 (4.22), 525 (4.02), 590 (3.60), 597 (3.50), 649 (3.28). UV-Vis (1% TFA-dichloromethane): λ_{max}/nm (log ε) 418 (5.24), 549 (3.89), 576 (3.96). ^{1}H NMR (500 MHz, $CDCl_3$): δ –3.87 (1H, br s, NH), 1.86 (6H, t, *J* = 7.7 Hz, 8,17-CH_2C*H*$_3$), 1.95 (6H, t, *J* = 7.7 Hz, 12,13-CH_2C*H*$_3$), 3.45 (6H, s, 7,18-Me), 3.93 (4H, q, *J* = 7.7 Hz, 8,17-C*H*$_2CH_3$), 4.23 (4H, q, *J* = 7.7 Hz, 12,13-C*H*$_2CH_3$), 10.13 (2H, s, 2,3-H), 10.15 (2H, s, 10,15-H), 10.72 (2H, s, 5,20-H). ^{1}H NMR (500 MHz, TFA-$CDCl_3$): δ 1.84 (6H, t, *J* = 7.8 Hz, 8,17-CH_2C*H*$_3$), 1.89 (6H, t, *J* = 7.8 Hz, 12,13-CH_2C*H*$_3$), 3.79 (6H, s, 7,18-Me), 4.23 (4H, q, *J* = 7.8 Hz,

8,17-C*H*$_2$CH$_3$), 4.32 (4H, q, *J* = 7.8 Hz, 12,13-C*H*$_2$CH$_3$), 10.60 (2H, s, 2,3-H), 10.97 (2H, s, 10,15-H), 11.66 (2H, s, 5,20-H). ^{13}C NMR (125 MHz, $CDCl_3$): δ 11.55, 17.85, 18.57, 20.05, 20.14, 99.16, 112.68, 133.11, 136.76, 138.28, 140.47, 145.98, 146.80, 153.76, 156.48. ^{13}C NMR (125 MHz, TFA-$CDCl_3$): δ 12.05, 16.50, 17.65, 20.36, 20.47, 100.90, 115.56, 139.31, 142.98, 142.99, 143.70, 145.34, 146.14, 147.18, 147.56, 147.57, 150.19. HR-MS (ESI) m/z: [M + H]+ calcd for $C_{30}H_{34}N_3S$ 468.2473, found 468.2481.

8,12,13,17-Tetratethyl-7,18,23-trimethyl-21-thiaporphyrin (**97b**). *N*-methyl tripyrrane **54d** (200 mg, 0.428 mmol) was dissolved in TFA (2 mL) and stirred under nitrogen for 2 minutes. The solution was diluted with dichloromethane (38 mL), followed by the immediate addition of 2,5-thiophendicarboxaldehyde (62.0 mg, 0.443 mmol), and left to stir for another 2 hours under nitrogen. The mixture was neutralized by the dropwise addition of triethylamine, DDQ (100 mg) was added, and the solution stirred for 1 hour. The mixture was washed with water and then with aqueous sodium bicarbonate solution, and the solvent removed under reduced pressure. The crude material was chromatographed twice on neutral grade 3 alumina eluting with dichloromethane and a dark brown band was collected each time. The product was vacuum dried overnight to give 23-methyl-21-thiaporphyrin (34.6 mg, 0.0718 mmol, 17%) as a dark blue/purple solid, mp > 300 °C. UV-Vis (1% Et_3N-dichloromethane): λ_{max}/nm (log ε) 412 (4.89), 505 (4.09), 533 (3.67), 607 (3.31), 640 (2.76), 668 (3.08). UV-Vis (1% TFA -dichloromethane): λ_{max}/nm (log ε) 425 (5.13), 556 (3.67), 587 (3.73). UV-Vis (5% TFA -dichloromethane): λ_{max}/nm (log ε) 423 (5.15), 554 (3.68), 584 (3.74). ^{1}H NMR (500 MHz, $CDCl_3$): δ -4.39 (3H, s, N-Me), 1.48 (6H, t, $^3J_{HH}$ = 7.7 Hz, 12,13-$CH_2C\mathit{H}_3$), 1.84 (6H, t, $^3J_{HH}$ = 7.7 Hz, 8,17-$CH_2C\mathit{H}_3$), 3.39 (6H, s, 7,18-Me), 3.67-3.74 (2H, m), 3.78-3.95 (6H, m) (4 x C*H*$_2$CH$_3$) 9.96 (2H, s, 10,15-H), 10.00 (2H, s, 2,3-H), 10.57 (2H, s, 5,20-H). ^{1}H NMR (500 MHz, TFA-$CDCl_3$): δ -4.84 (3H, s, N-Me), -4.12 (2H, br s, 2 x NH), 1.40

(6H, t, $^3J_{HH}$ = 7.7 Hz, 12,13-CH_2CH_3), 1.84 (6H, t, $^3J_{HH}$ = 7.7 Hz, 8,17-CH_2CH_3), 3.75 (6H, s, 7,18-Me), 3.76-3.82 (2H, m), 3.85-3.92 (2H, m), 4.14-4.22 (4H, m) (4 x CH_2CH_3) 10.39 (2H, s, 2,3-H), 10.72 (2H, s, 10,15-H), 11.48 (2H, s, 5,20-H). ^{13}C NMR (125 MHz, $CDCl_3$): δ 11.44, 17.22, 17.78, 20.11, 20.14, 31.20 (N-CH_3), 103.41, 113.15, 133.88, 134.25, 137.64, 146.66, 149.05, 149.81, 153.39, 157.25. ^{13}C NMR (125 MHz, TFA-$CDCl_3$): δ 12.05, 16.40, 16.53, 20.45, 20.50, 30.46 (N-CH_3), 102.32, 111.07, 113.34, 114.79, 115.60, 117.87, 139.03, 142.30, 142.97, 145.06, 145.81, 147.44, 150.99, 158.27. HR-MS (ESI) *m/z*: $[M + H]^+$ calcd for $C_{31}H_{36}N_3S$ 482.2630, found 482.2616.

2,3,8,12,13,17-Hexaethyl-7,18,21-trimethylporphyrin (**99b**). *N*-methyl tripyrrane **54d** (265 mg, 0.567 mmol) was dissolved in TFA (2.5 mL) and stirred under nitrogen for 2 minutes. The solution was diluted with dichloromethane (50 mL), followed by the immediate addition of 2,5-pyrroledicarboxaldehyde (104.7 mg, 0.585 mmol), and left to stir for another 2 hours under nitrogen. The mixture was neutralized by the dropwise addition of triethylamine, DDQ (132.5 mg) was added, and the solution stirred for 1 hour. The mixture was washed with water, and then with aqueous sodium bicarbonate solution, and the solvent removed under reduced pressure. The crude material was chromatographed on neutral grade 3 alumina, eluting with chloroform, and a red/pink band was collected. Recrystallization from chloroform-hexanes gave pure 23-methylporphyrin (148 mg, 0.284 mmol, 50%) as dark purple/blue crystals, mp 238-242°C. UV-Vis (1% Et_3N-dichloromethane): λ_{max}/nm (log ε) 379 (4.76), 410 (5.06), 505 (4.07), 535 (3.71), 585 (3.57), 615 (2.85), 641 (3.43). UV-Vis (1% TFA-dichloromethane): λ_{max}/nm (log ε) 404 (5.51), 550 (4.14), 596 (3.91). UV-Vis (5% TFA-dichloromethane): λ_{max}/nm (log ε) 404 (5.51), 551 (4.12), 596 (3.86). ^{1}H NMR (500 MHz, $CDCl_3$): δ -4.76 (3H, s, N-Me), -3.22 (1H, br s, NH), 1.48 (6H, t, $^3J_{HH}$ = 7.7 Hz), 1.85 (6H, t, $^3J_{HH}$ = 7.7 Hz), 1.92 (6H, t, $^3J_{HH}$ = 7.7 Hz) (6 x CH_2CH_3), 3.49 (6H, s, 7,18-

Me), 3.67-3.74 (2H, m), 3.78-3.85 (2H, m), 3.88-4.02 (4H, m), 4.07-4.19 (4H, m) (6 x C*H*$_2$CH$_3$), 9.90 (2H, s, 5,20-H), 9.94 (2H, s, 10,15-H). ^{1}H NMR (500 MHz, TFA-CDCl$_3$): δ -5.59 (3H, s, N-Me), -3.52 (2H, br s, 2 x NH), 1.41 (6H, t, $^3J_{HH}$ = 7.7 Hz), 1.80 (6H, t, $^3J_{HH}$ = 7.8 Hz), 1.88 (6H, t, $^3J_{HH}$ = 7.8 Hz) (6 x CH$_2$C*H*$_3$), 3.73 (6H, s, 7,18-Me), 3.70-3.86 (4H, m), 4.13-4.27 (8H, m) (6 x C*H*$_2$CH$_3$), 10.61 (2H, s, 5,20-H), 10.73 (2H, s, 10,15-H). ^{13}C NMR (125 MHz, CDCl$_3$): δ 11.75, 17.27, 17.97, 18.54, 19.87, 19.96, 20.94, 32.80 (N-*C*H$_3$), 96.72, 101.59, 132.03, 136.61, 137.30, 139.13, 145.58, 148.65, 151.96, 155.28. ^{13}C NMR (125 MHz, TFA-CDCl$_3$): δ 12.01, 16.53, 16.62, 17.70, 20.13, 20.20, 20.54, 29.96 (N-*C*H$_3$), 99.94, 100.86, 138.59, 140.03, 141.19, 142.15, 143.02, 145.75, 146.06, 154.55. HR-MS (ESI) *m/z*: [M + H]$^+$ calcd for $C_{35}H_{45}N_4$ 521.3644, found 521.3641.

9,13,14,18-Tetraethyl-8,19,24-trimethyloxybenziporphyrin (**100a**). *N*-methyl tripyrrane **54d** (185 mg, 0.396 mmol) was dissolved in TFA (2 mL) and stirred under nitrogen for 2 minutes. The solution was diluted with dichloromethane (33 mL), followed by immediate addition of 5-formylsalicylaldehyde (58 mg, 0.386 mmol), and left to stir for another 2 hours under nitrogen. The mixture was neutralized by the dropwise addition of triethylamine, DDQ (88 mg) was added, and the solution stirred for 1 hour. The mixture was washed with water and then with aqueous sodium bicarbonate solution, and the solvent removed under reduced pressure. The crude material was chromatographed on neutral grade 3 alumina, eluting with dichloromethane and then 50% chloroform-dichloromethane, and a dark green band was collected. Recrystallization from chloroform-hexanes gave pure 24-methyloxybenziporphyrin (24.8 mg, 0.0504 mmol, 13%) as dark blue/purple crystals, mp > 300°C. IR: ν_{CO}/cm^{-1} 1618 (C=O). UV-Vis (1% Et$_3$N-dichloromethane): λ_{max}/nm (log ε) 331 (4.47), 441 (4.86), 473 (4.73), 564 (3.65), 621 (4.16), 725 (3.79). UV-Vis (1% TFA-dichloromethane): λ_{max}/nm (log ε) 317 (4.24), 351 (4.60), 434 (4.80),

556 (3.54), 602 (3.84), 698 (3.65), 760 (3.77). UV-Vis (5% TFA-dichloromethane): λ_{max}/nm (log ε) 319 (4.25), 351 (4.60), 433 (4.80), 511 (2.93), 554 (3.55), 601 (3.85), 693 (3.65), 764 (3.78). ^{1}H NMR (500 MHz, $CDCl_3$): δ –4.14 (1H br s, 22-H), -3.63 (3H, s, N-Me), 1.45-1.50 (6H, m, 13,14-CH_2CH_3), 1.73 (6H, t, $^{3}J_{HH}$ = 7.7 Hz, 9,18-CH_2CH_3), 3.33 (3H, s, 8-Me), 3.43 (3H, s, 19-Me), 3.52-3.68 (4H, m, 13,14-CH_2), 3.74-3.86 (4H, m, 9,18-CH_2), 7.36 (1H, d, $^{3}J_{HH}$ = 9.4 Hz, 3-H), 8.72 (1H, dd, $^{3}J_{HH}$ = 9.5 Hz, $^{4}J_{HH}$ = 2.2 Hz, 4-H), 9.20 (1H, s, 16-H), 9.37 (2H, s, 6,11-H), 10.50 (1H, s, 21-H). ^{1}H NMR (500 MHz, TFA-$CDCl_3$): δ –0.52 (3H, s, N-Me), 0.82 (1H, s, 22-H), 1.33 (6H, q, *J* = 7.7 Hz,), 1.43-1.47 (6H, m) (4 x CH_2CH_3), 2.95 (3H, s), 2.96 (3H, s) (8,19-Me), 3.02-3.13 (4H, m), 3.23-3.35 (4H, m) (4 x CH_2CH_3), 5.49 (1H, s), 5.52 (1H, s) (2 x NH), 7.62 (1H, d, *J* = 8.8 Hz, 3-H), 7.93 (1H, s), 7.99 (1H, s) (11,16-H), 8.58 (1H, dd, *J* = 8.9 Hz, *J* = 2.0 Hz, 4-H), 8.80 (1H, s, 6-H), 9.46 (1H, s, 21-H). ^{13}C NMR (125 MHz, $CDCl_3$): δ 11.61, 11.85, 16.69, 16.84, 17.08, 17.44, 19.78, 19.79, 19.87, 33.25 (N-CH_3), 93.69, 98.97, 111.18, 118.86, 120.52, 120.56, 124.21, 127.50, 130.03, 135.28, 137.33, 138.09, 139.04, 139.72, 140.60, 141.82, 144.53, 145.72, 145.76, 146.92, 148.18, 149.02, 151.22, 189.33. ^{13}C NMR (125 MHz, TFA-$CDCl_3$): δ 11.16, 11.21, 15.33, 15.36, 15.42, 18.96, 19.14, 19.17, 37.17 (N-CH_3), 94.30, 95.66, 116.55, 119.76, 120.51, 122.20, 123.85, 127.46, 140.13, 140.57, 140.69, 141.18, 143.85, 146.49, 147.52, 149.71, 154.36, 155.90, 159.26, 172.76. HR-MS (ESI) *m/z*: $[M + H]^+$ calcd for $C_{33}H_{38}N_3O$ 492.3015, found 492.3025.

[9,13,14,18-Tetraethyl-8,19,24-trimethyloxybenziporphyrinato] palladium(II) (**102**). Palladium(II) acetate (10 mg, 0.0445 mmol) was added to a solution of 23-methyloxybenziporphyrin (10 mg, 0.0203 mmol) in acetonitrile (10 mL) and the solution was reacted under reflux for 30 minutes. The mixture was then diluted with chloroform and washed with water, and the solvent was removed under reduced pressure. The crude material was

chromatographed on grade 3 neutral alumina eluting with chloroform, and a green band was collected and recrystallized from chloroform-methanol to give palladium(II) 23-methyloxybenziporphyrin (4.4 mg, 0.00738 mmol, 36%) as emerald green crystals, mp 180-185 °C, dec. IR: ν_{CO}/cm^{-1} 1555 (C=O). ^{1}H NMR (500 MHz, $CDCl_3$): δ -2.36 (3H, s, N-Me), 1.61-1.65 (6H, m), 1.69-1.73 (6H, m) (4 x CH_2CH_3), 3.27 (3H, s, 8-Me), 3.32 (3H, s, 19-Me), 3.64-3.84 (8H, m, 4 x CH_2CH_3), 7.10 (1H, d, $^{3}J_{HH}$ = 9.0 Hz, 3-H), 8.47 (1H, d, $^{3}J_{HH}$ = 9.2 Hz, 4-H), 9.22 (1H, s, 6-H), 9.46 (1H, s), 9.52 (1H, s) (11,16-H), 10.58 (1H, s, 21-H). ^{13}C NMR (125 MHz, $CDCl_3$): δ 11.42, 11.70, 16.24, 16.30, 17.12, 17.33, 20.01, 20.03, 20.05, 46.28 (N-CH_3), 98.70, 100.16, 123.45, 123.56, 125.78, 126.57, 128.61, 136.58, 136.89, 139.47, 139.78, 140.19, 140.87, 140.93, 141.40, 141.50, 143.78, 146.14, 149.64, 150.14, 151.70, 190.17. HR-MS (ESI) *m/z*: $[M + H]^+$ calcd for $C_{33}H_{36}N_3OPd$ 596.1893, found 596.1874.

9,13,14,18-Tetraethyl-8,19,24-trimethyloxypyriporphyrin (**100b**). *N*-methyl tripyrrane **54d** (177 mg, 0.379 mmol) was dissolved in TFA (2 mL) and stirred under nitrogen for 2 minutes. The solution was diluted with dichloromethane (33 mL), followed by immediate addition of 5-formylsalicylaldehyde (57.4 mg, 0.380 mmol), and left to stir for another 2 hours under nitrogen. The mixture was neutralized by the dropwise addition of triethylamine, DDQ (86 mg) was added, and the solution stirred for 1 hour. The mixture was washed with water and then with aqueous sodium bicarbonate solution, and the solvent removed under reduced pressure. The crude material was chromatographed twice on neutral grade 3 alumina, eluting with chloroform and then 2% methanol-chloroform, and a dark green band was collected each time. The product was dried overnight under vacuum to give 24-methyloxybenziporphyrin (66.7 mg, 0.135 mmol, 36%) as a dark blue/purple solid, mp > 300°C. IR: ν_{CO}/cm^{-1} 1625 (C=O). UV-Vis (1% Et_3N-dichloromethane): λ_{max}/nm (log ε) 324 (4.14), 434 (4.56), 546 (3.51), 581 (3.56), 625 (3.87), 673

(3.70). UV-Vis (1% TFA-dichloromethane): λ_{max}/nm (log ε) 324 (4.13), 425 (4.90), 453 (4.61), 549 (3.57), 588 (3.78), 629 (4.07). UV-Vis (5% TFA-dichloromethane): λ_{max}/nm (log ε) 323 (4.19), 426 (4.82), 550 (3.61), 599 (3.74), 627 (3.93), 648 (3.80). ^{1}H NMR (500 MHz, $CDCl_3$): δ -4.20 (3H, s, N-Me), -1.26 (1H, br s, NH), 1.37 (3H, t, *J* = 7.7 Hz, 14-CH_2CH_3) 1.41 (3H, t, *J* = 7.7 Hz, 13-CH_2CH_3), 1.79 (3H, t, *J* = 7.7 Hz, 9-CH_2CH_3), 1.83 (3H, t, *J* = 7.7 Hz, 18- CH_2CH_3), 3.44 (3H, s, 8-Me), 3.58 (3H, s, 19-Me), 3.59-3.64 (2H, m, 13-CH_2), 3.69-3.77 (2H, m, 14-CH_2), 3.82-3.93 (2H, m, 9-CH_2), 3.94-4.02 (2H, m, 18-CH_2), 7.91 (1H, d, *J* = 9.4 Hz), 9.33 (1H, d, *J* = 9.4 Hz), 9.64 (1H, s, 16-H), 9.68 (1H, s, 6-H), 9.73 (1H, s, 11-H), 10.89 (1H, s, 21-H). ^{1}H NMR (500 MHz, TFA-$CDCl_3$): δ -2.92 (3H, s, N-Me), 0.30 (2H, br s, 2 x NH), 1.41-1.46 (6H, m, 13,14-CH_2CH_3) 1.63-1.66 (6H, m, 9,18-CH_2CH_3), 3.35 (3H, s), 3.38 (3H, s) (8,19-Me), 3.39-3.50 (4H, m, 13,14-CH_2), 3.71-3.79 (4H, m, 9,18-CH_2), 8.57 (1H, d, *J* = 9.1 Hz, 3-H), 9.24 (1H, s), 9.63 (1H, d, *J* = 9.1 Hz, 4-H), 9.78 (1H, s, 6-H), 10.70 (1H, s, 21-H). ^{13}C NMR (125 MHz, $CDCl_3$): δ 11.83, 11.93, 16.82, 16.98, 17.32, 17.61, 19.71, 19.83, 20.08, 20.11, 33.19 (N-CH_3), 95.49, 101.51, 106.21, 115.07, 131.69, 133.37, 135.40, 138.72, 139.52, 141.04, 143.29, 146.50, 150.10, 150.71, 151.24, 185.23. ^{13}C NMR (125 MHz, TFA-$CDCl_3$): δ 11.49, 11.58, 15.93, 16.11, 19.62, 34.54 (N-CH_3), 96.83, 97.33, 113.31, 119.83, 127.91, 127.93, 139.37, 139.62, 140.17, 140.58, 142.31, 142.60, 142.93, 144.78, 145.64, 147.79, 149.46, 149.74, 159.10, 159.63, 173.83 (br). HR-MS (ESI) *m/z*: $[M + H]^+$ calcd for $C_{32}H_{37}N_4O$ 493.2967, found 493.2965.

tert-Butyl 23-methylazuliporphyrin dihydrochloride (**103**H_2^{2+}). *N*-methyl tripyrrane **54d** (103 mg, 0.221 mmol) was dissolved in TFA (1 mL) and stirred for 2 minutes under nitrogen. The mixture was diluted with dichloromethane (99 mL), followed by the immediate addition of 6-*tert*-butylazulene-1,3-dicarbaldehyde (57.6 mg, 0.240 mmol), and the solution was left to stir overnight under nitrogen. The mixture was oxidized by vigorous washing with ferric chloride (0.1%, 200

mL), and then washed with 10% aqueous hydrochloric acid. The solvent was evaporated off under reduced pressure and the residue was recrystallized twice from chloroform-hexanes to give *tert*-butyl 23-methylazuliporphyrin dihydrochloride (113 mg, 0.194 mmol, 78%) as dark crystals, mp > 300 °C. UV-Vis (1% Et_3N-dichloromethane): λ_{max}/nm (log ε) 363 (4.47), 401 (4.37), 459 (4.44), 482 (4.52) 669 (3.89). UV-Vis (1% TFA-dichloromethane): λ_{max}/nm (log ε) 368 (4.50), 443 (sh, 4.46), 469 (4.77), 587 (3.88), 647 (4.19), 686 (sh, 3.93), 750 (3.62). ^{1}H NMR (500 MHz, TFA-d_6-DMSO): δ -3.38 (1H, s, CH), -3.36 (3H, s, N-Me), -0.36 (2H, br s, 2 x NH), 1.26 (6H, t, J = 7.7 Hz) 1.57 (6H, t, J = 7.7 Hz) (4 x CH_2CH_3), 1.64 (9H, s, 2^3-$C(CH_3)_3$), 3.46 (6H, s, 7,18-Me), 3.44-3.53 (2H, m), 3.64-3.71 (2H, m), 3.75-3.83 (2H, m), 3.85-3.92 (2H, m) (4 x CH_2CH_3), 8.89 (2H, d, J = 10 Hz, 2^2, 3^2-CH), 9.66 (2H, s), 10.39 (2H, d, J = 10 Hz, 2^1, 3^1-CH), 10.72 (2H, s). ^{13}C NMR (125 MHz, TFA-d_6-DMSO): δ 11.62, 16.25, 16.51, 19.56, 19.59, 31.50 ($C(CH_3)_3$), 32.25 (N-CH_3), 40.78 ($C(CH_3)_3$), 97.16, 110.95, 125.63, 129.15, 141.07, 141.46, 141.53, 142.01, 142.19, 142.31, 146.18, 153.68, 156.74. HR-MS (ESI) m/z: [M + H]+ calcd for $C_{41}H_{48}N_3$ 582.3848, found 582.3847.

CHAPTER V: CONCLUSIONS

Investigations into the modification of porphyrinoid systems are of interest in order to analyze the effects they may have on these macrocyclic molecules. By altering atoms within the porphyrinoid cavity, changing the external substituents, or inserting one or more different rings into the system, changes in the electronic properties, structure stability and reactivity can be assessed. Carbaporphyrinoids are a common type of porphyrin analogue that involve a core modification where one or more of the internal nitrogen atoms are replaced by carbon atoms. Metalation of carbaporphyrins has been widely studied, demonstrating that these compounds can still act as versatile ligands and bind with a number of late transition metals, despite the inclusion of internal carbon atoms.

Among the carbaporphyrinoid systems that form stable metal complexes are benzocarbaporphyrins, which have previously been shown to form organometallic complexes with Rh(III), Ir(III), Au(III) and Ag(III) metal cations. The work reported in this thesis demonstrates that internal alkylation alters the coordination chemistry of benzocarbaporphyrins and allows them to form stable complexes with metals in the 2+ oxidation state. When reacted with $Pd(OAc)_2$, 23-methylbenzocarbaporphyrin formed a 23-methyl palladium(II) complex that rearranged to give a C-methyl palladium(II) complex. This was proposed to occur via an oxidative addition of the alkyl group onto the palladium metal center, followed by a reductive elimination that transfers the methyl onto the 21-carbon. Internally methylated benzocarbaporphyrins, as well as a carbaporphyrin diester and a naphthocarbaporphyrin, were also shown to form rhodium complexes. It was found that 21- and 22-methylbenzocarbaporphyrins reacted with $[Rh(CO)_2Cl]_2$

to give stable rhodium(I) complexes, but reaction with a 23-methylbenzocarbaporphyrin gave a very different result. Specifically, the 23-methyl compound did not produce a rhodium(I) species, but instead formed a rhodium(III) complex accompanied by the unexpected formation of an internal methylene bridge. Hence, the introduction of the internal methyl substituent drastically affects how benzocarbaporphyrins coordinate to rhodium. A carbaporphyrin diester and a naphthocarbaporphyrin were also shown to react with $[Rh(CO)_2Cl]_2$ to give rhodium(I) complexes. However, unlike the rhodium(I) derivatives of 21- and 22-methylbenzocarbaporphyrins, these compounds generated rhodium(III) complexes in refluxing pyridine, thereby demonstrating that the carbaporphyrin platform can bind rhodium in two oxidation states. Four of the rhodium complexes were characterized by X-ray crystallography, and this provided information on the bonding frameworks that were obtained. Furthermore, the formation of the rhodium(III) system with a bridging methylene unit demonstrates how a 23-methylbenzocarbaporphyrin can rearrange when rhodium is incorporated into the macrocycle. This rearrangement also highlights the capability of rhodium(III) porphyrinoids to promote C-H bond activation.

Carbaporphyrinoid systems are commonly synthesized using the '3+1' variant of the MacDonald Condensation. This methodology allows for alteration of either the tripyrrane unit or the dialdehyde unit, making it simple to design a multitude of modified porphyrinoids. The insertion of an internal methyl group had dramatic effects on benzocarbaporphyrin systems, and therefore it was of interest to investigate the effects of internal substituents on other porphyrinoids. A series of *N*-methylated porphyrin analogues were synthesized using the '3+1' approach, and the characterization of these modified porphyrinoids is reported in this thesis. The introduction of an internal methyl group affected all of the porphyrinoid systems, where the most dramatic of changes were observed in the UV-Vis spectra. The alkyl substituent may distort the π-system of the

macrocycle, and consequently this results in bathochromic shifts to the absorption bands for the methylated derivatives compared to their non-methylated counterparts. In the case of the 24-methyloxybenzi- and oxypyriporphyrins, the UV-Vis spectra show drastic weakening and broadening in the absorption bands. For the other methylated derivatives, the shift to longer wavelengths was the most evident change, with a slight broadening of the bands in some cases. Metalation of *N*-methyloxybenziporphyrin with $Pd(OAc)_2$ gave a stable palladium(II) complex, where the internal methyl remained in its original position. This result demonstrated that the presence of an internal methyl group facilitates the formation of a stable palladium(II) complex.

Although the introduction of an internal alkyl substituent greatly affected the chromophores of porphyrinoid systems, the porphyrin analogues fully retained their aromatic characteristics. The global aromatic properties of these systems were assessed by proton NMR spectroscopy and in every case the diamagnetic ring currents were not significantly altered by introducing internal alkyl substituents. Nevertheless, the dramatic changes observed in the electronic spectra upon alkylation, and the modification of the systems' ability to form organometallic derivatives, demonstrates that incorporation of *N*-alkyl substituents provides a valuable strategy for adjusting the properties of porphyrinoid structures.

REFERENCES

1. Thompson, S. J.; Brennan, M. R.; Lee, S. Y.; Dong, G. Synthesis and applications of rhodium porphyrin complexes. *Chem. Soc. Rev.* **2018**, *47*, 929-981.
2. Fleischer, E. B. Structure of porphyrins and metalloporphyrins. *Acc. Chem. Res.*, **1970**, *3*, 105–112.
3. Smith, K. M. *Porphyrins and Metalloporphyrins: A New Edition Based on the Original Volume by J. E. Falk*, Elsevier, 1975.
4. Wasielewski, M. R. Photoinduced electron transfer in supramolecular systems for artificial photosynthesis. *Chem. Rev.* **1992**, *92*, 435–461.
5. Sheldon, R. A. *Metalloporphyrins in Catalytic Oxidations*; Taylor & Francis: United Kingdom, 1994.
6. Lash, T. D. Synthesis of novel porphyrinoid chromophores. In *The Porphyrin Handbook*, Kadish, K. M.; Smith, K. M.; Guilard, R., Eds.; Academic Press: New York, 2000; Vol. 2, pp. 125
7. *The Porphyrin Handbook*, Kadish, K. M.; Smith, K. M.; Guilard, R., Eds.; Academic Press: New York, 2000; Vol. 6.
8. Bonnett, R. Photosensitizers of the porphyrin and phthalocyanine series for photodynamic therapy. *Chem. Soc. Rev.* **1995**, *24*, 19–33.
9. Ogoshi, H.; Mizutani, T. Multifunctional and Chiral Porphyrins: Model Receptors for Chiral Recognition. *Acc. Chem. Res.* **1998**, *31*, 81–89.

10. Chandra, R. M.; Tiwari, P.; Kaur, M.; Sharma, Jain, R.; Dass, S. Metalloporphyrins-Applications and clinical significance. *Indian J. Clin. Biochem.* **2000**, *15*, 183–199.
11. Suslick, K. S.; Rakow, N. A.; Kosal, M. E.; Chou, J-H. The materials chemistry of porphyrins and metalloporphyrins. *J. Porphyrins Phthalocyanines* **2000**, *4*, 407–413.
12. (a) Brown, S. B.; Truscott, T. G. New light on cancer therapy. *Chem. Br.* **1993,** *29*, 955. (b) Milgrom, L. R.; MacRobert, S. Light years ahead. *Chem. Br.* **1998,** *34* (35), 45.
13. Mironov, A. Transition Metal Complexes of Porphyrins and Porphyrinoids. *Handbook of Porphyrin Science- With Applications to Chemistry, Physics, Material Science, Engineering, Biology and Medicine,* Kadish, K. M.; Smith, K. M.; Guilard, R., eds.; World Scientific Publishing, 2012, Vol. 18, pp. 303-413.
14. Sanders, J. K. M.; Bampos, N.; Clyde-Watson, Z.; Darling, S. L.; Hawley, J. C.; Kim, H-J.; Mak, C. C.; Webb, S. J. Introduction, In *The Porphyrin Handbook*, Kadish, K. M.; Smith, K. M.; Guilard, R., Eds.; Academic Press: New York, 2000; Vol. 3, pp. 3.
15. Lash, T.D. Carbaporphyrins and Related Systems. Synthesis, Characterization, Reactivity and Insights into the Nature of Porphyrinoid Aromaticity. *Handbook of Porphyrin Science-With Applications to Chemistry, Physics, Material Science, Engineering, Biology and Medicine,* Kadish, K. M.; Smith, K. M.; Guilard, R., eds.; World Scientific Publishing, 2012, Vol. 16, pp. 1-329.
16. Lash, T. D.; Hayes, M. J. Conjugated macrocycles related to porphyrins. Part 9. Carbaporphyrins. *Angew. Chem. Int. Ed. Engl.* **1997**, *36*, 840-842.
17. Lash, T. D. Recent advances on the synthesis and chemistry of carbaporphyrins and related porphyrinoid systems. *Eur. J. Org. Chem.* **2007**, *33*, 5461-5481.

18. Lash, T .D.; Hayes, M. J.; Spence, J. D.; Muckey, M. A.; Ferrence, G. M.; Szczepura, L. F. Conjugated Macrocycles Related to the Porphyrins. 21. Synthesis, Spectroscopy, Electrochemistry, and Structural Characterization of Carbaporphyrins. *J. Org. Chem.* **2002**, *67*, 4860-4874.
19. Lash, T. D. Out of the Blue! Azuliporphyrins and Related Carbaporphyrinoid Systems. *Acc. Chem. Res.* **2016**, *49*, 471-482.
20. Lash, T. D. Benziporphyrins, a Unique Platform for Exploring the Aromatic Characteristics of Porphyrinoid Systems. *Org. Biomol. Chem.* **2015**, *9*, 682-705.
21. (a) Srinivasan, A.; Furuta, H. Confusion Approach to Porphyrinoid Chemistry. *Acc. Chem. Res.* **2005**, *38*, 10-20. (b) Toganoh, M.; Furuta, H. Blooming of Confused Porphyrinoids — Fusion, Expansion, Contraction, and More Confusion. *Chem. Commun.* **2012**, *48*, 937-954.
22. Lash, T. D. Oxybenziporphyrin, a fully aromatic semiquinone porphyrin analog with pathways for 18π-electron delocalization. *Angew. Chem. Int. Ed. Engl.* **1995**, *34*, 2533–2535.
23. Lash, T. D.; Chaney, S. T.; Richter, D. T. Conjugated Macrocycles Related to Pophyrins. 12. Oxybenzi- and Oxypyriporphyrins: Aromaticity and Conjugation in Highly Modified Porphyrinoid Structures. *J. Org. Chem*. **1998**, *63*, 9076–9088.
24. Richter, D. T.; Lash T. D. Conjugated macrocycles related to the porphyrins. Part 18: Synthesis and spectroscopic characterization of electron-rich benzi- and oxybenziporphyrins: influence of steric and electronic factors on porphyrinoid aromaticity. *Tetrahedron* **2001**, *57*, 3659–3673.

25. (a) Lash, T. D.; Chaney, S. T. Conjugated macrocycles related to the porphyrins. Part 7. Tropiporphyrin: tropylium versus porphyrinoid aromaticity. *Tetrahedron Lett.* **1996**, *37*, 8825− 8828. (b) Bergman, K. M.; Ferrence, G. M.; Lash, T. D. Conjugated Macrocycles Related to the Porphyrins. Part 36. Tropiporphyrins, Cycloheptatrienyl Analogues of the Porphyrins: Synthesis, Spectroscopy, Chemistry, and Structural Characterization of a Silver(III) Derivative. *J. Org. Chem.* **2004**, *69*, 7888−7897.
26. Lash, T. D. Metal Complexes of Carbaporphyrinoid Systems. *Chem. Asian J.* **2014**, *9*, 682-705.
27. Muckey, M. A.; Szczepura, L. F.; Ferrence, G. M.; Lash, T. D. Silver(III) Carbaporphyrins: The First Organometallic Complexes of True Carbaporphyrins. *Inorg. Chem.* **2002**, *41*, 4840-4842.
28. Lash, T. D.; Colby, D. A.; Szczepura, L. F. New Riches in Carbaporphyrin Chemistry: Silver and Gold Organometallic Complexes of Benzocarbaporphyrins. *Inorg. Chem.* **2004**, *43*, 5258-5267.
29. Sahota, N.; Ferrence, G. M.; Lash, T. D. Synthesis and Properties of Carbaporphyrin and Carbachlorin Dimethyl Esters Derived from Cyclopentanedialdehydes. *J. Org. Chem.* **2017**, *82*, 9715-9730.
30. Adiraju, V. A. K.; Ferrence, G. M.; Lash, T. D. Rhodium(I), Rhodium(III) and Iridium(III) Carbaporphyrins. *Dalton Trans.* **2016**, *45*, 13691-13694.
31. Stepien, M.; Latos-Grazynski, L. Benziporphyrins: Exploring Arene Chemistry in s Macrocyclic Environment. *Acc. Chem. Res.* **2005**, *38*, 88-98.

32. (a) Graham, S. R.; Ferrence, G. M.; Lash, T. D. Organometallic Chemistry of Carbaporphyrinoids: Synthesis and Characterization of Nickel(II) and Palladium (II) Azuliporphyrins. *Chem. Commun.* **2002**, *38*, 894-895. (b) Lash, T. D.; Colby, D. A.; Graham, S. R.; Ferrence, G. M.; Szczepura, L. F. Organometallic Chemistry of Azuliporphyrins: Synthesis, Spectroscopy, Electrochemistry and Structural Characterization of Nickel(II), Palladium(II) and Platinum(II) Complexes of Azuliporphyrins. *Inorg. Chem.* **2003**, *42*, 7326-7338.

33. Bialek, M. J.; Latos-Grazynski, L. Merging of Inner and Outer Ruthenium Organometallic Coordination Motifs within an Azuliporphyrin Framework. *Chem. Commun.* **2014**, *50*, 9270-9272.

34. Stateman, L. M.; Ferrence, G. M.; Lash, T. D. Rhodium(III) Azuliporphyrins. *Organometallics* **2015**, *34*, 3842-3848.

35. Lash, T. D.; Pokharel, K.; Zeller, M.; Ferrence, G. M. Iridium(III) azuliporphyrins. *Chem. Commun.* **2012**, *48*, 11793-11795.

36. (a) Toganoh, M.; Furuta, H. In *Handbook of Porphyrin Science – With Applications to Chemistry, Physics, Material Science, Engineering, Biology and Medicine*, Kadish, K. M.; Smith, K. M.; Guilard, R., eds.; World Scientific Publishing: Singapore, 2010, Vol. 2, pp 295-367. (b) Harvey, J. D.; Ziegler, C. J. Developments in the metal chemistry of N-confused porphyrin. *Coord. Chem. Rev.* **2003**, *247*, 1-19.

37. Chmielewski, P. J.; Latos-Grazynski, L.; Rachlewicz, K.; Glowiak, T. Tetra-p-tolylporphyrin with an Inverted Pyrrole Ring: A Novel Isomer of Porphyrin. *Angew. Chem. Int. Ed. Engl.* **1994**, *33*, 779 – 781.

38. Furuta, H.; Ogawa, T.; Uwatoko, Y.; Araki, K. N-Confused Tetraphenylporphyrin-Silver(III) Complex. *Inorg. Chem.* **1999**, *38*, 2676 – 2682.

39. Lash, T. D.; Rasmussen, J. M.; Bergman, K. M.; Colby, D. A. Conjugated Macrocycles Related to the Porphyrins. Part 33. Carbaporphyrinoid Chemistry Has a Silver Lining! Silver(III) Oxybenzi-, Oxynaphthi-, Tropi-, and Benzocarbaporphyrins. *Org. Lett.* **2004**, *6*, 549.

40. Stepien, M.; Latos-Grazynski, L.; Lash, T. D.; Szterenberg, L. Palladium(II) Complexes of Oxybenziporphyrin. *Inorg. Chem.* **2001**, *40*, 6892.

41. Pokharel, K. Synthesis and Metalation of Porphyrin Analogues. M.S. Thesis, Illinois State University, Normal, IL, May 2007.

42. El-Beck, J. A.; Lash, T. D. Tetraphenyloxybenziporphyrin, a New Organometallic Ligand for Silver(III) and Gold(III). *Org. Lett.* **2006**, *8*, 5263−5266.

43. Szymanski, J. T.; Lash, T. D. Dimethoxytetraphenylbenziporphyrins. *Tetrahedron Lett.* **2003**, *44*, 8613−8616.

44. Lash, T. D.; Szymanski, J. T.; Ferrence, G. M. Tetraaryldimethoxybenziporphyrins at the Edge of Carbaporphyrinoid Aromaticity. *J. Org. Chem.* **2007**, *72*, 6481−6492.

45. Fosu, S. C.; Ferrence, G. M.; Lash, T. D. Synthesis and Metalation of Dimethoxybenziporphyrins, Thiabenziporphyrins and Dibenziporphyrins. *J. Org. Chem.* **2014**, *79*, 11061−11074.

46. Lash, T. D.; Ferrence, G. M. Metalation and Selective Oxidation of Diphenyl-23-oxa-, thia-, and Selena-21-carbaporphyrins. *Inorg. Chem.* **2017**, *56*, 11426−11434.

47. Chatterjee, T.; Shetti, V. S.; Sharma, R.; Ravikanth, M. Heteroatom-Containing Porphyrin Analogues. *Chem. Rev.* **2017**, *117*, 3254−3328.

48. Latos-Grazyński, L. Core modified Heteroanalogues of Porphyrins and Metalloporphyrins. In *The Porphyrin Handbook*; Kadish, K. M., Smith, K. M., Guilard, R., Eds.; Academic Press: New York, 2000; Vol. 2, pp 361−416.

49. Latos-Grazyński, L.; Lisowski, J.; Olmstead, M. M.; Balch, A. L. Five-Coordinate Complexes of 21-Thiaporphyrin. Preparation, Spectra, and Structures of Iron(II), Nickel (II) and Copper(II) Complexes. *Inorg. Chem*. **1989**, *28*, 1183−1188.

50. Latos-Grazyński, L.; Lisowski, J.; Olmstead, M. M.; Balch, A. L. Preparation and Structural Characterization of a Six-Coordinate 21- Thiaporphyrin Complex: RhIII(STPP)Cl2 (STPP = Tetraphenyl-21- thiaporphyrin Anion). *Inorg. Chem*. **1989**, *28*, 3328−3331.

51. Chuang, C. H.; Ou, C. K.; Liu, S. T.; Kumar, A.; Ching, W. M.; Chiang, P. C.; Dela Rosa, M. A. C.; Hung, C. H. Ruthenium Complexes of Thiaporphyrin and Dithiaporphyrin. *Inorg. Chem*. **2011**, *50*, 11947− 11957.

52. Gebauer, A.; Schmidt, J. A. R.; Arnold, J. Synthesis, Characterization, and Properties of a Lithium 21-Thiaporphyrin Complex. *Inorg. Chem*. **2000**, *39*, 3424−3427.

53. Tung, J. Y.; Liau, B. C.; Elango, S.; Chen, J. H.; Hsieh, H. Y.; Liao, F. L.; Wang, S. L.; Hwang, L. P. Preparation and Structural Characterization of mercury 21-thiaporphyrin complex: HgII(Stpp)CI (Stpp = tetraphenyl-21-thiaporphyrin anion). *Inorg. Chem. Commun*. **2002**, *5*, 150−155.

54. Ghosh, A.; Ravikanth, M. Rhenium (I) Tricarbonyl Complexes of 5,10,15,20-Tetraphenyl-21-thia and 21-Oxaporphyrins. *Inorg. Chem*. **2012**, *51*, 6700−6709.

55. Chmielewski, P. J.; Latos-Grazyński, L.; Olmstead, M. M.; Balch, A. L. Nickel Complexes of 21-Oxaporphyrin and 21, 23-Dioxaporphyrin. *Chem. Eur. J.* **1997**, *3*, 268−278.

56. Pawlicki, M.; Latos-Grazyński, L. Iron Complexes of 5,10,15,20- Tetraphenyl-21-oxaphyrin. *Inorg. Chem.* **2002**, *41*, 5866−5873.

57. Broadhurst, M. J.; Grigg, R.; Johnson, A. W. Synthesis of Porphin Analogues Containing Furan and/or Thiophen Rings. *J. Chem. Soc. C* **1971**, *0*, 3681–3690.

58. Ambre, R.; Yu, C. Y.; Mane, S. B.; Yao, C. F.; Hung, C. H. Toward carboxylate group functionalized A4, A2B2, A3B oxaporphyrins and zinc complex of oxaporphyrins. *Tetrahedron* **2011**, *67*, 4680−4688.

59. Stute, S.; Gotzke, L.; Meyer, D.; Merroun, M. L.; Rapta, P.; Kataeva, O.; Seichter, W.; Gloe, K.; Dunsch, L.; Gloe, K. Molecular Structure, UV/Vis Spectra, and Cyclic Voltammograms of Mn(II), Co(II), and Zn(II) 5,10,15,20-Tetraphenyl-21-oxaporphyrins. *Inorg. Chem.* **2013**, *52*, 1515−1524.

60. Bond, A. D.; Sanders, J. K. M.; Stulz, E. Ruthenium(II) and rhodium(III) porphyrin phosphine complexes: influence of substitution pattern on structure and electronic properties. *New J. Chem.* **2011**, *35*, 2691–2696.

61. Olguin, J.; Muller-Bunz, H.; Albrecht, M. Springloaded porphyrin NHC hybrid rhodium(III) complexes: carbene dissociation and oxidation catalysis. *Chem. Commun.*, **2014**, *50*, 3488–3490.

62. Anding, B. J.; Ellern, A.; Woo, L. K. Comparative Study of Rhodium and Iridium Porphyrin Diaminocarbene and N-Heterocyclic Carbene Complexes. *Organometallics* **2014**, *33*, 2219–2229.

63. Chan, K. S.; Lau, C. M. Syntheses of Acyl Rhodium Porphyrins by Aldehydic Carbon-Hydrogen Bond Activation with Rh(III) Porphyrin Chloride and Methyl. *Organometallics* **2006,** *25,* 260−265.

64. Chan, K. S.; Chiu, P. F.; Choi, K. S. Base-Promoted Selective Activation of Benzylic Carbon-Hydrogen Bonds of Toluenes by Rhodium(III) Porphyrins. *Organometallics* **2007,** *26,* 1117−1119.

65. (a) Chan, Y. W.; Chan, K. S. Base-promoted carbon-hydrogen bond activation of alkanes with rhodium(III) porphyrin complexes. *Organometallics* **2008,** *27,* 4625− 4635. (b) Fung, H. S.; Chan, Y. W.; Cheung, C. W.; Choi, K. S.; Lee, S. Y.; Qian, Y. Y.; Chan, K. S. Reactivity Studies of Rhodium(III) Porphyrins with Methanol in Alkaline Media. *Organometallics* **2009**, *28,* 3981−3989.

66. Aoyama, Y.; Yoshida, T.; Sakurai, K.; and Ogoshi, H. Activation of arene carbon-hydrogen bonds. Direct electrophilic aromatic metalation with a rhodium-porphyrin complex. *J. Chem. Soc., Chem. Commun.* **1983**, *8*, 478–479.

67. Aoyama, Y.; Yoshida, T.; Sakurai, K.; and Ogoshi, H. Activation of arene carbon-hydrogen bonds. Highly regioselective, electrophilic aromatic metalation with rhodium(III) porphyrin and subsequent cleavage of carbon-rhodium bond. *Organometallics* **1986**, *5*, 168–173.

68. Hurej, K.; Pawlicki, M.; Szterenberg, L.; Latos-Grazynski, L. A Rhodium-Mediated Contraction of Benzene to Cyclopentadiene: Transformations of Rhodium(III) *m*-Benziporphyrins. *Angew. Chem. Int. Ed.* **2016,** *55,* 1427-1431.

69. Sondheimer F, Wolovsky R and Amiel Y. Unsaturated Macrocyclic Compounds. XXIII. The Synthesis of the Fully Conjugated Macrocyclic Polyenes Cyclooctadecanonaene ([18]Annulene), Cyclotetracosadodecaene ([24]Annulene), and Cyclotriacontapentadecaene([30]Annulene). *J. Am. Chem. Soc*. **1962**, *84*, 274–284.

70. Vogel, E.; Pretzer, W.; Boll, W. A. 1.6-imino-cyclodecapentaen (1.6-imino-[10]-annulen). *Tetrahedron Lett*. **1965**, *6*, 3613–3617.

71. Vogel E. J. Novel porphyrinoid macrocycles and their metal complexes. *Heterocyclic Chem.* **1996**, *33*, 1461– 1487.

72. Cyranksi, M. K.; Krygowski, T. N.; Wisiorowski, M.; Hommes, N. J. R.; Schleyer, P. V. R. Global and Local Aromaticity in Porphyrins: An Analysis Based on Molecular Geometries and Nucleus-Independent Shifts. *Angew. Chem. Int. Ed.* **1998,** *37,* 177-180.

73. Lash, T. D. Origin of aromatic character in porphyrinoid systems. *J. Porphyrins Phthalocyanines* **2011,** *15,* 1094–1115.

74. Webb, L. E.; Fleisher, E. B. The Structure of Porphine. *J. Am. Chem. Soc*. **1965**, *87*, 667–669.

75. (a) Vogel, E.; Röhrig, P.; Sicken, M.; Knipp, B.; Herrmann, A.; Pohl, M.; Schmickler, H.; Lex, J. The Thiophene Analogue of Porphyrin: Tetrathiaporphyrin Dication. *Angew. Chem. Int. Ed. Engl*. **1989**, *28*, 1651–1654. (b) Vogel, E.; Pohl, M.; Herrmann, A.; Wiss, T.; König, C.; Lex, J.; Gross, M.; Gisselbrecht, J. P. Porphyrinoid Macrocycles Based on Thiophene—The Octaethyltetrathiaporphyrin Dication. *Angew. Chem. Int. Ed. Engl.* **1996**, *35*, 1520–1524.

76. Medforth, C. J. NMR Spectroscopy of Diamagnetic Porphyrins. In *The Porphyrin Handbook*, Kadish K. M., Smith, K. M., Guilard, R., Eds.; Academic Press: New York, 2000; Vol. 5, pp 1–80.

77. Lash, T. D.; Chaney, S. T. Conjugated macrocycles related to the porphyrins. 6. Oxypyriporphyrin, the first fully aromatic porphyrinoid macrocycle with a pyridine subunit. *Chem. Eur. J*. **1996**, *2*, 944–948.

78. (a) Adams K. R.; Bonnett, R.; Burke, P. J.; Salgado, A.; Vallés, M. A. Cleavage of (octaethyl-2,3-dihydroxychlorinato)nickel(II) to give the novel 2,3-dioxo-2,3-secochlorin system. *J. Chem. Soc., Perkin Trans. I* **1997**, *0*, 1769–1772. b) Kozyrev, A. N.; Alderfer, J. L.; Dougherty, T. J.; Pandey, R. K. Synthesis of Mono- and Di (oxopyri) porphyrins: A New Approach through Ring Enlargement with Diazomethane. *Angew. Chem. Int. Ed.* **1999**, *38*, 126–128. (c) Ryppa, C.; Niedzwiedzki, D.; Morozowich, N. L.; Srikanth, R.; Zeller, M.; Frank, H. A.; Brückner, C. Stepwise Conversion of Two Pyrrole Moieties of Octaethylporphyrin to Pyridin-3-ones: Synthesis, Mass Spectral, and Photophysical Properties of Mono and Bis(oxypyri)porphyrins. *Chem. Eur. J*. **2009**, *15*, 5749–5762.

79. Lash, T. D.; El-Beck, J. A.; Ferrence, G. M. Synthesis and Reactivity of *meso*-Unsubstituted Azuliporphyrins Derived from 6-*tert*-Butyl- and 6-Phenylazulene. *J. Org. Chem*. **2007**, *72*, 8402–8415.

80. Lash, T. D.; Chaney, S. T. Azuliporphyrin: A Case of Borderline Aromaticity. *Angew. Chem. Int. Ed. Engl*. **1997**, *36*, 839–840.

81. Lash, T. D.; Colby, D. A.; Graham, S. R.; Chaney, S. T. Synthesis, Spectroscopy and Reactivity of *meso*-Unsubstituted Azuliporphyrins and Their Heteroanalogues. Oxidative Ring Contractions to Carba-, Oxacarba-, Thiacarba-, and Selenacarbaporphyrins. *J. Org. Chem.* **2004**, *69*, 8851–8864.
82. Richter, D. T.; Lash, T. D. Conjugated macrocycles related to the porphyrins. Part 18: Synthesis and spectroscopic characterization of electron-rich benzi- and oxybenziporphyrins: influence of steric and electronic factors on porphyrinoid aromaticity. *Tetrahedron* **2001**, *57*, 3659–3673.
83. Campomanes, P.; Menéndez, M. I.; Cárdenas-Jirón, G. I.; Sordo, T. L. Molecular magnetic properties of heteroporphyrins: a theoretical analysis. *Phys. Chem. Chem. Phys.* **2007**, *9*, 5644–5648.
84. Rothemund, P.; Menotti, A. R. The synthesis of α,β,γ,δ-tetraphenylporphine. *J. Am. Chem. Soc.* **1941**, *63*, 267–270.
85. Rothemund, P. Formation of porphyrins from pyrrole and aldehydes. *J. Am. Chem. Soc.* **1935**, *57*, 2010–2011.
86. Sessler, J. L.; Mozaffari, A.; Johnson, M. R. 3,4-Diethylpyrrole and 2,3,7,8,12,13,17,18-octaethylporphyrin. *Org. Synth.* **1991**, *70*, 68–77.
87. Taniguchi, M.; Lindsey, J. S. Enumeration of isomers of substituted tetrapyrrole macrocycles: from classical problems in biology to modern combinatorial libraries. In *Handbook of Porphyrin Science*; Kadish, K. M, Smith, K. M, Guilard R., Eds.; World Scientific Press; Singapore, 2012; Vol. 23, pp 3–80.
88. Mauzerall, D. The thermodynamic stability of porphyrinogens. *J. Am. Chem. Soc.* **1960**, *82*, 2601–2603.

89. Vicente, M. D.; Smith, K. M. Syntheses and Functionalizations of Porphyrin Macrocycles. *Curr Org Synth*. **2014**, *11*, 3-28.

90. Arsenault, G. P.; Bullock, E.; MacDonald, S. F. Pyrromethanes and porphyrins therefrom. *J. Am. Chem. Soc*. **1960**, *82*, 4384–4389.

91. Lash, T. D. What's in a Name? The MacDonald Condensation. *J. Porphyrins Phthalocyanines* **2016,** *20,* 855–888.

92. (a) Sessler, J. L.; Lynch, V.; Johnson, M. R. Synthesis and crystal structure of a novel tripyrrane-containing porphyrinogen-like macrocycle. *J. Org. Chem*. **1987**, *52*, 4394–4397. (b) Sessler, J.L.; Cyr, M. J.; Lynch, V. Synthetic and structural studies of sapphyrin, a 22π-electron pentapyrrolic "expanded porphyrin". *J. Am. Chem. Soc*. **1990**, *112*, 2810–2813.

93. Jiao,W.; Lash, T. D. *tert*-Butyl-Substituted Tripyrranes: Insights into the Steric and Conformational Factors that Influence Porphyrinoid Ring Formation in the "3 + 1" Methodology. *J. Org. Chem.* **2003**, *68,* 3896–3901.

94. Lash, T. D.; Bergman, K. M. Further Observations on Conformational and Substituent Effects in Acid-Catalyzed "3 + 1" Cyclizations of Tripyrranes with Aromatic Dialdehydes. *J. Org. Chem.* **2012**, *77*, 9774–9783.

95. Chmielewski, P. J.; Latos-Grazynski, L. *N*-methyltetraphenylporphyrin with an inverted *N*-methylpyrrole ring: the first isomer of *N*-methyltetraphenylporphyrin. *J. Chem. Soc. Perkin Trans. 2* **1995**, *0*, 503-509.

96. Xiao, Z.; Dolphin, D. Facile synthesis of *N*,*N*′-dimethylated *N*-confused porphyrins. *Tetrahedron* **2002**, *58*, 9111-9116.

97. Lash, T. D.; Miyake, K.; Xu, L.; Ferrence, G. M. Synthesis of a Series of Aromatic Benziporphyrins and Heteroanalogues via Tripyrrane-Like Intermediates Derived from Resorcinol and 2-Methylresorcinol. *J. Org. Chem.* **2011**, *76,* 6295-6308.

98. Chmielewski, P. J.; Latos-Grazynski, L.; Glowiak, T. Reactions of Nickel(II) 2-Aza-5,10,15,20-tetraphenyl-21- carbaporphyrin with Methyl Iodide. The First Structural Characterization of a Paramagnetic Organometallic Nickel(II) Complex. *J. Am. Chem. Soc.* **1996**, *118,* 5690–5701.

99. Lash, T. D. Carbaporphyrinoid Systems. *Chem. Rev*. **2017**, *117*, 2313−2446.

100. Lavallee, D. K. *The Chemistry and Biochemistry of N-Substituted Porphyrins*, VCH Verlagsgesellschaft: Weinheim, Germany,1987; p. 313

101. Lash, T. D. Unexpected Alkyl Group Migration in Palladium(II) Benzocarbaporphyrins. *Org. Lett.* **2011**, *13,* 4632-4635.

102. Shears, B.; Hambright, P. A novel metal ion catalyzed demethylation of an N-methyl etioporphyrin. *Inorg. Nucl. Chem. Lett*. **1970**, *6,* 679-680.

103. Lavallee, D. K. Metal ion promoted demethylation of N-methyltetraphenyl-porphinatocopper(II). *Inorg. Chem*. **1976**, *15,* 691-694.

104. Lavallee, D. K. Metal ion promoted demethylation of N-Methyltetraphenyl-porphyrin by nickel(II), zinc(II) and manganese(II). *Inorg. Chem*. **1977**, *16,* 955-957.

105. Kuila, D.; Lavallee, D. K. Kinetics and mechanisms of dealkylation reactions of N-methylporphyrin complexes. 3. Effects of porphyrin ring substituents and reaction media. *Inorg. Chem*. **1983**, *22,* 1095-1099.

106. Szyszko, B.; Latos-Grazynski, L.; Szterenberg, L. A Facile Palladium-Mediated Contraction of Benzene to Cyclopentadiene: Transformations of Palladium(II) *p*-Benziporphyrin. *Angew. Chem., Int. Ed.* **2011**, *50*, 6587–6591.

107. Li, D.; Lash, T. D. Synthesis and Reactivity of Carbachlorins and Carbaporphyrins. *J. Org. Chem.* **2014**, *79*, 7112-7121.

108. Grabowski, E. Y.; AbuSalim, D. I.; Lash, T. D. Naphtho[2,3-*b*]carbaporphyrins. *J. Org. Chem.* **2018**, *83*, 11825-11838

109. Pacholska-Dudziak, E.; Skonieczny, J.; Pawlicki, M.; Szterenberg, L.; Ciunik, Z.; Latos-Grazyński, L. Palladium Vacataporphyrin Reveals Conformational Rearrangements Involving Hückel and Möbius Macrocyclic Topologies. *J. Am. Chem. Soc.* **2008**, *130*, 6182-6195.

110. Yoneda, T.; Saito, S.; Yorimitsu, H.; Osuka, A. Palladium(II)-Triggered Rearrangement of Heptaphyrins to *N*-Confused Porphyrins. *Angew. Chem., Int. Ed.* **2011**, *50*, 3475-3478.

111. Latham, A. N.; Ferrence, G. M.; Lash, T. D. Metalation and Methyl Group Migration in 21-, 22-, and 23-Methylcarbaporphyrins: Synthesis and Characterization of Palladium(II), Rhodium(I), and Rhodium(III) Derivatives. *Organometallics* **2019**, *38*, 575-585.

112. Chapelle, J. P.; Elguero, J.; Jacquier, R.; Tarrago, G. Enehydrazines [(alk-1-en-1-yl)hydrazines]. III. Reaction of 1,2-Dimethylhydrazine with Carbonyl Compounds; Formation of *N*-Methylpyrroles and 3-Pyrazolines. *Bull. Soc. Chim. Fr.* **1970**, 3147-3155.

113. Boudif, A.; Momenteau, M. A New Convergent Method for Porphyrin Synthesis Based on a '3 + 1' condensation. *J. Chem. Soc., Perkin Trans. 1* **1996**, 1235-1242.

114. Lash, T. D. Porphyrins with Exocyclic Rings. Part 9. Porphyrin Synthesis by the "3 + 1" Approach. *J. Porphyrins Phthalocyanines* **1997**, *1*, 29-44.

115. Jackson, A. H.; Pandey R. K.; Roberts, E. Total Synthesis of an *N*-Methylporphyrin. *J. Chem. Soc., Chem. Commun.* **1985**, 470–471.

116. Pandey, R. K.; Jackson A. H.; Smith, K. M. Ring Syntheses of the Four *N*-Methylprotoporphyrin Isomers and of Related *N*-Methyl and *N,N'*-Dimethylporphyrins. *J. Chem. Soc., Perkin Trans. 1* **1991**, 1211-1220.

117. Bruno, I. J.; Cole, J. C.; Kessler, M.; Luo, J.; Motherwell, W. D. S.; Purkis, L. H.; Smith, B. R.; Taylor, R.; Cooper, R. I.; Harris, S. E.; Orpen, A. G. Retrieval of Crystallographically-derived Molecular Geometry Information. *J. Chem. Inf. Comput. Sci.* **2004**, *44*, 2133-2144.

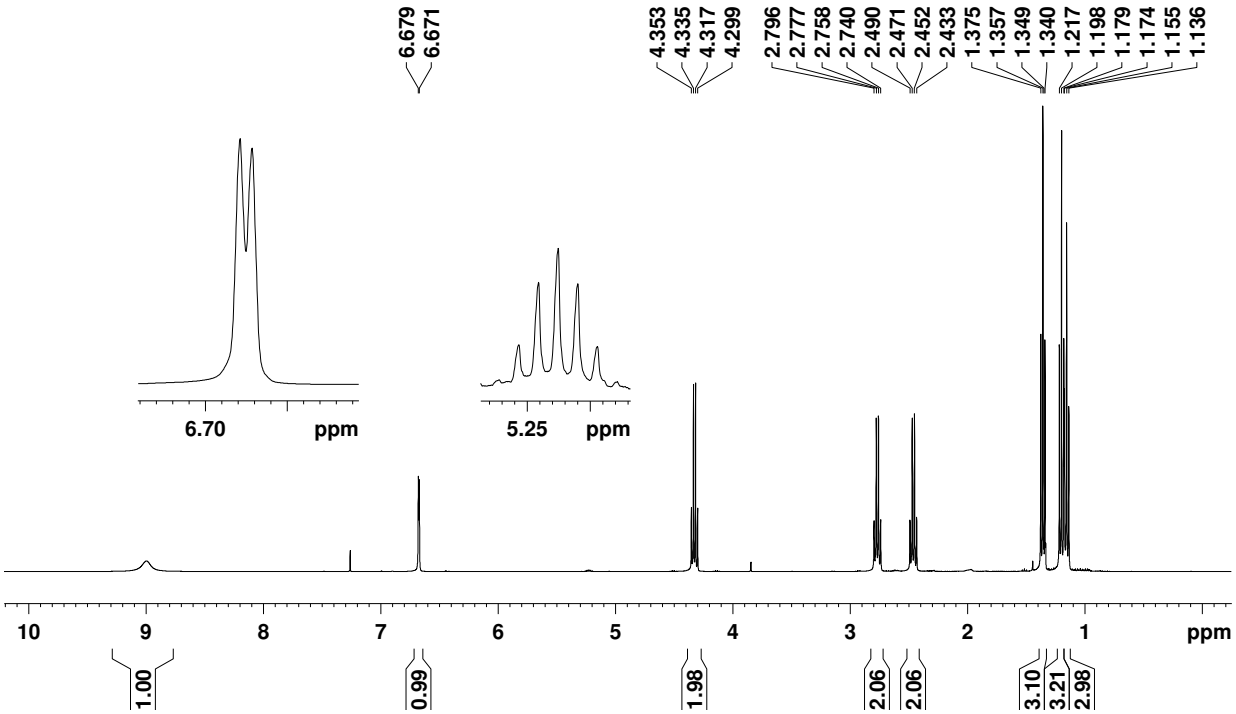

Figure A-1. 400 MHz ^{1}H NMR spectrum of pyrrole ethyl ester **79** in $CDCl_3$. The small multiplet at 5.23 ppm corresponds to a small amount of the related isopropyl ester (ca. 3%) that results from transesterification with the solvent 2-propanol.

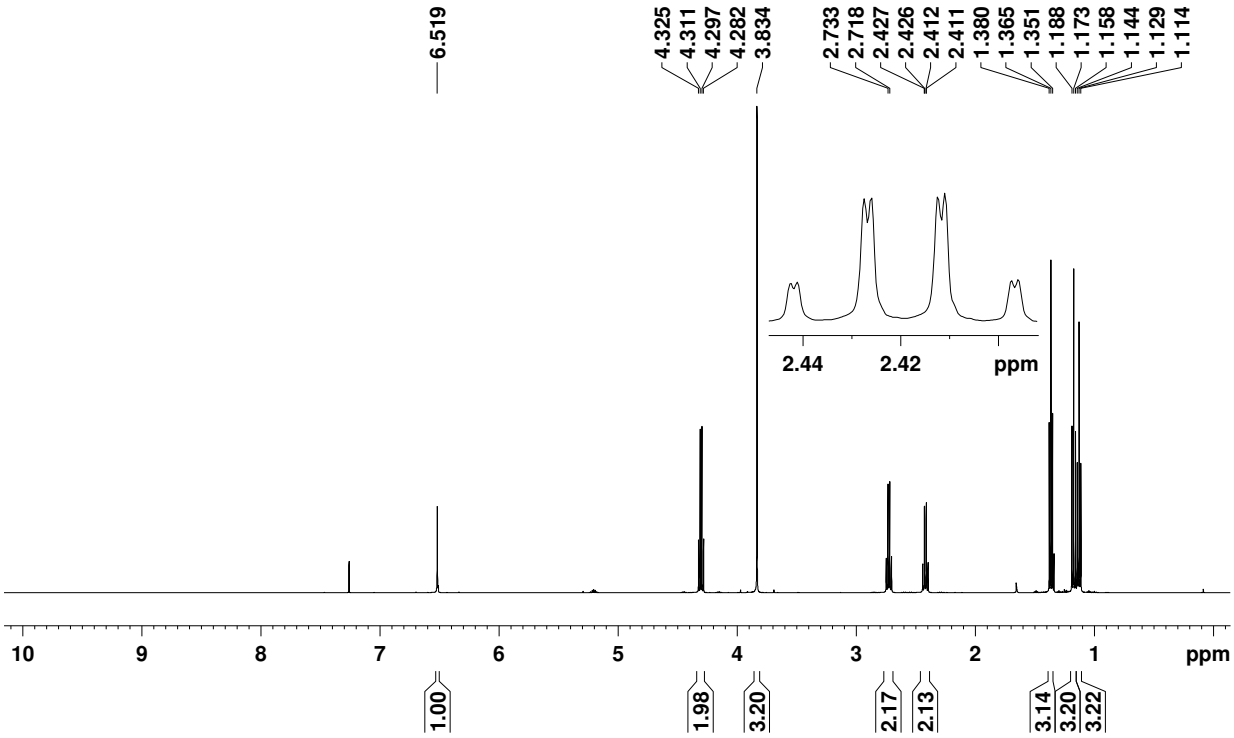

Figure A-2. ^{1}H NMR spectrum of *N*-methylpyrrole ethyl ester **79** in $CDCl_3$.

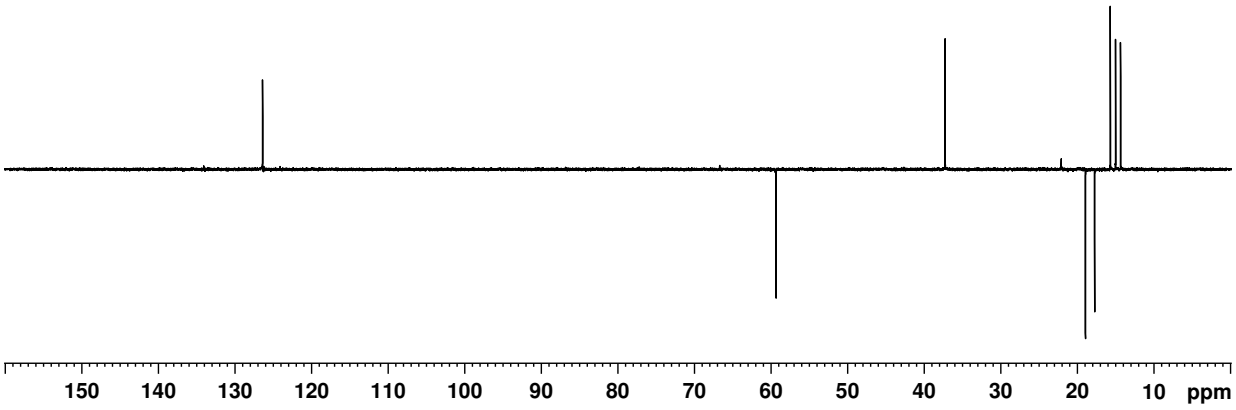

Figure A-3. DEPT-135 NMR spectrum of *N*-methylpyrrole ester **17b**.

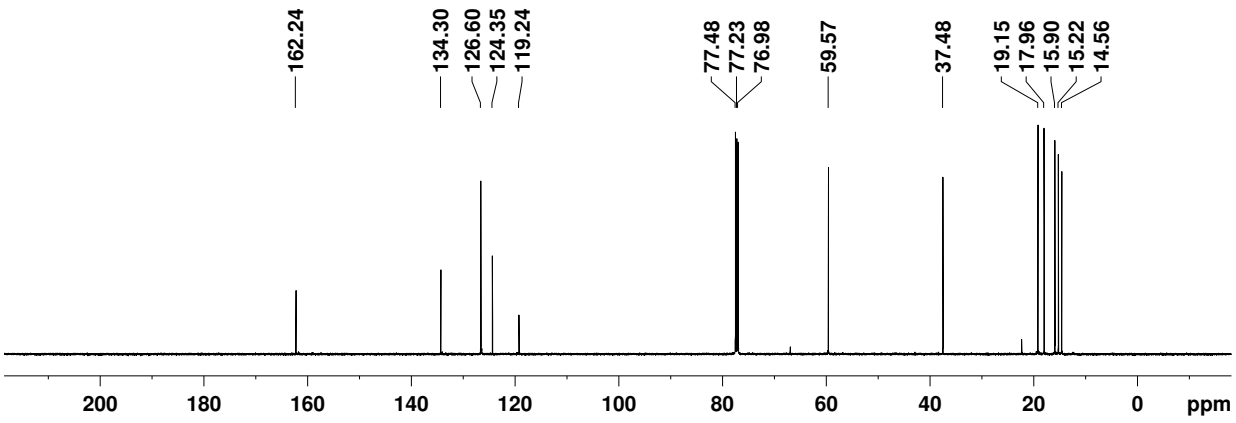

Figure A-4. 125 MHz ^{13}C NMR spectrum of *N*-methylpyrrole ethyl ester **79** in $CDCl_3$. The small peaks showing up at 22.3 and 66.9 ppm correspond to the presence of the related isopropyl ester.

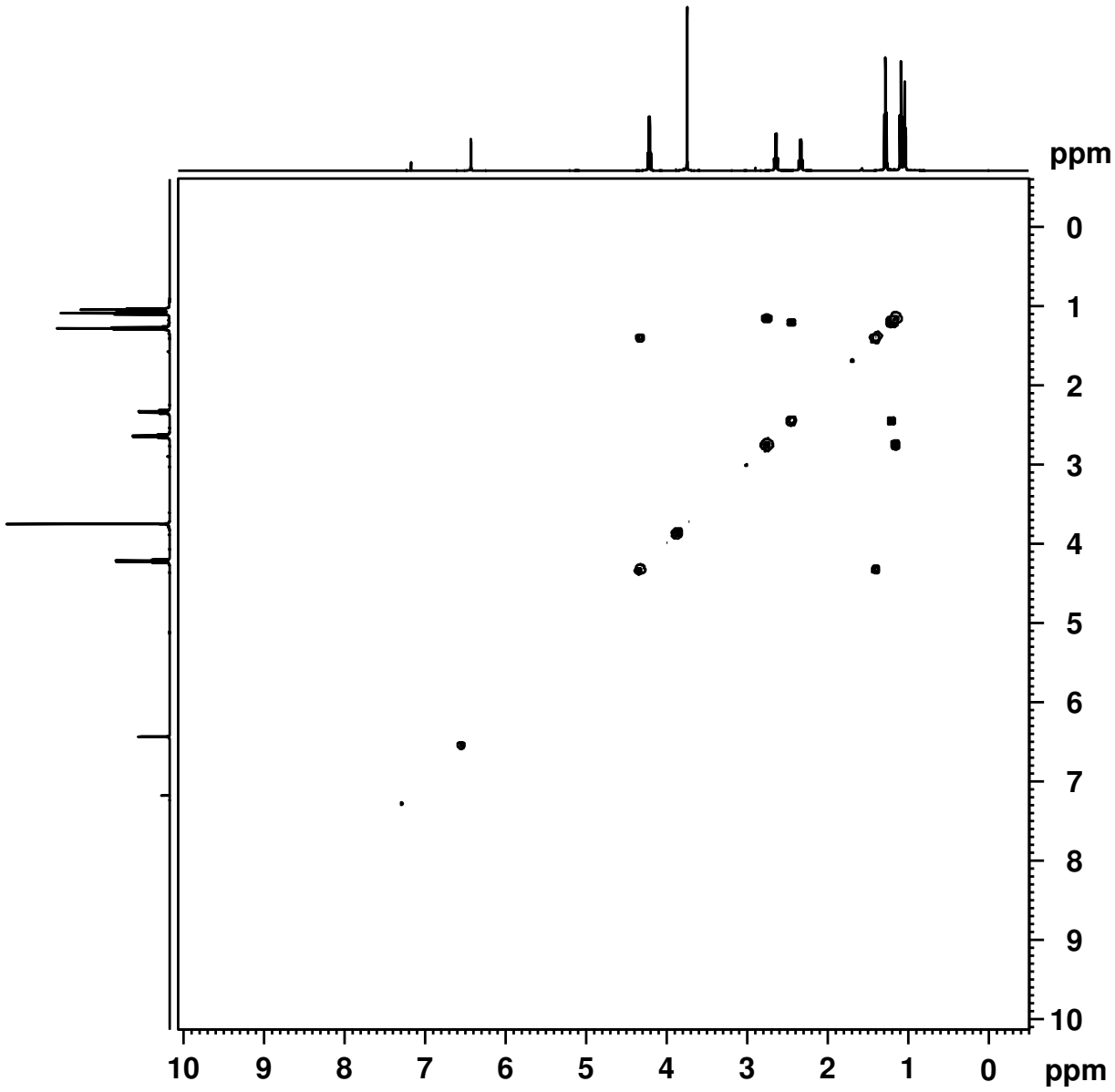

Figure A-5. ^{1}H-^{1}H COSY NMR spectrum of *N*-methylpyrrole ethyl ester **79** in $CDCl_3$.

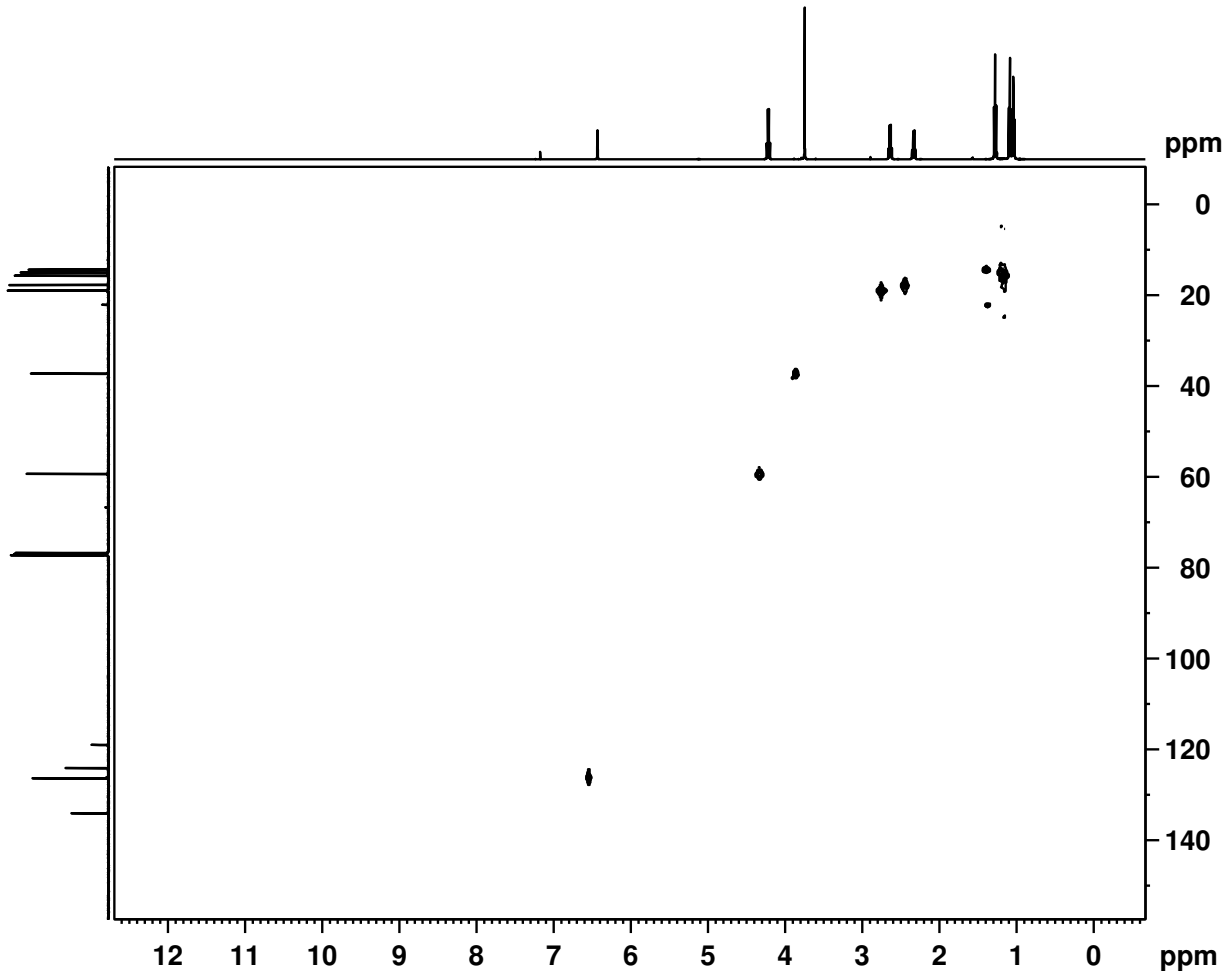

Figure A-6. HSQC NMR spectrum of *N*-methyl pyrrole ester **79**.

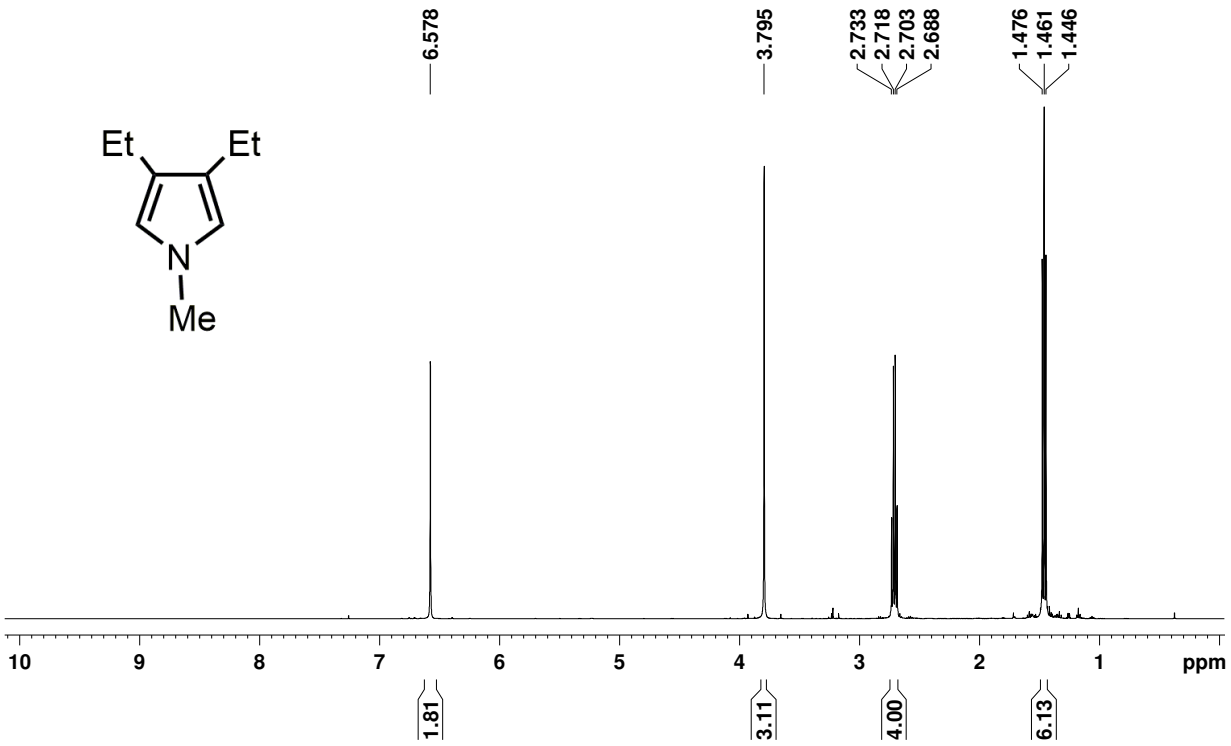

Figure A-7. 500 MHz ^{1}H NMR spectrum of 3,4-diethyl-1-methylpyrrole (**53b**) in $CDCl_3$.

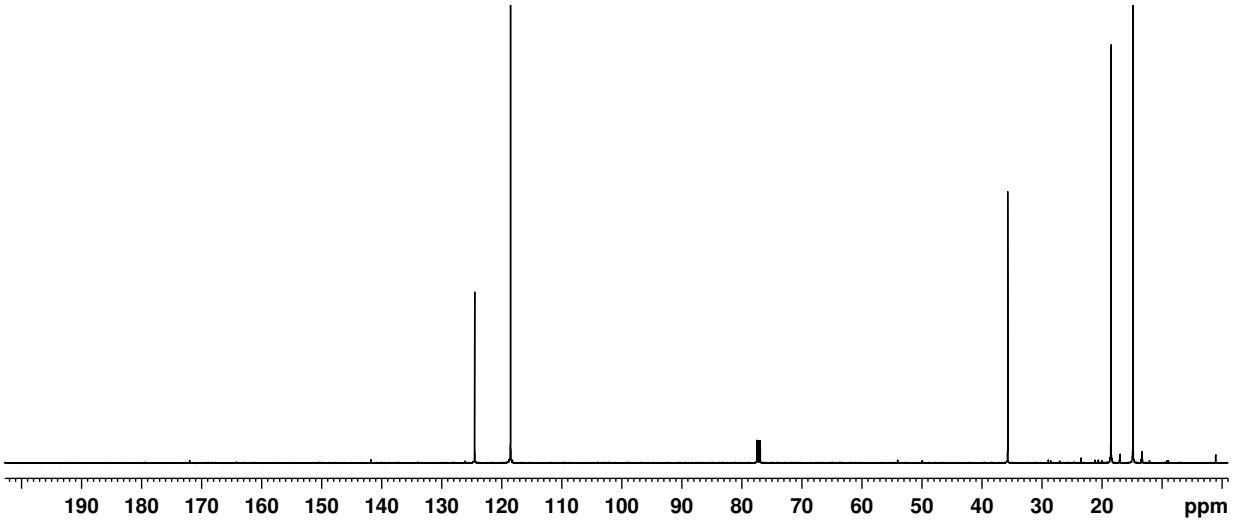

Figure A-8. 125 MHz ^{13}C NMR spectrum of 3,4-diethyl-1-methylpyrrole (**53b**) in $CDCl_3$.

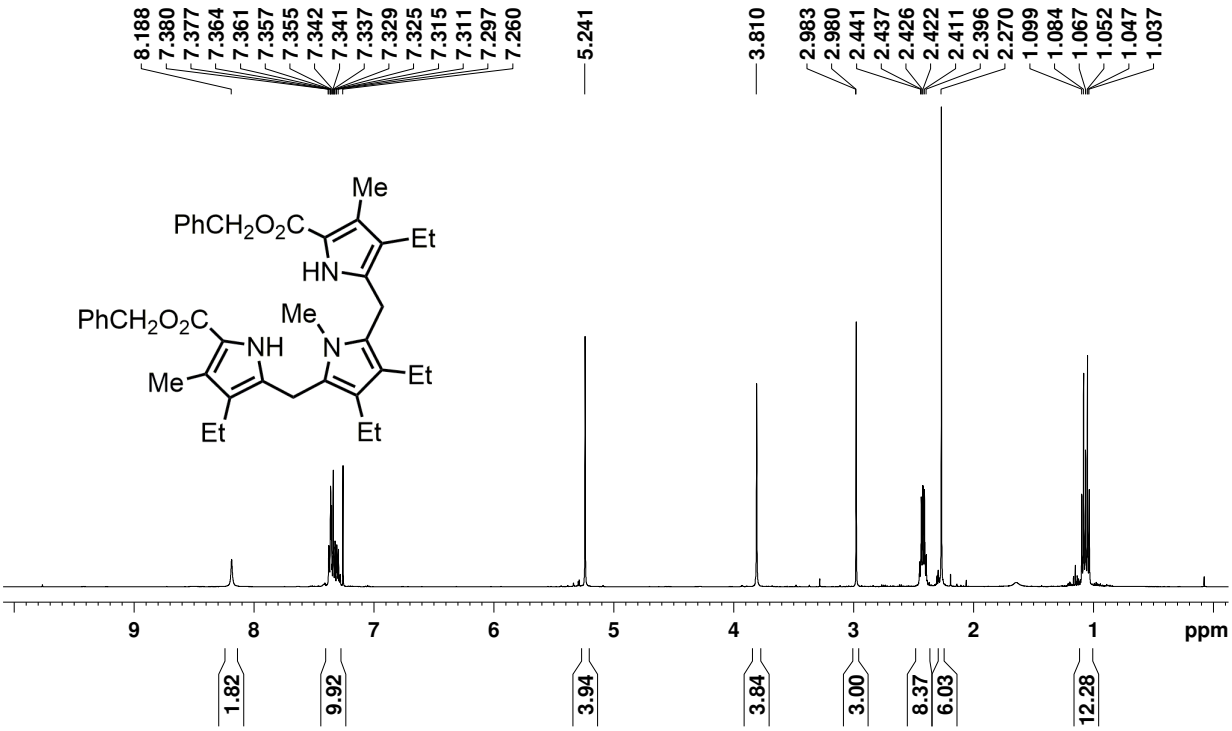

Figure A-9. 500 MHz ^{1}H NMR spectrum of *N*-methyltripyrrane dibenzyl ester **54c** in $CDCl_3$.

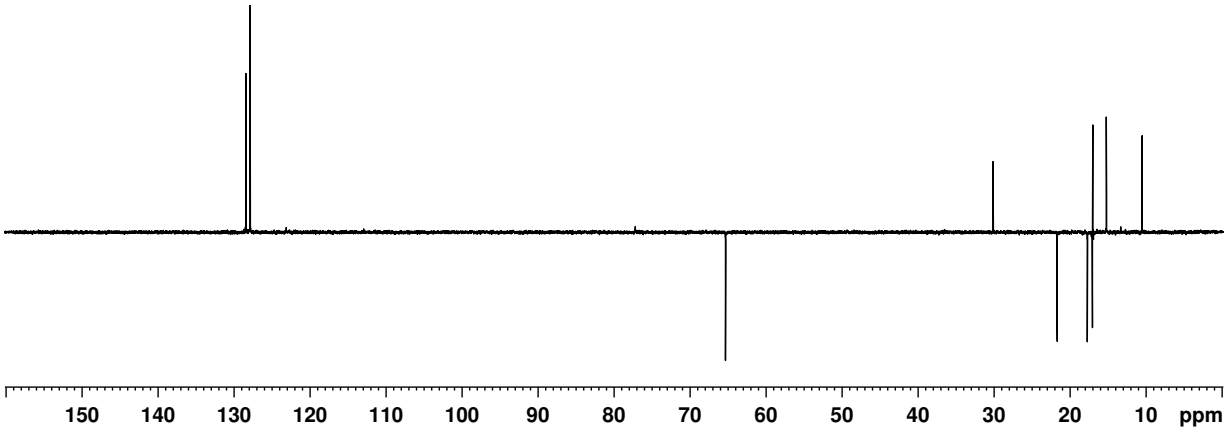

Figure A-10. 125 MHz ^{1}H NMR spectrum of *N*-methyltripyrrane dibenzyl ester **54c** in $CDCl_3$.

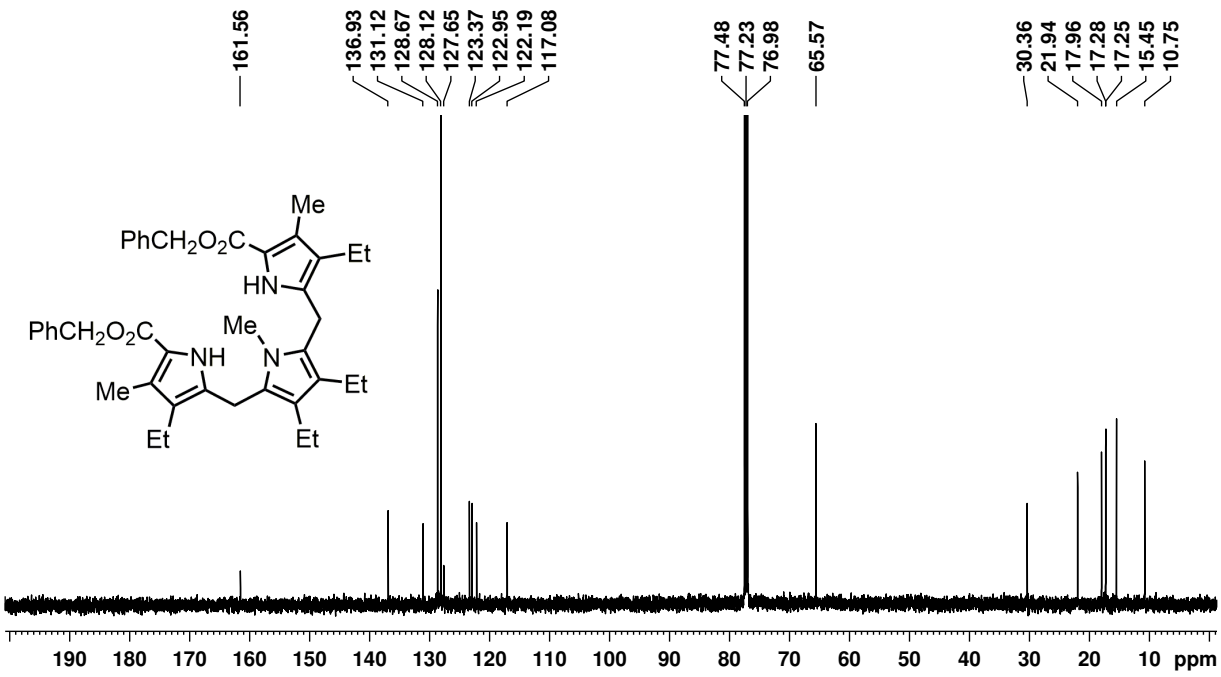

Figure A-11. 125 MHz ^{1}H NMR spectrum of *N*-methyltripyrrane dibenzyl ester **54c** in $CDCl_3$.

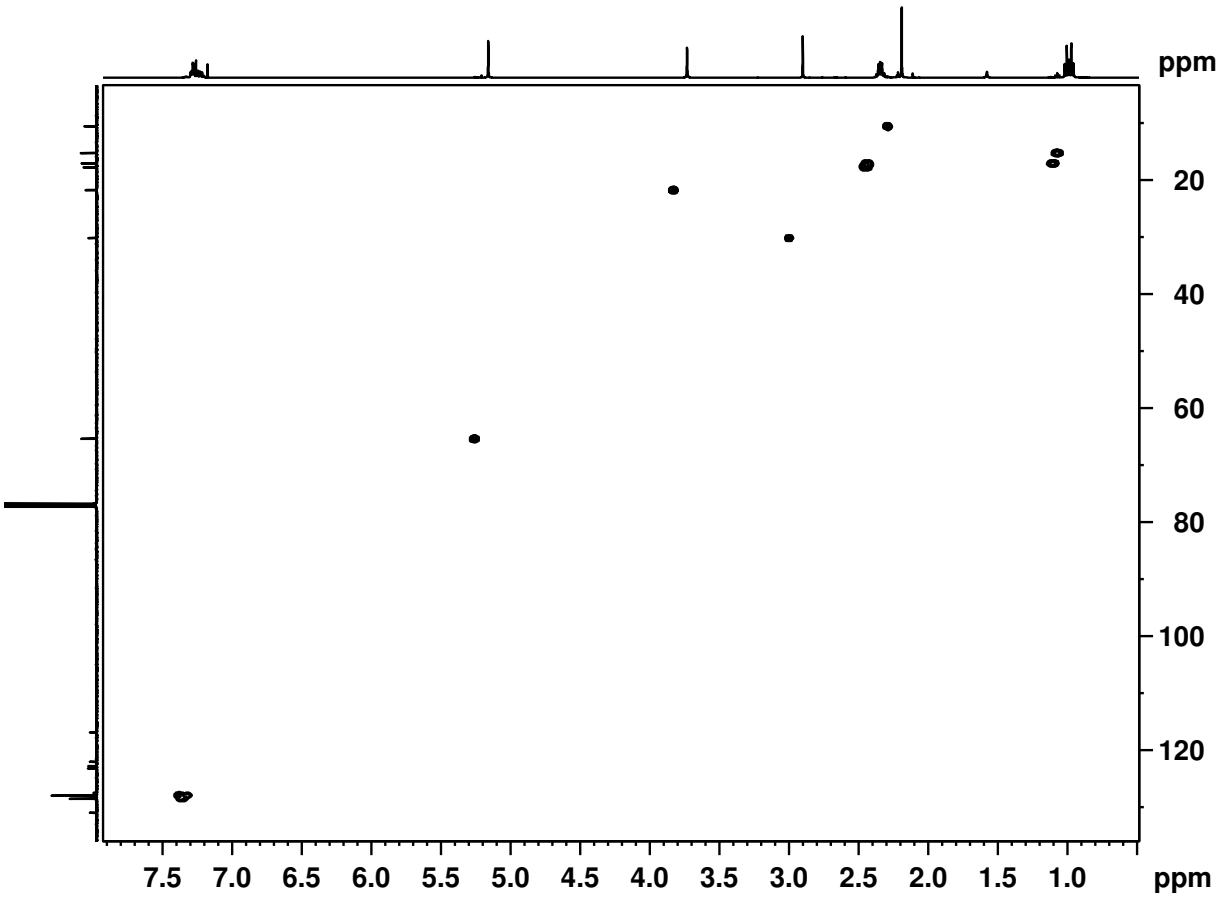

Figure A-12. HSQC NMR spectrum of *N*-methyltripyrrane dibenzyl ester **54c** in $CDCl_3$.

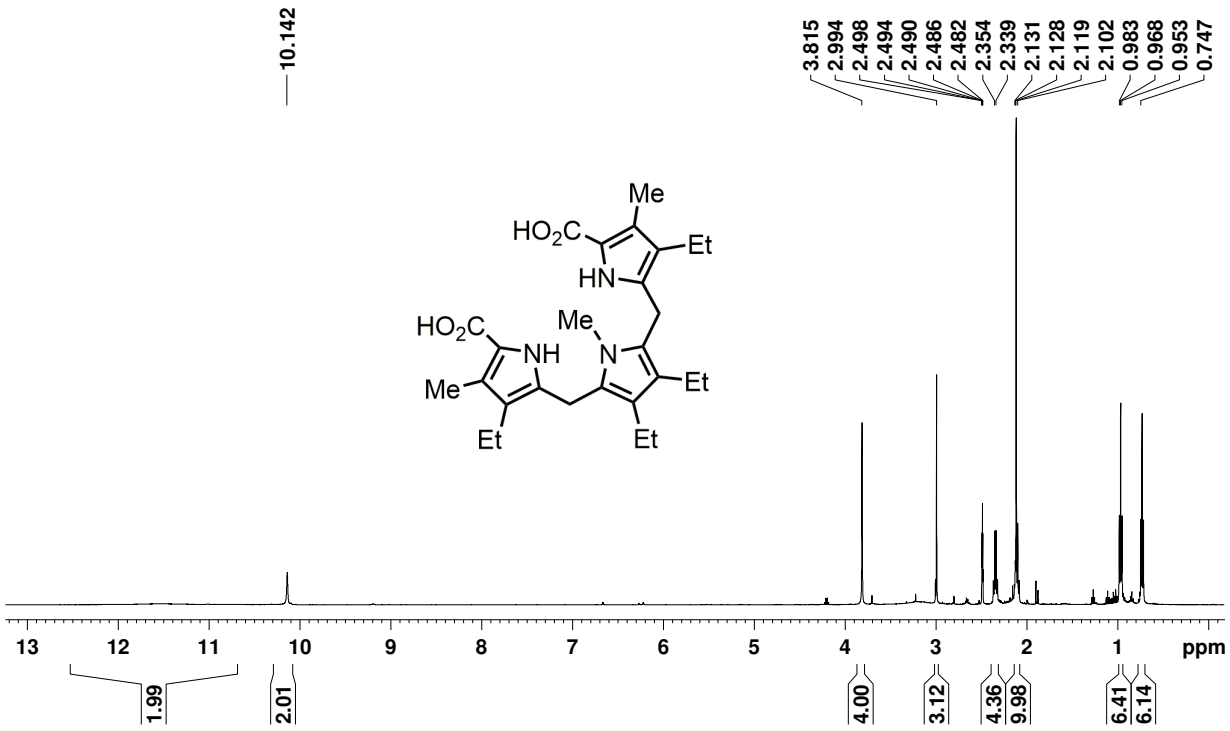

Figure A-13. 500 MHz ^{1}H NMR spectrum of *N*-methyltripyrrane dicarboxylic acid **54d** in d_6-DMSO.

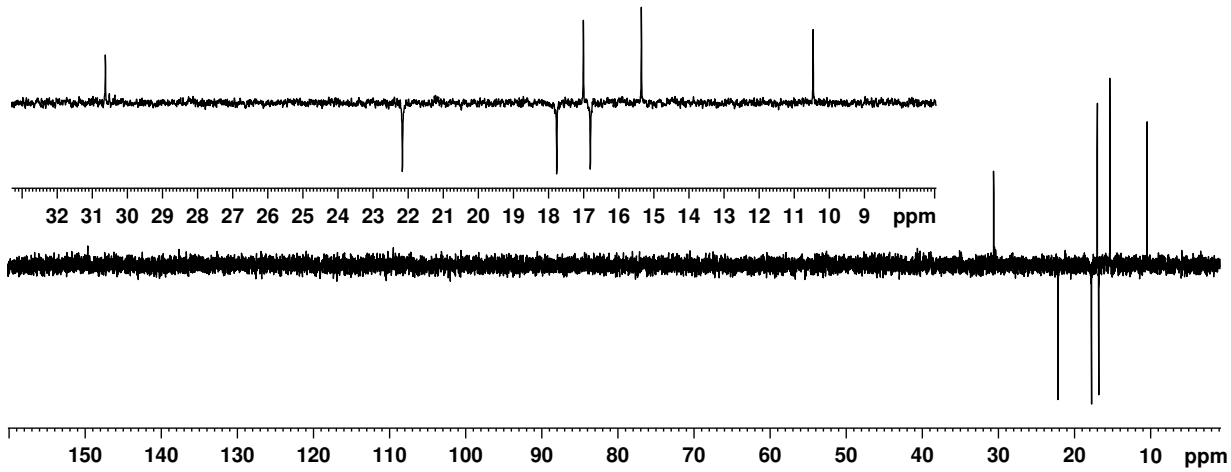

Figure A-14. DEPT-135 NMR spectrum of *N*-methyltripyrrane dicarboxylic acid **54d** in d_6-DMSO.

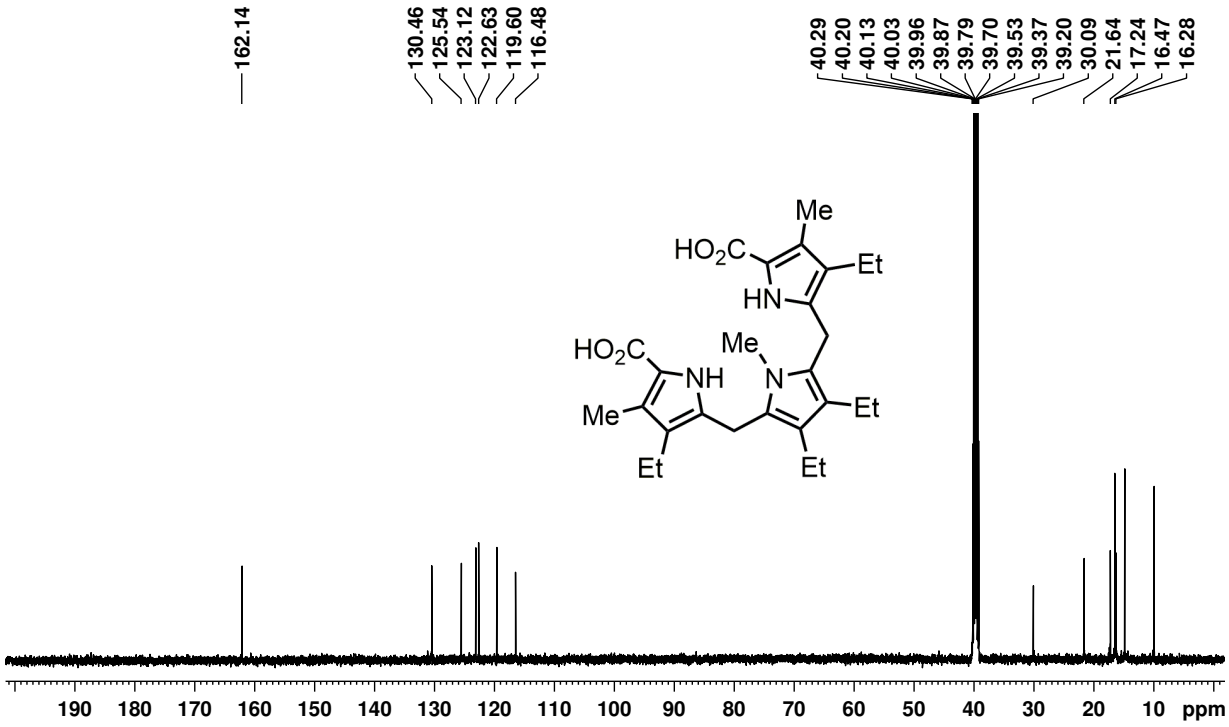

Figure A-15. 125 MHz ^{13}C NMR spectrum of *N*-methyltripyrrane dicarboxylic acid **54d** in d_6-DMSO.

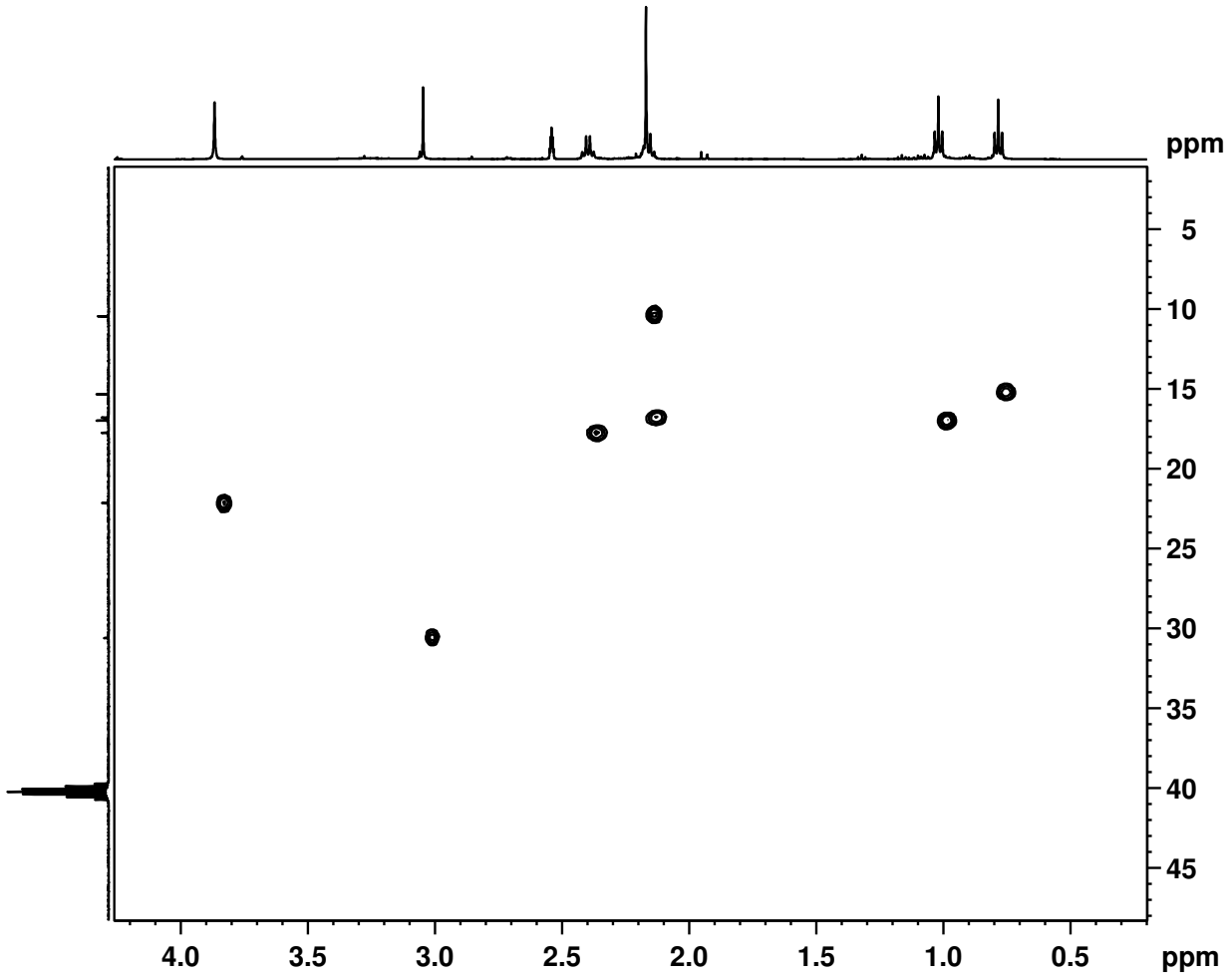

Figure A-16. HSQC NMR spectrum of *N*-methyltripyrrane dicarboxylic acid **54d** in d_6-DMSO.

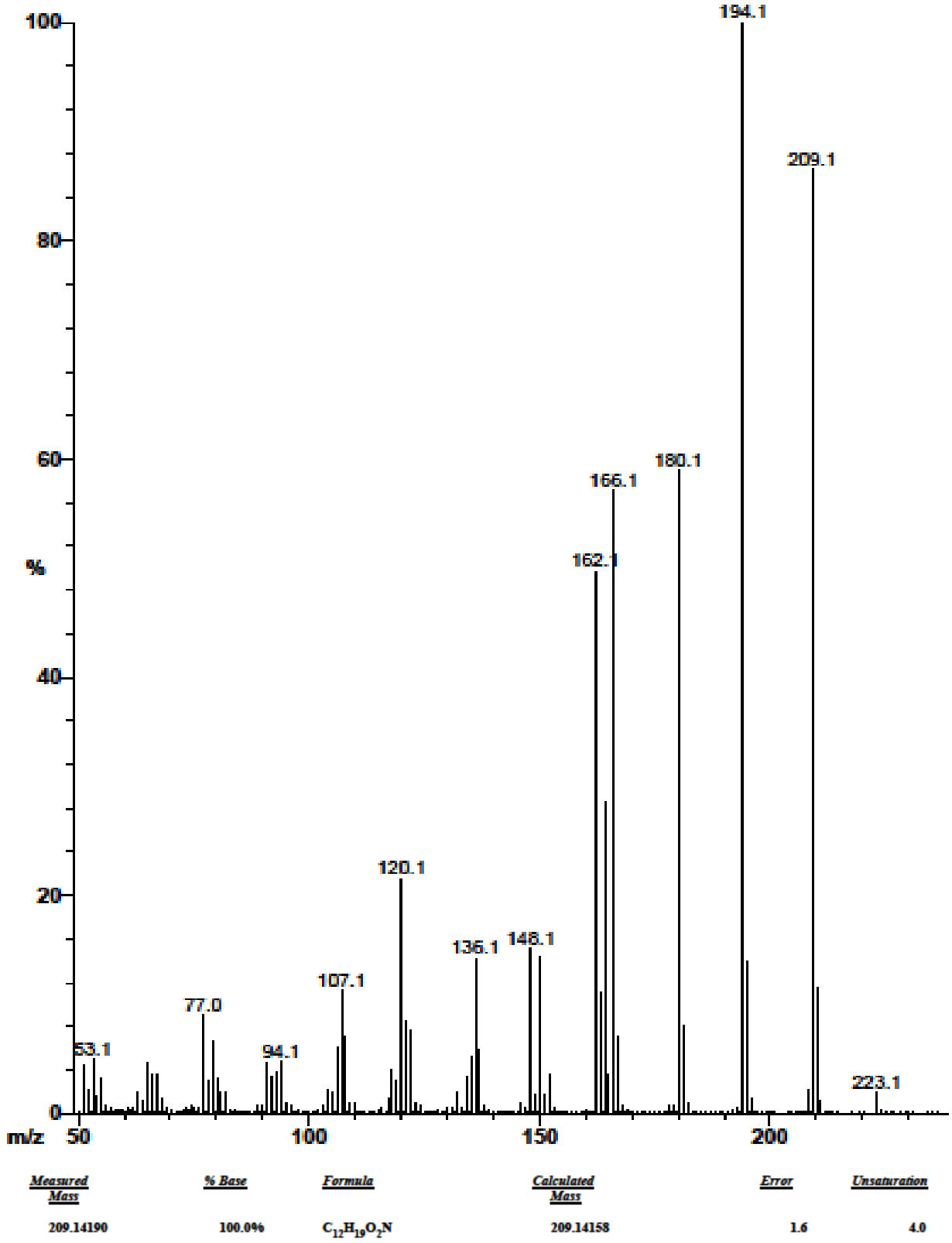

Figure A-17. EI MS of *N*-methylpyrrole ester **79**.

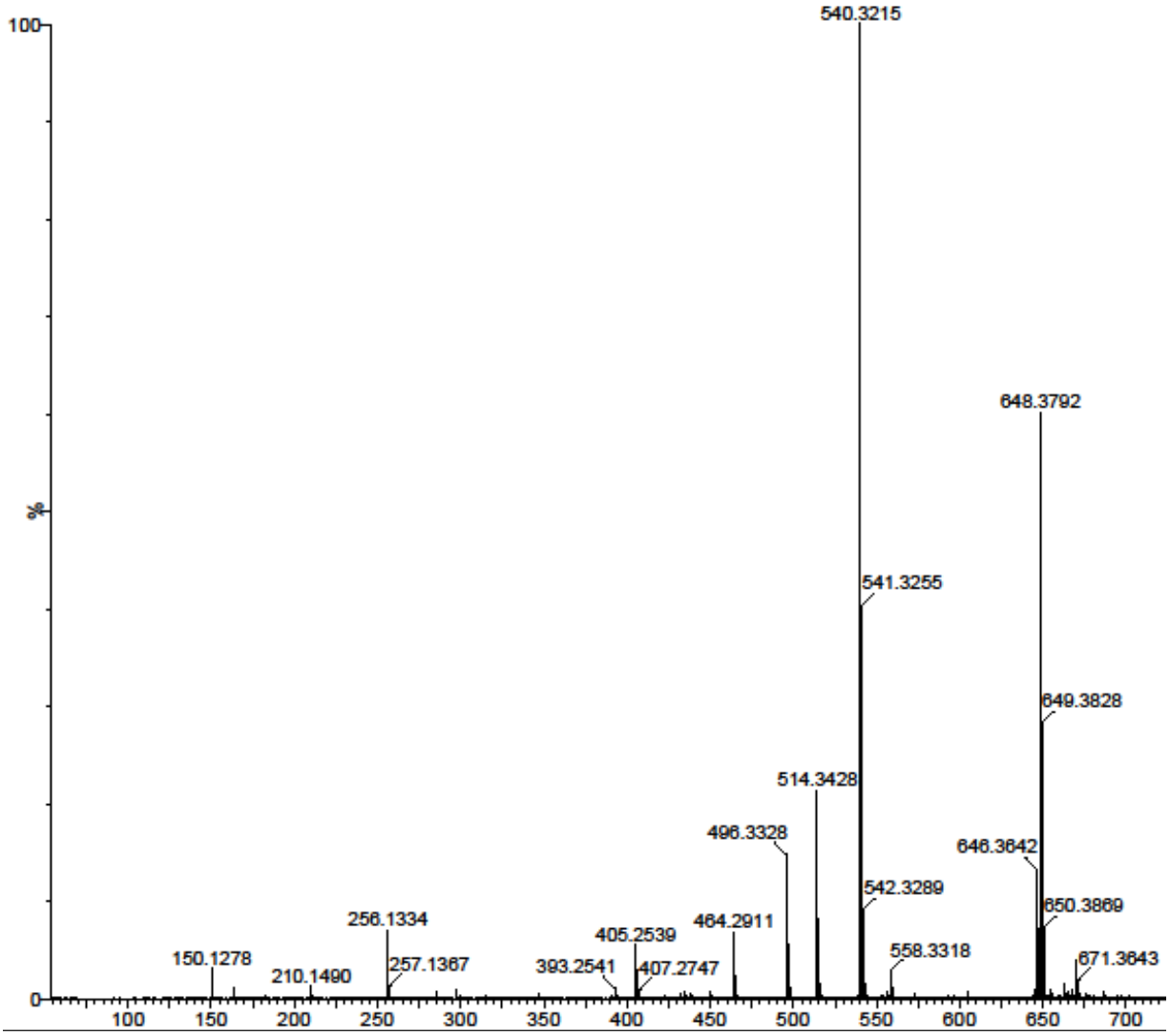

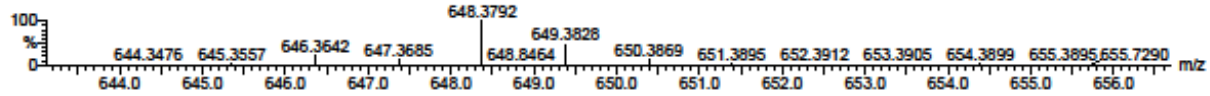

Minimum:				-1.5		
Maximum:		5.0	5.0	100.0		
Mass	**Calc. Mass**	**mDa**	**PPM**	**DBE**	**i-FIT**	**Formula**
648.3792	648.3801	-0.9	-1.4	18.5	1.7	C41 H50 N3 O4
	648.3777	1.5	2.3	15.5	22.0	C39 H51 N3 O4 Na
	648.3818	-2.6	-4.0	19.5	33.8	C44 H51 N O2 Na
	648.3761	3.1	4.8	14.5	88.8	C36 H50 N5 O6

Figure A-18. ESI MS of *N*-methyltripyrrane dibenzyl ester **54c**.

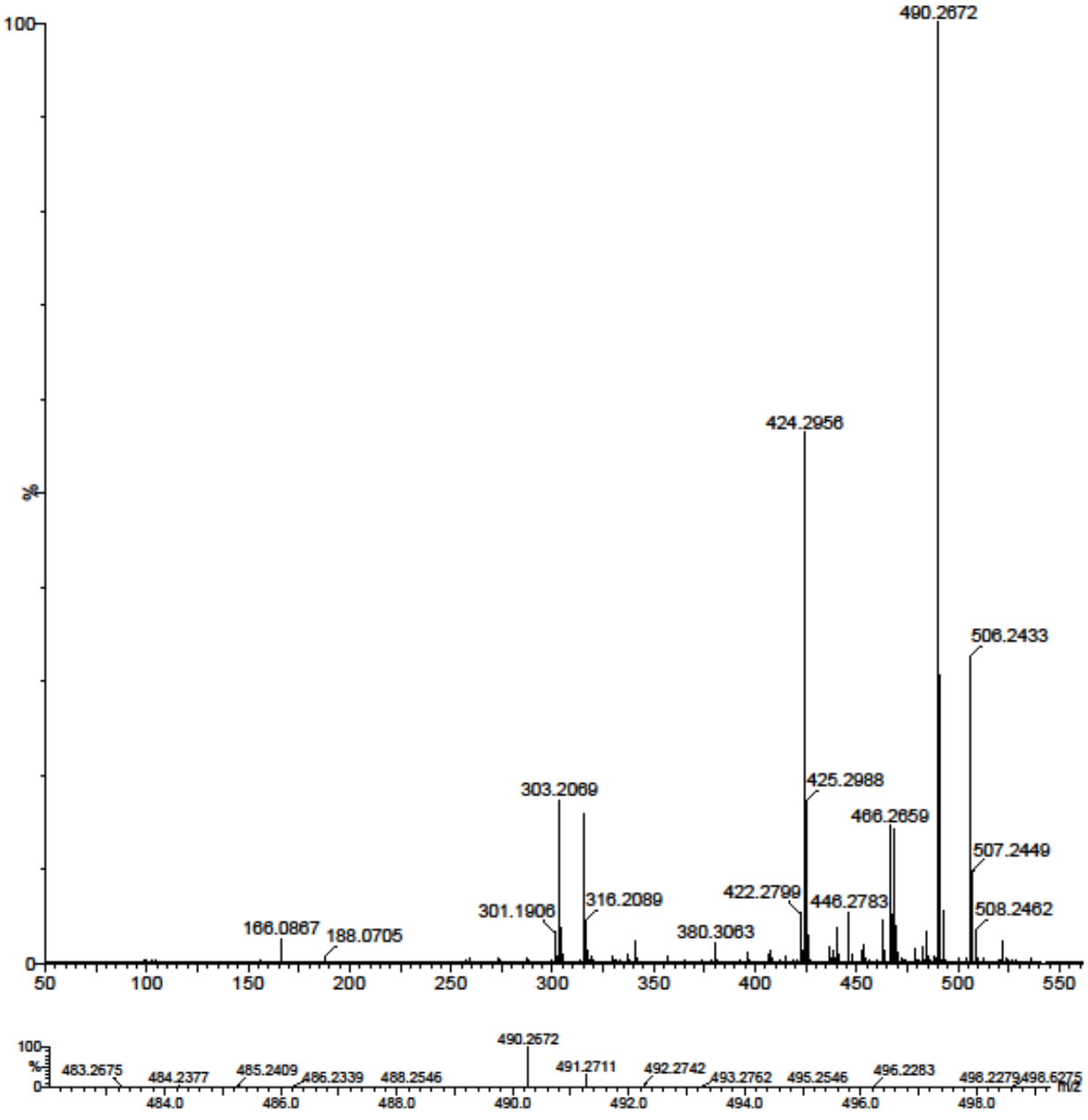

Minimum:				-1.5		
Maximum:		5.0	5.0	100.0		
Mass	Calc. Mass	mDa	PPM	DBE	i-FIT	Formula
490.2672	490.2666	0.6	1.2	9.5	3.0	C24 H36 N5 O6
	490.2682	-1.0	-2.0	10.5	2.4	C27 H37 N3 O4 Na

Figure A-19. ESI MS of *N*-methyltripyrrane dicarboxylic acid **54d**.

APPENDIX B: SPECTROSCOPIC DATA FOR 23-METHYLBENZOCARBAPORPHYRIN AND PALLADIUM(II) COMPLEXES

Table B-1. Summary of framework bond distances (Å) and angles (°) for **72** and **76**.

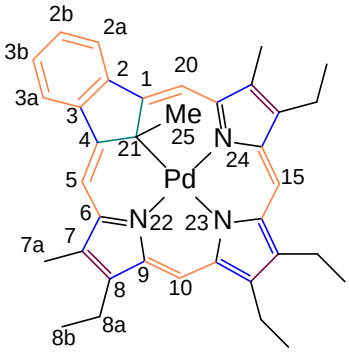

72

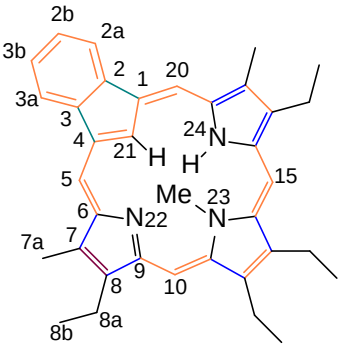

76

	72	**76**
C21-C25	1.577(2)	--
M-C21	2.0576(16)	--
M-N22	2.0363(14)	--
M-N23	2.0697(14)	--
M-N24	2.0352(14)	--
M-C25	--	--
C1-C21	1.491(2)	1.406(2)
C1-C2	1.450(2)	1.4822(19)
C2-C3	1.414(2)	1.4136(19)
C3-C4	1.449(2)	1.4753(19)
C4-C21	1.498(2)	1.4077(19)
C4-C5	1.367(2)	1.3977(19)
C5-C6	1.412(2)	1.4015(19)
C6-N22	1.364(2)	1.3668(17)
C6-C7	1.446(2)	1.4590(19)
C7-C8	1.361(2)	1.3574(19)
C8-C9	1.455(2)	1.4577(19)
C9-N22	1.387(2)	1.3638(17)
C9-C10	1.378(2)	1.4001(19)
C10-C11	1.402(2)	1.3928(19)
C11-N23	1.363(2)	1.3991(17)
C11-C12	1.448(2)	1.4302(18)
C12-C13	1.374(2)	1.3784(19)
C13-C14	1.446(2)	1.4301(18)

C14-N23	1.368(2)	1.4037(17)
C14-C15	1.396(2)	1.3924(19)
C15-C16	1.384(2)	1.3968(19)
C16-N24	1.390(2)	1.3711(17)
C16-C17	1.451(2)	1.4369(19)
C17-C18	1.363(2)	1.3781(19)
C18-C19	1.449(2)	1.4422(19)
C19-N24	1.365(2)	1.3724(17)
C19-C20	1.412(2)	1.3937(19)
C1-C20	1.366(2)	1.3971(19)
C1-C21-C4	103.80(13)	111.55(13)
C21-M-N22	89.67(6)	--
C21-M-N23	170.06(6)	--
C21-M-N24	90.12(6)	--
N22-M-N23	90.34(6)	--
N22-M-N24	177.98(6)	--
N23-M-N24	90.22(6)	--
C25-C21-M	98.06(10)	--
C25-C21-C1	107.20(13)	--
C25-C21-C4	107.75(13)	--

Purple more double bond like (≤1.37 Å), orange – more aromatic (1.38-1.41 Å), blue – more single bond like (1.42-1.45 Å), green – single bond limit (≥1.46 Å).

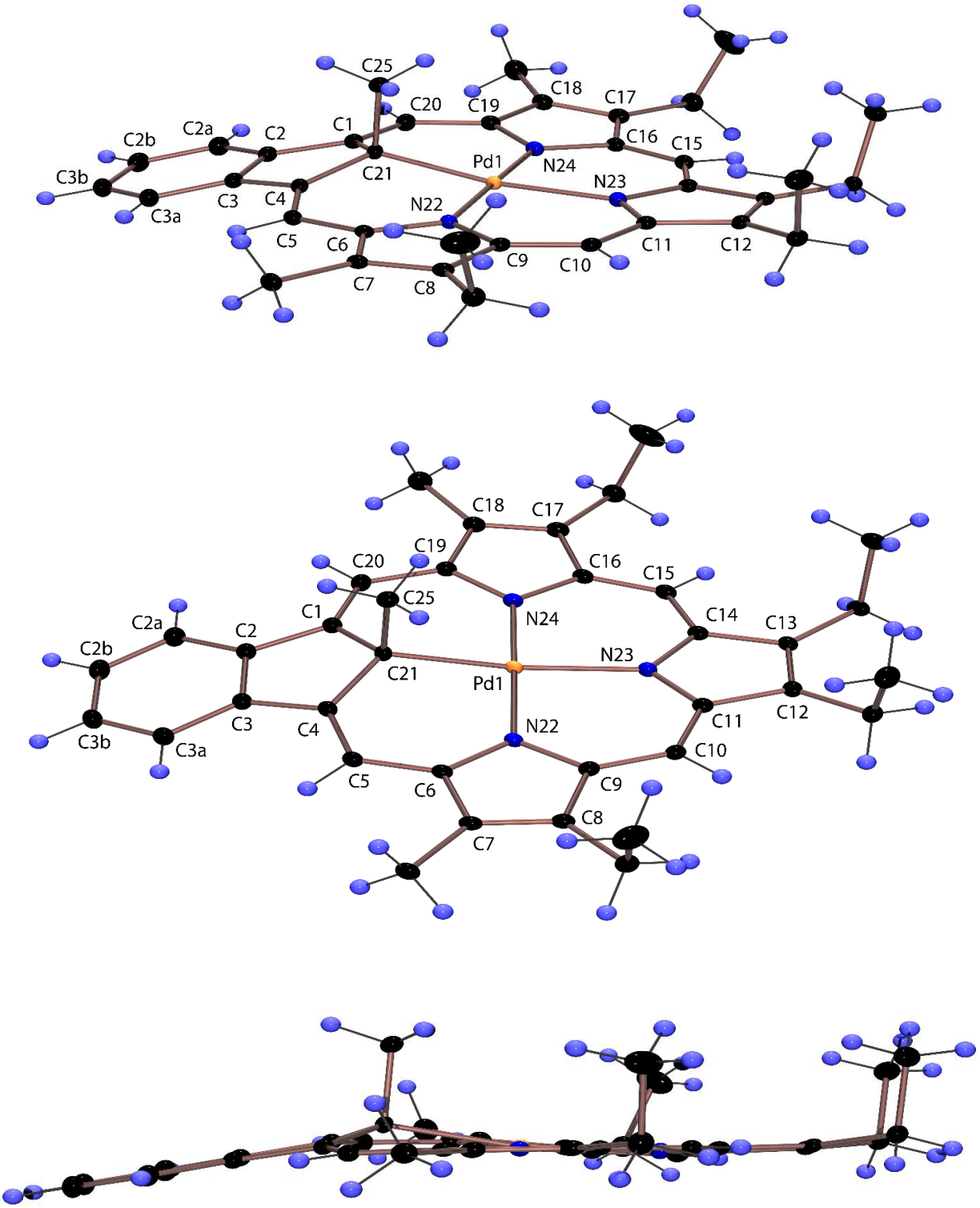

Figure B-1. Color POV-Ray rendered ORTEP III drawings (50% probability level, hydrogen atoms rendered arbitrarily small for clarity) showing three views of palladium(II) derivative **72**.

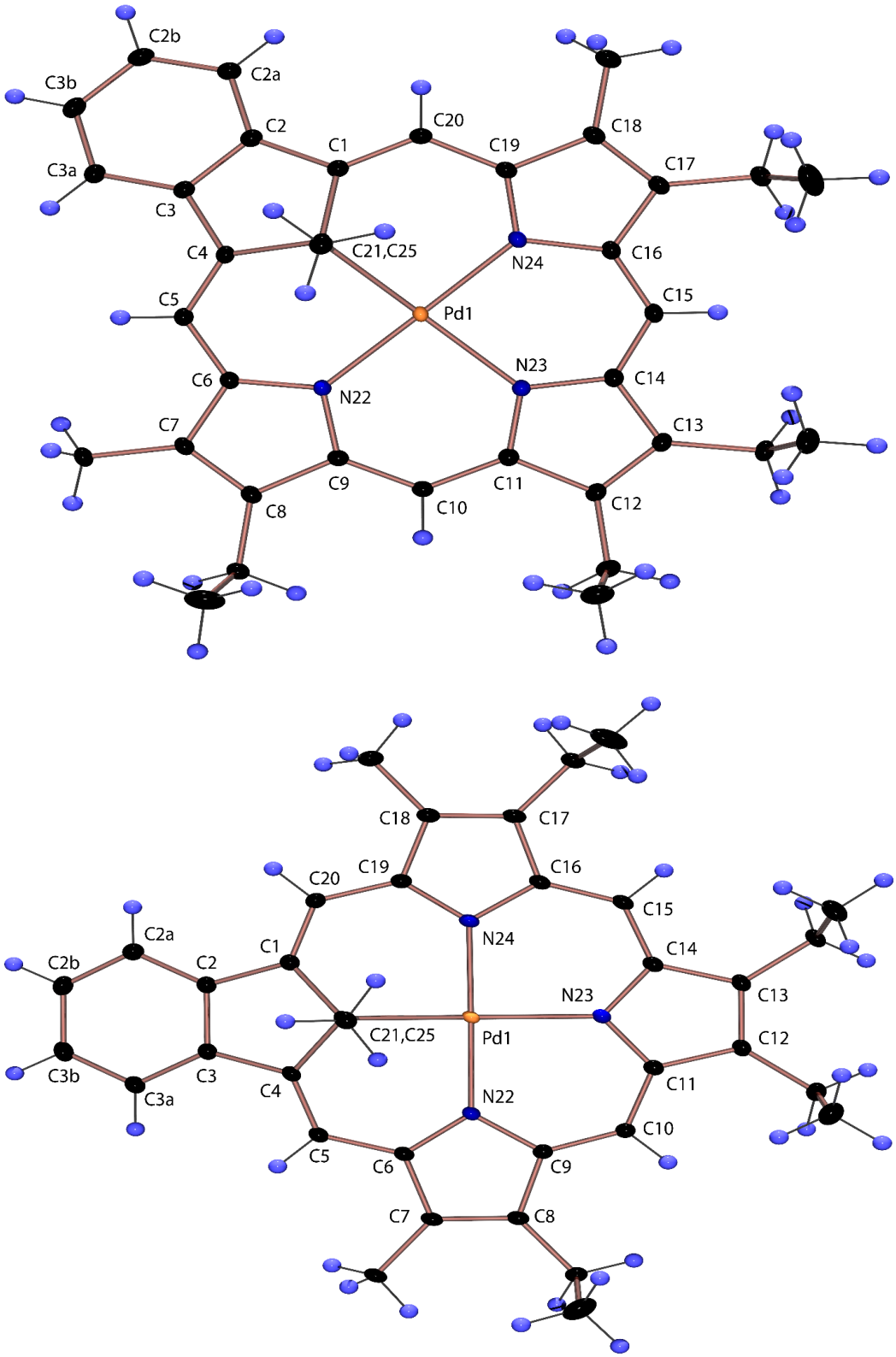

Figure B-2. Color POV-Ray rendered ORTEP III drawing (50% probability level, hydrogen atoms rendered arbitrarily small for clarity) showing two additional views of compound **72**.

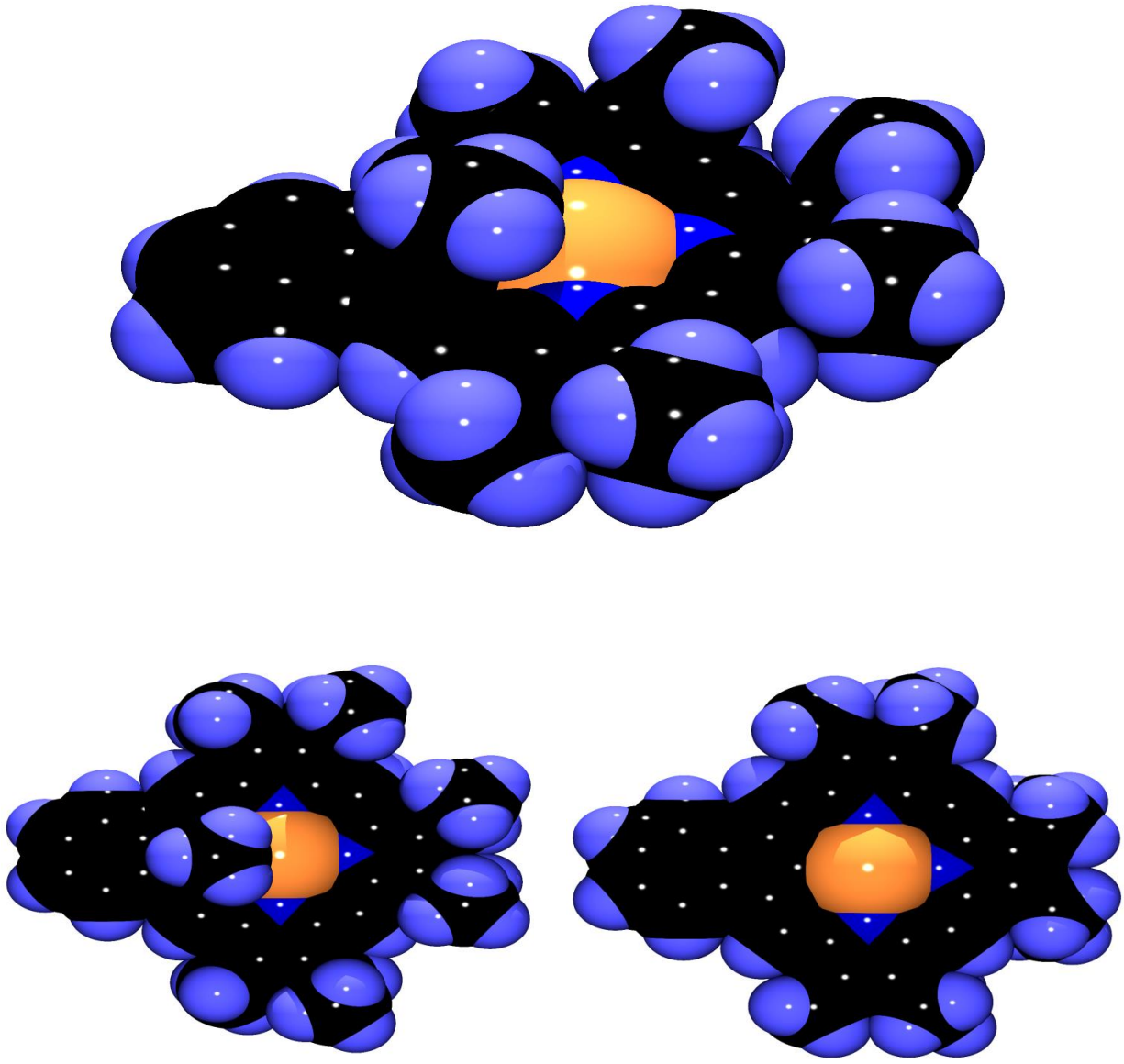

Figure B-3. Color POV-Ray rendered space-filling drawings of palladium complex **72**.

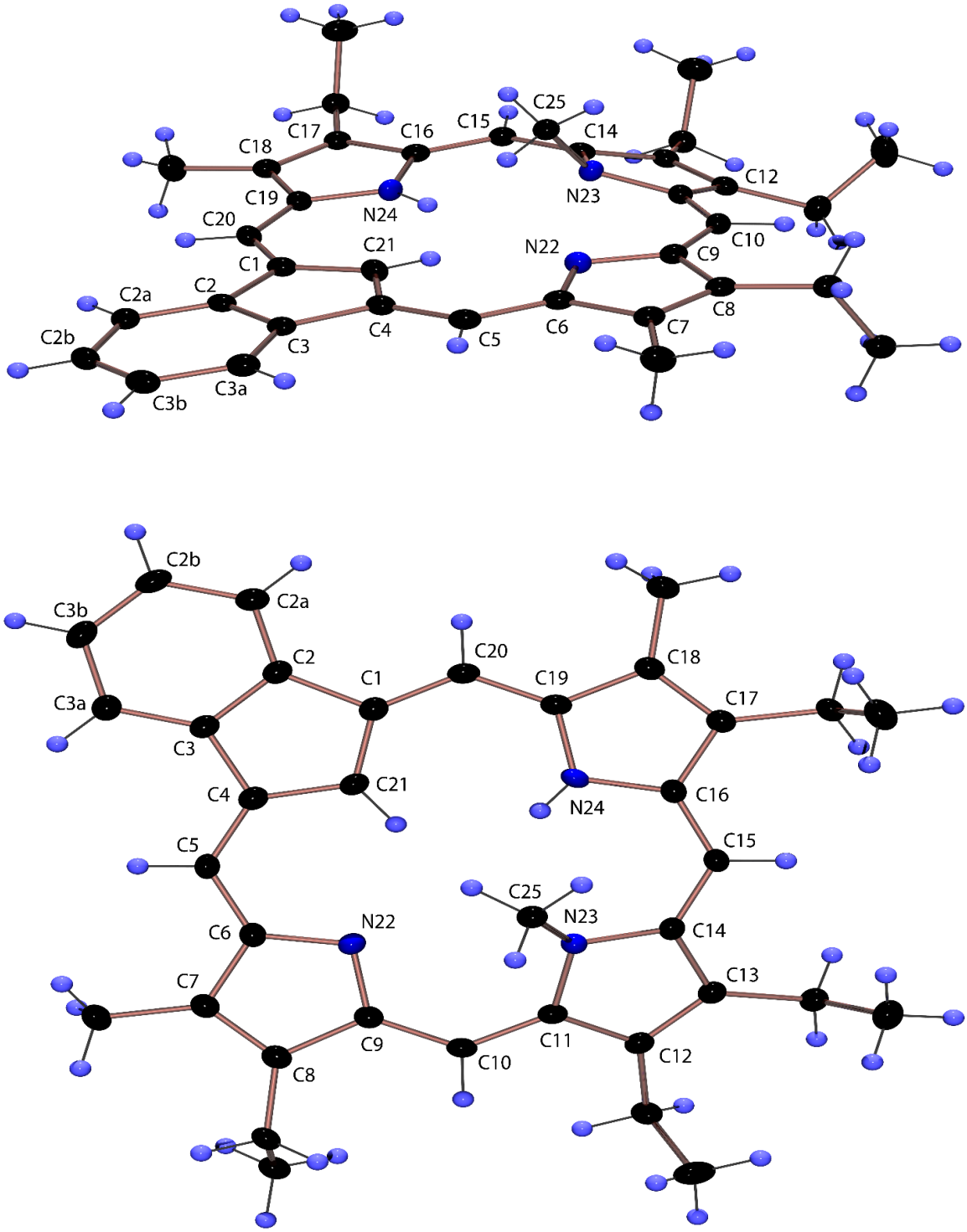

Figure B-4. Color POV-Ray rendered ORTEP III drawings (50% probability level, hydrogen atoms rendered arbitrarily small for clarity) showing two views of 23-methylcarbaporphyrin **76**.

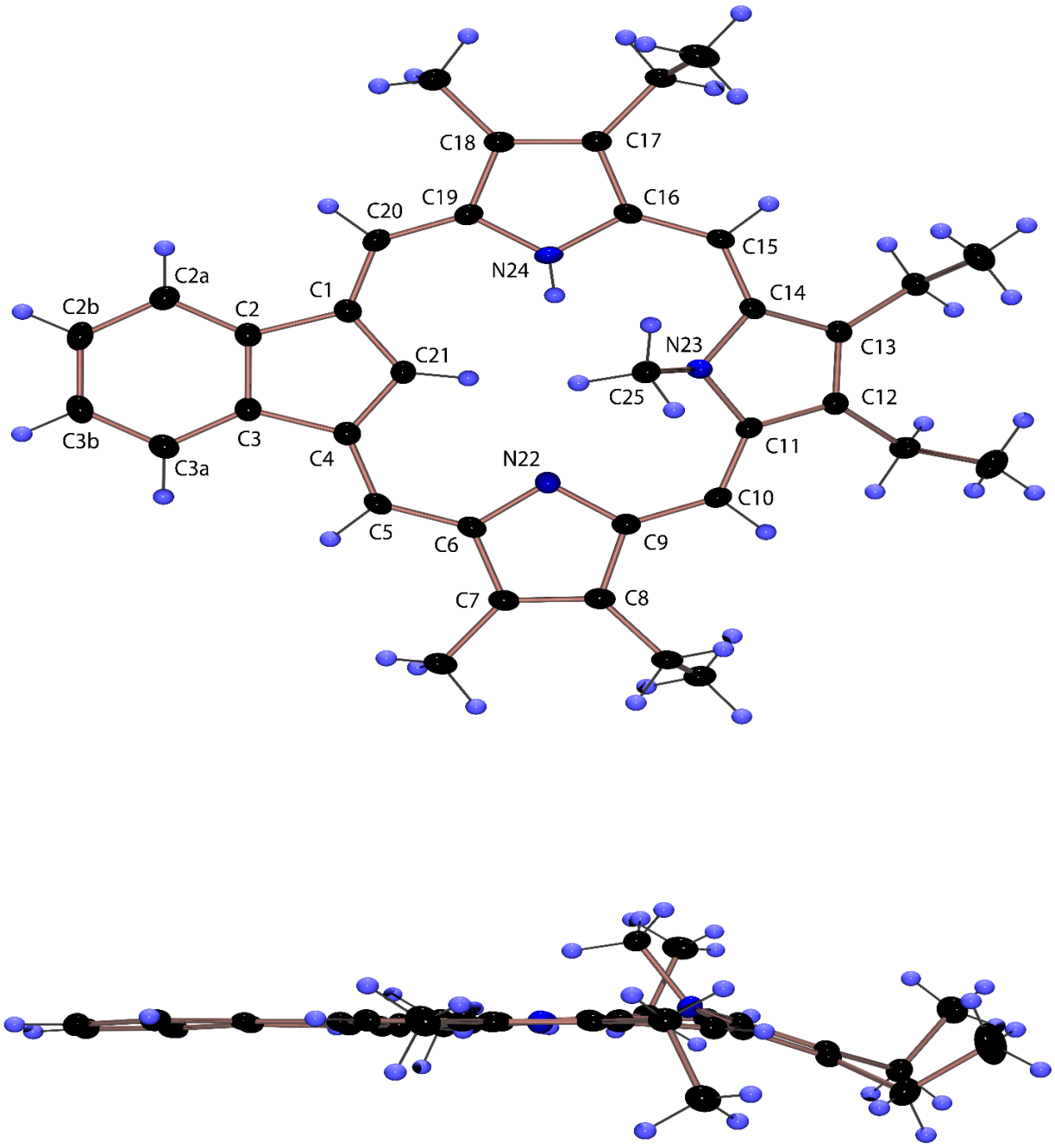

Figure B-5. Color POV-Ray rendered ORTEP III drawings (50% probability level, hydrogen atoms rendered arbitrarily small for clarity) showing two further views of 23-methylcarbaporphyrin **76**.

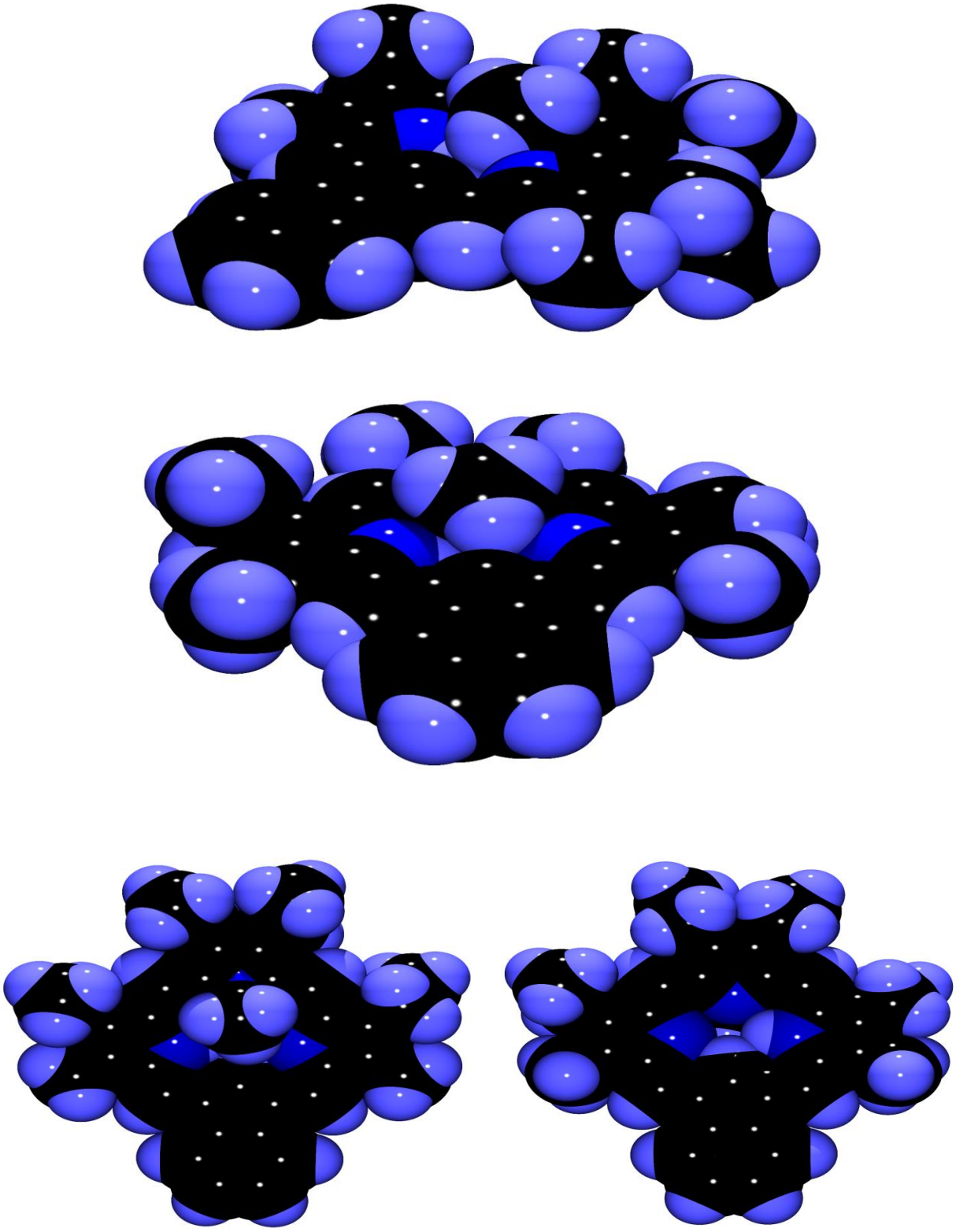

Figure B-6. Color POV-Ray rendered space-filling drawings showing 4 views of compound 23-methylcarbaporphyrin **76**.

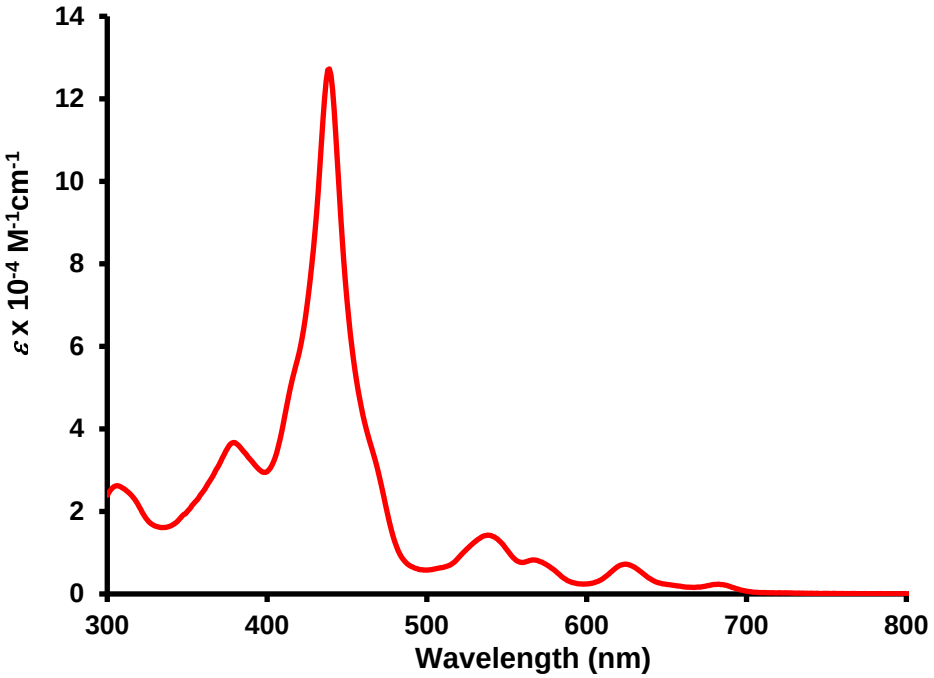

Figure B-7. UV-vis spectrum of 23-methylcarbaporphyrin **76** in 1% Et_3N-dichloromethane.

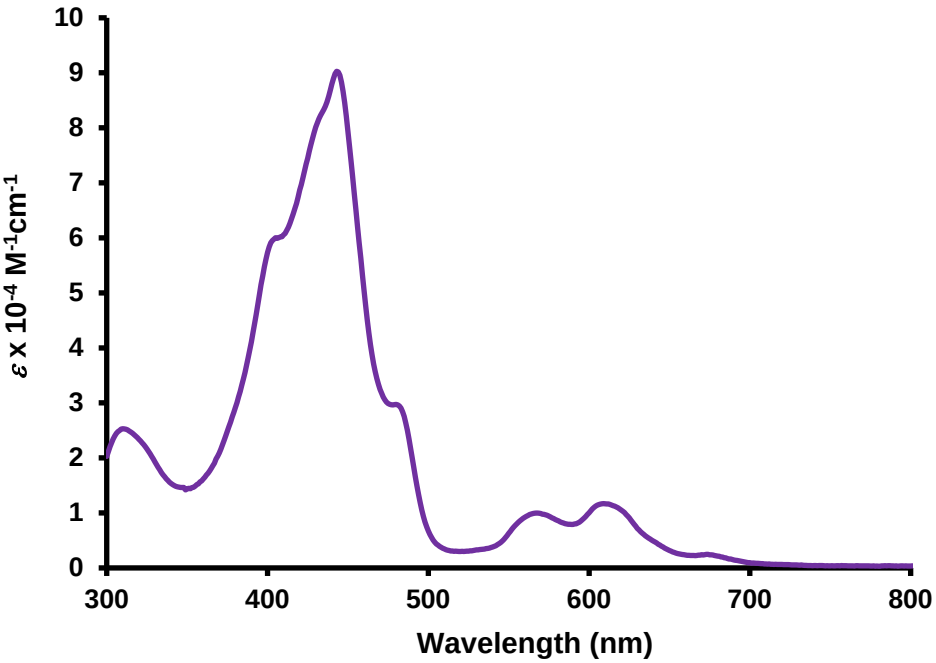

Figure B-8. UV-vis spectrum of monocation **76**H^+ in 1% TFA-dichloromethane.

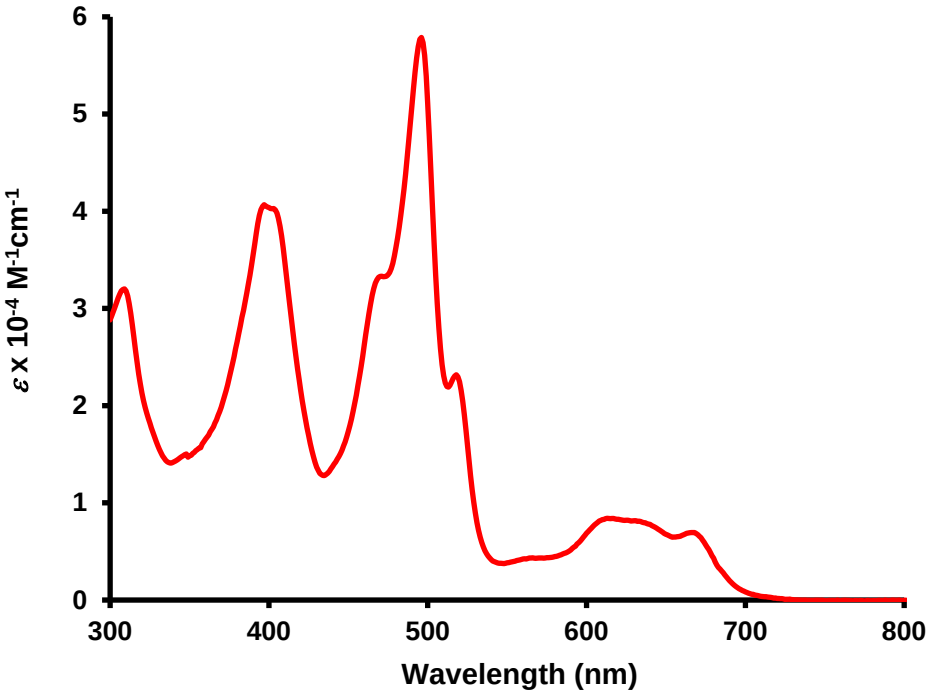

Figure B-9. UV-vis spectrum of palladium(II) complex **84** in dichloromethane.

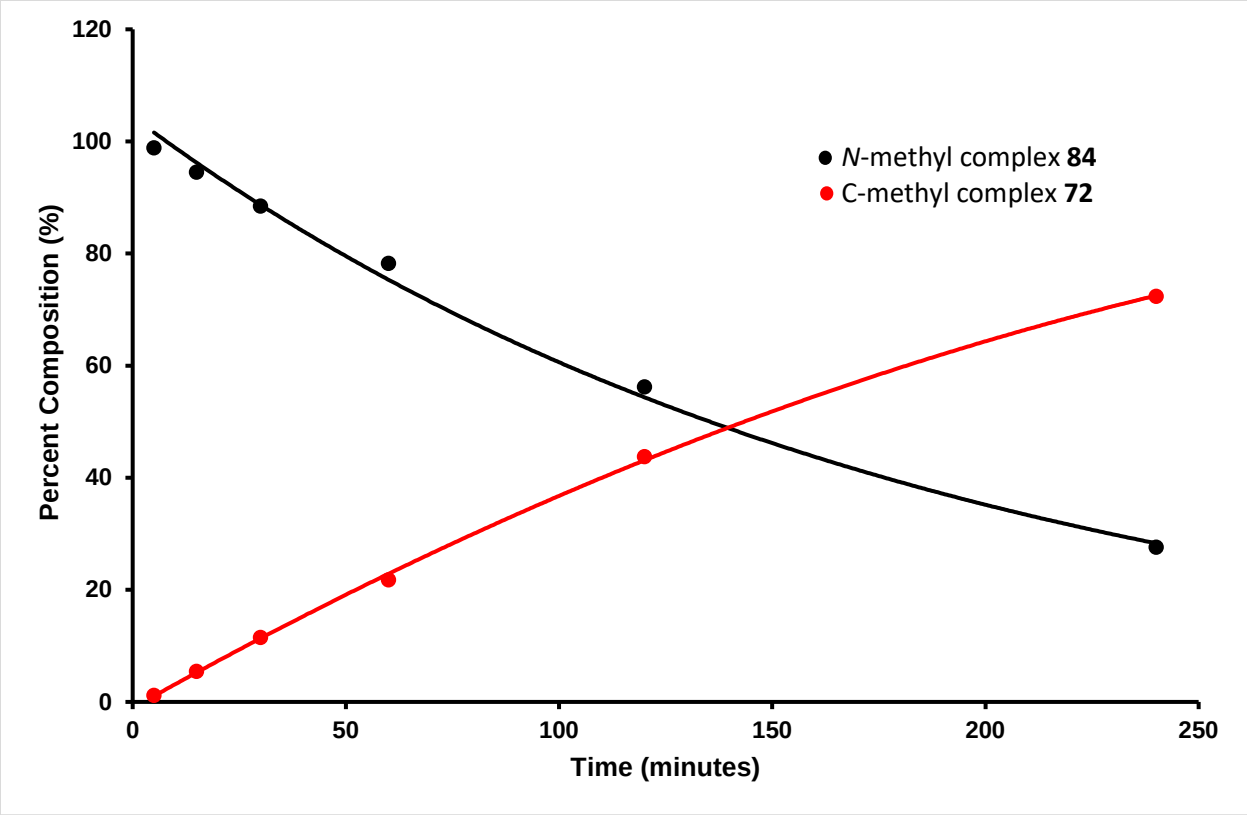

Figure B-10. Reflux reactions time course study for the metalation of **76** with palladium(II) acetate showing the conversion of **84** into **72**.

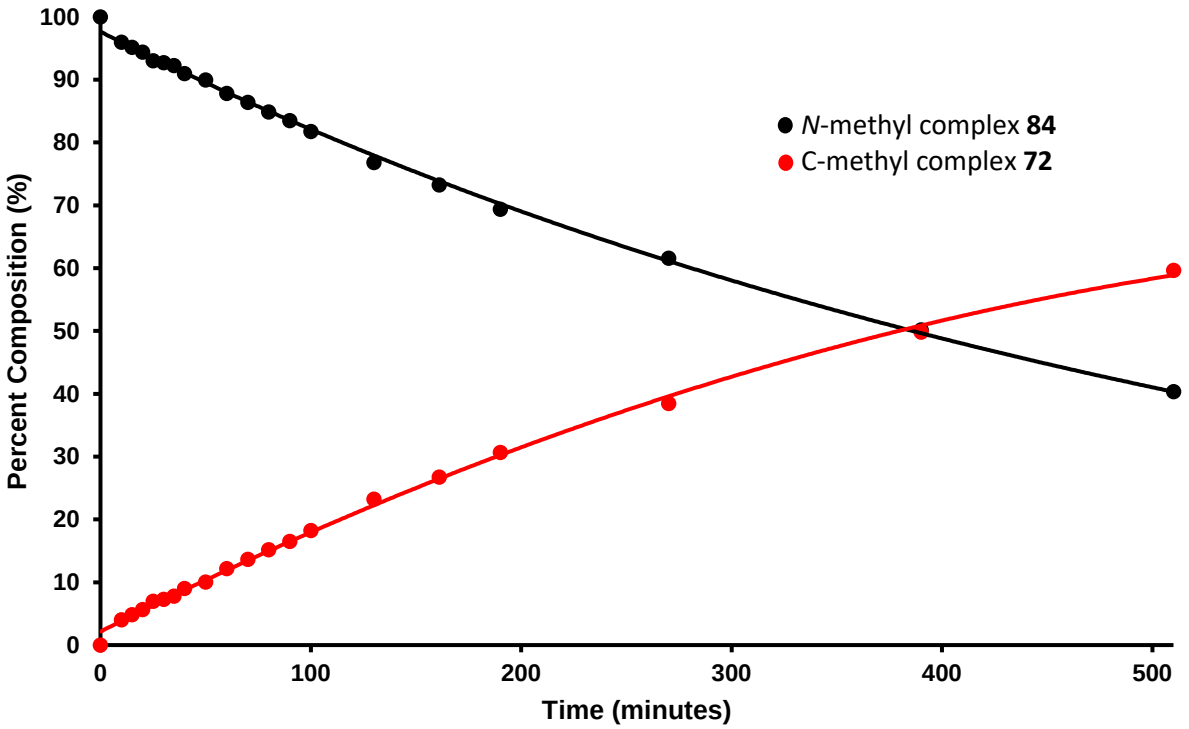

Figure B-11. Proton-NMR time course study for the metalation of **76** with palladium(II) acetate showing the conversion of **84** into **72**.

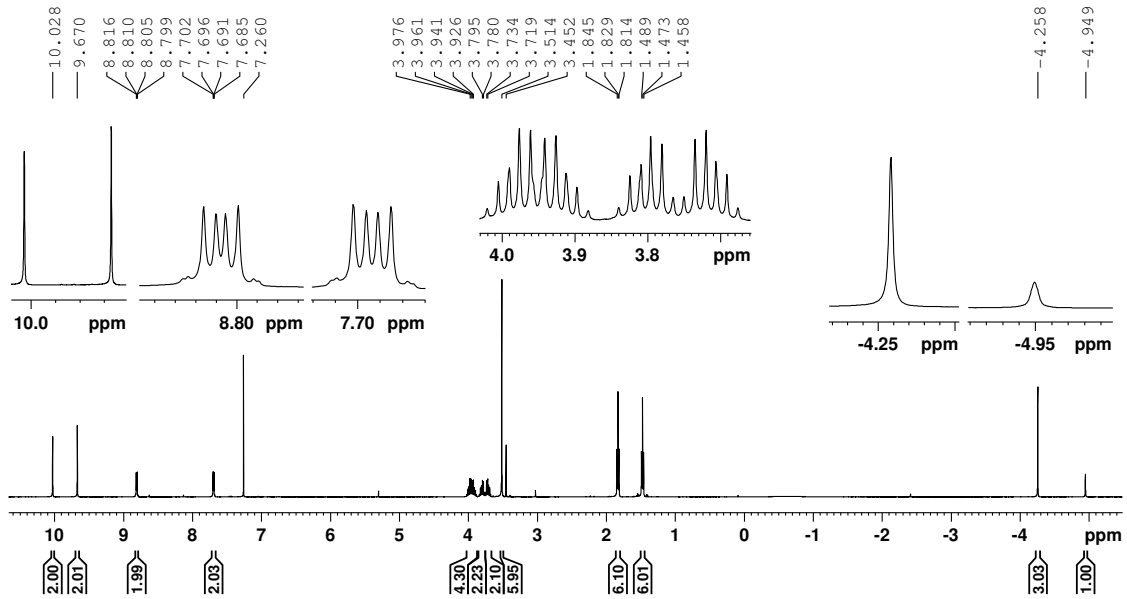

Figure B-12. 500 MHz ^{1}H NMR spectrum of 23-methylbenzocarbaporphyrin **76** in $CDCl_3$.

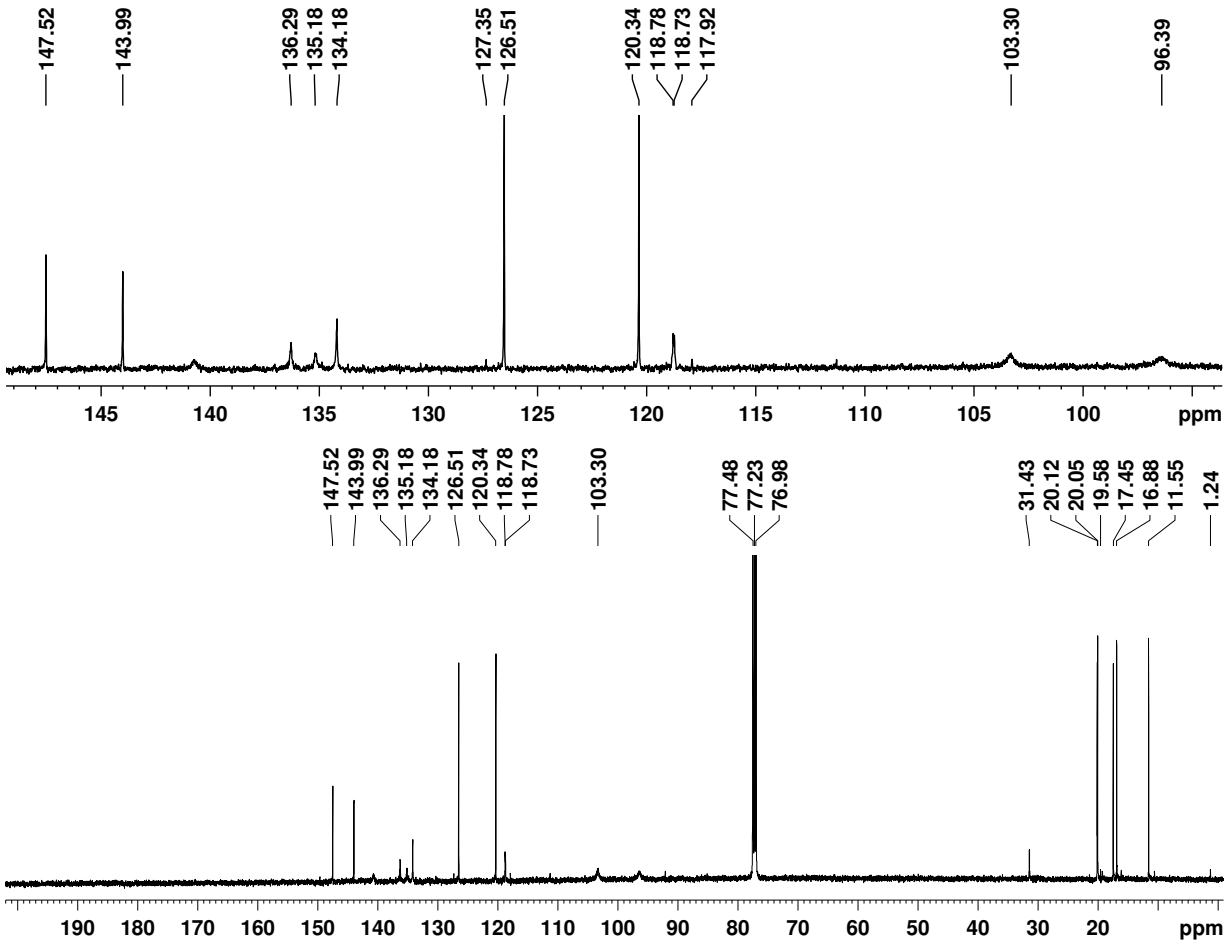

Figure B-13. 125 MHz ^{13}C NMR spectrum of 23-methylcarbaporphyrin **76** in $CDCl_3$.

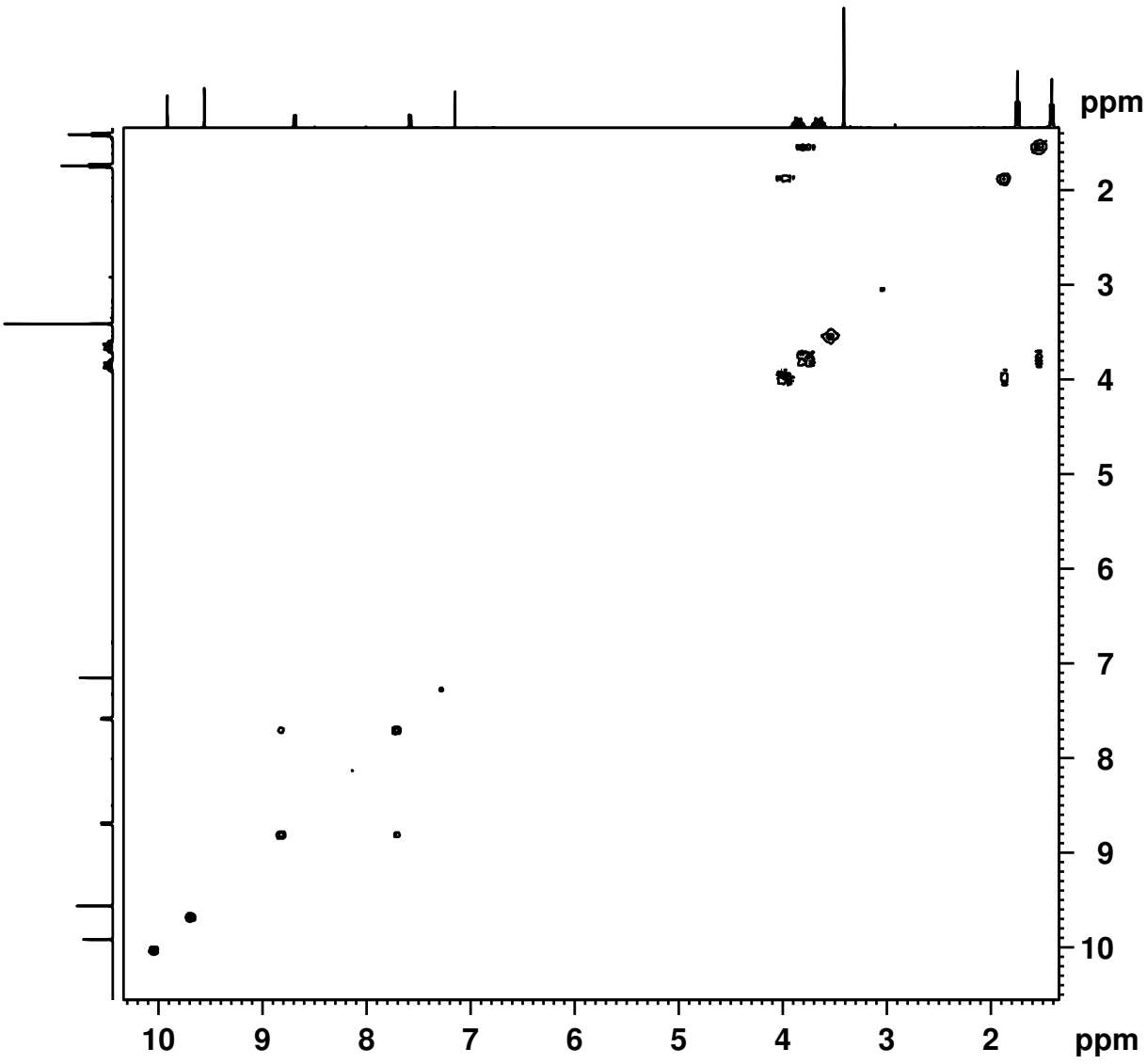

Figure B-14. ^{1}H-^{1}H COSY NMR spectrum of 23-methylcarbaporphyrin **76** in $CDCl_3$.

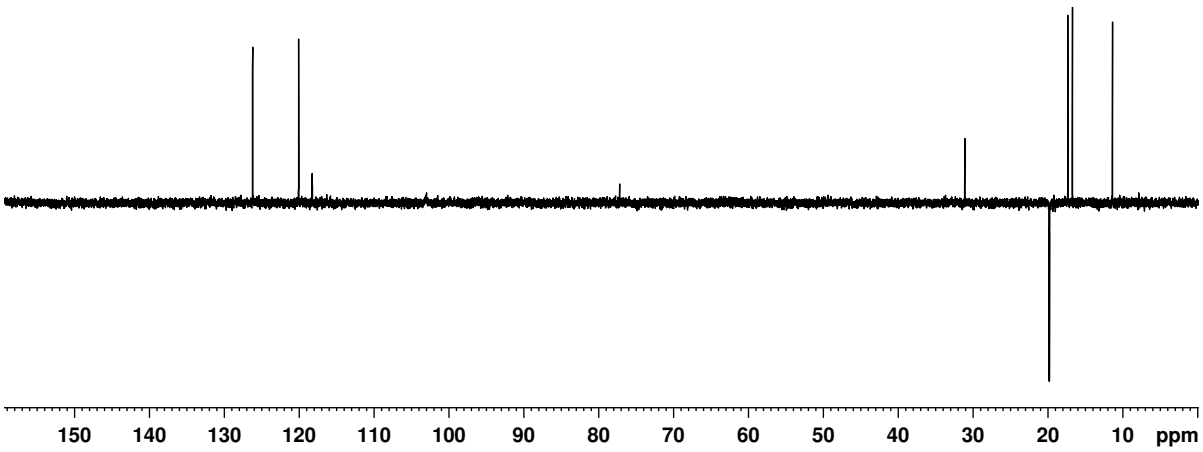

Figure B-15. DEPT-135 NMR spectrum of 23-methylcarbaporphyrin **76** in $CDCl_3$.

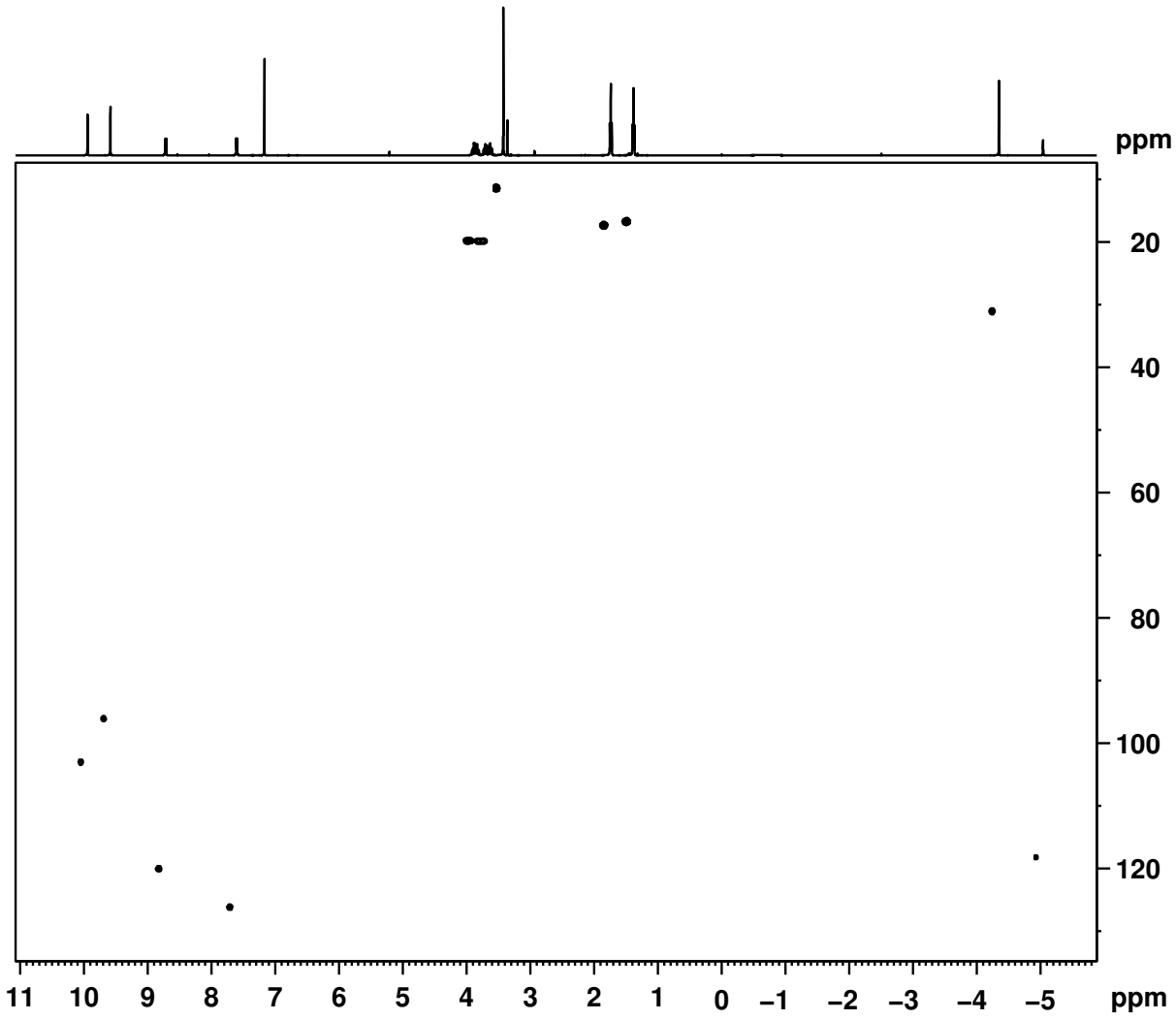

Figure B-16. HSQC NMR spectrum of 23-methylcarbaporphyrin **76** in $CDCl_3$.

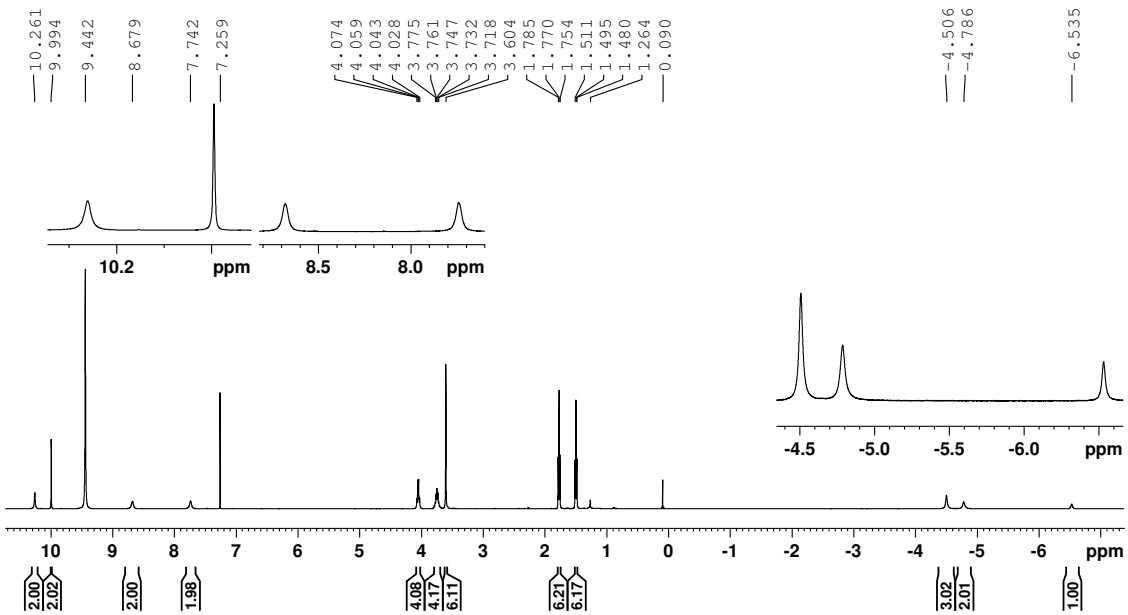

Figure B-17. 500 MHz ^{1}H NMR spectrum of 23-methylbenzocarbaporphyrin monocation **76**H^{+} in TFA-$CDCl_3$.

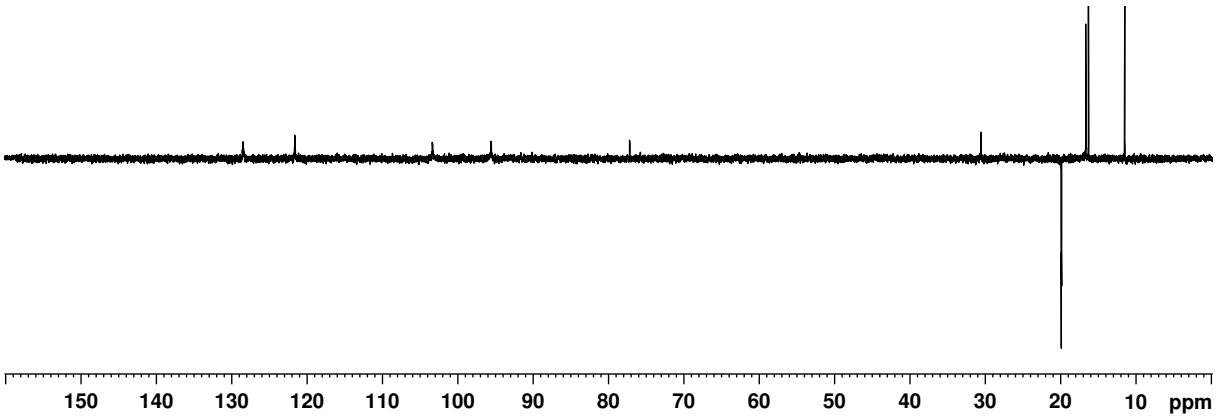

Figure B-18. DEPT-135 NMR spectrum of 23-methylcarbaporphyrin monocation **76**H^+ in TFA-$CDCl_3$.

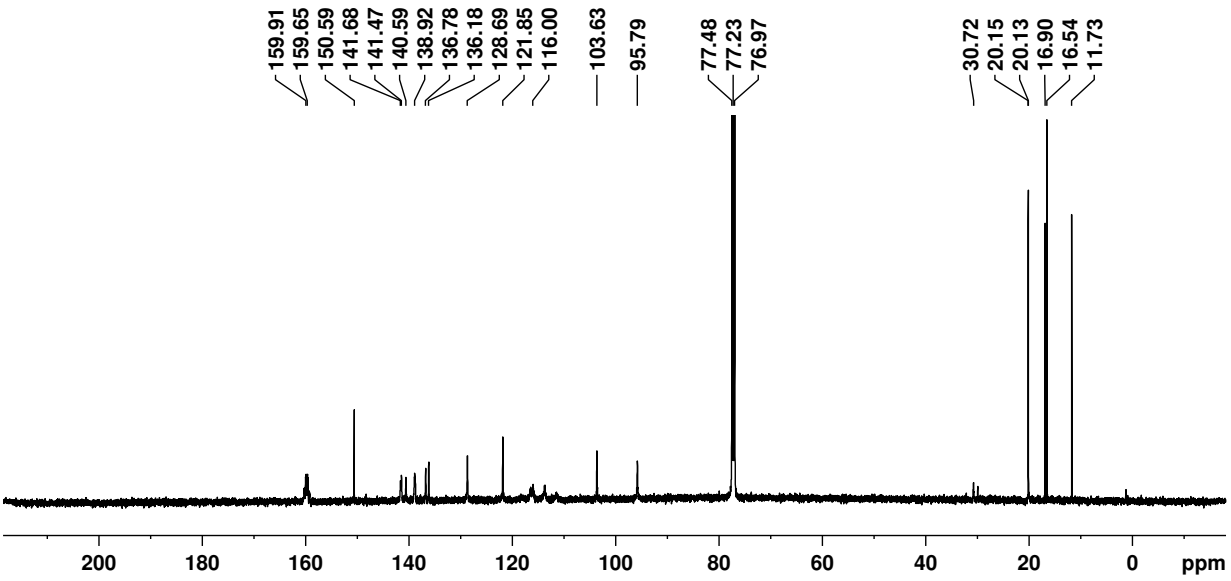

Figure B-19. 125 MHz ^{13}C NMR spectrum of 23-methylcarbaporphyrin monocation **76**H^+ in TFA-$CDCl_3$.

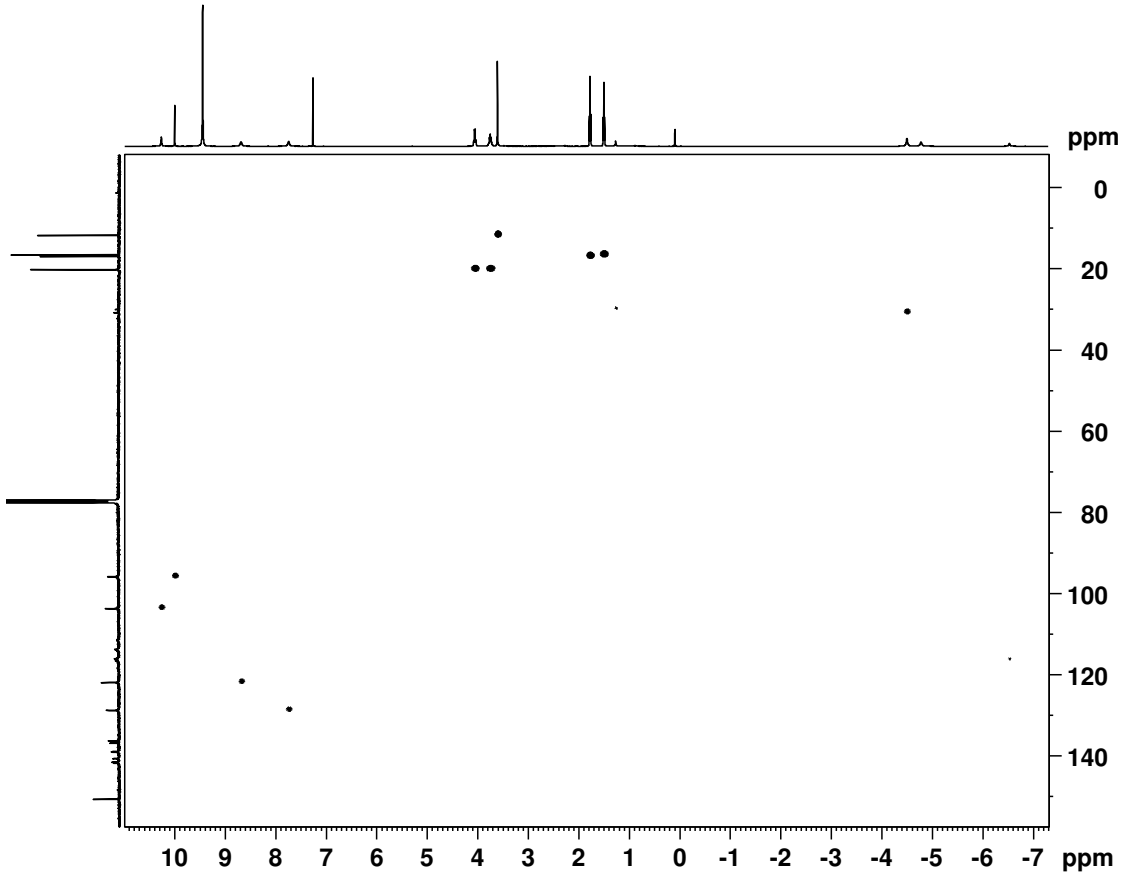

Figure B-20. HSQC NMR spectrum of 23-methylbenzocarbaporphyrin monocation **76**H^+ in TFA-$CDCl_3$.

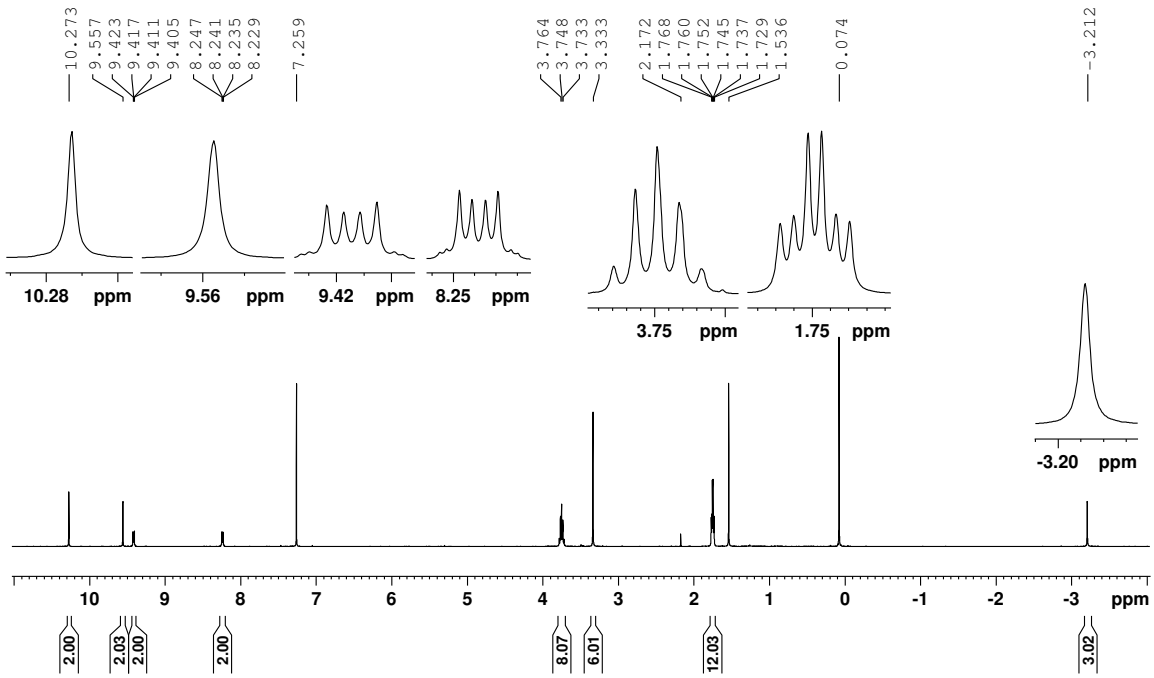

Figure B-21. 500 MHz ^{1}H NMR spectrum of palladium(II) 21-methylcarbaporphyrin **72** in $CDCl_3$.

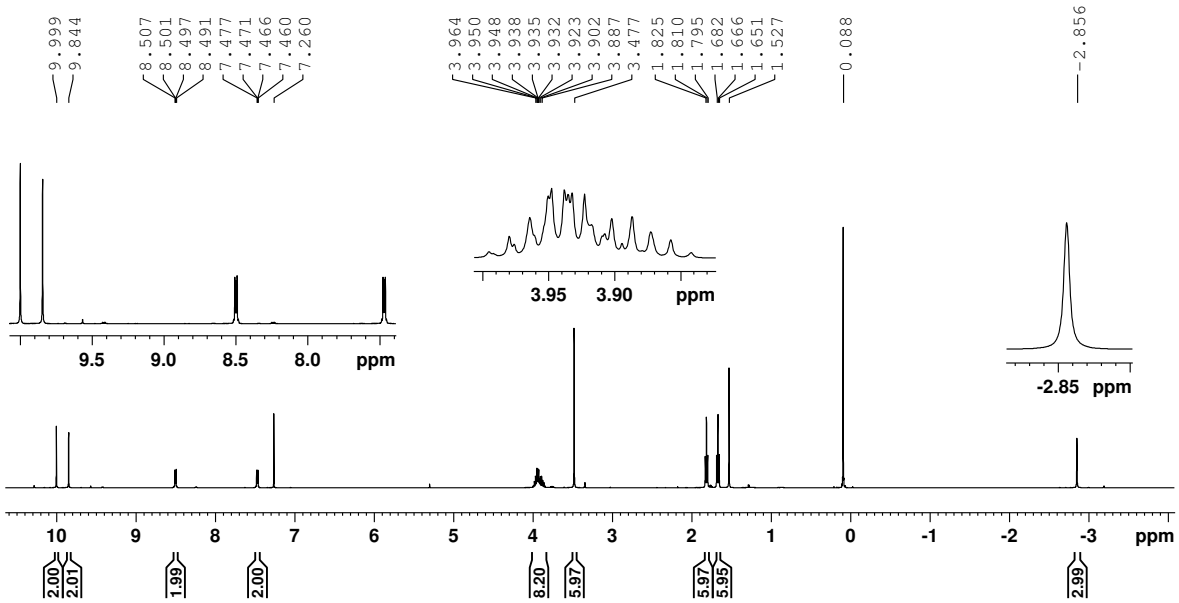

Figure B-22. 500 MHz ^{1}H NMR spectrum of palladium(II) 23-methylcarbaporphyrin **84** in $CDCl_3$.

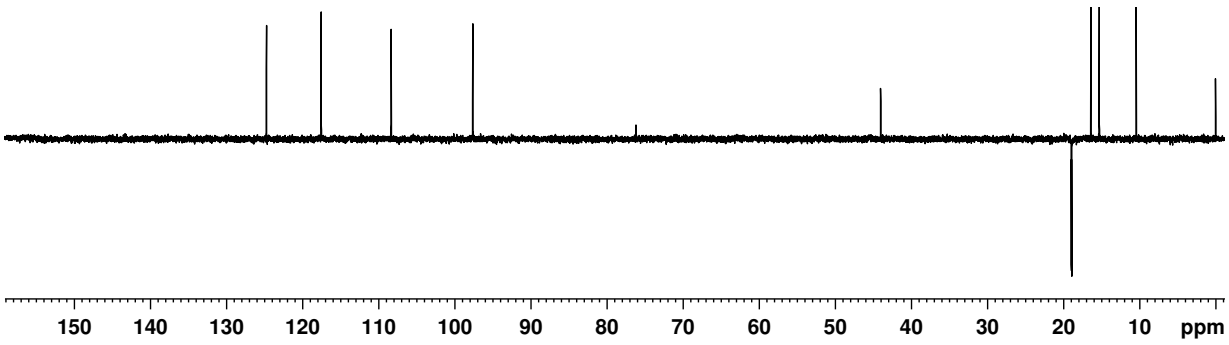

Figure B-23. DEPT-135 NMR spectrum of palladium(II) 23-methylcarbaporphyrin **84** in $CDCl_3$.

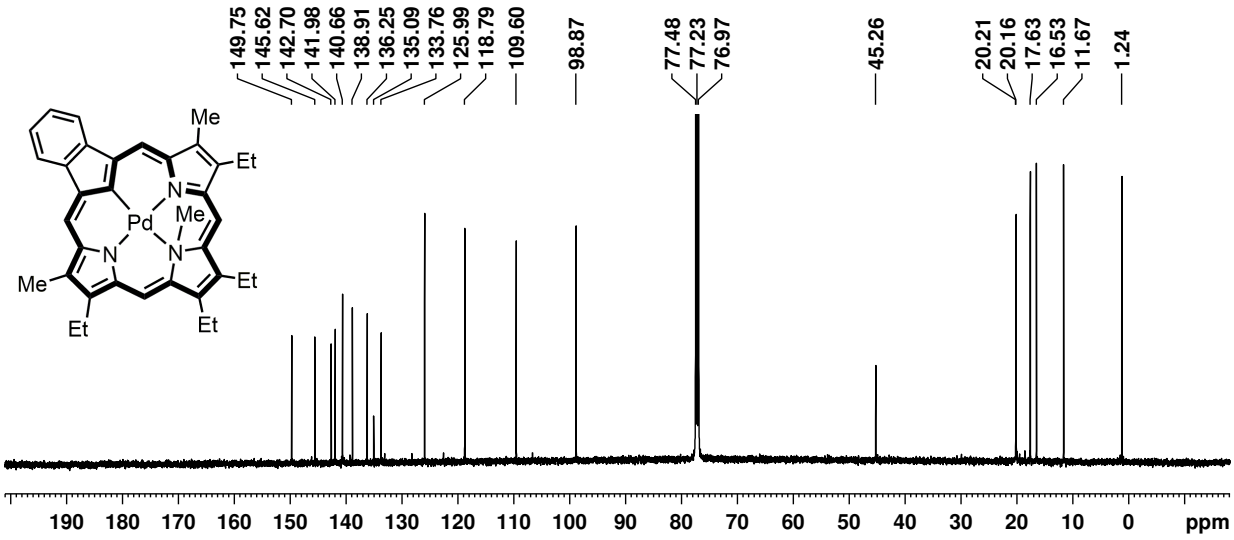

Figure B-24. 125 MHz ^{13}C NMR spectrum of palladium(II) 23-methylcarbaporphyrin **84** in $CDCl_3$.

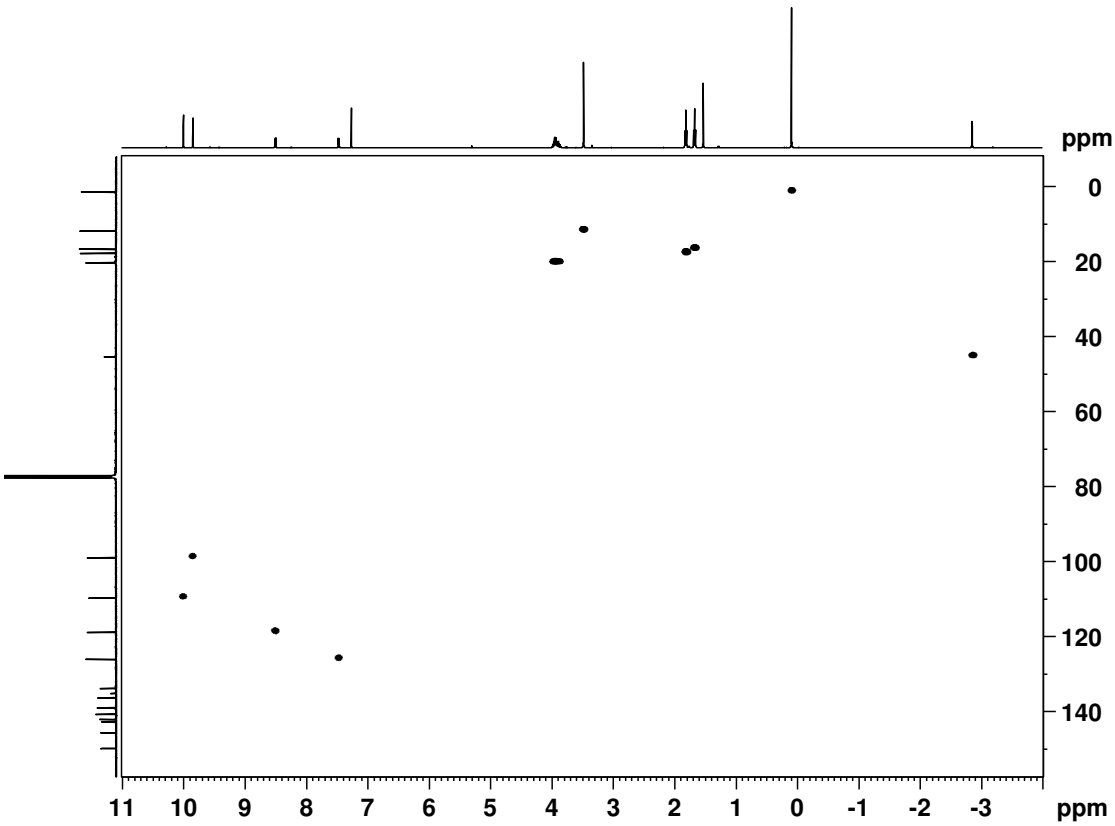

Figure B-25. HSQC NMR spectrum of palladium(II) 23-methylcarbaporphyrin **84** in $CDCl_3$.

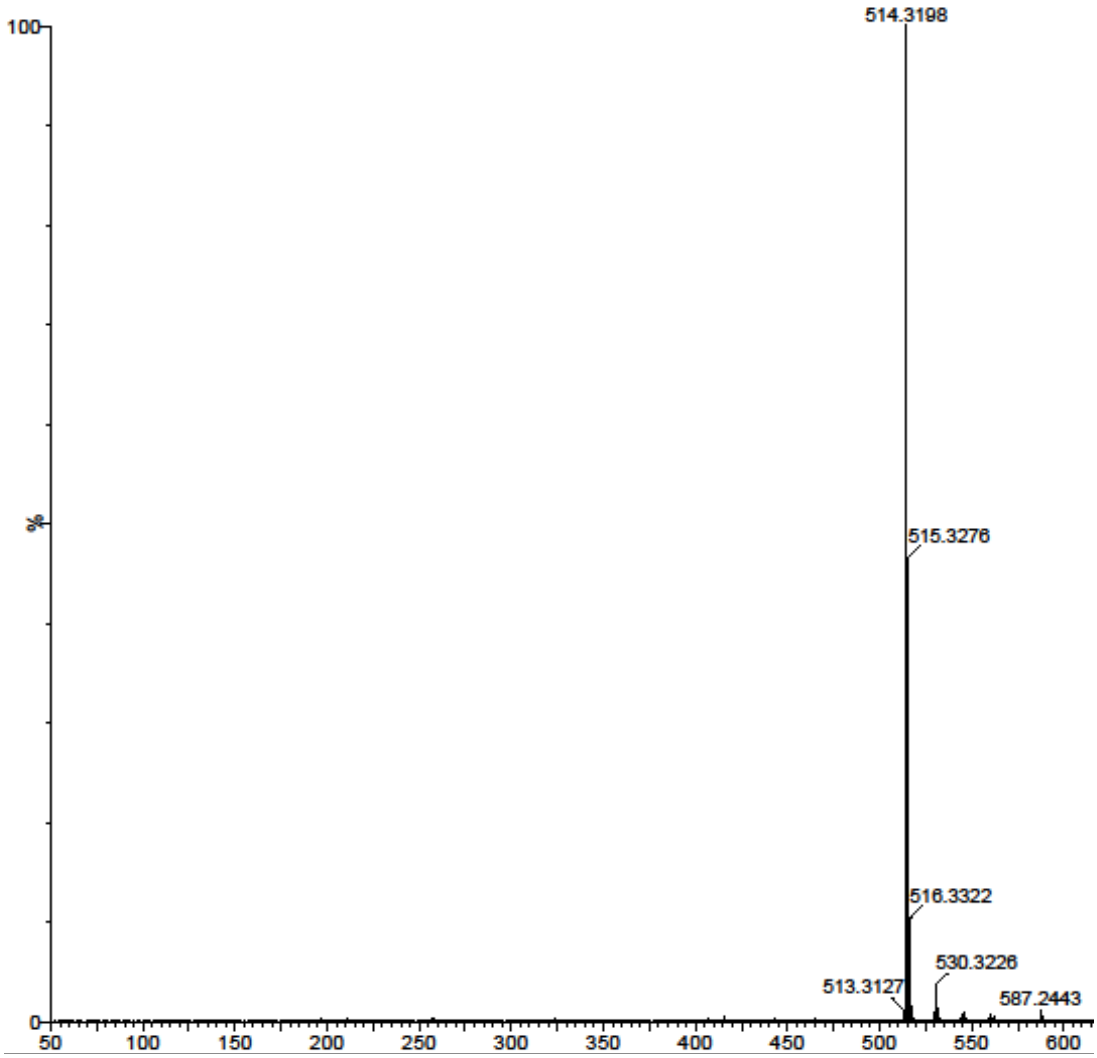

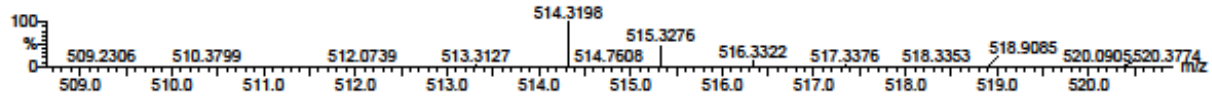

Minimum:				-1.5		
Maximum:		5.0	5.0	100.0		
Mass	Calc. Mass	mDa	PPM	DBE	i-FIT	Formula
514.3198	514.3182	1.6	3.1	14.5	74.8	C31 H40 N5 O2
	514.3222	-2.4	-4.7	18.5	19.5	C36 H40 N3

Figure B-26. ESI MS of *N*-methylcarbaporphyrin **76**.

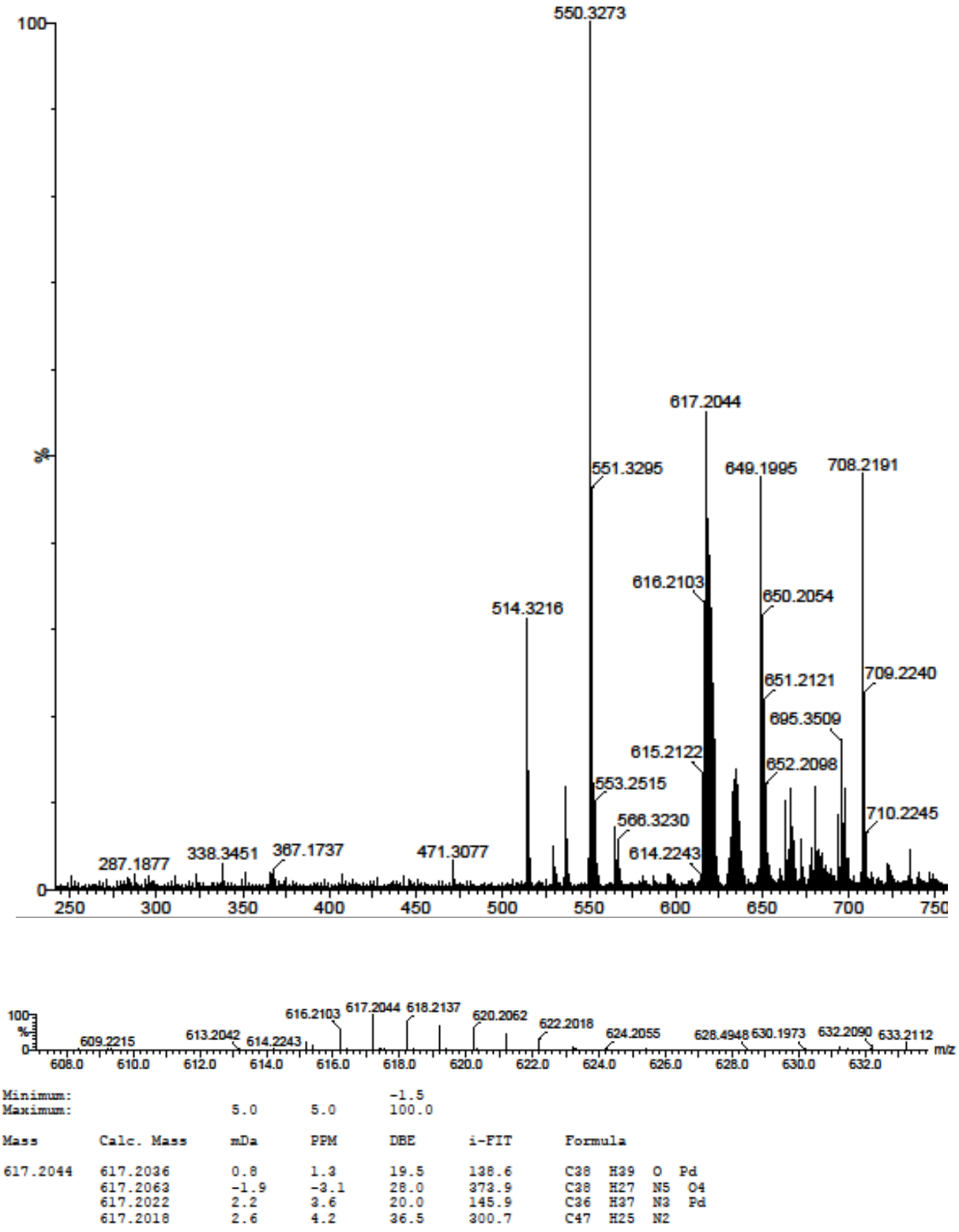

Minimum:				-1.5		
Maximum:		5.0	5.0	100.0		
Mass	**Calc. Mass**	**mDa**	**PPM**	**DBE**	**i-FIT**	**Formula**
617.2044	617.2036	0.8	1.3	19.5	138.6	C38 H39 O Pd
	617.2063	-1.9	-3.1	28.0	373.9	C38 H27 N5 O4
	617.2022	2.2	3.6	20.0	145.9	C36 H37 N3 Pd
	617.2018	2.6	4.2	36.5	300.7	C47 H25 N2

Figure B-27. ESI MS of palladium(II) complex **84**.

APPENDIX C: SPECTROSCOPIC DATA FOR RHODIUM COMPLEXES

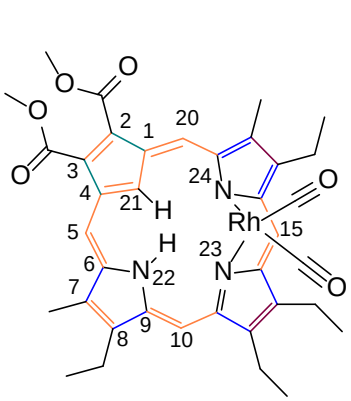

89

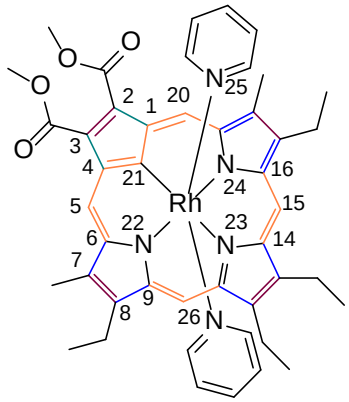

90

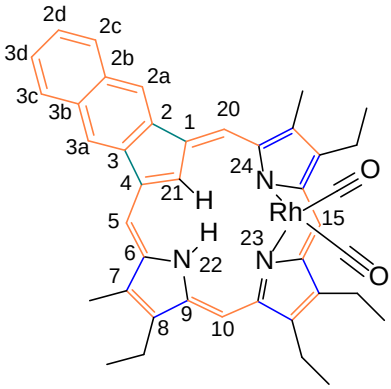

91

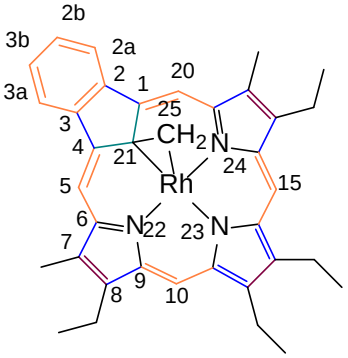

95

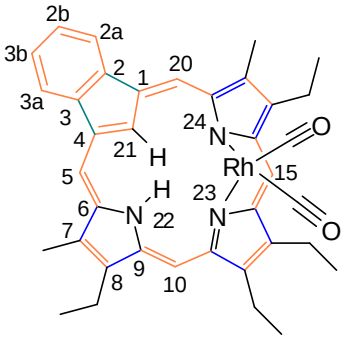

86

Table C-1. Summary of framework bond distances (Å) and angles (°) for **86**,[30] **89**, **90**, **91** and **95**.

	89•0.5 C_5H_{12}	**90•$CHCl_3$**	**91**	**95**	**86**[30]
C25-O25	1.133(3)	--	1.1372(19)	--	1.1356(14)
C26-O26	1.138(3)	--	1.134(2)	--	1.1370(14)
Rh-C25(orN25)	1.866(2)	2.0641(18)	1.8529(16)	1.9932(11)	1.8636(12)
Rh-C26(orN26)	1.856(2)	2.0720(18)	1.8677(16)	--	1.8536(11)
Rh-C21	--	1.986(2)	--	2.1329(11)	--
Rh-N22	--	2.0454(18)	--	2.0369(9)	--
Rh-N23	2.0895(18)	2.1046(19)	2.0894(12)	2.0431(9)	2.0920(9)
Rh-N24	2.0806(18)	2.0485(18)	2.0836(12)	2.0410(9)	2.0847(9)
C1-C21	1.407(3)	1.416(3)	1.4130(19)	1.4632(15)	1.4098(14)
C1-C2	1.462(3)	1.464(3)	1.4751(19)	1.4468(15)	1.4744(13)
C2-C3	1.377(3)	1.362(3)	1.4385(19)	1.4178(16)	1.4141(14)
C2-C2a	--	--	1.370(2)	--	1.3901(14)
C2a-C2b	--	--	1.425(2)	--	1.3997(14)
C2b-C3b	--	--	1.428(2)	--	1.3909(16)
C3b-C3a	--	--	1.422(2)	--	1.3986(16)

C3a-C3	--	--	1.3686(19)	--	1.3900(14)
C3-C4	1.471(3)	1.469(3)	1.4760(19)	1.4470(15)	1.4762(14)
C4-C21	1.401(3)	1.413(3)	1.3995(19)	1.4624(15)	1.4054(14)
C4-C5	1.410(3)	1.397(3)	1.4076(19)	1.3779(15)	1.4038(15)
C5-C6	1.384(3)	1.391(3)	1.3916(19)	1.4085(15)	1.3899(15)
C6-N22	1.380(3)	1.387(3)	1.3785(17)	1.3777(14)	1.3742(13)
C6-C7	1.440(3)	1.443(3)	1.445(2)	1.4496(15)	1.4372(14)
C7-C8	1.378(3)	1.364(3)	1.377(2)	1.3644(16)	1.3812(14)
C8-C9	1.445(3)	1.452(3)	1.444(2)	1.4540(15)	1.4383(14)
C9-N22	1.359(3)	1.376(3)	1.3695(18)	1.3802(13)	1.3668(13)
C9-C10	1.391(3)	1.404(3)	1.389(2)	1.3864(15)	1.3914(14)
C10-C11	1.401(3)	1.382(3)	1.4081(19)	1.3983(15)	1.4028(14)
C11-N23	1.386(3)	1.368(3)	1.3811(18)	1.3718(13)	1.3814(13)
C11-C12	1.455(3)	1.459(3)	1.4447(19)	1.4510(15)	1.4480(14)
C12-C13	1.362(3)	1.362(3)	1.372(2)	1.3702(15)	1.3698(14)
C13-C14	1.443(3)	1.458(3)	1.4414(19)	1.4485(15)	1.4427(14)
C14-N23	1.386(3)	1.367(3)	1.3859(18)	1.3665(14)	1.3859(12)
C14-C15	1.387(3)	1.393(3)	1.395(2)	1.3949(15)	1.3931(14)
C15-C16	1.397(3)	1.402(3)	1.395(2)	1.5353(17)	1.3991(14)
C16-N24	1.376(3)	1.366(3)	1.3770(18)	1.3791(14)	1.3756(12)
C16-C17	1.447(3)	1.455(3)	1.442(2)	1.4524(15)	1.4389(14)
C17-C18	1.370(3)	1.359(3)	1.375(2)	1.3614(15)	1.3772(14)
C18-C19	1.441(3)	1.440(3)	1.4440(19)	1.4538(15)	1.4460(13)
C19-N24	1.388(3)	1.391(3)	1.3782(18)	1.3791(14)	1.3813(13)
C19-C20	1.397(3)	1.387(3)	1.409(2)	1.4051(15)	1.4055(13)
C1-C20	1.404(3)	1.394(3)	1.3930(19)	1.3791(15)	1.3950(14)
C1-C21-C4	110.26(19)	107.78(19)	111.63(12)	107.31(9)	--
C6-N22-C9	111.53(18)	106.65(18)	111.43(12)	--	--
C21-Rh-N22	--	90.10(8)	--	89.43(4)	--
C21-Rh-N23	--	178.59(8)	--	168.60(4)	--
C21-Rh-N24	--	90.57(8)	--	89.05(4)	--
C21-Rh-N25	--	89.29(8)	--	--	--
C21-Rh-N26	--	89.09(8)	--	--	--
N22-Rh-N23	--	89.97(7)	--	90.46(4)	--
N22-Rh-N24	--	179.27(8)	--	177.62(3)	--
N22-Rh-N25	--	89.00(7)	--	--	--
N22-Rh-N26	--	90.21(7)	--	--	--
N23-Rh-N24	85.43(7)	89.35(7)	85.79(5)	90.66(4)	85.90(3)
N24-Rh-C25(orN25)	91.43(8)	90.70(7)	91.96(6)	--	91.86(4)
N24-Rh-C26(orN26)	175.36(9)	90.11(7)	176.68(6)	--	173.99(4)
N23-Rh-C25(orN25)	176.27(8)	89.30(7)	175.90(6)	--	177.11(4)
N23-Rh-C26(orN26)	94.62(9)	92.32(7)	93.41(6)	--	92.26(4)
C25-Rh-C26	88.35(10)	--	88.64(7)	--	89.78(5)
C25-C21-Rh	--	--	--	64.09(6)	--
C25-C21-C1	--	--	--	120.47(10)	--

C25-C21-C4	--	--	--	120.52(10)	--
N25-Rh-N26	--	178.19(8)	--	--	--
Rh-C25-O25	177.3(2)	--	177.43(15)	--	178.59(11)
Rh-C26-O26	176.2(2)	--	176.25(15)	--	176.81(10)

Purple more double bond like (≤1.37), orange – more aromatic (1.38-1.41), blue – more single bond like (1.42-1.45), green – single bond limit (≥1.46).

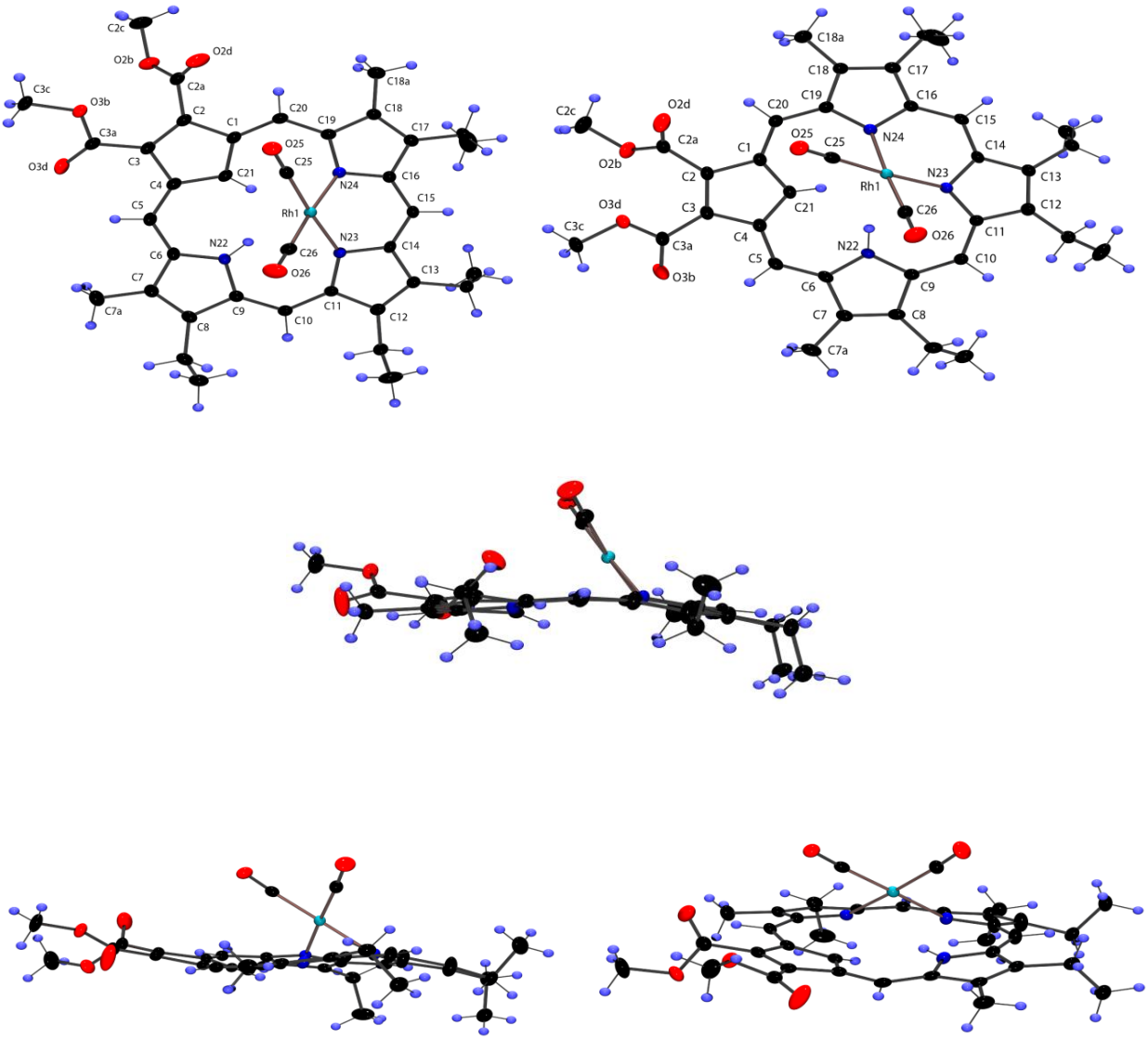

Figure C-1. Color POV-Ray rendered ORTEP III drawings (50% probability level, hydrogen atoms rendered arbitrarily small for clarity) showing a variety of views for rhodium(I) carbaporphyrin complex **89**.

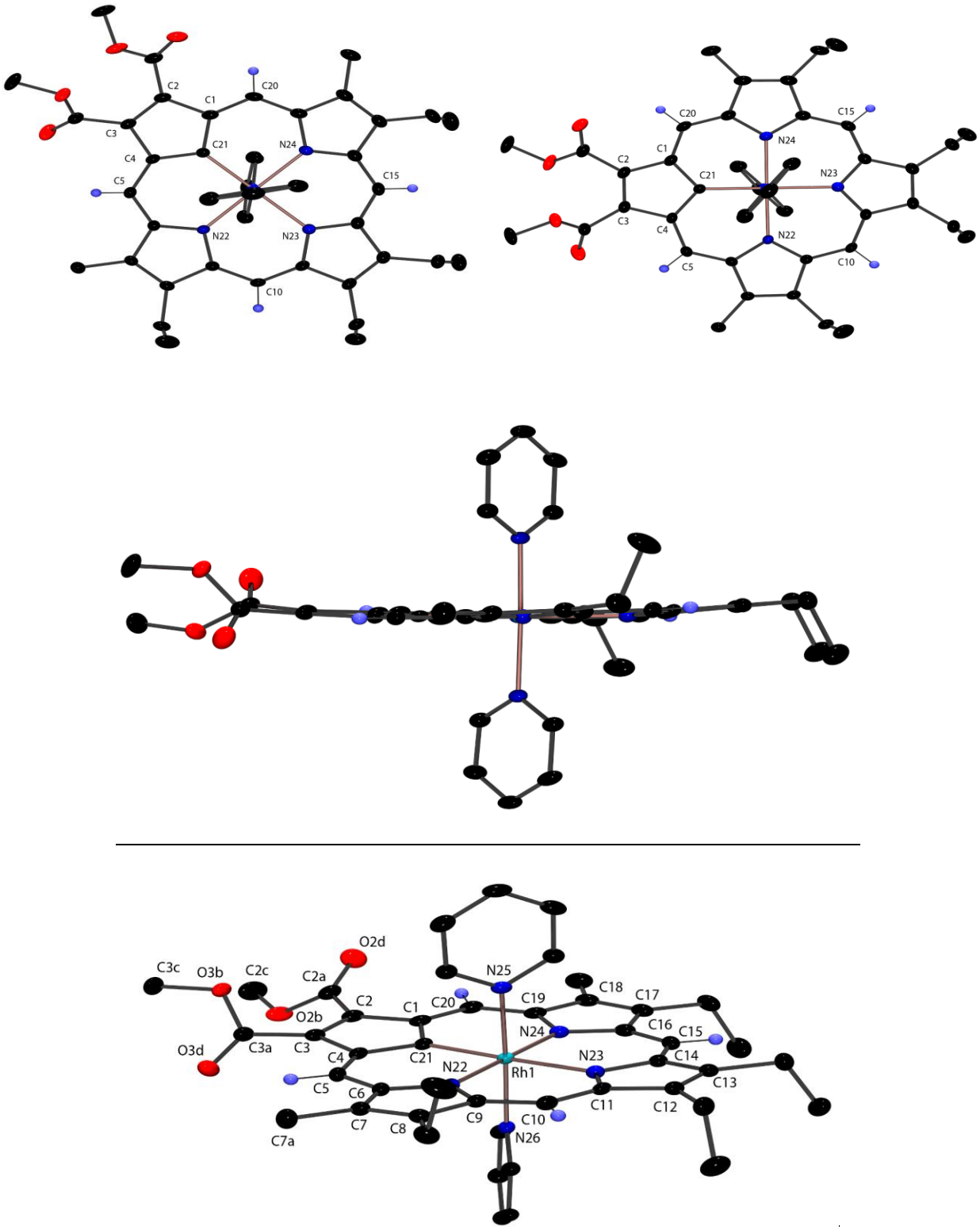

Figure C-2. Color POV-Ray rendered ORTEP III drawing (50% probability level, hydrogen atoms rendered arbitrarily small or omitted for clarity) showing a variety of views for rhodium(III) carbaporphyrin **90**.

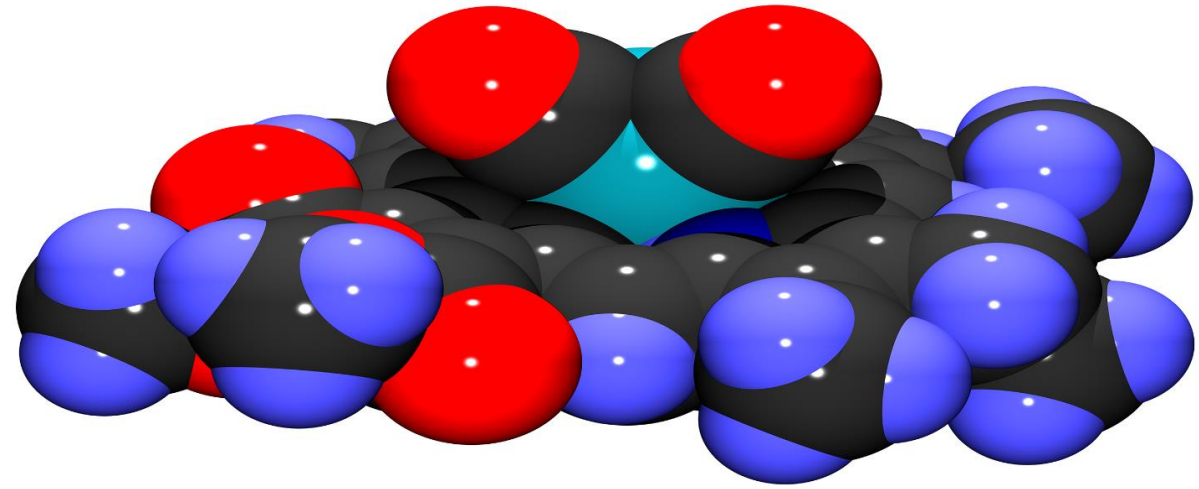

Figure C-3. Color POV-Ray rendered ORTEP III drawing (50% probability level, hydrogen atoms rendered arbitrarily small for clarity) showing a space-filling representation of rhodium(I) carbaporphyrin complex **89**.

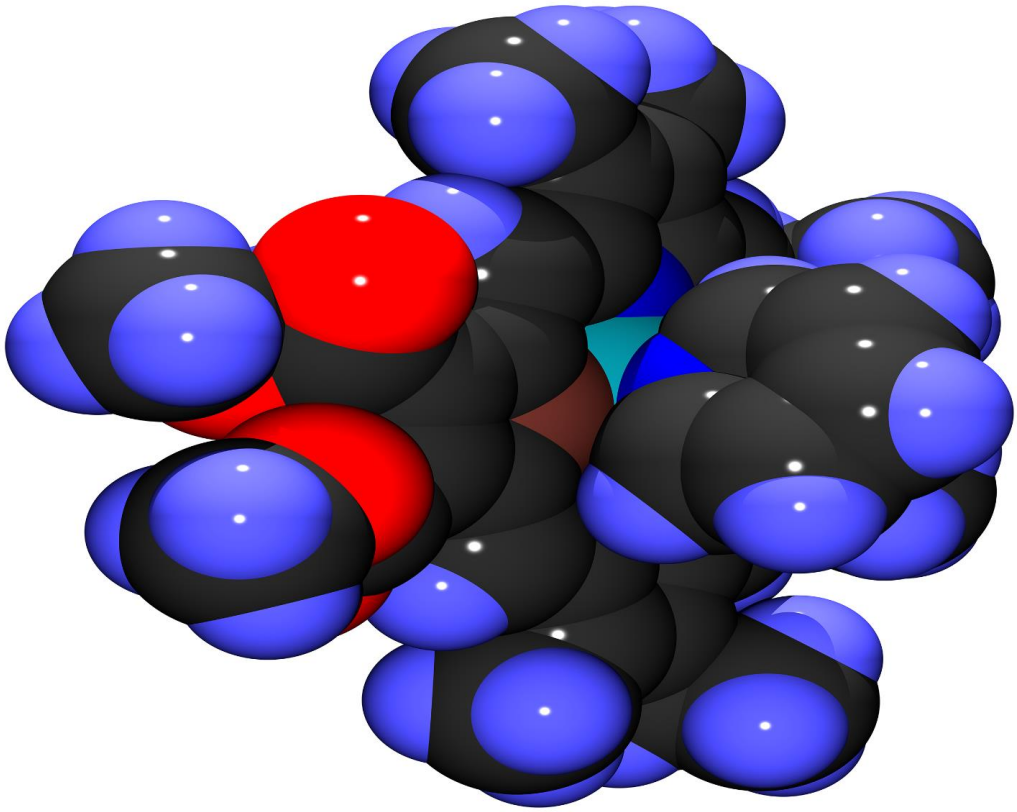

Figure C-4. Color POV-Ray rendered space-filling drawing of rhodium(III) carbaporphyrin **90**, carbon atom attached to rhodium highlighted in brown.

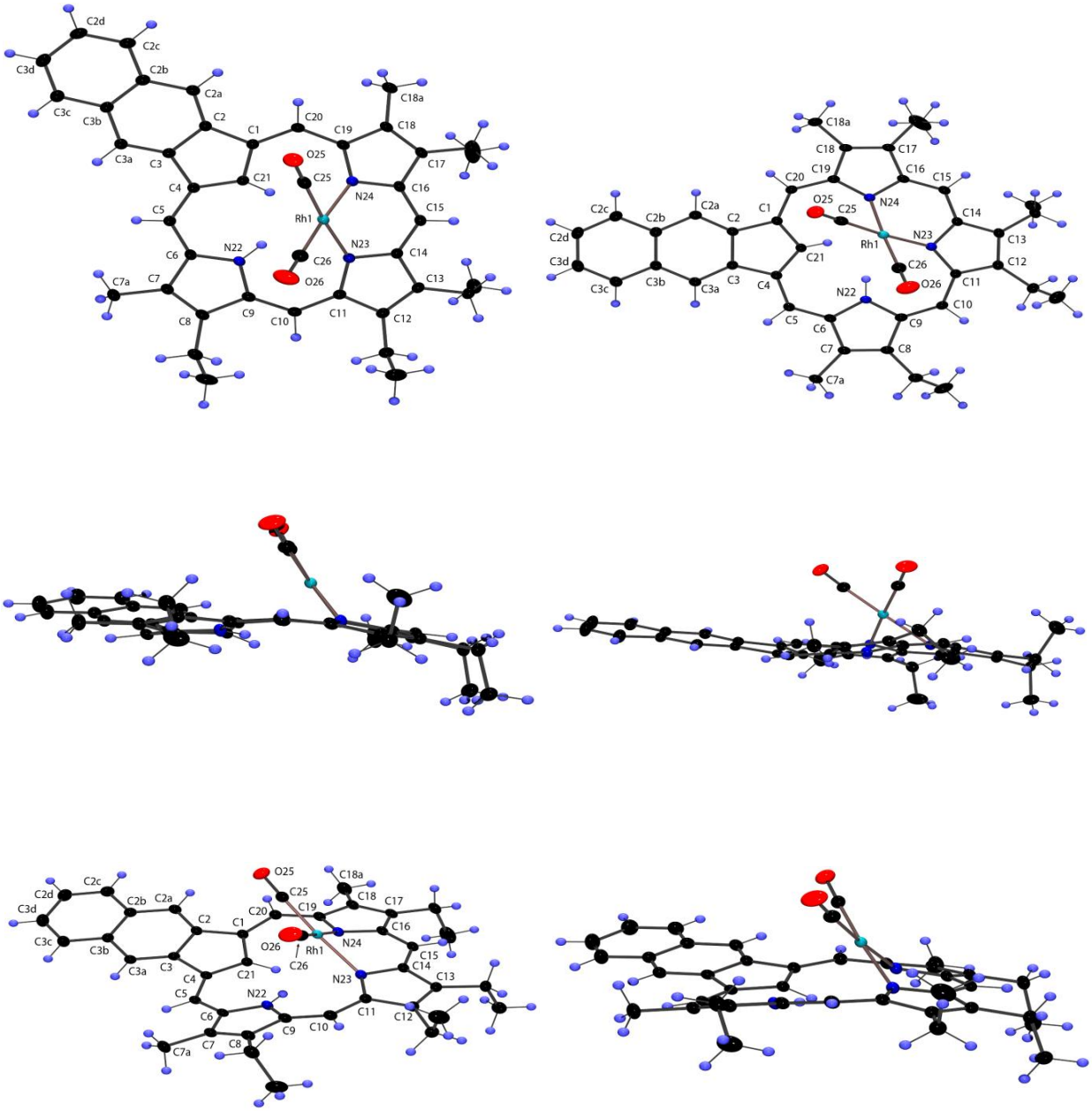

Figure C-5. Color POV-Ray rendered ORTEP III drawing (50% probability level, hydrogen atoms rendered arbitrarily small for clarity) showing a variety of views for rhodium(I) naphthocarbaporphyrin **91**.

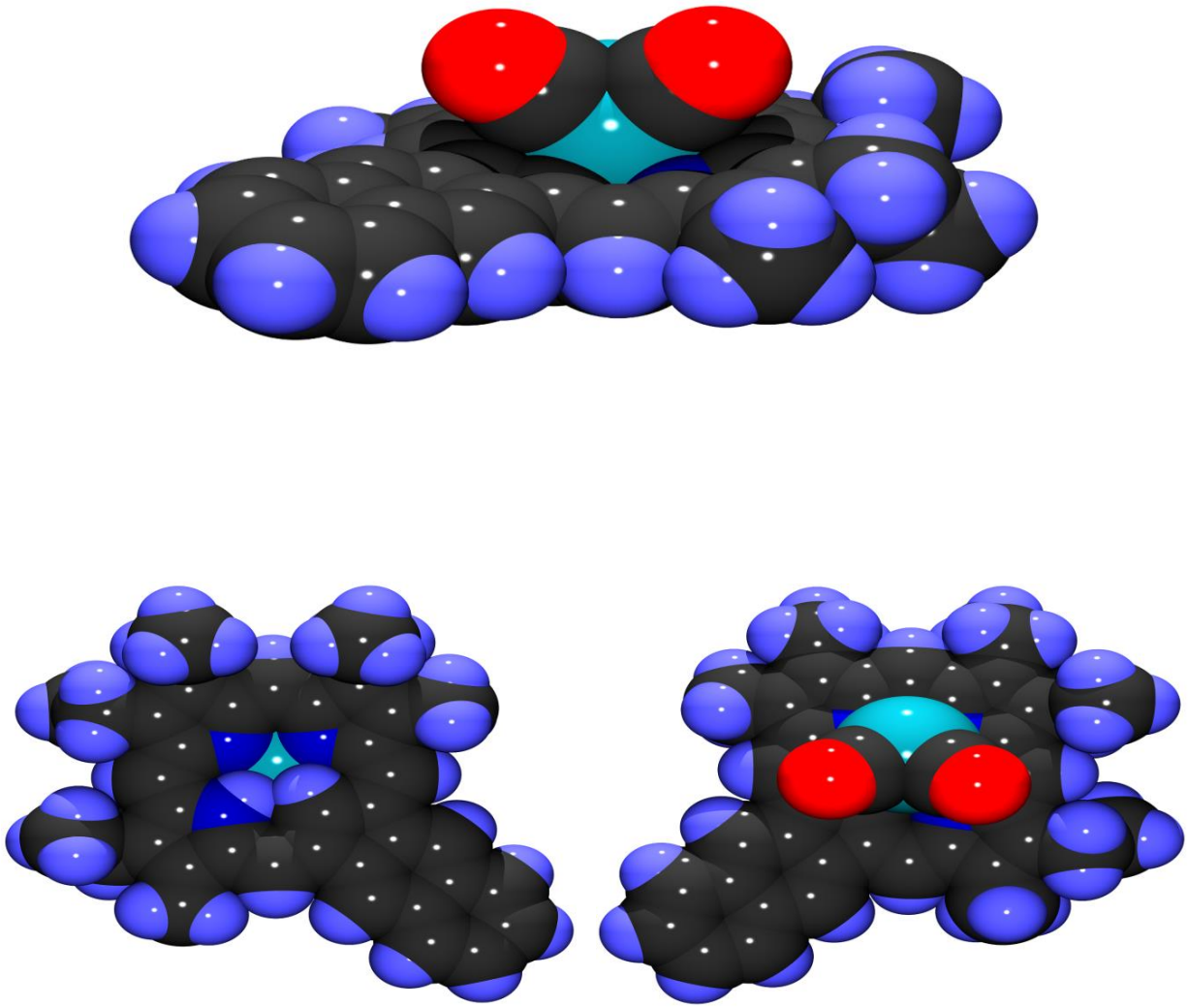

Figure C-6. Color POV-Ray rendered space-filling drawings of rhodium(I) naphthocarbaporphyrin **91**.

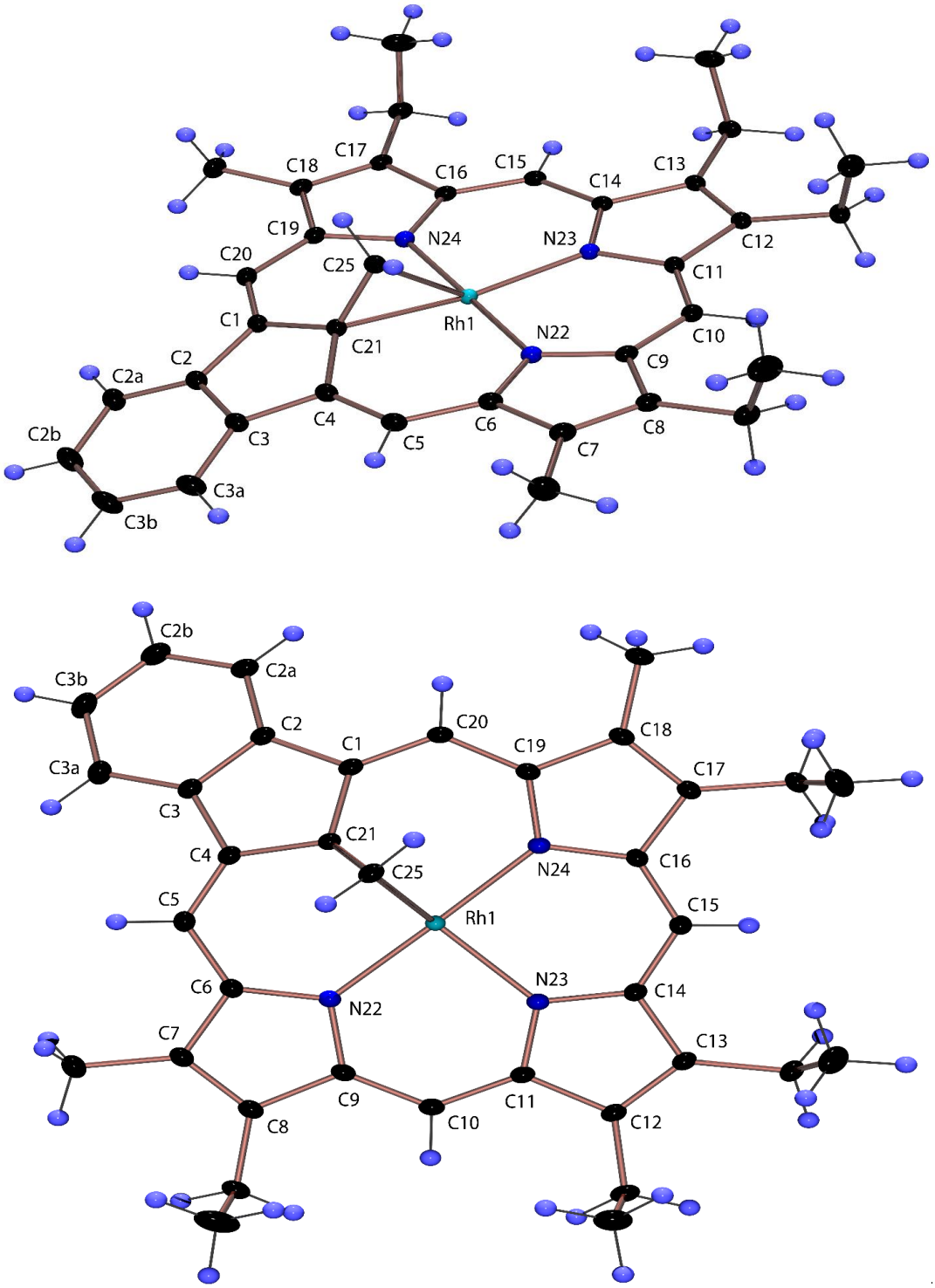

Figure C-7. Color POV-Ray rendered ORTEP III drawing (50% probability level, hydrogen atoms rendered arbitrarily small for clarity) showing two views of rhodium(III) complex **95**.

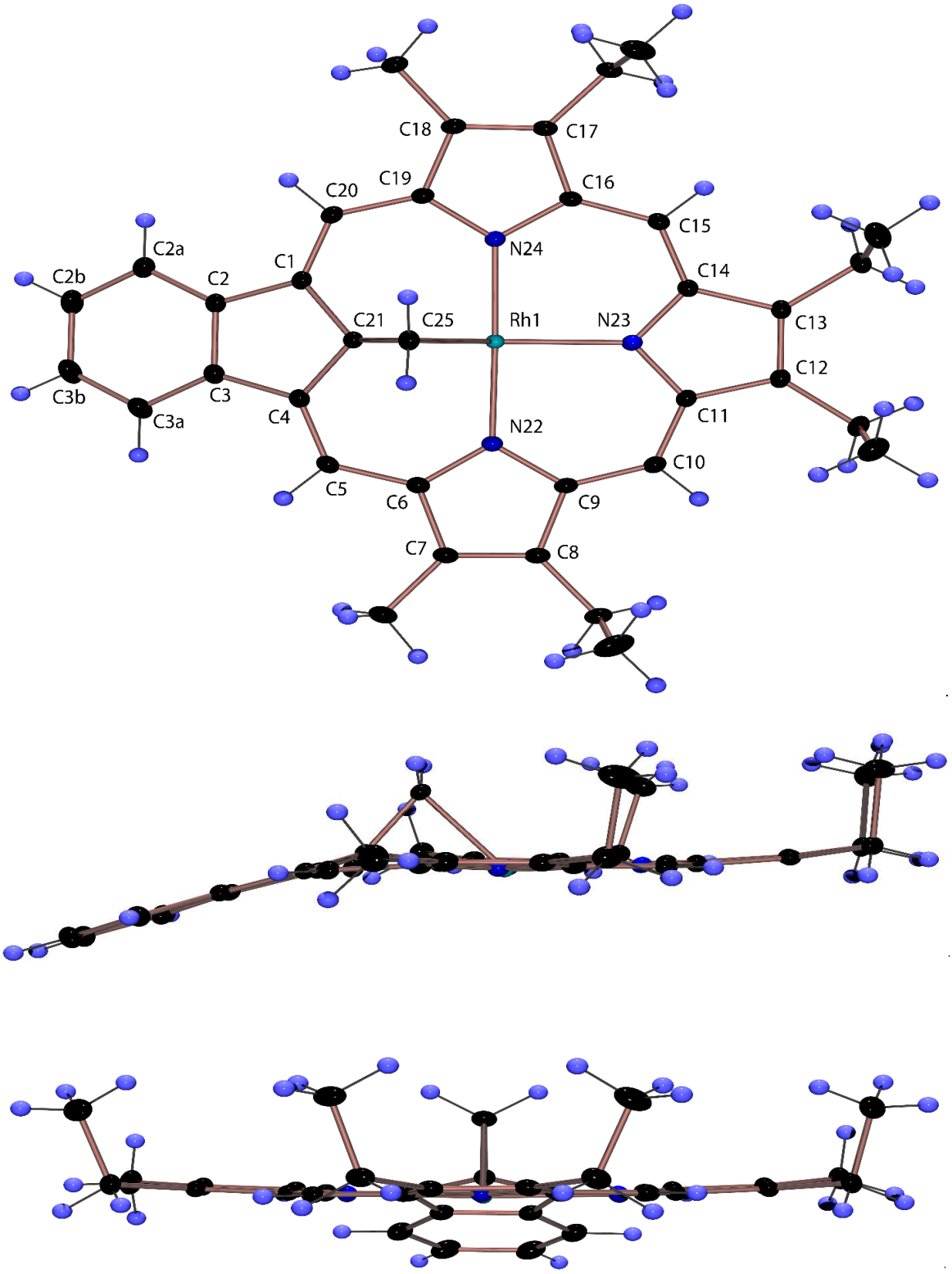

Figure C-8. Color POV-Ray rendered ORTEP III drawing (50% probability level, hydrogen atoms rendered arbitrarily small for clarity) showing three further views of rhodium(III) complex **95**.

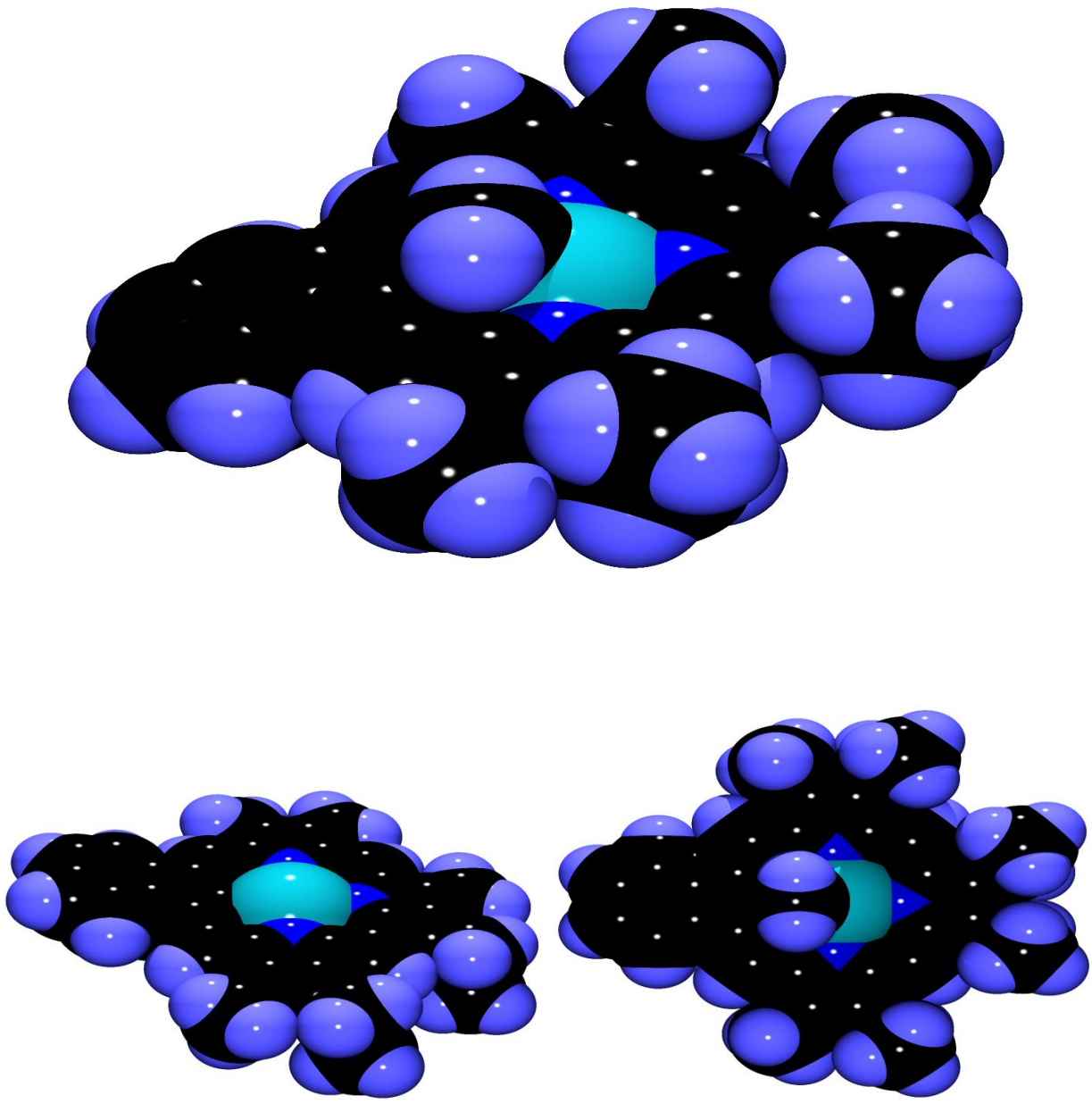

Figure C-9. Color POV-Ray rendered space-filling drawings showing three different views of methylene-bridged rhodium(III) complex **95**.

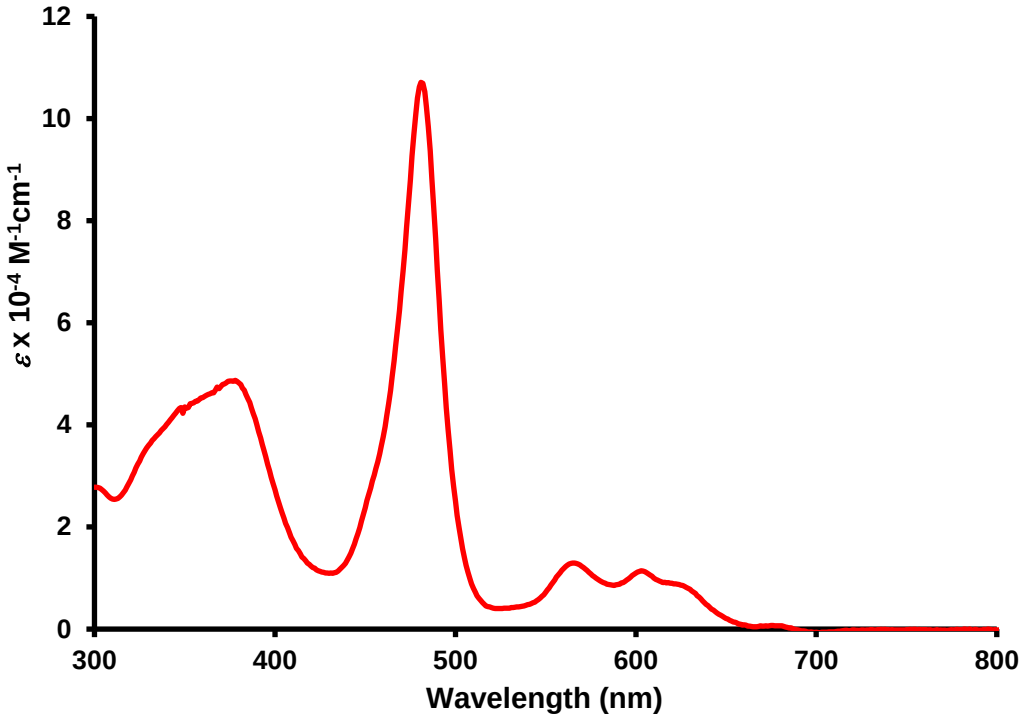

Figure C-10. UV-vis spectrum of rhodium(I) naphthocarbaporphyrin **91** in CH_2Cl_2.

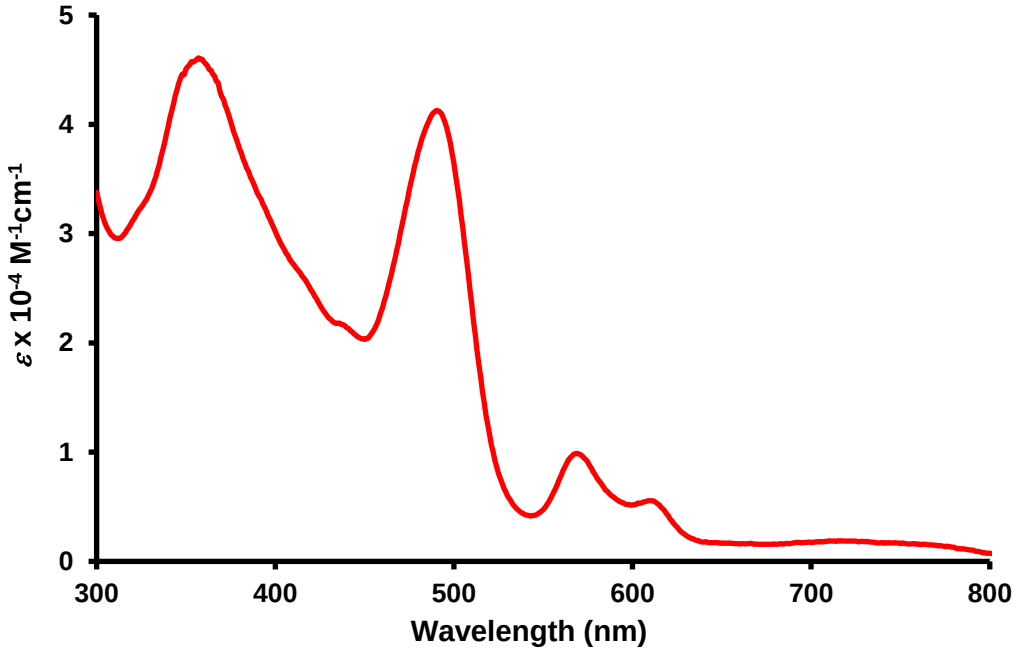

Figure C-11. UV-vis spectrum of rhodium(I) carbaporphyrin **89** in CH_2Cl_2.

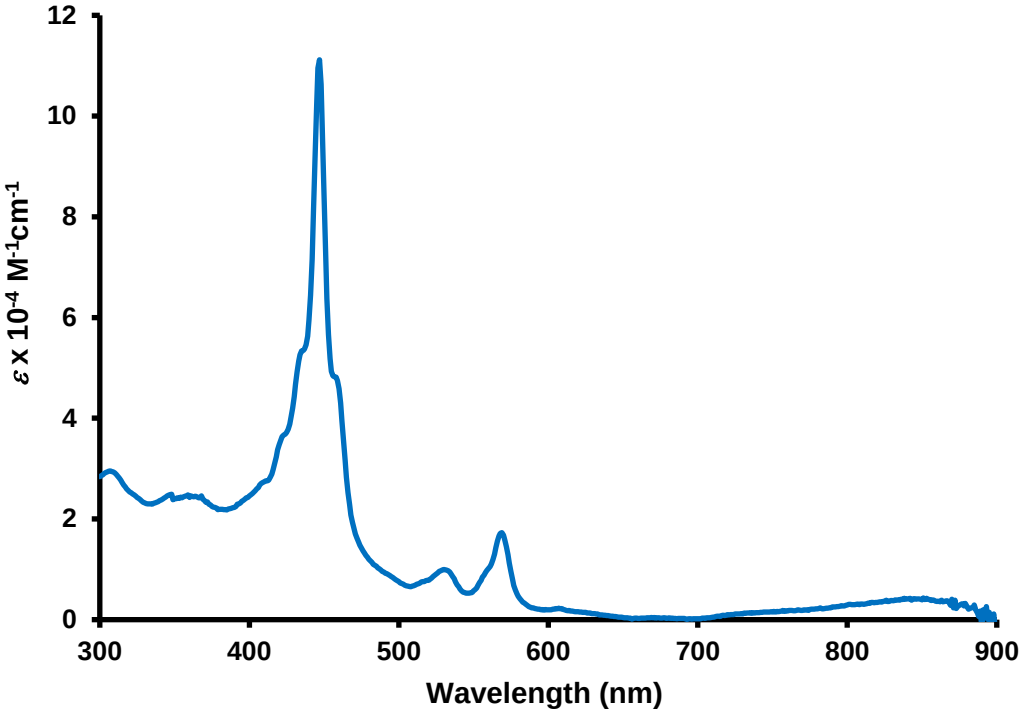

Figure C-12. UV-vis spectrum of rhodium(III) naphthocarbaporphyrin **92** in CH_2Cl_2.

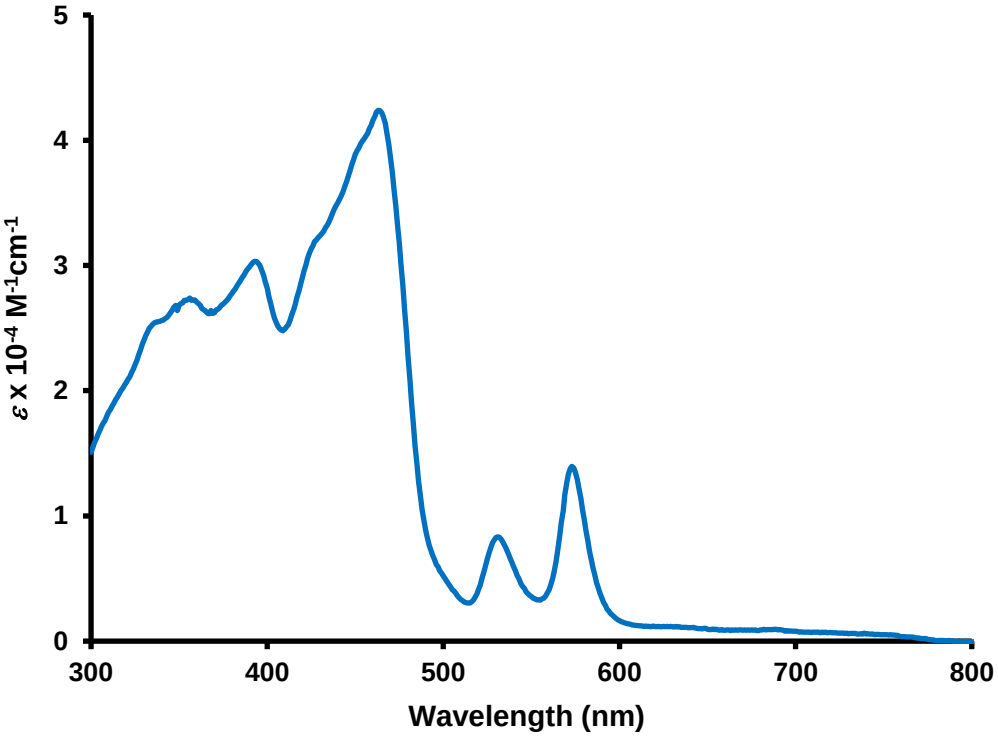

Figure C-13. UV-vis spectrum of rhodium(III) carbaporphyrin **90** in CH_2Cl_2.

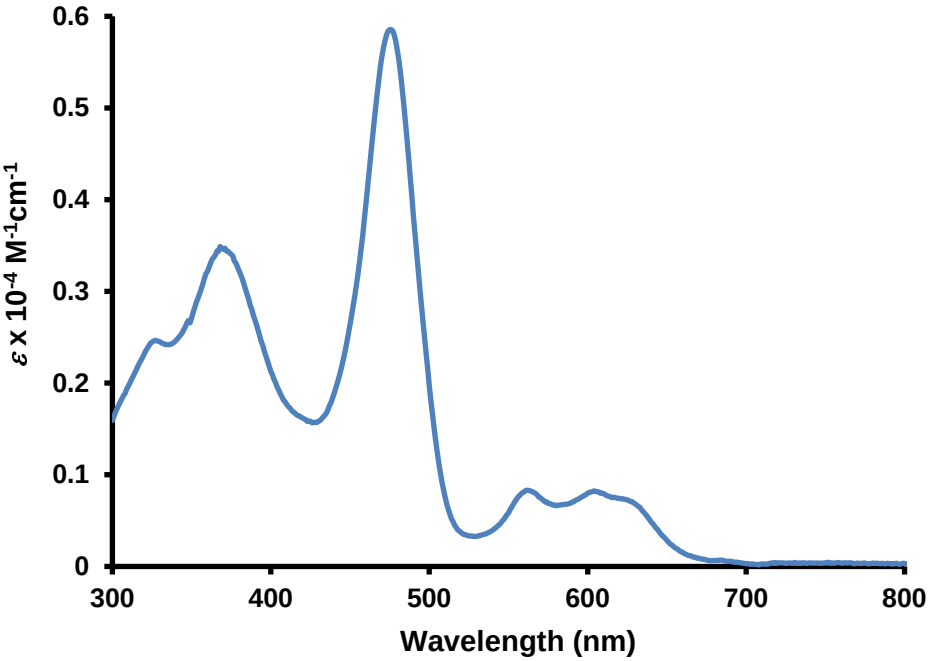

Figure C-14. UV-vis spectrum of rhodium(I) 21-methylcarbaporphyrin complex **94** in CH_2Cl_2.

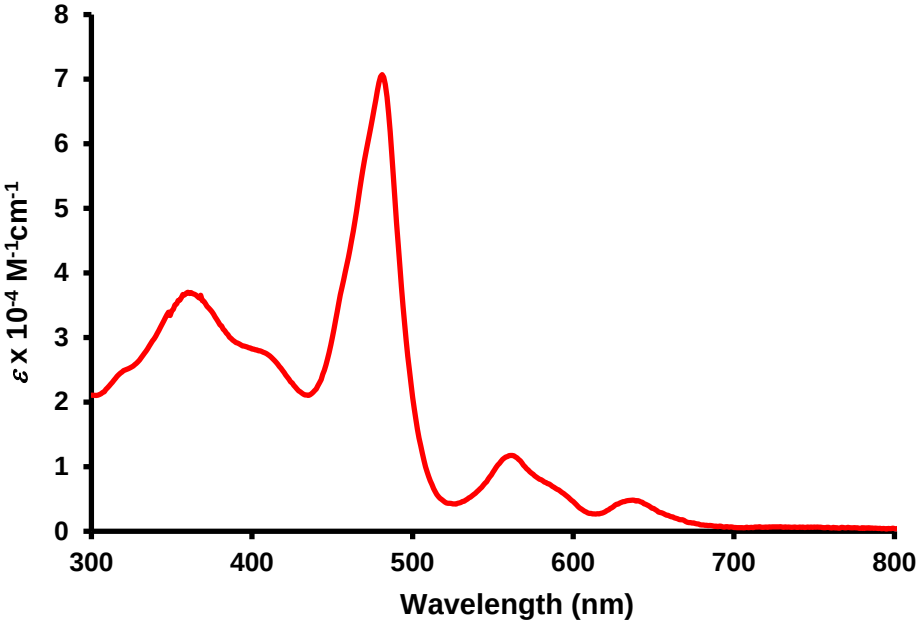

Figure C-15. UV-vis spectrum of rhodium(I) 22-methylcarbaporphyrin complex **93** in CH_2Cl_2.

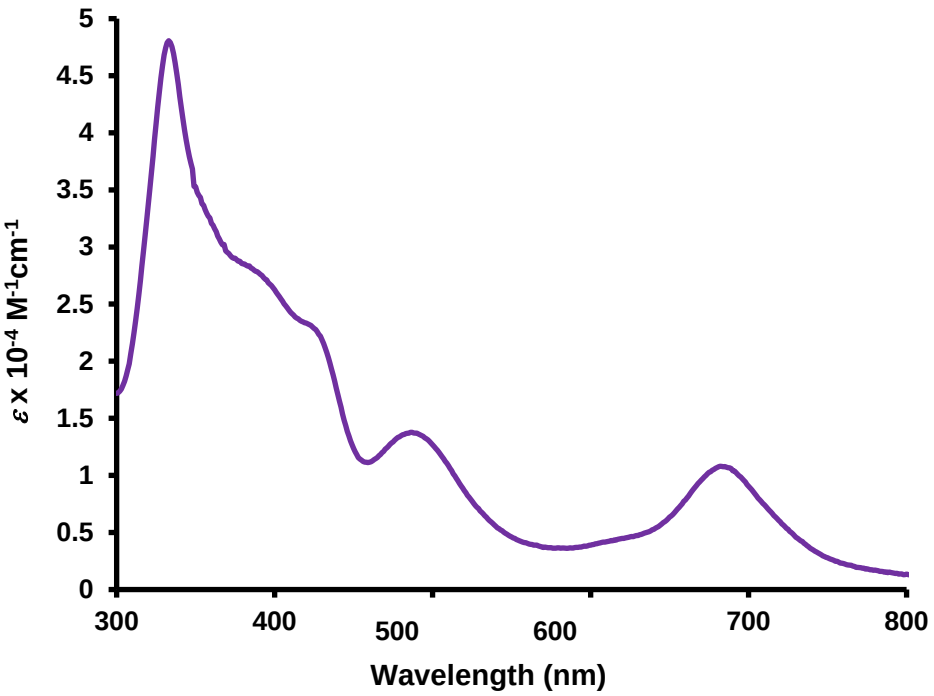

Figure C-16. UV-vis spectrum of rhodium(III) carbaporphyrin complex **95** in CH_2Cl_2.

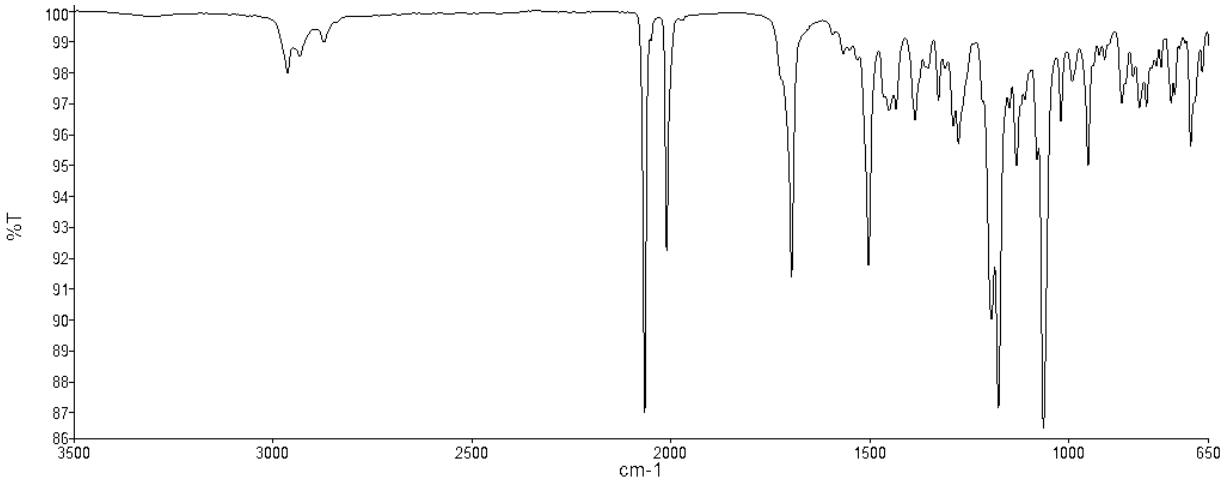

Figure C-17. IR spectrum of rhodium(I) carbaporphyrin **89**.

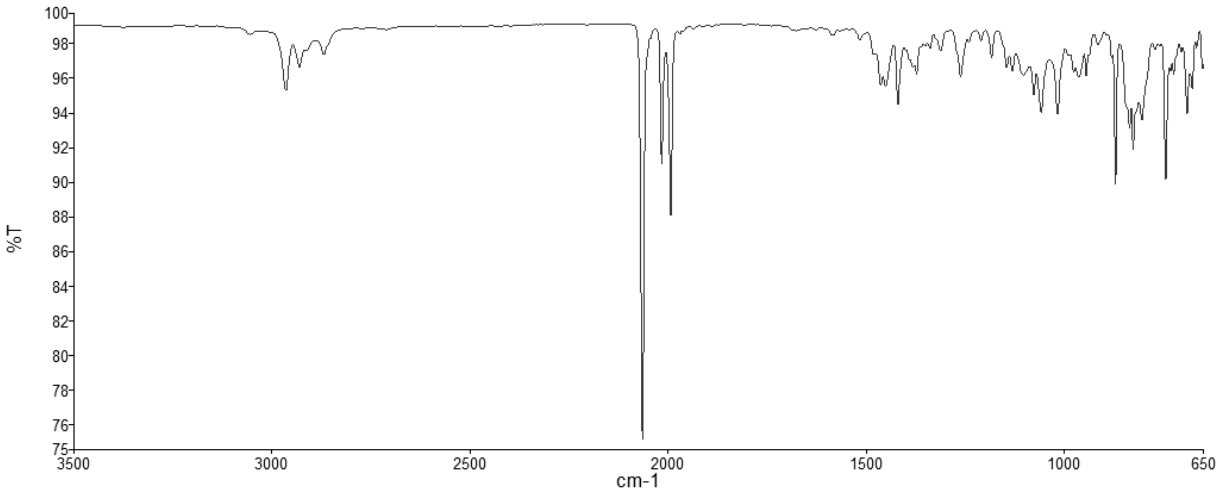

Figure C-18. IR spectrum of rhodium(I) naphthocarbaporphyrin **91**.

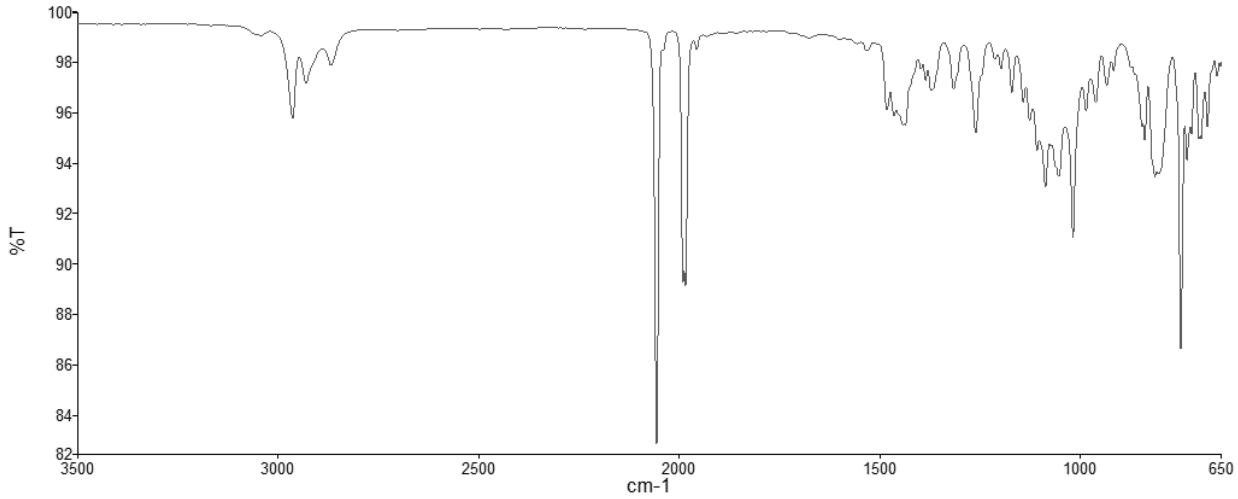

Figure C-19. IR spectrum of rhodium(I) 22-methylcarbaporphyrin **93**.

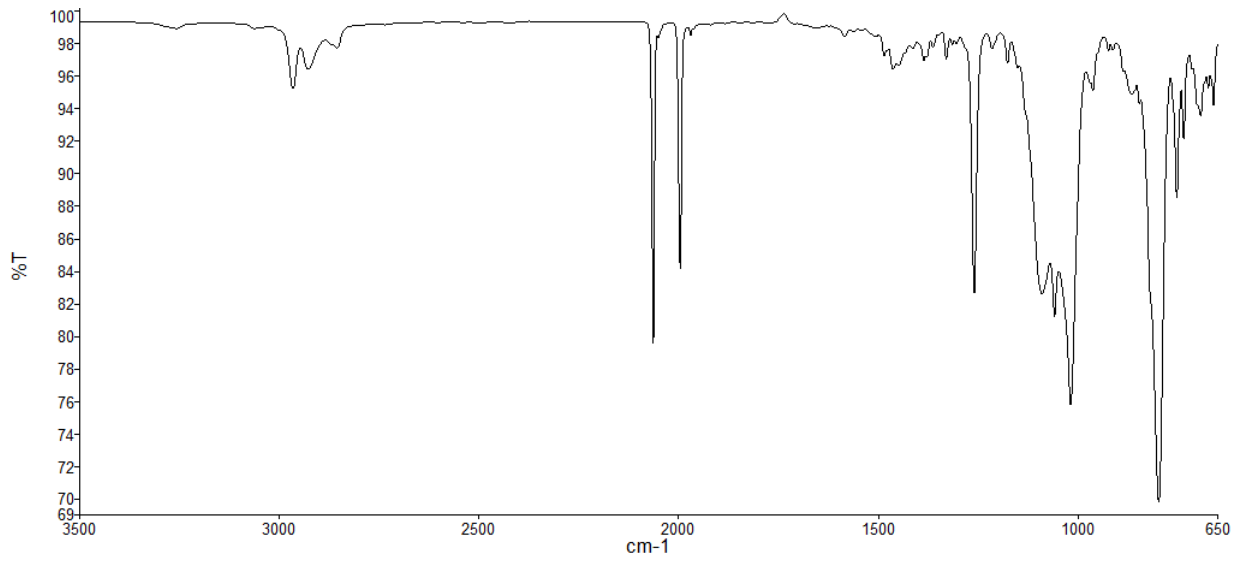

Figure C-20. IR spectrum of rhodium(I) 21-methylcarbaporphyrin **94**.

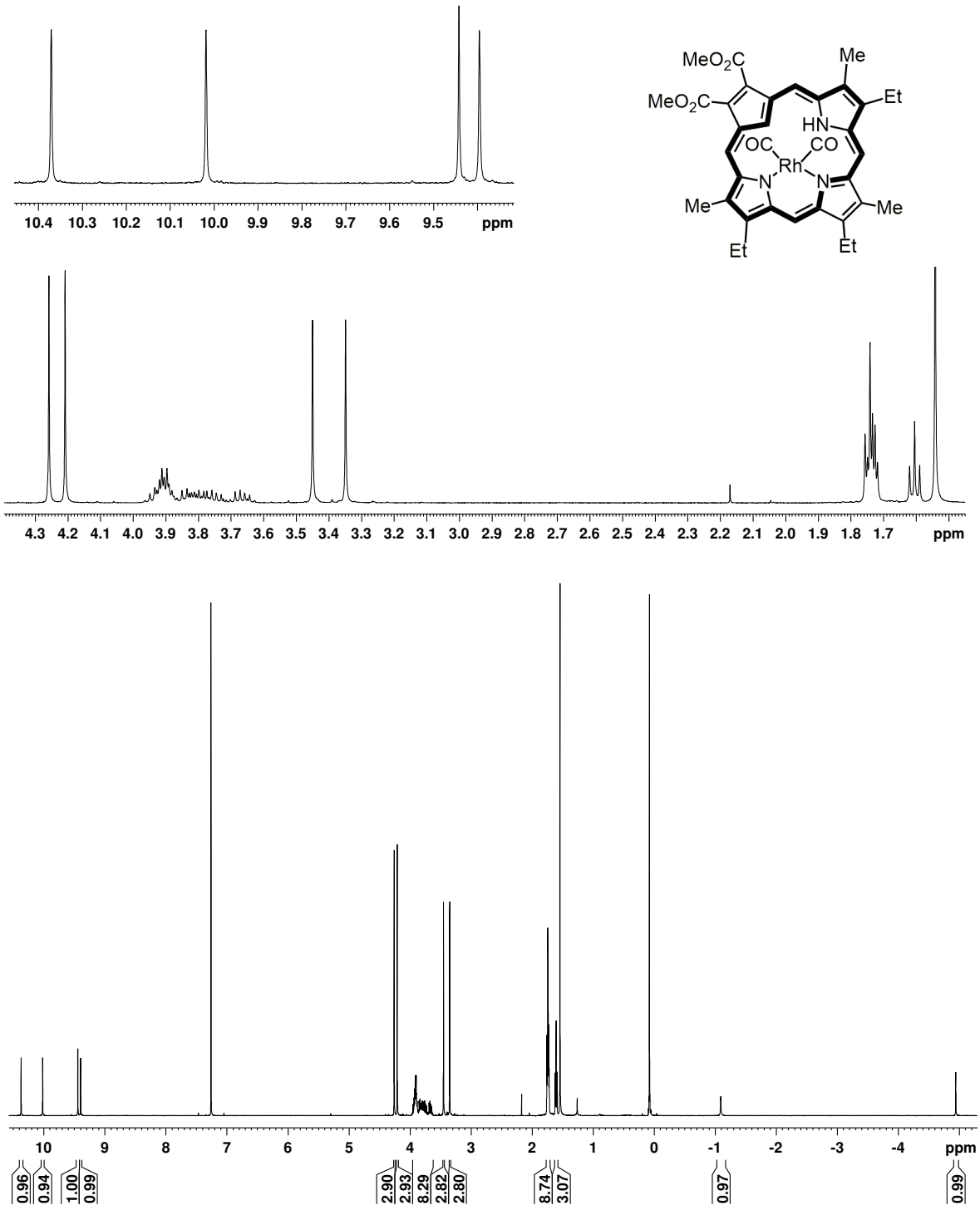

Figure C-21. 500 MHz ^{1}H NMR spectrum of rhodium(I) carbaporphyrin **89** in $CDCl_3$.

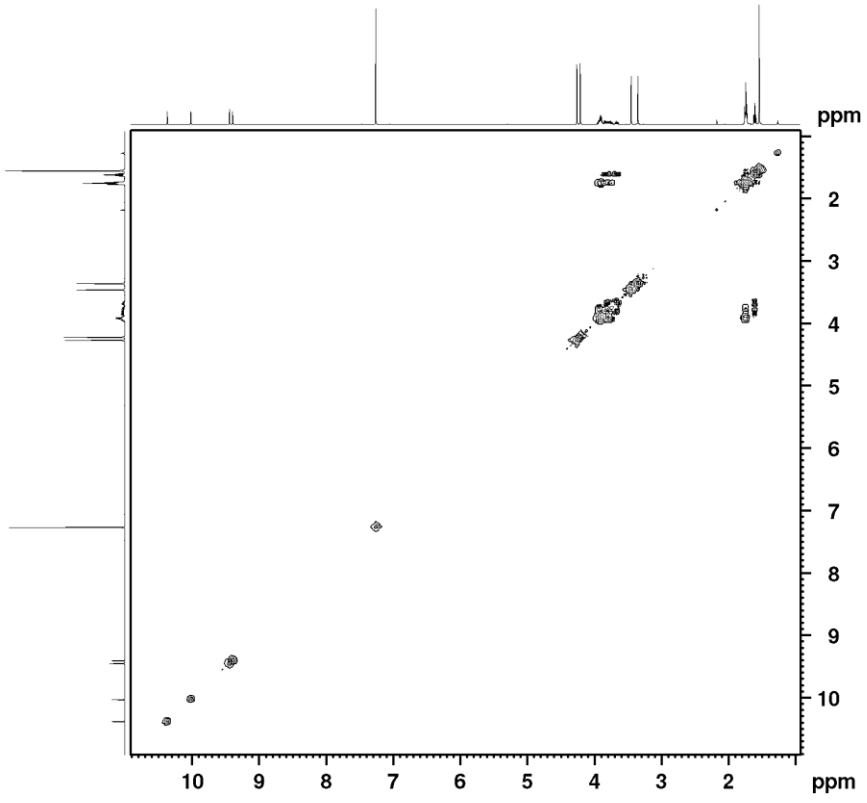

Figure C-22. ^{1}H-^{1}H COSY NMR spectrum of rhodium(I) carbaporphyrin **89** in $CDCl_3$.

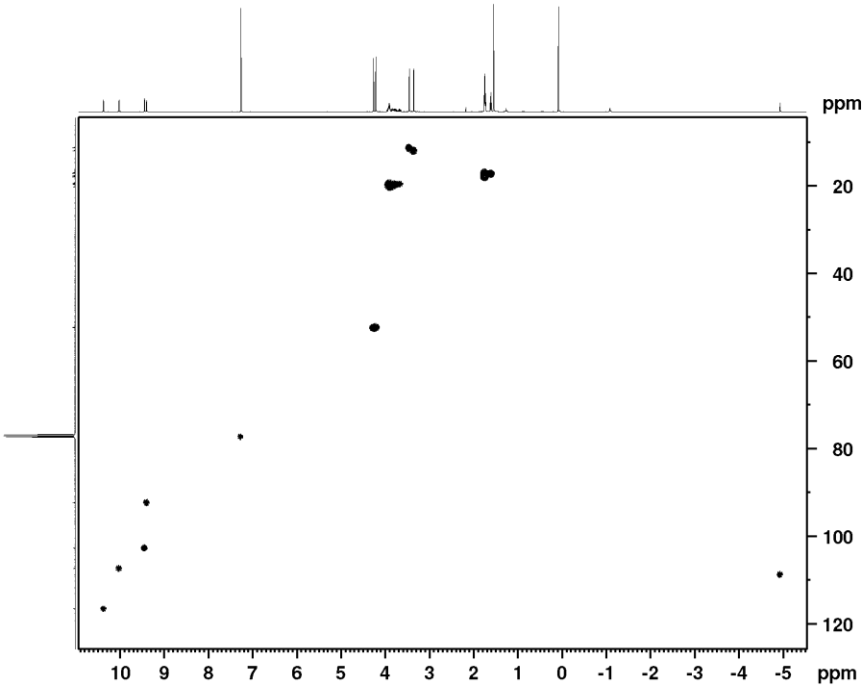

Figure C-23. HSQC NMR spectrum of rhodium(I) carbaporphyrin **89** in $CDCl_3$.

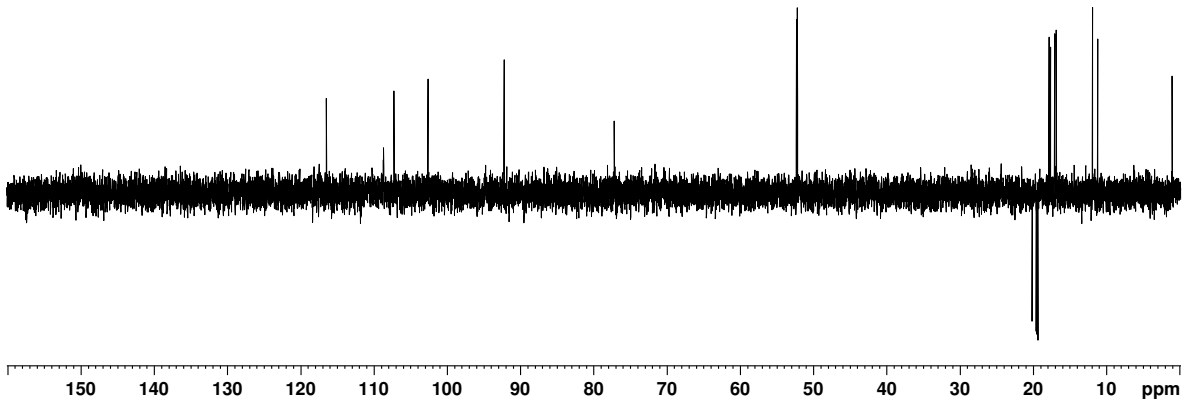

Figure C-24. DEPT-135 NMR spectrum of rhodium(I) carbaporphyrin **89** in $CDCl_3$.

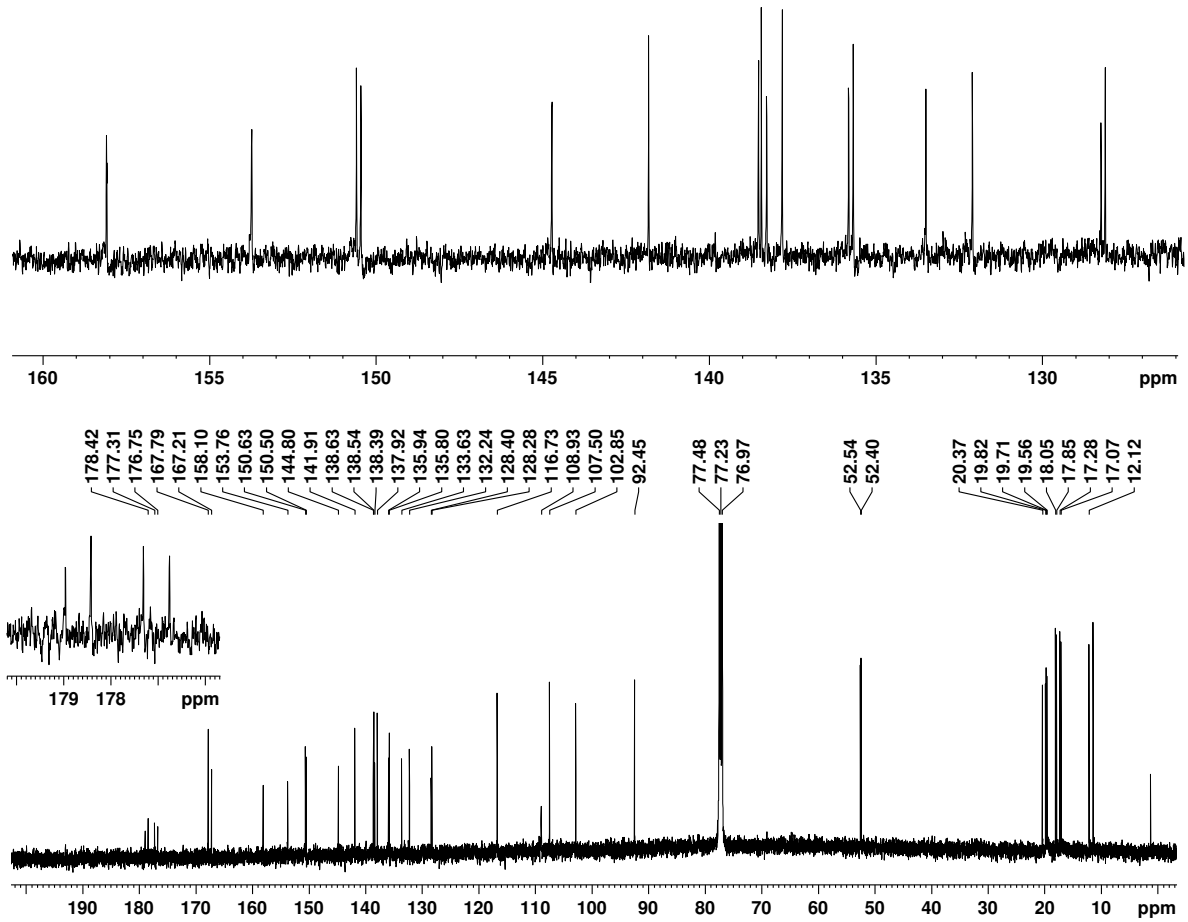

Figure C-25. 500 MHz ^{1}H NMR spectrum of rhodium(I) carbaporphyrin **89** in $CDCl_3$.

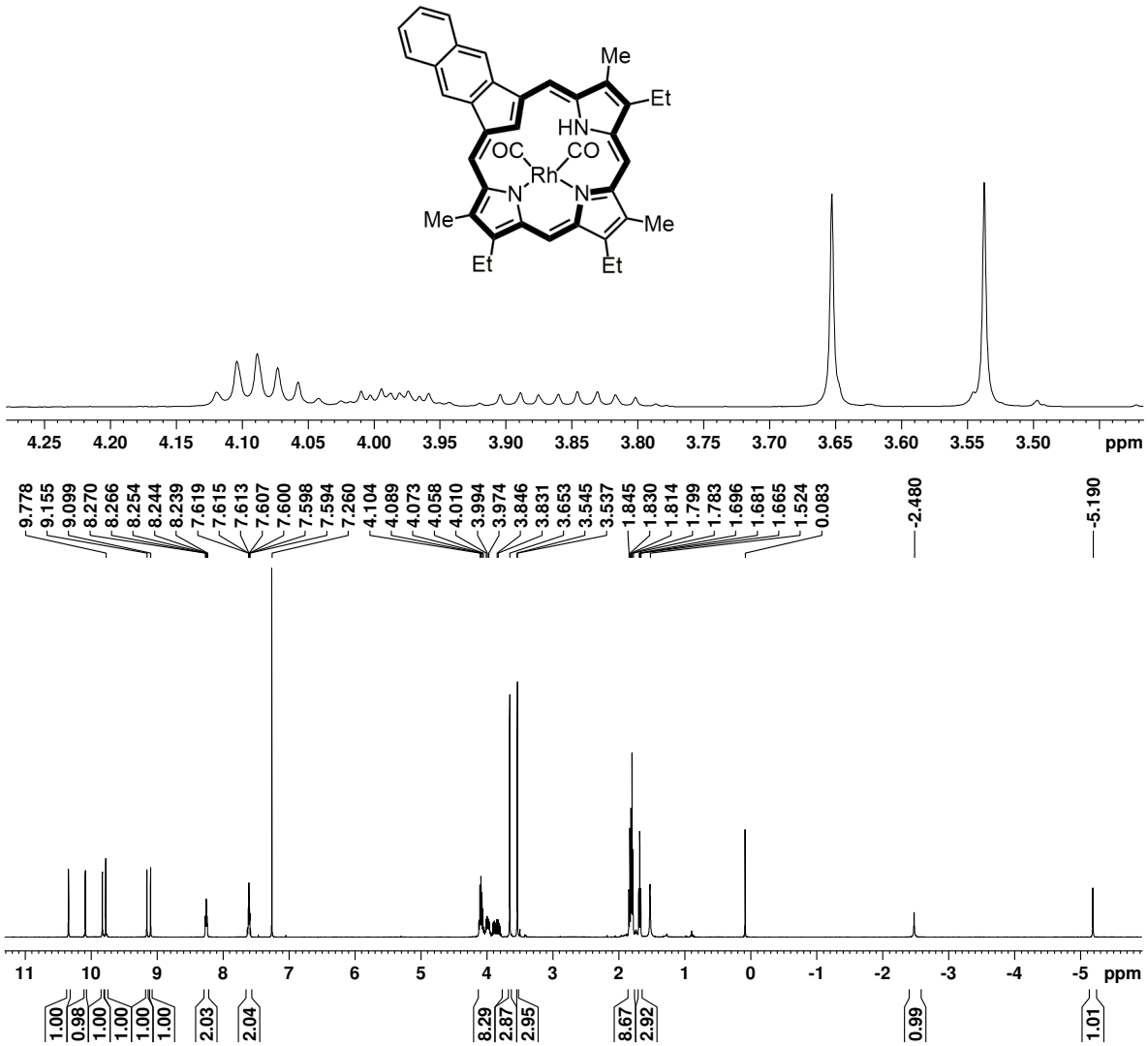

Figure C-26. 500 MHz ^{1}H NMR spectrum of rhodium(I) naphthocarbaporphyrin **91** in CDCl$_3$.

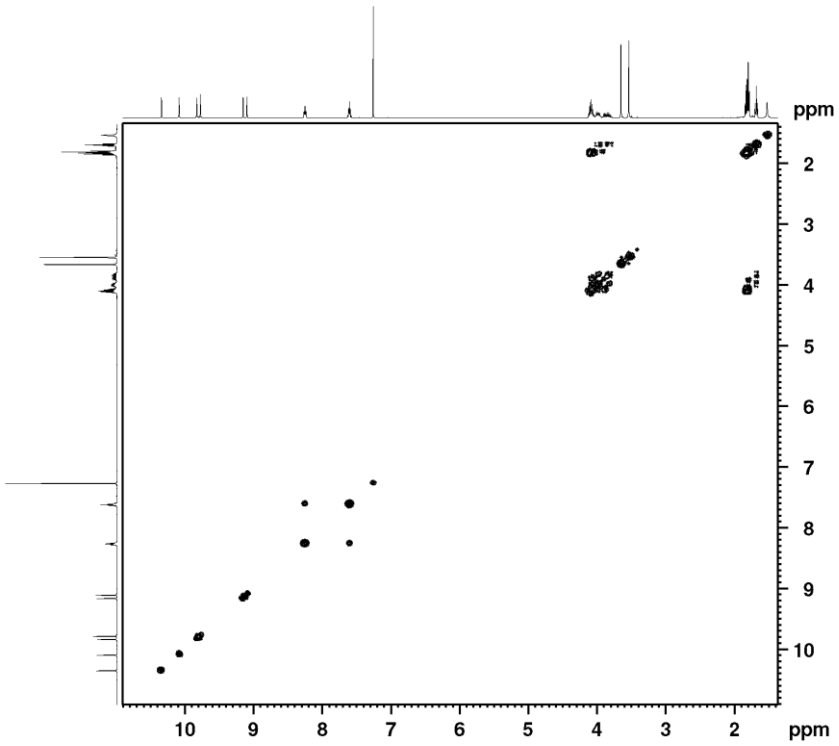

Figure C-27. ^{1}H-^{1}H COSY NMR spectrum of rhodium(I) naphthocarbaporphyrin **91** in $CDCl_3$.

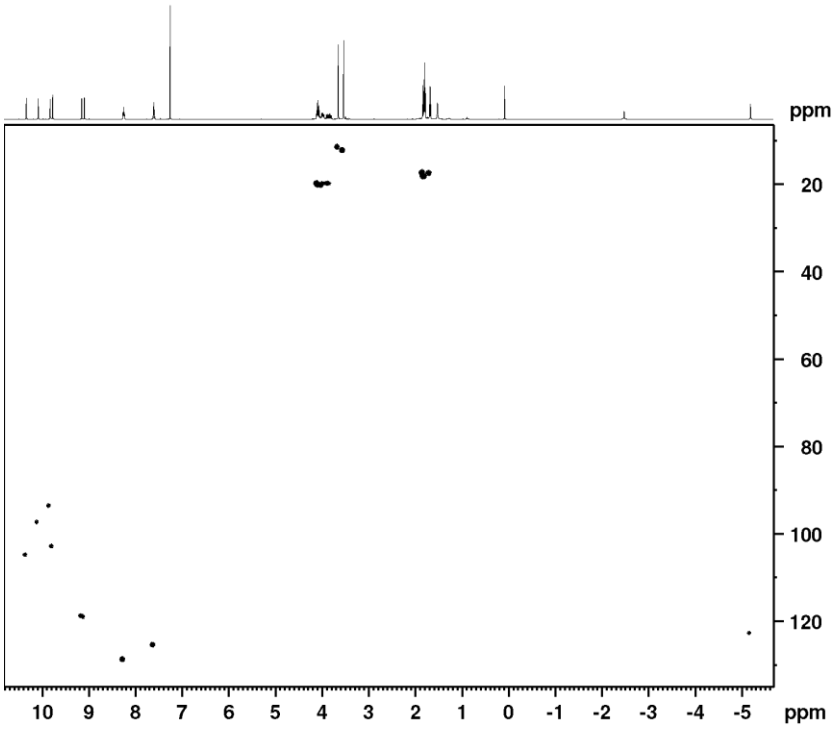

Figure C-28. HSQC NMR spectrum of rhodium(I) naphthocarbaporphyrin **91** in $CDCl_3$.

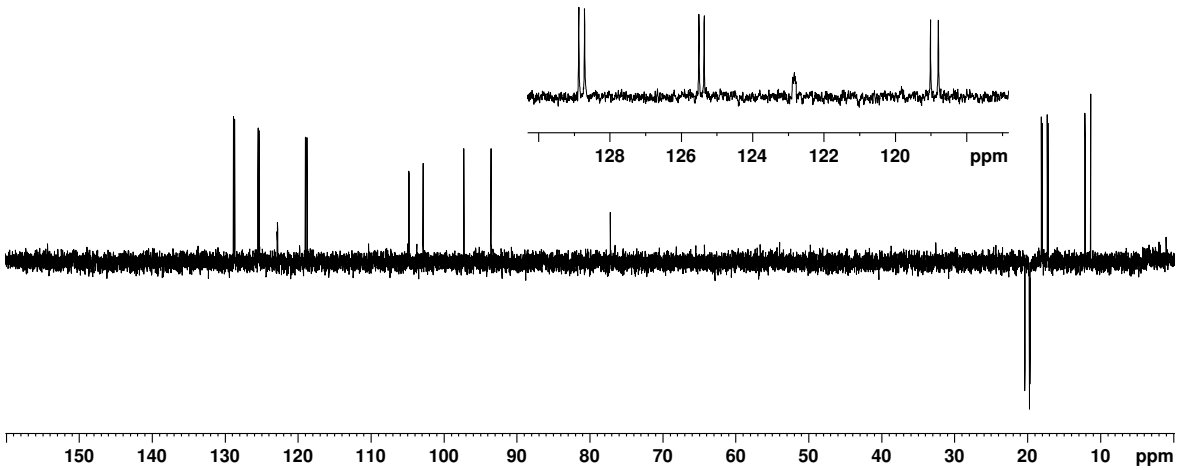

Figure C-29. DEPT-135 NMR spectrum of rhodium(I) naphthocarbaporphyrin **91** in $CDCl_3$.

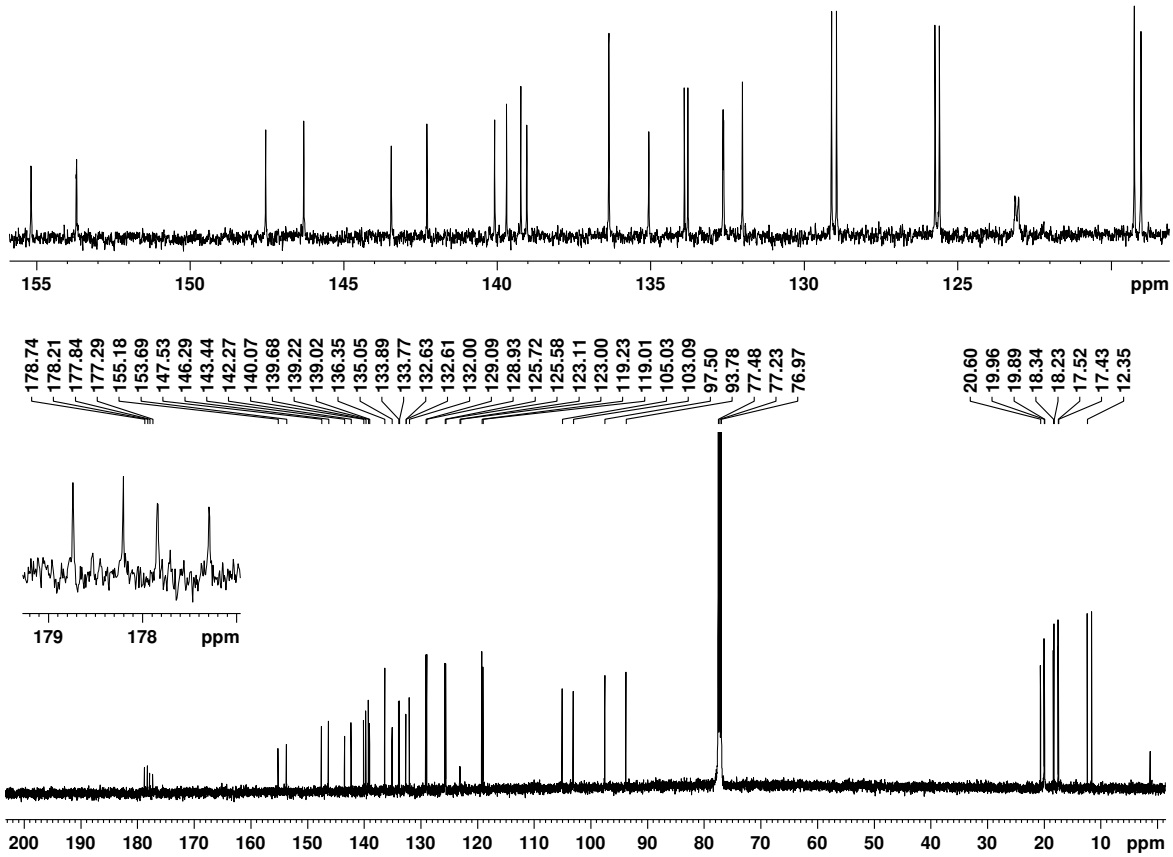

Figure C-30. 125 MHz ^{13}C NMR spectrum of rhodium(I) naphthocarbaporphyrin **91** in $CDCl_3$.

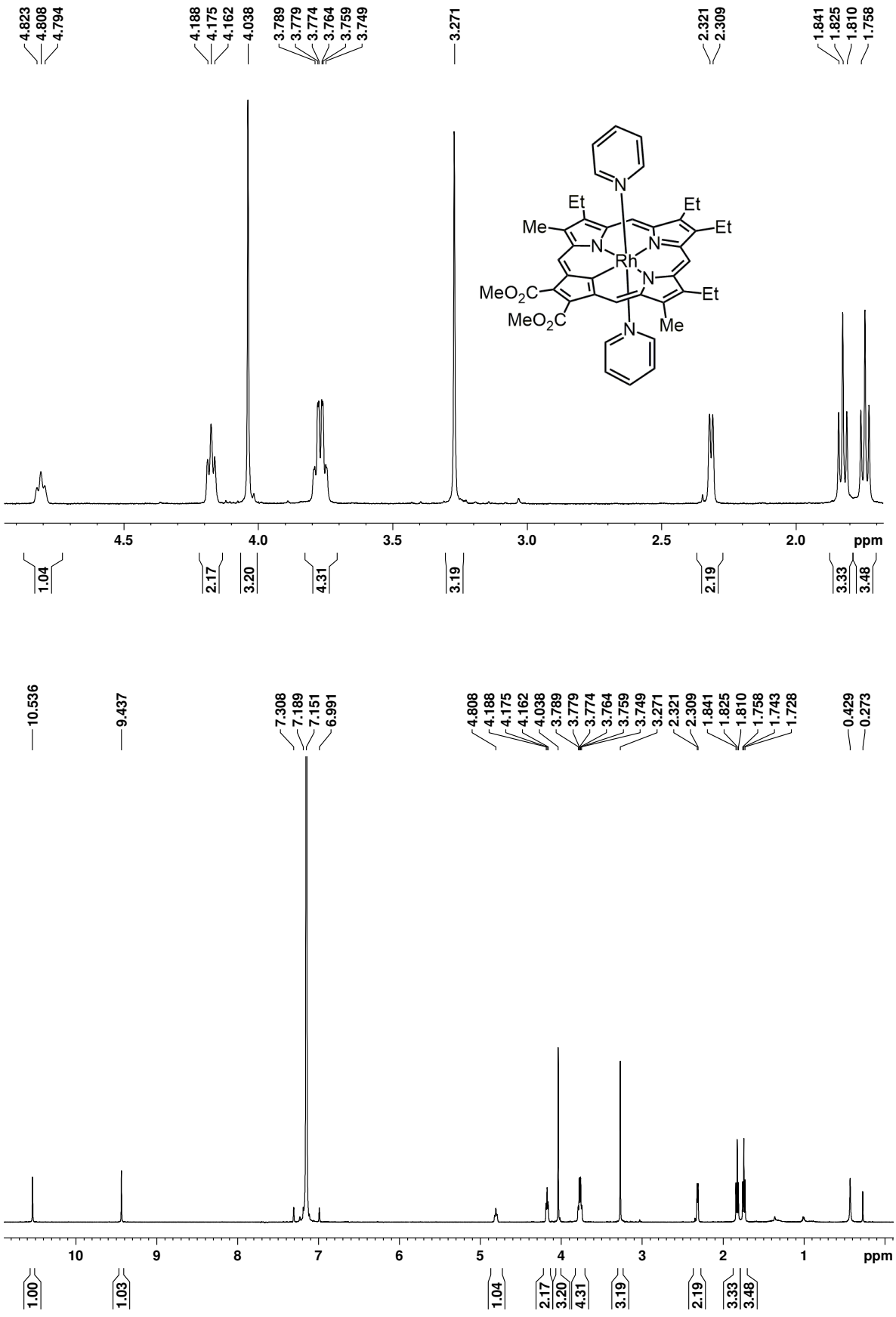

Figure C-31. 500 MHz ^{1}H NMR spectrum of rhodium(III) carbaporphyrin **90** in C_6D_6.

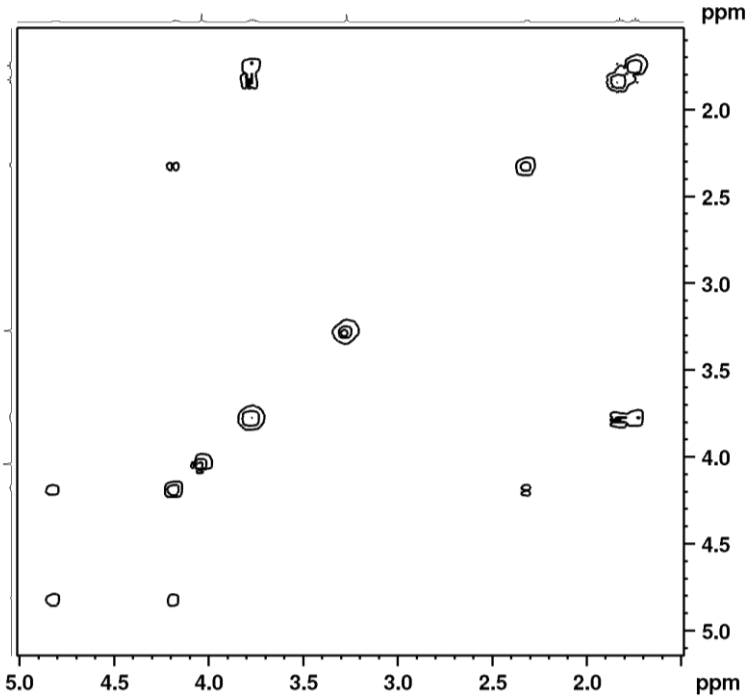

Figure C-32. ^{1}H-^{1}H COSY NMR spectrum of rhodium(III) carbaporphyrin **90** in C_6D_6 at 60 ^{o}C.

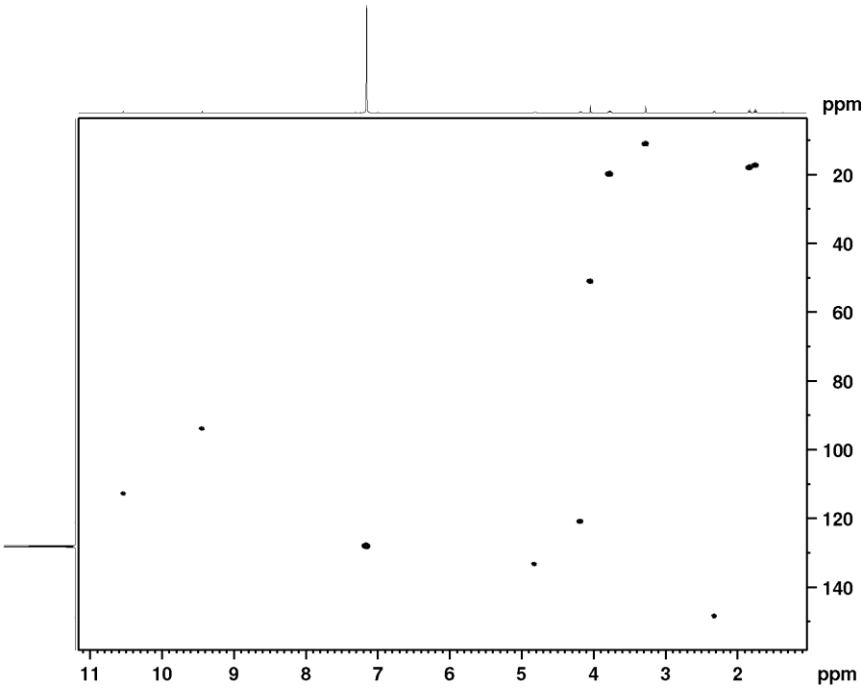

Figure C-33 HSQC NMR spectrum of rhodium(III) carbaporphyrin **90** in C_6D_6 at 60 ^{o}C.

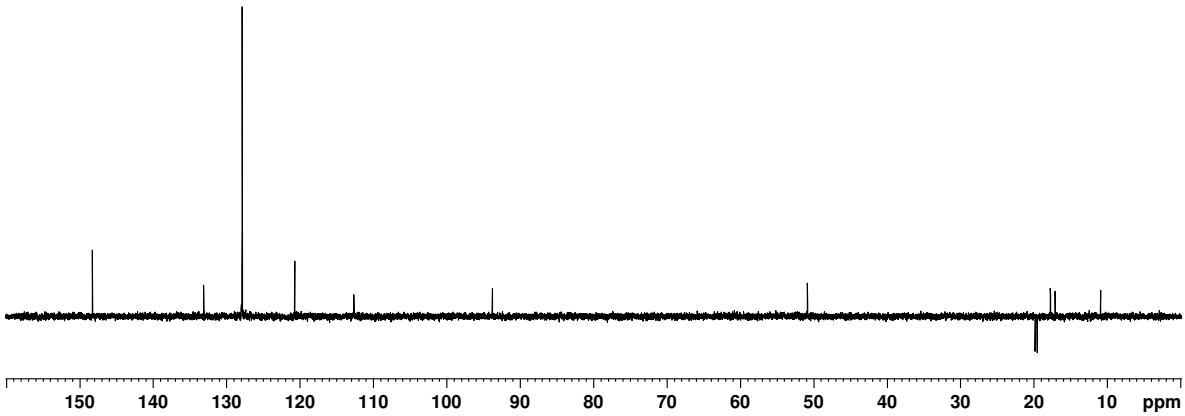

Figure C-34. DEPT-135 NMR spectrum of rhodium(III) carbaporphyrin **90** in C_6D_6.

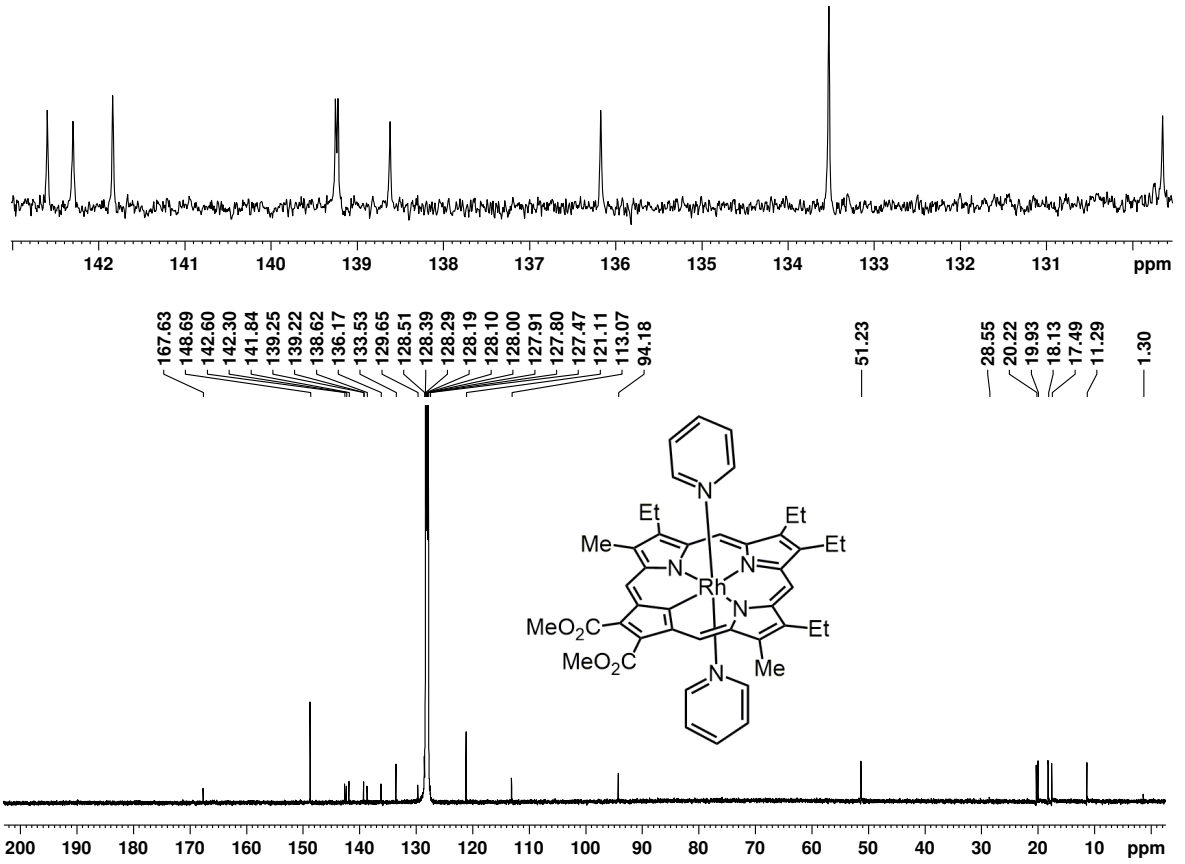

Figure C-35. 125 MHz ^{13}C NMR spectrum of rhodium(III) carbaporphyrin **90** in C_6D_6.

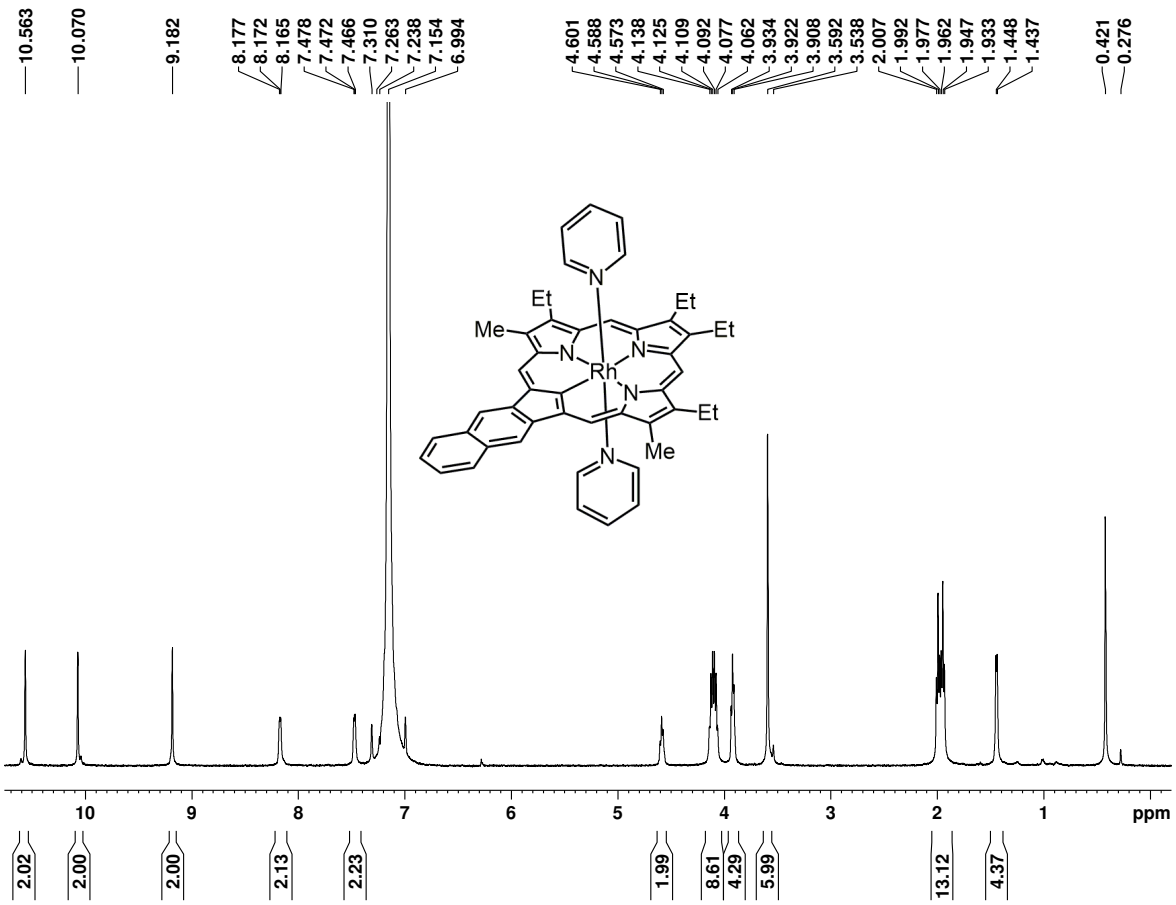

Figure C-36. 500 MHz ^{1}H NMR spectrum of rhodium(III) naphthocarbaporphyrin **92** in d_6-benzene at 60 °C.

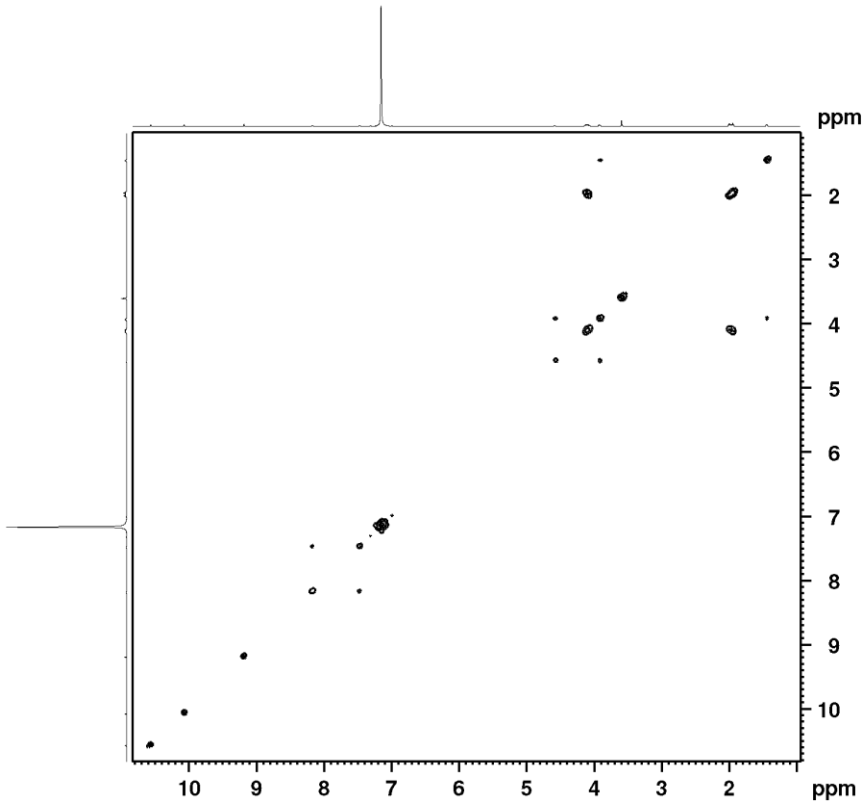

Figure C-37. ^{1}H-^{1}H COSY NMR spectrum of rhodium(III) naphthocarbaporphyrin **92** in C_6D_6 at 60 ^{o}C.

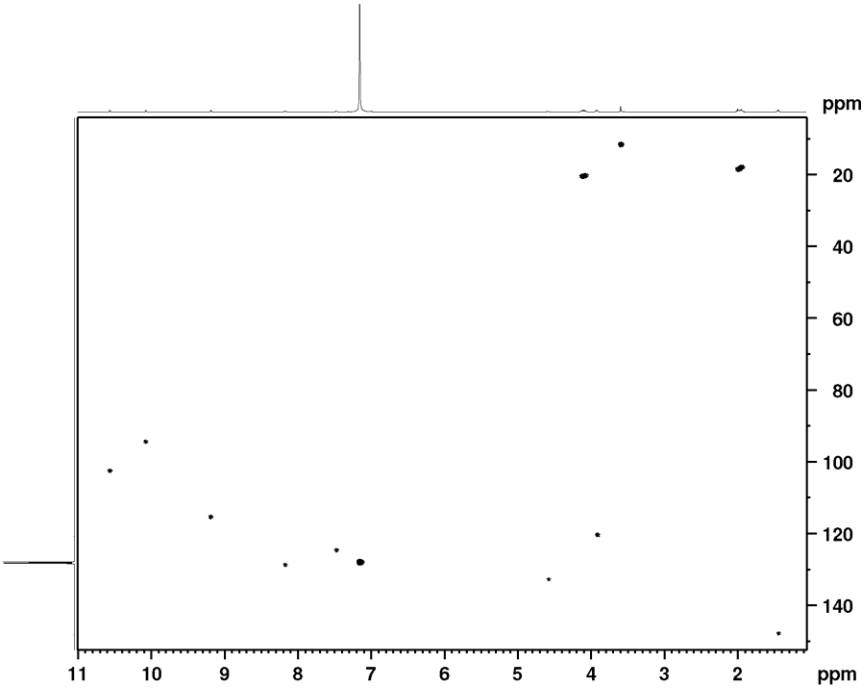

Figure C-38. HSQC NMR spectrum of rhodium(III) naphthocarbaporphyrin **92** in C_6D_6 at 60 ^{o}C.

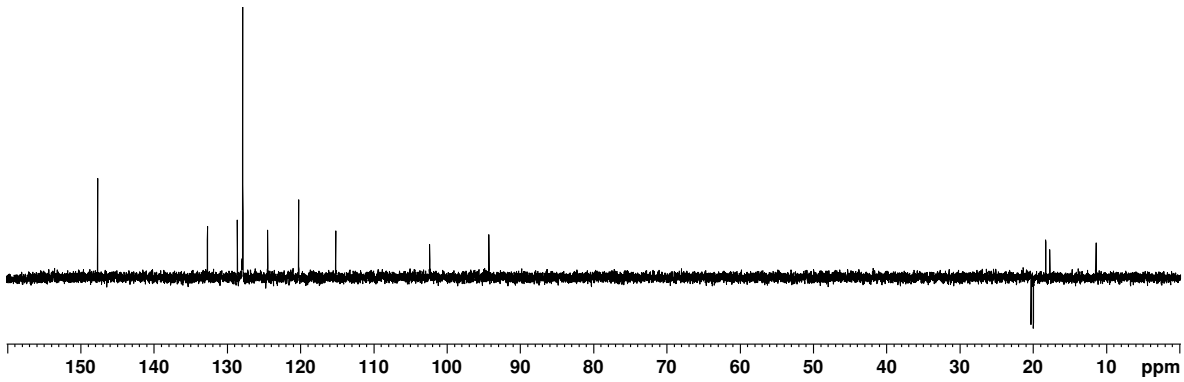

Figure C-39. DEPT-135 NMR spectrum of rhodium(III) naphthocarbaporphyrin **92** in d_6-benzene at 60 °C.

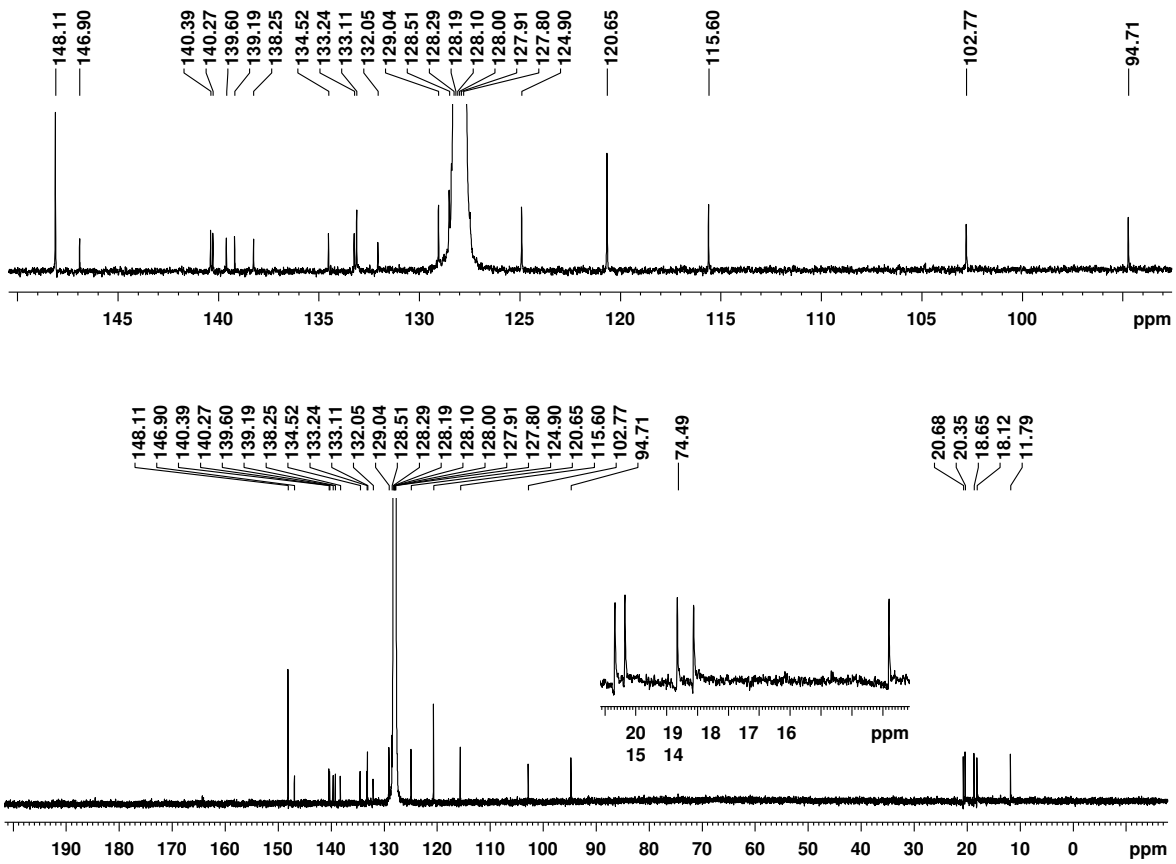

Figure C-40. 125 MHz ^{13}C NMR spectrum of rhodium(III) naphthocarbaporphyrin **92** in d_6-benzene at 60 °C.

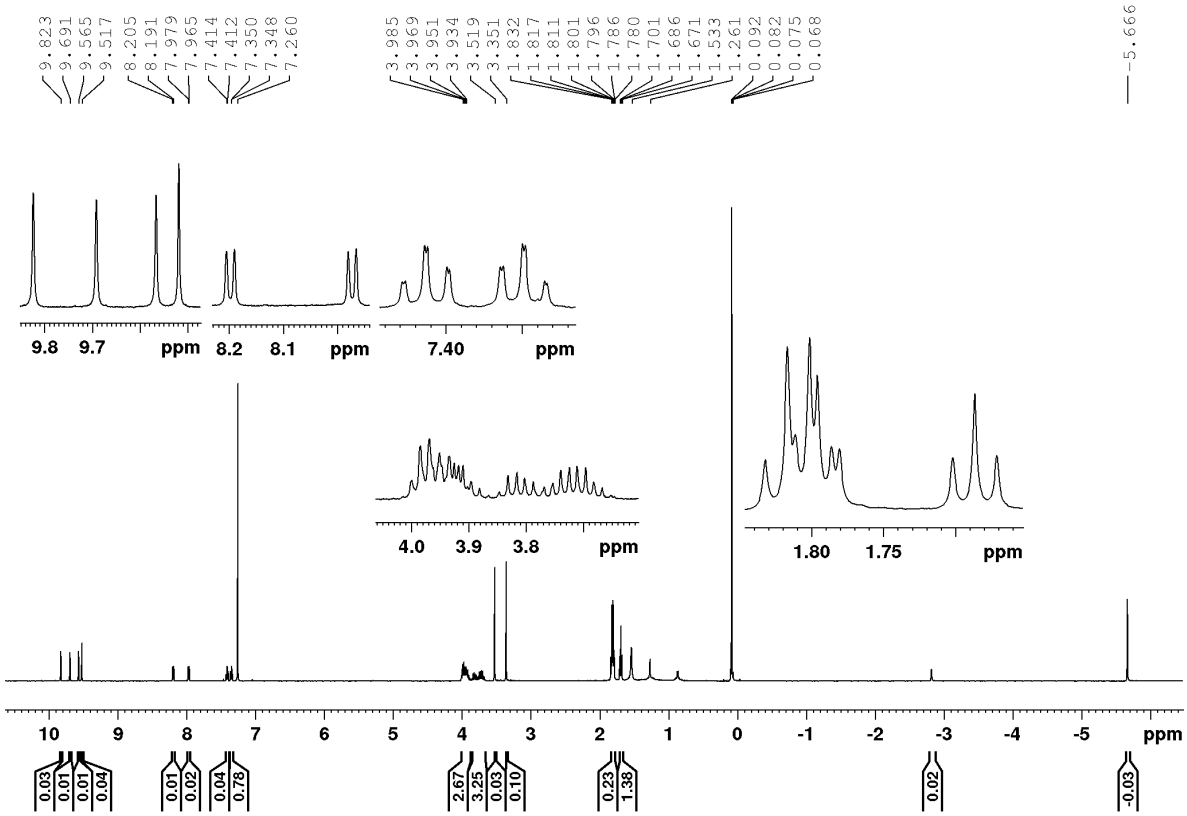

Figure C-41. 500 MHz ^{1}H NMR spectrum of rhodium(I) 21-methylcarbaporphyrin **94** in $CDCl_3$.

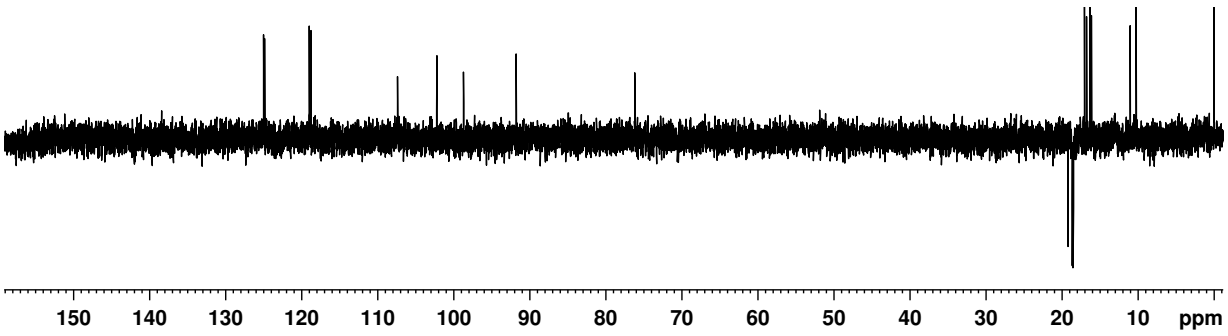

Figure C-42. DEPT-135 NMR spectrum of rhodium(I) 21-methylcarbaporphyrin **94** in $CDCl_3$.

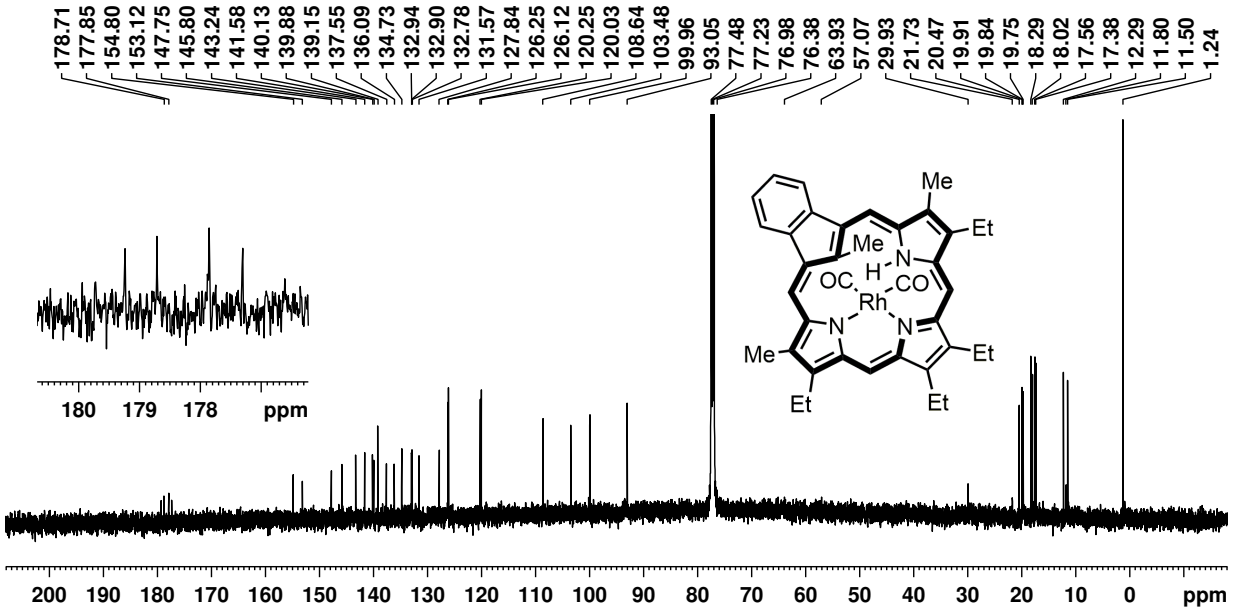

Figure C-43. 125 MHz carbon-13 NMR spectrum of rhodium(I) 21-methylcarbaporphyrin **94** in $CDCl_3$.

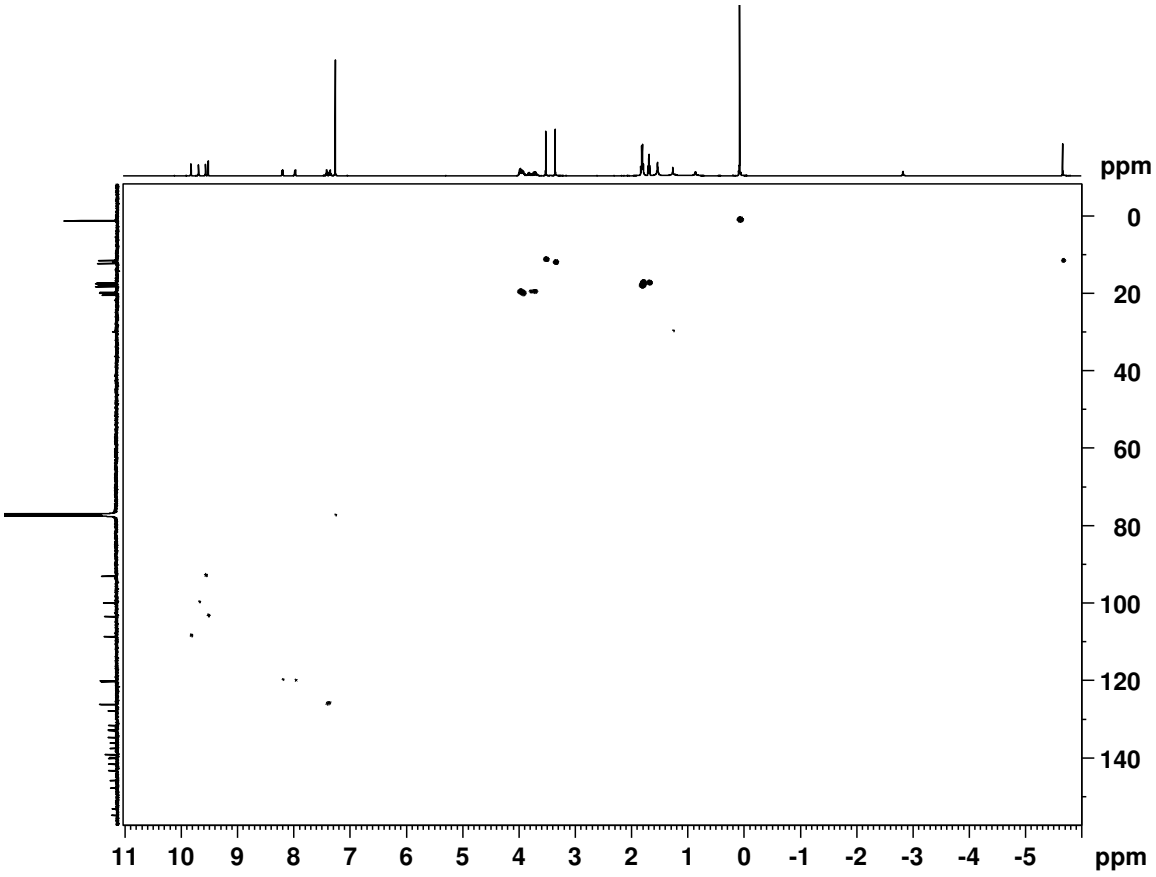

Figure C-44. HSQC NMR spectrum of rhodium(I) 21-methylcarbaporphyrin **94** in $CDCl_3$.

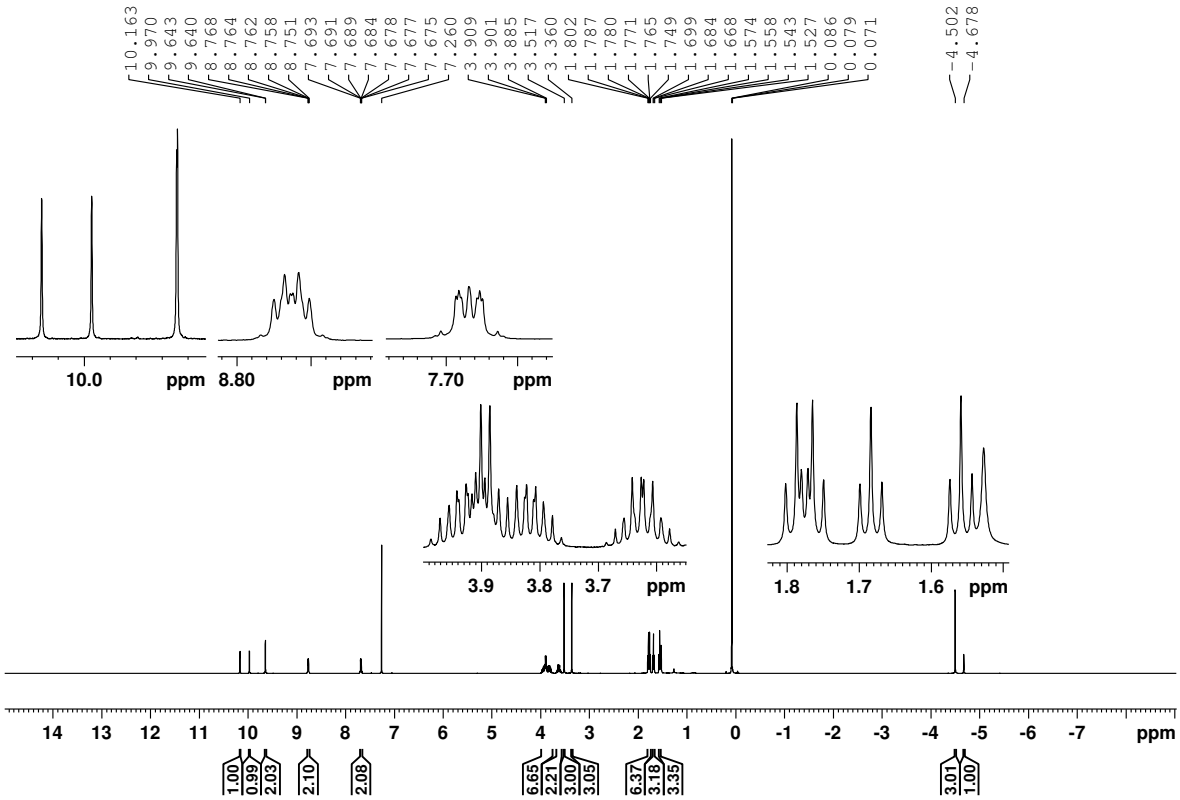

Figure C-45. 500 MHz ^{1}H NMR spectrum of rhodium(I) 22-methylcarbaporphyrin **93** in $CDCl_3$.

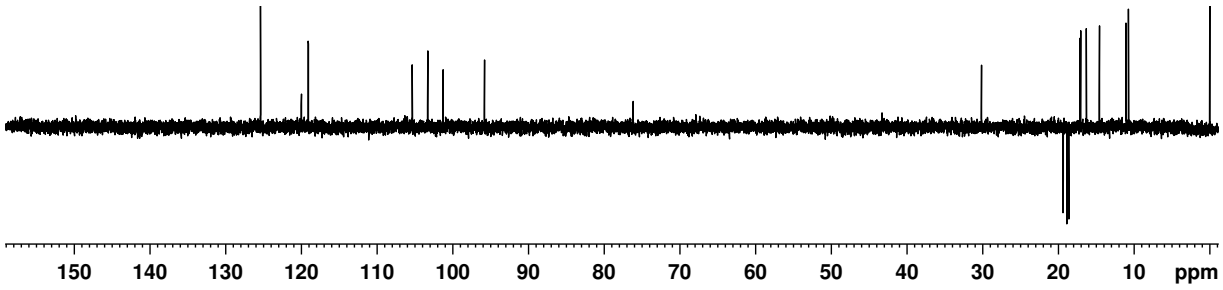

Figure C-46. DEPT-135 NMR spectrum of rhodium(I) 22-methylcarbaporphyrin **93** in $CDCl_3$.

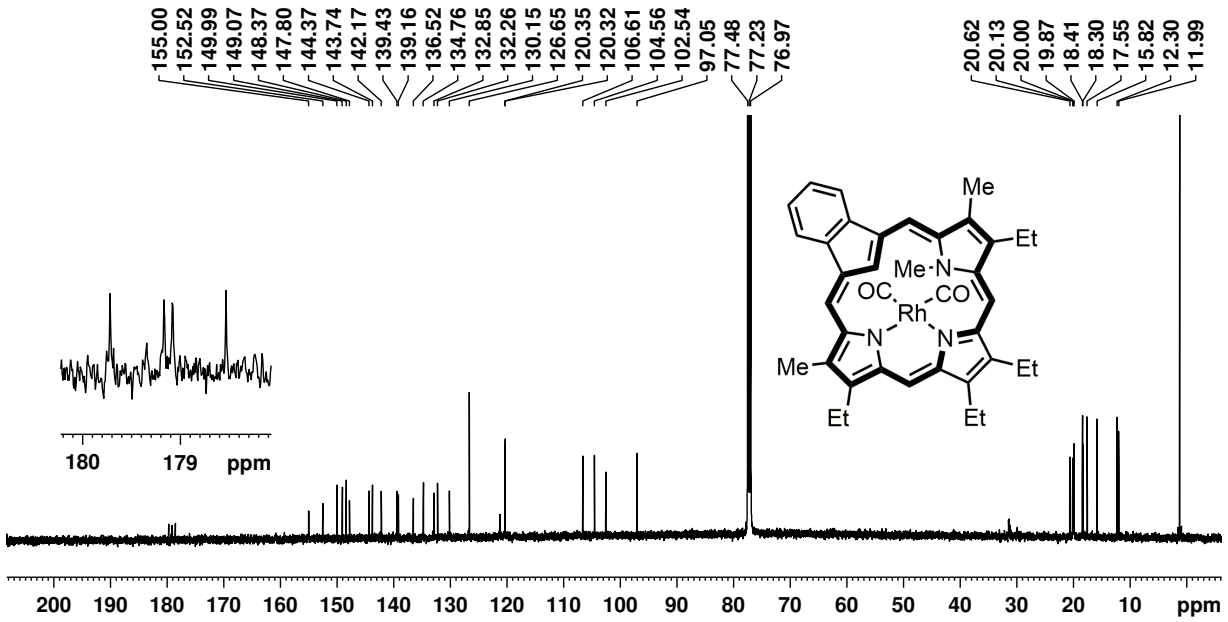

Figure C-47. 125 MHz ^{13}C NMR spectrum of rhodium(I) 22-methylcarbaporphyrin **93** in $CDCl_3$.

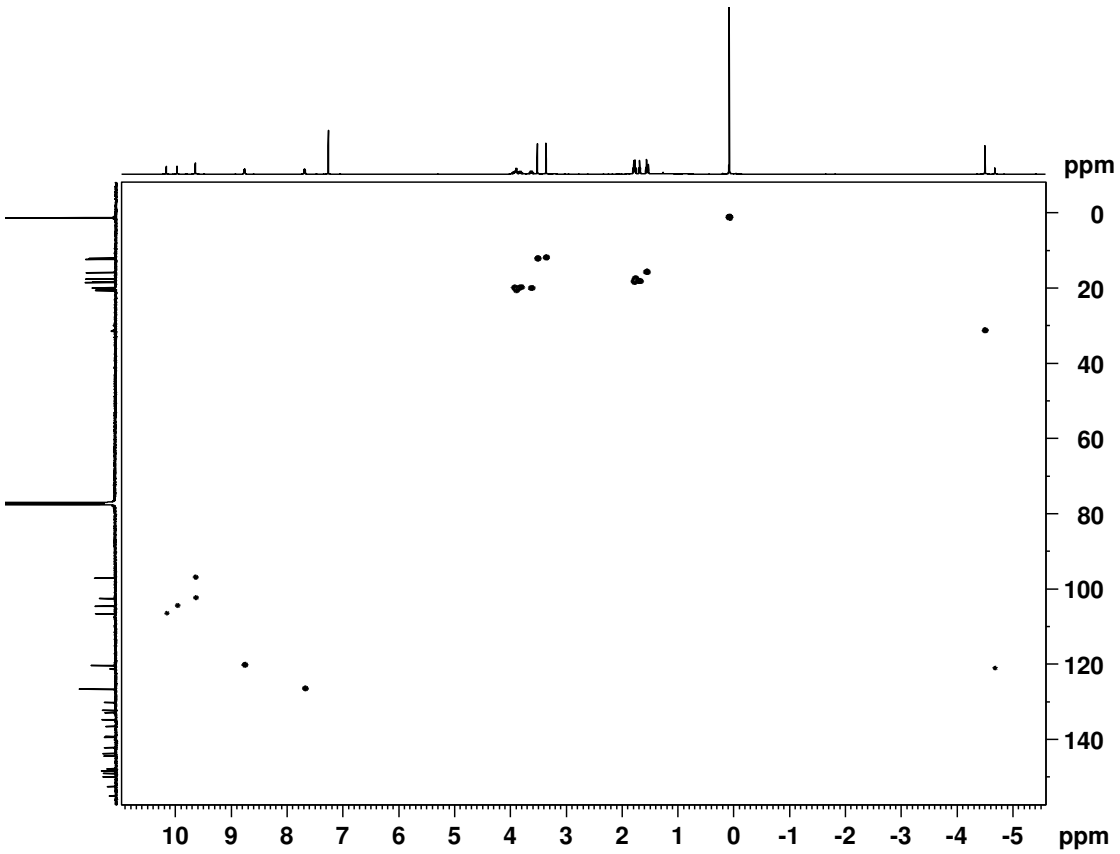

Figure C-48. HSQC NMR spectrum of rhodium(I) 22-methylcarbaporphyrin **93** in $CDCl_3$.

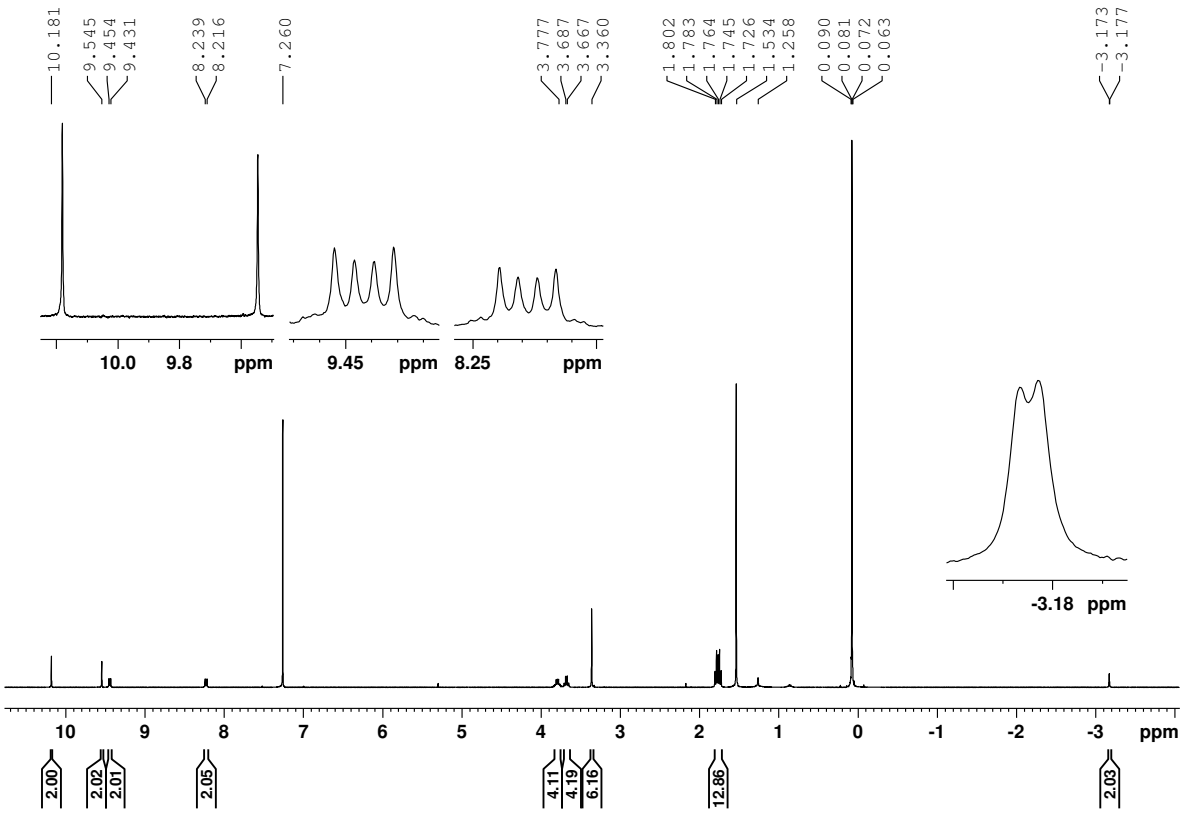

Figure C-49. 400 MHz ^{1}H NMR spectrum of rhodium(III) methylene-bridged complex **95** in $CDCl_3$.

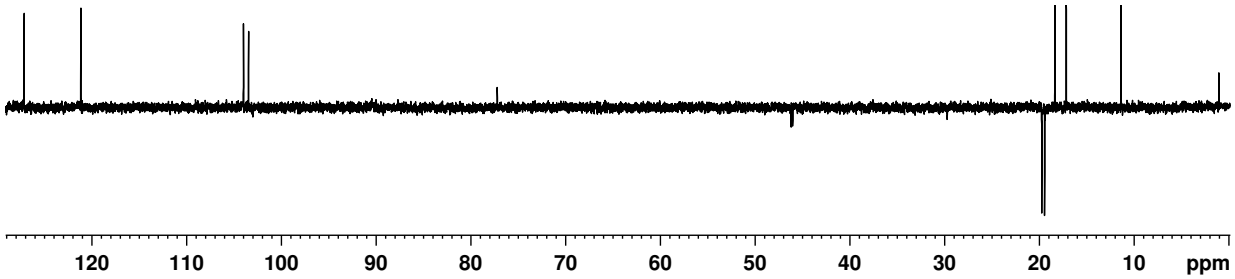

Figure C-50. DEPT-135 NMR spectrum of rhodium(III) methylene-bridged complex **95** in $CDCl_3$.

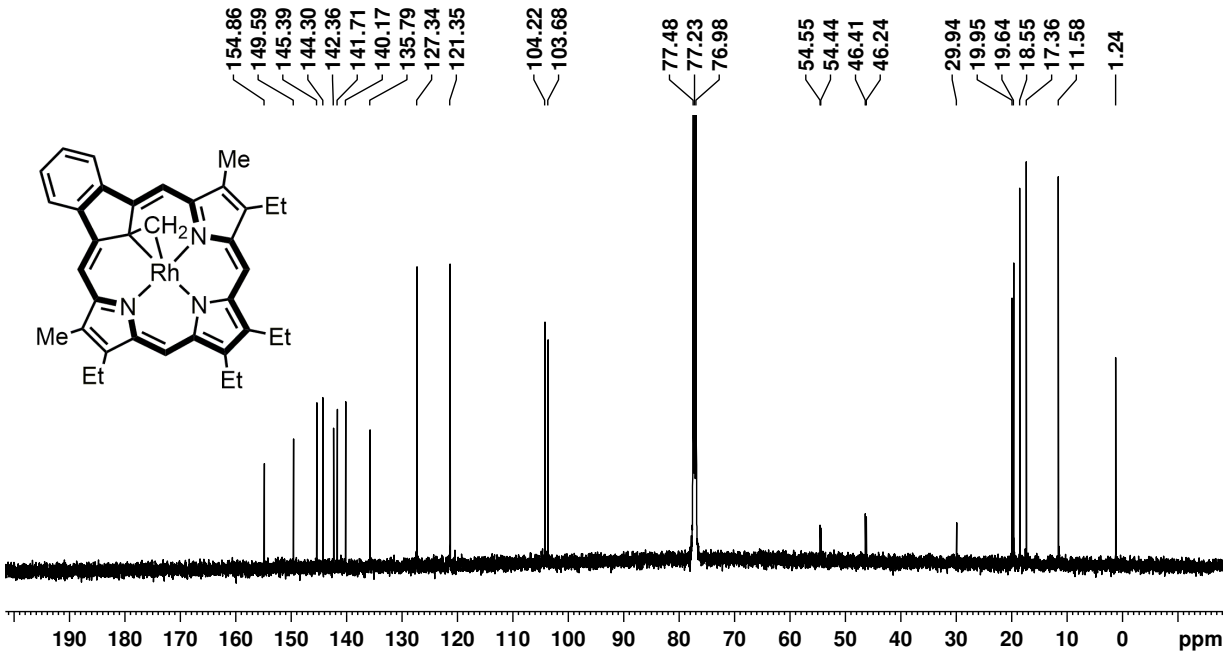

Figure C-51. 125 MHz ^{13}C NMR spectrum of rhodium(III) methylene-bridged complex **95** in $CDCl_3$.

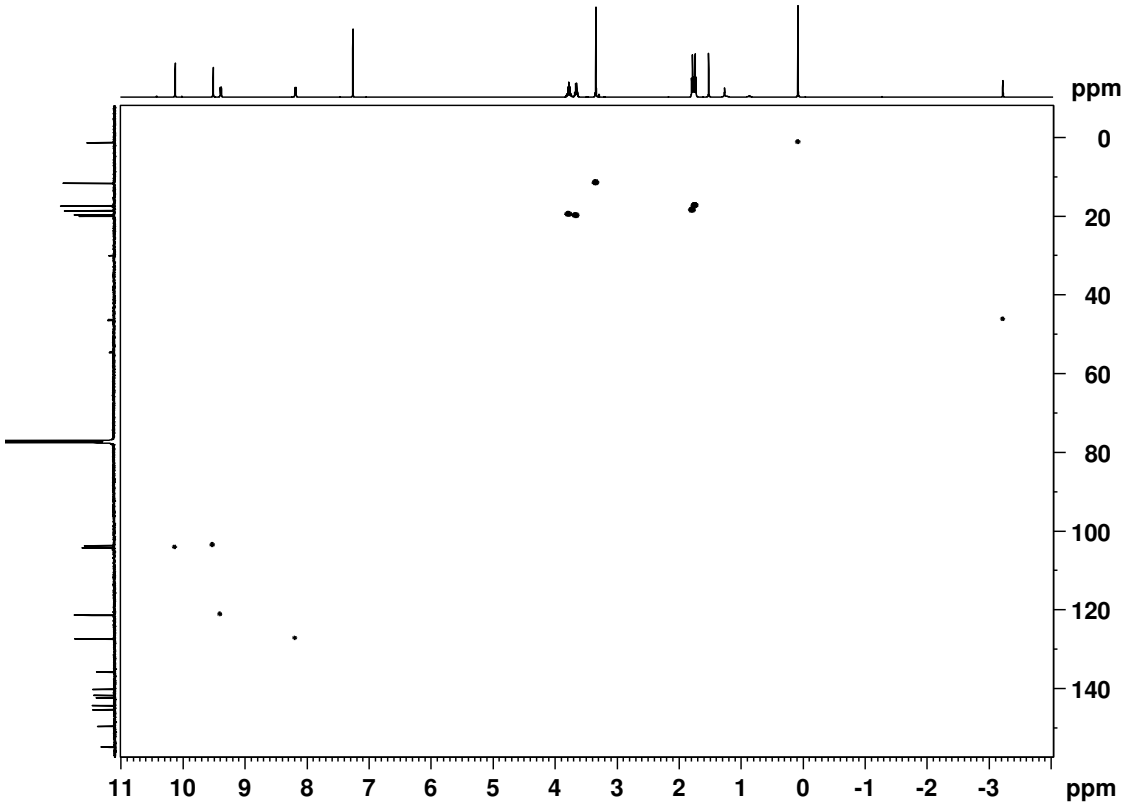

Figure C-52. HSQC NMR spectrum of rhodium(III) methylene-bridged complex **95** in $CDCl_3$.

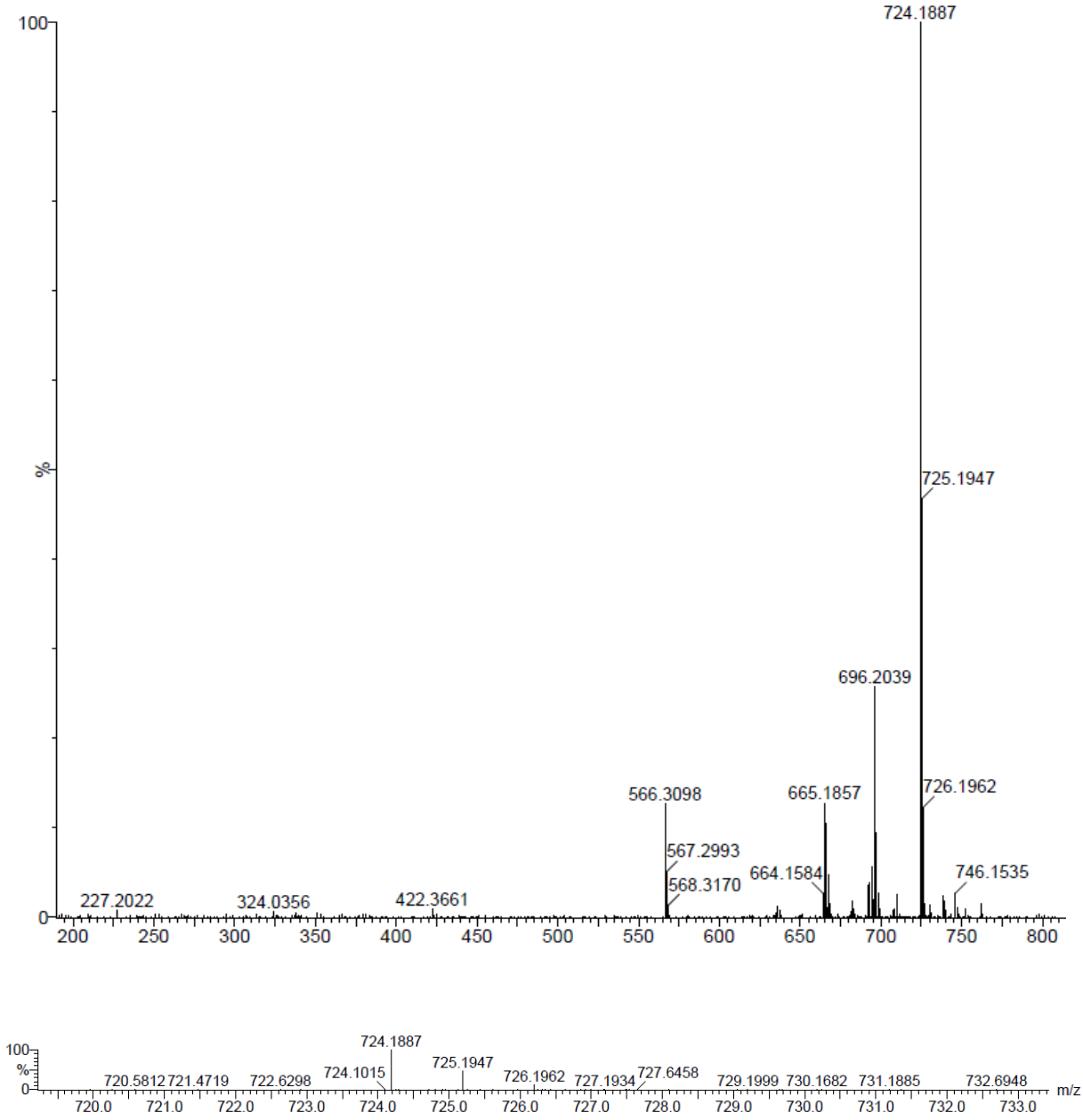

Figure C-53. ESI MS of rhodium(I) carbaporphyrin **89**.

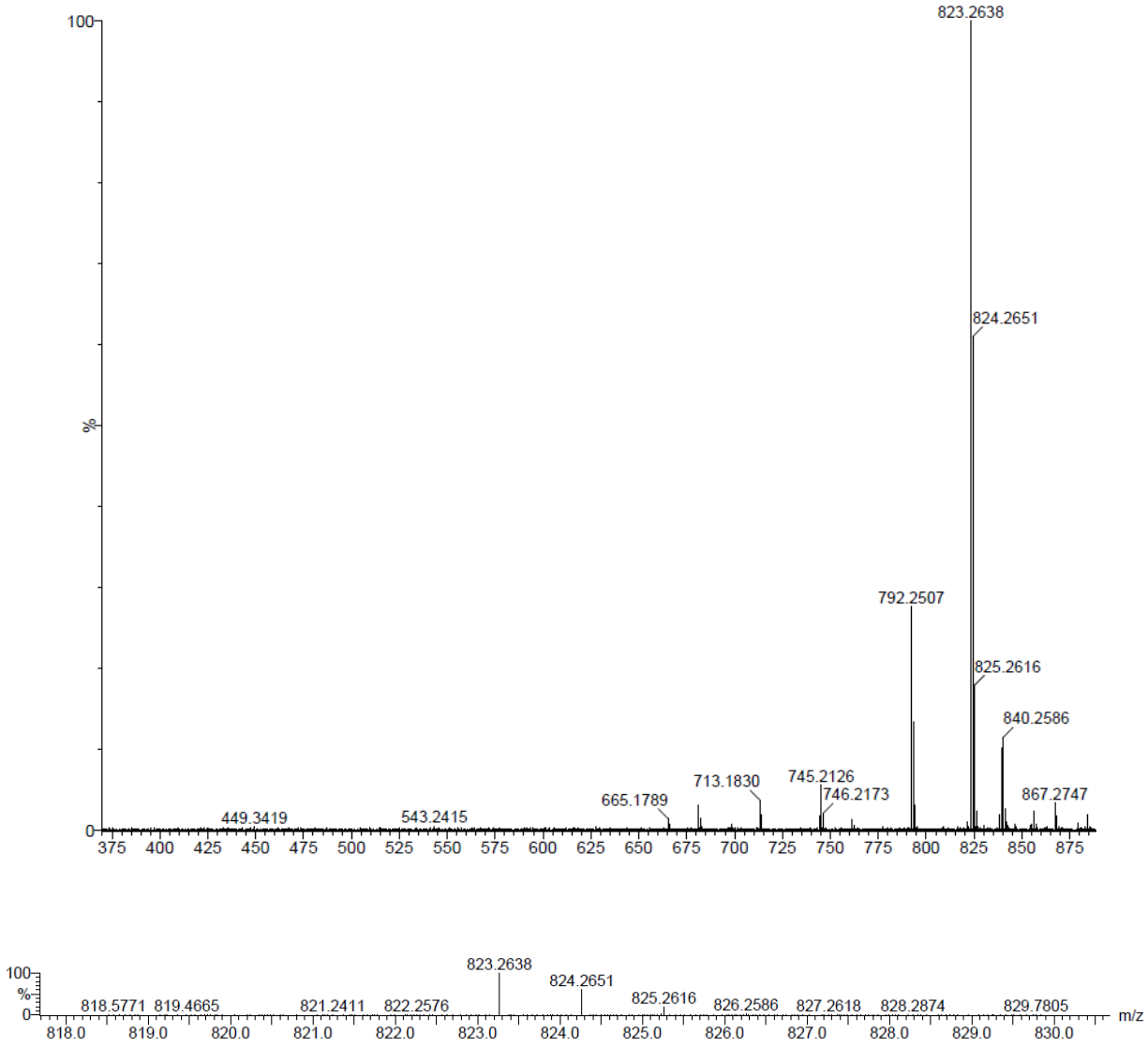

Figure C-54. ESI MS of rhodium(I) carbaporphyrin **91**.

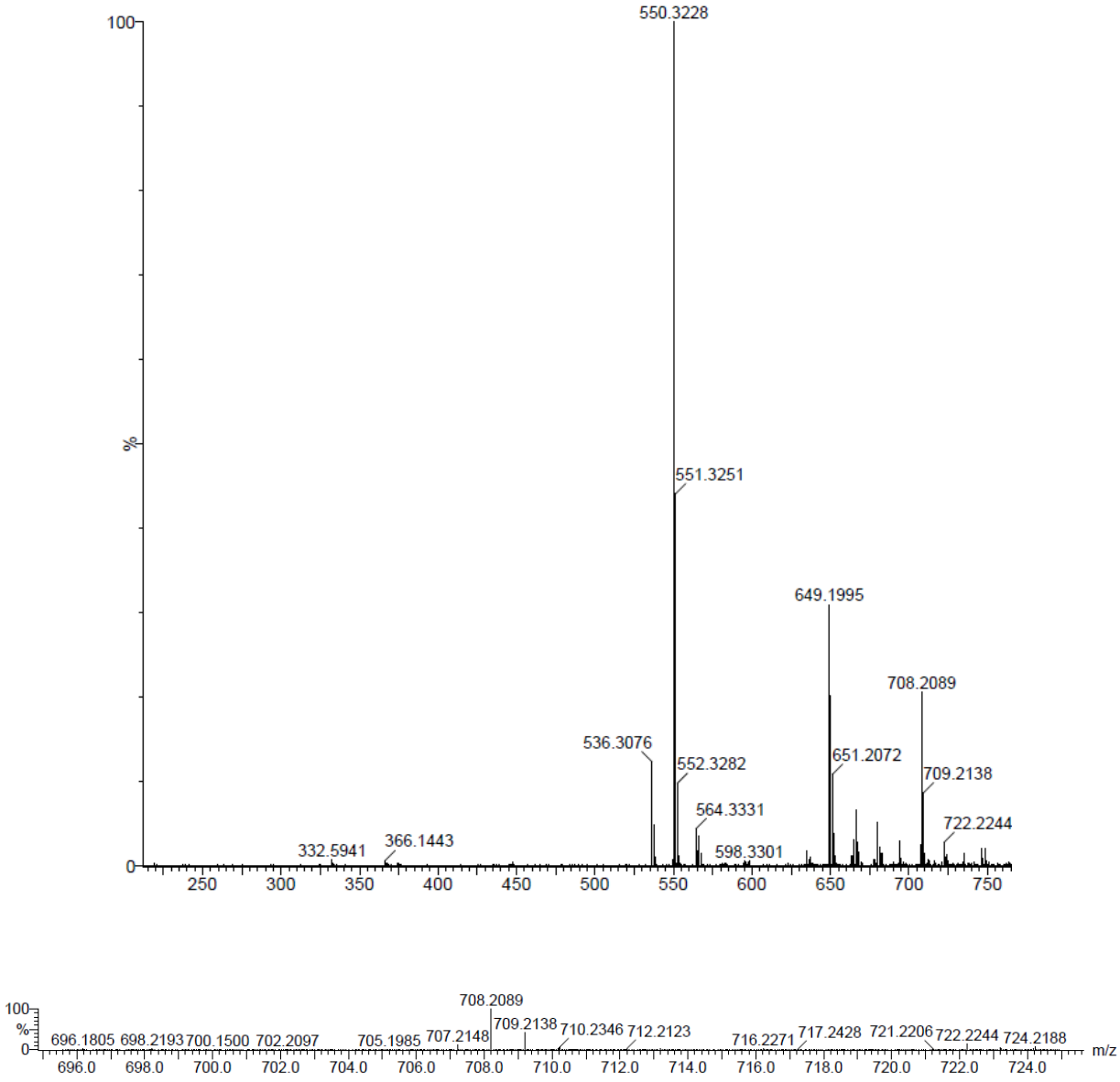

Figure C-55. ESI MS of rhodium(III) carbaporphyrin diester **91**.

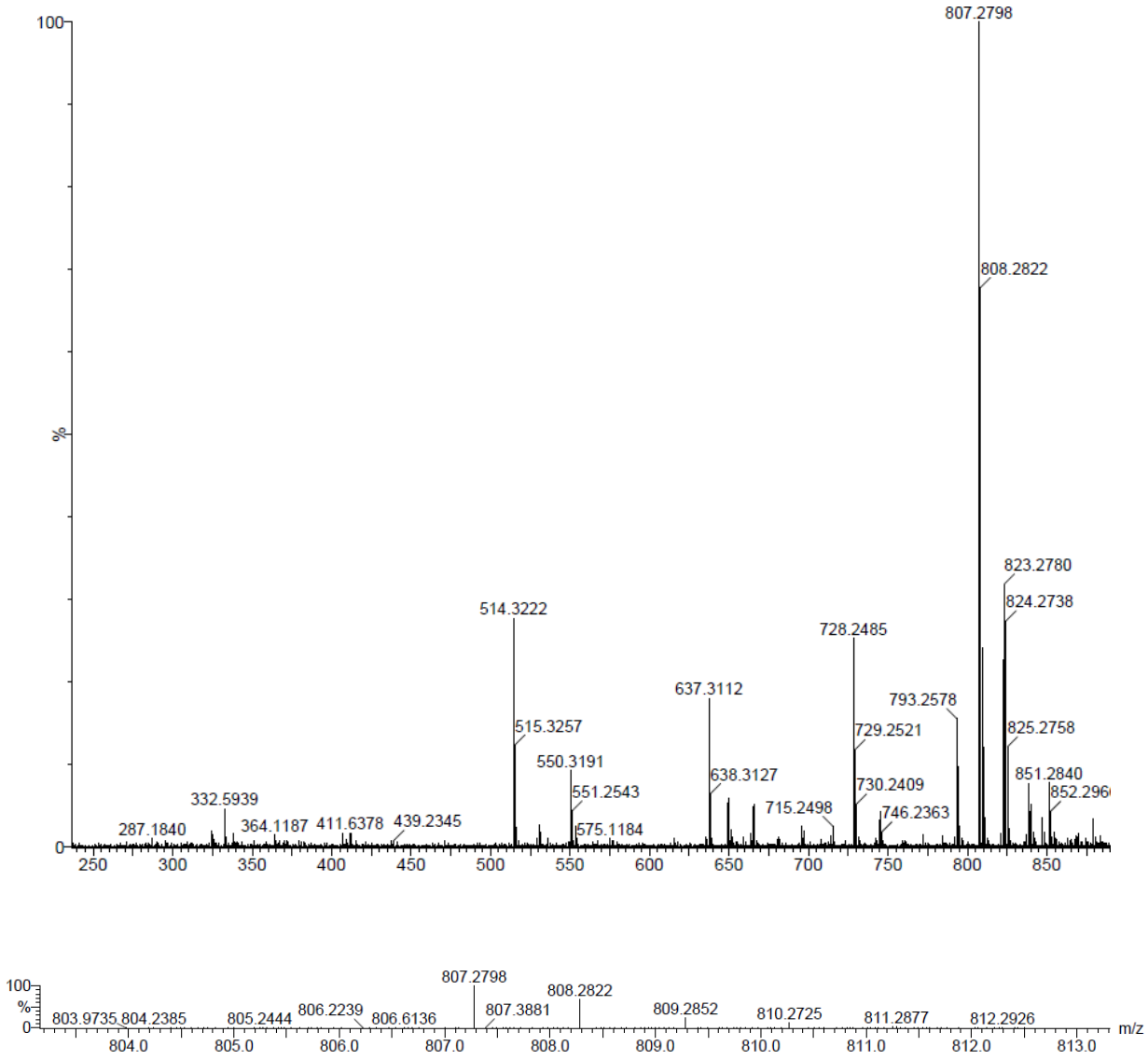

Figure C-56. ESI MS of rhodium(III) naphthocarbaporphyrin **92**.

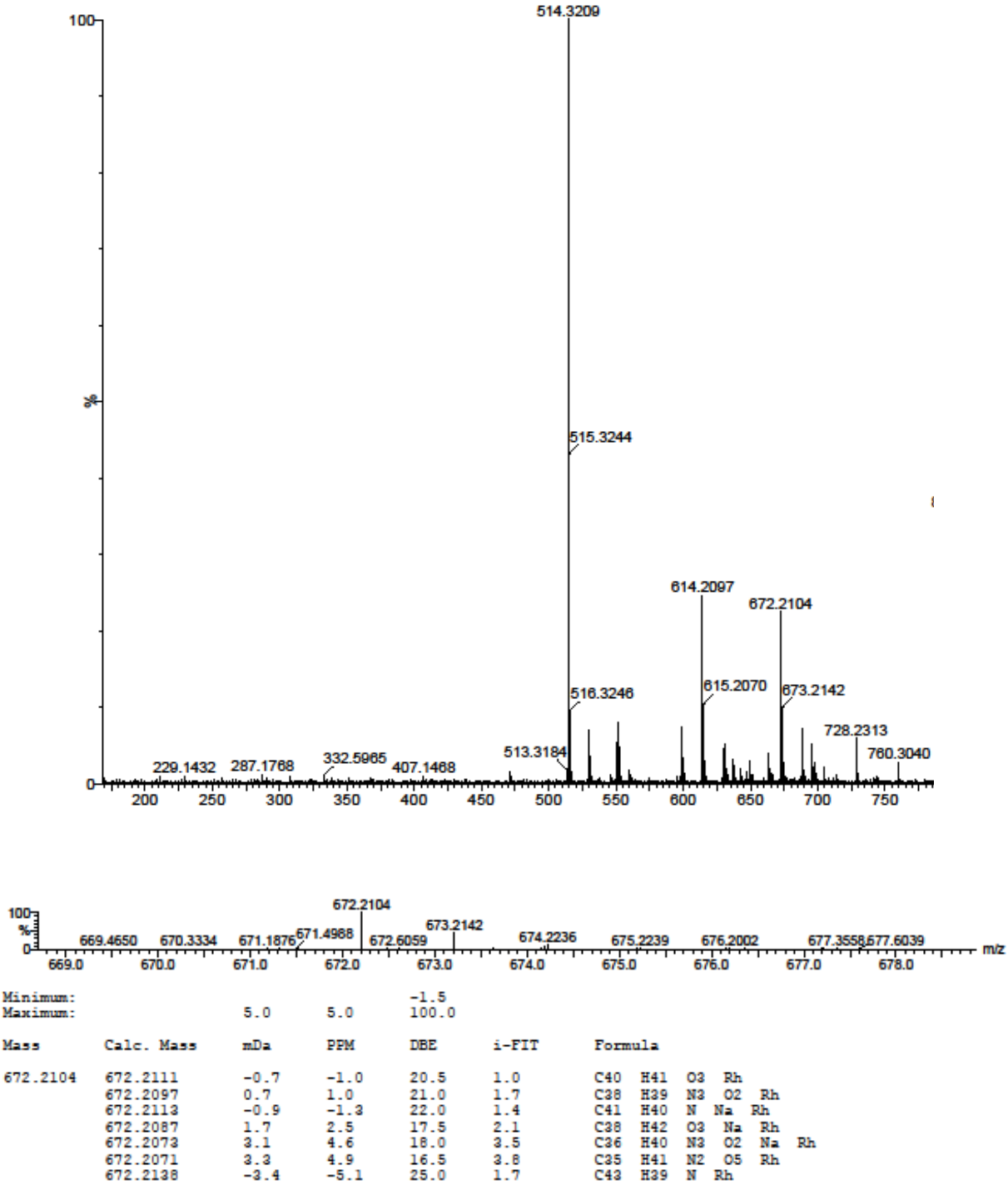

Minimum:				-1.5		
Maximum:		5.0	5.0	100.0		
Mass	**Calc. Mass**	**mDa**	**PPM**	**DBE**	**i-FIT**	**Formula**
672.2104	672.2111	-0.7	-1.0	20.5	1.0	C40 H41 O3 Rh
	672.2097	0.7	1.0	21.0	1.7	C38 H39 N3 O2 Rh
	672.2113	-0.9	-1.3	22.0	1.4	C41 H40 N Na Rh
	672.2087	1.7	2.5	17.5	2.1	C38 H42 O3 Na Rh
	672.2073	3.1	4.6	18.0	3.5	C36 H40 N3 O2 Na Rh
	672.2071	3.3	4.9	16.5	3.8	C35 H41 N2 O5 Rh
	672.2138	-3.4	-5.1	25.0	1.7	C43 H39 N Rh

Figure C-57. ESI MS of rhodium(I) complex **94**.

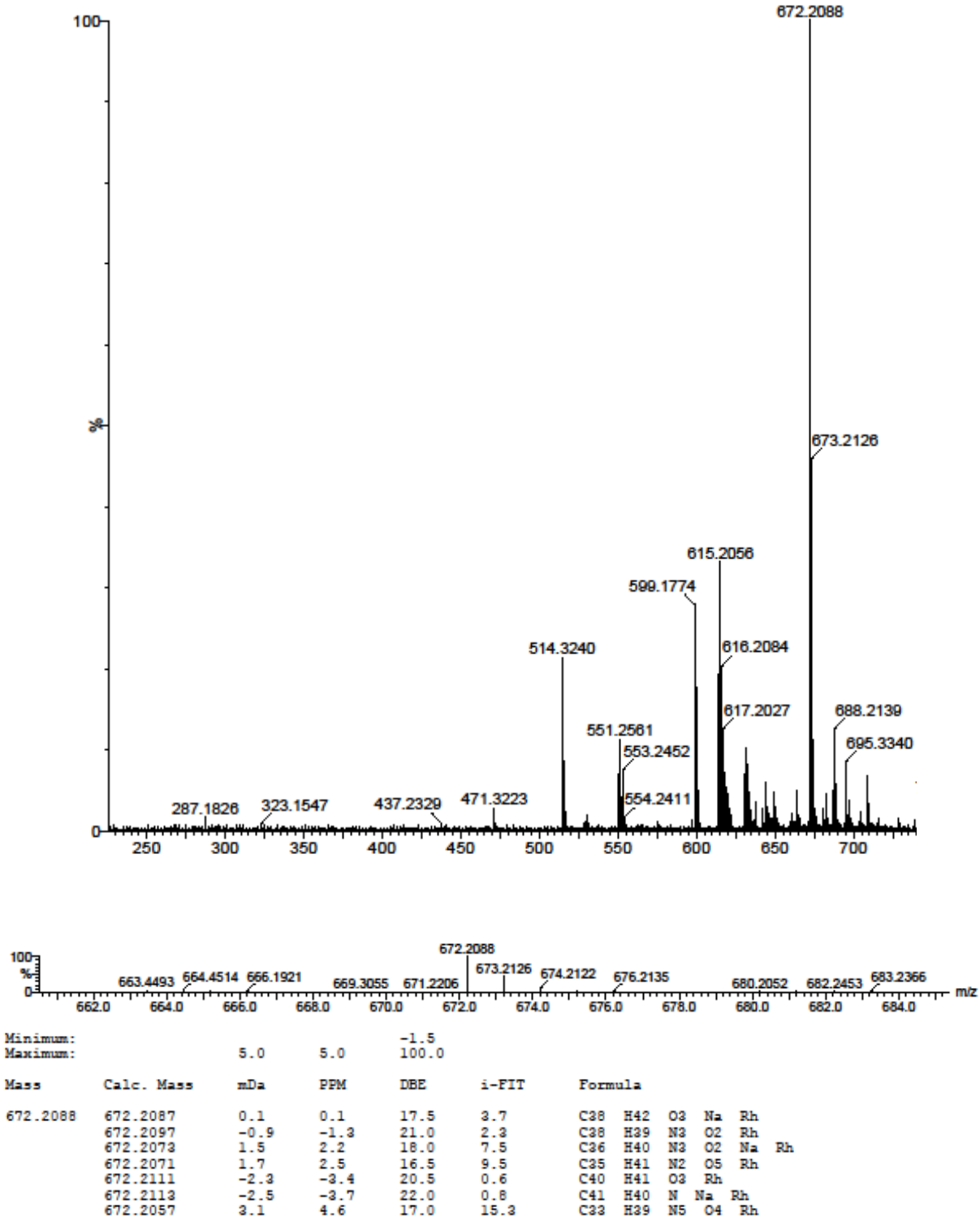

Minimum:				-1.5		
Maximum:		5.0	5.0	100.0		
Mass	**Calc. Mass**	**mDa**	**PPM**	**DBE**	**i-FIT**	**Formula**
672.2088	672.2087	0.1	0.1	17.5	3.7	C38 H42 O3 Na Rh
	672.2097	-0.9	-1.3	21.0	2.3	C38 H39 N3 O2 Rh
	672.2073	1.5	2.2	18.0	7.5	C36 H40 N3 O2 Na Rh
	672.2071	1.7	2.5	16.5	9.5	C35 H41 N2 O5 Rh
	672.2111	-2.3	-3.4	20.5	0.6	C40 H41 O3 Rh
	672.2113	-2.5	-3.7	22.0	0.8	C41 H40 N Na Rh
	672.2057	3.1	4.6	17.0	15.3	C33 H39 N5 O4 Rh

Figure C-58. ESI MS of rhodium(I) complex **93**.

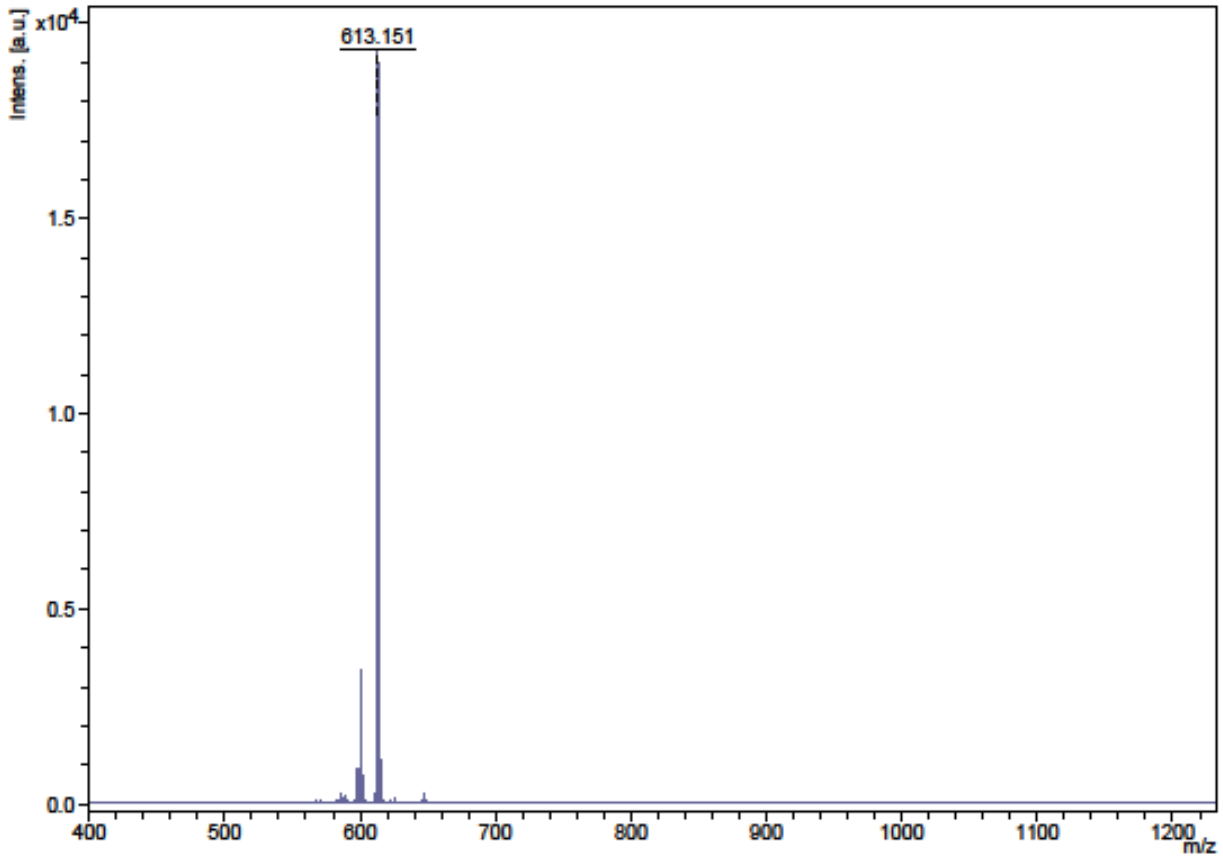

Figure C-59. Electron impact mass spectrum of rhodium(III) complex **95**.

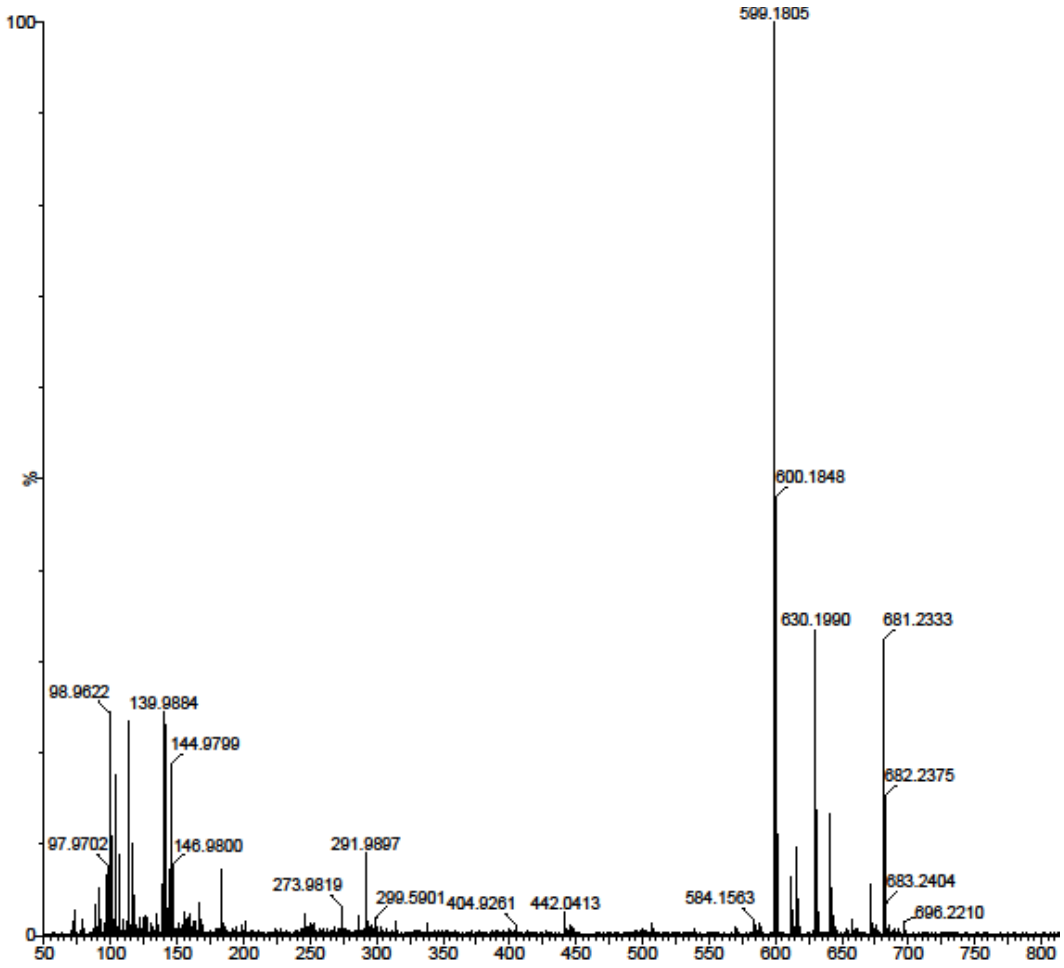

Mass	Calc. Mass	mDa	PPM	DBE	i-FIT	Norm	Conf(%)	Formula
599.1805	599.1808	-0.3	-0.5	20.5	1978.1	5.163	0.57	C35 H34 N3 Rh
	599.1800	0.5	0.8	37.5	1972.9	0.006	99.43	C48 H23

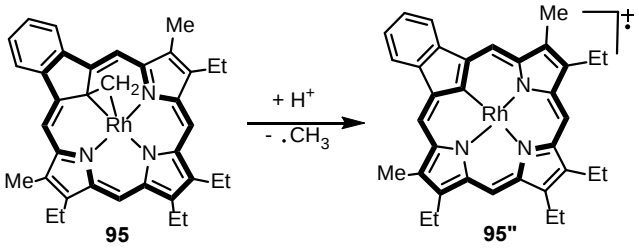

Figure C-60. Electrospray ionization mass spectrum of rhodium(III) complex **95** showing that complete degradation had occurred. The molecular ion corresponds to rhodium complex **95"**.

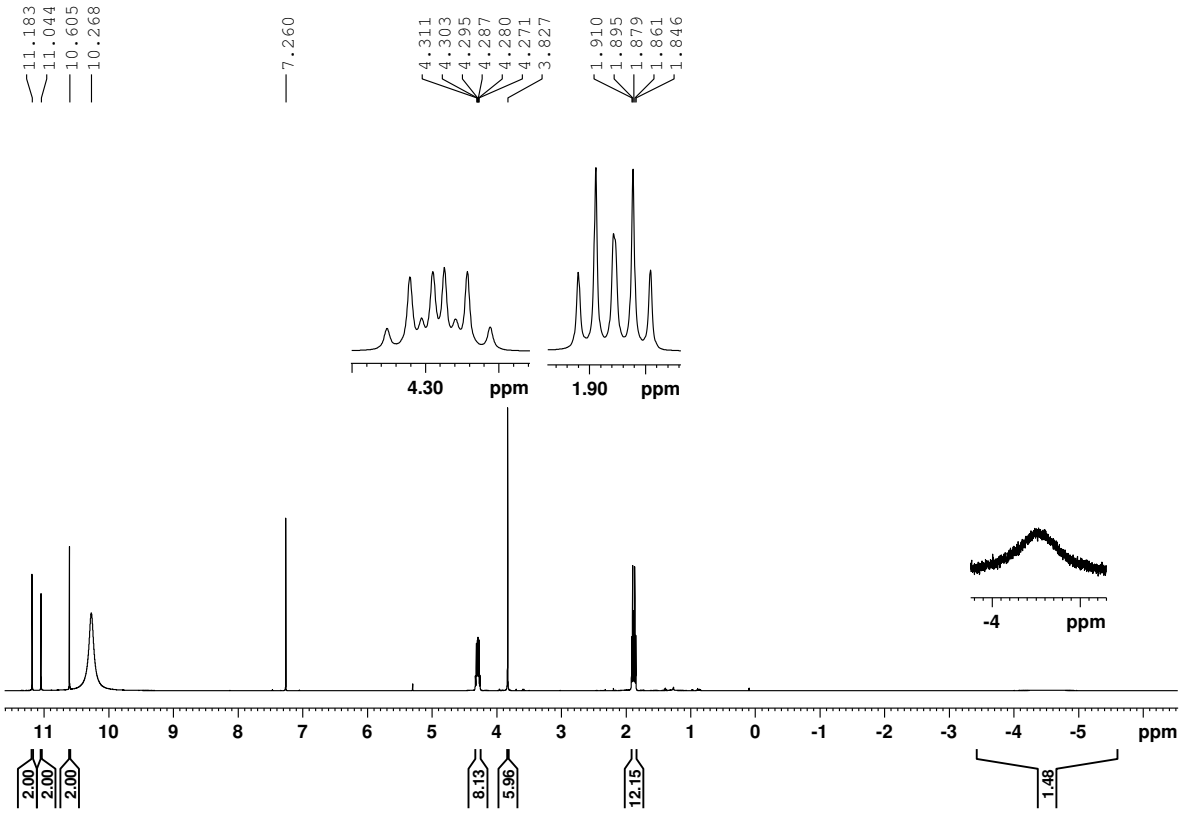

Figure D-1. 500 MHz ^{1}H NMR spectrum of 21-oxaporphyrin **96a**H_2^{2+} in TFA-$CDCl_3$

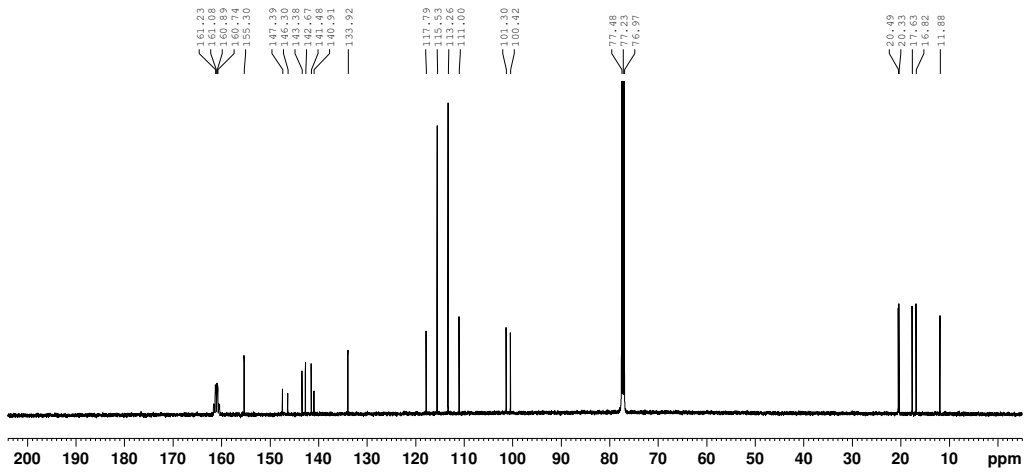

Figure D-2. 125 MHz ^{13}C NMR spectrum of 21-oxaporphyrin **96a**H_2^{2+} in TFA-$CDCl_3$

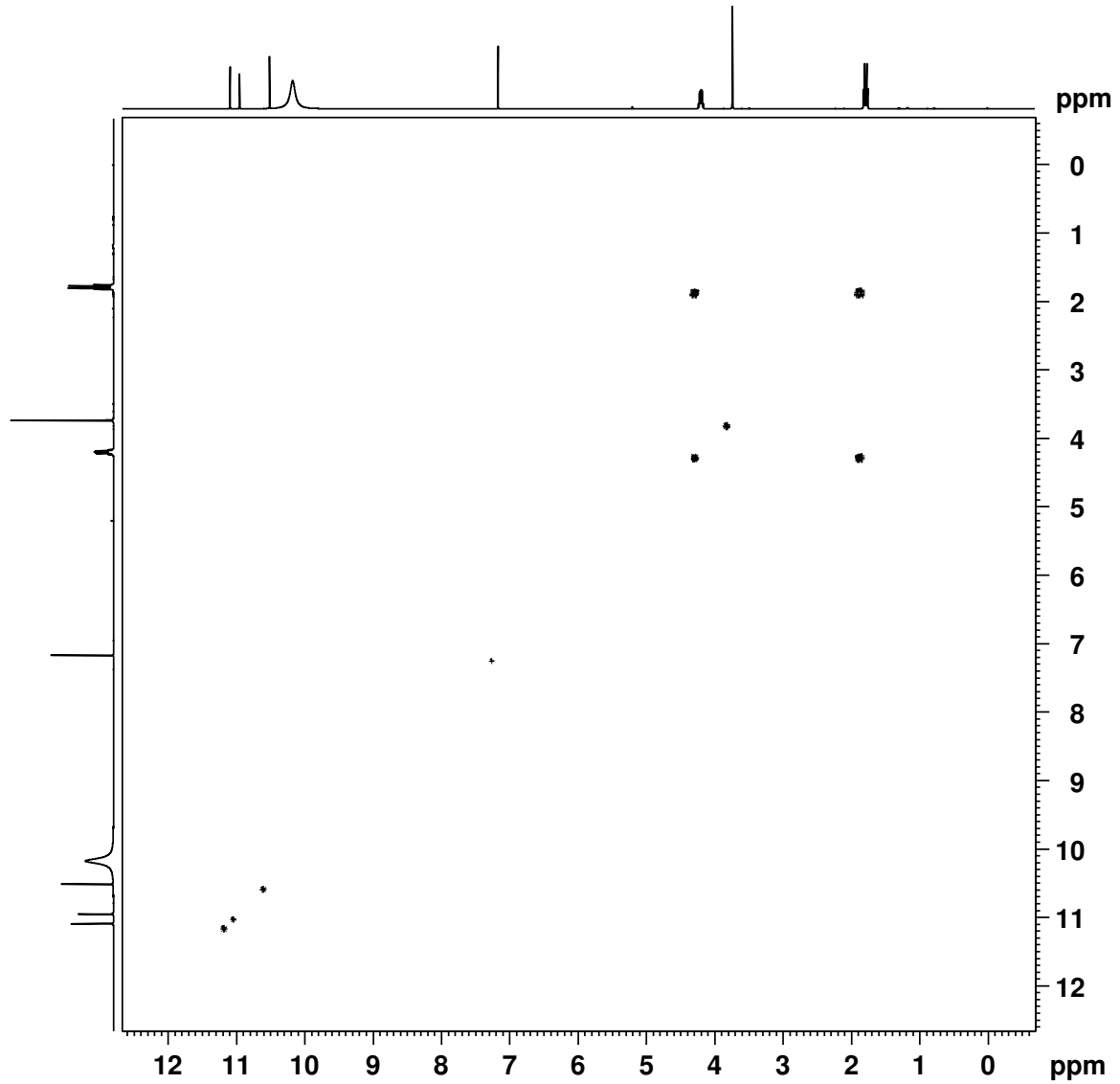

Figure D-3. ^{1}H-^{1}H COSY NMR spectrum of 21-oxaporphyrin **96a**H_2^{2+} in TFA-$CDCl_3$

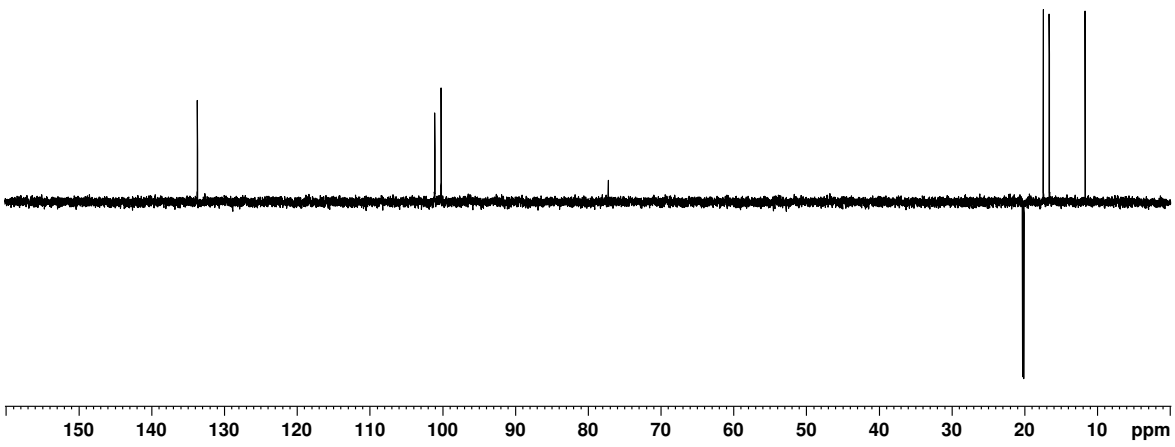

Figure D-4. DEPT-135 NMR spectrum of 21-oxaporphyrin **96a**H_2^{2+} in TFA-$CDCl_3$

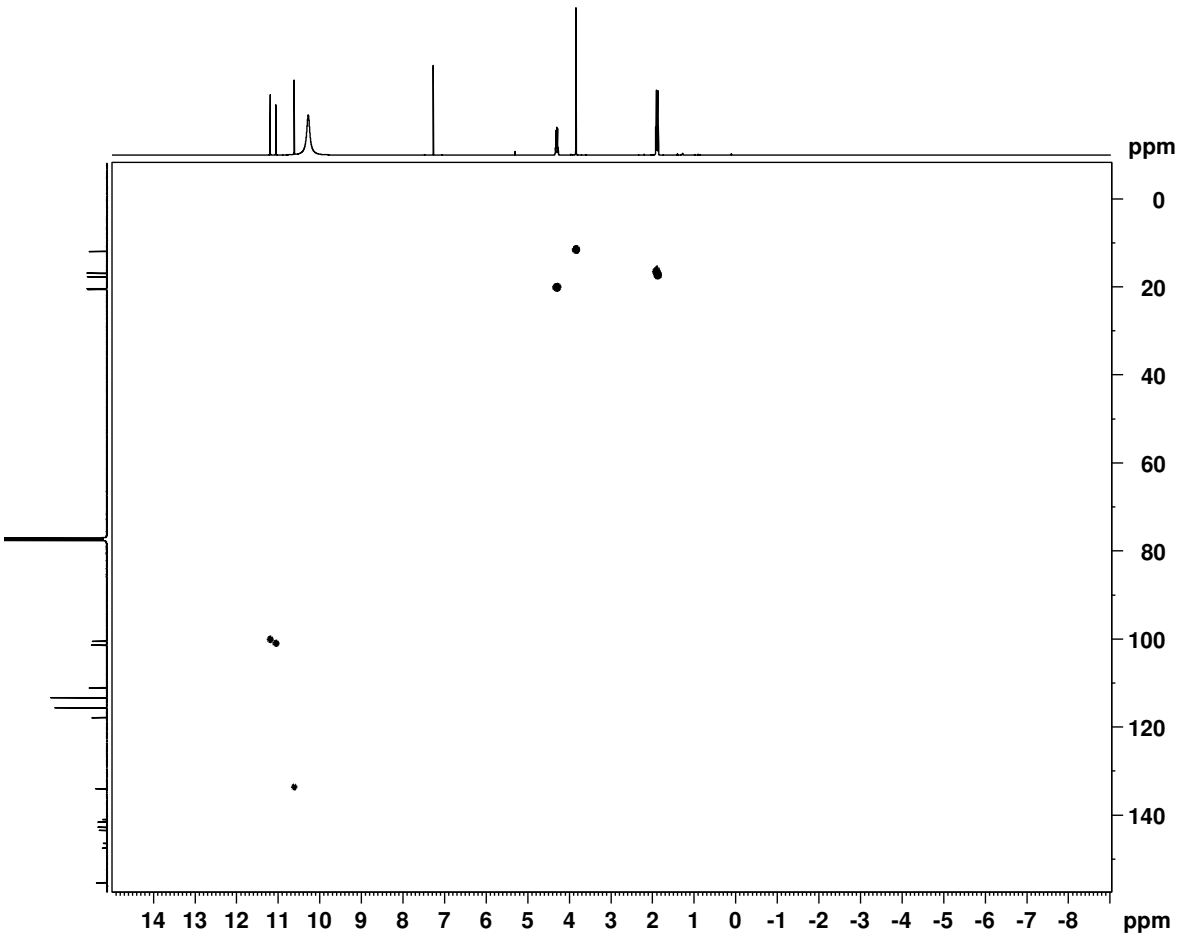

Figure D-5. HSQC NMR spectrum of 21-oxaporphyrin **96a**H_2^{2+} in TFA-$CDCl_3$

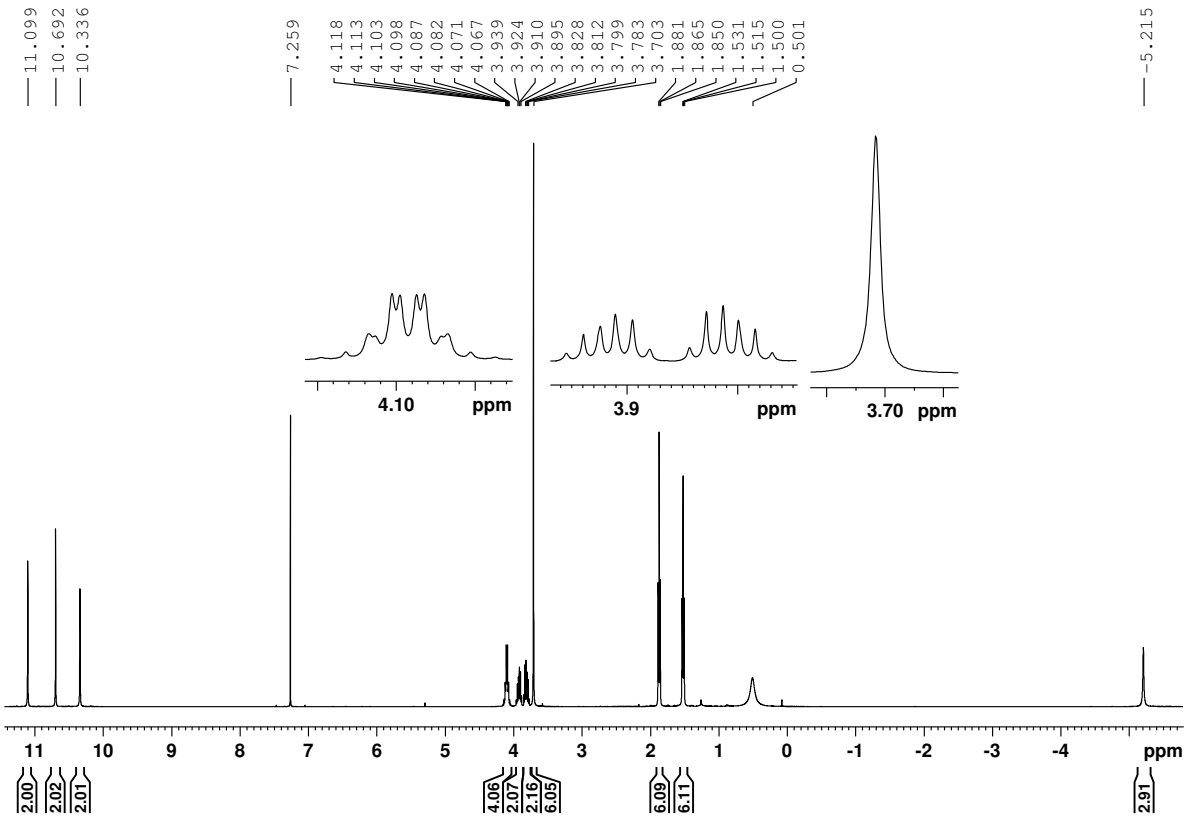

Figure D-6. 500 MHZ ^{1}H NMR spectrum of *N*-methyl oxaporphyrin **96b** in $CDCl_3$

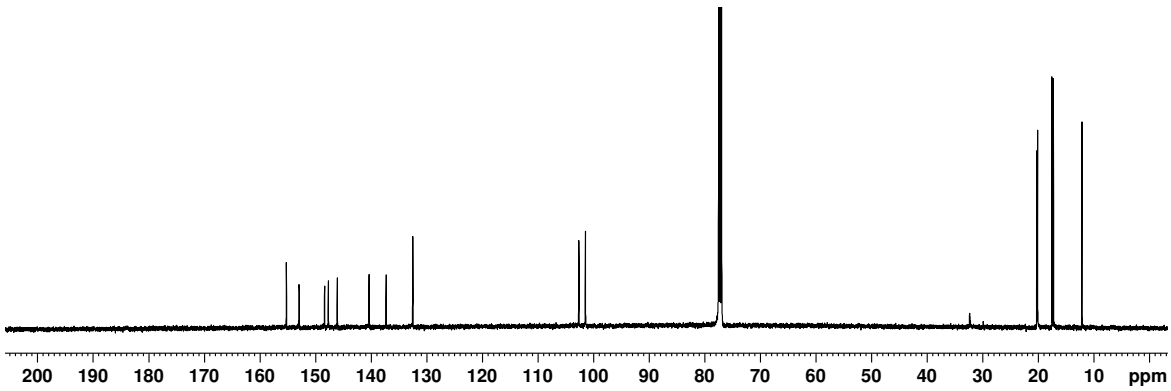

Figure D-7. 125 MHz ^{13}C NMR spectrumof *N*-methyl oxaporphyrin **96b** in $CDCl_3$

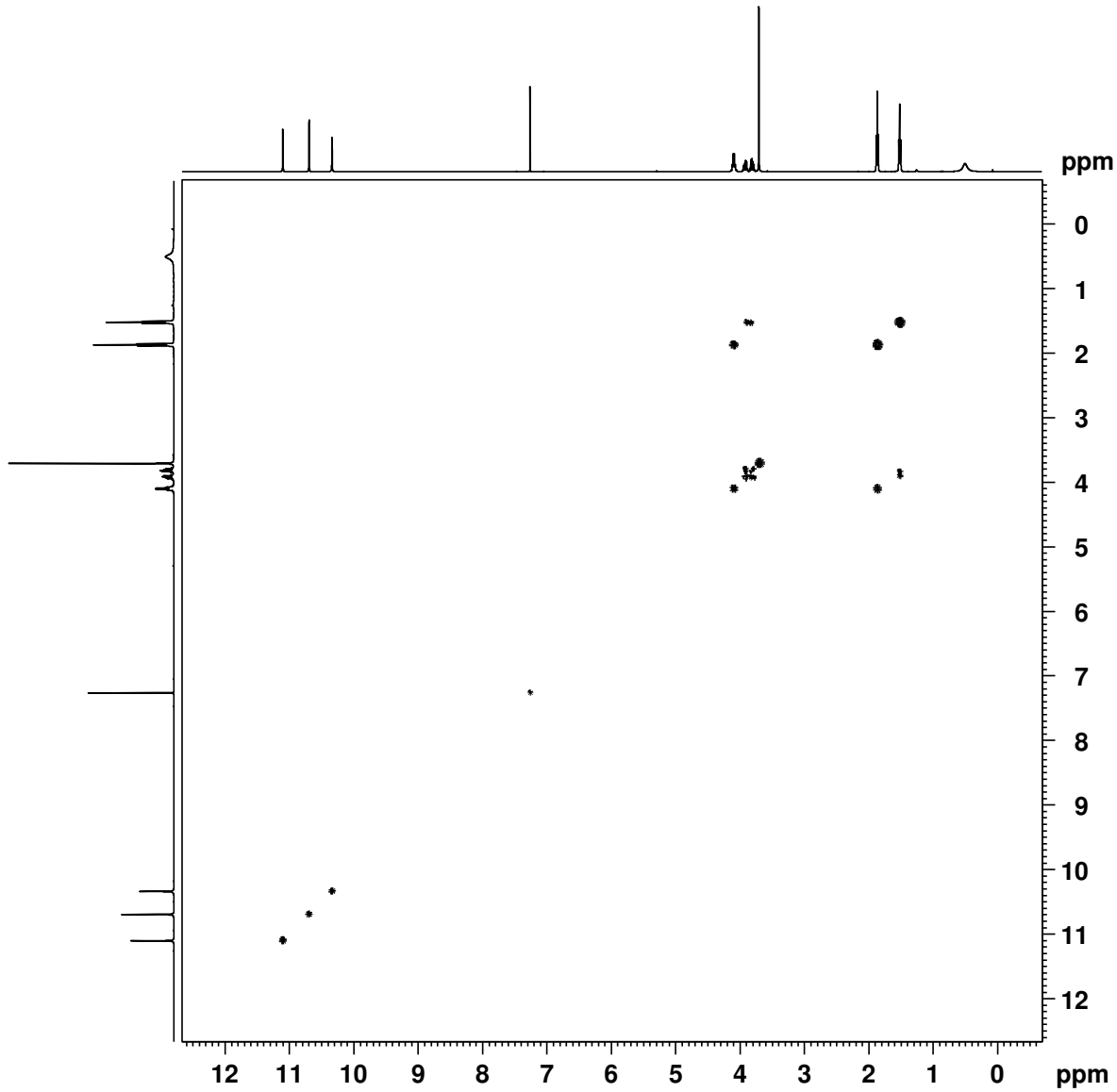

Figure D-8. ^{1}H-^{1}H COSY NMR spectrum of *N*-methyl oxaporphyrin **96b** in $CDCl_3$

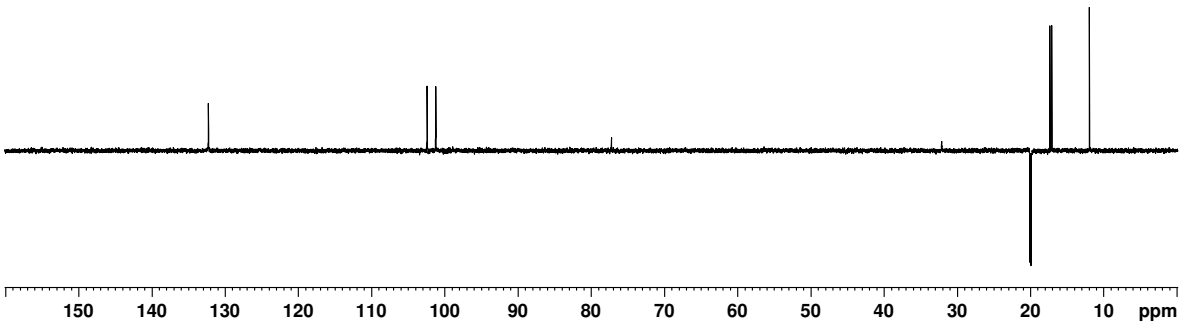

Figure D-9. DEPT-135 NMR spectrum of *N*-methyl oxaporphyrin **96b** in $CDCl_3$

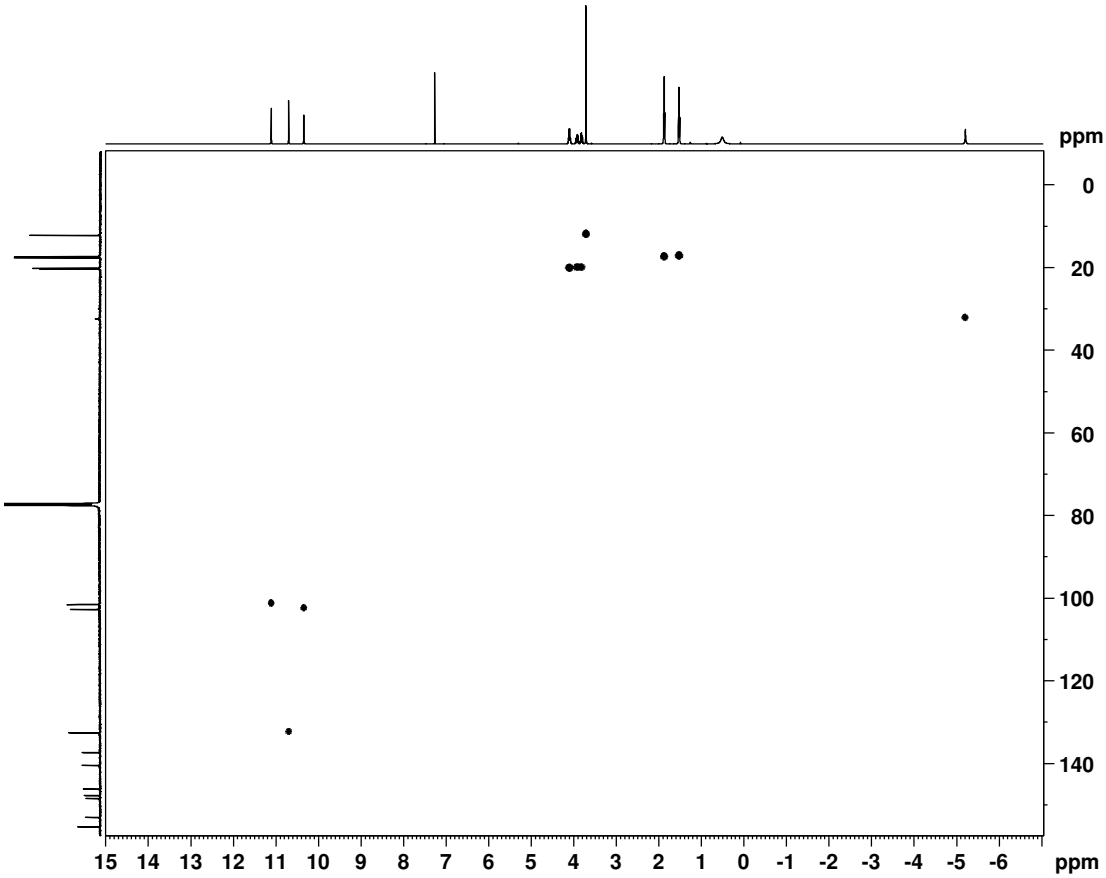

Figure D-10. HSQC NMR spectrum of *N*-methyl oxaporphyrin **96b** in $CDCl_3$

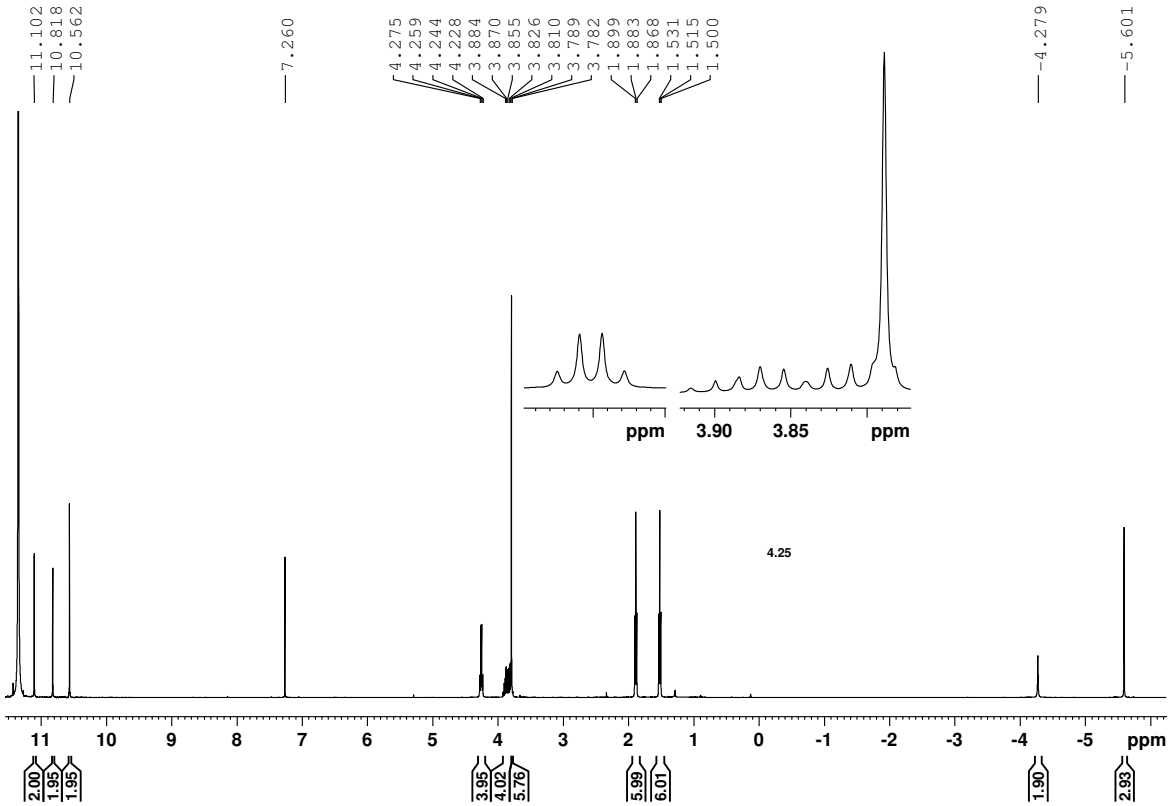

Figure D-11. 500 MHz ^{1}H NMR spectrum of *N*-methyl oxaporphyrin **96b** in TFA-$CDCl_3$

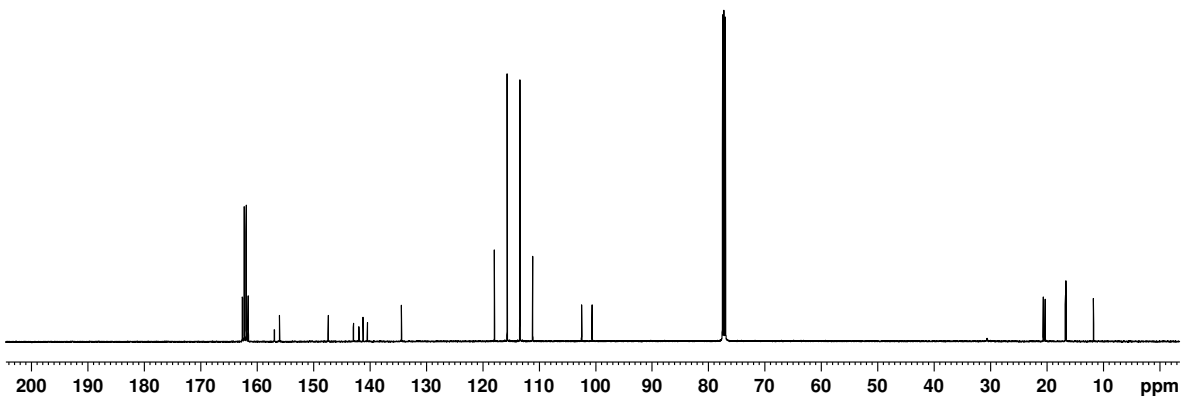

Figure D-12. 125 MHz ^{13}C NMR spectrum of *N*-methyl oxaporphyrin **96b** in TFA-$CDCl_3$

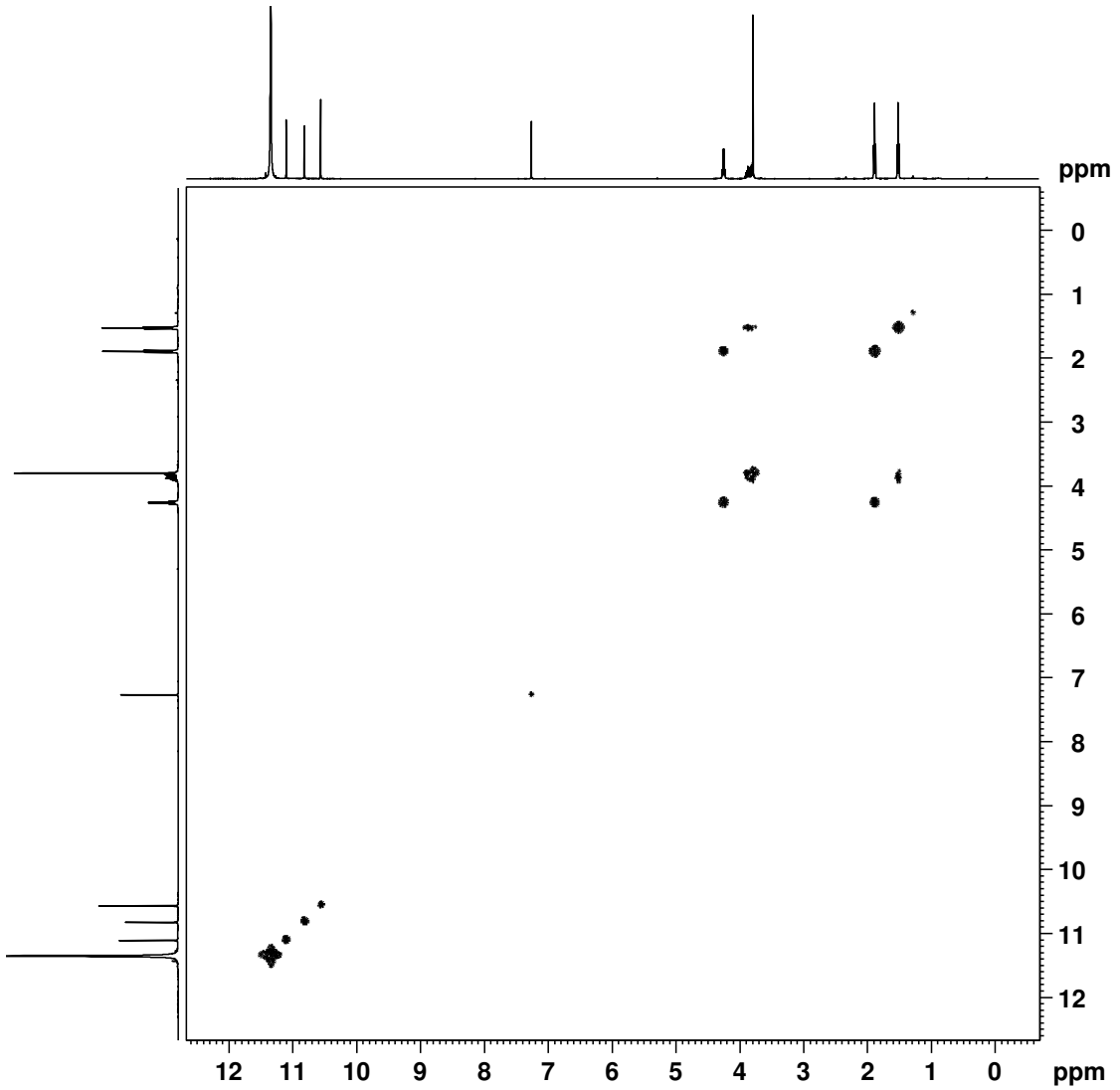

Figure D-13. ^{1}H-^{1}H COSY NMR spectrum of *N*-methyl oxaporphyrin **96b** in TFA-$CDCl_3$

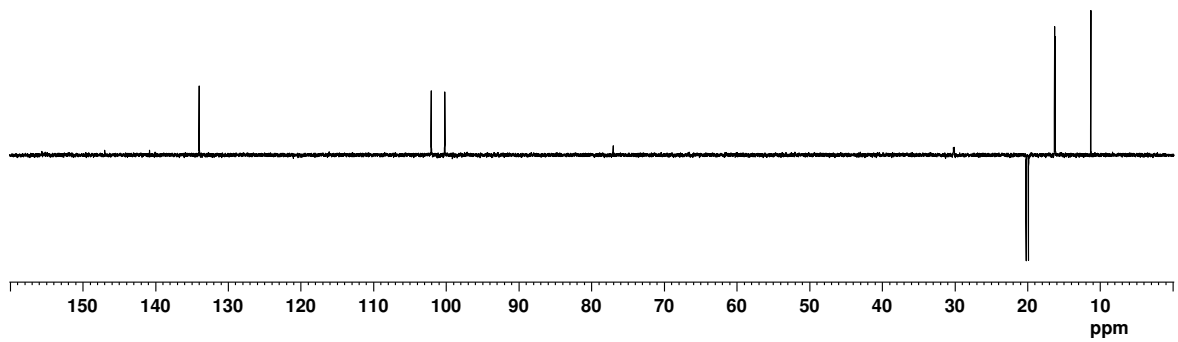

Figure D-14. DEPT-135 NMR spectrum of *N*-methyl oxaporphyrin **96b** in TFA-$CDCl_3$

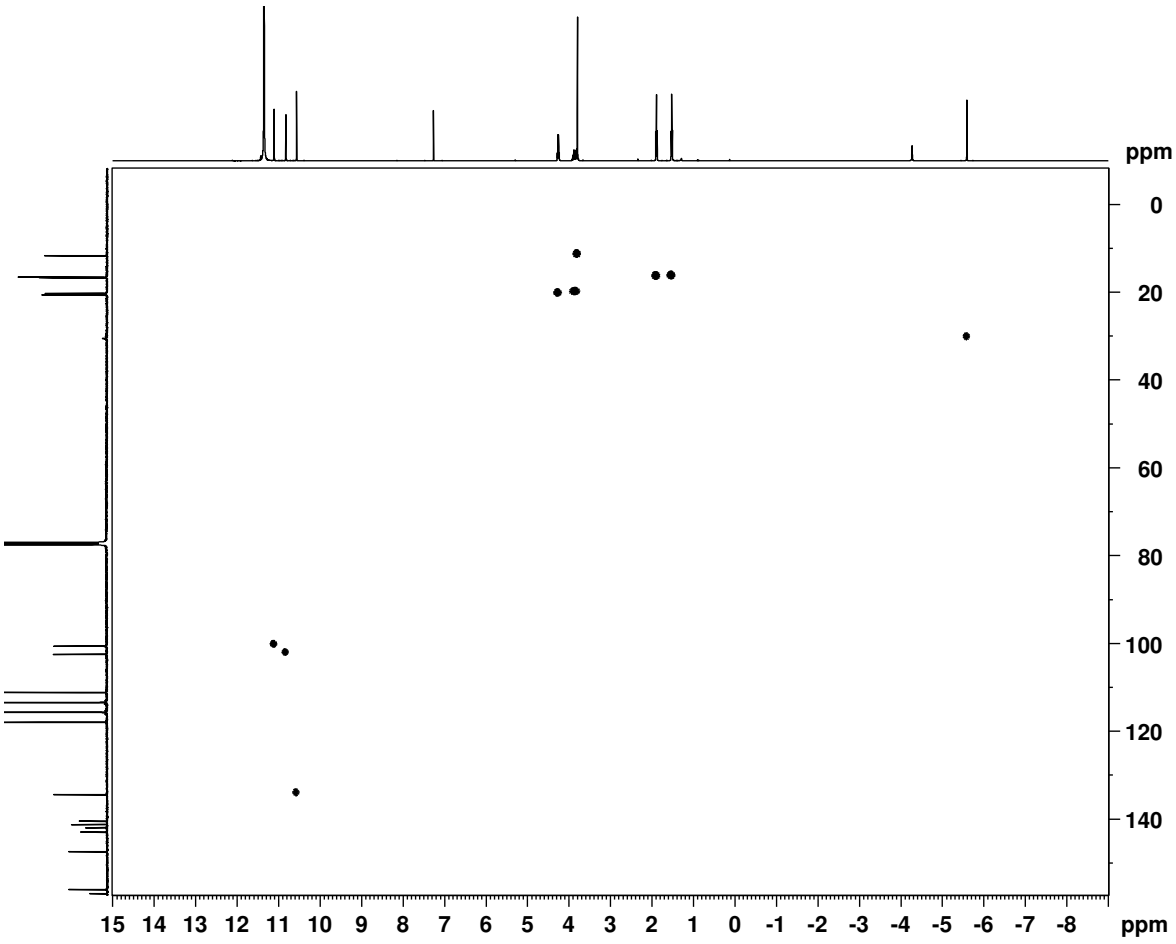

Figure D-15. HSQC NMR spectrum of *N*-methyl oxaporphyrin **96b** in TFA-$CDCl_3$

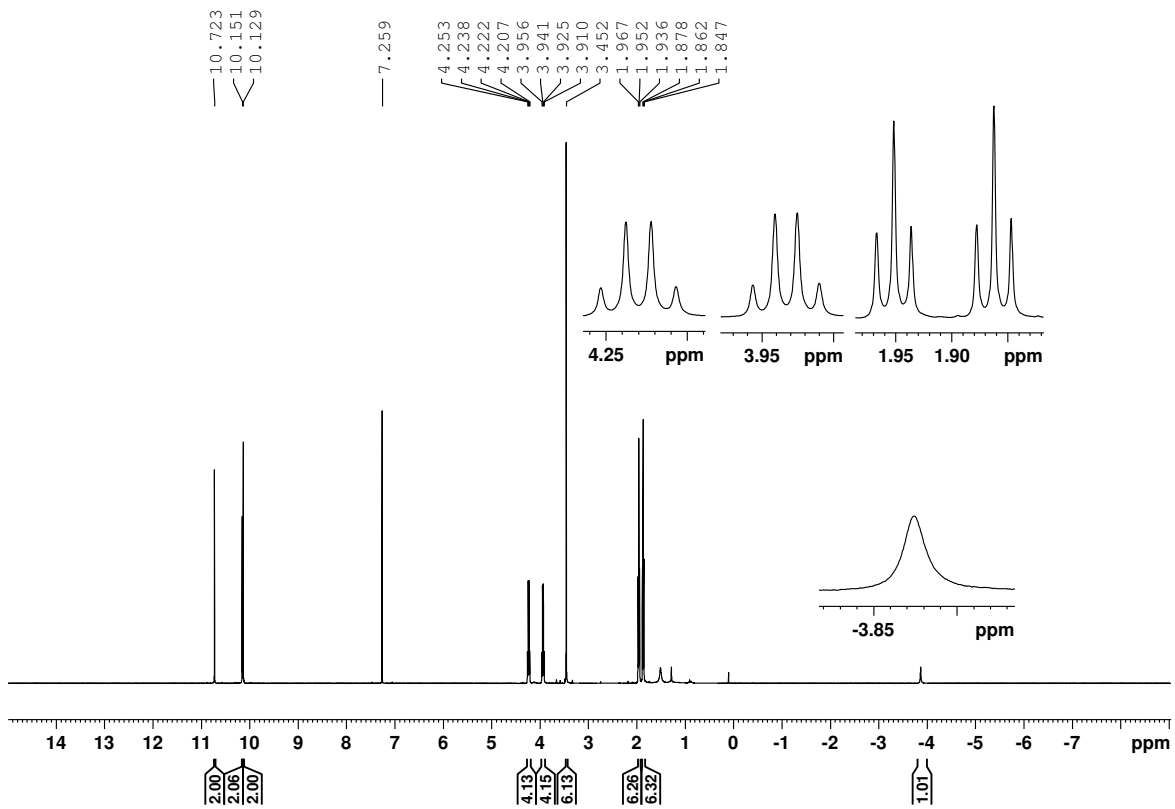

Figure D-16. 500 MHz ^{1}H NMR spectrum of 21-thiaporphyrin **97a** in $CDCl_3$

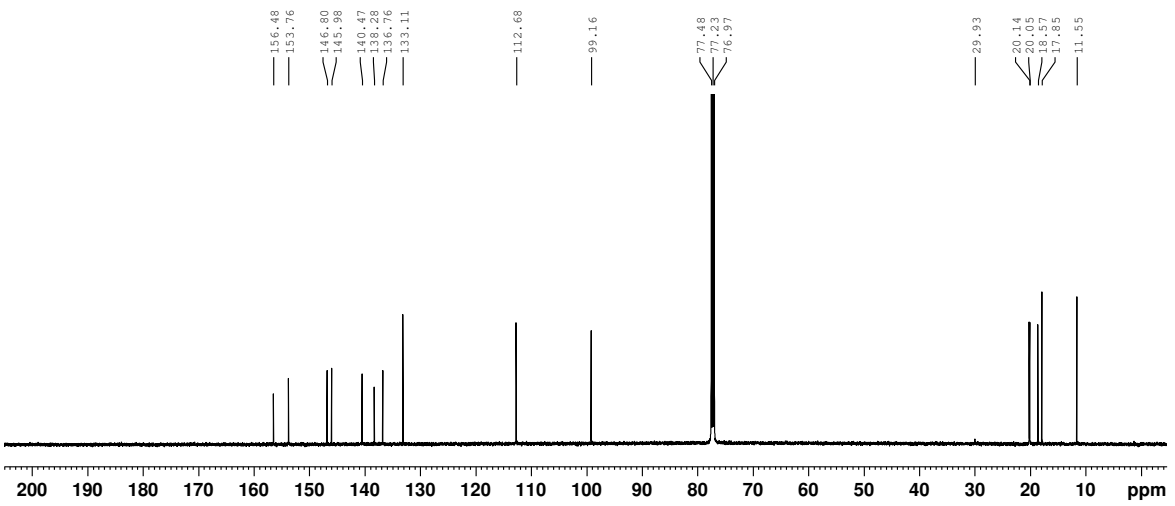

Figure D-17. 125 MHz ^{13}C NMR spectrum of 21-thiaporphyrin **97a** in $CDCl_3$

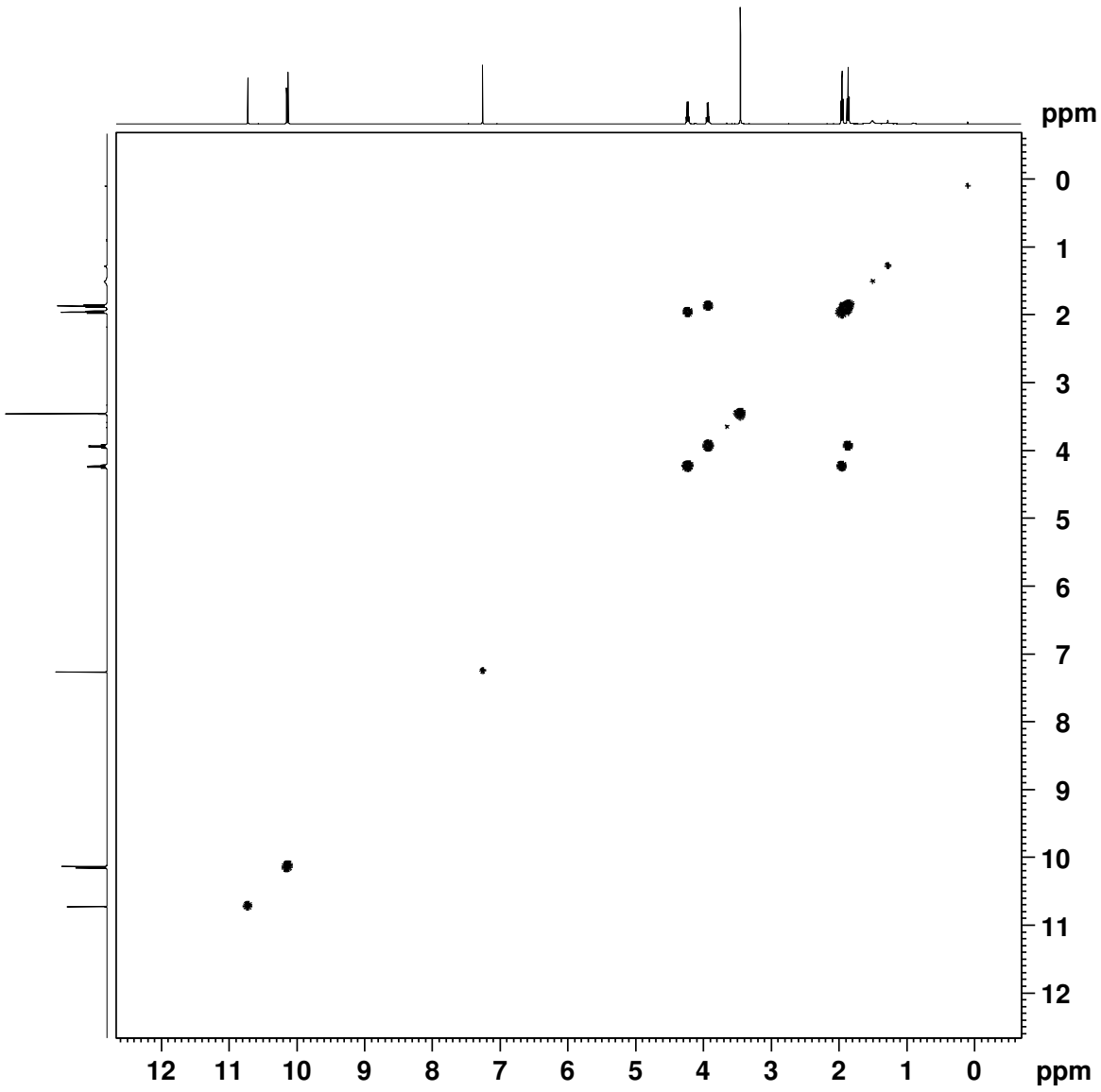

Figure D-18. ^{1}H-^{1}H COSY NMR spectrum of 21-thiaporphyrin **97a** in $CDCl_3$

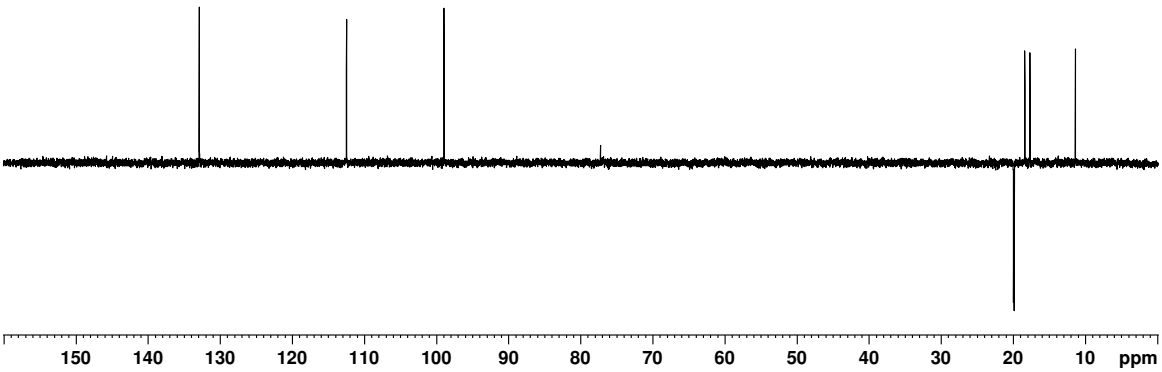

Figure D-19. DEPT-135 NMR spectrum of 21-thiaporphyrin **97a** in $CDCl_3$

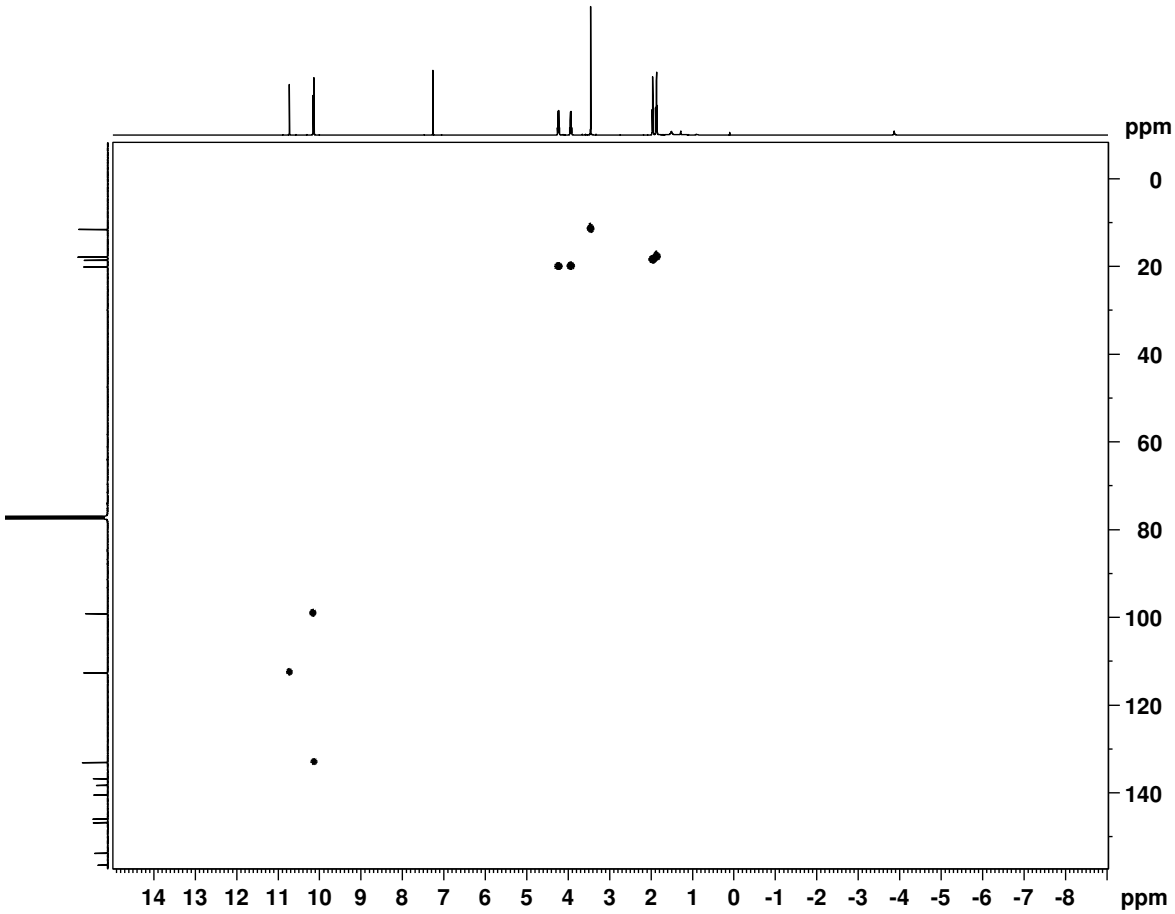

Figure D-20. HSQC NMR spectrum of 21-thiaporphyrin **97a** in $CDCl_3$

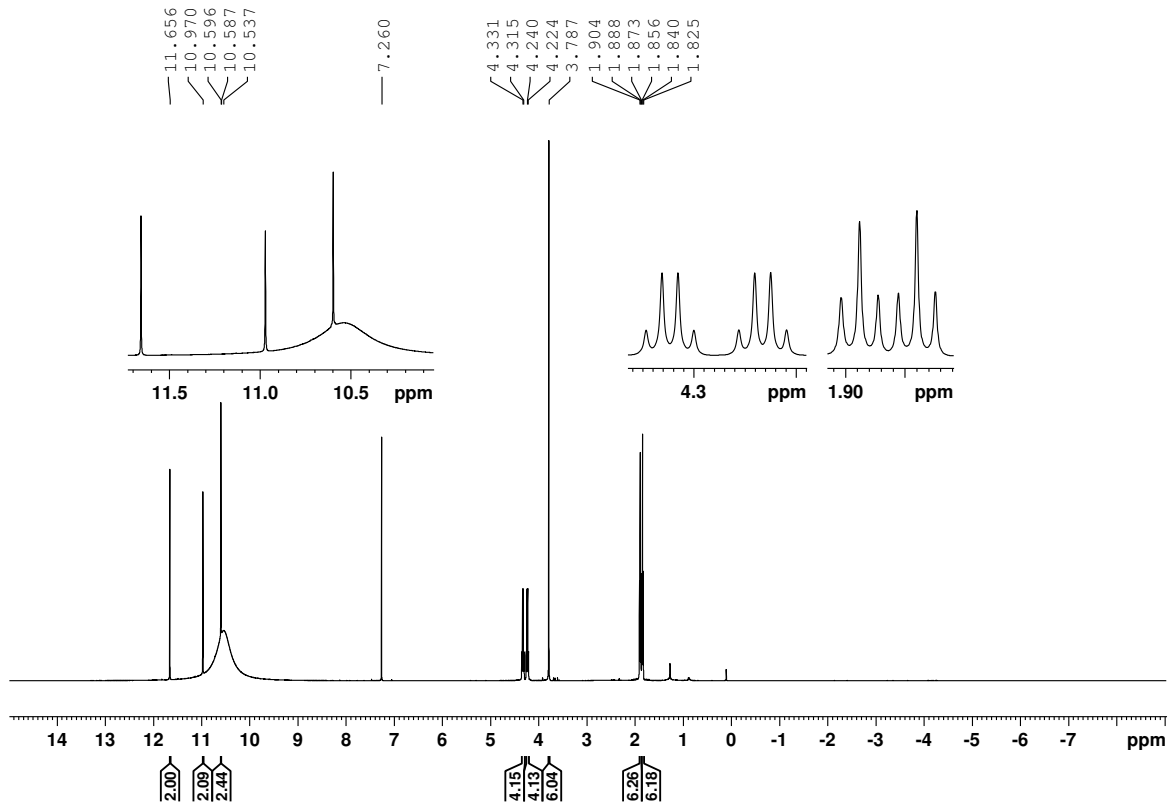

Figure D-21. 500 MHz ^{1}H NMR spectrum of 21-thiaporphyrin **97a**H_2^{2+} in TFA-$CDCl_3$

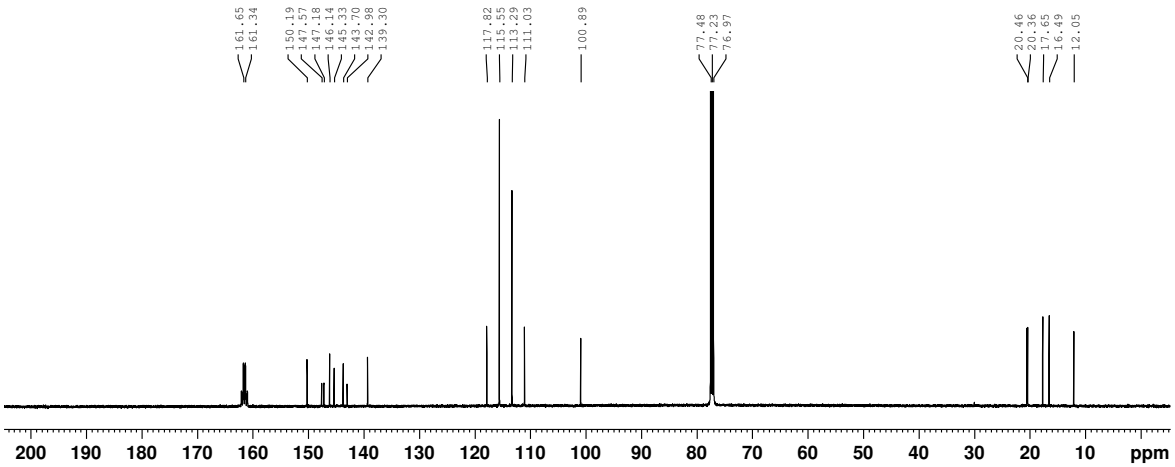

Figure D-22. 125 MHz ^{13}C NMR spectrum of 21-thiaporphyrin **97a**H_2^{2+} in TFA-$CDCl_3$

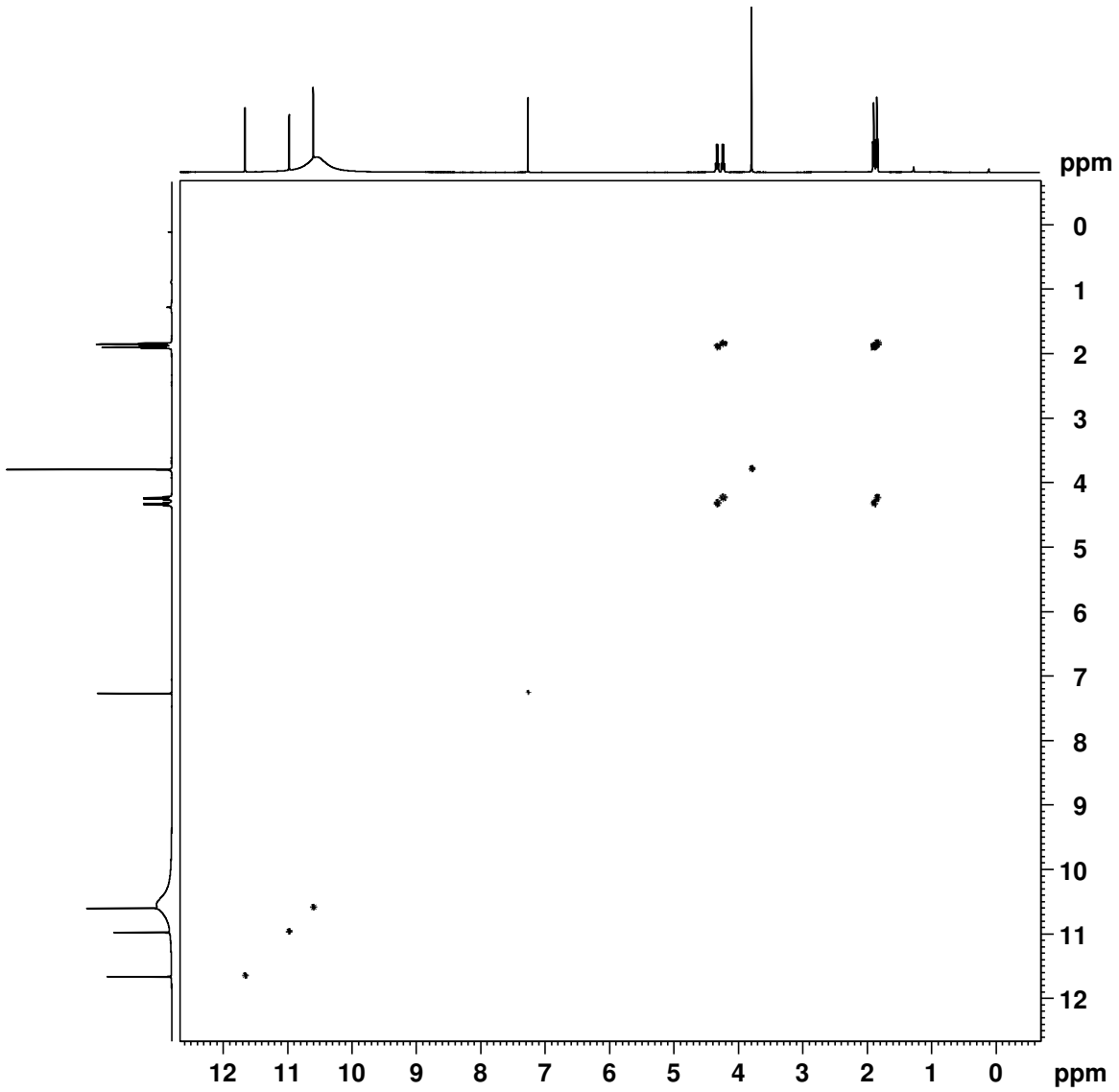

Figure D-23. ^{1}H-^{1}H COSY NMR spectrum of 21-thiaporphyrin **97a**H_2^{2+} in TFA-$CDCl_3$

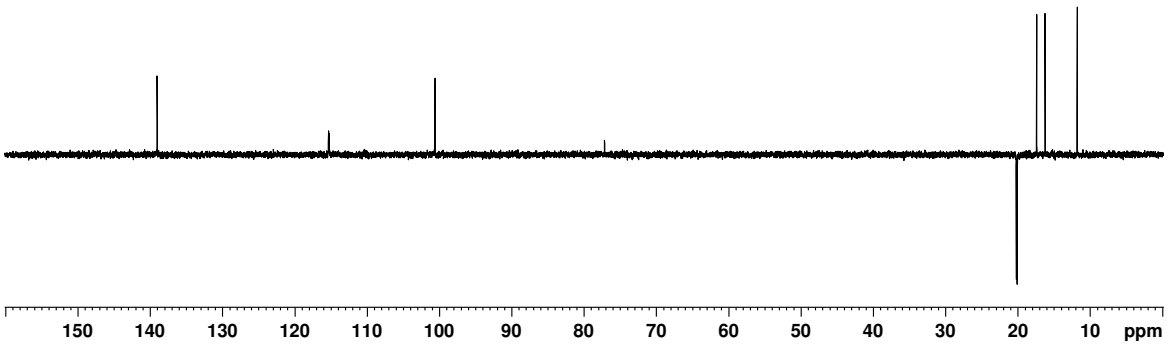

Figure D-24. DEPT-135 NMR spectrum of 21-thiaporphyrin **97a**H_2^{2+} in TFA-$CDCl_3$

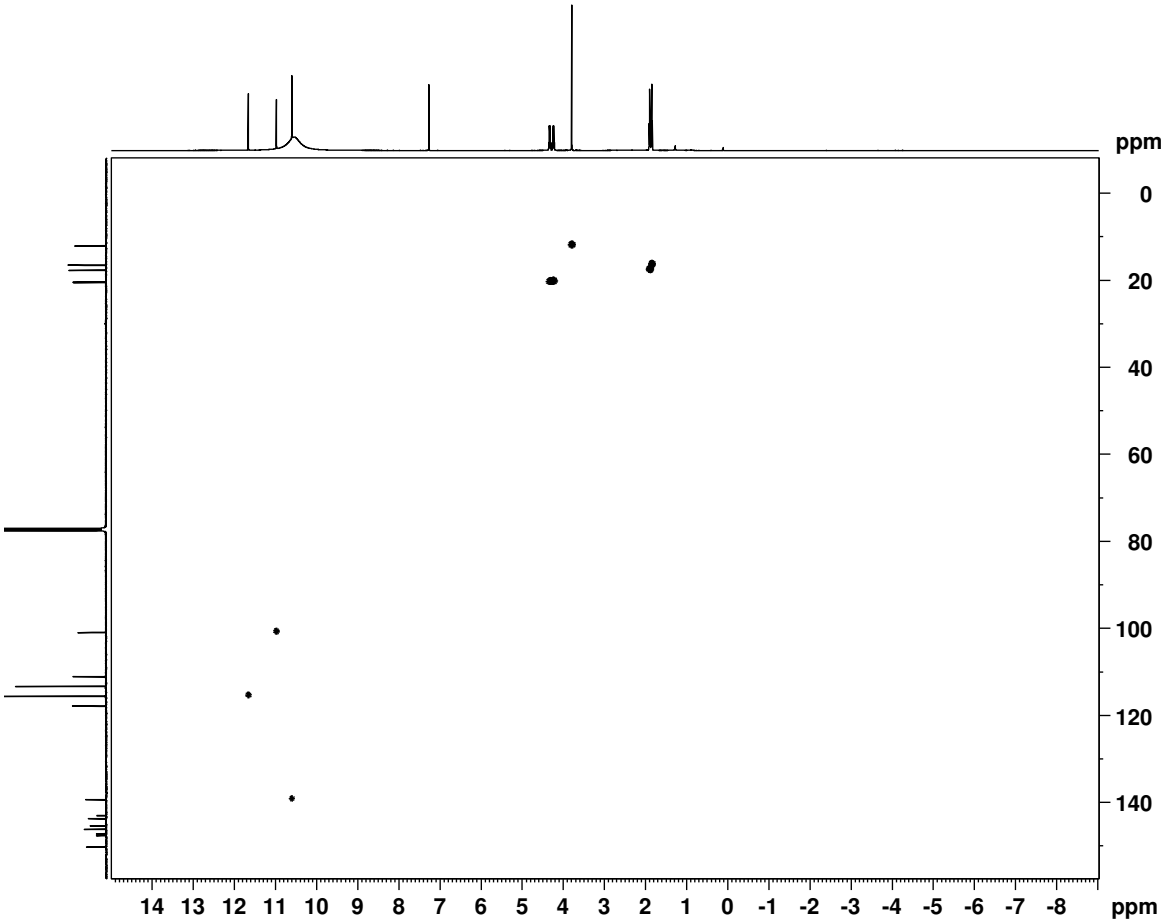

Figure D-25. HQSC NMR spectrum of 21-thiaporphyrin **97a**H_2^{2+} in TFA-$CDCl_3$

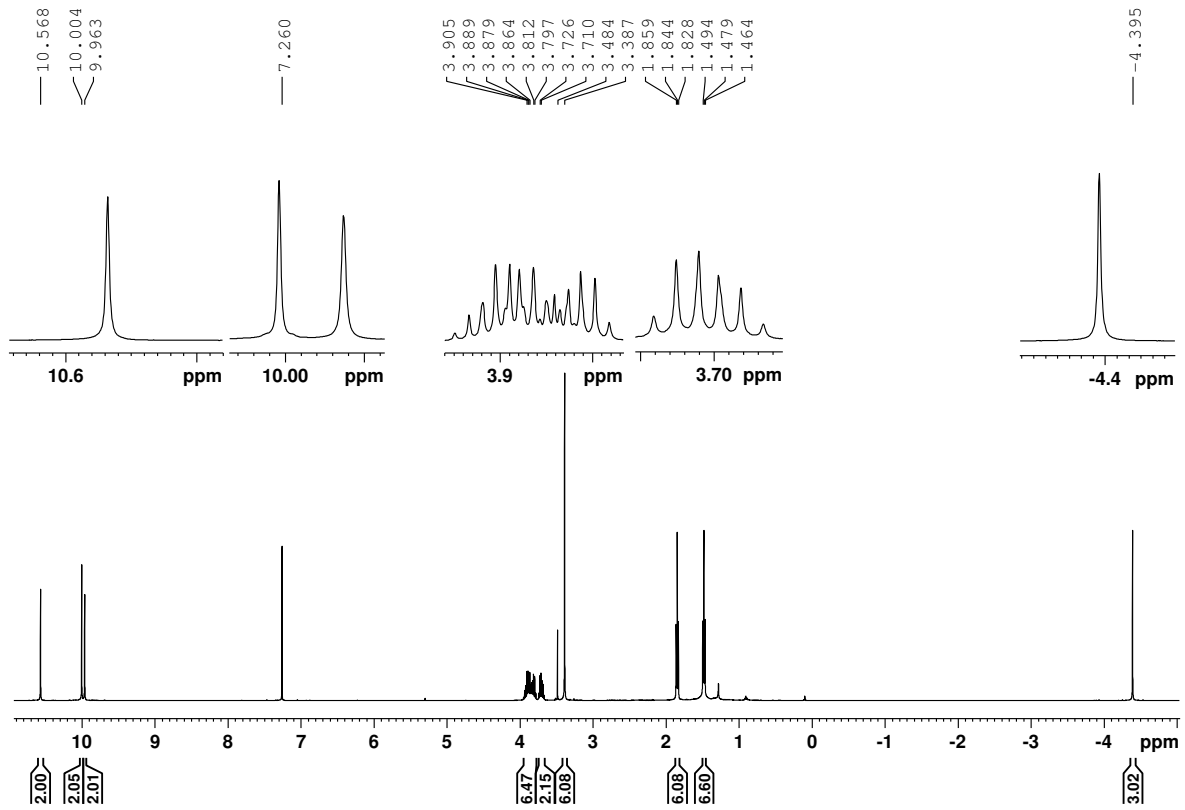

Figure D-26. 500 MHz ^{1}H NMR spectrum of *N*-methyl thiaporphyrin **97b** in $CDCl_3$

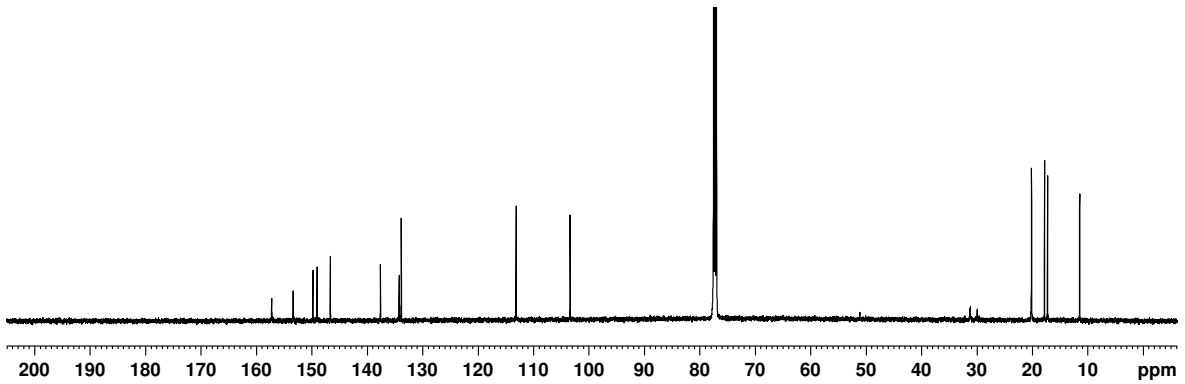

Figure D-27. 125 MHz ^{13}C NMR spectrum of *N*-methyl thiaporphyrin **97b** in $CDCl_3$

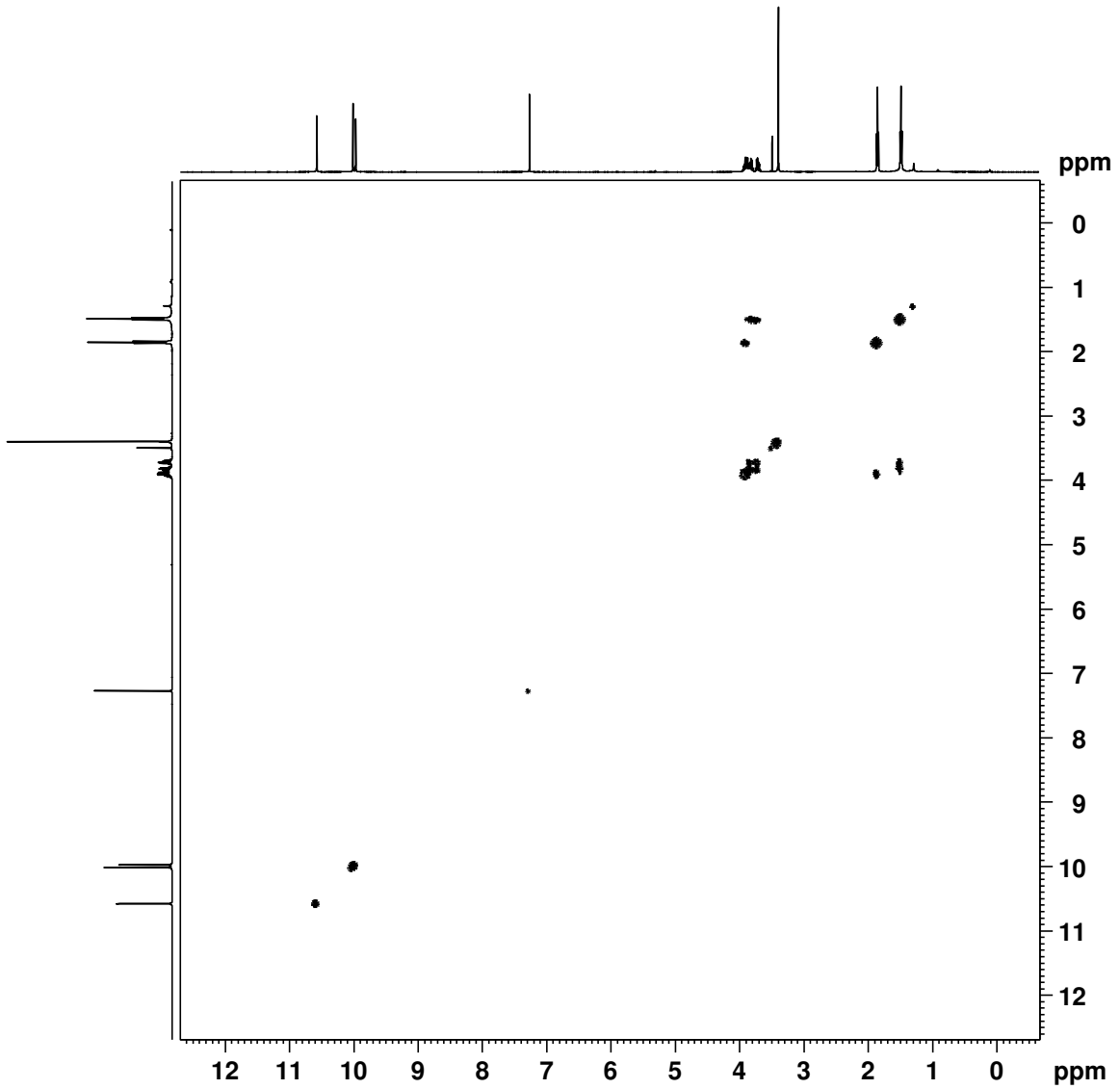

Figure D-28. ^{1}H-^{1}H COSY NMR spectrum of *N*-methyl thiaporphyrin **97b** in $CDCl_3$

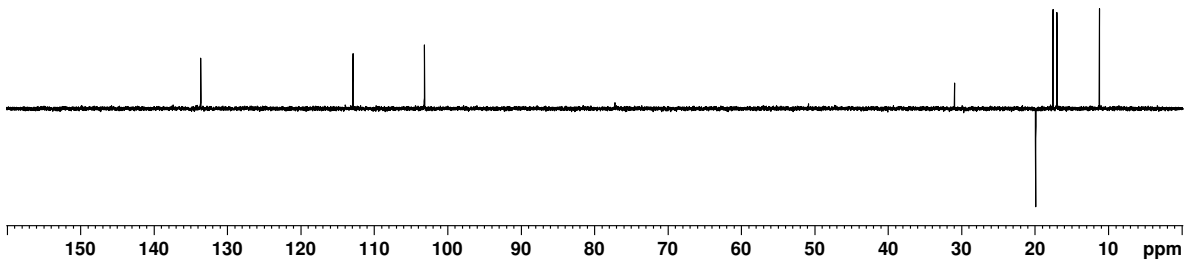

Figure D-29. DEPT-135 NMR spectrum of *N*-methyl thiaporphyrin **97b** in $CDCl_3$

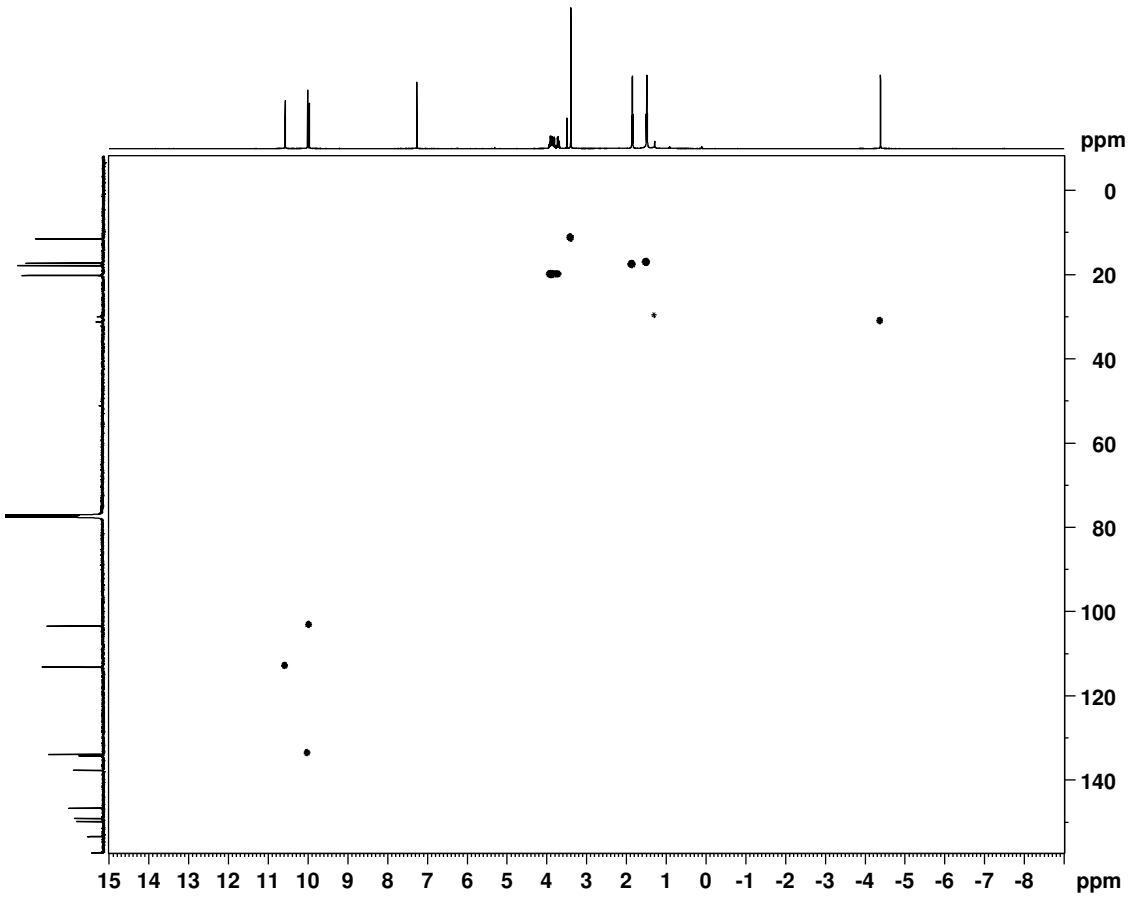

Figure D-30. HSQC NMR spectrum of *N*-methyl thiaporphyrin **97b** in $CDCl_3$

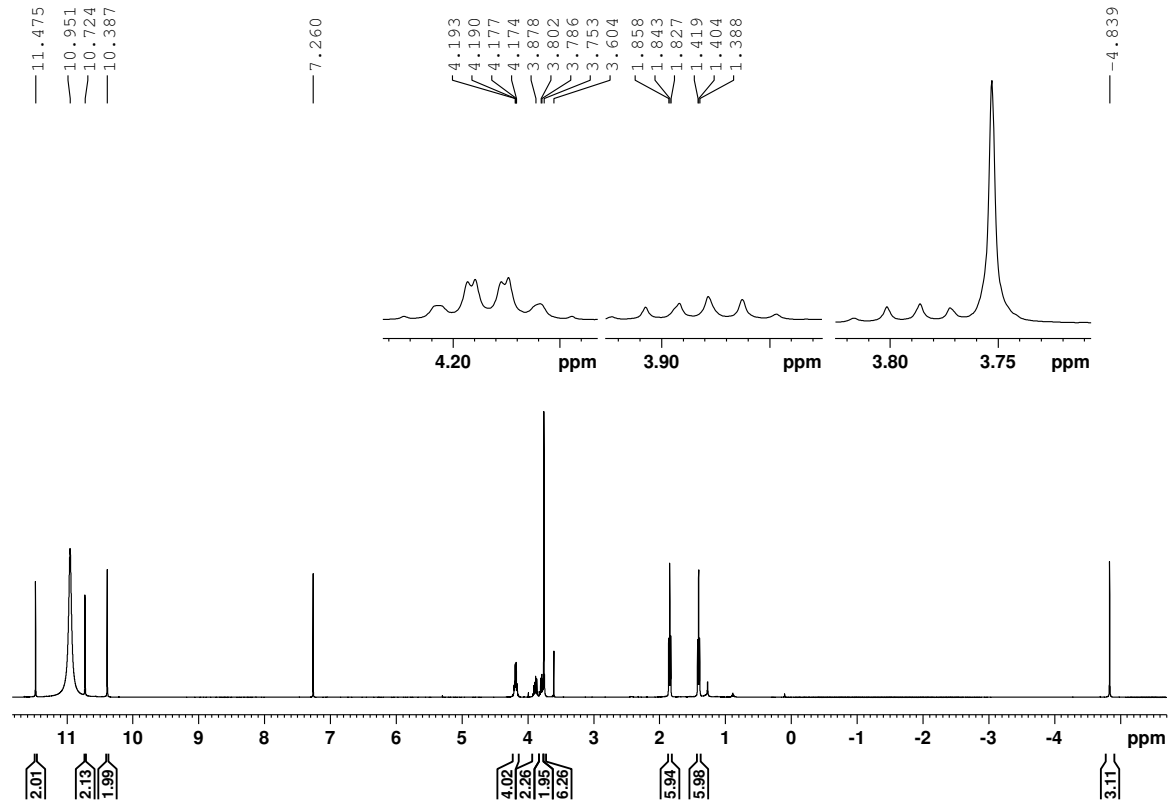

Figure D-31. 500 MHz ^{1}H NMR spectrum of *N*-methyl thiaporphyrin **97b** in TFA-$CDCl_3$

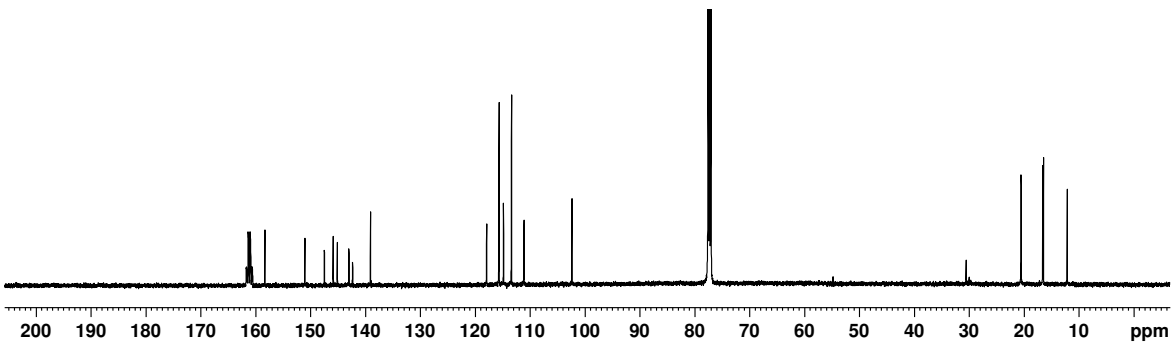

Figure D-32. 125 MHz ^{13}C NMR spectrum of *N*-methyl thiaporphyrin **97b** in TFA-$CDCl_3$

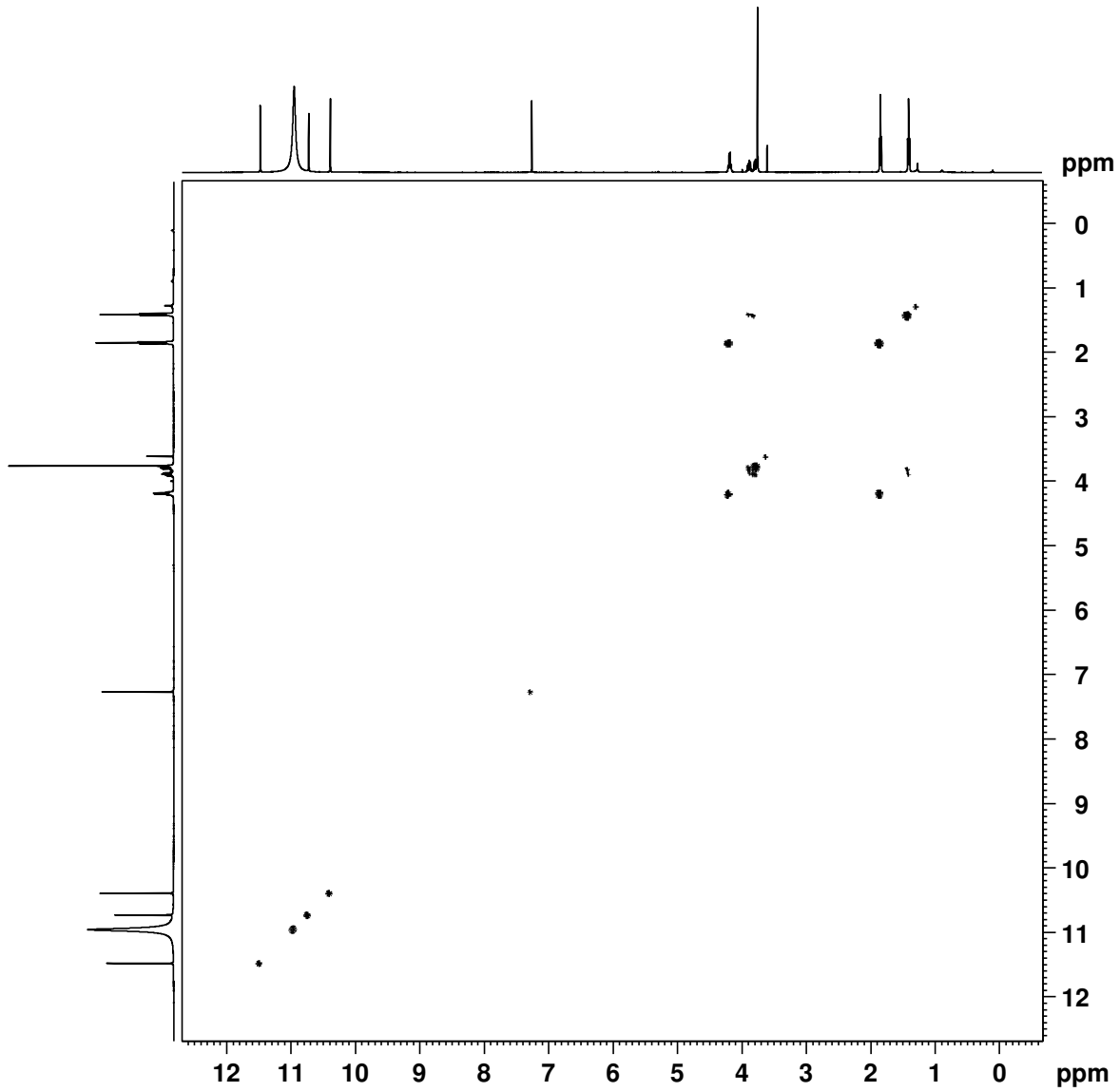

Figure D-33. ^{1}H-^{1}H COSY NMR spectrum of *N*-methyl thiaporphyrin **97b** in TFA-$CDCl_3$

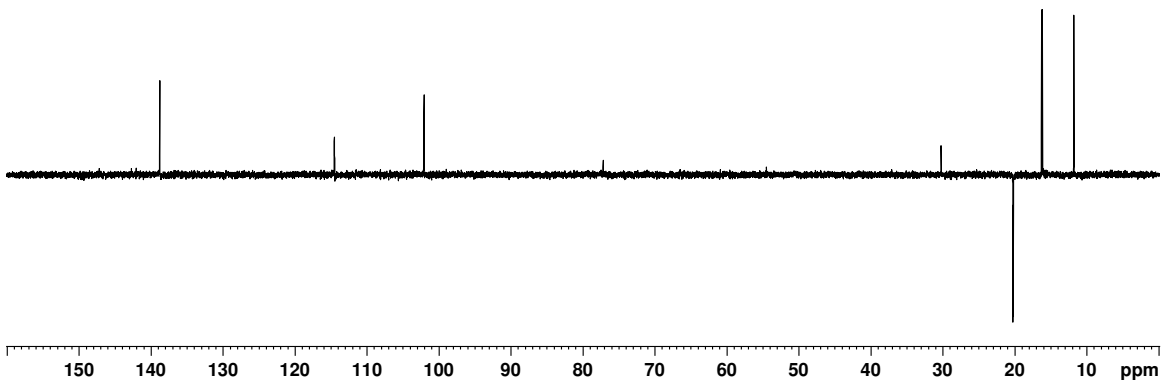

Figure D-34. DEPT-135 NMR spectrum of *N*-methyl thiaporphyrin **97b** in TFA-$CDCl_3$

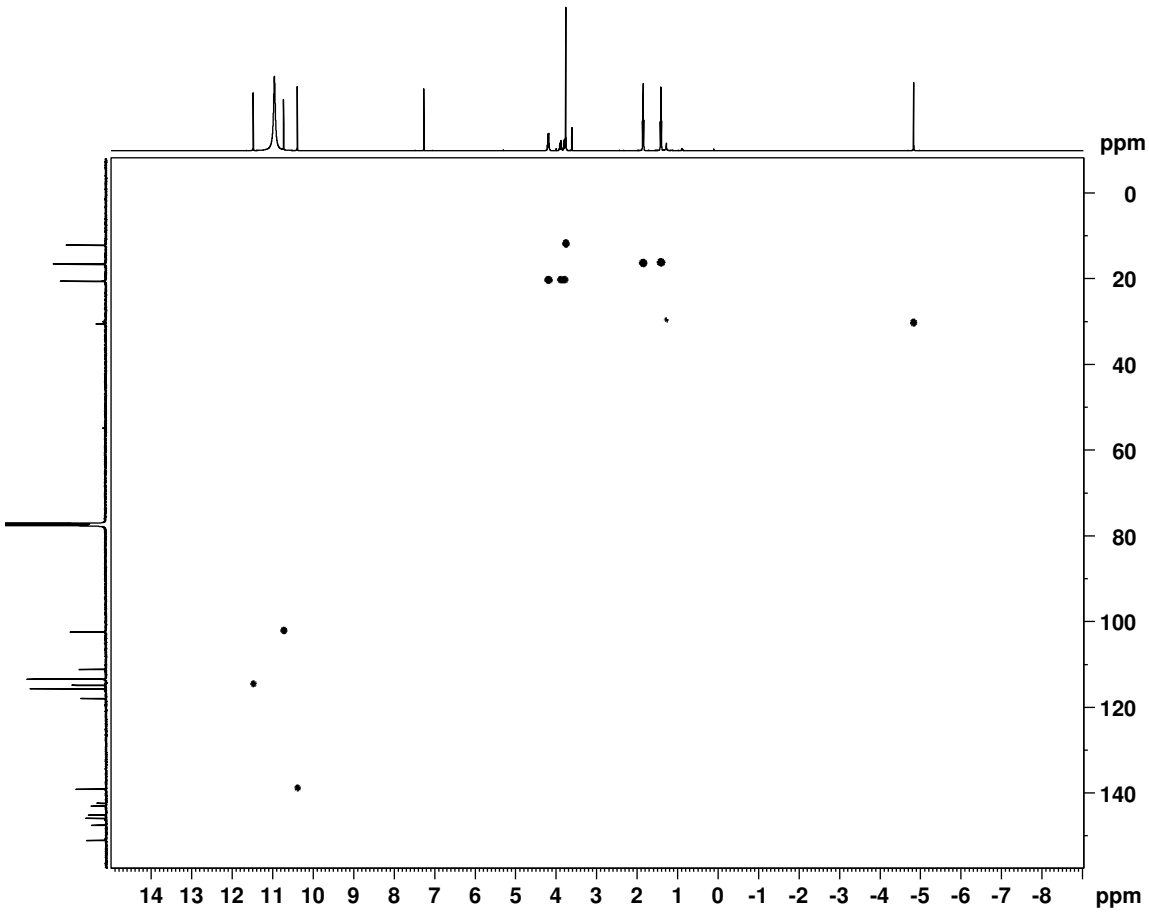

Figure D-35. HSQC NMR spectrum of *N*-methyl thiaporphyrin **97b** in TFA-$CDCl_3$

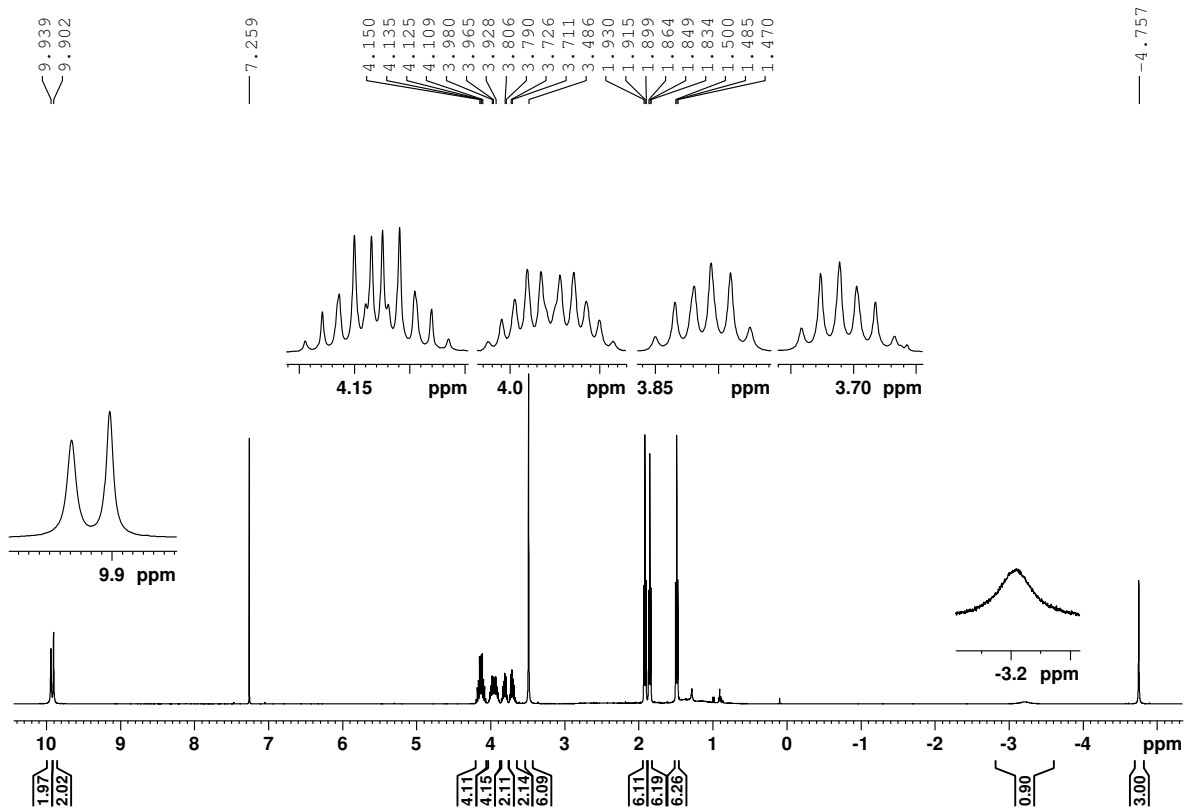

Figure D-36. 500MHz ^{1}H NMR spectrum of *N*-methyl porphyrin **99b** in $CDCl_3$

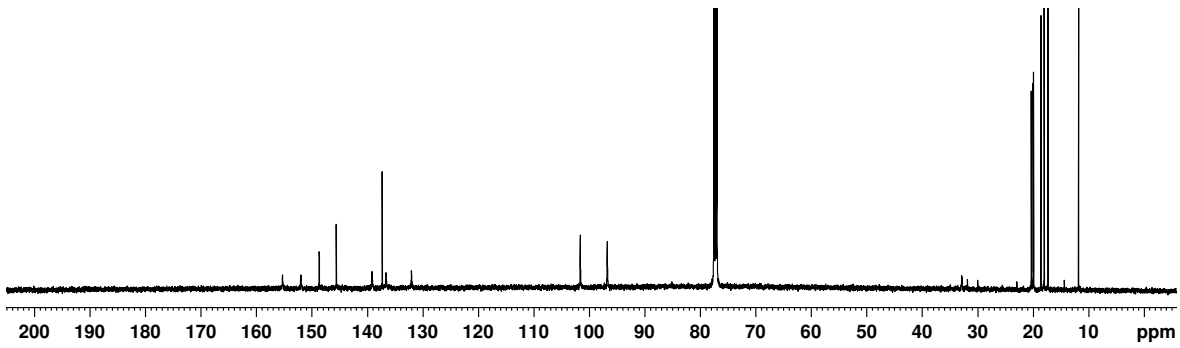

Figure D-37. 125 MHz ^{13}C NMR spectrum of *N*-methyl porphyrin **99b** in $CDCl_3$

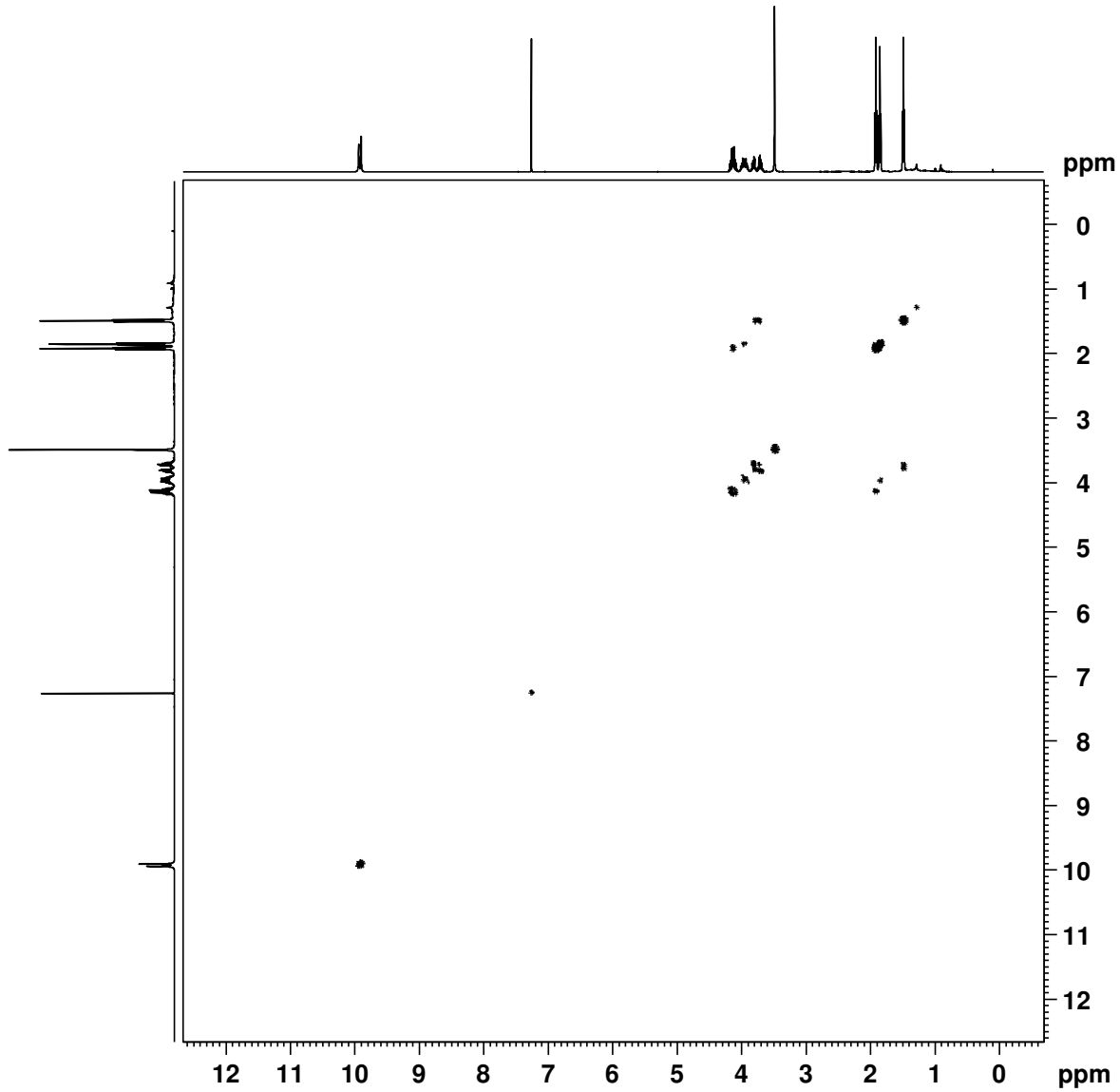

Figure D-38. ^{1}H-^{1}H COSY NMR spectrum of *N*-methyl porphyrin **99b** in $CDCl_3$

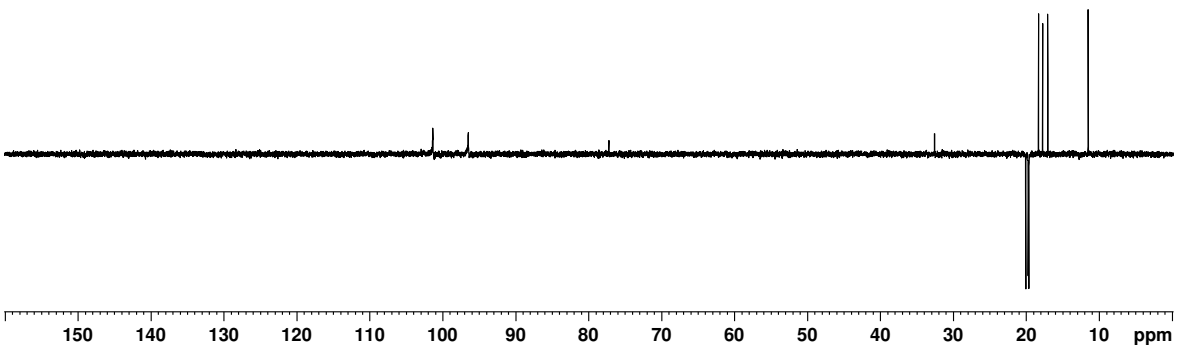

Figure D-39. DEPT-135 NMR spectrum of *N*-methyl porphyrin **99b** in $CDCl_3$

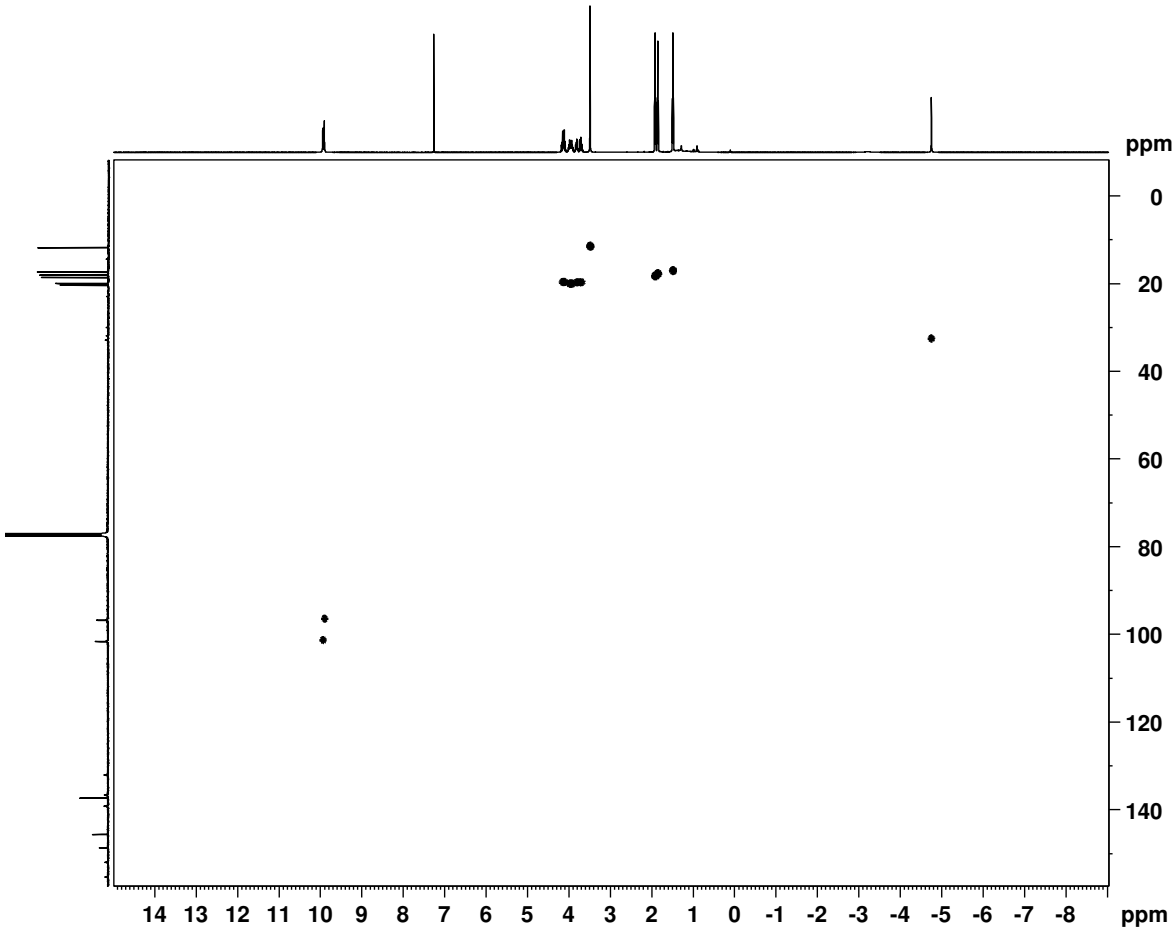

Figure D-40. HSQC NMR spectrum of *N*-methyl porphyrin **99b** in $CDCl_3$

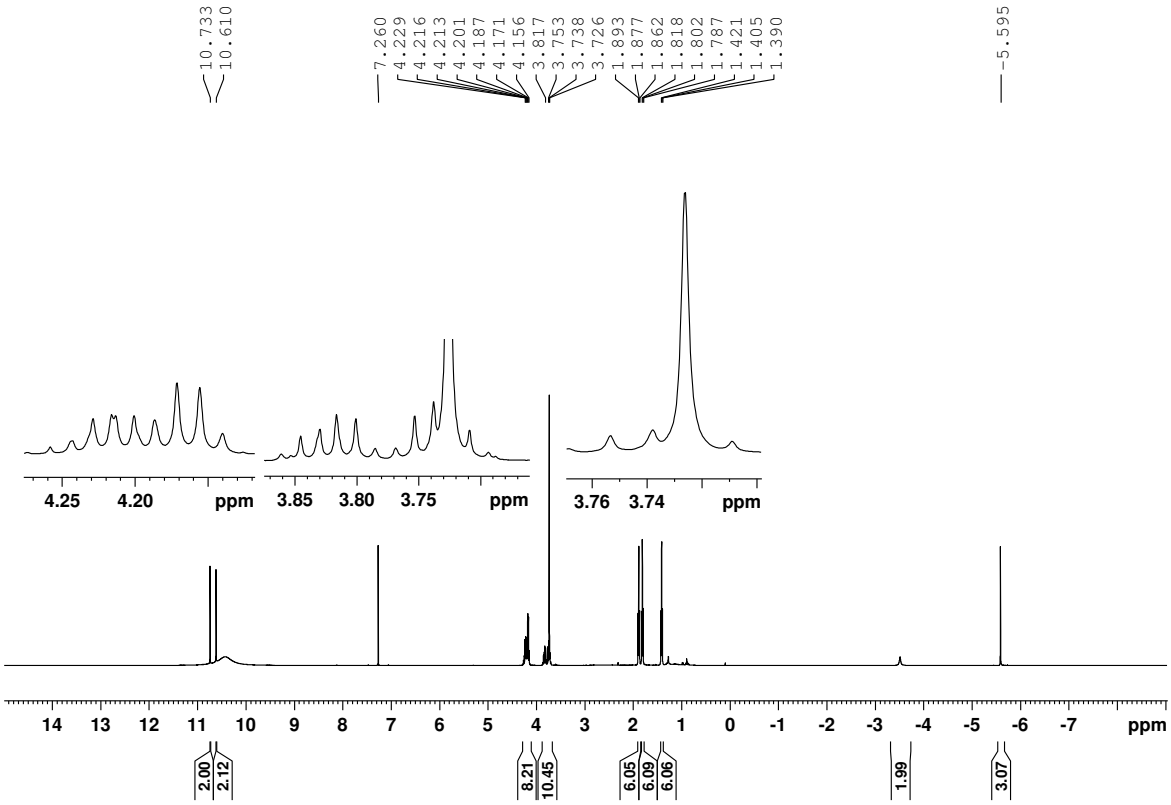

Figure D-41. 500 MHz ^{1}H NMR spectrum of *N*-methyl porphyrin **99b** in TFA-$CDCl_3$

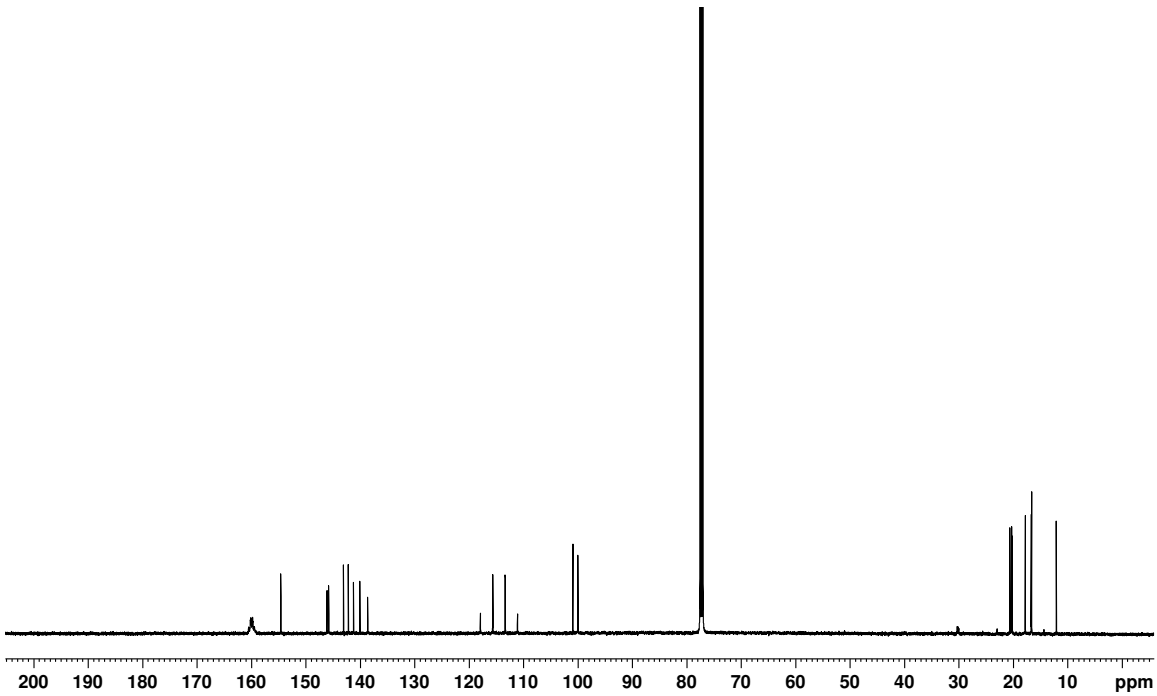

Figure D-42. 125 MHz ^{13}C NMR spectrum of *N*-methyl porphyrin **99b** in TFA-$CDCl_3$

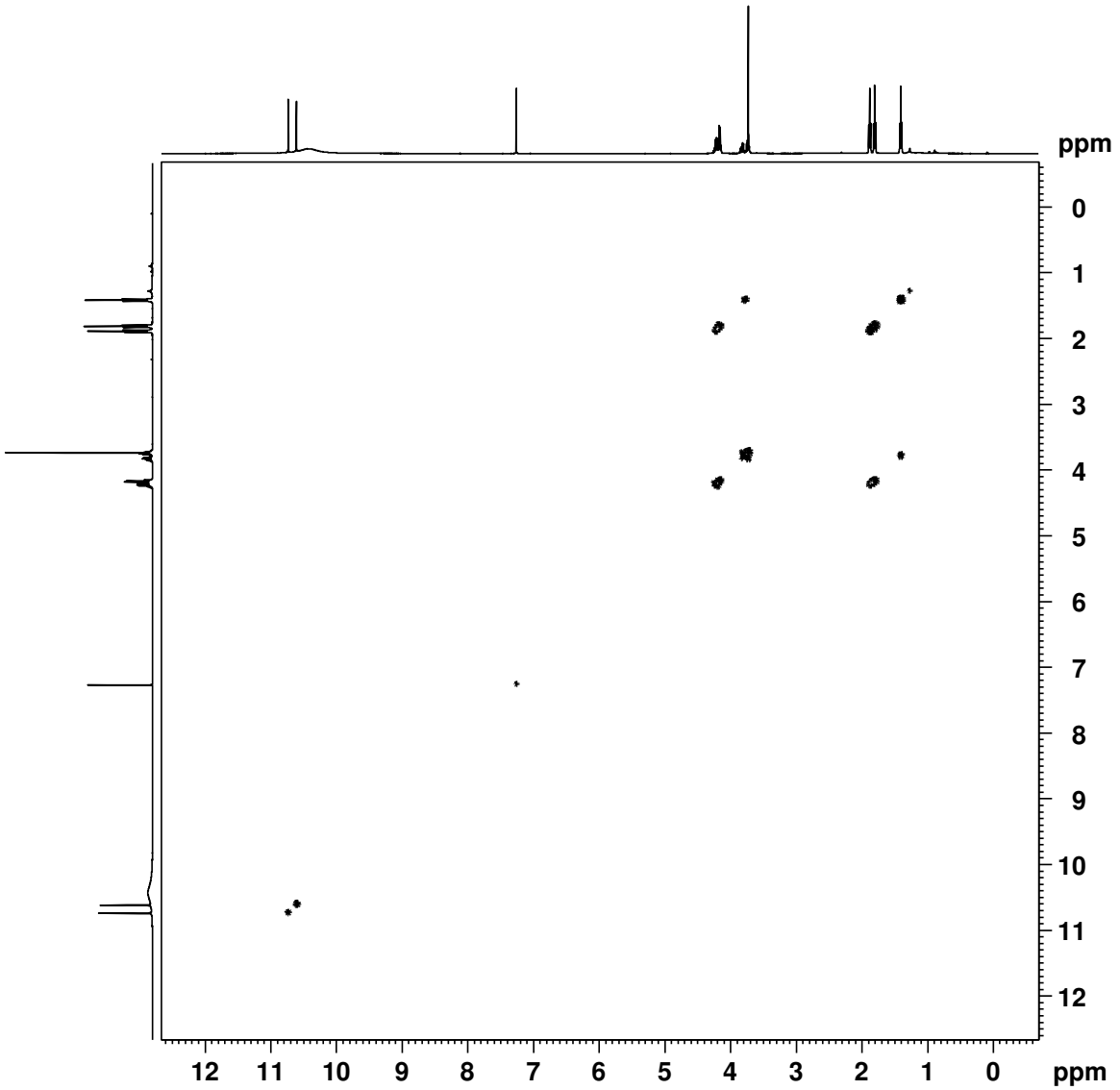

Figure D-43. ^{1}H-^{1}H COSY NMR spectrum of *N*-methyl porphyrin **99b** in TFA-$CDCl_3$

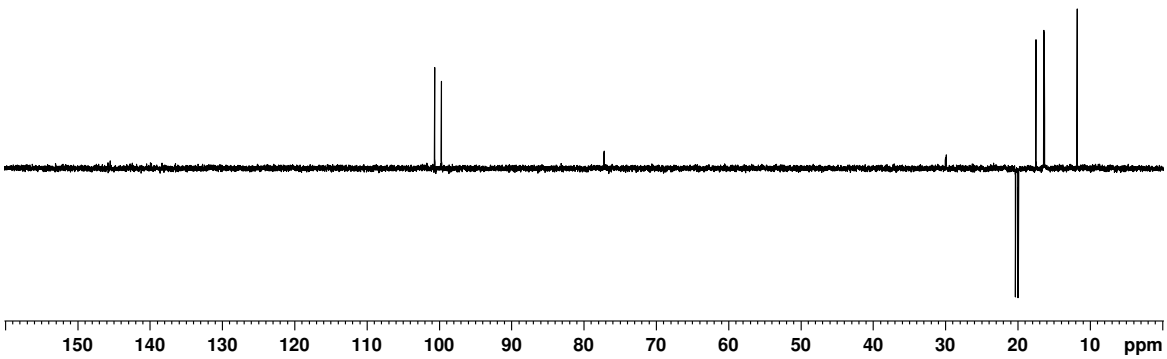

Figure D-44. DEPT-135 NMR spectrum of *N*-methyl porphyrin **99b** in TFA-$CDCl_3$

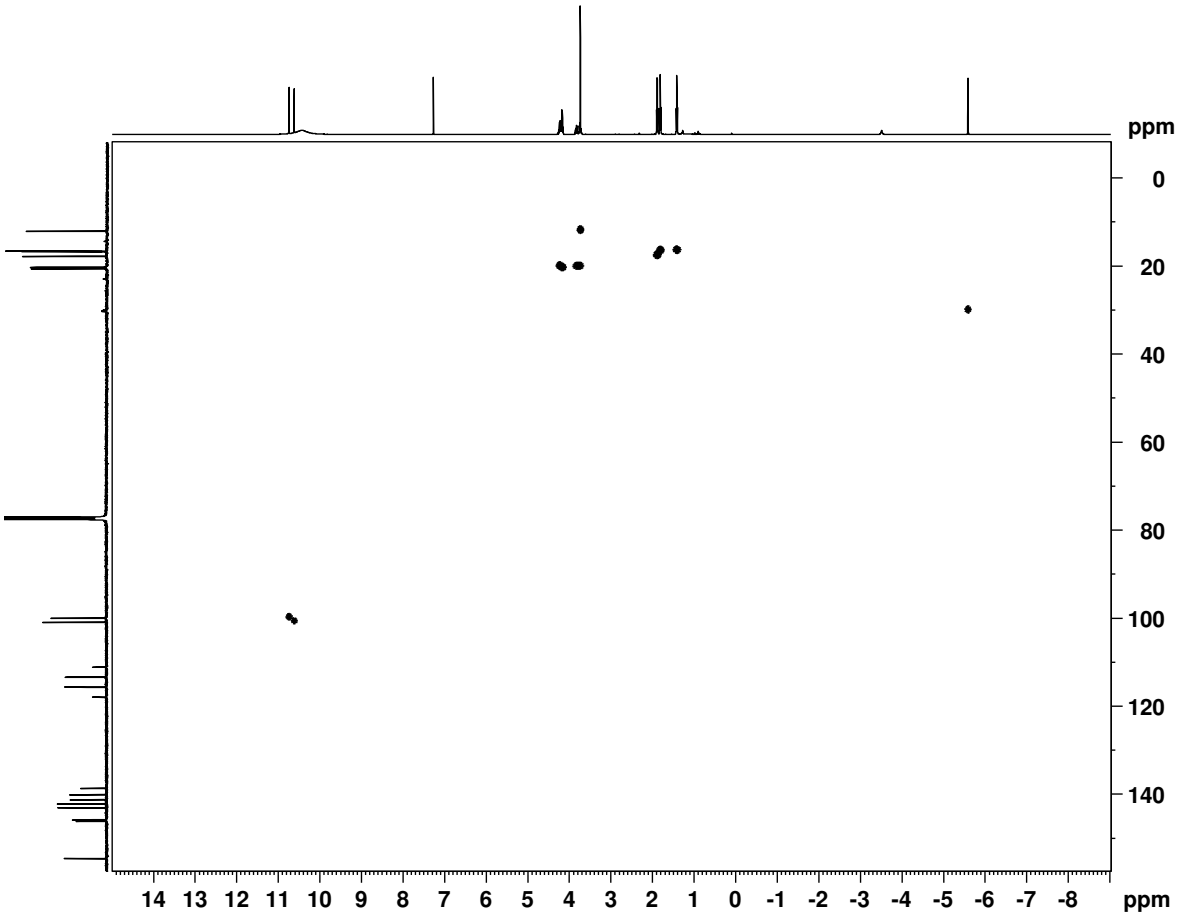

Figure D-45. HSQC NMR spectrum of *N*-methyl porphyrin **99b** in TFA-$CDCl_3$

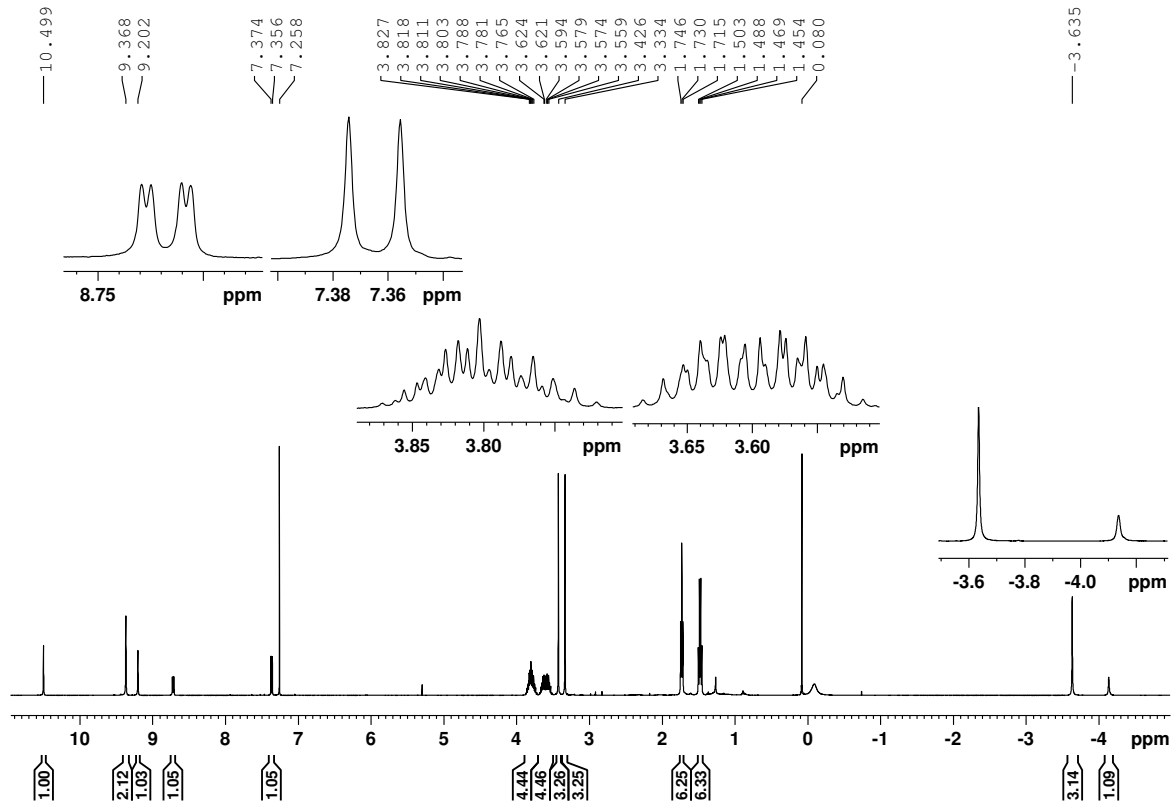

Figure D-46. 500 MHz ^{1}H NMR spectrum of *N*-methyl oxybenziporphyrin **100a** in $CDCl_3$

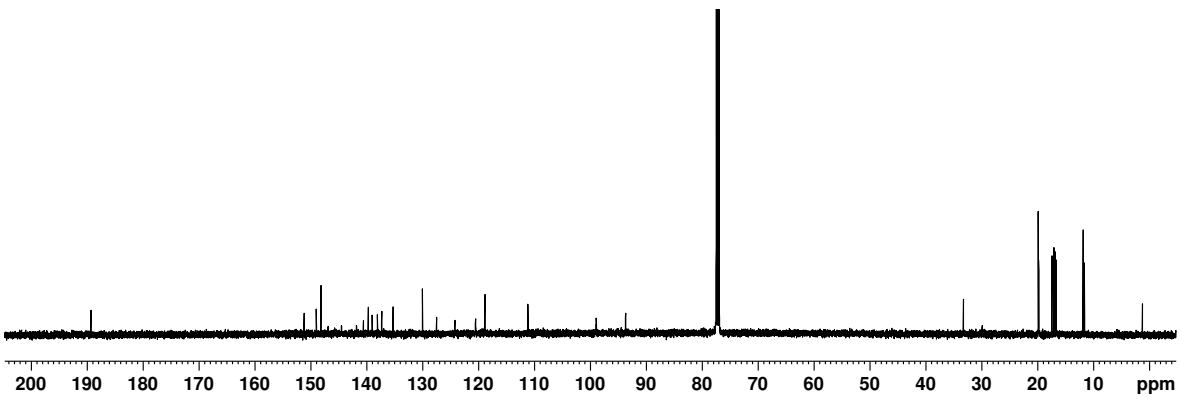

Figure D-47. 125 MHz ^{13}C NMR spectrum of *N*-methyl oxybenziporphyrin **100a** in $CDCl_3$

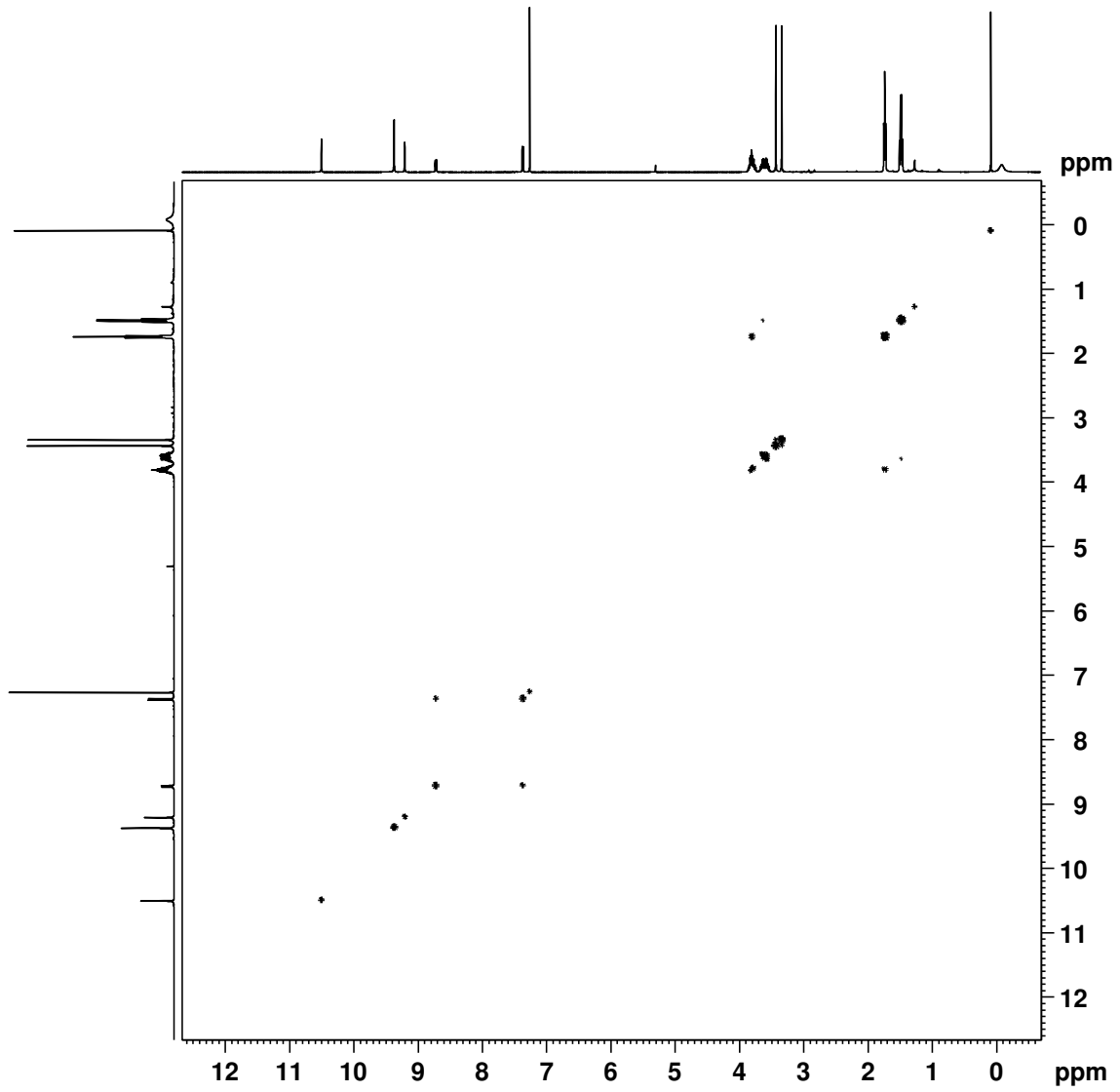

Figure D-48. ^{1}H-^{1}H COSY NMR spectrum of *N*-methyl oxybenziporphyrin **100a** in $CDCl_3$

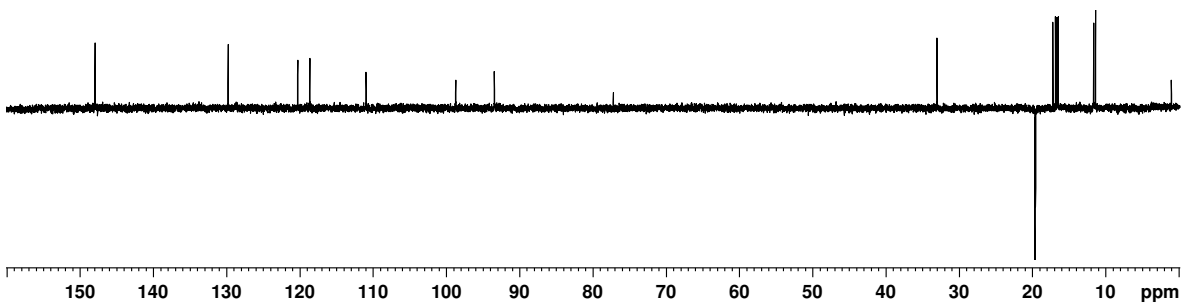

Figure D-49. DEPT-135 NMR spectrum of *N*-methyl oxybenziporphyrin **100a** in $CDCl_3$

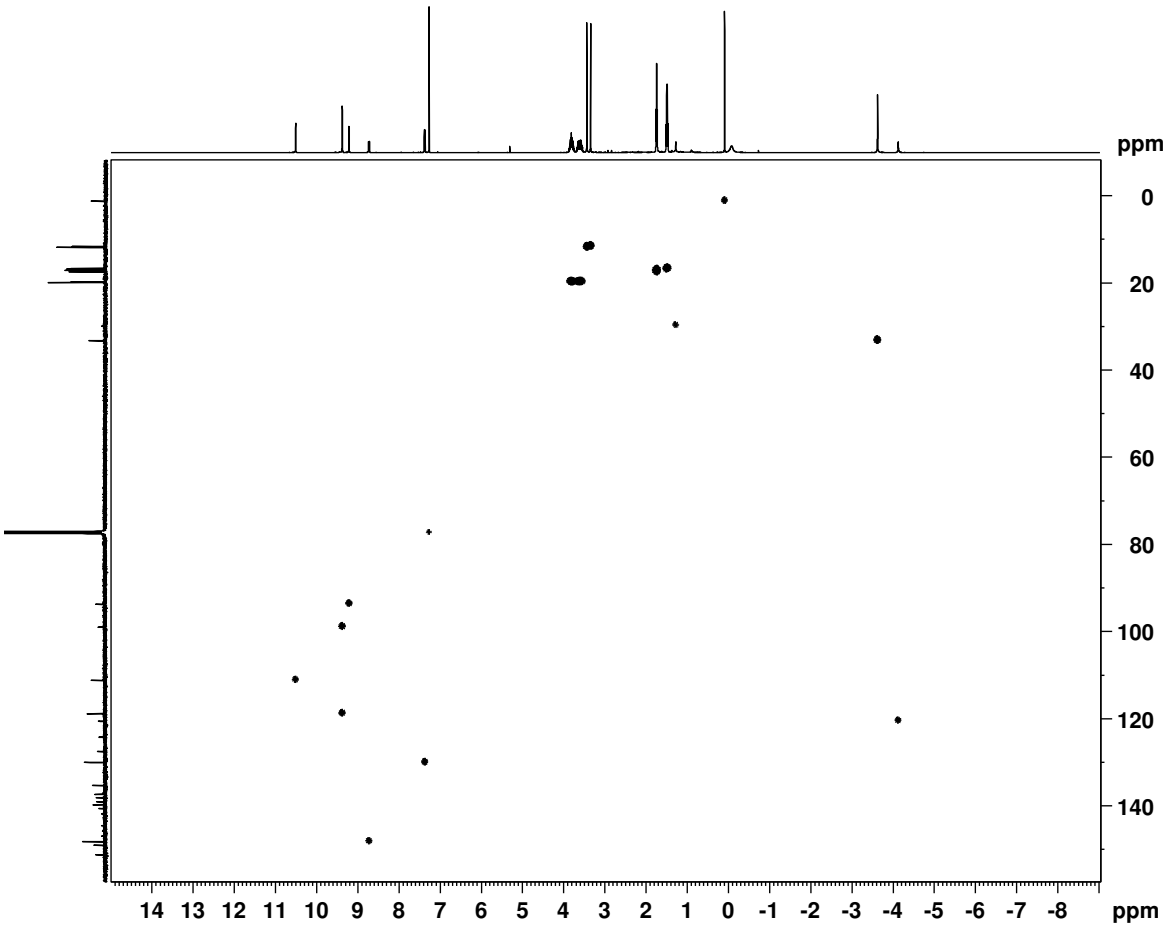

Figure D-50. HSQC NMR spectrum of *N*-methyl oxybenziporphyrin **100a** in $CDCl_3$

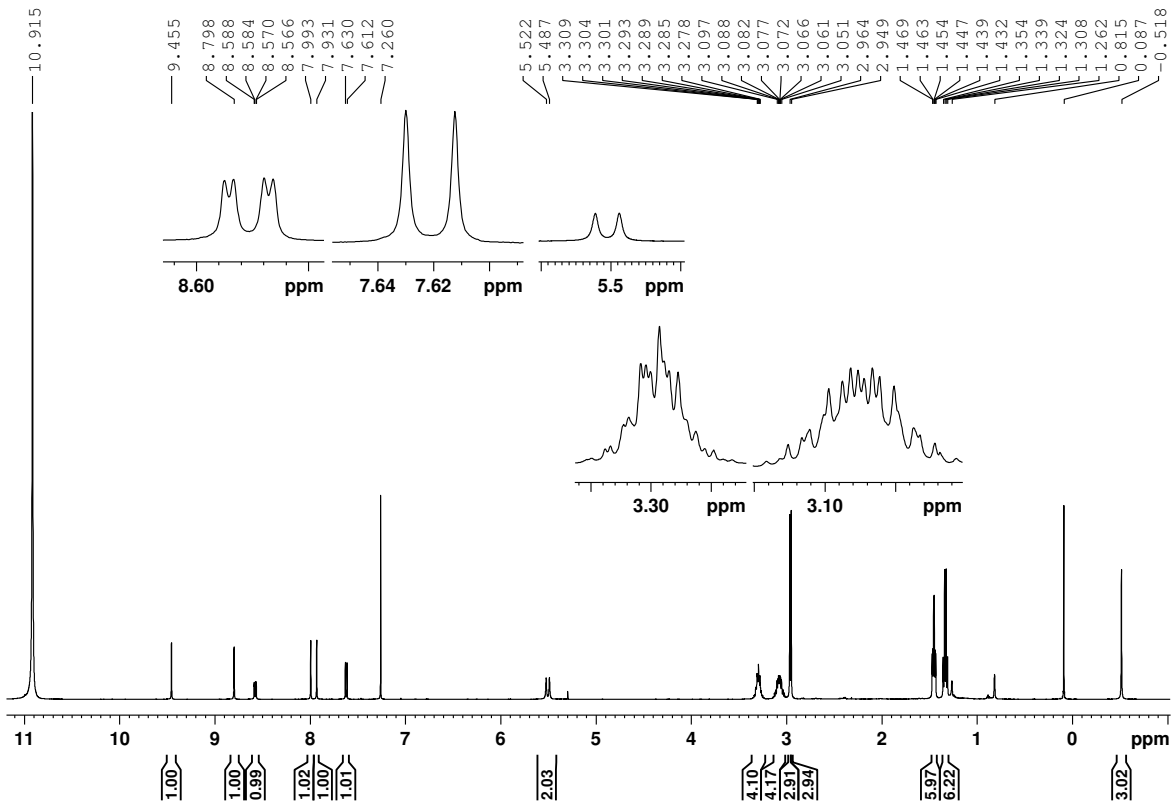

Figure D-51. 500 MHz ^{1}H NMR spectrum of *N*-methyl oxybenziporphyrin **100a** in TFA-CDCl$_3$

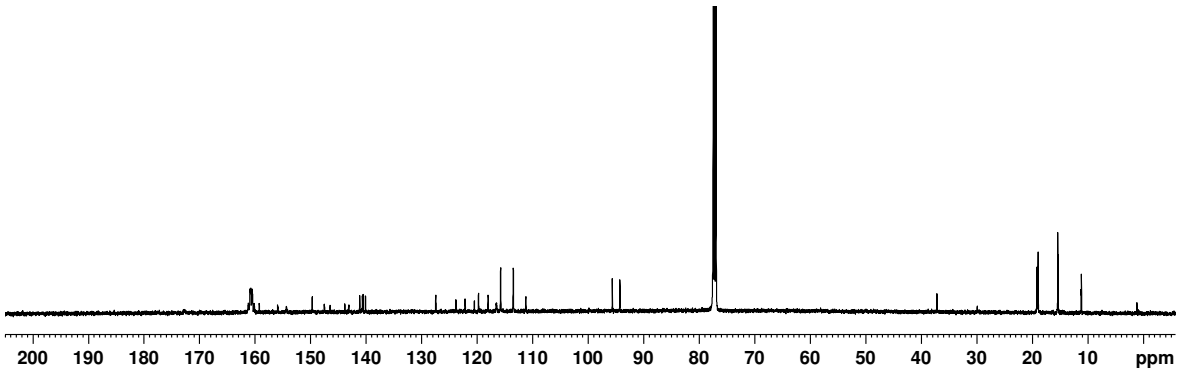

Figure D-52. 125 MHz ^{13}C NMR spectrum of *N*-methyl oxybenziporphyrin **100a** in TFA-CDCl$_3$

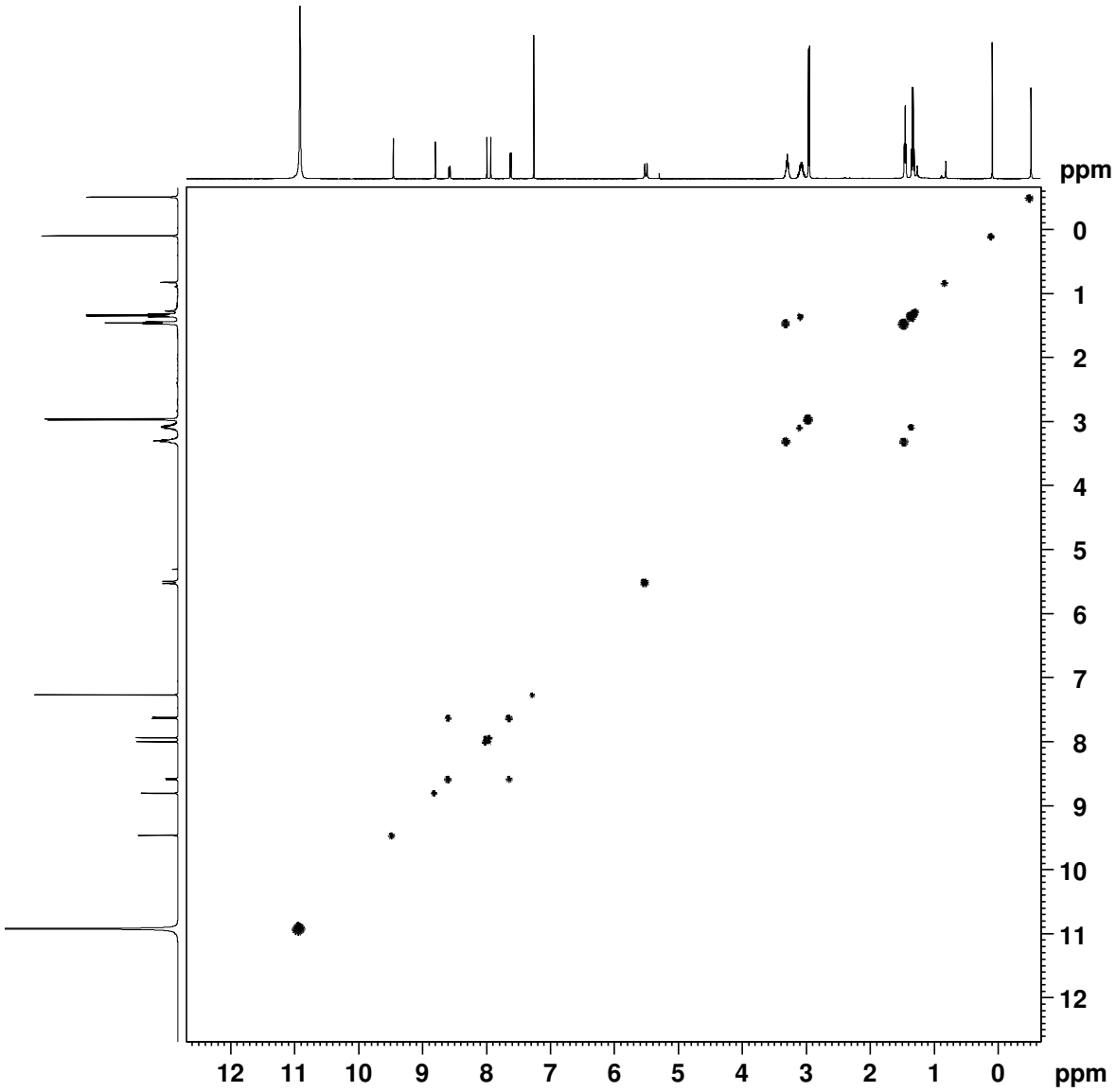

Figure D-53. ^{1}H-^{1}H COSY NMR spectrum of *N*-methyl oxybenziporphyrin **100a** in TFA-$CDCl_3$

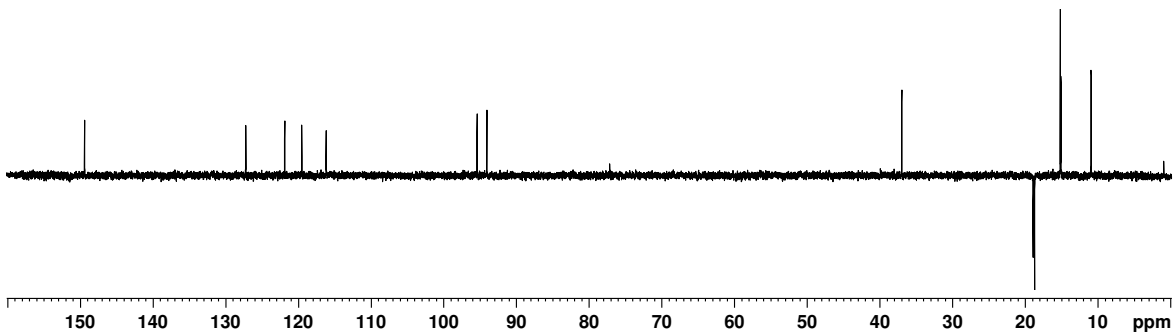

Figure D-54. DEPT-135 NMR spectrum of *N*-methyl oxybenziporphyrin **100a** in TFA-$CDCl^3$

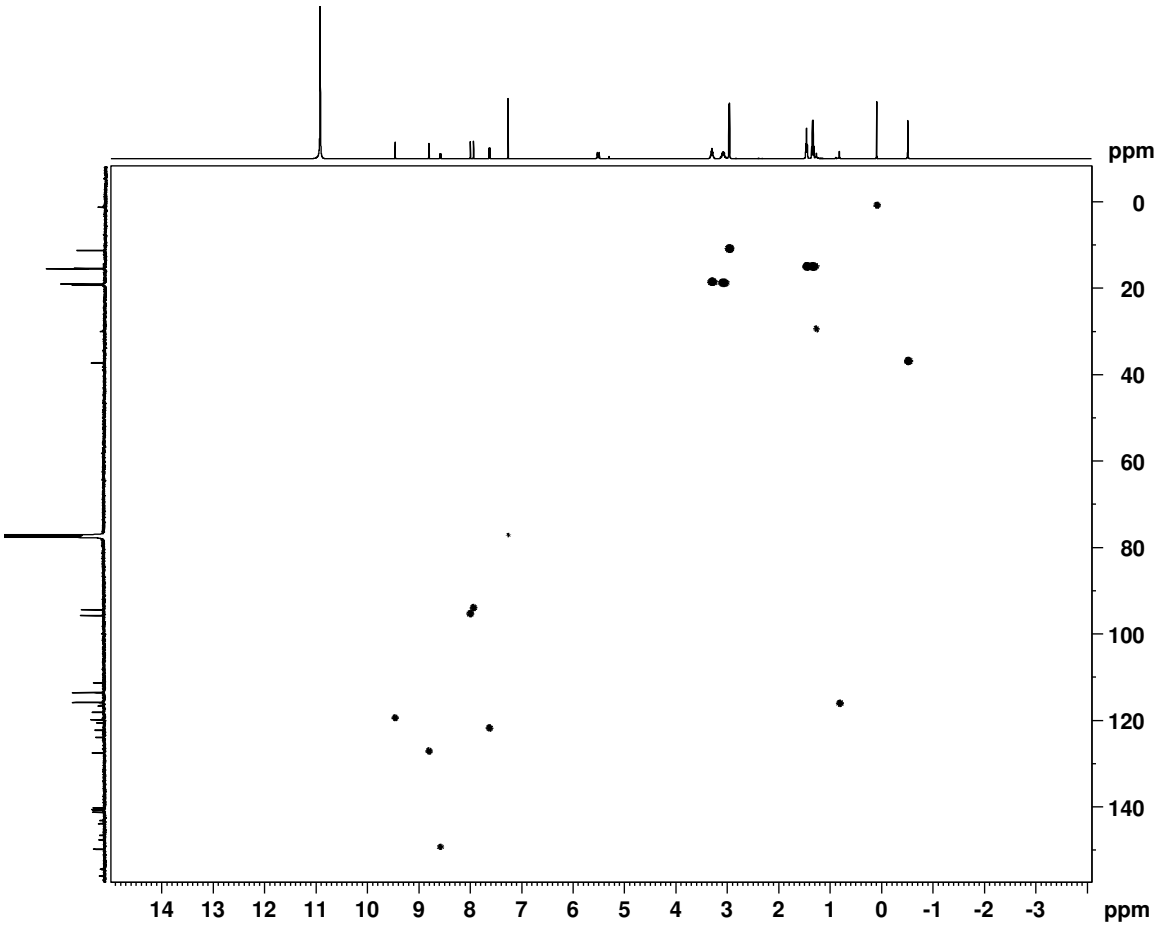

Figure D-55. HSQC NMR spectrum of *N*-methyl oxybenziporphyrin **100a** in TFA-$CDCl^3$

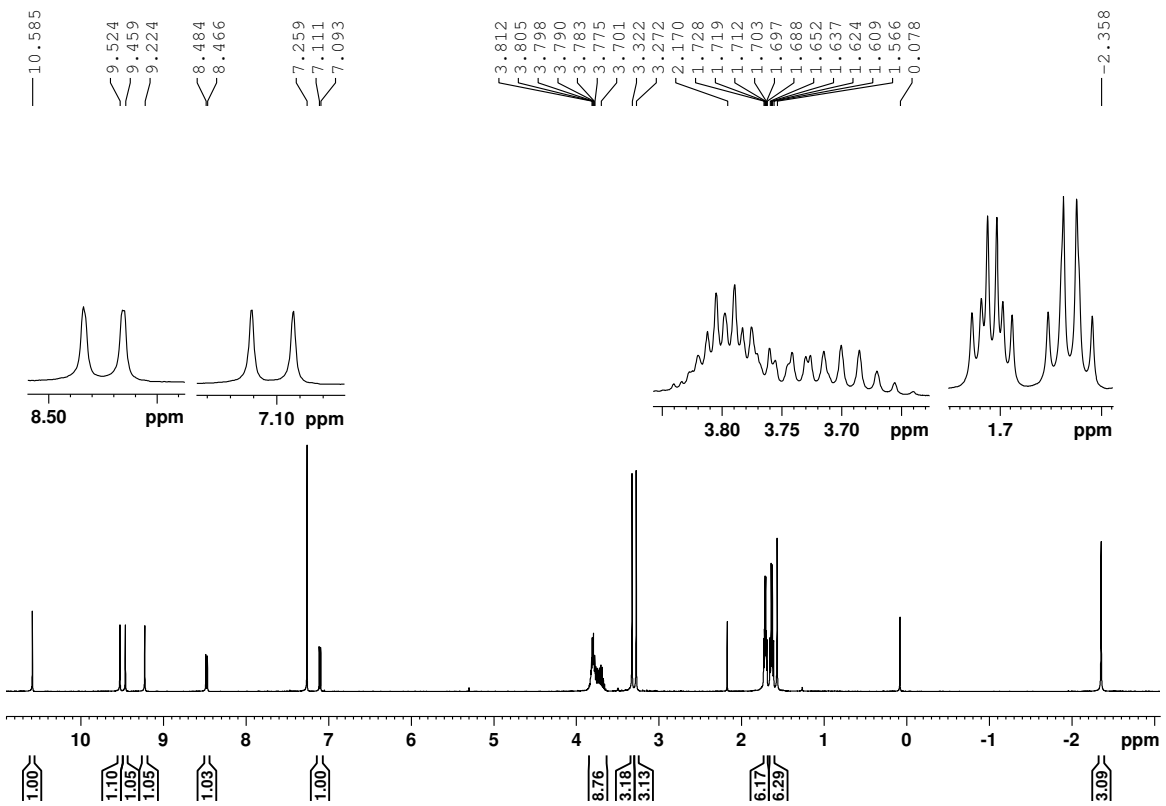

Figure D-56. 500 MHz ^{1}H NMR spectrum of *N*-methyl palladium(II) oxybenziporphyrin **102** in CDCl$_3$

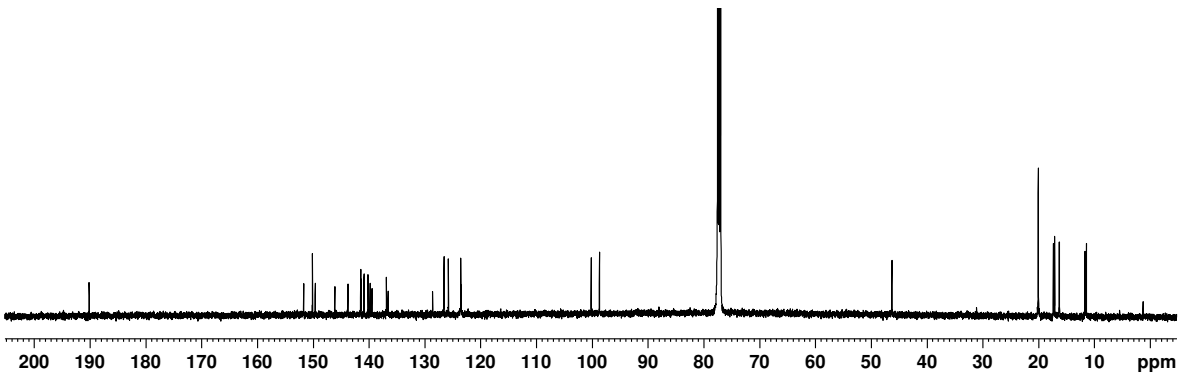

Figure D-57. 125 MHz ^{13}C NMR spectrum of *N*-methyl palladium(II) oxybenziporphyrin **102** in CDCl$_3$

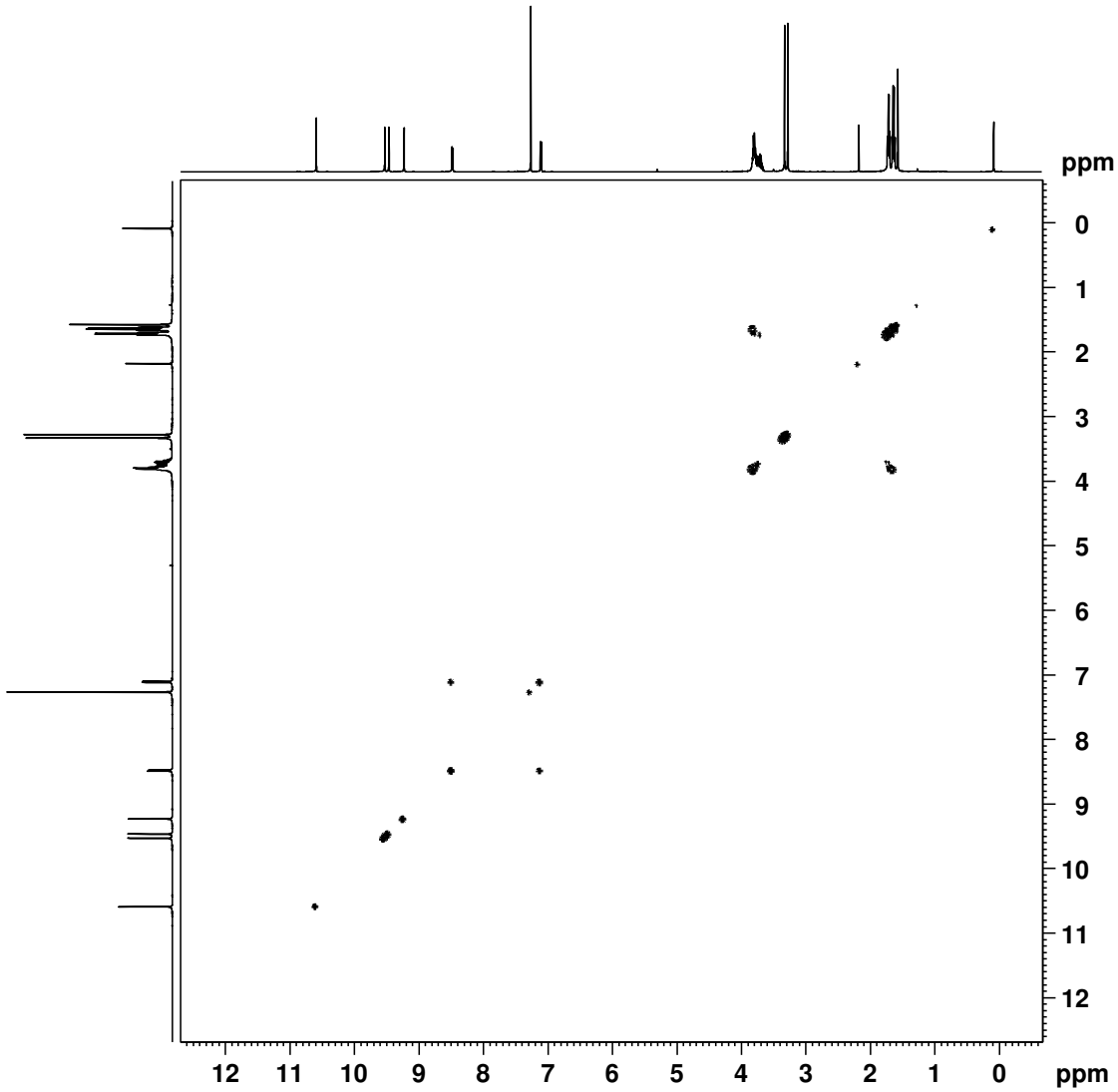

Figure D-58. ^{1}H-^{1}H COSY spectrum of *N*-methyl palladium(II) oxybenziporphyrin **102** in $CDCl_3$

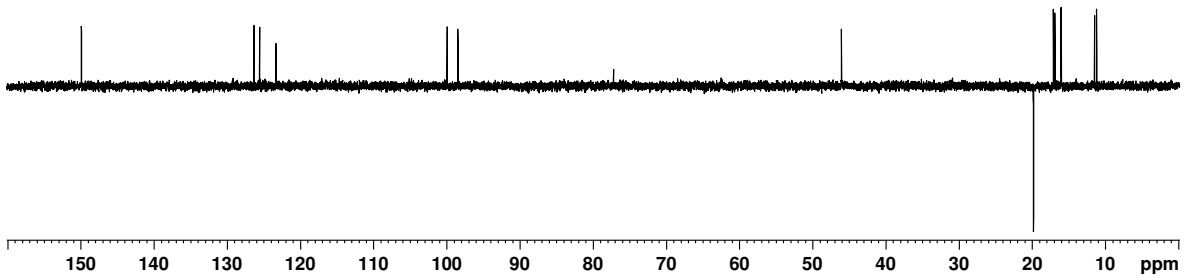

Figure D-59. DEPT-135 NMR spectrum of *N*-methyl palladium(II) oxybenziporphyrin **102** in $CDCl^3$

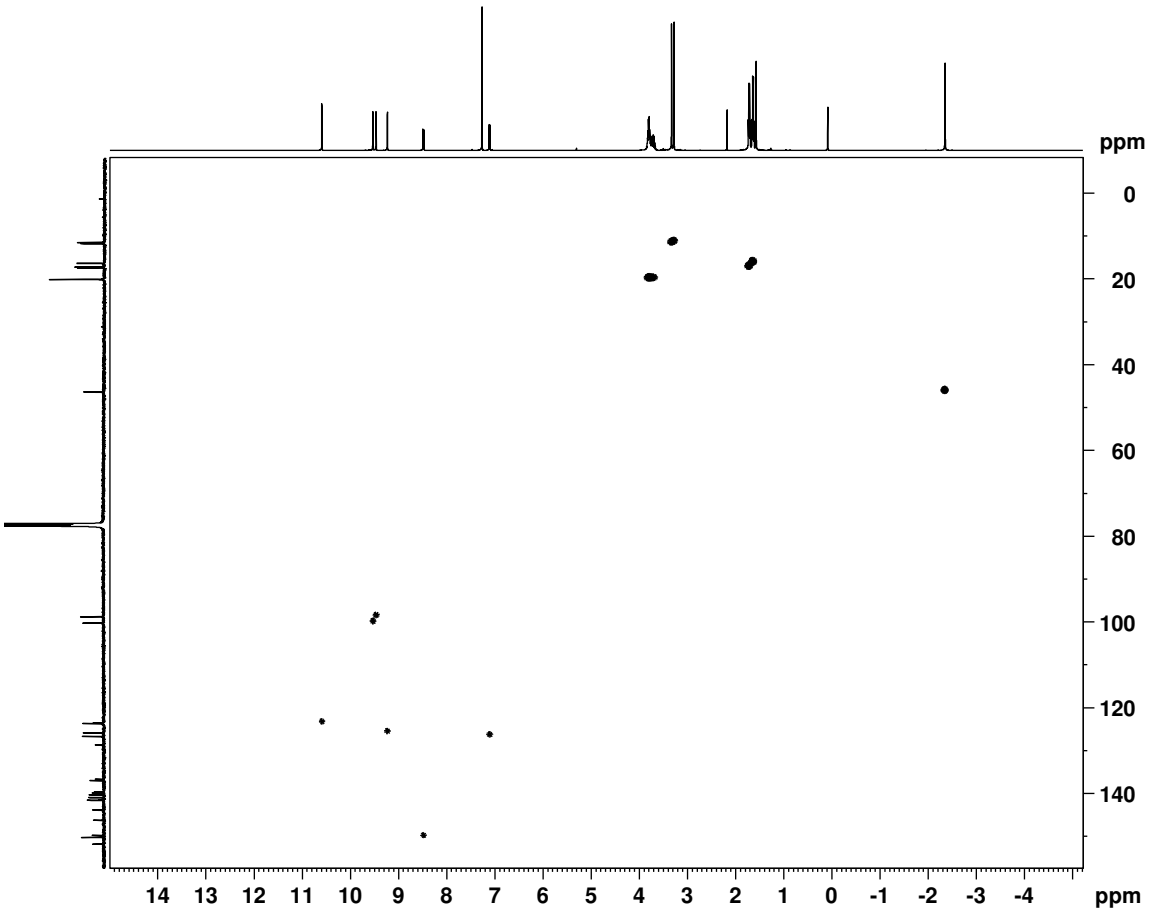

Figure D-60. HSQC NMR spectrum of *N*-methyl palladium(II) oxybenziporphyrin **102** in $CDCl_3$

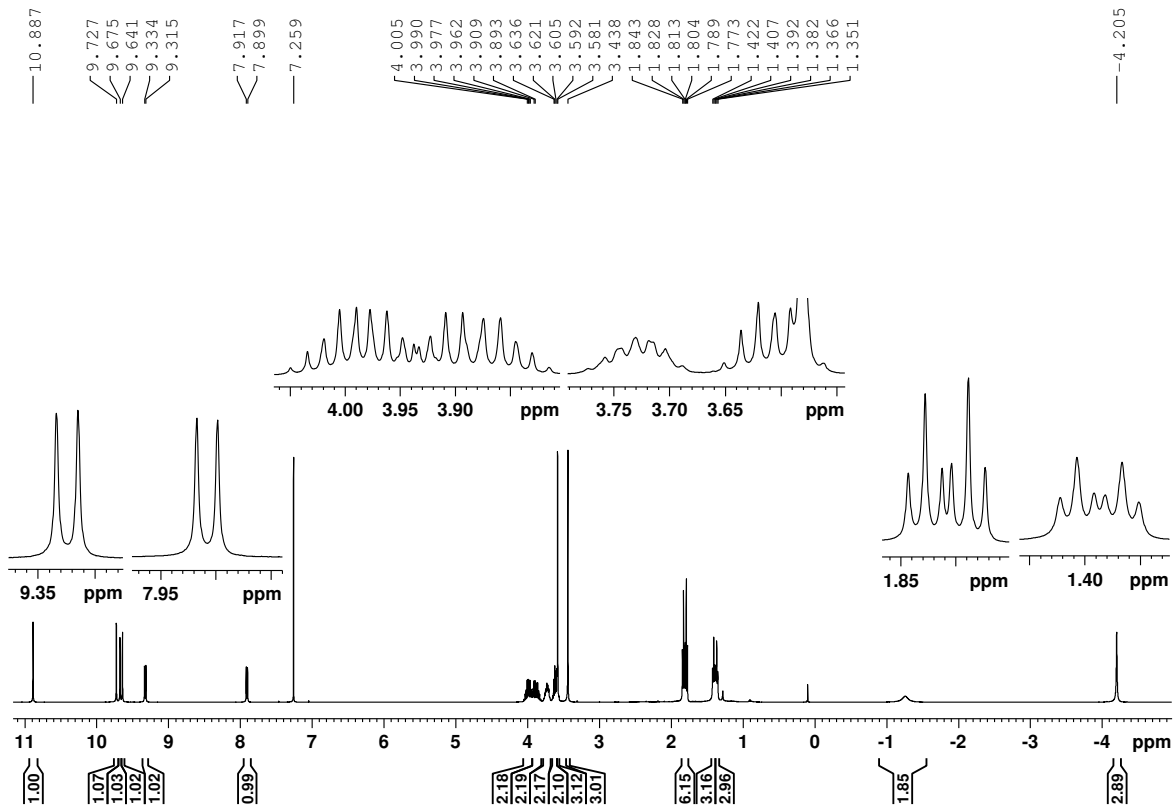

Figure D-61. 500 MHz ^{1}H NMR spectrum of *N*-methyl oxypyriporphyrin **100b** in $CDCl_3$

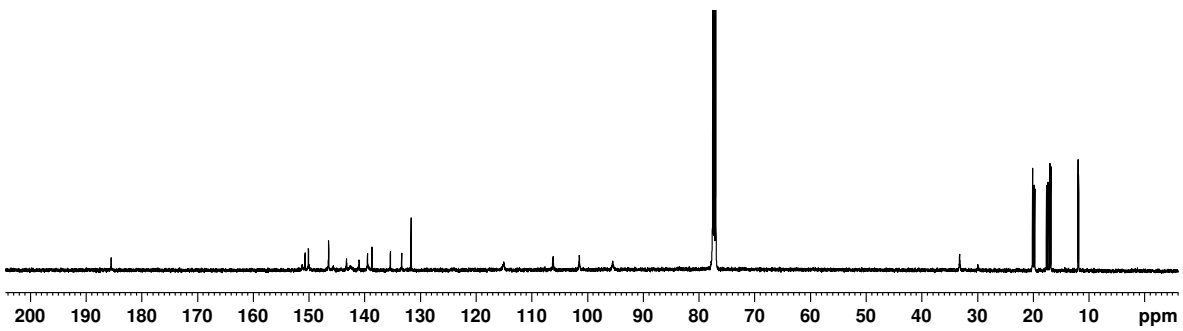

Figure D-62. 125 MHz ^{13}C NMR spectrum of *N*-methyl oxypyriporphyrin **100b** in $CDCl_3$

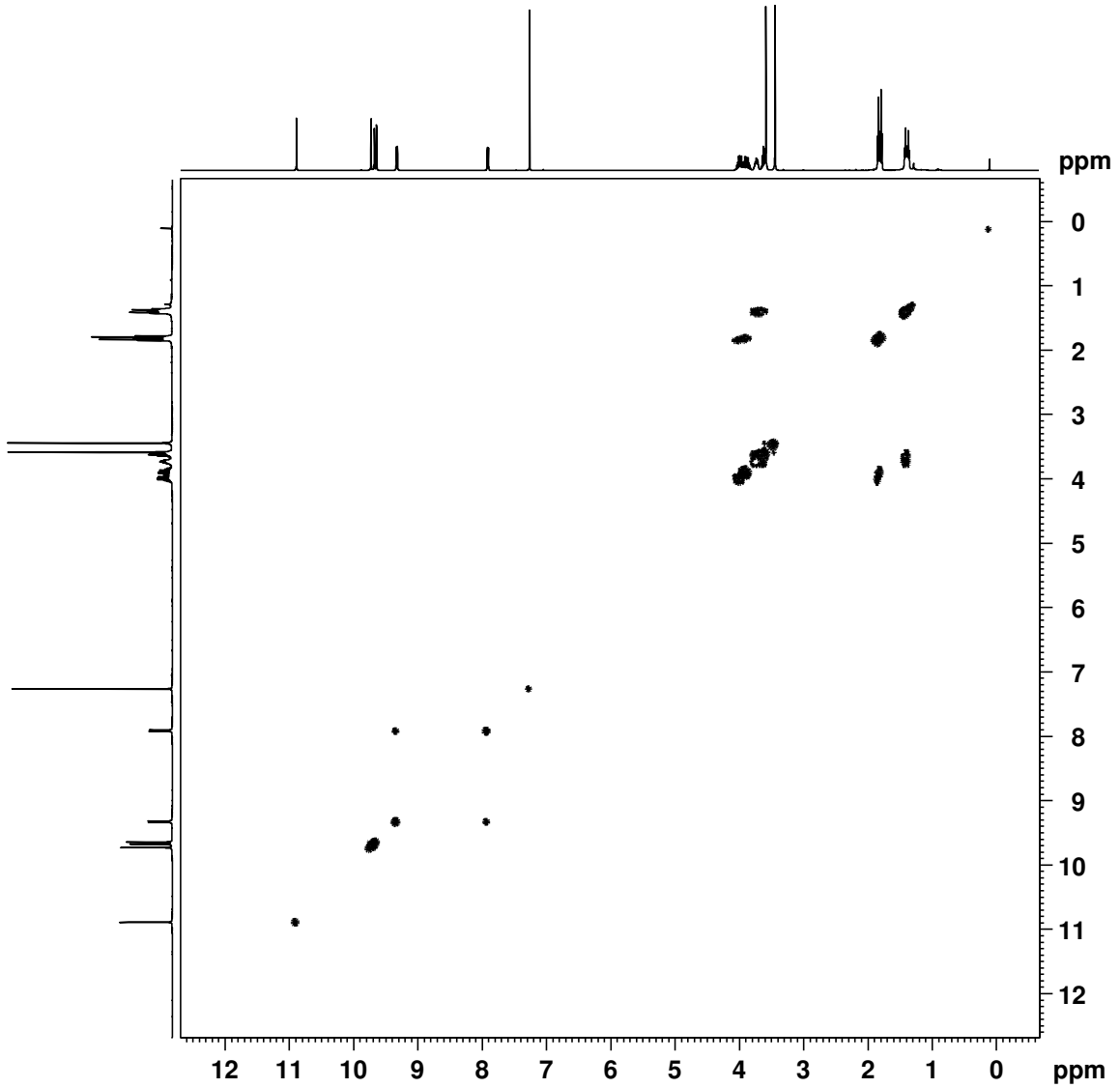

Figure D-63. ^{1}H-^{1}H COSY NMR spectrum of *N*-methyl oxypyriporphyrin **100b** in $CDCl_3$

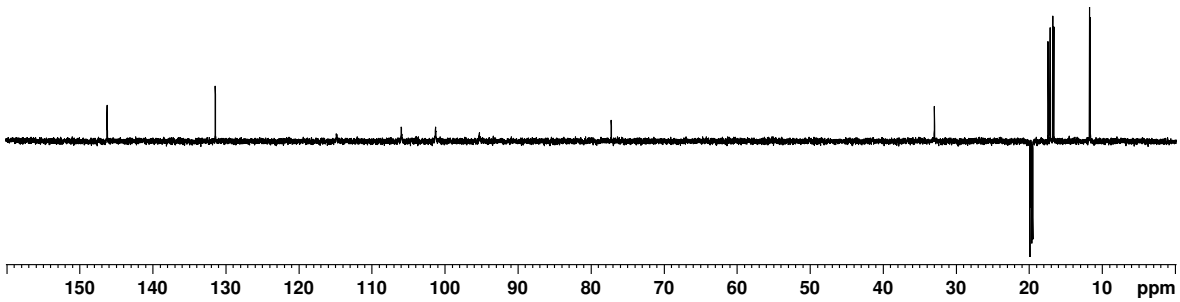

Figure D-64. DEPT-135 NMR spectrum of *N*-methyl oxypyriporphyrin **100b** in $CDCl_3$

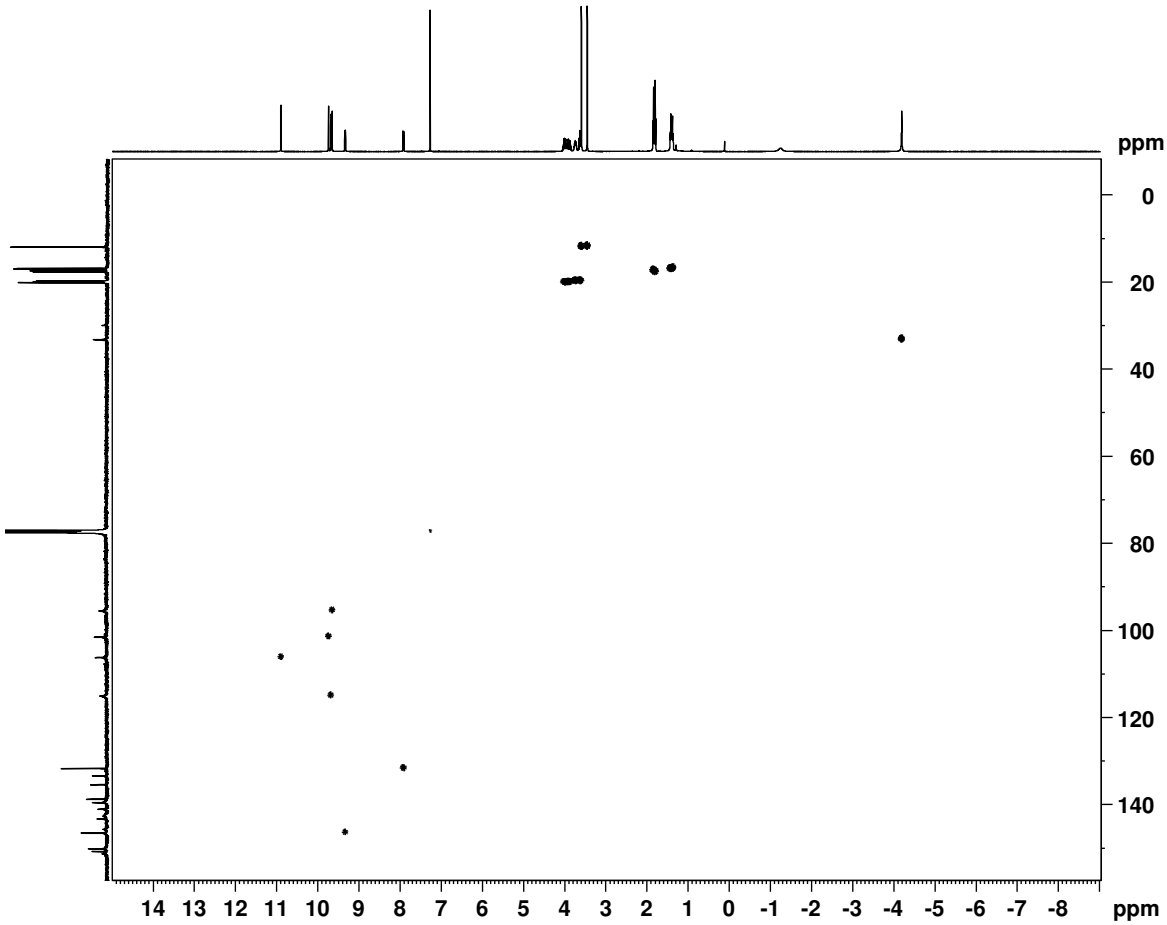

Figure D-65. HSQC NMR spectrum of *N*-methyl oxypyriporphyrin **100b** in $CDCl_3$

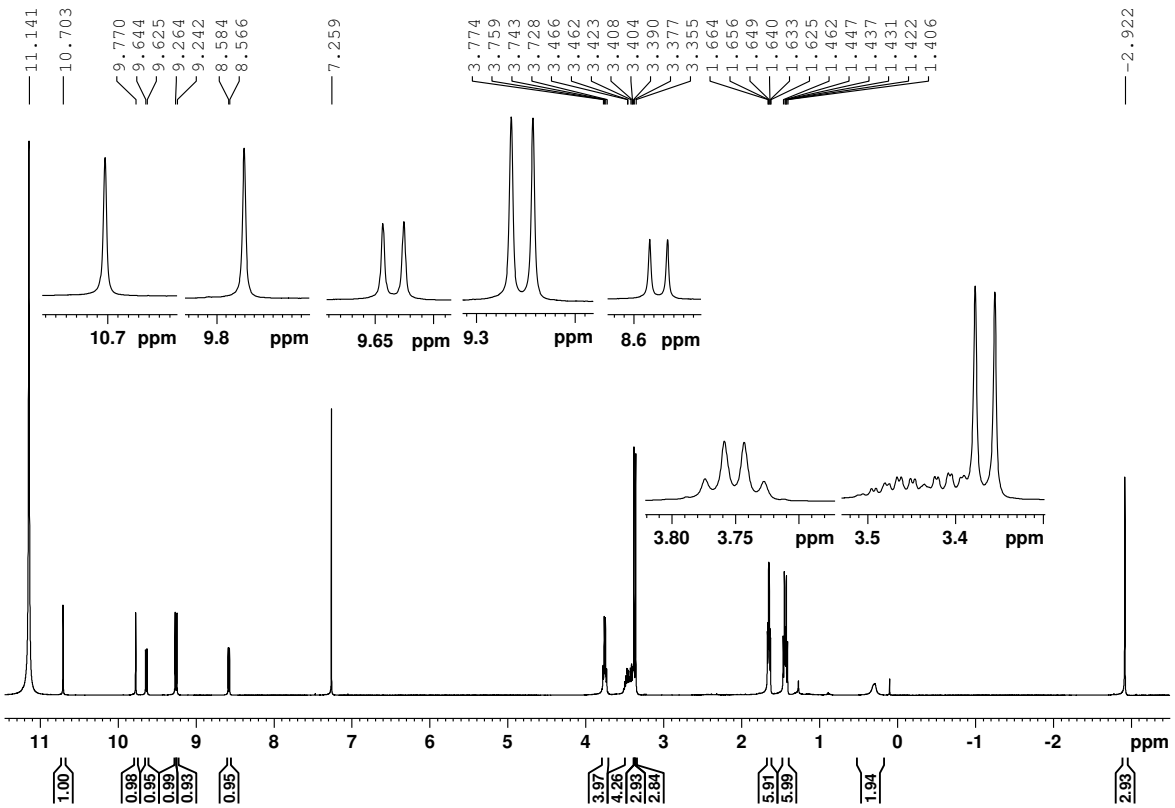

Figure D-66. 500 MHz ^{1}H NMR spectrum of *N*-methyl oxypyriporphyrin **100b** in TFA-CDCl$_3$

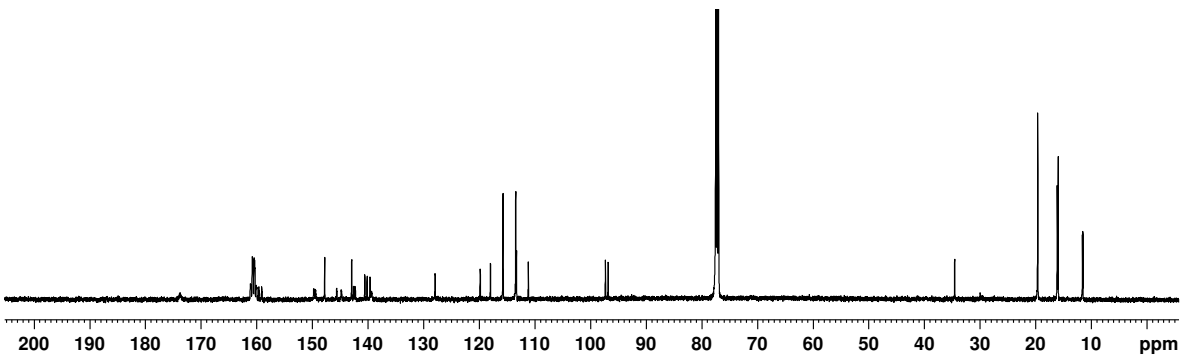

Figure D-67. 125 MHz ^{13}C NMR spectrum of *N*-methyl oxypyriporphyrin **100b** in TFA-CDCl$_3$

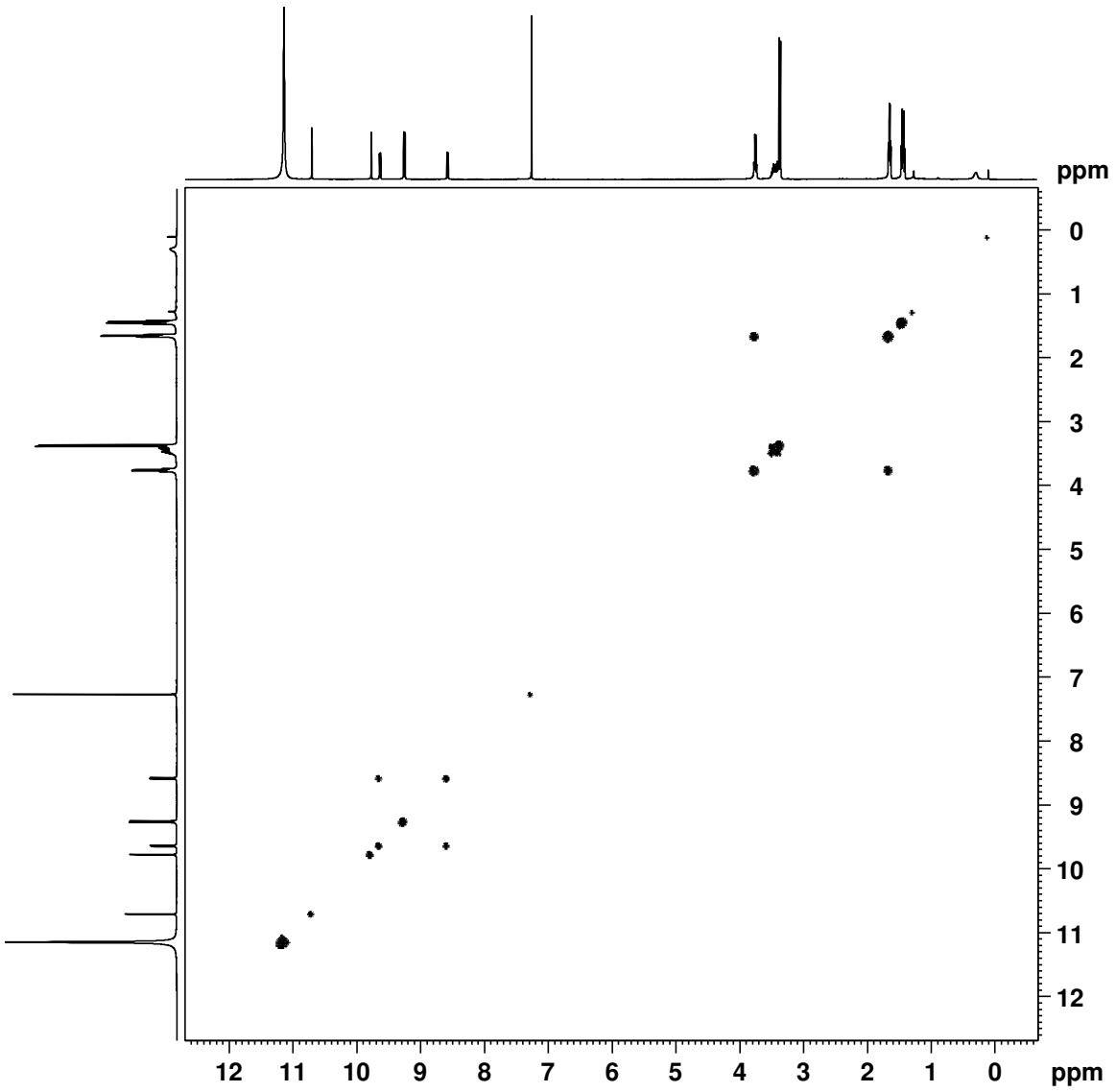

Figure D-68. ^{1}H-^{1}H COSY NMR spectrum of *N*-methyl oxypyriporphyrin **100b** in TFA-$CDCl_3$

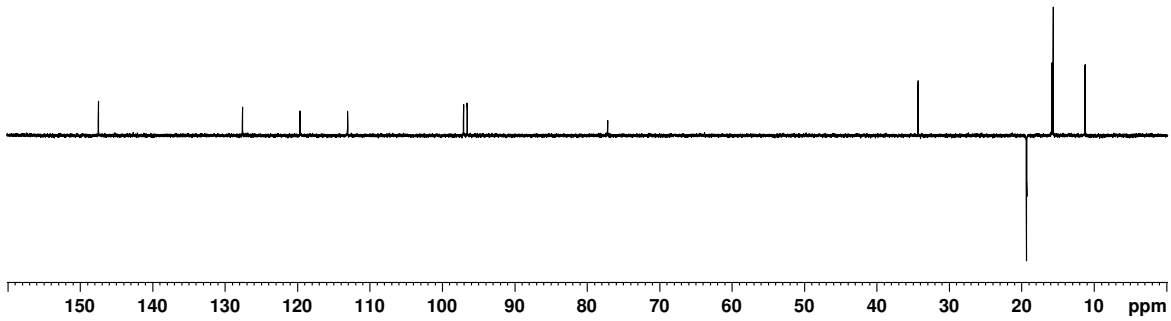

Figure D-69. DEPT-135 NMR spectrum of *N*-methyl oxypyriporphyrin **100b** in TFA-$CDCl_3$

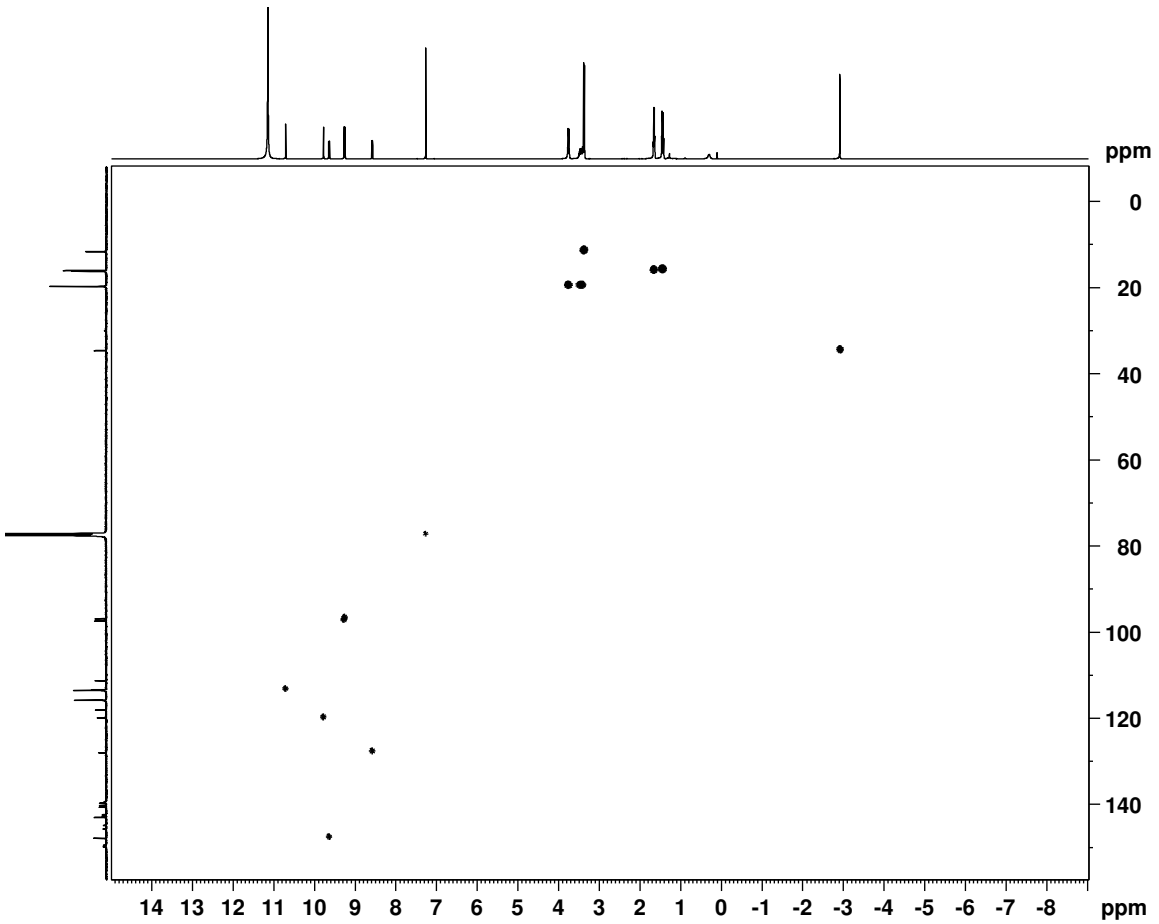

Figure D-70. HSQC NMR spectrum of *N*-methyl oxypyriporphyrin **100b** in TFA-$CDCl_3$

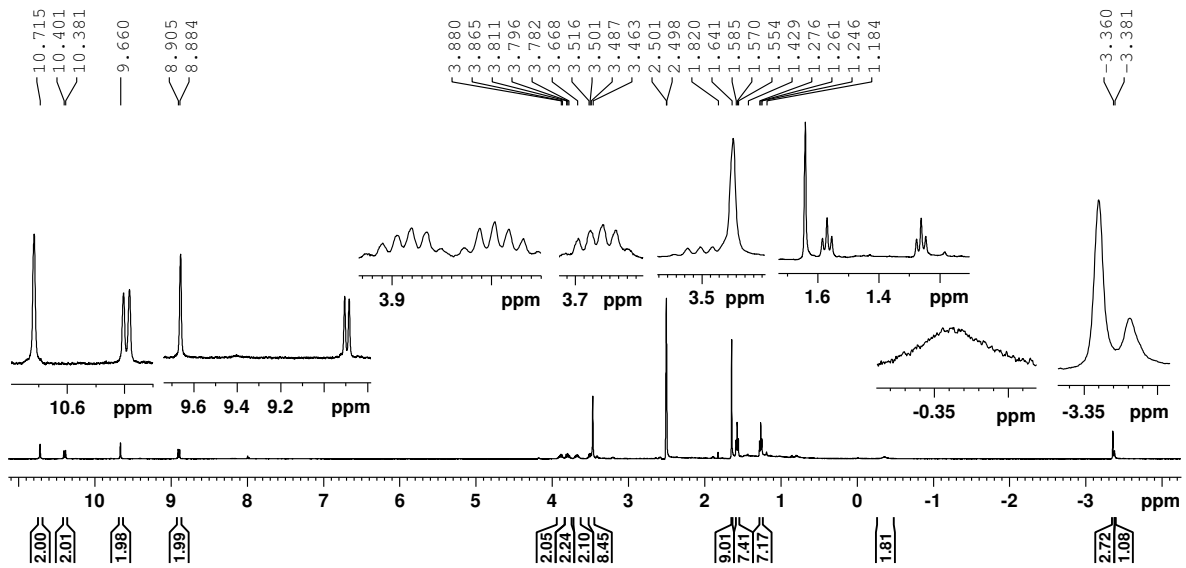

Figure D-71. 500 MHz ^{1}H NMR spectrum of *N*-methyl *tert*-butyl azuliporphyrin **103**H_2^{2+} in TFA-*d*^{6}-DMSO

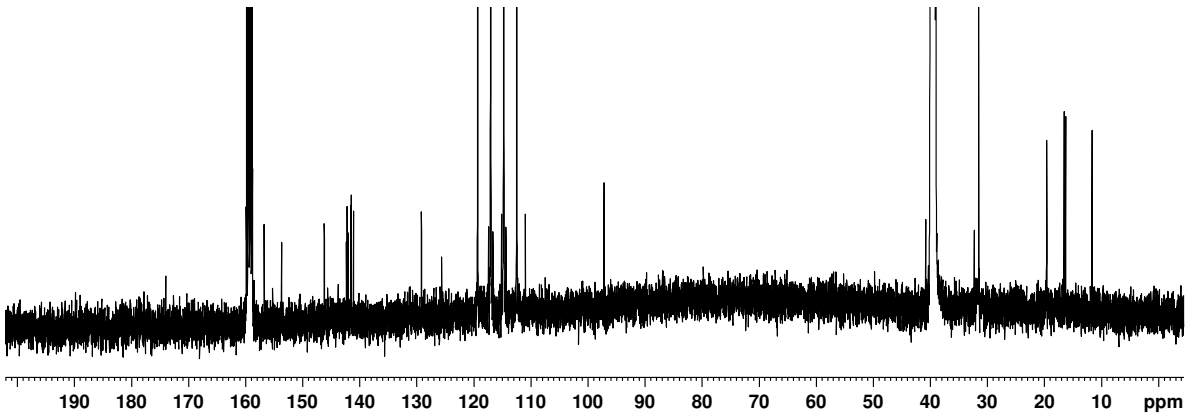

Figure D-72. 125 MHz ^{13}C NMR spectrum of *N*-methyl *tert*-butyl azuliporphyrin **103**H_2^{2+} in TFA-*d*^{6}-DMSO

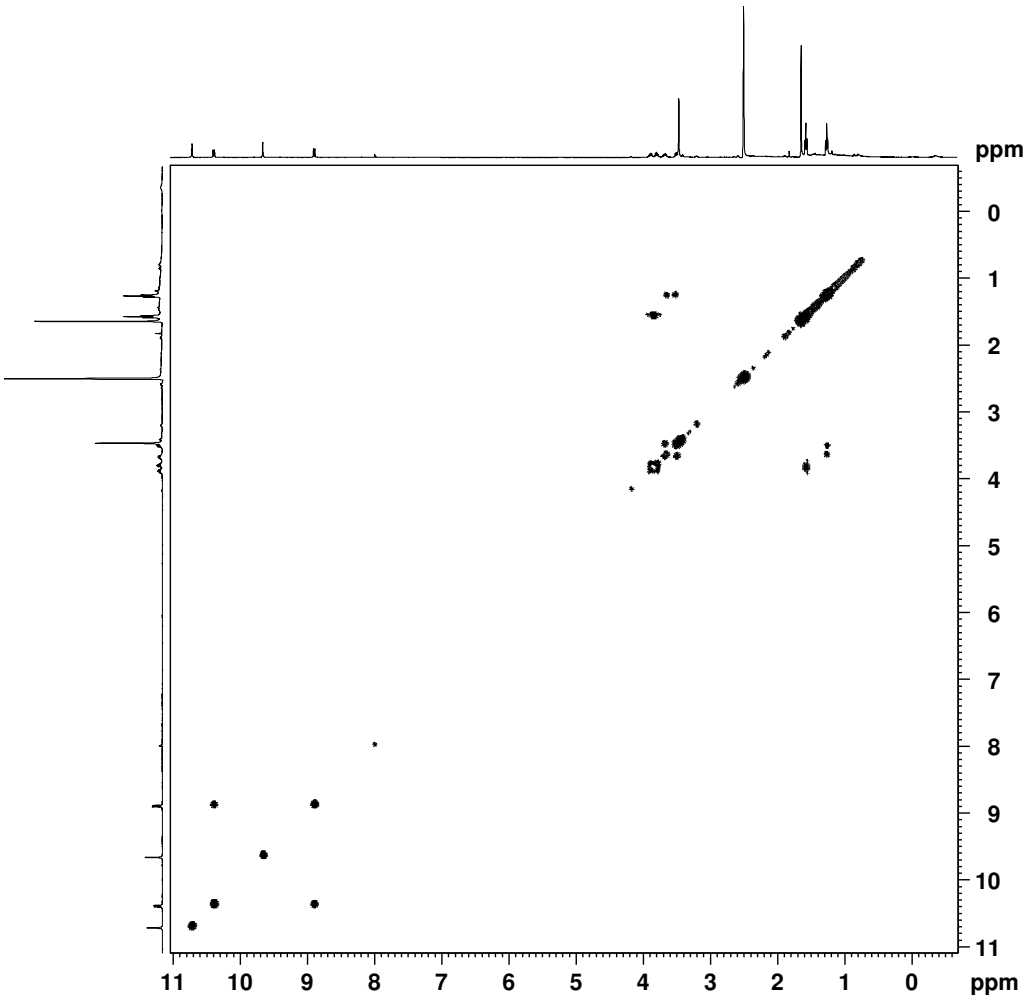

Figure D-73. ^{1}H-^{1}H COSY NMR spectrum of *N*-methyl *tert*-butyl azuliporphyrin **103**H_2^{2+} in TFA-*d*6-DMSO

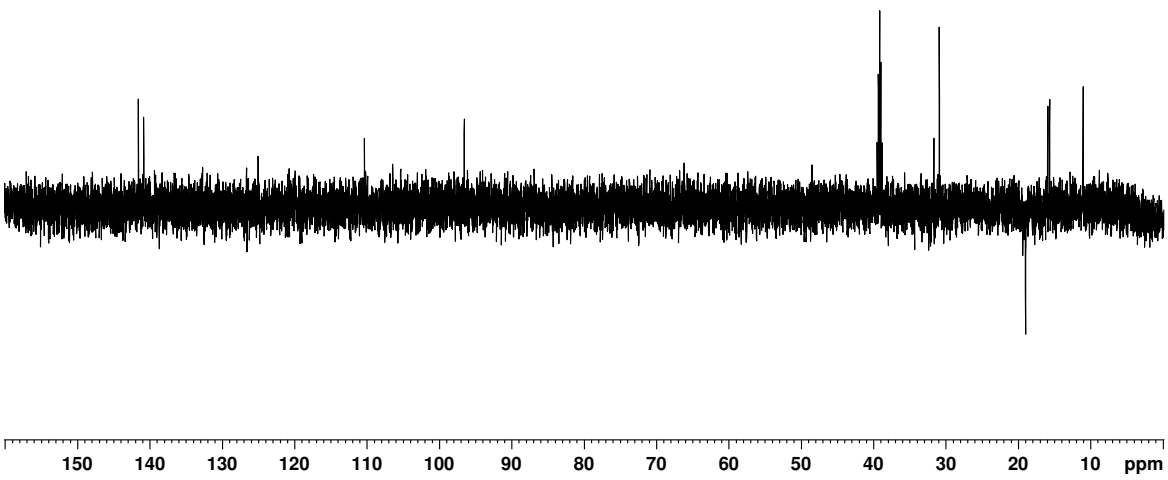

Figure D-74. DEPT 135 NMR spectrum of *N*-methyl *tert*-butyl azuliporphyrin **103**H_2^{2+} in TFA-*d*6-DMSO

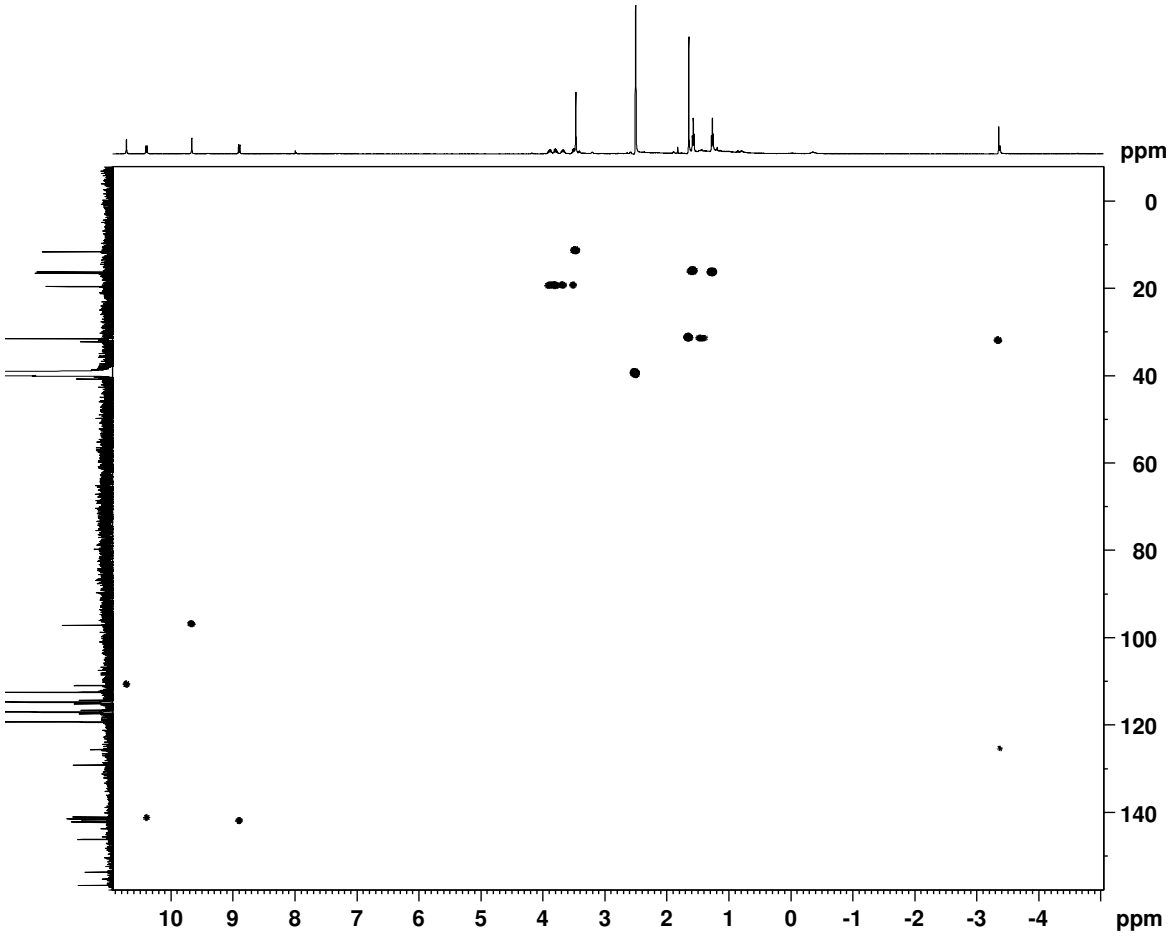

Figure D-75. HSQC NMR spectrum of *N*-methyl *tert*-butyl azuliporphyrin **103**H_2^{2+} in TFA-*d*^{6}-DMSO

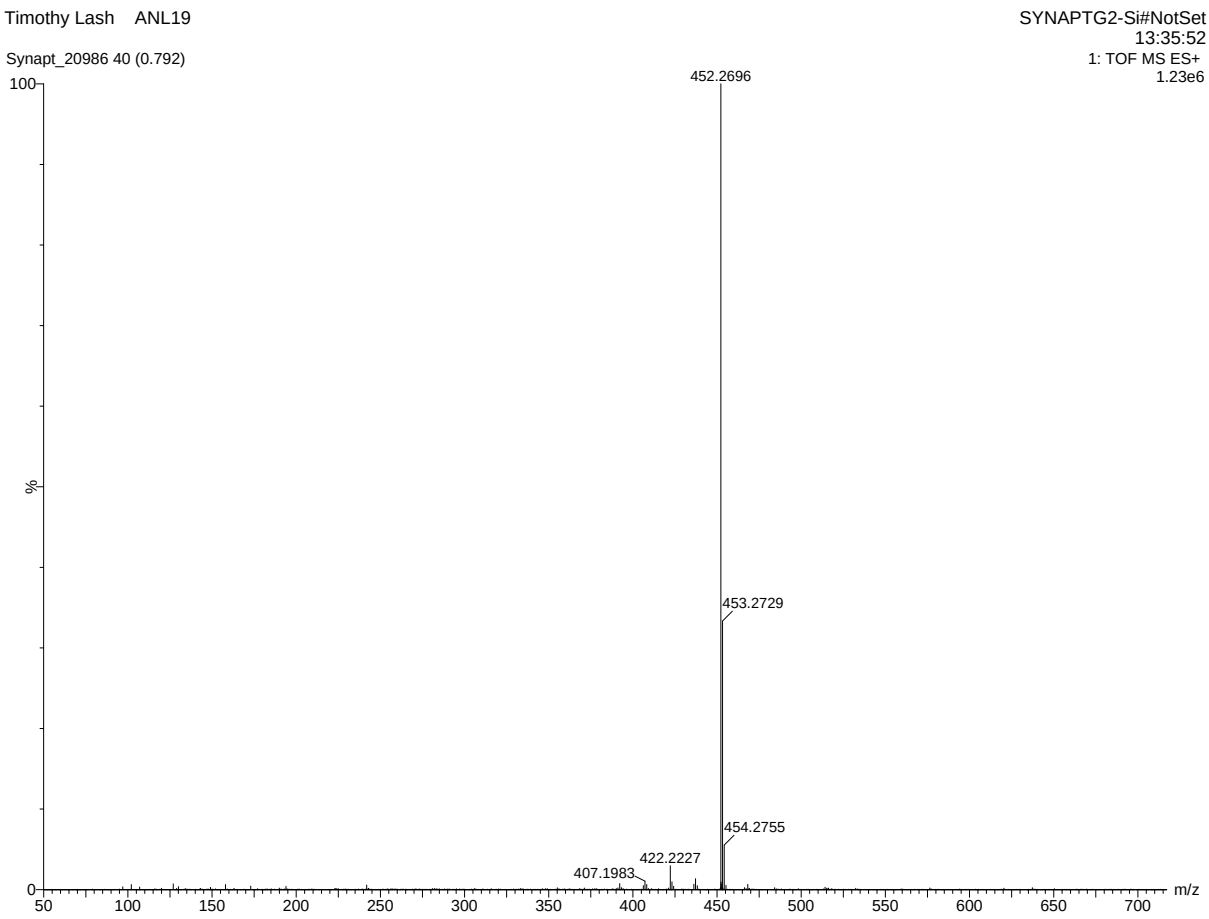

Figure D-76. ESI MS of 21-oxaporphyrin **96a**

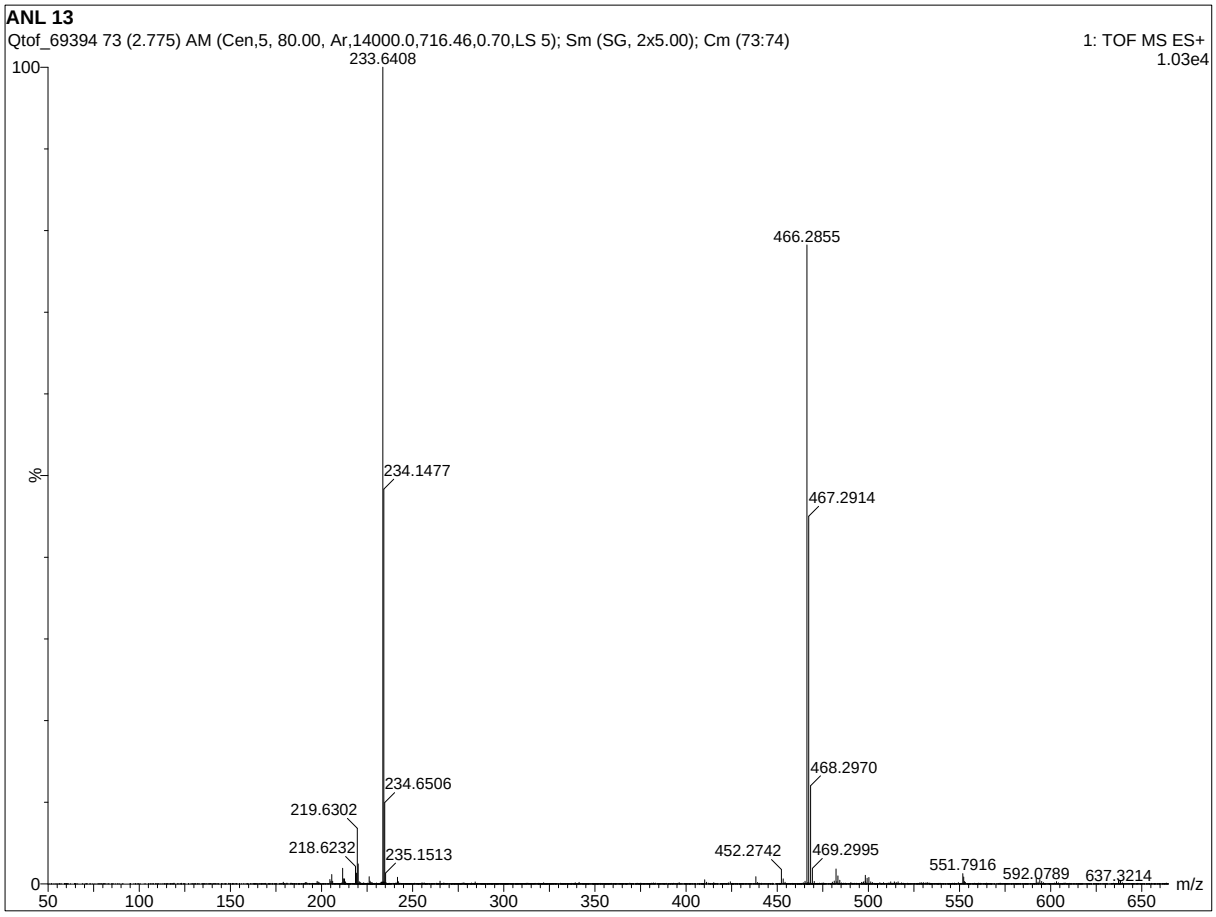

Figure D-77. ESI MS of *N*-methyl oxaporphyrin **96b**

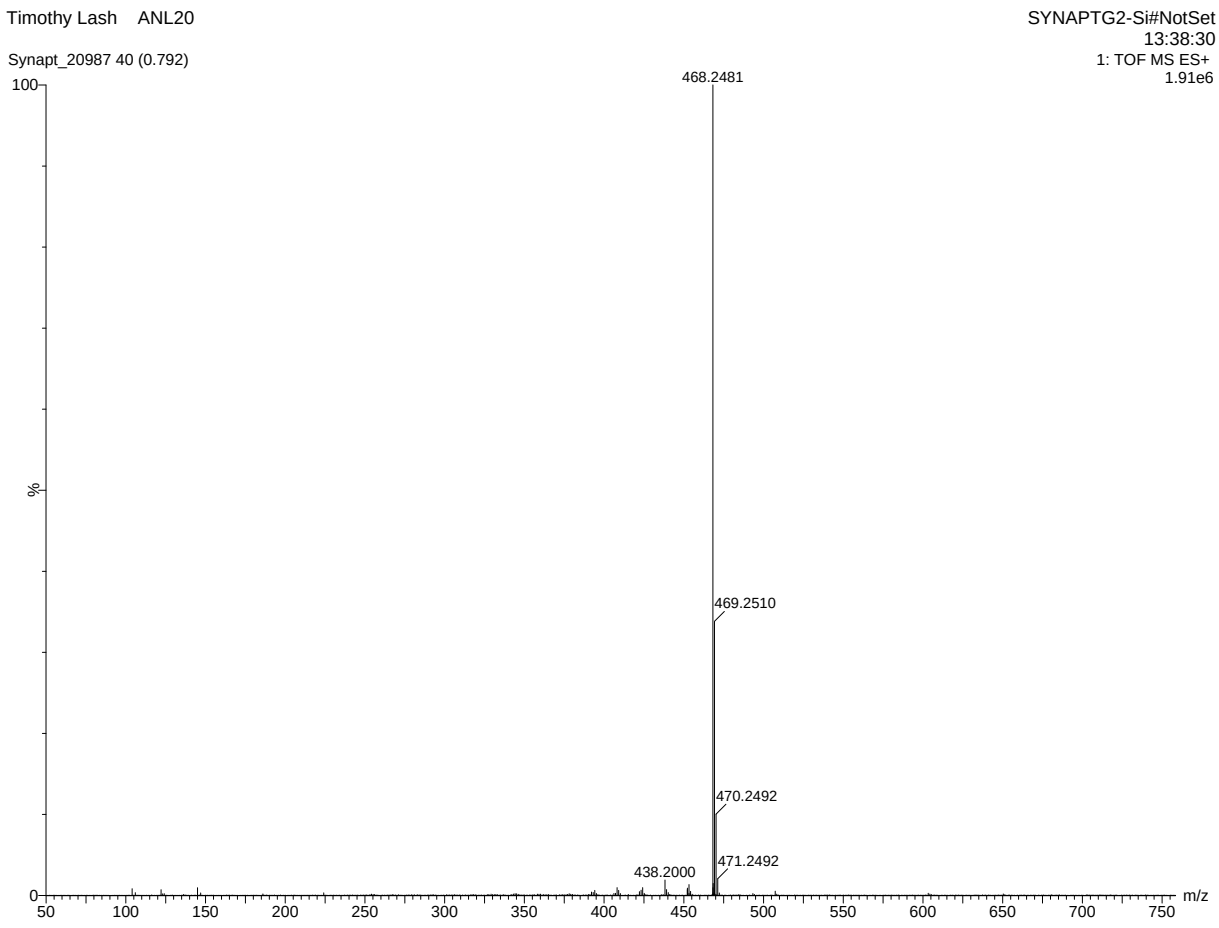

Figure D-78. ESI MS of 21-thiaporphyrin **97a**

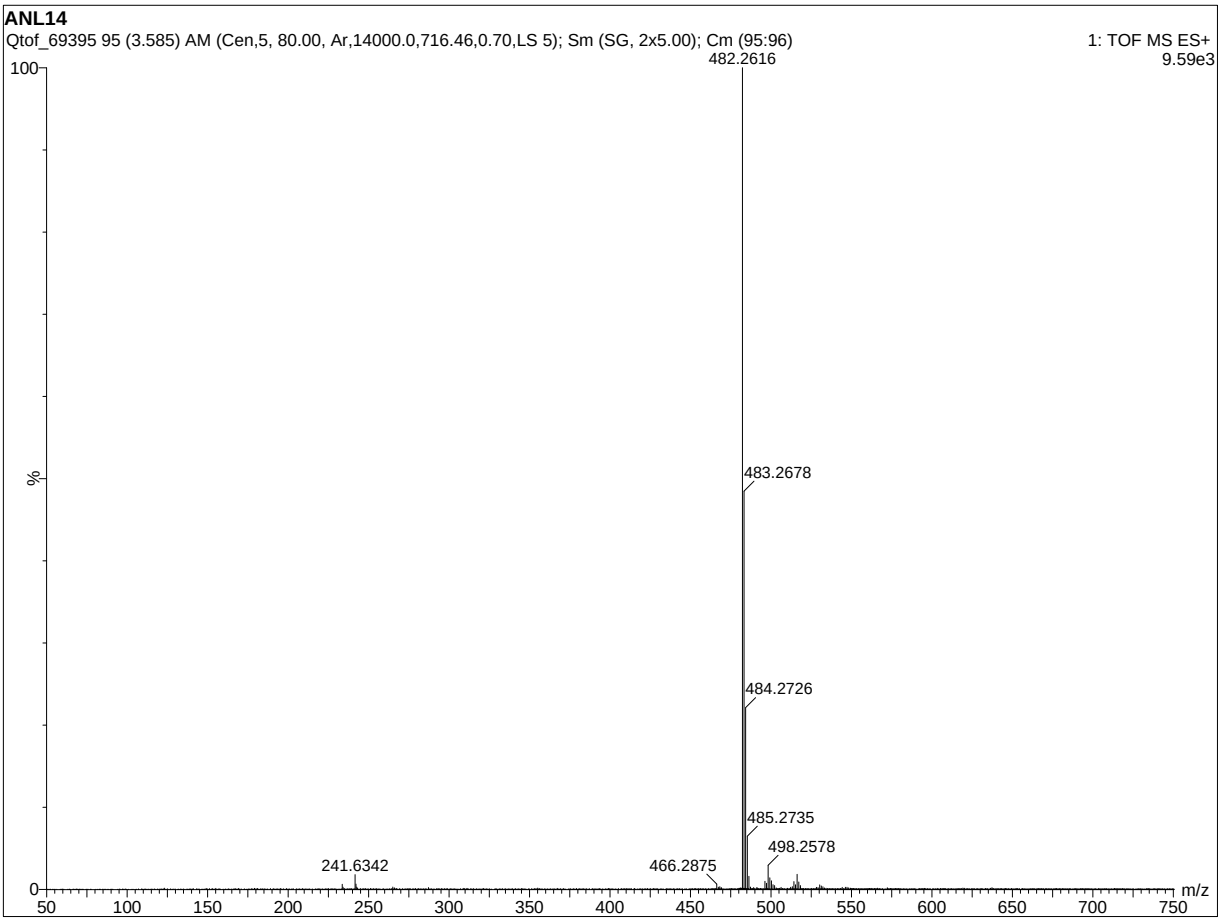

Figure D-79. ESI MS of *N*-methyl thiaporphyrin **97b**

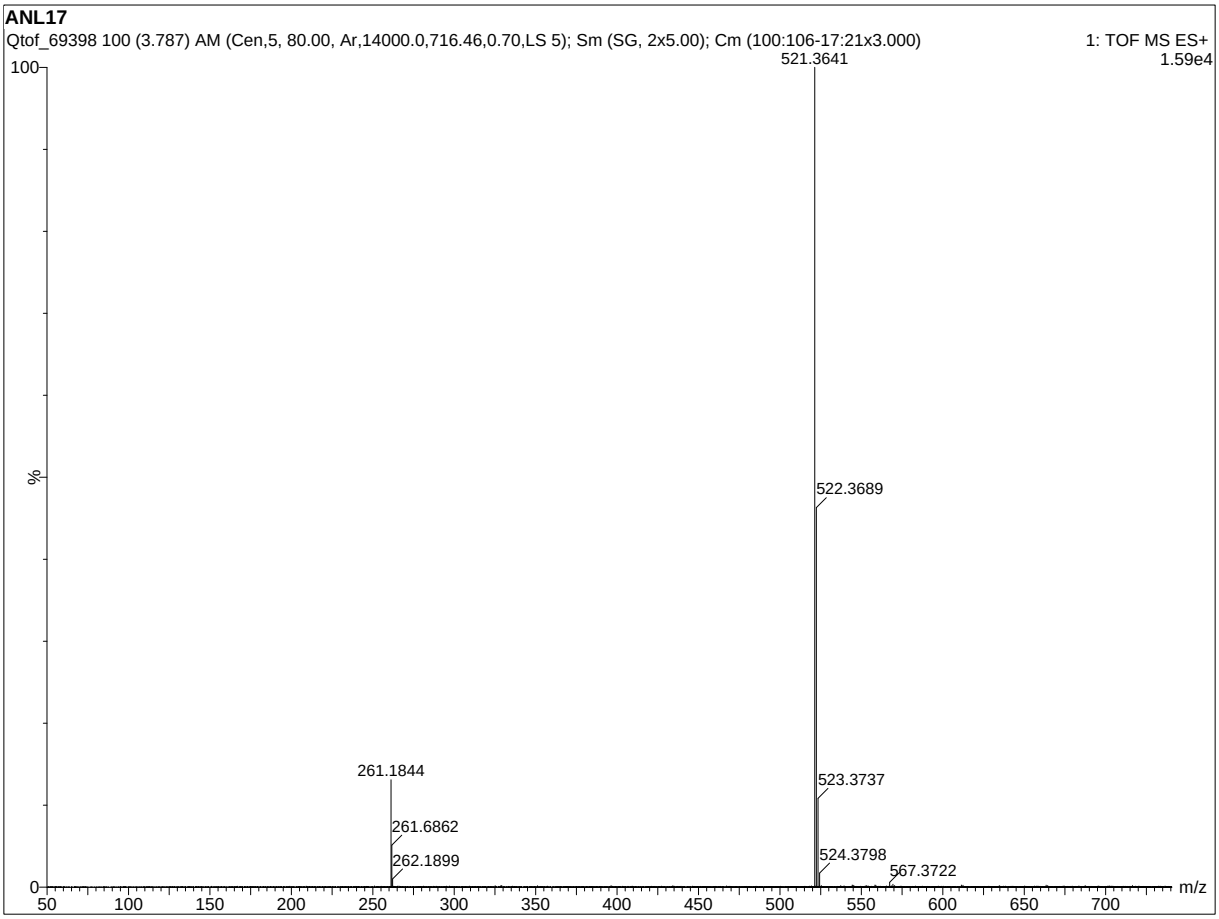

Figure D-80. ESI MS of *N*-methyl porphyrin **99b**

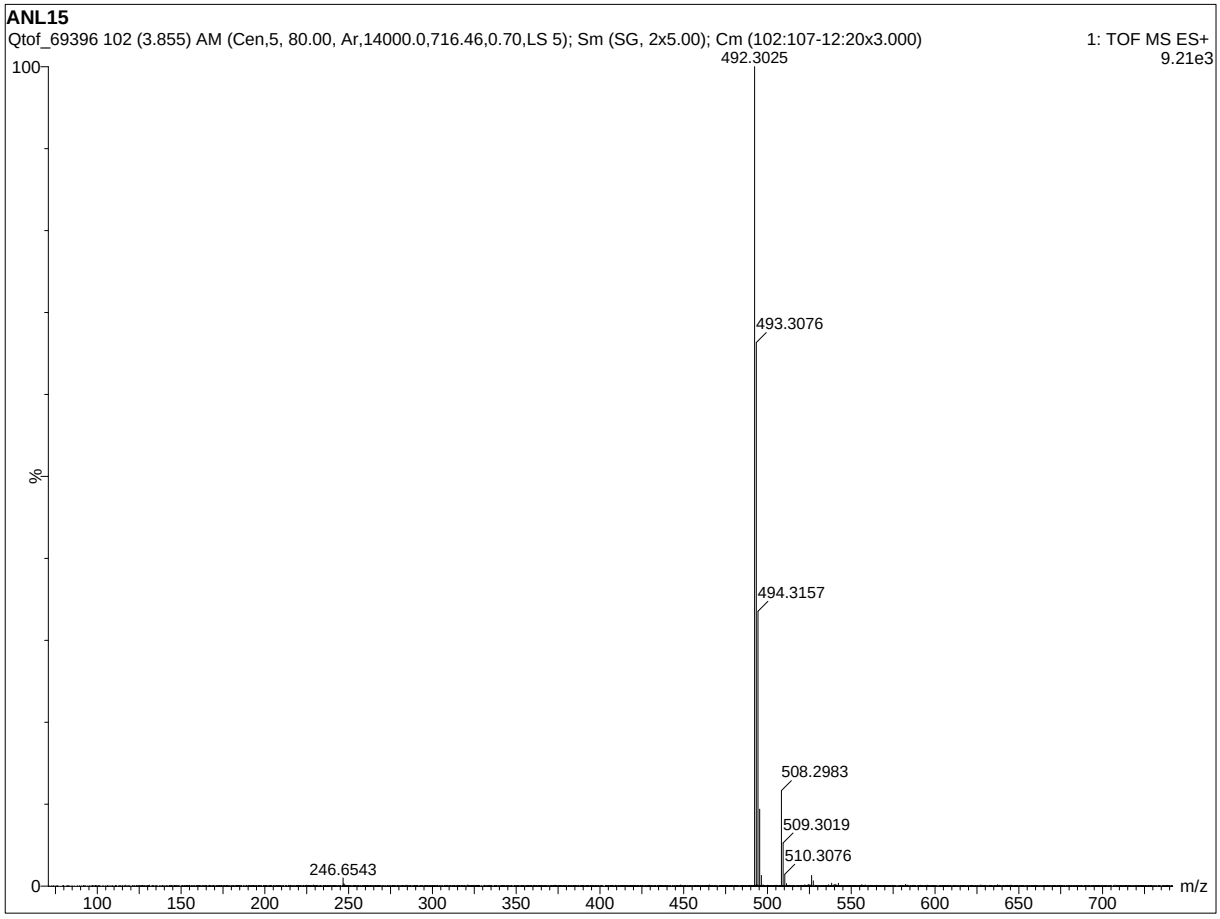

Figure D-81. ESI MS of *N*-methyl oxybenziporphyrin **100a**

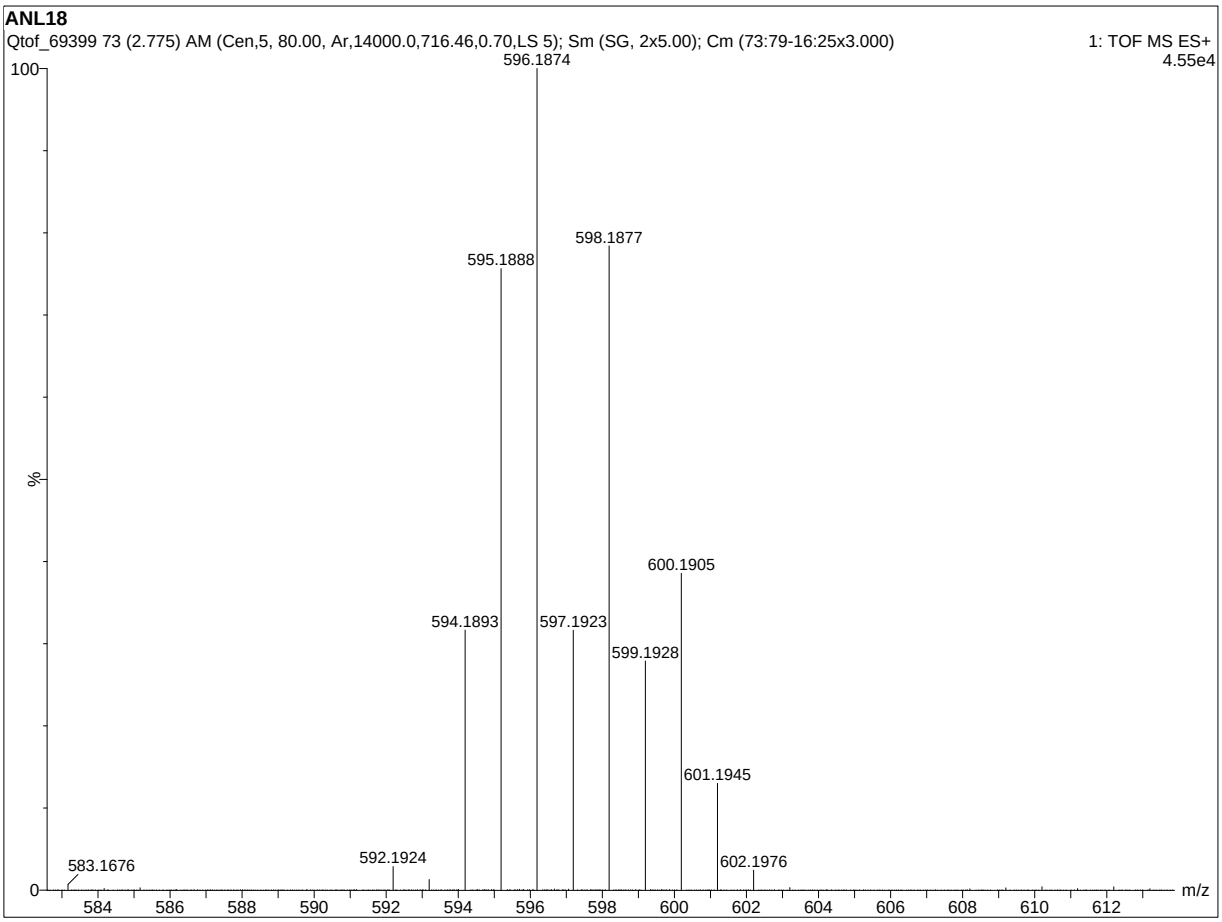

Figure D-82. ESI MS of *N*-methyl palladium(II) oxybenziporphyrin **102**

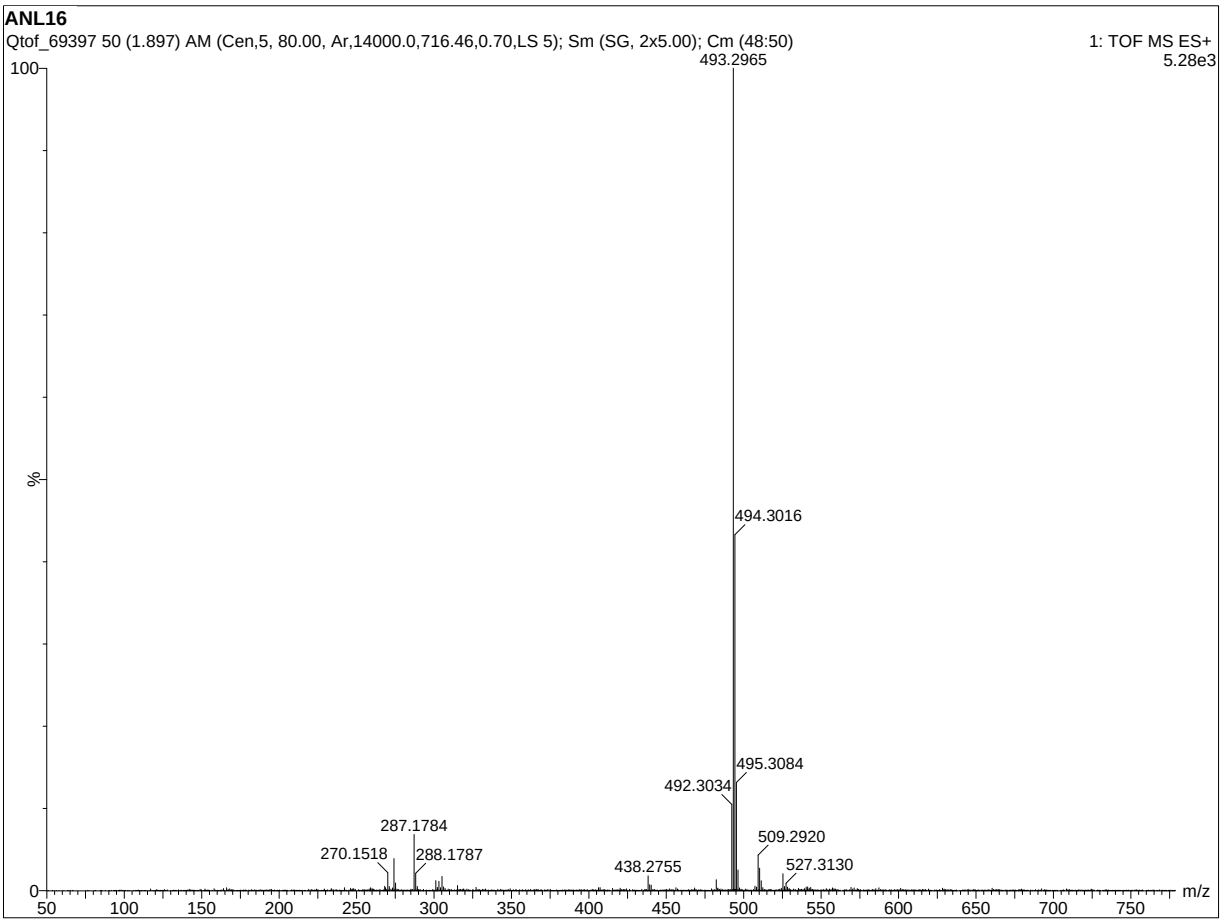

Figure D-83. ESI MS of *N*-methyl oxypyriporphyrin **100b**

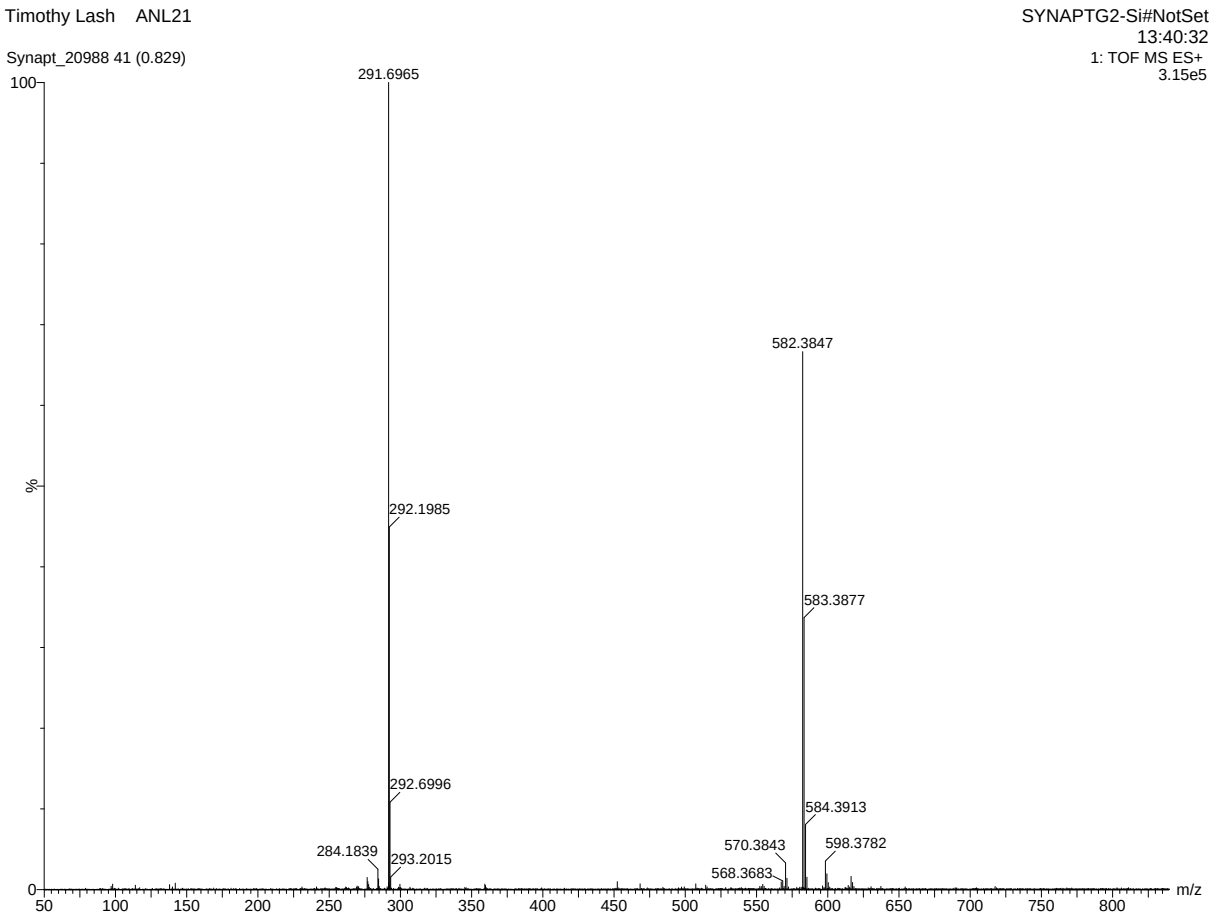

Figure D-84. ESI MS of *N*-methyl *tert*-Butyl azuliporphyrin **103**H_2^{2+}

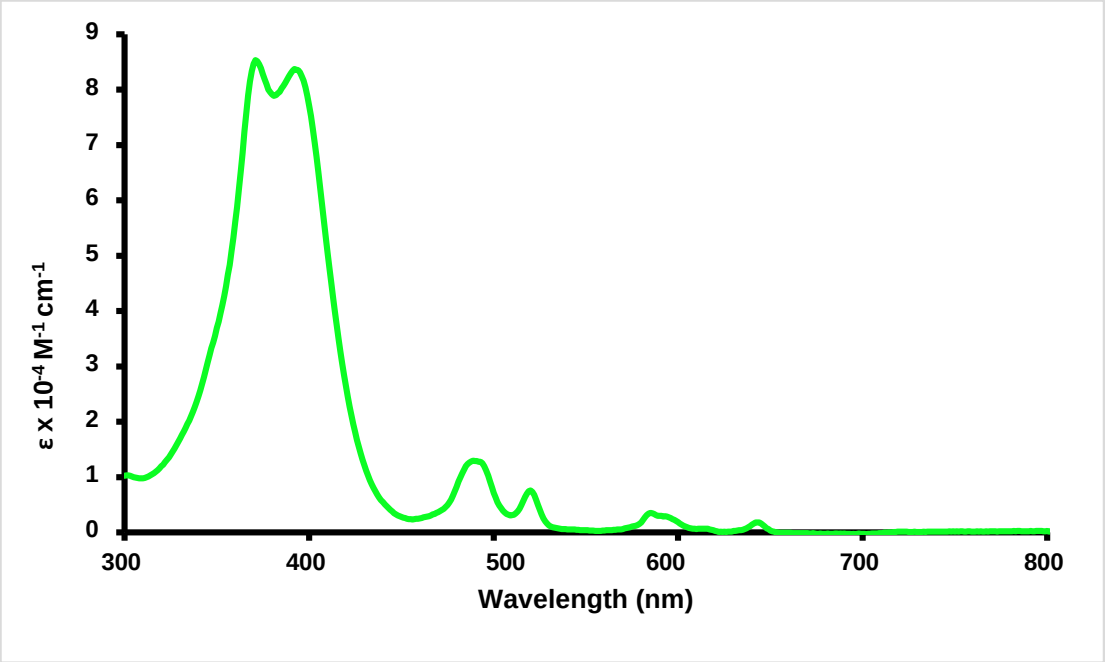

Figure D-85. UV-Vis spectrum of 21-oxaporphyrin **96a** in 1% triethylamine-dichloromethane

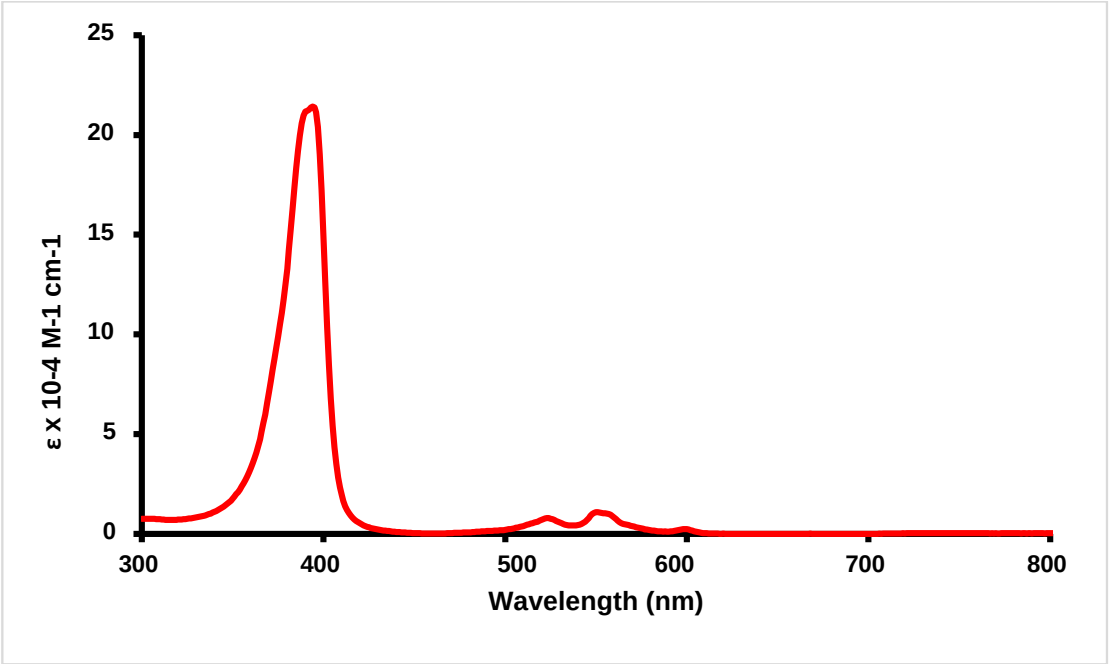

Figure D-86. UV-Vis spectrum of 21-oxaporphyrin **96a** in 1% TFA-dichloromethane

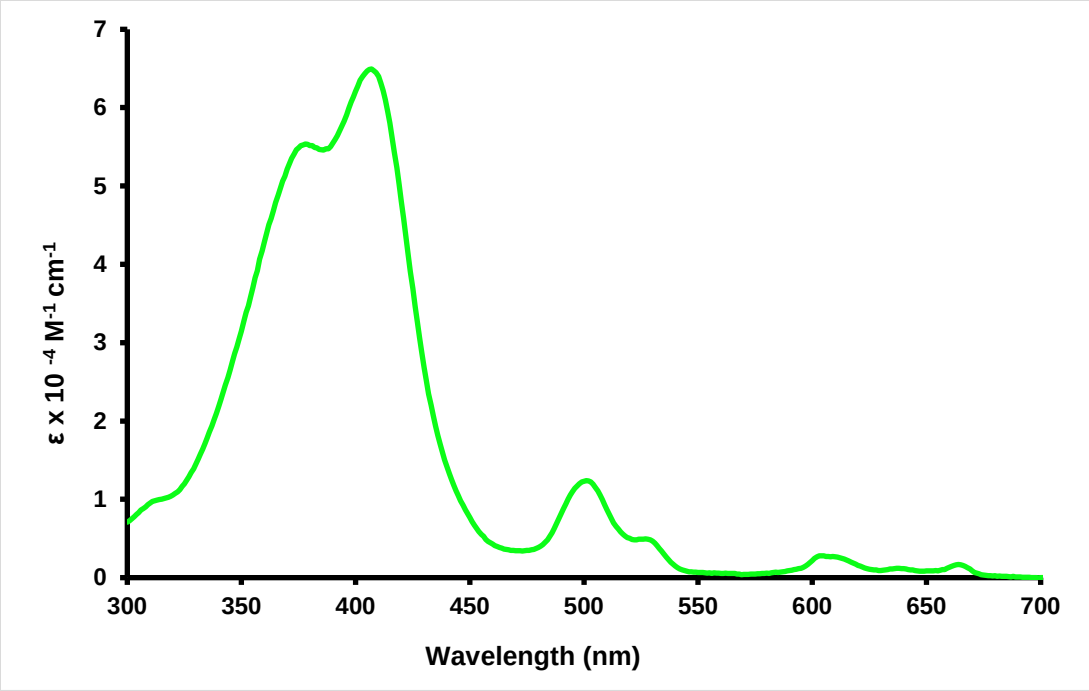

Figure D-87. UV-Vis spectrum of *N*-methyl oxaporphyrin **96b** in 1% triethylamine-dichloromethane.

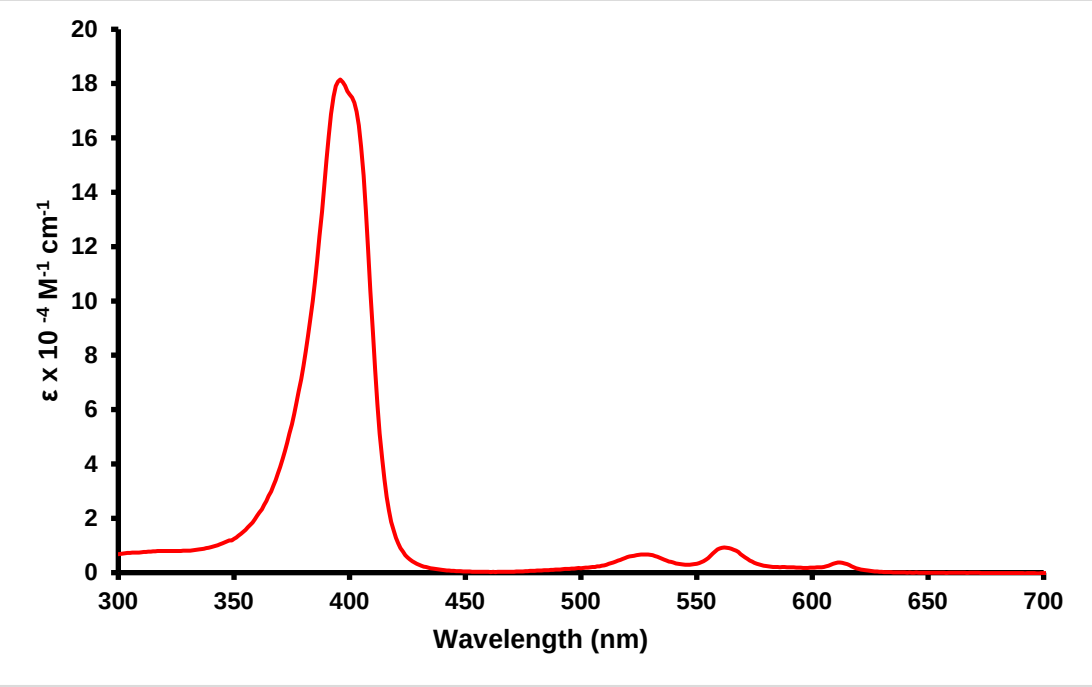

Figure D-88. UV-Vis spectrum of *N*-methyl oxaporphyrin **96b** in 1% TFA-dichloromethane.

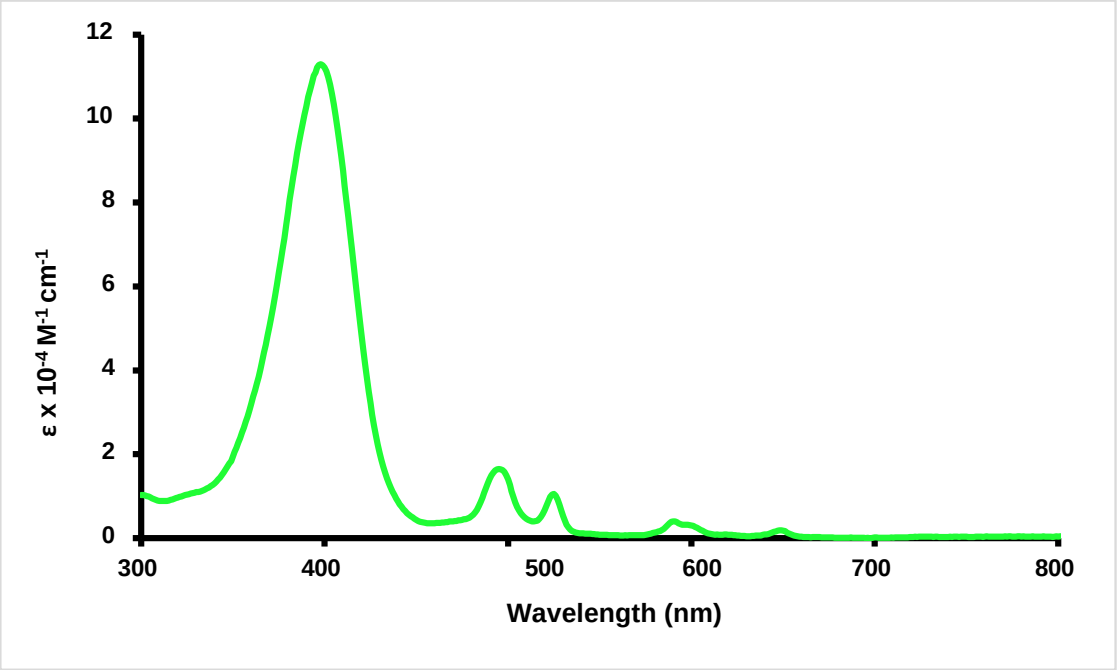

Figure D-89. UV-Vis spectrum of 21-thiaporphyrin **97a** in 1% triethylamine-dichloromethane

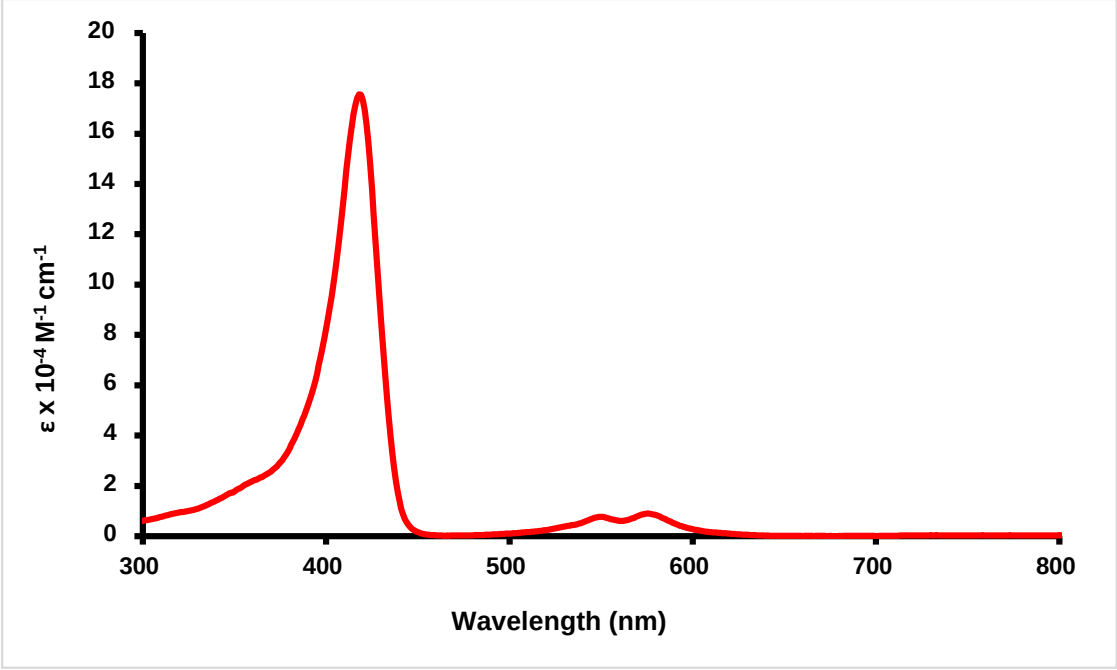

Figure D-90. UV-Vis spectrum of 21-thiaporphyrin **97a** in 1% TFA-dichloromethane

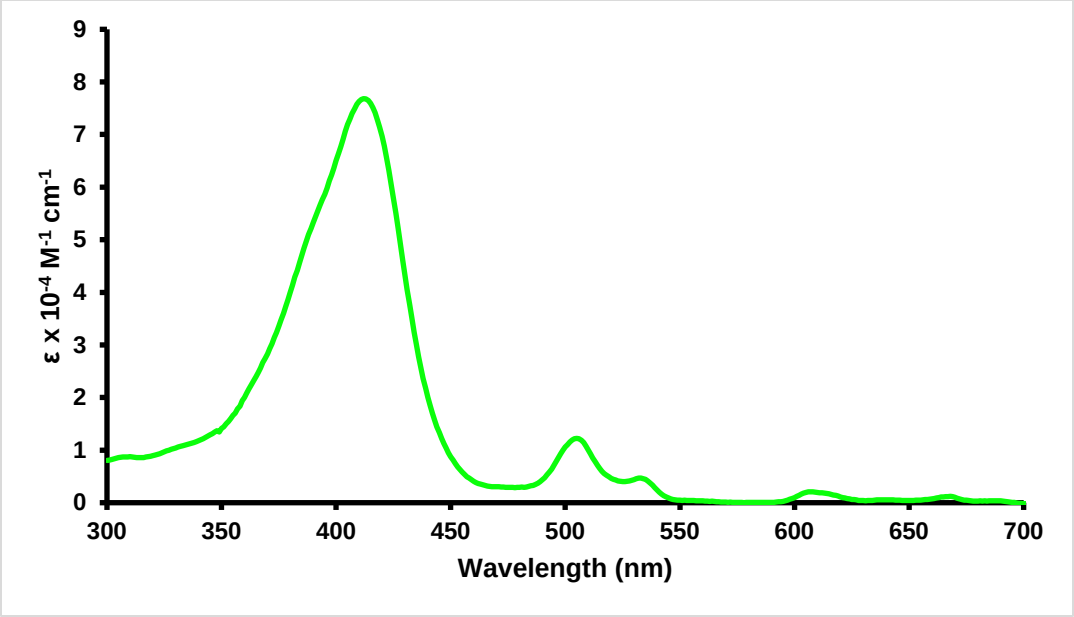

Figure D-91. UV-Vis spectrum of *N*-methyl thiaporphyrin **97b** in 1% triethylamine-dichloromethane.

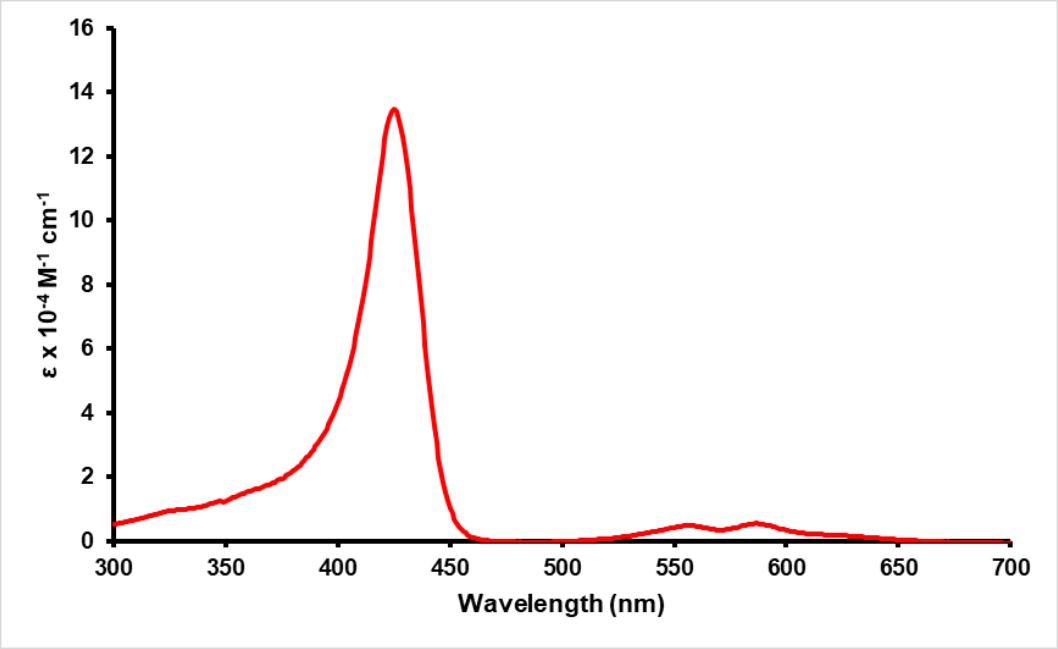

Figure D-92. UV-Vis spectrum of *N*-methyl thiaporphyrin **96b** in 1% TFA-dichloromethane.

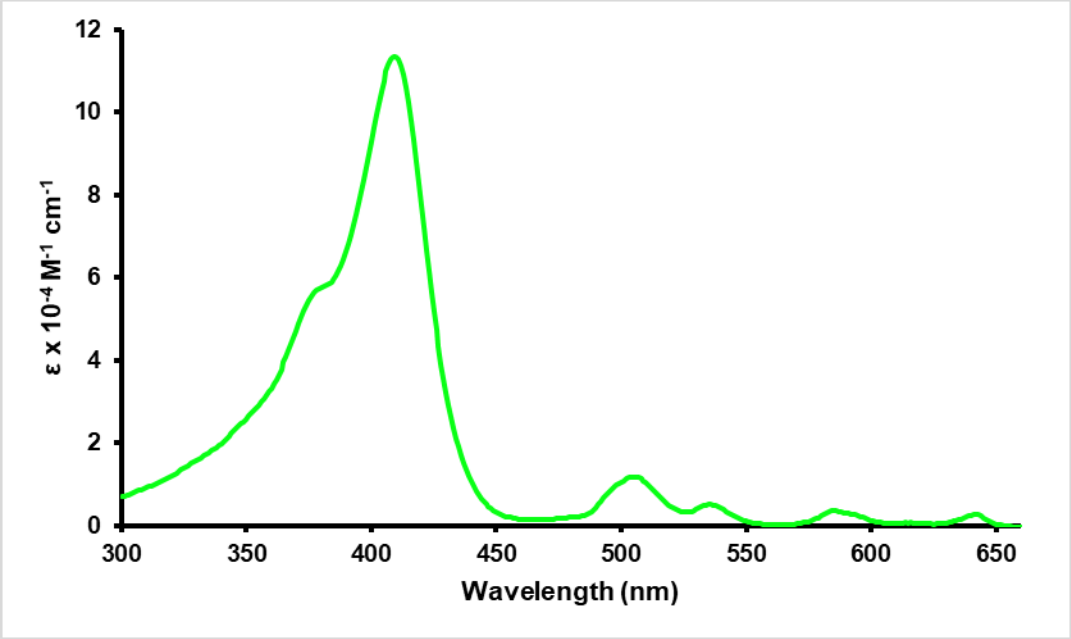

Figure D-93. UV-Vis spectrum of *N*-methyl porphyrin **99b** in 1% triethylamine-dichloromethane.

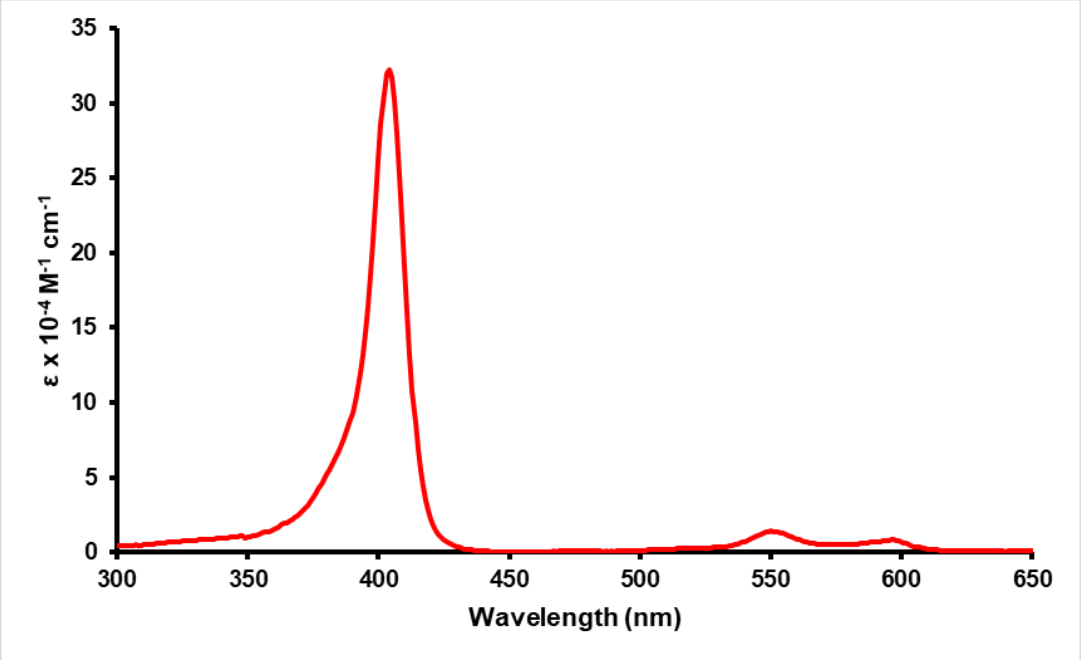

Figure D-94. UV-Vis spectrum of *N*-methyl porphyrin **99b** in 1% TFA-dichloromethane.

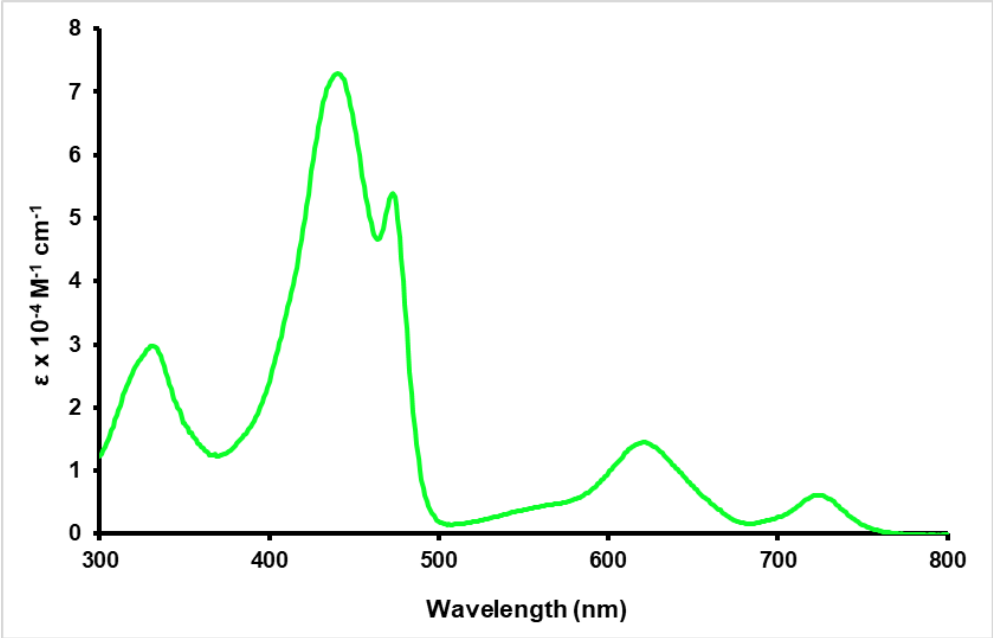

Figure D-95. UV-Vis spectrum of *N*-methyl oxybenziporphyrin **100a** in 1% triethylamine-dichloromethane.

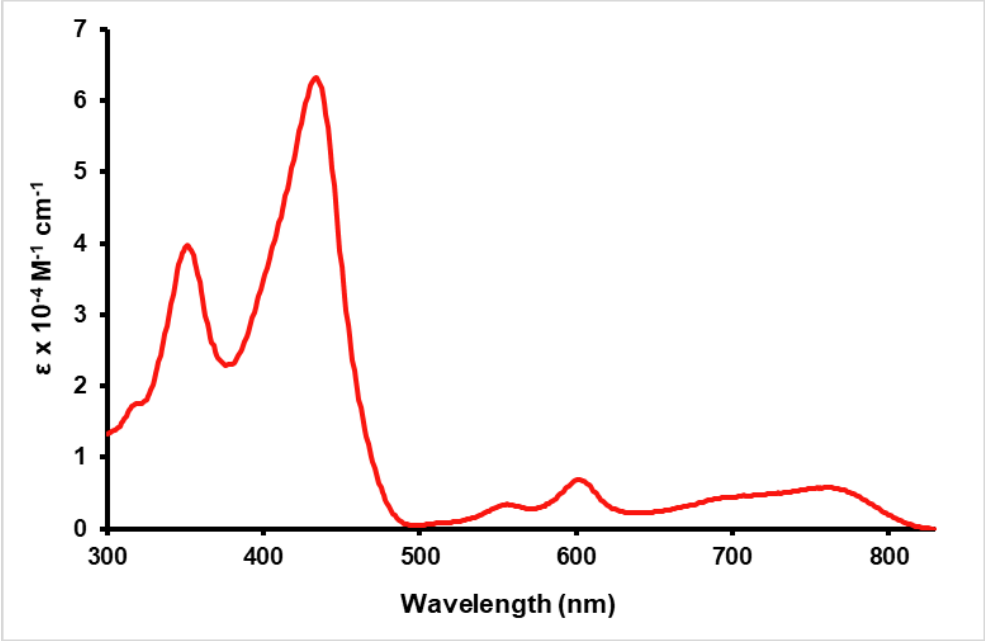

Figure D-96. UV-Vis spectrum of *N*-methyl oxybenziporphyrin **100a** in 1% TFA-dichloromethane.

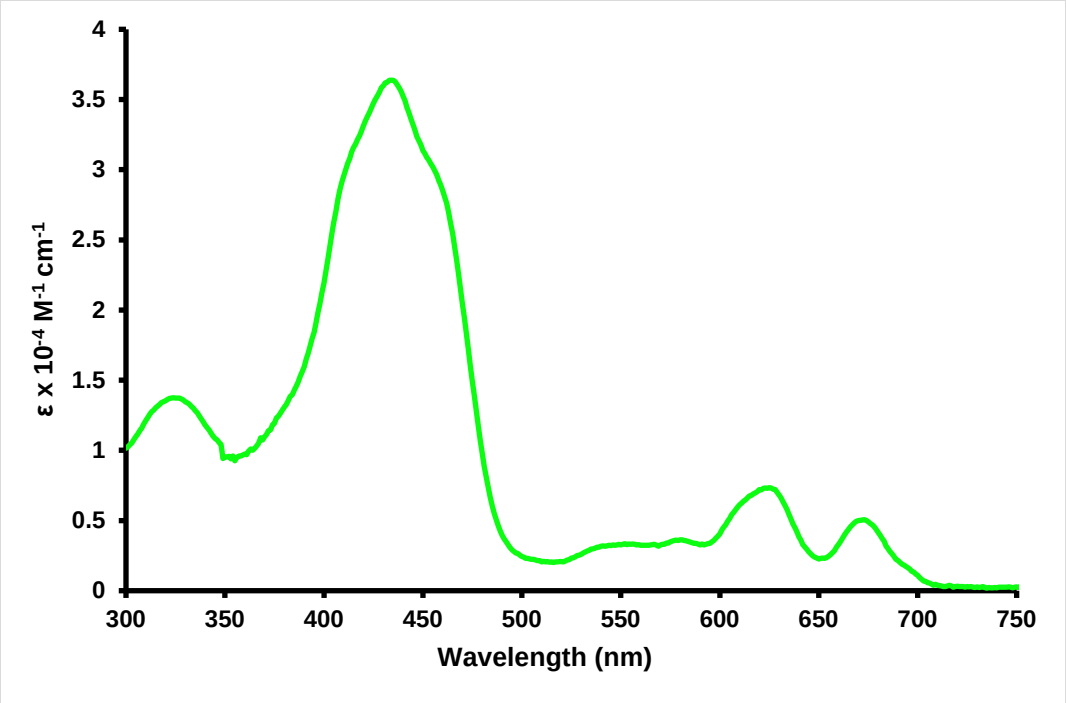

Figure D-97. UV-Vis spectrum of *N*-methyl oxypyriporphyrin **100b** in 1% triethylamine-dichloromethane.

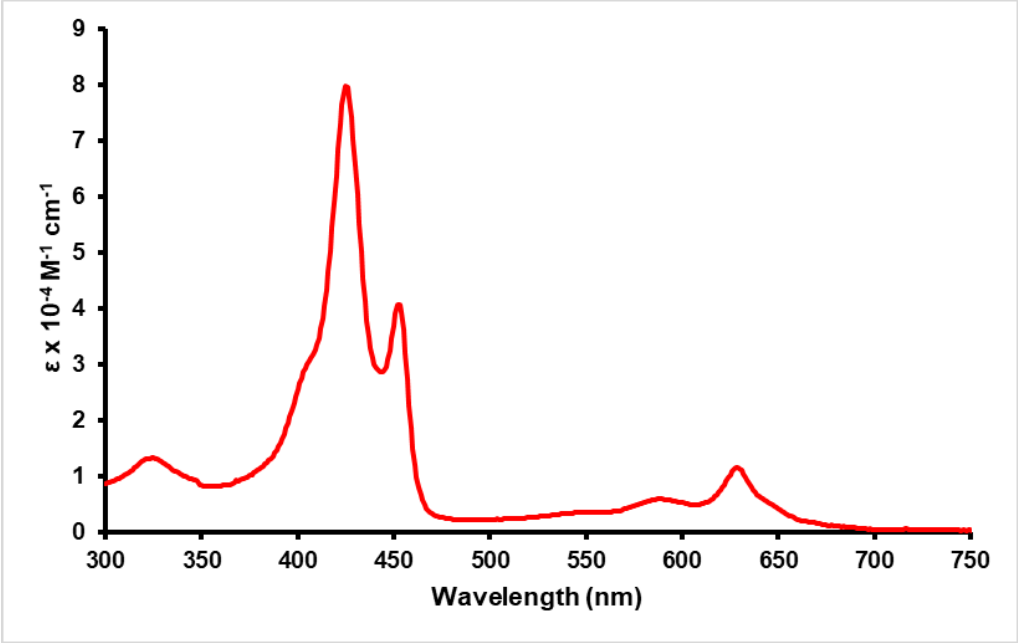

Figure D-98. UV-Vis spectrum of *N*-methyl oxypyriporphyrin **100b** in 1% TFA-dichloromethane.

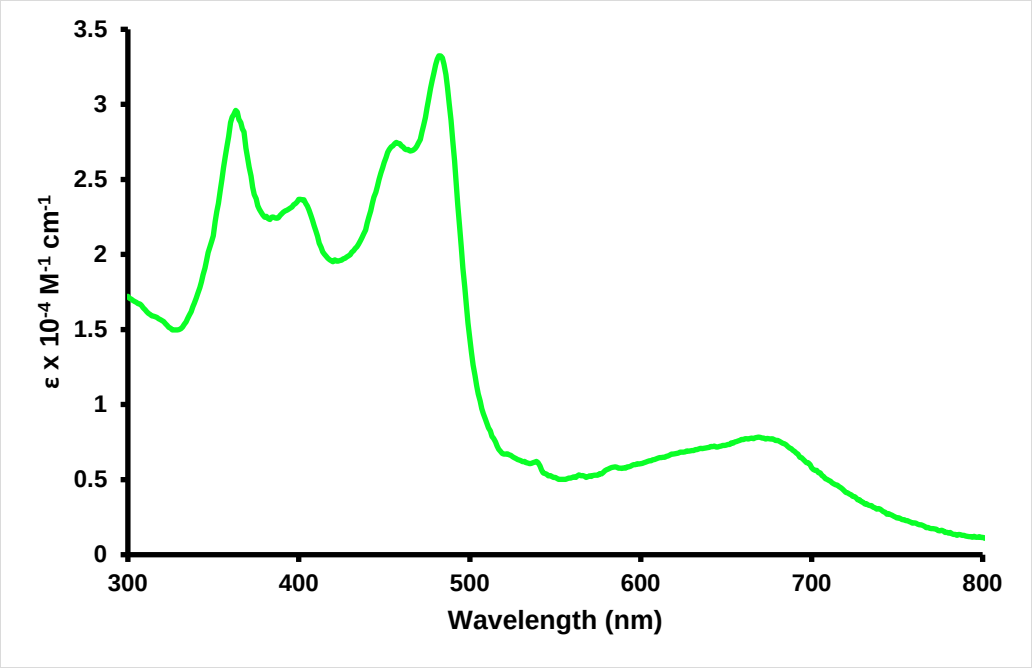

Figure D-99. UV-Vis spectrum of *N*-methyl *tert*-butyl azuliporphyrin **103**H_2^{2+} in 1% triethylamine-dichloromethane.

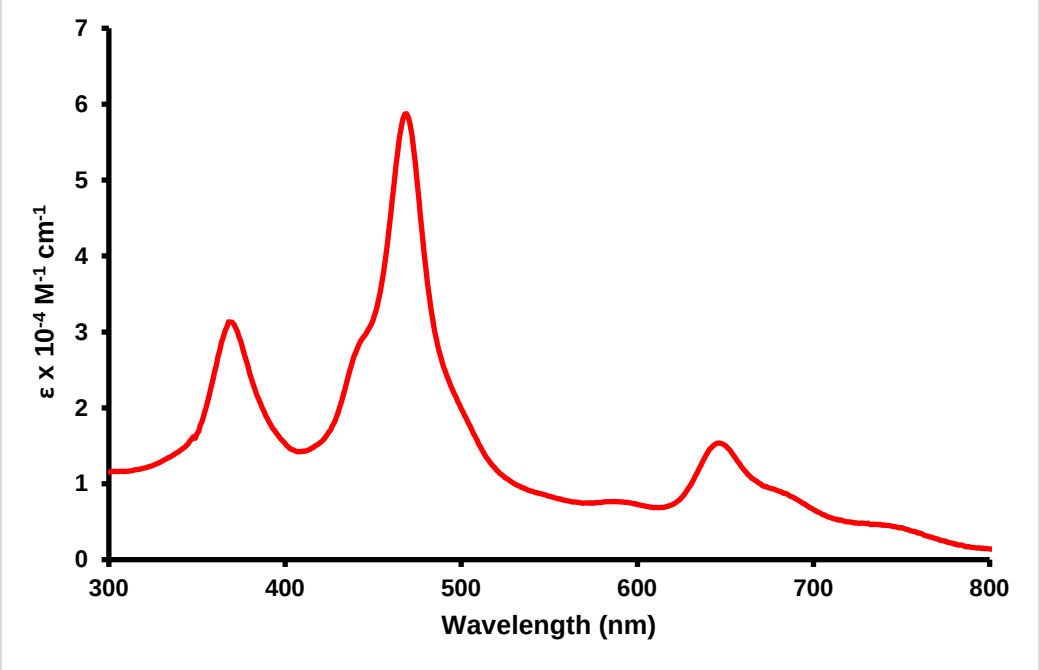

Figure D-100. UV-Vis spectrum of *N*-methyl *tert*-butyl azuliporphyrin **103**H_2^{2+} in 1% TFA-dichloromethane.